ORGANISATION EUROPÉENNE POUR LA RECHERCHE NUCLÉAIRE

CERN EUROPEAN ORGANIZATION FOR NUCLEAR RESEARCH

PHYSICS AT LEP2

Editors: G. Altarelli, T. Sjöstrand and F. Zwirner

Vol. 2

GENEVA
1996

ORGANISATION EUROPÉENNE POUR LA RECHERCHE NUCLÉAIRE

CERN EUROPEAN ORGANIZATION FOR NUCLEAR RESEARCH

PHYSICS AT LEP2

Editors: G. Altarelli, T. Sjöstrand and F. Zwirner

Vol. 2

GENEVA
1996

ABSTRACT

This is the final report of the Workshop on Physics at LEP2, held at CERN during 1995. The first part of vol. 1 is devoted to aspects of machine physics of particular relevance to experiments, including the energy, luminosity and interaction regions, as well as the measurement of beam energy. The second part of vol. 1 is a relatively concise, but fairly complete, handbook on the physics of e^+e^- annihilation above the WW threshold and up to $\sqrt{s} \approx 200$ GeV. It contains discussions on WW cross-sections and distributions, W mass determination, Standard Model processes, QCD and gamma–gamma physics, as well as aspects of discovery physics, such as Higgs, new particle searches, triple gauge boson couplings and Z'. The second volume contains a review of the existing Monte Carlo generators for LEP2 physics. These include generators for WW physics, QCD and gamma–gamma processes, Bhabha scattering and discovery physics. A special effort was made to co-ordinate the different parts, with a view to achieving a systematic and balanced review of the subject, rather than just publishing a collection of separate contributions.

CONTENTS

Volume 1

Volume 2

EVENT GENERATORS

EVENT GENERATORS FOR WW PHYSICS

Conveners: D. Bardin and R. Kleiss

Working group: E. Accomando, H. Anlauf, A. Ballestrero, F.A. Berends, E. Boos,
F. Caravaglios, D. van Dierendonck, M. Dubinin, V. Edneral, F.C. Erné, J. Fujimoto,
V. Ilyin, T. Ishikawa, S. Jadach, T. Kaneko, K. Kato, S. Kawabata, Y. Kurihara, D. Lehner,
A. Leike, R. Miquel, G. Montagna, M. Moretti, T. Munehisa, O. Nicrosini, T. Ohl,
A. Olchevski, G.J. van Oldenborgh, C.G. Papadopoulos, G. Passarino, D. Perret-Gallix,
F. Piccinini, R. Pittau, W. Płaczek, A. Pukhov, V. Savrin, M. Schmitt, S. Shichanin,
Y. Shimizu, T. Sjöstrand, M. Skrzypek, H. Tanaka, Z. Wąs

Contents

4

1 Introduction: the need for Monte Carlo

In this report we shall deal with the practical implementation of the theoretical results described in the WW study group report. There, many important results and formulae have been given which have to find their way into the analysis of the LEP2 data, in particular those dealing with the measurement of the W mass and couplings. It is our aim to describe the current state of the art of this implementation.

The simplest detectable final states of relevance are those consisting of four fermions (when we disregard the complications arising from photon bremsstrahlung, gluon bremsstrahlung and hadronization effects), and consequently the phase space has seven dimensions (eight, if we also include the overall azimuthal distribution of events around the beam axis – this distribution, however, is trivial as long as no transversely polarized beams are considered). Obviously, the sets of diagrams that contribute to a given final state is also quite complicated. Below, we shall present a classification of the various sets of diagrams that we have found useful in discussing and comparing results. When we also take into account the complicated peaking structures resulting from the many different Feynman diagrams, it becomes clear that the only way in which we can arrive at experimentally meaningful results in which all cuts can be accommodated is that of Monte Carlo simulation of the full event. This feature is even more pronounced than at LEP1, where the important events have a two-fermion final state, with only one relevant angular variable, and little peaking structure at given energy. There are, of course, processes such as $e^+e^- \to W^+W^- \to q\bar{q}\mu\nu_\mu$ where experimental cuts tend to be not very drastic, but even is such cases the estimate of a given experiment's acceptance and efficiency will probably have to rely on Monte Carlo simulation, even if the final fits are performed in some semi-analytic fashion. This is even more the case if in the above process we replace the muon by the electron.

1.1 Semianalytics versus event generators

Notwithstanding all this, it is very desirable to have at our disposal also calculations that do not rely on explicit event generation. As is the case in LEP1 physics, a number of semi-analytical results have been obtained, mainly in the form of the GENTLE code, which extends the formalism of [1] to integrate analytically over a number of variables, and performs the few remaining integrations using standard numerical packages (see [2] and references therein). Although in this way neither all diagrams nor all possible experimental cuts can be incorporated, we feel that the existence of such results, with an inherently much smaller numerical error as well as excellent control over the theoretical input, establishes an important benchmark for the Monte Carlo programs. As will be clear from our comparisons of the results of the various programs, GENTLE indeed serves, in many cases, as such a benchmark, especially in the 'tuned comparisons' we describe below.

Essentially all Monte Carlo codes presented here consist of two main ingredients, incorporated in (usually) three steps to produce numerical output. The ingredients are:

- a set of routines that, for given values of the fermions' four-momenta, produce the value of the matrix element, squared, and summed/averaged over the appropriate spins and colors. A wide number of techniques are used to obtain the matrix elements. For example, the `ALPHA` code takes as input the effective action of the theory, and numerically computes the saddle point of the path integral for given external momenta, without explicit reference to Feynman diagrams. The `ERATO`, `EXCALIBUR`, `WTO`, `WPHACT`, and `WWGENPV` codes (among many) use different kinds of helicity techniques, where the relevant diagrams are either put in 'by hand' or generated by some semi-automatic procedure. Yet other codes such as the `CompHEP` and `grc4f` programs employ a fully automated diagram-generating-and-evaluating code. The fact that such disparate treatments manage to come up with agreeing numbers can be viewed as important checks on the correctness of the various individual procedures. Some programs (in particular `ALPHA` and `WWFT`) also incorporate explicit photons into the computation of the matrix element, while the `grc4f`, `PYTHIA` and `WOPPER` programs use 'parton shower' techniques to generate photons, the `KORALW` code employs the so-called YFS approach, and WWGENPV uses a p_T-dependent structure-functions-inspired formulation. It should also be stressed that not all programs can compute all contributing Feynman diagrams: this important fact should be kept in mind when we discuss the results.

- a set of routines that transform uniformly distributed pseudo-random numbers into phase space variables, taking as much of the peaking structure as possible into account by a number of mappings and branch choices. Again, different programs employ widely different techniques to this end. In particular for processes with electrons or positrons in the final state the occurrence of t-channel photon exchange calls for a very careful treatment.

Obviously, the distinction between these two ingredients is not always completely straightforward, especially in codes that employ 'showering', where the phase space generation should itself induce the correct matrix elements. Also, not all programs use pseudo-random numbers as a basis for the phase space generation: some codes employ 'black box' integrators such as provided by the NAG library, while the `WTO` uses quasi-random, deterministic number sets (technically known as shifted Korobov sets).

The running of a typical Monte Carlo consists of three steps:

- initialization: here the input parameters are read in, and various preparatory steps are undertaken. For instance, `EXCALIBUR` will, at this stage, determine the contributing Feynman diagrams and print them, and work out which peaking structures contribute.

- generation: here a event-generating routine is called the desired number of times to arrive at a phase space point together with its matrix element. Also the necessary filling of histograms and other bookkeeping is performed in this step.

- evaluation: when the desired number of events has been produced, the total cross section

7

is computed as the average event weight, where the event weight is defined as the ratio of the matrix element squared over the phase space Jacobian.

For details about the workings of the various different programs we refer to the next subsection, where more information is given for each individual program, together with the necessary references.

1.2   The Ultimate Monte Carlo

The above rough description does, of course, no justice to the effort that has already gone into all the existing codes: but it is only fair to say that, at this moment, none of them can be considered as the definitive program. This 'Ultimate Monte Carlo' (which may remain out of reach) is approached, by different authors, in different ways, and some programs have desirable features (for instance, explicit, finite-p_T photons), that are not shared by other programs, which however have their own attractions (for instance, inclusion of all Feynman diagrams). As we have already indicated, it must be always kept in mind, when comparing programs, that such differences in approach will unavoidably result in differences in results; *but such differences should **not** be regarded as any kind of theoretical uncertainty, but rather as an indication of the importance of the different ingredients.* In fact, the real theoretical uncertainty (due, for example, to unknown higher-order corrections) is quite distinct from the differences between programs. It may be instructive to give a list of the features of the Ultimate Monte Carlo, in order for the user to appreciate to what extent a given program satisfies her/his needs in a particular analysis. The Ultimate Monte Carlo should:

- treat all possible four-fermion final states, with all relevant Feynman diagrams (possibly with the option to restrict the set of diagrams).

- produce gauge-invariant results. If one describes off-shell, unstable W pair production using only the three Feynman diagrams in the *CC03* sector, then gauge dependence will result. Fortunately, at LEP2 energies these effects are very small provided a suitable gauge such as the unitary or 't Hooft-Feynman gauge is chosen: but, especially when t-channel photon exchange takes place, the gauge cancellations can be very delicate. Related to this is the requirement that the various coupling constants are chosen in a consistent manner.

- have a correct treatment of the bosonic widths. This is closely related to the previous point: if one just inserts a running width, gauge invariance is lost, with dramatic results for final states with electrons or positrons. This problem, and its various possible resolutions, are described in detail in [3].

- have the fermion masses taken into account. For instance, EXCALIBUR treats the fermions as strictly massless, which accelerates the computation of the matrix elements considerably, but imposes the need to avoid phase space singularities by explicit cuts, and makes it impossible to incorporate Higgs production and decay consistently.

8

- have explicit, p_T-carrying photons. This is of particular importance for a distinction of "initial" and "final" state radiation in an M_W measurement, as well as the search for anomalous couplings.

- have the higher-order photonic radiative corrections taken into account properly. This probably does not mean, given the experimental accuracy to be expected at LEP2, that very high orders or very high precision are required, but it would be very useful to be able to prove that radiative effects are small for a particular quantity. For instance, the Coulomb singularity which modifies the WW intermediate state is an important effect.

- should have good control over the non-QED radiative correction, preferably in the form of the complete $\mathcal{O}(\alpha)$ corrections, and resummed higher-order effects where necessary.

- incorporate QCD effects, both in the W self-energy and in the gluonic corrections to quark final states. Also relevant is the interference between electroweak and QCD channels in the production of four-quark final states. In this place it should be remarked that it is of course trivial to add the 'naive' QCD correction $1 + \alpha_s/\pi$ to the total cross section, but in the presence of cuts this may be less appropriate: the particular strategy adopted must depend on the interface with a hadronization routine.

- have a good interface to hadronization packages. This is especially relevant to the W mass measurement, together with the next point:

- give information, for each generated event, on how much of the matrix element is contributed by each subset of Feynman diagrams, and/or each color configuration. This is important for problems of color reconnection and Bose-Einstein effects.

- have Higgs production and decay implemented.

- have the possibility of anomalous couplings. This allows for the study of the effects of such couplings to good precision using control-variate techniques (that is, switching the anomalous couplings on and off for a given event sample, thereby avoiding statistical fluctuations that might wash out the small anomalous effects).

1.3   Comparison generalities

The rest of this contribution deals with the description and the comparison of the different codes and their results. It must again be stressed, that the field is still in a state of flux, and probably not one of the programs has taken on its final form. We can, therefore, only present results as they are at this particular moment (December 1995), with the remark that most of the discrepancies are well-understood and are expected to decrease significantly in the near future. There are several ways in which we have compared the various codes:

9

- **by ingredients**

  To this end, we just compare which of the features of the Ultimate Monte Carlo are part of the different codes. Again, we stress that the choice of code depends to a large extent on the user's particular problem. For instance, background studies will require a code that contains all Feynman diagrams, while high-precision studies of inclusive quantities may be better of with a semi-analytical program such as GENTLE. In the next section we present what we feel to be the most relevant information on each program.

- **by 'tuned' comparison**

  This means that we have chosen a minimal process described by a minimal set of diagrams (*CC03* and *CC10*), for which we have computed several quantities. The idea of this exercise is that *all programs should agree on these numbers*. Of course, one must make sure that the physical parameters of the theory such as masses and widths in propagators, and the coupling constants in the Lagrangian, are constructed to be identical in all codes. The aim is twofold. In the first place it allows to establish the *technical precision* of the various codes, and we have come (as will be shown) to a satisfactory number of one per mille or better, at least for a large cluster of dedicated codes. In the second place, such a tuned comparison is a good bug hunting ground, as we have found. Many small differences usually can be traced back either to small bugs or small differences in input parameters or cuts.

- **by 'best you can do' comparison**

  The tuned comparison, useful as it is, is not of direct experimental relevance since it relies on switching off all features in which one program is better than another. The real physics results must of course incorporate more than this bare minimum, and therefore we have computed a number of quantities, for one class of processes, in which (apart from agreed-upon input parameters) each code provides us with its own 'best answer'. Again, we want to stress that these results do not agree, nor should they be expected to: differences in these results reflect differences in the physics approach. Comparisons apart, in the end the programs will have to provide the community with explicit predictions, and this 'best you can' should give an idea of the extent to which these predictions depend on the various pieces of physics input. Whereas the results of the tuned comparison are not expected to change appreciably in the near future, the 'best you can' results must, and probably will, converge over time as more physics input is incorporated into more programs.

- **by 'all you can do' comparison**

  finally, we have let the programs pass an 'all you can do' comparison phase, where each program has computed essentially all the processes it is able to treat. Of course, only some out of all the codes can do *all* four-fermion processes: but from such a game should arise a coherent picture of what the current state-of-the-art is. Another goal of the 'all you can do' comparison, which is also 'tuned', is to provide precision benchmarks for *all four-fermion processes*.

1.4 A classification of 4-fermion processes

For the various four-fermion final states produced in e^+e^- annihilation, the numbers of contributing Feynman diagrams are quite different. On top of double-pole (WW or ZZ) diagrams there are, in general, a lot of so-called background diagrams with different intermediate states, which are single-resonant or non-resonant. In this section we present a classification of all four-fermion final states in the Standard Model [1]. This classification was originally proposed in [5]. The tables presented below are borrowed from papers [2] and [6], while their description is updated.

In general all possible final states can be subdivided into two classes. The first class comprises production of (up, anti-down) and (down, anti-up) fermion pairs,

$$(U_i \ \bar{D}_i) \ + \ (D_j \ \bar{U}_j) \,,$$

where i, j are generation indices. The final states produced via virtual W-pairs belong to this class. Therefore, we will call these 'CC'-type final states. The second class is the production of two fermion-antifermion pairs,

$$(f_i \ \bar{f}_i) \ + \ (f_j \ \bar{f}_j) \,, \ \ f = U, \ D.$$

As it is produced via a pair of two virtual neutral vector bosons we will call this a final state of 'NC'-type. Obviously these two classes overlap for certain final states.

The number of Feynman diagrams in the CC classes are shown in table 1.

	$\bar{d}u$	$\bar{s}c$	$\bar{e}\nu_e$	$\bar{\mu}\nu_\mu$	$\bar{\tau}\nu_\tau$
$d\bar{u}$	*43*	**11**	20	**10**	**10**
$e\bar{\nu}_e$	20	20	*56*	18	18
$\mu\bar{\nu}_\mu$	**10**	**10**	18	*19*	**9**

Table 1: *Number of Feynman diagrams for 'CC' type final states.*

Three different cases occur in the table 1 [2]:

(i) The *CC11* family.
   The two fermion pairs are different, the final state does not contain identical particles nor electrons or electron neutrinos (numbers in table 1 in **boldface**). The corresponding eleven diagrams are shown in figures 1 and 2. There are less diagrams if neutrinos are produced (`CC9, CC10` processes).

(ii) The *CC20* family.
   The final state contains one $e^\pm$ together with its neutrino (Roman numbers in table 1); compared to case (i), the additional diagrams have a t channel gauge boson exchange. For a purely leptonic final state, a *CC18* process results.

---

[1] The classification is done with the help of `CompHEP` [4].

[2] In [7], a slightly different classification has been introduced; the relation of both schemes is discussed in [5].

(iii) The *CC43/mix43* family and *CC56/mix56* process.

Two mutually charge conjugated fermion pairs are produced (*italic* numbers in table 1). Differing from cases (i) and (ii), the diagrams may proceed via both, WW- and ZZ-exchanges. For this reason, we will also call them *mix*-ed class. There are less diagrams in the *mix43* process if neutrinos are produced (*mix19* process). With the two charge conjugated ($\bar{e}\nu_e$) doublets, one has *mix56* process.

Each of these classes contains the *CC03* process, which is described by the usual three 'double W-pole' Feynman diagrams, figure 1. From the *CC11* set of diagrams only 10 contribute
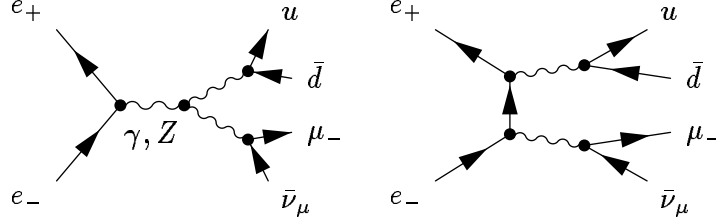
Figure 1: The *CC03* set of Feynman diagrams

to the process $e^+e^- \to \mu^- \bar{\nu}_\mu u\bar{d}$, because the photon doesn't couple to the neutrino (cf. fig. 2).
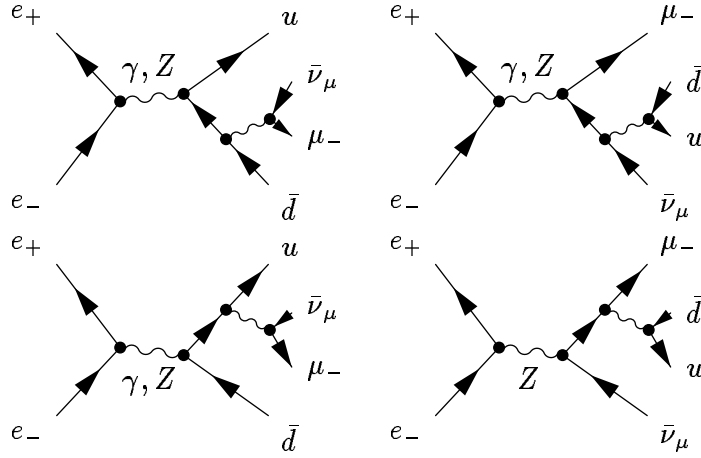
Figure 2: The *CC11* set of Feynman diagrams

For the final states corresponding to the NC class the number of Feynman diagrams is presented in table 2.

(i) The *NC32* family.

The simplest case (numbers in **boldface**) does not contain electrons or identical fermions[3].

---

[3] We exclude the Higgs boson exchange diagrams from the classification in the tables.

	$\bar{d}d$	$\bar{u}u$	$\bar{e}e$	$\bar{\mu}\mu$	$\bar{\nu}_e\nu_e$	$\bar{\nu}_\mu\nu_\mu$
$\bar{d}d$	4·16	*43*	48	**24**	21	**10**
$\bar{s}s, \bar{b}b$	**32**	*43*	48	**24**	21	**10**
$\bar{u}u$	*43*	4·16	48	**24**	21	**10**
$\bar{e}e$	48	48	4·36	48	*56*	20
$\bar{\mu}\mu$	**24**	**24**	48	4·12	19	*19*
$\bar{\tau}\tau$	**24**	**24**	48	**24**	19	**10**
$\bar{\nu}_e\nu_e$	21	21	*56*	19	4·9	12
$\bar{\nu}_\mu\nu_\mu$	**10**	**10**	20	*19*	12	4·3
$\bar{\nu}_\tau\nu_\tau$	**10**	**10**	20	**10**	12	6

Table 2: *Number of Feynman diagrams for 'NC' type final states.*

(ii) The *NC48* and *NC21* families.
   The numbers in roman correspond to the final states which include $f = e, \nu_e$ except for cases covered by item (iv). The large number of diagrams here is due to additional t-channel exchange.

(iii) The *NC4·16* family.
   With identical fermions f ($f \neq e, \nu_e$), the number of diagrams grows drastically due to the necessity to satisfy the Pauli principle, i.e. to anti-symmetrize the amplitude. For purely leptonic processes this number of diagrams reduces to *4·12* since the gluon exchange doesn't contribute.

(iv) The *NC4·36* and *NC4·9* processes, with the two e^+e^- or $\bar{\nu}_e\nu_e$ pairs in the final state. The corresponding numbers are shown sans serif.

(v) The *mix43* and *mix56* processes.
   The numbers in *italic* correspond to final states which are also present in table 1, case (iii).

2 Descriptions of 4-fermion codes

2.1 ALPHA

Authors:

Francesco Caravaglios   caravagl@thphys.ox.ac.uk
Mauro Moretti   moretti@hep1.phys.soton.ac.uk

Description

In ref.[8], we suggested an *iterative* algorithm to compute automatically the scattering matrix elements of any given effective Lagrangian, Γ. By exploiting the relation between Γ and the

connected Green's function generator, Z, we obtained a formula which does not require the use of Feynman graphs, and is suitable to implementation in a numerical routine. The problem of computing the scattering matrix element can be reformulated as the problem of finding the minimum of Z with respect to a *finite* set of variables. Once the stationary conditions for Z are written down, they can be solved iteratively and, truncating the series after a proper number of steps, one obtains the solution. Using this algorithm we have been able to build a Fortran code, ALPHA, for the automatic computation of matrix elements. When the initial and final states of the process are specified (type, momenta and spin of the external particles) the program prepares an array b_j for all the possible degrees of freedom (the label j refers to internal and external momenta and to the particles type, color and spin). As shown in [8], the scattering matrix element $\mathcal{A}$ is obtained as

$$\mathcal{A} = a_i b_i + \frac{1}{2} K_{lm} b_l b_m + \frac{1}{6} O_{ijk} b_i b_j b_k. \tag{1}$$

where the b_j are obtained from the equation of motion in presence of a source term a_i.

$$a_i = K_{im} b_m + \frac{1}{2} O_{ijk} b_j b_k, \tag{2}$$

which can be solved iteratively.

The matrix O_{ijk} contains the physical couplings between the degrees of freedom b_j of the fields entering the scattering process and the matrix K_{lm} accounts for the kinetic terms in the Lagrangian. In the Fortran code the matrix elements O_{ijk} and K_{lm} are returned by some subroutines as a function of the finite set of possible momenta P_m.

The ALPHA code includes all the electroweak interactions and the whole flavor content of the Standard Model (SM) (presently it does not account for the strong interactions) and it can perform all possible electroweak matrix elements in the SM regardless of the initial or final state type. In addition, due to its simple logic, it allows for modification of the Lagrangian with no excessive effort (by adding the proper subroutines to compute the new O_{ijk} interactions and/or adding the relevant variables for the new particles). Since the algorithm is purely numerical, the output can be immediately used for an integration procedure.

Features of the program

The numerical integration is performed by mean of the package VEGAS [9]. The variables have been chosen in such a way that each singularity corresponds to an integration variable allowing VEGAS to cope effectively with the pole structure of the physical process. The phase space is factorized as a multiple decay process using the formula

$$d\Phi(P; q_1, q_2, q_3, ..., q_n) = d\Phi(Q = q_1 + q_2; q_1, q_2) d\Phi(P; Q, q_3, ..., q_n)(2\pi)^3 d^2 Q \tag{3}$$

where the squared momenta Q^2 corresponds to the physical singularities. For some final states there are multiple channels exhibiting a pole structure. In these cases it is difficult to obtain a good convergence of the integral with a single choice of phase space variables. Therefore we

split the integration domain in different regions, and in each of them we make a different choice of physically motivated variables. One additional real variable is used to map the discrete set of spin configurations. At least for the processes we have considered, the VEGAS algorithm has adequately performed a selection of the relevant spin configurations.

In principle, all possible final states can be treated. For most of them the corresponding phase space routines are also implemented: an exception being processes with electrons in the final state. All possible choices of spin configurations can be selected, for instance polarized initial states are immediately available.

The Monte Carlo does not include initial/final-state radiation (ISR/FSR). We have instead used ALPHA to compute the rates for the process $e^+e^- \rightarrow 4 \; fermions \; + \; \gamma$; all the Standard Model diagrams are evaluated with a finite (constant) width of the electroweak gauge bosons and the physical fermion masses.

Anomalous couplings can be easily added, even with momentum dependent form factors, running widths etc.

Since the method of calculation does not rely on Feynman graphs technique it is not possible, in general, to isolate the contribution of a single graph. Turning on/off each single interactions, the contribution of many subsets of diagrams can be extracted but this might be not practical enough.

Program layout

The program requires as input the center of mass energy and the number of external particles: for each type (*i.e.* top, strange,...Z) we have to enter a number which can be 0 if no particle of that type exists, or 1,2,... as required. A subroutine generates the momenta and the spin configurations according to a phase space preselected among a list of prepared ones. All the couplings of the theory are collected in a single subroutine which is adequately commented and is called only once at the beginning of the run. A subroutine is provided which has as input the external momenta and as output a flag which when set to zero forces the program to ignore the given phase space point, thereby allowing for any kind of cut. Another subroutine is provided to make it possible to produce plots. Each variable to be plotted must be normalized between 0 and 1 and as output a file is produced which registers for each variable N (input number) equispatiated bins containing the (unnormalized) integral and variance. As output the cross section (in picobarn) is also given with its statistical error.

With few modifications, we can therefore provide a code for the computation of *all* processes listed in tables 1 and 2 allowing the user to implement any cuts to change the numerical values of the electroweak couplings and to record all the data required to produce a plot.

Other operations, like allowing the user to compute an arbitrary process or to change the Lagrangian of the model are not completely user-friendly at the moment.

Input parameters and the Lagrangian

We used the common set of Standard Model parameters (as discussed in section 3). All the fermions are massive. The gauge boson propagators include the width, which is constant in order to obtain gauge invariant matrix elements. The inclusion of the proper, physical, running width for the gauge bosons in a gauge invariant way, namely including the relevant corrections to the three and four point Green Functions, is straightforward in our approach and it will be done in a near future. The cuts applied to the four final fermions are the common one used for the comparison tests.

Availability:
The program is available upon e-mail request from the authors.

2.2   CompHEP 3.0

Authors:

E.Boos	boos@theory.npi.msu.su
M.Dubinin	dubinin@theory.npi.msu.su
V.Edneral	edneral@theory.npi.msu.su
V.Ilyin	ilyin@theory.npi.msu.su
A.Pukhov	pukhov@theory.npi.msu.su
V.Savrin	savrin@theory.npi.msu.su
S.Shichanin	shichanin@m9.ihep.su

Description

The main idea in `CompHEP` [10] was to enable on to go directly from the Lagrangian to cross sections and distributions effectively, with a high level of automation.

Version 3.0 has 4 built-in physical models. Two of them are versions of the Standard Model (SU(3)xSU(2)xU(1)) in the unitary and 't Hooft-Feynman gauges with the parameters corresponding to the standard LEP2 input.

The general structure of the `CompHEP` package is represented in Figures 3, 4. It consists of symbolical and numerical modules. The main tasks solved by the symbolical module (written in C) are :

1. to select a process by specifying *in-* and *out-* particles. Any type of five particle final state for decays and five particle final state for collisions can be defined;

2. to generate and display Feynman diagrams. It is possible to delete some diagrams from the further consideration, leaving only limited subsets;

4. to generate and display squared Feynman diagrams (corresponding to squared S-matrix elements);

5. to calculate analytical expressions corresponding to squared diagrams with the help of a fast built-in symbolic calculator. Traces of gamma matrices products are calculated, summing over the final state polarizations. Masses of initial and final particles can be kept nonzero in the squared amplitude calculation and phase space integration;

6. to save symbolic results corresponding to the squared diagrams calculated in the `REDUCE` and `MATHEMATICA` codes for further symbolical manipulations;

7. to generate the optimized `FORTRAN` code for the squared matrix elements for further numerical calculations.

Program layout

The numerical part of the `CompHEP` package is written in `FORTRAN`. It uses the `CompHEP FORTRAN` output, the `BASES&SPRING` package [11] for adaptive Monte-Carlo integration and unweighted event generation. The main tasks solved by the numerical module are :

1. to choose phase-space kinematical variables. Exact parameterizations of three, four and five particle phase space in the case of massive particles are used [12];

2. to introduce kinematical cuts over any squared momenta transferred and squared masses for any groups of outgoing particles. Any kinematical cuts for noninvariant variables can be introduced using explicit restrictions on the four-momenta;

3. to perform a kinematical regularization (mapping) to remove sharp peaks in the squared matrix elements. The package has a rich choice of optimizing possibilities (various combinations of phase space parameterizations and mappings);

4. to change the `BASES` parameters for Monte-Carlo integration;

5. to change numerical values of model parameters;

6. to calculate distributions, cross sections or particle widths by the Monte-Carlo method. The output for a cross section value (sequence of MC iterations) and distributions (set of histograms) has the standard `BASES` form;

7. to perform the same integration taking into account structure function for incoming particles. Initial state radiation (ISR) is implemented in the structure function approach [13]. An interface to the standard PDF library is available. Final state radiation and the Coulomb term are not implemented. Photon radiation from the initial and final states can be introduced by calculation of exact amplitude for $2 \rightarrow 5$ process (4 fermions + photon).

8. to generate events and to get histograms simulating the signal and background. `SPRING` [11] is used for unweighted event generation.

`CompHEP` is a menu-driven program with a context HELP facility. Each of two variants of the Standard Model (unitary or and 't Hooft-Feynman gauges) is defined by four tables:

17

menu 1

QED
Fermi model
St. model (unit. gauge)
St. model (Feyn. gauge)
NEW MODEL

menu2

Enter process
Edit model
Delete changes

menu3

Variables
Constraints
Particles
Lagrangian

menu 4

Squaring
View diagrams

menu 5

View squared diagrams
Symbolic calculation
Write results
REDUCE program
Numerical calculator
Enter new process
Interface

menu 6

FORTRAN code
REDUCE code
MATHEMATICA code

menu 7

View/change data
(Set angular range)
(Set precision)
(Angular dependence)
Parameter dependence

menu 8

Show plot
Save results in a file
Recalculate

menu 9

(Total cross section)
(Asymmetry)

menu 10

Show plot
Save results in a file

Figure 3: The menu system for the CompHEP symbolic part

Main menu

1. Calculation	2. IN state
3. Model parameters	4. Invariant cuts
5. Kinematics	6. MC parameters
7. Regularization	8. Task formation
9. View results	10. User's menu

In state

1. StructF(1) = *OFF*
2. SQRTS = *1000*
3. StructF(2) = *OFF*

Invariant cuts

1. Insert new cut
2. Delete cut
3. Change cut

MC parameters

1. Ncall = *10000*	2. Acc1= *0.1*
3. Itmx1= *5*	4. Acc2= *0.1*
5. Itmx2=*0*	6. Event generator OFF
7. Number of events = *1000*	

Regularization

1. Insert new regularization
2. Delete regularization
3. Change regularization

Task formation

1. Table parameters
2. Set default session
3. Add session to batch

View results

1. session # to view - *3*	2. View result file
3. View protocol file	4. View histogram file

Figure 4: The menu system for the CompHEP numerical part

Variables	list of parameters (masses, widths, couplings, mixings)
Constraints	list of functionally dependent parameters
Particles	list of particles and quantum numbers
Lagrangian	list of Feynman rules for vertices

At present, versions for different platforms exist: HP Apollo 9000, IBM RS 6000, DECstation 3000, SPARC station, Silicon Graphics and VAX.

Availability
The package is available from
internet host: theory.npi.msu.su
directory: pub/comphep-3.0
files: 30.tar.Z, install.doc, manual.ps.Z

2.3   ERATO

Author:[4]

Costas G Papadopoulos	papadopo@cernvm.cern.ch
	C.G.Papadopoulos@durham.ac.uk and
	papadopo@alice.nrcps.ariadne-t.gr

Description

ERATO[14]-[15] is a four-fermion Monte Carlo[5] . This program is an evolution of an older code where single-W production, $e^-e^+ \rightarrow e^- \bar{\nu}_e W$ was calculated including all possible non-standard couplings of the three-boson interactions[14], $WW\gamma$ and WWZ. This code has now been updated in order to include all background graphs for the processes $e^-e^+ \rightarrow \ell \bar{\nu}_\ell u \bar{d}$ with $\ell = e, \mu, \tau$. The actual version of the program can now produce results for any four-fermion final state. As far as the matrix element calculation is concerned, the program uses a representation of the basic fermion current $\bar{u}_\lambda(p_1)\gamma^\mu u_\lambda(p_2)$, the 'E-vector',which is given as follows:

$$E_\lambda^\mu(p_1, p_2) \equiv \bar{u}_\lambda(p_1)\gamma^\mu u_\lambda(p_2) \tag{4}$$

where

$$E_-^0 = \sqrt{p_1^+ p_2^+} + \frac{(p_{1x} + ip_{1y})(p_{2x} - ip_{2y})}{\sqrt{p_1^+ p_2^+}}$$

$$E_-^x = \sqrt{\frac{p_2^+}{p_1^+}}(p_{1x} + ip_{1y}) + \sqrt{\frac{p_1^+}{p_2^+}}(p_{2x} - ip_{2y})$$

---

[4]In several aspects of the program the following people have contributed:

Mark Gibbs, Liverpool	gibbs@afsmail.cern.ch
Robert Sekulin, DRAL	robert@vax2.rutherford.ac.uk
Spyros Tzamarias, Liverpool	tzamaria@cernvm.cern.ch

[5]In ancient Greek mythology EPATΩ was the muse of Music. By accident the name of the program is also part of the genERATOr group.

20

$$E_-^y = -i\left(\sqrt{\frac{p_2^+}{p_1^+}}(p_{1x}+ip_{1y}) - \sqrt{\frac{p_1^+}{p_2^+}}(p_{2x}-ip_{2y})\right)$$

$$E_-^z = \sqrt{p_1^+p_2^+} - \frac{(p_{1x}+ip_{1y})(p_{2x}-ip_{2y})}{\sqrt{p_1^+p_2^+}} \tag{5}$$

with $p^{\pm} = p^0 \pm p^3$. The above representation is valid only for massless fermions. All matrix elements have been tested against `MadGraph`[16] calculations under the same conditions, and the agreement was at least 13 digits using a `REAL*8` declaration.

In addition to the amplitude calculation, we have implemented a Monte Carlo integration algorithm which is essentially identical to the multichannel approach of references [7, 18]. The problem is that the amplitude we have to integrate over is a very complicated function of the kinematical variables, peaking at different regions of phase space. The idea is to define different kinematical mappings, corresponding to different peaking structures of the amplitude and then use an optimization procedure to adjust the percentage of the generated phase-space points, according to any specific mapping, in such a way that the total error is minimized.

Special care has also been taken in order to include in a gauge-invariant way the width effects. As is well known the introduction of an s-dependent width leads to gauge-violation in the $s-$ and $t-$ channel. This is because the s-dependent width violates the Ward identities at the one loop. The solution is to include consistently all one loop corrections. More precisely, if one restricts oneself to fermionic corrections, one has to include the one-loop fermion 'triangle' to the three-boson vertex function. This way, the gauge-invariance is restored. Bosonic corrections are much more subtle due to the gauge-parameter dependence, but in the case of W and Z line-shape parameters their contribution is suppressed compared to the fermionic one, due to simple kinematical reasons. In `ERATO` the imaginary part at the one-loop level of both two-point and three-point functions of vector bosons is implemented in a very compact analytic form[3].

Leading higher order corrections are also included in `ERATO`, in the form of initial-state radiation (ISR), using the structure function approach with all possible ISR-radiator functions available (β or η option).

An other important feature of `ERATO` is the incorporation of all CP conserving non-standard couplings. In fact the way the program is written enables us to include any non-standard couplings, for instance $ZZ\gamma$ or CP-violating $WW\gamma$ and WWZ parameters.

Features of the program
The main features of the program are the following: it can be used both as an event generator and as an integrator: all final states, and all possible cuts, are in principle allowed. Initial-state radiation is implemented using structure functions; final-state radiation and the Coulomb correction are not implemented. All possible anomalous couplings are implemented, the fermions are assumed to be massless, with a leading-log approximation for the structure functions.

Interface
The output from the `ERATO` generator for the semi-leptonic and four-jet channels contains

colored partons, and consequently it is desirable to include models of QCD effects such as hadronization in the simulation procedure. One way to include these phenomena is to pass the four-momenta generated by ERATO to an existing simulation package. This approach is attractive as there are a number of such packages in existence.

The ERATO generator has been interfaced successfully to the JETSET [28] and HERWIG [17] packages. T he procedure is the same in both cases and can be easily extended to other simulation packages.

Firstly, the event configurations produced by ERATO are not of equal probability and have to be selectively used in such a way so as to respect the correct distributions of kinematic variables. This is achieved by unweighting the events; events are used at random with a probability given by the weight of the event divided by the maximum weight. The efficiency of this procedure is typically of order 0.1%.

Secondly, the particle content of the ERATO final state has to be selected. At present, this is determined at the start of a simulation run but in principle can be performed on an event- by event- basis.

Thirdly, the ERATO program assumes that all the fermions are massless. As a result, the four-momenta of a final state configuration have to be shifted in order to place massive fermions on shell. This is achieved by shifting the three-momenta slightly. As the energies in a typical LEPII event are high compared to the particle masses the change in momenta is a negligible effect. Following these steps, the simulation package is then used for the parton showering and hadronization stages of event generation.

Program layout
The structure of the program will be described in detail in a future publication in CPC.

Input parameters
Any set of input parameters can be implemented. In the most usual version the LEP2 standard input is used. Preferred and comparison values are identical.

Output
In the present form of the program any histogram can be obtained very easily. Cross sections for left and right incoming electrons are given separately. Error estimates are the standard ones.

Availability
From ftp://alice.nrcps.ariadne-t.gr/pub/papadopo/erato/

2.4 EXCALIBUR

Authors:

F.A. Berends   berends@rulgm0.leidenuniv.nl
R. Kleiss   t30@nikhefh.nikhef.nl
R. Pittau   pittau@psw218.psi.ch

Short description:
The program `EXCALIBUR` [7, 18] evaluates cross sections for electron-positron scattering into four final-state fermions. This is done by Monte Carlo simulation, in which events are generated over a phase space determined by a number of a-priori cuts (in many cases, the whole phase space is accessible). Each event carries a weight such that the average event weight gives the total cross section. The distribution of events over the phase space is generated by employing a large number of mappings of random numbers. Given an event, additional cuts can be imposed by hand by setting the weight of unwanted events to zero; and, of course, any number of differential distributions can also be constructed. Since the matrix elements are computed on the level of helicity amplitudes, as sums of distinct diagrams, the contributions of subsets of diagrams and of particular helicity configurations can also be studied.

Program features:

1. **method of integration:**
   the program is a strict Monte-Carlo one, in the sense that no phase space variables are integrated over analytically. This means that *all* phase space variables are amenable to any kind of cut. The generated events come with a non-constant weight: a sample of unweighted events can be selected from the generated sample by the usual rejection techniques. The efficiency of this procedure is in many cases of the order of a few per cent, depending on the final state of choice and the phase space cuts.

2. **possible final states:**
   all possible four-fermion final states are included: the user supplies the choice in the input file. An important restriction is that the fermions are considered to be strictly massless, and therefore Higgs exchange is not included.

3. **possible cuts:**
   since every event is completely specified, in principle any conceivable phase space cut can be implemented. It must be noted that, since all fermion masses are taken to be zero, singularities can occur in photon exchange channels, and these have to be excised by user-supplied a-priori cuts. Therefore, when a final state e^+ or e^- occurs, a cut on its scattering angle and energy is necessary, and when a charged particle-antiparticle pair is produced, a cut on its invariant mass is in order. These cuts are specified in the input file (see discussion below). For calculations based on a restricted set of Feynman graphs without photon exchange (e.g. the *CC03* diagrams) such cuts are of course not necessary.

4. **treatment of ISR:**
ISR is implemented in the form of two structure functions, *i.e.* two energy fractions x_1 and x_2 are generated, but no bremsstrahlung p_T. The four-fermion event is then generated in the reduced-center-of-mass frame. The actual photon structure functions used are the 'type 2' ones of the W-pair report.

5. **treatment of FSR:**
No FSR is at the moment included.

6. **treatment of final state decays:**
since the fermions are considered massless, they are stable and no decay is provided: moreover, the fermions' density matrix is strictly diagonal.

7. **treatment of the Coulomb singularity:**
the Coulomb term can be easily implemented by multiplying the appropriate WW diagrams by the correct factor, but is not yet included in the standard version.

8. **treatment of anomalous couplings:**
a version of `EXCALIBUR` is available which includes anomalous triple-gauge-boson couplings. Six CP-conserving anomalous contributions can be put to a nonzero value: these correspond to the quantities x_γ, y_γ, x_Z, δ_Z, y_Z, and z_Z defined in ref. [19]. For zero values of these numbers the minimal Standard Model predictions are recovered.

9. **treatment of fermion masses:**
as mentioned, these are zero, both in the matrix element and in the phase space momenta.

10. **treatment of hadronization:**
no interface with hadronization routines are provided in the standard version; but since the momenta are completely specified the necessary `COMMON` can easily be constructed.

11. **subsets of diagrams etc:**
since in `EXCALIBUR` all diagrams and helicities are explicit, it is simple, for a given final state, to select subsets of diagrams or helicity combinations. There exists the possibility to select, using the input file, only those diagrams that correspond to the WW, ZZ, $We\nu$, Zee or $Z\nu_e\bar{\nu}_e$ final states, or include all tree diagrams.

Program layout
The working of `EXCALIBUR` can be divided into three parts: initialization, generation, and evaluation. The two main parts of the event generation stage are the choosing of a random phase space point, and the computation of the matrix element at that point.

The initialization is performed by the routine `SETPRO`. It reads the data from the input file, and determines from these which are the Feynman tree graphs that will be considered. There are two distinct diagram topologies: 'abelian' graphs, with only fermion-boson couplings, and 'nonabelian' ones with also triple-boson couplings. The program considers all possible permutations of the external momenta over these diagrams, and determines, by quantum numbers

24

conservation, if they can contribute. Then, also the most significant phase space mappings (so-called *channels*) are determined.

Upon the calling of an event, first the two energies $x_{1,2}$ of the incoming $e^{\pm}$ are generated. Then, in the center of mass frame after this ISR, one particular channel is picked, by which uniform random numbers are mapped into a phase space point. The various channels are constructed from a limited number of explicit mappings, each with its own subroutine: this modular structure ensures transparency of coding, easy debugging, and the possibility of implemented additional channels when necessary. The probability of picking a particular channel is given by its *a-priori weight*: the final cross section is by construction independent of the values of this weights. After this, the event weight is computed, as the ration of the matrix element squared to the generated phase space density. For the computation of the matrix element, we use the fact that every contributing nonabelian graph can, in the minimal standard model, be simply expressed as a combination of two contributing abelian ones. These are computed, for definite helicities, by spinor techniques. The phase space density consists of a sum of the densities appropriate to each contributing channel, weighted with their a-priori weights. At several points during a run of generating events, the a-priori weights are optimized so as to approximate the weight distribution with the minimum possible variance for the available set of channels, as described in [18].

The evaluation stage consists of the estimate of the average weight and its estimated error (and, in fact, the estimated error on the error estimate). Also, the distribution of all nonzero weights is plotted, together with some information on the a-priori weight optimization. More information can be found in [7].

Input parameters
We have used the following sets of input parameters, one for the tuned comparison with the other codes, and one that reflects what (in our view) is the most accurate prediction possible with EXCALIBUR. They are given in the table below.

parameter	'comparison'	'best'
Z mass (GeV)	91.1888	91.1546
Z width (GeV)	2.4974	2.49646
W mass (GeV)	80.23	80.02042
W width (GeV)	2.0366	2.03302
$\sin^2\theta_W$	0.231031	0.231031
$1/\alpha$	128.07	128.07
α_s	0	0.103

The following remarks are in order here. The 'best values' for the boson masses and widths are chosen so as to take into account the running of the widths, using the transform described in [20]. The value of α is used for the four-fermion system, but for the ISR the value $1/137$ is of course used. The use of α_s is relevant for four-quark and qq-two gluon final states, where the QCD four-jet production diagrams are also included. These values are set internally by the

program. In addition, there are a number of other input parameters, set in the input file:

NPROCESS	the number of processes to be treated
N	The number of events to be generated
ISTEPMAX	the number of times the a-priori weights are to be optimized
OUTPUTNAME	name of the output file
KREL	the set of diagrams to be considered: 0 all diagrams, 1 WW, 2: ZZ, 3: $We\nu$, 4: Zee, 5: $Z\nu_e\bar{\nu}_e$
LQED	0: no ISR, 1: ISR included.
ROOTSMUL	the total energy
SHCUT	minimum invariant mass after ISR
ECUT	minimum energy for the outgoing particles (4 values)
SCUT	minimum invariant mass for outgoing particle pairs (6 values)
CMAX	maximum value of $\cos\theta$ between two particles (14 values)
PAR	labels of the produced fermions (4 character*3 values)

All these values are reproduced in the output file.

Output

The output prints the process considered, with the labeling of the various particle momenta. Also a complete list of all abelian and nonabelian diagrams is given, and a list of all generation channels that will be used. Upon evaluation, information on the weight distribution is given, and the results of the weight optimization procedure.

Availability

The program is available from the authors upon request, as well as from the CPC library.

2.5   GENTLE/4fan

Authors:

D. Bardin[a]	BARDINDY@CERNVM.CERN.CH
M. Bilenky[a]	bilenky@ifh.de
D. Lehner[b]	lehner@ifh.de
A. Leike[a]	LEIKE@CERNVM.CERN.CH
A. Olchevski[a]	OLSHEVSK@VXCERN.CERN.CH
T. Riemann[a]	riemann@ifh.de

[a] FORTRAN code gentle_4fan.f
[b] FORTRAN code gentle_nc_qed.f

Description of the package

The GENTLE/4fan package is designed to compute selected total four-fermion production cross-sections and final-state fermion pair invariant mass distributions for charged current (CC) and neutral current (NC) mediated processes within the Standard Model (SM). For the $CC03$ subprocess, the W production angular distribution is also accessible. In the NC case, SM

Higgs Production is included. The phase space integration is carried out by a semi-analytical technique, which is described below. The GENTLE/4fan package is written in Fortran. It consists of two branches. The basic branch gentle_4fan.f contains all features of the package but complete initial-state radiation (ISR) to NC processes. The subroutine fourfan.f called by gentle_4fan.f performs the computation of NC cross-sections and is described in [21]. The (as yet) independent branch gentle_nc_qed.f includes complete ISR to $NC02$ and $NC08$ and will soon be merged into gentle_4fan.f.

Program features:

1. **Method of integration:**
   The package is a *semi-analytical* one. Without (with) ISR, the phase space is parametrized by five (seven) angular variables and the final state fermion pair invariant masses (plus the reduced center of mass energy squared). All angular variables are integrated analytically. The resulting formulae are input to the package. Invariant masses are subsequently integrated numerically with a self-adaptive Simpson algorithm. Optionally, for the $CC03$ subprocess, the W production angle may also be numerically integrated. The method is numerically stable and usually very fast.

2. **Possible final states:**
   The package may treat all four-fermion final states which do not contain identical particles, electrons, or electron neutrinos. This means that the package accesses all final states that are described by *annihilation* and *conversion* type Feynman diagrams (see [5] for a classification):

   (1) $CC03$ (with complete ISR) [22]

   (2) $NC02$, $NC08$ (with complete ISR) [23]

   (3) $CC9$, $CC10$, $CC11$ [2]

   (4) $NC06$, $NC10$, $NC24$, $NC32$ [24]

   (5) NC + Higgs [6]

   Via flags, cross-sections for subsets of Feynman diagrams may be extracted.

3. **Cuts**
   Cuts may be imposed on invariant masses of fermion pairs and on the invariant mass of the final state four-fermion system. Using the structure function approach in gentle_4fan.f, cuts on the electron/positron momentum fraction can be imposed. For the $CC03$ subprocess, cuts on the W production angle are enabled.

4. **Initial state radiation**
   ISR is implemented into the package. *Universal* ISR is present for all processes [2]. In addition, the package includes complete, i.e. *universal* and *non-universal* ISR for the $CC03$, $NC02$, and $NC08$ processes [22, 23]. *Non-universal* ISR does not contribute to *annihilation* diagrams. It may be argued that *non-universal* ISR is very small, $\mathcal{O}(10^{-3})$,

for *conversion-annihilation* interferences. The speed of the package is slowed down, if *non-universal* ISR is included, due to its complex analytical structure.

5. **Final state radiation**
   Final state radiation is not implemented.

6. **Treatment of final state decays**
   Final state decays are not accounted for.

7. **Treatment of the Coulomb Singularity**
   The Coulomb singularity is included according to reference [25].

8. **Treatment of the Anomalous Couplings**
   Anomalous couplings are not included.

9. **Treatment of masses**
   In general, final-state masses are neglected in the matrix elements. Where needed, however, masses are retained in the phase space. In addition, masses of heavy particles coupling to the Higgs boson are taken into account where appropriate.

10. **Hadronization**
    No interface to hadronization is foreseen.

Input parameters

All input parameters are set inside the **Fortran** code. **gentle_4fan.f** uses the following flags, set in the subroutine **WWINOO**:

IBCKGR: *CC03* case (**IBCKGR=0**) or *CC11* case (**IBCKGR=1**)

IBORNF: Tree level (**IBORNF=0**) or ISR corrected (**IBORNF=1**) quantities

ICHNNL: *CC03* (**ICHNNL=0**), *CC11* with specific final state [$l_1\nu_1 l_2\nu_2$ (**ICHNNL = 1**), $l\nu q\bar{q}$ (**ICHNNL = 2,3**), $q_1\bar{q}_1 q_2\bar{q}_2$ (**ICHNNL = 4**)], and inclusive *CC11* (**ICHNNL=5**)

ICOLMB: Inclusion of Coulomb singularity (**ICOLMB=1,...,5**) or not (**ICOLMB=0**)
                Recommended value: **ICOLMB=2**

ICONVL: Flux function (**ICONVL=0**) or structure function apporach (**ICONVL=1**)
                Recommended value: **ICONVL=0**

IGAMZS: Constant Z width (**IGAMZS=0**) or s-dependent Z width (**IGAMZS=1**)

IINPT: Input for tuned comparison (**IINPT=0**) or preferred Input (**IINPT=1**)

IIQCD: Naive inclusive QCD corrections are included (**IIQCD=1**) or not (**IIQCD=0**)

IMMIM: Minimal number of a moment requested by **IREGIM**

IMMAX: Maximal number of a moment requested by **IREGIM**

IONSHL: On-shell (**IONSHL=0**) or off-shell heavy bosons (**IONSHL=1**)

IPROC :   *CC* case (**IPROC=1**) or *NC* case (**IPROC=2**, call to **fourfan.f** is initialized)

IQEDHS: Determination of the *universal* ISR radiator:
           $\mathcal{O}(\alpha)$ exponentiated (**IQEDHS=-1,0**);
           $\mathcal{O}(\alpha)$ exponentiated plus different $\mathcal{O}(\alpha^2)$ contributions (**IQEDHS=1,...,4**)
                Recommended value: **IQEDHS=3**

IREGIM: Calculation of the total cross-section (**IREGIM=0**), the moments of the radiative loss of final state four-fermion invariant mass (**IREGIM=1**), the moments of the radiative energy loss (**IREGIM=2**), the moments of the W mass shift $\left(\sqrt{s_+} + \sqrt{s_-} - 2M_W\right)$ (**IREGIM=3**), and the first moments of $\cos\left(n\theta_W\right)$, $n = 1, ..., 4$ (**IREGIM=4**)

IRMAX : Maximum value of **IREGIM**

IRSTP : Step in a DO loop over **IREGIM**

ITVIRT: *Non-universal* virtual ISR included (**ITVIRT=1**) or not (**ITVIRT=0**)

ITBREM: *Non-universal* bremsstrahlung included (**ITBREM=1**) or not (**ITBREM=0**)

IZERO : See equation (4.5) of [2]. Recommended value: **IZERO=1**

IZETTA: See equation (4.21) of [2]. Recommended value: **IZETTA=1**

In the **gentle_nc_qed.f** branch, only the flags **IBORNF, IONSHL, ITVIRT, ITBREM** are used. The additional flag **IBOSON** in **gentle_nc_qed.f** distinguishes between the *NC02* and the **NC8** process.

The center of mass energy squared is chosen by setting the variable **IREG** and the parameters **ISMAXA** or **ISMAXB** in the main program. The following input may be changed by the user:

$$
\begin{array}{rclcl}
\texttt{GFER} & = & G_\mu & = & 1.16639 \times 10^{-5} \text{ GeV}^{-2}, \text{ the Fermi coupling constant} \\
\texttt{ALPW} & = & \alpha(2M_W) & = & 1/128.07, \text{ the running fine structure constant at } 2\,M_W \\
\texttt{AME} & = & m_e & = & 0.51099906 \times 10^{-3} \text{ GeV, the electron mass} \\
\texttt{AMZ} & = & M_Z & = & 91.1888 \text{ GeV, the } Z \text{ mass,} \\
\texttt{AMW} & = & M_W & = & 80.230 \text{ GeV, the } W \text{ mass} \\
\texttt{GAMZ} & = & \Gamma_Z & = & 2.4974 \text{ GeV, the } Z \text{ width} \\
\texttt{ALPHS} & = & \alpha_s(2M_W) & = & 0.12
\end{array}
$$

Output

The following derived quantities are computed in **gentle_4fan.f** and printed in the output:

$$
\begin{aligned}
\texttt{GAMW} &= \Gamma_W = \frac{9}{6\sqrt{2}\pi} G_\mu M_W^3 \left(1 + \frac{2\alpha_s(2M_W)}{3\pi}\right) \\
\texttt{SIN2W} &= \sin^2\theta_W = 1 - M_W^2/M_Z^2 \\
\texttt{GAE} &= -\frac{e}{4s_W c_W} = -\frac{\sqrt{4\pi\alpha(2M_W)}}{4s_W c_W} \\
\texttt{GVE} &= \texttt{GAE} \cdot (1 - 4s_W) \\
\texttt{GWF} &= \frac{g}{2\sqrt{2}} = -\texttt{GAE} \cdot \sqrt{2}c_W \\
|\texttt{GWWG}| &= \sqrt{4\pi\alpha(2M_W)} \\
|\texttt{GWWZ}| &= |\texttt{GWWZ}| \cdot \frac{c_W}{s_W}
\end{aligned}
$$

GVE and **GAE** are the electron vector and axial vector couplings, **GWF** is the fermion-W coupling, and |**GWWG**| and |**GWWZ**| are the trilinear gauge boson couplings for the photon and the Z

respectively. Further the output repeats the flag settings. After the cross-section calculation, the following output is printed:

$$\begin{aligned} \texttt{SQS} &= \sqrt{s} \\ \texttt{XSECO} &= \sigma_{\text{tot}}(s) \quad \text{in nanobarns} \end{aligned} \tag{6}$$

In addition, the calculated `MOMENTS` are printed. In the first column `IREGIM` is printed. The second column is arranged in blocks of three lines each. The first line contains the integer n. The second line contains the nth moment of the physical quantity indicated by `IREGIM`. The third line contains the dimensionless n^{th} moment obtained through division of the nth moment by the proper power of $\sqrt{s}/2$.

Although variable names are slightly different, `gentle_nc_qed.f` uses the same derived quantities as `gentle_4fan.f`. For one run, `gentle_nc_qed.f` outputs the used flag values together with the fermion code numbers `IFERM1/IFERM2`, the color factors `RNCOU1/RNCOU2`, the masses `AM1/AM2`, and the invariant pair mass cuts `CUTM12,CUTM34` for the final state fermion pairs. In addition, the lower cut `CUTXPR` on the ratio of the four-fermion invariant mass squared over the center of mass energy squared, s'/s is output. The main output, however, is an array of center of mass energies and the corresponding total cross-sections.

Availability
The codes are available from the authors upon E-Mail request or via WWW

`gentle_4fan.f`	from	`http://www.ifh.de/~bardin/gentle_4fan.uu`
`gentle_nc_qed.f`	from	`http://www.ifh.de/~lehner/gentle_nc_qed.uu`

2.6   grc4f 1.0

Authors:

J. Fujimoto	junpei@minami.kek.jp
T. Ishikawa	tishika@gal.kek.jp
T. Kaneko	kaneko@minami.kek.jp
K. Kato	kato@sin.cc.kogakuin.ac.jp
S. Kawabata	kawabata@minami.kek.jp
Y. Kurihara	kurihara@minami.kek.jp
D. Perret-Gallix	perretg@cernvm.cern.ch
Y.Shimizu	shimiz@minami.kek.jp
H.Tanaka	tanakah@minami.kek.jp
e-mail:	grc4f@minami.kek.jp

Program features

The program `grc4f` is a Monte Carlo generator for all final 4-fermion states generated by `GRACE`[26].

Several experimental cuts are implemented in default.

QED radiative corrections are implemented with structure functions for the ISR; in several processes QED parton shower (QEDPS) [27] is also an option, also for FSR.

Other final-state decays are implemented using JETSET, [28]. Color base information (related to the issue of color reconnection) is available.

The Coulomb term, and anomalous couplings, are both implemented.

Fermion masses can be kept nonzero everywhere.

Program layout

Integration

The numerical integration of the differential cross section over the phase space is carried out by the program BASES [29]. The probability information is automatically produced and saved in the file bases.data, according to which the event generation is done. An example is as follows:

```
call bsinit                          initialization of BASES/SPRING.
call userin                          initialization of parameters.
call bases( func, estim, sigma, ctime, it1, it2 )  integration
lun = 23
open(lun,file='bases.data',status='unknown',form='unformatted')
call bswrit( lun )                   saving the information to a file.
close ( lun )
```

In the arguments of subroutine bases, func is the name of a function program, estim is the cumulative estimate of the integral, sigma is the standard deviation of the estimate of the integral, ctime is the computing time in seconds and it1 and it2 is the number of iterations made in the grid optimization step and integration step.

Event generation

The event generation program SPRING[29] samples a hypercube according to bases.data, and tests if this point is accepted by comparing the probability at the point to the maximum probability in the hypercube. When SPRING accepts a point, the event corresponding to the point is generated with weight one. An example is as follows:

```
implicit real*8 (a-h,o-z)
parameter( nextrn = 6 )
common /sp4vec/ vec(4,nextrn)
....
real*4  p,v
common /lujets/ n,k(4000,5),p(4000,5),v(4000,5)
.....
call bsinit                          initialization of BASES/SPRING.
call userin                          initialization of parameters.
lun = 23
open(lun,file='bases.data',status='old',form='unformatted')
```

```
        call bsread( lun )                  reading the probability information.
        close( lun )

        call gr2lnd                         setting parameters for JETSET from GRACE.

  *===> Event generation loop
        mxtry  = 50                         number of maximum trials.
        mxevnt = 10000                      number of events.
        do 100 nevnt = 1, mxevnt
          call spring( func , mxtry )
          ( Four-momentum is stored in array vec.)
          ( The event information is converted into common block /lujets/.)
    100 continue
```

Input parameters

In the program **grc4f** the menu modes are supported using the command interpreter **KUIP**[30] developed at CERN and the identical environment to **PAW++**[31] is furnished to users, who select the menu and type parameters in menu windows.

- Selection of 4 fermion process.

- Center of mass energy:$\sqrt{s}$

- Mass and width of all particles.

- Experimental cuts

    - Minimum and maximum angle cuts for each particles (in the laboratory frame) (**coscut**).

    - Minimum and maximum energy cuts for each particles(**engyct**).

    - Minimum and maximum invariant mass cuts(**amasct**). ($Q_1 = (p_3 + p_4)^2$, $Q_2 = (p_5 + p_6)^2$)

    - Resonance mass and width in case of $1/Q_i$-singularity.

- Flag for Coulomb term.

- Flag for anomalous couplings in some processes.

- Selection of the calculation: no-radiation case, structure functions, or QEDPS.

- Parameters for integration step: number of iteration steps and number of sample points.

- Parameters for event generation step: maximum number of trials and number of events.

The general parameters in GRACE can be found in the GRACE manual[26] (spin polarization, graph selection and so on).

Output:

- Total cross section, the standard deviations and the convergence behavior in the integration steps.

- Histograms:

    - $d\sigma/dE_i, i = 3,4,5,6$:Energy distributions of each final particles
    - $d\sigma/d\cos\theta_i, i = 3,4,5,6$
    - Invariant Masses Q_1 and Q_2.

- Scatter plots:

    - $\cos\theta_i - E_i$
    - $Q_1 - Q_2$.

The contents of histograms and scatter plots are copied into the HBOOK format file[32].

Availability
By anonymous ftp to ftp location: **/kek/minami/grc4f** at **ftp.kek.jp**

2.7   KORALW 1.03

Authors:

M. Skrzypek	skrzypek@hpjmiady.ifj.edu.pl
S. Jadach	jadach@cernvm.cern.ch
W. Płaczek	placzek@hephp02.phys.utk.edu
Z. Wąs	wasm@cernvm.cern.ch

Description
This program includes not only QED effects in the initial state but also in leptonic decays of W and secondary decays, i.e. in the τ lepton decays. Hadronization of quarks is also performed. The effects of spin are included in combined W-pair production and decay. The τ polarization is also taken into account in its decays. Any experimental cut and apparatus efficiency may be introduced easily by rejecting some of the generated events.

Program changes from version 1.02 to 1.03

Here we describe the main properties of the generator KORALW. We do not present the program, which was published in [33]-[34]. The present version 1.03 features all properties of the previous version 1.02:

- The matrix element for W-pair production and W-pair decay into four fermions (the *CC03* group) with a proper W-spin treatment and finite W width,

- All W decay channels into pairs of leptons or quarks,

- Initial-state multi-photon emission in the full photon phase space (i.e. with finite transverse photon momenta),

- Simulation of the decay of polarized τ leptons (from W decay) in all possible channels, taking into account spin polarization and QED bremsstrahlung [35].

- Photon emission by leptons in W decay, up to double bremsstrahlung [36].

- Arrangement of quarks from W decay into colored strings and fragmentation into hadrons according to the LUND model using JETSET [28].

- Massive kinematics with exact four-momentum conservation for the entire $W^- W^+$ production and decay process.

In version **1.03** the following four major improvements have been introduced:

- Coulomb correction, in a form useful close to the WW threshold.It is taken from ref. [37] and it can be activated in straightforward way, as explained in the program documentation. Starting from the present KORALW version 1.03, the KeyCul component of the program input parameter NPAR(1) is thus *not* dummy anymore.

- KORALW now includes an interface to the external library calculating the correction-weight due to a more complete matrix element (so called background processes). At present, an interface to the GRACE library [26] calculating multi-diagram matrix elements is available. On occasion, one may wish to replace the matrix element by a different one, for instance including special combinations of anomalous couplings. Due to the modular structure of KORALW and, in particular, due to the full factorizability of the approximate QED matrix element into a Born matrix element and the QED part, it is straightforward to replace the existing Born-level matrix element with any other one, provided that the external library is able to calculate the corresponding matrix elements out of the externally generated four-momenta. To this end an external program, calculating the ratio of the matrix element squared of the particular choice to the basic matrix element squared of the program, has to be provided by the user.

  A pre-defined interface, now included in KORALW, will activate those routines with the help of Key4f component of KORALW input parameter NPAR(4)= 100*KeyACC +10*Key4f +KeyMix. For Key4f=0 no external matrix element is included and for Key4f=1 it is active. The new position of the weight switch, KeyWgt=NPAR(3) is also introduced. For KeyWgt=2 the program works as for the old and not modified KeyWgt=0 setting, but the external weights are calculated and transmitted to the common block wgtall.

34

In our distribution directory (see section 4 of program documentation) the additional fortran file is introduced in the directory `interfaces`. On the user side, his own directory has to replace the directory `ampli4f`. The following two routines have to be provided: `AMPINI(XPAR,NPAR)` which should initialize the external matrix element library. Standard `KORALW` input parameter matrices `XPAR` and `NPAR` can be used there for the initialization purposes. The `SUBROUTINE AMP4F(Q1,IFBM1,Q2,IFBM2,P1,IFL1,P2,IFL2,P3,IFL3,P4,IFL4, WTMD4F,WT4F)` should calculate ratio `WTMD4F`, of the new matrix element squared, and the one of the standard `KORALW`. The `Q1,IFBM1,Q2,IFBM2,P1,IFL1,P2,IFL2,P3, IFL3, P4,IFL4` denote respectively four momenta and identifiers (accordingly to the PDG conventions [38]) of initial state effective beams and the final state fermion states before final state bremsstrahlung generation. The additional vector weight `WT4F(I), I=1,9` may optionally be filled by routine `AMP4F`. It is not used in the program but only transmitted to the `KORALW` optional weights common block `wgtall` as `wtset(40+I)`. The `WTMD4F` is set into `wtset(40)`.

An example of the interfaced external matrix-element, based on the `GRACE` code [26], can be obtained upon request from the authors of `KORALW`. In the distribution version we include a dummy `ampli4f` library. It sets the external weight to 1 and prints a warning message.

We found it useful to introduce the `KeyWu` switch which controls the level of sophistication of the W width implementation. Like for the Z (`KeyZet`) case `KeyWu`=0,1,2 denotes respectively $(s/M_W)\Gamma_W$, constant and zero W width. Note that `NPAR(2)`= `100000*KeyWu +10000*KeyRed +1000*KeySpn+100*KeyZet +10*KeyMas +KeyBra`.

- Anomalous couplings for the WWV, $V = Z, \gamma$ vertices in the built-in matrix element are parameterized by 2×7 variables $g_1^V, g_4^V, g_5^V, \lambda_V, \kappa_V, \tilde{\lambda}_V, \tilde{\kappa}_V$ as defined in [41]. They can be reached by `KeyACC` component of `KORALW` input parameter `NPAR(4)`=`100*KeyACC+10*Key4f` `+KeyMix`. `KeyACC`=1 activates their values as set by the user via `KORALW` input parameter vector `xpar` (see routine `KORALW` for more details) and prints them to the output. `KeyACC`=0 enforces the Standard Model values.

- The semianalytical part of the program `KORWAN` was enlarged with two functions `s1wan(s1)` and `s1s2wan(s1,s2)` for the one and two dimensional distribution of the single or double W invariant masses. These functions require standard initialization of the `KORWAN` routine with the input parameters as explained in `KORALW` manual. Optionally, if the `KORWAN` input parameter `keymod` is increased by 10000 the calculations in `KORWAN` are not executed and the initialization is performed only.

Still remaining limitations of the program are:

- A simplified matrix element for the QED photon emission,

- Lack of electroweak non-QED corrections[6],

_____

[6]Most probably these corrections are small in comparison with the experimental precision and it is not

- A simplified "color arrangement" for four quark jets.

The above and other shortcomings of the program will be systematically addressed in the forthcoming versions of the program.

Availability
The Version: 1.03 is available from
www: http://hpjmiady.ifj.edu.pl/programs/programs.html

2.8   LEPWW

Author:

F.C. Erné   z63@nikhef.nl

Description

The original `LEPWW` event generator[39] contains *CC03* and *NC02* tree-level diagrams for the processes $e^-e^+ \rightarrow u\bar{u}u\bar{u}$, $e^-e^+ \rightarrow u\bar{u}d\bar{d}$ and $e^-e^+ \rightarrow u\bar{u}d\bar{d}$, with massless fermions and W and Z poles. Its present name and version is 'egwwv208.car' in the L3 event generator library. A FORTRAN file is available.

Features of the program

A complete set of final state fermions is available.

Order α initial-state radiation, allowing transverse momentum, is implemented following the procedure in the REMT routines[40].

Final state radiation from electrons, muons and τ's can be switched on optionally, according to the `PHOTOS` package[36].

For τ decay final lepton states of definite helicity are projected out, which allows decay through an adapted version of the `TAUOLA` routines[35].

Non-SM couplings have been implemented with the parameterization of Hagiwara et al[41].

Quark fragmentation proceeds through `JETSET` routines[28].

QCD effects on the boson widths and branching ratios can be taken into account.

No Coulomb term is implemented.

The program aims at a 1 to 2% precision in the description of total and differential processes. The program has been available throughout the LEP2 workshop. The development has been completed.

---

necessary to include them in the Monte Carlo program – it is enough if they are in the auxiliary semi-analytical program.

Input parameters: data cards

FAW, FAZ	fudge factors for W and Z width
PROC	Generate WW or ZZ
DKW1,DKW2	Decay of W^+, W^- into $q\bar{q}$, $e\nu$, $\mu\nu$, $\tau\nu$
DKZ1,DKZ2	Decay of $Z1, Z2$ into $q\bar{q}$, $\nu\bar{\nu}$, e^+e^-, $\mu^+\mu^-$, $\tau^+\tau^-$
IRAD,FRAD	Flags for initial and final-state radiation
WMAX	Maximum weight
F1G-F7Z	Fourteen variables for the Triple Boson Vertex
LEP2	LEP2 workshop parameters; it overrules the other data cards

Availability

http://www.fys.ruu.nl/~dieren/LEPWW.html

2.9 LPWW02

Authors

Ramon Miquel   miquel@alws.cern.ch

Michael Schmitt   schmitt@vxaluw.cern.ch

General description

LPWW02 is a Monte Carlo program for the simulation of four-fermion final states at LEP2. It contains the Feynman diagrams with two resonating W's and Z's and features, among other things, initial- and final-state radiation, Coulomb singularity effects and effective couplings. It is interfaced to the JETSET package to handle gluon radiation, hadronization and decays.

The generator is based on a complete Monte Carlo calculation of the cross section for the process $e^+e^- \rightarrow f_1\bar{f}_2f_3\bar{f}_4$ through a pair of heavy bosons, WW and/or ZZ [42]. Initial- and final- state radiation are incorporated with structure functions. The Monte Carlo algorithm for event generation uses two subgenerators to generate the WW and ZZ topologies. Suitable approximants are used in the generation step to increase its efficiency using the importance sampling technique. At the end, a rejection algorithm ensures that the unweighted events produced are distributed according to the exact matrix element. A complete description of the physics in the program, with results and comparisons with other calculations is available [43].

Features of the program

- LPWW02 is a Monte Carlo event generator of unweighted events. Any cut can be applied to the generated events.

- The accessible final states are those that can be produced in e^+e^- collisions from intermediate states consisting on two W bosons or two Z bosons: $u\bar{d}\mu^-\bar{\nu}_\mu$, $u\bar{u}\mu^+\mu^-$, $u\bar{u}d\bar{d}$,... In flavor configurations like the last one, the interference between the WW and ZZ diagrams is properly taken into account. In a given run, the user can either specify a fixed final

37

state or get directly the correct flavor mix for events produced through two W's and/or two Z's.

- Initial state radiation is simulated using the structure-function approach [44, 45]. The Born-like cross section at the reduced center-of-mass energy after initial-state radiation is convoluted with the structure functions of the electron and positron, which take into account their probabilities to radiate. The electron structure function, $D_e(z,s)$, taken from ref. [45], includes soft-photon exponentiation and leading-logarithmic corrections up to $\mathcal{O}(\alpha^2)$. The structure function approach is used in the collinear approximation and, hence, the photon direction is assumed to be that of the incoming beams. Consequently, no real photon four-momenta are generated inside the experimentally accessible regions of phase space. Since the radiation not only changes the effective center-of-mass energy of the event, but also the center-of-mass momentum with respect to the laboratory system, a boost is applied to the generated particles to take this into account.

- We employ the PHOTOS package [36] to simulate radiation from final state electrons and muons. Radiation from quarks is taken care of by the JETSET package [28] Radiation from taus or their decay products is neglected. The algorithm in PHOTOS provides full kinematic information for the splitting $f \to f'\gamma$. It is based on an implementation of $\mathcal{O}(\alpha^2)$ bremsstrahlung calculation in the leading-log approximation. This means that final-state radiation does not influence the total cross section calculation in any way.

- In the first stage, the program produces a final state consisting on four-fermion plus a number of photons. The interface with JETSET takes care of hadronization and subsequent decays of hadrons. JETSET also takes care of decaying the tau leptons.

- We have implemented the Coulomb correction in the production of two W's following ref. [46]. It is numerically equivalent to the treatment of ref. [25].

- At this time, the possibility of anomalous couplings is not contemplated in the program.

- The fermions are generated with their appropriate masses. However the matrix element is computed in the massless limit.

- LPWW02 is interfaced with JETSET.

- It is straight-forward to get the information on the contributions from different sets of diagrams in view of a possible simulation of the effect of color recombination.

Program layout

The structure of the program can be summarized as follows:

- Initialization. It includes the computation of the maximum weight for the rejection algorithm that will be used later and the initialization of the PHOTOS package used for final-state radiation.

38

- Event Loop. A fixed number of unweighted events are generated. There are a number of steps:

    - The electron and positron effective energies at collision point after radiation are generated.

    - The final state flavor is chosen randomly according to some approximate probabilities that take into account Cabibbo mixing. Alternatively, the final state can be fixed to a particular combination of flavors.

    - One of two subgenerators is chosen randomly to generate the event kinematics. One of them maps the peaks for the WW channel, the other for the ZZ channel.

    - The exact matrix element squared is computed. A weight is assigned to each event according to the ratio of the exact matrix element squared to the approximate weights used in the generation stage, including the ones for choice of flavor composition and initial-state radiation.

    - A rejection algorithm is applied to the final weight to get unweighted events.

    - The four momenta are given their corresponding masses, readjusting the kinematics of the event. The event is boosted to the lab frame according to the incoming electron and positron effective energies.

    - PHOTOS is called to provide final-state radiation off electrons and muons only.

    - JETSET is invoked to take care of hadronization, decays and final state radiation off quarks or hadrons.

    - Four-vectors are stored in the standard Lund common block.

- Final: The cross section is computed with statistical error. A summary of the run is given.

Input Parameters and Flags

The following is a description of the input parameters and flags together with the values used for the tuned comparisons:

- XMZ=91.1888, mass of the Z (GeV).

- XMW=80.23, mass of the W (GeV).

- ALFA0=137.0359895, $1/\alpha_{QED}(0)$. Used for the photon radiation.

- ALFA=128.07, $1/\alpha_{QED}(s)$.

- GF= 1.16639E-5, Fermi constant.

- ALFAS=0., $\alpha_s(M_W^2)$. Set to zero for the tuned comparisons.

- `WWUSER=2.03367`, user value for W width. Ignored if UWFLAG=0.

- `ZWUSER=2.4974`, user value for Z width. Ignored if UWFLAG=0.

- `IRFLAG=1`, generate initial-state radiation (1) or not (0).

- `CSFLAG=0`, include the Coulomb correction (1) or not (0)

- `BWFLAG=1`, Breit-Wigner with mass-dependent (1) or constant (0) width.

- `ASFLAG=0`, apply α_s correction for widths (1) or not (0).

- `FRFLAG=0`, generate final-state radiation (1) or not (0) (`PHOTOS`).

- `IZFLAG=0`, include contributions from ZZ diagrams (1) or not (0).

- `ILFLAG=0`, invoke `JETSET` for showers, fragmentation, and decay (1) or not (0).

- `UWFLAG=1`, use total W and Z widths from the user (1) or the SM (0).

The preferred values would differ from the previous ones in the following:

- `ALFAS=0.12`

- `CSFLAG=1`

- `ASFLAG=1`

- `FRFLAG=1`

- `IZFLAG=1`

- `ILFLAG=1`

- `UWFLAG=0`

Output

The program's output consists on the result of the cross section for the required final state. An estimate of the statistical error is also provided. The four-momenta of the generated particles are available in the event loop through the standard Lund common block.

Availability of the program
LPWW02 is available from the authors.

2.10   PYTHIA 5.719 / JETSET 7.4

Author:

Torbjörn Sjöstrand   torbjorn@thep.lu.se

Description

PYTHIA/JETSET is a general-purpose event generator for a multitude of processes in e^+e^-, ep and pp physics [47, 48]. The emphasis is on the detailed modeling of hadronic final states, i.e. QCD parton showers, string fragmentation and secondary decays. The electroweak description is normally restricted to improved Born-level formulae, and so is not competitive for high-precision studies.

Features of the program

- Monte Carlo event generator.

- By default any final state allowed for a process is included in the generation, but it is possible to select a specific combination of final states with large flexibility.

- Several cuts are available, if desired. Examples include the mass ranges for the hard scattering process and for resonances. It is not possible to set cuts directly on the four final fermions, however.

- ISR is implemented in a two-stage process. First structure functions are used to select x_1 and x_2 values for the hard scattering. Currently the structure function is the one recommended for LEP 1 [49], but it would be easy to expand to more alternatives. Thereafter a backwards evolution scheme is used to reconstruct explicit sequences of $e\rightarrow e\gamma$ branchings, including $p_\perp$ recoils. The algorithm used is essentially the same as originally developed for QCD applications [50].

- FSR is implemented inside each gauge boson system separately. For a W this means as it would have been obtained in the formal limit $\Gamma_W \rightarrow 0$. Again a parton-shower description is used, with explicit matching to the first-order matrix elements, as for final-state QCD radiation [51]. Quarks can radiate both photons and gluons.

- For the hard process $e^+e^- \rightarrow W^+W^-$, only x_1, x_2, the two W masses and one relative angle are selected [2], [22]. FS decays are considered in a second step, using the formulae of [52] to calculate the conditional probability for a set of four decay angles (two for each W). The philosophy is the same for other processes.

- Several optional Coulomb formulae are available [53]; the recommended one is the first-order expression in [54].

- No anomalous couplings.

- Finite fermion masses are included in the phase-space factors for partial widths.

41

- Hadronization comes built-in.

- Since the program does not include interference e.g. between the WW and ZZ processes, each individual event is uniquely assigned to a specific process, and this information is available to the user.

Program layout

At initialization, coefficients are optimized in the analytical expressions subsequently used to select kinematical variables (i.e. phase-space points will be picked more often in those regions where the matrix elements are peaked), and the corresponding maxima of differential cross sections are found. For each event, a process type and a phase-space point is selected by hit-or-miss Monte Carlo. That is, events come with unit weight (but an option with weighted events exists). The maximum found in the initialization is increased if one encounters a larger differential cross-section value. (Formally this introduces an error in the method, but when the increase occurs early in the run and/or is small, this error is negligible.) The cross-section information is improved with increasing statistics. After its selection, the hard scattering is gradually dressed up, by the addition of initial-state radiation, resonance decays, final-state radiation and hadronization.

Note that Γ_Z is not set independently in PYTHIA; rather it is given by electroweak relations and is thus too small when one asks for $\alpha_s = 0$.

Each event is listed in full in COMMON/LUJETS/ (optionally also in COMMON/HEPEVT/), so any experimentally definable quantity can be extracted. Also other pieces of event information is available in common blocks. A table of cross sections can be obtained, but this does not include error estimates.

Availability and documentation
The master copies of the programs, documentation and sample main programs are available at web address http://thep.lu.se/tf2/staff/torbjorn/.

The main reference is [47]. A full manual and physics description (over 320 pages) is [48]. An overview, with a table of the most interesting subprocesses, is given in the QCD generators section of this report.

2.11 WOPPER 1.4

Authors:

Harald Anlauf   anlauf@crunch.ikp.physik.th-darmstadt.de
Thorsten Ohl   Thorsten.Ohl@Physik.TH-Darmstadt.de

General description:
WOPPER is a fairly standard Monte Carlo event generator for *un*weighted $e^+e^- \rightarrow 4f$ events [55]-[57]. Emphasis is put on leading logarithmic radiative corrections to $W^\pm$ pair production

(i.e. doubly resonant four-fermion production at LEP2). An extension to singly resonant four-fermion production is being tested and will be released as WOPPER version 1.5. WOPPER is interfaced with fragmentation and hadronization Monte Carlos to allow full simulation of event samples at LEP2.

Features:

- WOPPER is a Monte Carlo event generator with *un*weighted events, suitable for full simulation of event samples.

- All possible four-fermion final states are generated.

- All cuts can be applied to the final states.

- Initial state QED radiation is implemented in leading logarithmic approximation. The leading logarithms $\propto (\alpha/\pi)(\ln(s/m_e^2) - 1)$ from collinear and soft emission are summed to all orders in a parton shower algorithm using the first order non-singlet splitting functions. A finite p_T for photons and the hard scattering center of mass system is generated according to the $1/pk$ pole.

- Final-state QED radiation is not implemented.

- Decays of final states are left to external packages. Standard interfaces are implemented.

- Coulomb corrections are implemented with finite width according to ref. [25].

- Anomalous couplings are not implemented.

- Finite fermion masses are implemented in the kinematics, but the matrix elements are calculated in the massless limit.

- Fragmentation and hadronization are left to dedicated QCD Monte Carlos. The standard W^+W^-–QCD event generator interface is implemented.

- Currently, only charged current diagrams are implemented, therefore information on color reconnection is neither needed nor available.

Algorithm:

- WOPPER's initialization phase starts with calculating the coupling constants from the input parameters according to the value of **scheme**. The maximum of the total hard cross section $\sigma(s, k_+^2, k_-^2)$ for off-shell $W^\pm$ pair production is determined to allow the generation of *un*weighted events. NB: $k_\pm^2$ do not really correspond to off-shell $W^\pm$'s for singly resonant contributions.

43

- For event generation, an off-shell $W^{\pm}$ pair is produced with the invariant mass reduced and the center of mass system boosted from radiative corrections. This pair is subsequently decayed, keeping all angular correlations among the four decay fermions.

- A Monte Carlo estimate of the total cross section based on the events generated so far can be requested at any time. In particular, it is produced in the clean-up phase.

Input parameters:

1. **Tuned comparison:**

   - `scheme`: 1, i.e. use G_F, M_W and $\alpha_{QED}(2M_W)$ as input and calculate $\sin^2\theta_W = \pi\alpha_{QED}(2M_W)/(\sqrt{2}G_F M_W^2)$ as well as $\Gamma_W = G_F M_W^3(3 + 2\alpha_{QCD}(2M_W)/\pi)/(\sqrt{8}\pi)$.
   - `mass1z`: $M_Z = 91.1888$
   - `gamm1z`: $\Gamma_Z = 2.4974$
   - `mass1w`: $M_W = 80.23$
   - `gfermi`: $G_F = 1.16639 \cdot 10^{-5}\,\mathrm{GeV}^{-2}$
   - `ahpla`: $1/\alpha_{QED}(2M_W) = 128.07$
   - `alphas`: $\alpha_{QCD} = 0$
   - `ckmvus`: $V_{us} = 0$
   - `ckmvcb`: $V_{cb} = 0$
   - `ckmvub`: $V_{ub} = 0$
   - `coulom`: `false`, i.e. no Coulomb correction

2. **Preferred input:** the input used in the *"Best You Can Do"* event samples is identical to the one used in the tuned comparison, except for

   - `alphas`: $\alpha_{QCD}(M_Z) = 0.123$
   - `ckmvus`: $V_{us} = 0.2196$
   - `ckmvcb`: $V_{cb} = 0.0400$
   - `ckmvub`: $V_{ub} = 0.0032$
   - `coulom`: `true`, i.e. apply Coulomb correction

In addition to the above G_F-scheme, the following schemes are available:

- `scheme` $= -1$: like `scheme` $= 1$, but for Γ_W, which is taken from the input parameter `gamm1w`

- `scheme` $= 2$: use `sin2w` ($\sin^2\theta_W$) as input and calculate $G_F = \pi\alpha_{QED}/(\sqrt{2}\sin^2\theta_W M_W^2)$

- scheme $= -2$: like scheme $= 2$, but for Γ_W, which is taken from the input parameter gamm1w

- scheme $= 3$: use sin2w ($\sin^2 \theta_W$) and gfermi (G_F) as independent input parameters and force $\alpha_{QED}(s) = \alpha_{QED}(0)$

- scheme $= -3$: like scheme $= 3$, but for Γ_W, which is taken from the input parameter gamm1w

Output:
After startup and initialization, WOPPER prints a version number and a description of the selected input parameter scheme to standard output. Additional print commands can be used to print some or all internal flags and parameters. Generated events are stored in the standard /HEPEVT/ common block and a user routine (by default "call hepawk('scan')") is called. At the end of the run, the total cross section and an error estimate is available in the last /HEPEVT/ record.

Availability:
The WOPPER distribution can be obtained directly from the authors or from the internet

- WWW: http://crunch.ikp.physik.th-darmstadt.de/
  monte-carlos.html#wopper

- Anonymous FTP from crunch.ikp.physik.th-darmstadt.de,
  in the directory pub/ohl/wopper

Ready-to-run versions are available in the experimental LEP2 collaborations.

2.12   WPHACT

W W and Higgs Physics with **PHACT**

Authors:

E. Accomando   accomando@to.infn.it
A. Ballestrero   ballestrero@to.infn.it

General description

WPHACT is a program created to study four-fermion, WW and Higgs physics at present and future e^+e^- colliders. In its present form, it can compute all SM processes with four fermions in the final state. For NC processes involving b quarks, and no electrons in the final state, finite b masses can be fully taken into account.

Full tree-level matrix elements for all CC and NC processes are computed by means of subroutines which make use of the helicity formalism of ref. [58]. Their code has been written

semi-automatically through the set of routines PHACT [59] (**P**rogram for **H**elicity **A**mplitudes **C**alculations with **T**au matrices) which implements the method in a fast and efficient way.

In the above formalism, eigenstates of the fermion propagators are used to simplify matrix expressions. These eigenstates are chosen to be generalizations of the spinors used in ref.[60]. Essentially, the numerator of fermion propagators are diagonalized in the massless lines and have very simple expressions in the massive ones. The computation of fermion lines reduces to evaluating the matrices corresponding to insertions of vector or scalar lines and combining them together. This is performed most efficiently with the so-called *tau matrices* [58]. The program PHACT writes automatically the optimized fortran code necessary for every insertion and every combination, given the names of the vectors, couplings, etc. From various comparisons made, we have been convinced that in fact the codes for the amplitudes written in this way run very fast, and this is the case also for WPHACT.

Different phase spaces, with different random number mappings, are employed in order to take into account the peak structure of the resonating diagrams for the different processes. The adaptive routine VEGAS[9] is used for integrating over the phase space.

For additional information, see also the section on event generators for Higgs physics.

Features of the program

WPHACT is a Monte Carlo program. For all phase spaces used, all momenta are explicitly computed in terms of the integration variables. This implies that any cut can be implemented, and it can be easily used also as an event generator. The events obtained in this way are of course weighted. VEGAS is an adaptive routine, which normally runs a few iterations (good efficiency is normally obtained with about three iterations), seeking for a better grid of the integration space. If one doesn't want to generate too many events, it is better to use the events of the last iteration. Distributions for any variable can also be implemented. Even if various distributions have already been produced, and examples are available, no automatic implementation of distributions has yet been introduced.

All SM final states with four fermions can be calculated. No W's or Z's or Higgs are allowed in the final state. They are always appropriately considered as virtual particles.

Any cut can be performed. Initial state QED radiation is included through Structure Functions $\mathcal{O}(\alpha^2)$. FSR is not implemented. The Coulomb term is implemented with the approach of ref. [25]. Anomalous couplings are available. No interface to hadronization is available.

So far the only fermion masses which can be different from zero are those of quarks in NC processes relevant for Higgs production, like e.g. $e^+e^- \rightarrow b\bar{b}b\bar{b}$, $e^+e^- \rightarrow \nu_e\bar{\nu}_e b\bar{b}$, etc. The nonzero masses are fully taken into account both in the matrix element and in the phase space. Just because of the helicity formalism adopted, the massive case does not cost much more than the massless one in cpu time.

It is easy to obtain the contributions from different set of diagrams, as every diagram is

evaluated individually for all helicity configurations and then summed to the others before squaring and summing over helicity configurations. Actually, in the case of mixed CC and NC processes the two contributions are evaluated and integrated separately.

As far as speed is concerned, we give some indicative values about the running time on ALPHA AXP 2100/4 OVMS:

CPU time per call for *CC03* without ISR: $\qquad\qquad$ 5.6×10^{-5} sec.

CPU time per call for *CC11* with ISR: $\qquad\qquad$ 1.2×10^{-4} sec.

At Lep2 energies, 30 M calls (about one hour) are used to obtain *CC11* with ISR cross section with a typical estimated error of about 1×10^{-4}. The same process can be evaluated in about 2 minutes with 1 M calls at permille level. For *CC03* without ISR 20 M calls (20 minutes) give an estimated error of about 1×10^{-4} and 1 M calls (1 minute) are necessary for permille precision. The same programs are about 5 times slower on a VAXstation 4000/90.

Program layout

The variables by which the phase spaces are described are the W masses for CC contributions, the Z masses for NC contributions, together with the angle of the two virtual particles with respect to the beam, the decay angles in their rest frames, and x_1, x_2, the fractions of momenta carried by the electrons. Appropriate change of variables to take care of peaks in x_1, x_2, M_W or M_Z lead to the real integration variables. For every point chosen by the integration routine, the full set of four-momenta is reconstructed and passed to the subroutine which evaluates the differential cross section with the helicity amplitude formalism. For every point in the integration variables, i.e. for every set of four momenta chosen, `VEGAS` gives a weight which must be used together with the value of the cross section for producing distributions.

Four phase spaces are available and have been used for the different matrix elements contributions, depending on the number of possible resonances. Every single phase space integrates better that particular contribution it has been constructed for. After various tests we however found that the phase space suitable for double resonant contributions is quite precise also in evaluating all contributions together. It turns out to be faster than splitting the contributions and integrating them separately with automatic determination of the relative precision. At present all contributions are normally evaluated together with one single kind of phase space. When mixed CC and NC are present, it is better to run the two contributions separately (adding the interference to the biggest one), as the change of variables necessary to take care of the resonances depends on their masses.

Input parameters, flags, etc.

Normal input parameters are M_W, M_Z, α, α_S. In the tuned comparisons $sin^2\theta_W$ has also been given as an input, while it is usually derived from the relation $sin^2\theta_W = 1 - M_W^2/M_Z^2$.

The main flag of the program is `ich`, which chooses among different final states. Other flags allow to compute with (when their value = 1) or without (when their value = 0) ISR,

Coulomb corrections and α_S corrections. They are respectively : `isr, icoul, iqcd`. The last option refers at present only to CC10 processes. A flag (`iterm`) allows using (`iterm = 1`) or not (`iterm = 0`) some iterations (normally one is enough) for thermalizing. The number of iterations (`itmx`) and of points for iteration (`ncalls`) for the thermalizing phase as well as for the normal one and the accuracy required (`acc`) are read from the input.

Output

The output is just the standard `VEGAS` output, from which one can read the final result and estimated statistical error, as well as the result and error for every iteration. Results with big oscillations among different iterations and corresponding big reported χ^2 simply mean that the number of evaluations per iteration was not sufficient for the integrand, and have to be discarded.

Concluding remarks

As already stated, `WPHACT` makes use of matrix elements which run fast. Speed is in our opinion a relevant issue, not only because it allows to perform complicated calculations, but also for rather short ones. In Monte Carlos, speed corresponds to the possibility of generating in the same time many more events, achieving a much better precision in integration.

The program , which does not make use of any library, has proved to be reliable over a vast range of statistical errors from the percent up to 10^{-5}. Thus it can be used both to obtain very precise results with high statistics runs and to get fast answers.

Availability:
The program is available from the authors or by anonymous ftp from
ftp.to.infn.it/pub/ballestrero.

2.13   WTO

Author:

Giampiero Passarino   giampiero@to.infn.it

`WTO` is a *quasi-analytical, deterministic* code for computing observables related to the process $e^+e^- \rightarrow \bar{f}_1 f_2 \bar{f}_3 f_4$. The full matrix elements are used and in the present version the following final states are accessible (see [5] for a general classification):

1. *CC03, CC11, CC20, NC21, NC24, NC32, mix43*

2. *NC23* (= *NC21* + Higgs signal), *NC25* (= *NC24* + Higgs signal)

Further extensions will be gradually implemented. To fully specify `WTO`'s setup an option must be chosen for the renormalization scheme (RS). One has the options commonly used for tuned comparisons or the default, i.e.

$$s_w^2 = \frac{\pi\alpha(2M_w)}{\sqrt{2}G_\mu M_w^2}, \qquad g^2 = \frac{4\pi\alpha(2M_w)}{s_w^2}, \tag{7}$$

$$s_w^2 = 1 - \frac{M_w^2}{M_z^2}, \qquad g^2 = 4\sqrt{2}G_\mu M_w^2 \tag{8}$$

where $\alpha^{-1}(2M_w) = 128.07$ and G_μ is the Fermi coupling constant. Final state QCD corrections are not taken into account in the present version, except for the Higgs signal (NC21-NC25) where the pole quark masses, $m_q(m_q^2)$, are in input. The code will compute the correct running, up to terms $\mathcal{O}(\alpha_s^2)$, i.e. $m_{b,c}(m_H^2)$ and will include 'effectively' a final state QCD correction.

The matrix elements are obtained with the helicity method described in ref.[61]. The whole answer is written in terms of invariants, i.e.

$$e^+(p_+)e^-(p_-) \rightarrow f(q_1)\bar{f}(q_2)f'(q_3)\bar{f}'(q_4), \tag{9}$$

$$x_{ij}s = -(q_{i-2} + q_{j-2})^2, \quad x_{1i}s = -(p_+ + q_{i-2})^2, \tag{10}$$

$$x_{2i}s = -(p_- + q_{i-2})^2, \quad s_1 s^2 = \epsilon(p_+, p_-, q_1, q_2), \dots \tag{11}$$

and the integration variables are chosen to be $m_-^2 = x_{24}$, $m_+^2 = x_{56}$, $M_0^2 = x_{45}$, $m_0^2 = x_{36}$, $m^2 = x_{35}$, $t_1 = x_{13}$, $t_w = x_{13} + x_{14}$. The convention for the final states in WTO is: $e^+e^- \rightarrow 1+2+3+4$. For CC processes $1 = d, 2 = \bar{u}, 3 = u', 4 = \bar{d}'$, with $u = \nu, u, c$ and $d = l, d, s, b$. For NC processes the adopted convention is $1 = f, 2 = \bar{f}, 3 = f'$ and $4 = \bar{f}'$. Initial state QED radiation is included through the Structure Function approach up to $O(\alpha^2)$. The code will return results according to three (pre-selected) options, i.e $\beta^2\eta$ (default) [62], β^3 [63] and $\beta\eta^2$ [7] where $\beta = 2\frac{\alpha}{\pi}\left(\log\frac{s}{m_e^2} - 1\right)$, $\eta = 2\frac{\alpha}{\pi}\log\frac{s}{m_e^2}$. QED corrections also include the Coulomb term correction [25] for the *CC03* part of the cross section. When initial-state QED radiation is included, there are two additional integrations over the fractions of the beam energies lost through radiation, $x_\pm$. This description of the phase space gives full cuts-availability through an analytical control of the boundaries of the phase space. Upon specification of the input flags it is therefore possible to cut on all final state invariant masses, all (LAB) final state energies $E_i, i = 1, 4$, all (LAB) scattering angles, $\theta_i, i = 1, 4$ all (LAB) final state angles, $\psi_{ij}, i, j = 1, 4$.

Both the matrix elements and the phase space are given for massless fermions. There is no interface with hadronization. The integration is performed with the help of the NAG [64] routine D01GCF. This routine uses the Korobov-Conroy number theoretic approach with a MC error estimate arising from converting the number theoretic formula for the n-cube $[0,1]^n$ into a stochastic integration rule. This allows a 'standard error' to be estimated. Prior to a call to D01GCF the peak structure of the integrand is treated with the appropriate mappings.

Whenever the program is called it will start the actual calculation of one of the following observables: cross section or a pre-selected sample of moments of distributions, for instance $< x_\gamma^n >$. Since WTO does not generate hard and non-collinear photons, E_γ is just the total radiated photon energy. There is no adaptive strategy at work since the routine D01GCF,

49

being a deterministic one, will use a fixed grid. The evaluation of the specified observable will be repeated NRAND times to give the final answer, however there is no possibility to examine the partial results but only the average and the resulting standard error will be printed. The error in evaluating , say, a cross section, satisfies $E < CK\, p^{-\alpha} \log^{\alpha\beta} p$, where $p = $NPTS, α and C are real numbers depending on the convergence rate of the Fourier series, β is a constant depending on the dimensionality n of the integral and K is a constant depending on α and n.

Numerical input parameters such as $\alpha(0), G_\mu, M_z, M_w, \ldots$ are stored in a BLOCK DATA. There are various flags to be initialized to run `WTO`. Here follows a short description of the most relevant ones:

NPTS - INTEGER, NPTS=1,10 chooses the actual number of points for applying the Korobov-Conroy number theoretic formulas. The built-in choices correspond to to a number of actual points ranging from 2129 up to 5,931,551.

NRAND - INTEGER, NRAND specifies the number of random samples to be generated in the error estimation (usually $5 - 6$).

OXCM - CHARACTER*1, the main decision branch for the process: [C(N)] for CC, (NC).

OTYPEM - CHARACTER*4,Specifies the process, i.e. *CC03, CC11, CC20* for CC processes and *NC19, NC24, NC21, NC25, NC32* for NC processes.

ITCM - INTEGER, the type of observable requested (0 for cross section). For *CC11* ($e^+e^- \to \mu^- \bar\nu_\mu u\bar d$) a number of distributions are available (for instance $< x_\gamma^n >$). If the n-th moment of a distribution is requested then

ITCNM - INTEGER, must be set to n.

OCOUL - CHARACTER*1, controls the inclusion of the Coulomb correction factor [Y/N].

IOS - INTEGER, two options $[1,2]$ (1 =default for tuned comparisons) for the renormalization scheme.

IOSF - INTEGER, three options $[1-3]$ for the $\eta - \beta$ choice in the structure functions.

CHDM. . . - REAL, Electric charges, third component of isospin for the final states.

`WTO` is a robust one call - one result code, thus in the output one gets a list of all relevant input parameters plus the result of the requested observable with an estimate of the numerical error. A very rough estimate of the theoretical error (very subjective to say the least) can be obtained by repeating runs with different IOS, IOSF options. A rough estimate of the requested CPU time (on a VAXstation $4000 \cdot 90$) vs precision can be inferred from the following table which refers to $\sigma(e^+e^- \to \mu^- \bar\nu_\mu u\bar d)$ at $\sqrt{s} = 161\,\mathrm{GeV}$

GENTLE			0.1269543
σ (nb)	0.1266300 $\pm$ 0.822D-03	0.1268430 $\pm$ 0.171D-03	0.1269526 $\pm$ 0.381D-05
W/G(%)	0.26	0.09	$1.\times 10^{-3}$
CPU	00:03:17.78	00:19:25.00	18:56:25.99

After initialization for the background process $e^+e^- \rightarrow \bar{\nu}_\mu \nu_\mu \bar{b}b$ with $M_z - 25\,\mathrm{GeV}< M_{\nu\nu} < M_z + 25$ GeV, $M_{\bar{b}b} > 30$ GeV and with the b angle with respect to the beams $> 20^o$, the typical output will look as follows:

```
This run is with:

NPTS           =  7
NRAND          =  6

E_cm (GeV) =           0.17500E+03
beta       =           0.11376E+00 sin^2      =         0.23103E+00
M_W  (GeV) =           0.80230E+02 M_Z (GeV) =          0.91189E+02
G_W  (GeV) =           0.20337E+01 G_Z (GeV) =          0.24974E+01

No QED Radiation
There are cuts on fs invariant masses, no cuts on fs energies,
cuts on scattering angles, no cut on fs angles

\emph{NC24}-diagrams : charges     -0.3333     0.0000
                 isospin    -0.5000     0.5000

On exit IFAIL = 0 - Cross-Section

CPU time  41 min  28 sec, sec per call    =      0.415E-02
# of calls        =      599946

sigma      =      0.1489801E-02   +-           0.1930508E-05

Rel. error of     0.130 %
```

2.14   WWF 2.2

Author:

Geert Jan van Oldenborgh   gj@rulkol.LeidenUniv.nl

Description

This Monte Carlo is the beginning of a full one-loop Monte Carlo [65]-[66]. At the moment it includes a tree level part (WWFT, which participated in the tuned comparisons), hard and soft bremsstrahlung (WWFTSH, exact matrix element, resummed in the forward and backward

region), and the factorizable virtual graphs (`WWFTSHV`, on request only). We are working on the missing parts, the non-factorizable loop graphs. t-channel graphs for electrons in the final state, and a shower algorithm for the forward/backward photons.

Features of the program

There are two forms of the program: an event generator (`wwfax`) and 'integrator' (`wwfmc`), the latter has a parallel option (`wwfpvmmc`, `wwfpvmslave`). Interfaces to `BASES/SPRING` are also provided.

The program can generate all final states which are reachable through two W bosons. The user can specify whether the final states should be leptonic, semileptonic and/or hadronic, and which leptons should be included in leptonic decays, for instance 'all semi-leptonic and leptonic channels with electrons and muons'. All cuts can be implemented after the event is generated. To optimize event generation one can specify the minimum photon energy, the minimum and maximum angle of photons to the beam, minimum angle to charged particles, and the maximum virtuality of the W's.

Two methods have been implemented to compute ISR: structure functions (Leiden 2-loop and YFS 3-loop leading logarithmic, with the possibility of giving the photon bunch a one-photon spectrum p_T), and the explicit 1-photon matrix element (for $CC03$ and $CC11$ processes), minus the leading log part of this matrix element, plus the resummed leading log structure functions mentioned above. In the latter case an estimate of the missing virtual corrections is included, which makes it unsuitable for total cross section predictions. For FSR we use the exact one-photon matrix element; there is an option to reduce the leading logarithmic part of this by an arbitrary factor to compensate for the excess near jets (which are described by on-shell quarks). The default event generation routine calls `JETSET` to do all the hadronization and τ decays. No polarization information is passed as yet, although all particles come from W bosons and the helicities are therefore fixed. There is a `JETSET` interface, which will soon be adapted to the proposed standard. There is no possibility to get information about subsets of diagrams yet, but this will be included in this interface.

We have the possibility to shift the Coulomb term from the virtual corrections to the the tree level terms (and therefore include it in the hard and soft radiation as well). For this we take the one-loop expression given in ref. [25]. Anomalous couplings are implemented only at the tree level, we follow the conventions of Jegerlehner [67]. In the hard radiation matrix element there is the option to include the full effect of finite fermion masses; the default is to include the leading effects only. The tree level ME can also include some mass effects. The phase space is always taken massive.

Program layout

The 'integrator' program `wwfmc` is a stand alone program, which reads its data from a file `wwf.dat`, which defines the input parameters, and `vegas.dat`, which gives the parameters for the integration by `VEGAS` (adaptive weighted integration) or `NVEGAS` (integrates many quantities, like the tuned comparison data).

tuned	best	description
80.23	80.26	W mass in GeV, LEP1 definition (running width)
−1	−1	W width, if < 0 it is computed
−1	−1	Z mass, if < 0 it is taken to be 91.188 GeV
−1	−1	Z width, if < 0 it is taken to be 2.4974 GeV
100	300	Higgs mass (only used in virtual corrections)
176	165	top quark mass (only used in virtual corrections)
2	0/2	0: constant width (use for hard & virtual corrections)
		2: s-dependent width (preferred for tree level only)
4	2	renormalization scheme: 1: α, 2: G_μ with α for soft radiation, 3: G_μ
		4: the tuned comparison scheme
2	2	1: narrow-width approximation, 2: full off-shell calculation
		(not defined with virtual), 3: pole scheme calculation
1	1	1: fast massless matrix element, 2: slower massive matrix element
0	0	0: include all diagrams
0	0	0: include corrections both to production and decay
0/1	0/1	0: only resonant tree level diagrams ($CC03$)
		1: same plus universal non-resonant diagrams ($CC11$)
0/1	0/1	same for radiative graphs
0	.123	α_s
2	0–7	decay channel, sum of 1: leptonic, 2: semileptonic, 4: hadronic
0	0–7	W^+ decay channels, sum of 1: $e^+\nu_e$, 2: $\mu^+\nu_\mu$, 4: $\tau^+\nu_\tau$, 8: $u\bar{d}$
2	0–7	W^- decay channels, sum of 1: $e^-\bar{\nu}_e$, 2: $\mu^-\bar{\nu}_\mu$, 4: $\tau^-\bar{\nu}_\tau$, 8: $\bar{u}d$
0	0.01	$E_\gamma^{\min}$ needed for hard/soft cut-off
0	0	$\theta_{\gamma,f}^{\min}$ used to optimize event generation
0	0	$\theta_{\gamma,e}^{\min}$ used to optimize event generation
180	180	$\theta_{\gamma,e}^{\max}$ used to optimize event generation
0	0	if $c > 0$ generate $\left|\sqrt{s_\pm} - M_W\right| < c$ GeV
0/1	0/1	0: no cuts, 1: canonical cuts, 2: require one observable photon
3	3	0: no extra initial-state radiation,
		1: use Leiden 2-loop structure functions,
		2: use YFS 3-loop structure functions.
180	180/10	cone around beam pipe where radiation is exponentiated
		(use 5–10 degrees when including explicit hard radiation)
1	1	1: use crude p_T algorithms for ISR photons
0	0	1: exclude leading logarithmic initial-state radiation
0	0/20	cone around final state particles where FSR is reduced
0	0/0.4	fraction of leading log final-state radiation off quarks to leave out
0	0/1	1: include explicit hard photon radiation matrix element
0	0/1	1: include explicit soft photon matrix element
0	0	1: include loop graphs (not yet complete)
1	1	1: include tree level matrix element
0	1	1: include the Coulomb term in tree

Table 3: Input file format of `WWF 2.2`

The event generator is a set of three routines:
– `axinit`: preparation, this also establishes the maximum of the function,
– `axeven`: generates one event
– `axexit`: finalization, prints statistics, gives cross section and weight per event.
The use of these routines is demonstrated in the program `wwfax`. The event generation does
not use any adaptive strategies. The event is presented in a subroutine `wwfeve`, the default
version of which calls `JETSET` and lists the event on standard output.

Input
The input parameters are expected to be in a file `wwf.dat` with the information described in
table 3

Output

The program `wwfax` (or the equivalent routines) will give call the routine `wwfeve` for each
event generated; the default is to list the event on standard output. Some informative
messages will also appear on standard output:
– while initializing: the current maximum, a measure of the progress towards this maximum
and the largest negative event found so far,
– at the end of initialization: the maximum used and a summary of the negative events,
– while generating: error messages (mainly inaccuracies and negative weights) and the
numbers of events generated at powers of two,
– at exit: the cross section, weight per event, efficiency, CPU time used and a summary of the
impact of the negative weight events. The program `wwfmc` integrates the cross section and the
tuned comparison quantities, and will dump these in this format. One can make plots by
editing wwfill and the file `h.dat`.

Availability
The programs can be obtained from
`ftp://rulgm4.LeidenUniv.nl/pub/gj`,
`http://rulgm4.LeidenUniv.nl`
either as a compressed archive `wwf.tar.gz` or separate files. The package includes a makefile
and is known to compile without problems on HP, DEC, Linux, NeXT and Sun workstations.

2.15   WWGENPV/HIGGSPV

Authors:

Guido Montagna   montagna@pv.infn.it
Oreste Nicrosini   nicrosini@vxcern.cern.ch, nicrosini@pv.infn.it
Fulvio Piccinini   piccinini@pv.infn.it

Description:
WWGENPV and HIGGSPV are four-fermion Monte Carlo codes, originally conceived for W-boson

and Higgs-boson physics, respectively. The present version of `WWGENPV` is an upgrade of the published version. A detailed description of the formalism adopted and the physical ideas behind it can be found in the original literature, namely ref. [63] and references therein. A detailed description of `HIGGSPV` can be found in the report of the "Event Generators for Discovery Physics" Working Group, these proceedings.

The programs are based on the exact tree-level calculation of several four-fermion final states. Any cut on the final state configuration can be implemented. Initial- and final-state QED corrections are taken into account at the leading logarithmic level by proper structure functions, including p_T/p_L effects. An hadronization interface is at present available for *CC03* processes, and is under development [68]. All the relevant presently known non-QED corrections are also taken into account.

Features of the programs:
The codes consist of three Monte Carlo branches, in which the importance-sampling technique is employed to take care of the peaking behavior of the integrand:

- Unweighted event generation. The codes provide a sample of unweighted events, defined as the components of the four final-state fermions momenta, plus the components of the initial- and final-state photons, plus $\sqrt{s}$, stored into proper n-tuples. The programs must be linked to CERNLIB for graphical interfaces.

- Weighted event integration. It is intended for computation only. In particular, the codes return the values of several observables together with a Monte Carlo estimate of the errors. The programs must be linked to CERNLIB for the evaluation of few special functions.

- Adaptive integration. It is intended for computation only, but offering high precision performances. On top of importance sampling, an adaptive Monte Carlo integration algorithm is used. The program must be linked to NAG library for the Monte Carlo adaptive routines. Full consistency between non-adaptive and adaptive integrations has been explicitly proven. Neither final-state radiation nor p_T splitting are taken into account in this branch.

The non-adaptive branches rely upon the random number generator RANLUX.

As far as the physical features are concerned, the most important items are:

- Several Charged Current (`WWGENPV`) and Neutral Current (`HIGGSPV`) processes are available, namely *CC11*, *CC20*, *NC21* (*NC23* = *NC21* + Higgs signals), *NC24* (*NC25* = *NC24* + Higgs signals), *NC32*, *NC48* (*NC50* = *NC48* + Higgs signals) and all their subsets. The extension to other classes is under development.

- Any kind of cuts can be imposed.

- Initial- and final-state photon radiation is implemented at the leading logarithmic level in the structure function formalism. The structure function used is explicitly written in [63]. Moreover, p_T/p_L effects are taken into account.

- The Coulomb correction is taken into account (see [63] and references therein), together with flavor mixing and the presently known QCD corrections.

- An interface to hadronization packages is available for *CC03* processes and the extension to other classes is under development [68].

- There is the possibility of getting information on the contribution of subsets of the diagrams by setting proper flags.

At present, neither final state decays nor anomalous couplings are implemented. Moreover, finite fermion mass effects are partially taken into account only at the phase space boundary.

Program layout
After the initialization of the Standard Model parameters and of the electromagnetic quantities, the independent variables are generated, according to proper importance samplings, within the allowed range for an extrapolated set-up. The analytical control of the phase-space boundaries allows to reach an efficiency which, for an extrapolated set-up, is unitary, and remains very high for a wide range of (reasonable) cuts. By means of the solution of the exact kinematics, the four-momenta of the outgoing fermions are reconstructed in the laboratory frame, together with the four-momenta of all the generated photons. If the event satisfies the cuts imposed by the user in SUBROUTINE CUTUSER, the matrix element is called, otherwise it is set to zero.

In the generation branch, an additional random number is generated in order to implement the hit-or-miss algorithm and if the event is accepted it is recorded into an n-tuple.

In the non-adaptive integration branch, the integration of several (see below) observables is performed in a single run, by cumulating in parallel all the contributions to the integrands.

In the adaptive integration branch (ref.: NAG routine D01GBF), on top of importance sampling the integration routine automatically subdivides the integration region into subregions and iterates the procedure where the integrand is found more variant. The program stops when a required relative precision is satisfied.

INPUT parameters and flags (WWGENPV):
A sample of the input flags that can be used is the following:

OGEN = I choice between integration [I] and generation [G] branch

RS = c.m. energy (GeV)

OFAST = N choice between adaptive [Y] or non adaptive [N] branch

NHITWMAX = number of weighted events

56

`IQED = 1` choice for Born [0] or QED corrected [1] predictions

`ODIS = T` choice for a total cross section [T] or an invariant mass distribution [W]

`OWIDTH = Y` W-boson width computed within the SM according to LEP2 standard input [Y] or input the preferred value [N]

`NSCH = 2` Renormalization Scheme choice (three possible choices)

`ALPHM1 = 128.07D0` $1/\alpha$ value (LEP2 standard input)

`OCOUL = N` option for Coulombic correction [Y] or not [N]

`SRES = Y` option for *CC11* [Y] or *CC03* [N] diagrams

A detailed account of the other relevant possibilities offered by the code (namely, command files for generation and adaptive integration branches) will be given elsewhere [68].

Description of the OUTPUT:
For all three branches the output contains the values of the Standard Model parameters and of the couplings appearing in the Feynman rules.

In the generation branch, besides the output file containing the value of the cross sections for unweighted events, together with a Monte Carlo estimate of the error, also an n-tuple containing the generated events is written.

In the adaptive branch, the values of the cross section with its numerical error plus (when ISR is included) the energy and invariant mass losses with their errors are then printed.

In the non-adaptive branch, together with the cross sections, the estimates of the moments used in the tuned comparisons and of the histograms are also printed, together with the Monte Carlo errors.

Availability:
The codes are available upon request to one of the authors.

2.16 Summary

We will now briefly summarize the features of the programs presented in the previous subsections. Table 4 gives an overview over the features of the programs participating in the comparisons. It is just intended as a brief digest and the short writeups in the previous section should be consulted for reference. Here is a description of the columns of table 4:

Type:
  one of the four types of programs: *EG*: (unweighted) event generator, *MC*: (weighted) Monte Carlo integration program, *Int.*: deterministic integration program, and *SA*: semi-analytical integration program.

Diagrams:

the subset(s) of Feynman diagrams implemented in the hard matrix element: *CC03*: the three basic $e^+e^- \to W^+W^-$ charged current diagrams from figure 1, *CC11*: the eleven charged current diagrams from figure 2, see table 1; *NC24* and *NC21* subsets of neutral current diagrams, see table 2; *NNC=NC32 / NC21 / NC48 / NC4 × 16*; *NCC=CC11 / CC20 / NC32 / NC21 / mix43 / NC48 / NC4 × 16*; *all*: all diagrams. We emphasize, that we have listed only those processes in this column for which participating codes have contributed at least one number, see also the tables in [69]. This entry may therefore differ from that presented in the program descriptions.

ISR:

the type of initial-state radiation implementation: *SF*: structure functions; *FF*: flux functions; *REMT*: REMT routines, see subsection 2.8. *PS*: parton showers; *YFS*: Yennie-Frautschi-Suura exponentiation; and *ME*: matrix element (exact lowest order bremsstrahlung matrix element and infrared divergent virtual contributions); *BME*: the one photon bremsstrahlung matrix element is available; no virtual contributions.

FSR:

the type of final-state radiation implemented, see also section 3.1.15; *PH*: FSR is implemented by making use of `PHOTOS` package; the other symbols are the same as in the ISR column.

NQCD:

naive, inclusive QCD correction to $W^\pm$ decays. A '+' does not imply that hard QCD radiation is implemented in the program (see page 69 for more details).

Coul.:

Coulomb correction (see page 68 for more details).

AC:

availability of anomalous couplings in the three gauge boson vertices. Since we have not compared predictions with anomalous couplings in this study, the entries in this column are identical to what is advertized in the program descriptions.

m_f:

treatment of fermion masses: +: all fermion masses taken into account, $\pm$: massless matrix elements with massive kinematics (mostly Källén λ-functions), and finally −: all fermions massless. It must be remarked here that 'all' does not necessarily mean that nonzero masses have been included in all processes presented in the comparisons.

Hadr.:

availability of an interface to hadronization libraries. With the exception of `PYTHIA`, no program includes hadronization code. All rely on `HERWIG` or `JETSET` to perform this task. The interface with hadronization packages and its interplay with final-state QCD radiation deserves a longer comment. For some codes a minus in this column is a direct consequence of the adopted strategy, e.g. semianalytical codes were never meant for this interface.

Program	Type	Diagrams	ISR	FSR	NQCD	Coul.	AC	m_f	Hadr.
ALPHA	MC	all	BME	−	−	−	−	+	−
CompHEP	EG	all	SF	−	−	−	−	+	−
ERATO	MC	CC11/CC20	SF	−	+	−	+	−	+
EXCALIBUR	MC	all	SF	−	+	+	+	−	−
GENTLE	SA	CC11/NC32	SF/FF	−	+	+	−	±	−
grc4f	EG	all	SF/PS	PS	+	+	+	+	+
HIGGSPV	EG	NNC	SF(p_T)	−	+		−	±	−
KORALW	EG	CC11	YFS	PH	+	+	+	±	+
LEPWW	EG	CC03	REMT	PH	+	−	+	−	+
LPWW02	EG	CC03	SF	PH	+	+	−	±	+
PYTHIA	EG	CC03	SF+PS	PS	+	+	−	±	+
WOPPER	EG	CC03	PS	−	+	+	−	±	+
WPHACT	MC	all	SF	−	+	+	+	+	−
WTO	Int.	NCC	SF	−	+	+	−	−	−
WWF	EG	CC11	SF+ME	ME	+	+	+	+	+
WWGENPV	EG	CC11/CC20	SF(p_T)	SF(p_T)	+	+	−	±	+

Table 4: Overview of the participating programs.

3   Comparisons of CC Processes

We now come to a detailed comparison of the Monte Carlo Event Generators and semianalytical programs available for the study of four-fermion processes at LEP2. The next subsection contains our most comprehensive study of *CC10* processes. Much shorter studies of *CC11* and *NC* processes are presented in the following subsection and the next section. Finally, the cross sections for *all* four-fermion processes are presented.

3.1   *CC10* processes

In a set of *tuned comparisons* of *CC* processes we have tested the implementation of the *CC10* family for a prescribed set of approximations. Because the *CC03* set (cf. fig. 1) is available in *all* programs, one of the *tuned comparison* has been restricted to this subset of all contributing diagrams.

It was then extended to the process $e^+e^- \rightarrow \mu^- \bar{\nu}_\mu u \bar{d}$, where from the *CC11* set of diagrams only 10 contribute, because the photon does not couple to the neutrino (cf. fig. 2).

59

In a second set of *unleashed comparisons* all the contributors have presented their preferred scenario for the process $(e^+e^- \to \mu^-\bar{\nu}_\mu u\bar{d})$ or, in short, they have produced the *best prediction they can give* at present. The latter comparison can show which part of the spread in predictions is due to the different approximations used.

3.1.1 Observables

In comparing of predictions for exclusive observables, we have concentrated on the prototypical "semileptonic" *CC10* process

$$e^+e^- \to \mu^-\bar{\nu}_\mu u\bar{d}\,, \tag{12}$$

which belongs to the *CC11* family. This choice is also partially motivated by the fact that the same process can be computed by restricting the calculation to the *CC03* class, thus allowing more codes to participate. Moreover, it is known that at LEP 2 energies the ratio of *CC03/CC10* cross sections is very near to one, although the difference is seen in some of the distributions. It should be mentioned that for the other semi-leptonic process $e^+e^- \to e^-\bar{\nu}_e u\bar{d}$ even the total cross section can not be well approximated by the *CC03* limit.

The following simple observables have received particular attention, because they are of prime importance for the measurement of the properties of the charged intermediate $W^\pm$ bosons at LEP2.

- The total cross section σ, with and without canonical cuts (see section 3.1.6 for a precise definition).

- The moments of the production angle θ_W of the W^+ with respect to the e^+-beam:

$$\langle \cos \theta_W \rangle_{1,2} = \frac{1}{\sigma} \int T_{1,2}(\cos \theta_W) d\sigma \tag{13}$$

  where the $T_n(\cos \theta) = \cos(n\theta)$ are the Chebyshev polynomials $T_1(x) = x$ and $T_2(x) = 2x^2 - 1$. The distribution of the production angle will be used in some studies of the non-abelian $W^\pm$ couplings. A precise description of the standard model prediction for this observable is therefore mandatory for this fundamental test of the non-abelian gauge structure of the standard model.

- From the invariant masses $s_\pm$ of the hadronic (W^+) and leptonic (W^-) decay products we have constructed the following moments:

$$\langle x_m \rangle_{1,2} = \frac{1}{\sigma} \int \left(\frac{\sqrt{s_+} + \sqrt{s_-} - 2M_W}{2E_B} \right)^{1,2} d\sigma \tag{14}$$

These quantities will of course be of prime importance for the $W^\pm$-mass measurement.

- The moments of the sum E_γ of the energies of all radiated photons

$$\langle x_\gamma \rangle_1 = \frac{1}{\sigma} \int \left(\frac{E_\gamma}{E_B} \right)^1 d\sigma \tag{15}$$

For constraint fits of the $W^\pm$-mass, a precise knowledge of the energy lost by initial-state radiation is mandatory. This quantity has to be described by all programs with high accuracy.

- Also, moments of the lost and visible photon energies $E_\gamma^{\text{lost/vis.}}$. The latter are accessible only in programs which generate non-vanishing p_T for ISR photons.

We have also looked at the following leptonic variables.

- The moments of the production angle θ_μ of the μ^- with respect to the e^--beam:

$$\langle \cos \theta_\mu \rangle_{1,2} = \frac{1}{\sigma} \int T_{1,2}(\cos \theta_\mu) d\sigma \tag{16}$$

- The moments of the decay angle θ_μ^* of the μ^- with respect to the direction of the decaying W^-, measured in the latter's rest frame:

$$\langle \cos \theta_\mu^* \rangle_{1,2} = \frac{1}{\sigma} \int T_{1,2}(\cos \theta_\mu^*) d\sigma \tag{17}$$

This is another quantity that can gainfully be used in the determination of the non-abelian $W^\pm$-couplings.

- The moments of the energy E_μ of the μ^-:

$$\langle x_\mu \rangle_{1,2} = \frac{1}{\sigma} \int \left(\frac{E_\mu}{E_B} \right)^{1,2} d\sigma \tag{18}$$

However, the numerical results will be given only for the first moments of leptonic variables.

During early stages of the comparison effort, we have additionally considered the third and fourth order moments of these observables. It turned out, however, that these moments typically receive very large statistical errors. They have therefore been dropped. Together with the moments, we have produced histograms for the observables. Presenting these histograms for all programs is next to impossible, however. It has turned out that the moments that have been just described are much more powerful tools for the sake of comparison. The histograms have therefore been dropped, together with the higher order moments. Towards the end of the comparison effort, some codes have also performed a study of various distributions, e.g. $d\sigma/dE_\gamma, d\sigma/ds_+(s_-)$ etc, where the relevant range of the variables has been divided in a large number of bins (typically $\approx 50 - 100$). Also for distributions we have registered a very good agreement, showing among other things that moments can be reconstructed to high precision from the distributions.

3.1.2 Tuned Comparisons

Our first task was to verify that all programs implement their advertised features correctly within the given statistical and numerical uncertainty, at least for *CC03, CC10*. Obviously, this is only straightforward, if all programs implement the same features. This is not the case, of course. Therefore we have performed a set of so-called *tuned comparisons* in which only a common subset of features has been enabled and identical inputs have been used, as far as possible. Actually a semi-tuned comparison has also been attempted by several codes for *all processes* and the results will be described in subsection 5.

Ideally, all programs would have options to emulate *all* other programs. Then all programs should give the same results (up to Monte Carlo errors), if running in the same mode and using the same input. This approach has been adopted in a study [70] of electroweak radiative corrections at the Z-resonance.

In the case at hand, this approach presents a more severe problem because electromagnetic radiative corrections are implemented in a variety of styles: some programs are using structure functions or flux functions, while other programs employ parton shower algorithms, see [71] for details. There are even hybrids of structure functions and matrix elements available. Since these algorithms are central to the respective programs, it is not possible to exchange them without destroying the identity of the programs. In any case one should be aware that there are different implementations of the QED corrections and that this issue is deeply related to a quest for a fully gauge-invariant description of QED radiation in 4f-processes; this goal has *not* been achieved so far.

3.1.3 Input parameters

The choice of input parameters is related to the choice of the electroweak renormalization scheme (RS). Actually, we have at our disposal the usual set of precisely measured parameters

$$\alpha(0), G_F, M_Z,$$
(19)

and we want to include M_W, [71]. Given the fact that the $\mathcal{O}(\alpha)$ electroweak corrections are not available for the *off-shell* case, we end up with an additional freedom in fixing the weak-mixing angle and the $SU(2)_L$ coupling constant. There are at least two *natural* choices, one of which had been adopted for the tuned comparisons, although it does not respect the proper Ward identities (more a question of principle than of numerical relevance). In this scheme, the effective weak mixing angle is determined as

$$\sin^2 \theta_W = \frac{\pi \alpha(2M_W)}{\sqrt{2} G_F M_W^2}.$$
(20)

In order to achieve agreement in a tuned comparison, all programs have to agree on the

Quantity	Value
M_Z	$91.1888\,\text{GeV}$
Γ_Z	$2.4974\,\text{GeV}$
M_W	$80.23\,\text{GeV}$
Γ_W	$3G_F M_W^3/(\sqrt{8}\pi)$
$\alpha(0)$	$1/137.0359895$
$\alpha(2M_W)$	$1/128.07$
G_F	$1.16639 \cdot 10^{-5}\ \text{GeV}^{-2}$
α_{QCD}	0
V_{CKM}	1

Table 5: Input parameters used in the *tuned comparisons*

effective coupling constants entering the hard matrix element; this has been controlled by printing out these constants, for which all the codes have registered an agreement up to computer precision: $g_V = -0.0141$, $g_A = -0.18579$, $g = 0.23041$, $g_{ZWW} = .057148$, $g_{\gamma WW} = 0.31324$.

The photonic corrections employed in the tuned comparisons are only those corresponding to a leading-logarithmic approximation of initial-state radiation, final-state radiation being implemented in only a few programs so far (for more details we refer to the section on FSR). The non-logarithmic QED radiative corrections have been fixed by demanding that structure functions and parton showers should use $\beta = \ln(s/m^2) - 1$ instead of $\eta = \ln(s/m^2)$. Other universal corrections should be left out, see page 70 for a brief discussion of flux functions. Such pragmatic renormalization schemes are not easily reconciled with the schemes used in $\mathcal{O}(\alpha)$ calculations. A complete calculation of this kind is, however, not available and it is important to resum the dominant contributions (cf. [71]), therefore this pragmatic approach has been taken.

3.1.4 Presentation

The comparisons are presented graphically in the style familiar from the comparisons of experimental LEP1 results. The predictions are aligned vertically with horizontal error bars. The scale at the bottom of each plot gives the absolute value of the observables.

We provide also two tools to simplify the interpretation of the results: at the top of each plot, a scale with the relative deviation from some (insignificant) central value is drawn. This can be used to gauge the numerical accuracy of the results, which is of particular importance for the tuned comparisons. It should be noted, however, that such a scale can be misleading for quantities that vanish in a first approximation. This 'fine tuning' occurs for $\langle x_m \rangle$: further comments are given below.
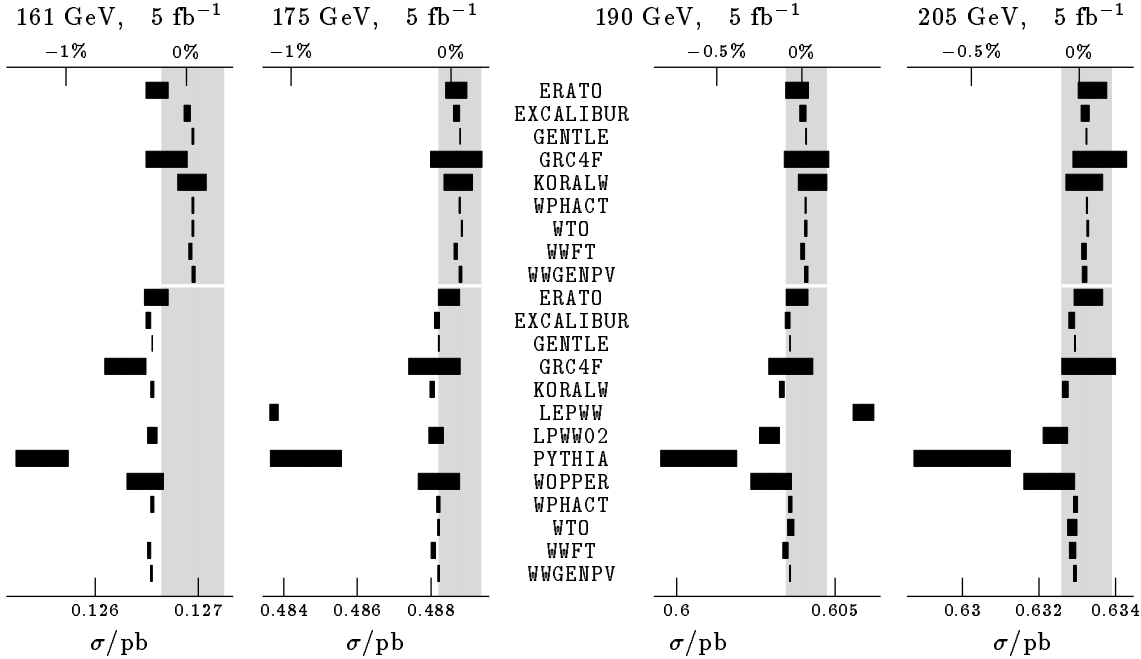
Figure 5: Tuned predictions for the total cross section for $e^+e^- \to \mu^-\bar{\nu}_\mu u\bar{d}$ without cuts.

In addition there is a gray band drawn around the central value, corresponding to a rough estimate of the experimental errors for a suitable integrated luminosity. This band is of particular importance for the *unleashed comparisons*, since it can be used by experimentalists to gauge the theorists' predictive power in relation to the experimental accuracy available at LEP2.

The results for both sets of Feynman diagrams are combined into one plot for the *tuned comparisons*. The upper half corresponds to the *CC10* set, while the *CC03* values are shown in the lower half, separated by a thin white line. This style of presentation clearly shows the effect of the *incompleteness error* caused by leaving out a class of diagrams. For the interpretation of the *incompleteness error* shown in the plots, two competing effects must be taken into account: the $e^+e^- \to \mu^-\bar{\nu}_\mu u\bar{d}$ final state under consideration is known to be less sensitive to "background" diagrams than final states with electrons. On the other hand, we have *not* applied any invariant mass cuts, which would reduce the contribution of "background" diagrams in an experimental analysis.

3.1.5 Experimental Errors

The statistical errors at an integrated luminosity of 500 pb^{-1} have been estimated by rescaling the errors from a high statistics ($\mathcal{O}(10^7)$ events) simulation using WOPPER[7]. For the error on the

---

[7]A change of even a few percent in this error estimate would have no impact on our conclusions. The choice of event generator is therefore completely irrelevant for our purposes and has been accidental.

total cross section, we use the naive statistical error

$$\frac{\Delta\sigma}{\sigma} \approx \frac{1}{\sqrt{N}} \tag{21}$$

from the event count $N = \sigma \cdot 500\,\mathrm{pb}^{-1}$ for *all* final states at $500\,\mathrm{pb}^{-1}$. This will *under*estimate the error on the cross section for the $\mu^- \bar{\nu}_\mu u\bar{d}$ final state by a factor of ≈ 5. At the same time it is a more realistic number for a cross section measurement in which events from a substantial fraction of all final states will be counted. The error on the moments is derived by rescaling the statistical errors of the high statistics `WOPPER` run by

$$\sqrt{\frac{N_{\text{generated}}}{N(500\,\mathrm{pb}^{-1})}} = \sqrt{\frac{\mathcal{L}_{\text{generated}}}{500\,\mathrm{pb}^{-1}}} \,. \tag{22}$$

Again, the event count for *all* final states is used, but also here the actual measurements will involve events of a variety of final states. The resulting relative errors are collected in table 6. It must be kept in mind that these errors are meant as order-of-magnitude estimates for gauging the accuracy of the theoretical predictions only. The actual measurement will be able to reduce these errors by intelligent use of constraints. At the same time, systematic errors will increase the experimental errors.

Some errors in table 6 appear suspiciously large, but their origin can be understood easily. The quantity $\langle x_m \rangle = \langle \sqrt{s_+} + \sqrt{s_-} - 2M_W \rangle / (2E_B)$ vanishes in the narrow width approximation. Therefore it is a *fine tuned* quantity for which the relative error can be of order one. The absolute error on $\langle \sqrt{s_+} + \sqrt{s_-} \rangle$ is about $70\,\mathrm{MeV}$ ($200\,\mathrm{MeV}$ at $161\,\mathrm{GeV}$). Experimentalists expect that the error on the W mass will be smaller by virtue of constraint fits. The errors on the photonic observables at $161\,\mathrm{GeV}$ are simply caused by the small radiated energy and the small number of hard, observable photons close to threshold.

In the plots below, the errors are presented for an integrated luminosity of $\mathcal{L}_0 = 500\,\mathrm{pb}^{-1}$. If the corresponding error is larger than the spread of the predictions, $\mathcal{L}_0$ is multiplied by an appropriate power of ten. According to the target set in [71], our predictions should have an error of less than one third of the expected experimental error. The spread of values in the plots below must therefore be inside a gray band corresponding to $5\,\mathrm{fb}^{-1}$.

At this point we should emphasize for the first time, that possible discrepancies in the *tuned comparisons* must *not* be mistaken for *theoretical* errors. They rather point to *incorrect* implementations and/or to still undiscovered bugs.

$\sqrt{s}$	161 GeV	175 GeV	190 GeV	205 GeV
σ	2.4%	1.2%	1.1%	1.1%
$\langle T_1(\cos\theta_W)\rangle$	6.8%	2.1%	1.4%	1.1%
$\langle T_2(\cos\theta_W)\rangle$	5.3%	3.7%	5.9%	15.3%
$\langle (x_m)^1\rangle$	3.2%	6.4%	38.1%	19.6%
$\langle (x_m)^2\rangle$	7.4%	5.8%	4.5%	4.0%
$\langle (x_\gamma)^1\rangle$	8.9%	2.9%	2.5%	2.4%
$\langle (x_\gamma)^2\rangle$	26.4%	6.3%	4.1%	3.7%
$\langle (x_\gamma^{\text{lost}})^1\rangle$	11.0%	3.7%	3.2%	3.0%
$\langle (x_\gamma^{\text{lost}})^2\rangle$	32.7%	7.9%	5.2%	4.8%
$\langle (x_\gamma^{\text{vis.}})^1\rangle$	14.9%	5.0%	4.2%	4.1%
$\langle (x_\gamma^{\text{vis.}})^2\rangle$	45.2%	10.6%	7.0%	6.3%
$\langle T_1(\cos\theta_\mu)\rangle$	4.1%	1.8%	1.3%	1.1%
$\langle T_2(\cos\theta_\mu)\rangle$	3.5%	2.1%	2.4%	3.1%
$\langle T_1(\cos\theta_\mu^*)\rangle$	16.6%	5.0%	3.2%	2.6%
$\langle T_2(\cos\theta_\mu^*)\rangle$	4.4%	2.4%	2.2%	2.3%
$\langle (x_\mu)^1\rangle$	0.4%	0.3%	0.3%	0.3%
$\langle (x_\mu)^2\rangle$	0.8%	0.5%	0.5%	0.6%

Table 6: Estimated statistical errors at $\mathcal{L}_0 = 500\,\text{pb}^{-1}$.

3.1.6 Canonical Cuts

Canonical cuts (a.k.a. ADLO/TH) have been defined in collaboration with ALEPH, DELPHI, L3 and OPAL. The following *acceptance cuts* define an optimistic union of the phase spaces that the four collaborations expect to cover:

- the energy of light charged leptons (e, μ) must be greater than $1\,\text{GeV}$;

- light charged leptons (e, μ) will be seen down to 10 degrees from either beam;

- the energy of a jet must be greater than $3\,\text{GeV}$. For the purpose of our study, jets will be identified with quarks;

- jets can be detected in the entire 4π of solid angle;

- photons must have an energy of at least $100\,\text{MeV}$ to be identified;

- photons will be seen down to 1 degree from either beam.

161 GeV, 5 fb^{-1} 175 GeV, 5 fb^{-1} 190 GeV, 5 fb^{-1} 205 GeV, 5 fb^{-1}

−1%   0%   −1%   0%   −0.5%   0%   −0.5%   0%

ERATO
EXCALIBUR
GRC4F
KORALW
WPHACT
WTO
WWFT
WWGENPV
ERATO
EXCALIBUR
GRC4F
KORALW
LEPWW
LPWW02
PYTHIA
WOPPER
WPHACT
WTO
WWFT
WWGENPV

0.124   0.125   0.475   0.48   0.588 0.59 0.592 0.594   0.615   0.62

σ_{CC}/pb σ_{CC}/pb σ_{CC}/pb σ_{CC}/pb
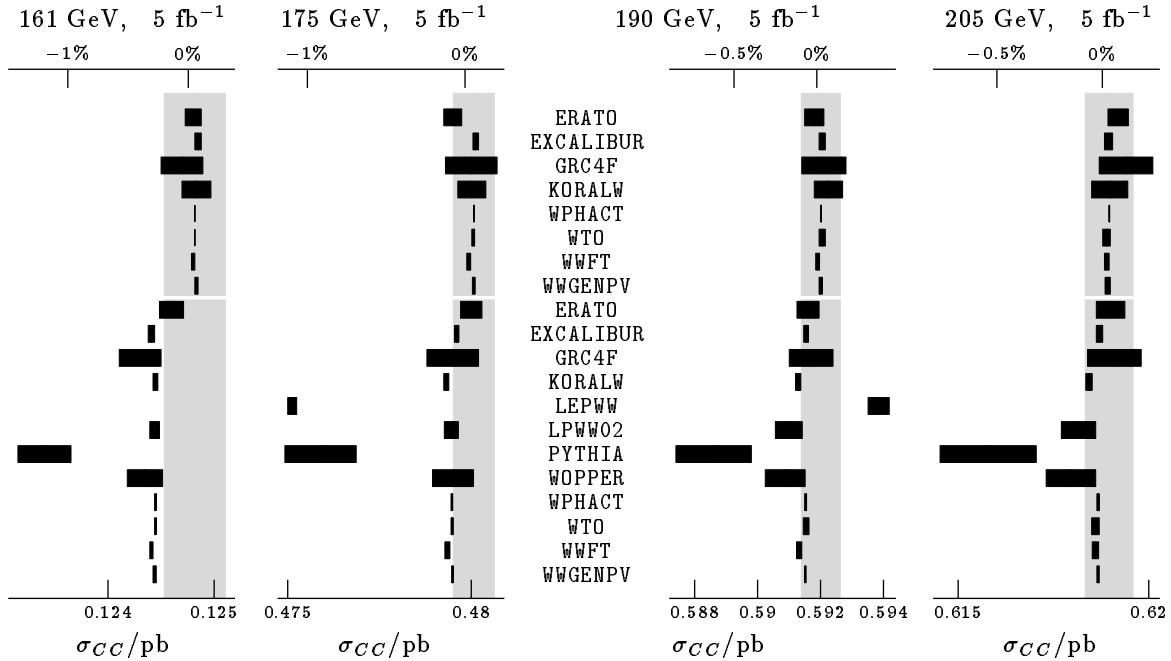
Figure 6: Tuned predictions for the total cross section for $e^+e^- \rightarrow \mu^-\bar{\nu}_\mu u\bar{d}$ after canonical (ADLO/TH) cuts.

These cuts do not address the issue of τ-identification. For the purpose of theoretical studies, τ's can be treated like the light charged leptons e and μ. It is understood that the programs considered here will have to be interfaced to external τ-decay packages. These *acceptance cuts* are supplemented by the following set of *separation cuts*:

- light charged leptons (e, μ) must be separated by at least 5 degrees from jets. Jets will again be identified with quarks.

- the invariant mass of two jets that are resolved as two separate jets must be greater than 5 GeV

- photons must be separated by at least 5 degrees from light charged leptons (e, μ) and jets

τ's will again be treated like the light charged leptons e and μ. If any of the charged particles of our final state fails any of these cuts, the event will be discarded.

Programs using the strict collinear limit for photons will count all photons as lost and assign them to initial-state radiation. If a program generates photons with a finite p_T, a more detailed treatment is necessary. Photons failing the separation cuts from charged final-state particles will not simply be discarded. Instead, their four momentum is added to the closest charged particle. Photons missing the acceptance cut around the beam pipe will be counted as lost

67
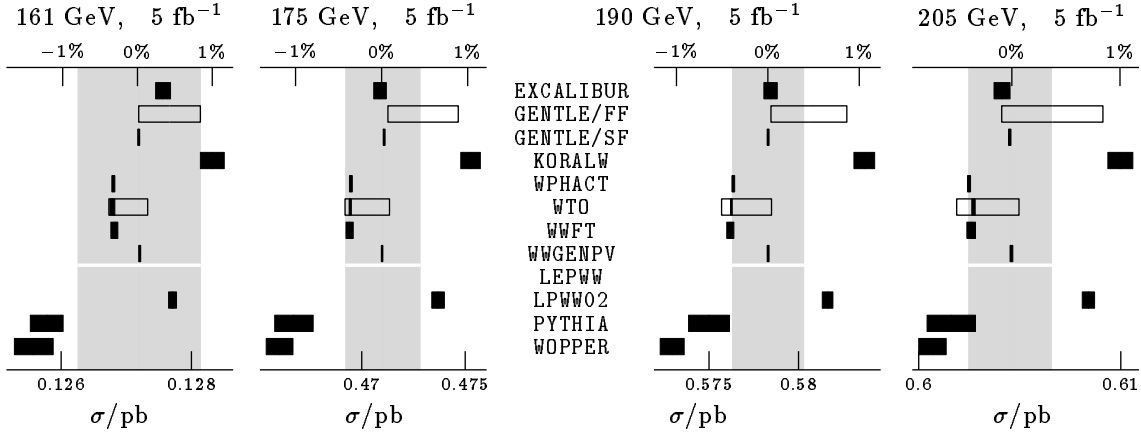
Figure 7: Unleashed predictions for the total cross section for $e^+e^- \rightarrow \mu^-\bar{\nu}_\mu u\bar{d}$ without cuts. The transparent, framed error bars are theoretical errors (cf. page 72).

and will be assigned to initial-state radiation. The question if this procedure is appropriate for dealing with final-state radiation will be discussed below in section 3.1.15. There the size of the separation cut will be discussed in more detail.

These cuts serve two purposes. Firstly they are important for testing programs under more realistic conditions. Secondly, they are required to give well-defined predictions without the need for internal technical cuts cutting out singular regions in phase space. However, for final states involving photons and for programs using massless fermions, some care must be taken in interpreting the results. Indeed, the canonical cuts when applied to a final-state l^+l^- allow for a minimum invariant l^+l^-- mass of $87.2\,\text{MeV}$ which is below $2\,m_\mu$.

Comparing figures 5 and 6, we observe that the effect of the canonical cuts are rather small. This shows that the effect of the internal technical cuts are very similar for all programs under consideration.

3.1.7 "Unleashed" Comparisons

Some numerically important corrections to the total cross section have been left out in the *tuned comparisons*. They have been studied in separate set of comparisons. In these *unleashed comparisons*, all program authors have been asked to provide the *"Best Prediction They Can Make"*. It is of course clear that this is a moving target and the data presented in this report must be viewed as a snapshot of the situation at the end of 1995. This is different from the *tuned comparisons*, which implement a fixed set of approximations and input parameters. These predictions should not change in time, unless bugs are found in some codes.

The *Coulomb correction* (see [71] for a detailed formula) is well established and can be implemented easily as a factor multiplying the part of the cross section emanating from the

68

161 GeV, 5 fb^{-1} 175 GeV, 500 pb^{-1} 190 GeV, 500 pb^{-1} 205 GeV, 500 pb^{-1}

−1%   0%   1%   −1%   0%   1%   −1%   0%   1%   −1%   0%   1%

EXCALIBUR
KORALW
WPHACT
WTO
WWFT
WWGENPV
LEPWW
LPWW02
PYTHIA
WOPPER

0.124   0.126   0.46   0.465   0.56   0.57   0.585 0.59 0.595

σ_{CC}/pb σ_{CC}/pb σ_{CC}/pb σ_{CC}/pb
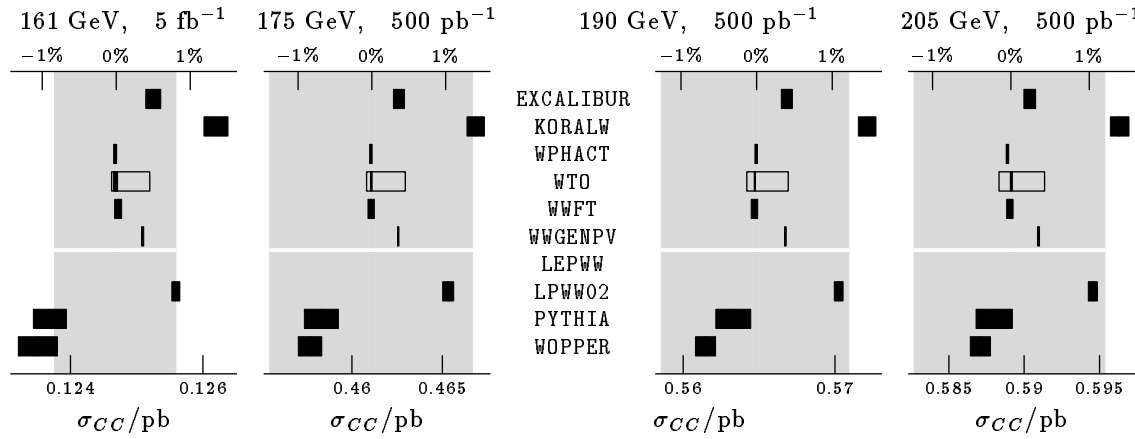
Figure 8: Unleashed predictions for the total cross section for $e^+e^- \to \mu^-\bar{\nu}_\mu u\bar{d}$ after canonical (ADLO/TH) cuts. The transparent, framed error bars are theoretical errors (cf. page 72).

CC03 subset of diagrams. Using a narrow-width approximation exaggerates the effect of the Coulomb correction.

The *QCD corrections* to the hadronic $W^\pm$ width, $\Gamma_W^{\mathrm{hadr.}}$, must be properly included in processes with $q\bar{q}$ pair(s). We have adopted a *naive QCD* factor (NQCD):

$$\Gamma^0_{W\to\mathrm{hadr.}} \to \sum_{\bar{q}q}\left(\Gamma^0_{W\to\bar{q}q} + \Gamma^1_{W\to\bar{q}q}\right) + \sum_{\bar{q}qg}\Gamma^1_{W\to\bar{q}qg} = \sum_{\bar{q}q}\Gamma^0_{W\to\mathrm{hadr.}} \cdot \left(1 + \frac{\alpha_{QCD}}{\pi}\right) \qquad (23)$$

It is certainly correct for inclusive quantities like the total cross section without cuts if only the CC03 diagrams are taken into account.

At the same time it is questionable for exclusive quantities and for diagrams that can not be factorized in the production and decay of a W^+W^- pair. Without a complete $\mathcal{O}(\alpha_{QCD})$ calculation including gluons in the final state, we can not prove that the correction is really of this magnitude in the presence of cuts. Similarly, we can not be sure about the CC11 diagrams without a calculation of the QCD box diagram corrections. Here, we are faced with the very familiar problem of whether we can shrink EW interactions to a point in the presence of gluon emission.

On the other hand, for our set of canonical (ADLO/TH) cuts with complete (4π) coverage of jets, the *"naive correction"* could be very close to the truth for the CC03 diagrams. Furthermore, even if the size of the correction to the CC11 diagrams has not been calculated, we know that it is a $\mathcal{O}(\alpha_{QCD})$ correction to a $\mathcal{O}(\Gamma_W/M_W)$ correction and it makes pragmatical sense to include the overall NQCD correction anyway. The factor (23) has therefore been included by all programs in the numbers below.

In connection with implementation of NQCD we emphasize that the effect of NQCD on some moments, typically $\langle x_m \rangle_n$, is quite large, i.e. of the order of few percent. For instance

69

both `WPHACT` and `WTO` have analyzed $\langle x_m \rangle_1$ with and without the inclusion of NQCD. The latter has a net effect of changing $\langle x_m \rangle_1$ of 1.5% at $\sqrt{s} = 161\,\mathrm{GeV}$ and of 2.6% at $\sqrt{s} = 175\,\mathrm{GeV}$. This is a considerable correction factor which, in general, calls for a better understanding of the QCD corrections to have full reliability of the order of magnitude of the effect.

Finally, the whole problem of the implementation of NQCD must be seen in the light of describing the relationship between the QCD matrix elements and the interface with hadronization. Ideally, we would have at our disposal a chain of cross checking programs starting from an exact semianalytical program, continuing with less precise but more flexible integration programs and ending with Monte Carlo event generators that can implement any cut and can be be interfaced with hadronization. In the last step *double-counting* should be carefully avoided. It must be kept in mind, however, that many hadronization codes will affect differential distributions only, without correcting the total cross section. Therefore such corrections have to be put in by hand. At the same time, hadronization may suffer from its own problems, connected with the identification of the proper *color-singlet* structure which is far from clear in the presence of complicated diagrams.

The *QED corrections*: Using the *current-splitting trick* [22], it is possible to identify a set of non-logarithmic universal QED radiative corrections and to implement them in so-called *flux functions*. In order to assess the effect from these contributions, `GENTLE` has contributed two numbers to the *unleashed comparisons*: one (`GENTLE/SF`) using structure functions, like most other programs and a second (`GENTLE/FF`) using flux functions. This also allows us to understand the apparent deviation of the `KORALW` number from the others: there, the so-called YFS form factor has been included, which is essentially equivalent with going from the SF to the FF description: indeed, the `GENTLE` result with FF is in good agreement with the `KORALW` one.

The *EW corrections* are the theoretically most demanding problem. There is a theoretical uncertainty from having to choose a particular resummation scheme. In the *tuned comparisons*, this uncertainty has artificially been removed by demanding a particular choice of input parameters. In the *unleashed comparisons*, the spread of predictions *can* point to a theoretical uncertainty. This is, however, not due to EW uncertainties because a sizeable fraction of the programs have used a scheme very similar to the *tuned comparisons*.

The *CKM quark mixing correction* is a trivial correction arising from non-trivial quark mixing:

$$\Gamma_W^{q\bar{q}} \propto |V_{q\bar{q}}|^2 \ . \tag{24}$$

Due to the unitarity of the CKM-matrix, the effects on the widths are negligible. If light quark flavors are summed over, as is required by experimental procedures anyway, the effect on exclusive final states will be small, except for the occasional b-quark. Since the range for $|V_{ud}|^2$ is larger than the uncertainties from other factors, the plots in figures 7 and 8 have been normalized to $|V_{ud}|^2 = 0.9518$.

The *fermionic masses* could, in principle, be included everywhere in the various calculations, but we point out that there are essentially three places where they become relevant. First of

70

all, the electron mass in $CC20$, whenever the $e^-(e^+)$ scattering angle is considered without cuts (gauge invariance is also involved here). Secondly, whenever a charged fermion-antifermion pair occurs in the final state, particular care should be devoted to study the threshold region in $\gamma^* \to f\bar{f}$. In the third place, the b-quark should be taken massive for a fully consistent study of Higgs boson production and of its background. For the last case, and for quarks in general, one should worry about which value to use, i.e. the pole mass or the running mass and, if the latter is chosen, at which scale. It is not at all an academic problem in view of the large difference between, say, $m_b(m_b)$ and $m_b(M_W)$ or $m_b(m_H)$.

Programs that implement the complete $CC10$ set of diagrams have contributed to the *unleashed comparisons* as well as programs restricted to the doubly resonant $CC03$ subset. In the context of a *"Best Prediction They Can Make"* the comparison of programs from both sets are justified. In order to help the reader, the $CC10$ programs have been collected at the top of each plot, while the $CC03$ programs are shown at the bottom, separated by a thin white line.

3.1.8 Theoretical uncertainties

At the level of our present knowledge, it is impossible to expect a common treatment of the *theoretical error*, something which is by definition highly subjective. However our preliminary investigations (mostly GENTLE and WTO) have shown that even the most crude and naive estimate of the theoretical error gives quite a wide spread of answers.

Ideally, a theoretical error should be inferred by estimating the differences originating from different treatments of leading higher order effects as well as from non-leading ones, whose size is notoriously much more difficult to guess. Obviously, a theoretical error is bound to disappear whenever real progress is achieved under the form of new and *complete* calculations. Most of the time, the potentialities claimed in the summary table only refer to some *naive* treatment of a particular effect. There is no particular harm in that, as long as *naive* estimates are kept well separated from the *precise* calculations. From this point of view the extension from $CC03$ to $CC10$ (or even better to $CC20$) is a well-established piece of work while the inclusion of final state QCD corrections is, at this stage, a *naive* although *educated* guess.

By referring to a *theoretical error* we can only admit a very partial attempt to understand the missing components of our calculations. Specifically, we can get a feeling of what is missing by allowing different implementations of the SF approach (η-scheme versus β-scheme or even the mixed one) and by judging in a very crude (and most probably underestimated) way the effect of terms of order $\alpha \times constant$. The same can be attempted by comparing the SF and the FF approaches. In the end the codes implementing SF have adopted the β-scheme for tuned comparisons (although it violates gauge invariance), since there are plausibility arguments showing that whenever the full answer is known in other processes then the β-scheme gives the best numerical approximation.

Very simple analyses of theoretical errors have been performed by GENTLE and WTO. They used different sets of *working options*.

GENTLE ran over 6 options: 5 `IZERO`×`IQEDHS` (see subsection 2.5) options using FF plus the standard SF treatment of ISR. In this way, the error due to different treatment of ISR was simulated. `GENTLE` results for σ, $\langle E_\gamma \rangle$ and $\langle 10 x_m \rangle_1$ are presented in table 7.

E_{cm} / `IZERO-IQEQHS`	0-0	0-1	0-2	0-3	1-3	SF
σ, pb						
161	0.13420	0.13366	0.13380	0.13379	0.13460	0.13364
175	0.49598	0.49522	0.49562	0.49561	0.49862	0.49493
190	0.60787	0.60801	0.60841	0.60838	0.61212	0.60758
205	0.63483	0.63558	0.63592	0.63590	0.63984	0.63512
$\langle (m, E)_\gamma \rangle$, GeV						
161	0.4671	0.4754	0.4746	0.4746	0.4749	0.4759
175	1.1055	1.1267	1.1248	1.1249	1.1254	1.1271
190	2.1052	2.1518	2.1473	2.1473	2.1488	2.1565
205	3.1388	3.2084	3.2010	3.2010	3.2041	3.2223
$\langle 10 x_m \rangle_1$						
161	-.38320	-.38410	-.38401	-.38401	-.38403	-.38400
175	-.066431	-.066714	-.066684	-.066684	-.066695	-.066701
190	-.012318	-.012516	-.012492	-.012492	-.012502	-.012508
205	.015638	.015478	.015501	.015501	.015489	.015450

Table 7: `GENTLE` theoretical errors

Two comments are in order here. First, since for `IQEDHS=0` only $\mathcal{O}(\alpha)$ exponentiated FF ISR corrections are used, while for `IQEDHS=1,2,3` different realizations of $\mathcal{O}(\alpha^2)$ are applied, one should consider the difference between `IQEDHS=0` and `IQEDHS`$\geq$`1` as an illustration of the importance of $\mathcal{O}(\alpha^2)$ corrections rather than as an estimate of theoretical errors. Second, in the FF method, one may access only $\langle m_\gamma \rangle$, whose difference from $\langle E_\gamma \rangle$ grows rapidly with energy, see [72]. So, in this case one should not consider the difference between FF and SF calculations as a theoretical uncertainty. The `GENTLE` theoretical errors are exhibited in figures 7 and 16 by a transparent, framed error bar.

`WTO` ran over $6 = 2 \times 3$ `IOS`×`IOSF` options. Two options, `IOS`, for the renormalization of the weak sector, see eqs. 7-8, and three options, `IOSF` for initial-state radiation structure functions implementations, adopted respectively in [7, 62, 63]. `WTO` results for σ and $\langle E_\gamma \rangle$ are given in table 8.

The largest uncertainty for $\langle E_\gamma \rangle$ is of $1.9, 3.2, 9.9, 20.5 \, \mathrm{MeV}$ for $E_{cm} = 161, 175, 190, 205 \, \mathrm{GeV}$ respectively.

In figures 7, 8 and 20 these uncertainties are exhibited by a transparent, framed error bar drawn around the black statistical error bar.

Inspecting figures 7 and 8, we see that the theoretical error derived this way nicely reproduces

E_{cm} / IOS-IOSF	1-1	1-2	1-3	2-1	2-2	2-3
σ, pb						
161	0.13206	0.13204	0.13250	0.13201	0.13198	0.13244
175	0.49207	0.49186	0.49358	0.49177	0.49156	0.49329
190	0.60240	0.60192	0.60404	0.60188	0.60139	0.60352
205	0.62828	0.62754	0.62977	0.62764	0.62691	0.62913
$\langle E_\gamma \rangle$, GeV						
161	0.4688	0.4673	0.4674	0.4685	0.4669	0.4670
175	1.1250	1.1219	1.1221	1.1251	1.1220	1.1222
190	2.1579	2.1484	2.1489	2.1583	2.1488	2.1493
205	3.2317	3.2119	3.2129	3.2324	3.2126	3.2135

Table 8: WTO theoretical errors

the range in predictions defined by WPHACT and WWF at the low end and EXCALIBUR, GENTLE (structure function) and WWGENPV at the high end. On the other hand we must not rush to the judgment that the theoretical error will always be given by the spread in predictions from different programs. A detailed analysis like the one performed by WTO is more reliable. In figure 20 below, we will see an example in which the theoretical error estimated from scanning the options is slightly larger than the spread in predictions.

3.1.9 Total Cross Sections

As can be seen in figures 5 and 6, the agreement among the programs is generally good for the total cross sections. As expected, the effect of the *CC11* diagrams is most notable at 161 GeV. Even though it will be hard to reach this level of experimental accuracy, the programs that are still restricted to the *CC03* subset should aim at implementing a more complete subset.

For most energies, the predictions of LEPWW have not been included in the plots because they are too far off from the other programs. This is caused by an insufficient implementation of initial state radiation in this program, which is of mostly historical interest.

The agreement of the predictions of PYTHIA with the rest of the programs is unsatisfactory.

It should come as no surprise that the spread of predictions is larger in the *unleashed comparisons*. It remains however at or below the expected experimental accuracy of LEP2.

The qualitative pictures with and without cuts are very similar. For this reason, we will show (with one exception) only results without cuts for the tuned comparisons and only results with cuts for the unleashed comparisons of exclusive observables below.
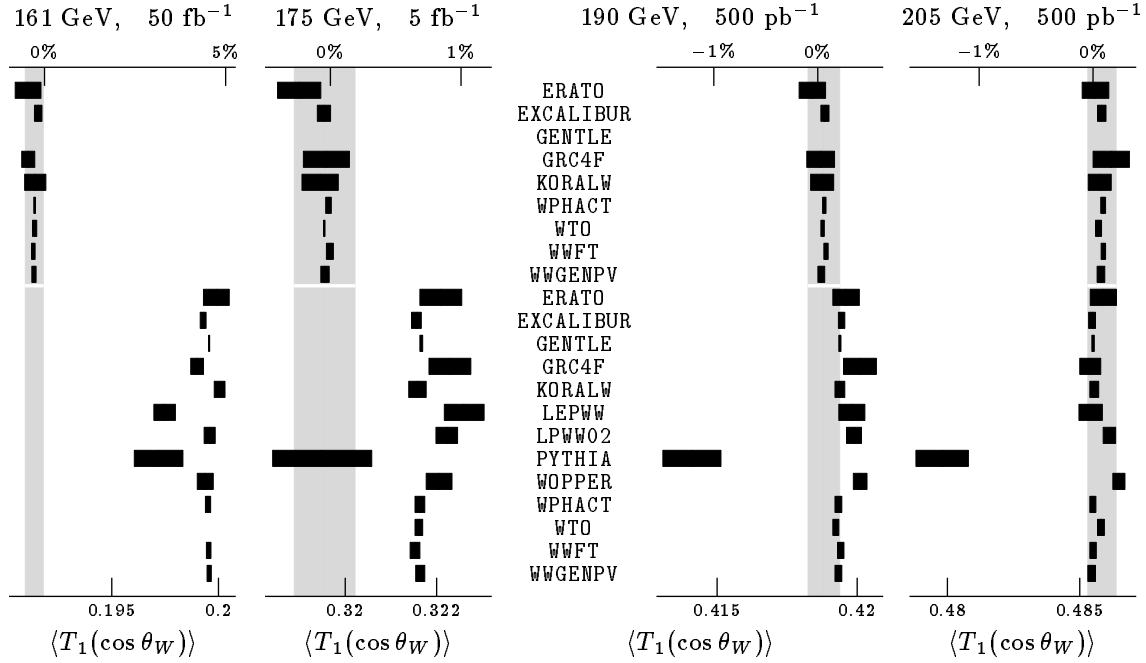
Figure 9: Tuned predictions for the first Chebyshev polynomial of the W production angle in $e^+e^- \to \mu^-\bar{\nu}_\mu u\bar{d}$ without cuts.
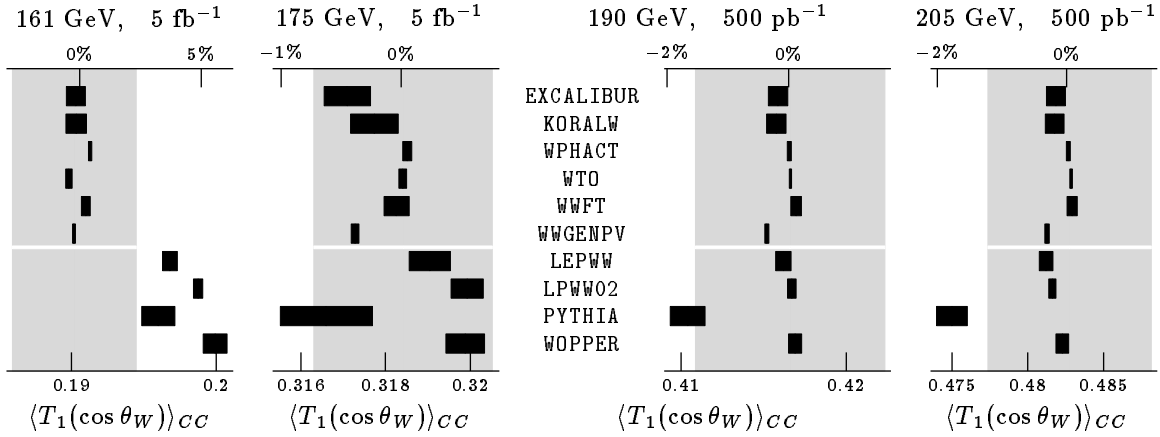
Figure 10: Unleashed predictions for the first Chebyshev polynomial of the W production angle in $e^+e^- \to \mu^-\bar{\nu}_\mu u\bar{d}$ with canonical (ADLO/TH) cuts.

3.1.10 W Production Angle

The trend observed in the total cross section continues in the moments of the W production angle. The deviations of PYTHIA's results are again not acceptable for precision measurements.

74
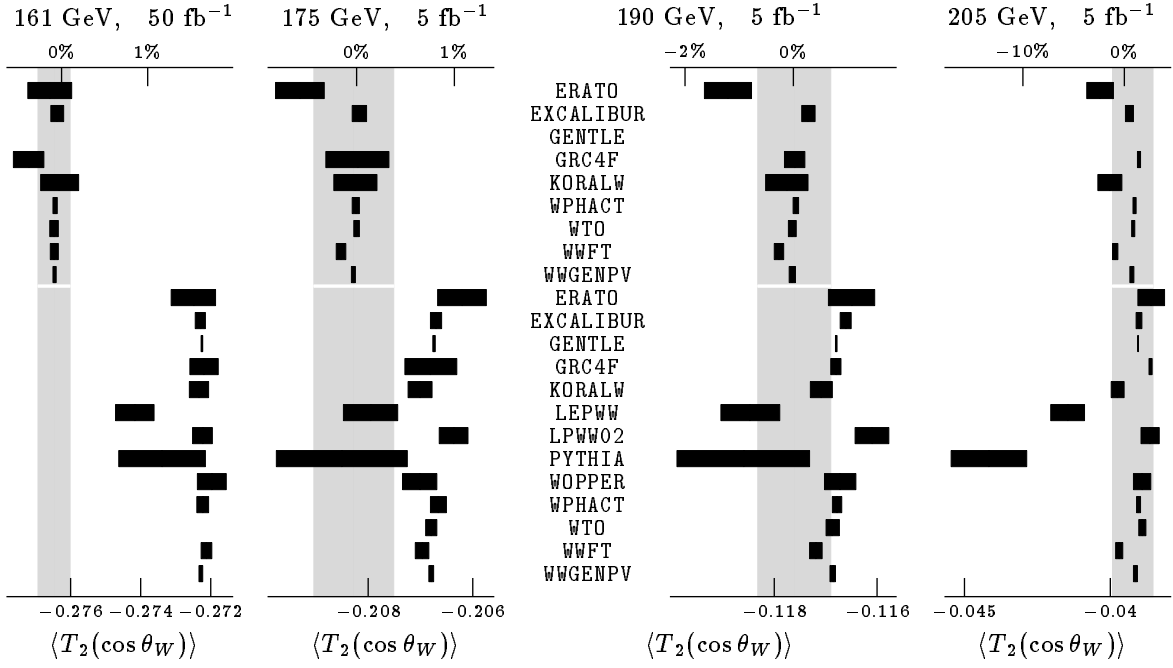
Figure 11: Tuned predictions for the second Chebyshev polynomial of the W production angle in $e^+e^- \to \mu^-\bar{\nu}_\mu u\bar{d}$ without cuts.
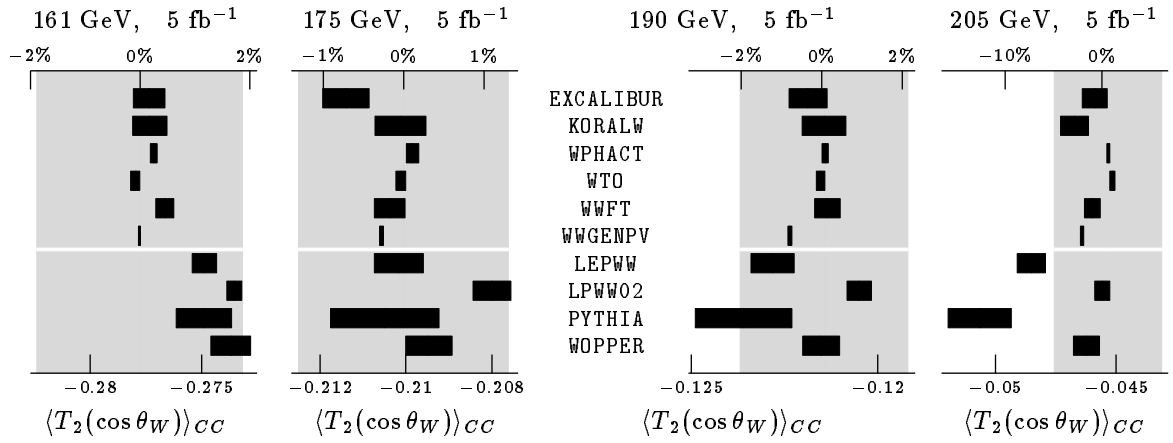

Figure 12: Unleashed predictions for the second Chebyshev polynomial of the W production angle in $e^+e^- \to \mu^-\bar{\nu}_\mu u\bar{d}$ with canonical (ADLO/TH) cuts.

75
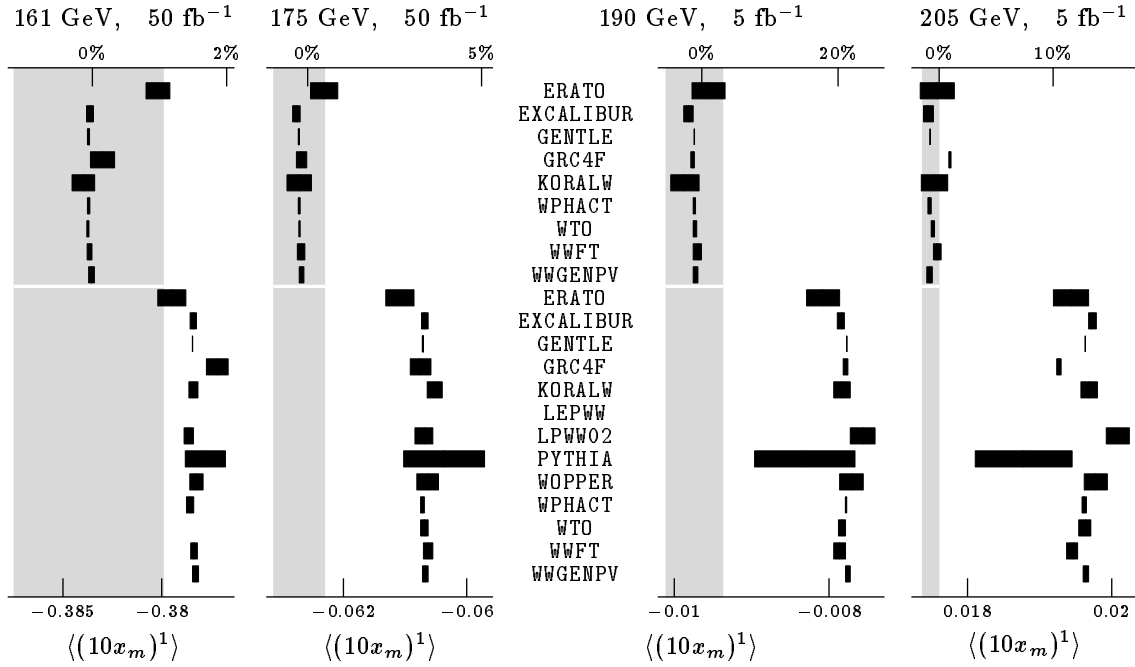
Figure 13: Tuned predictions for the deviation of the sum of invariant W-masses from $2M_W$ in $e^+e^- \to \mu^-\bar{\nu}_\mu u\bar{d}$ without cuts.
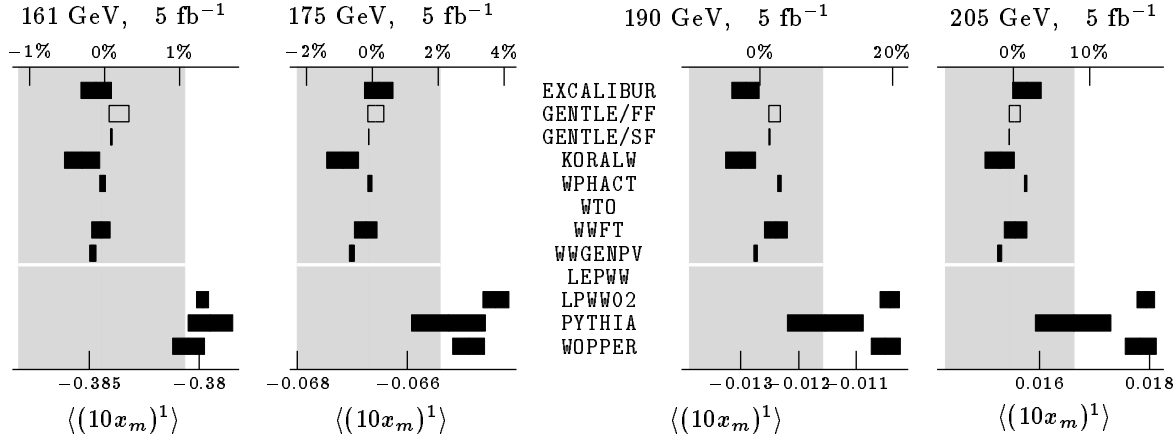
Figure 14: Unleashed predictions for the deviation of the sum of invariant W-masses from $2M_W$ in $e^+e^- \to \mu^-\bar{\nu}_\mu u\bar{d}$ without cuts. The transparent, framed error bars are theoretical errors (cf. page 72).

3.1.11 Invariant Masses

The effect of the *incompleteness error* of leaving out the *CC10* diagrams is of course most drastic in this observable. While the effect will be reduced somewhat by the necessary invariant mass
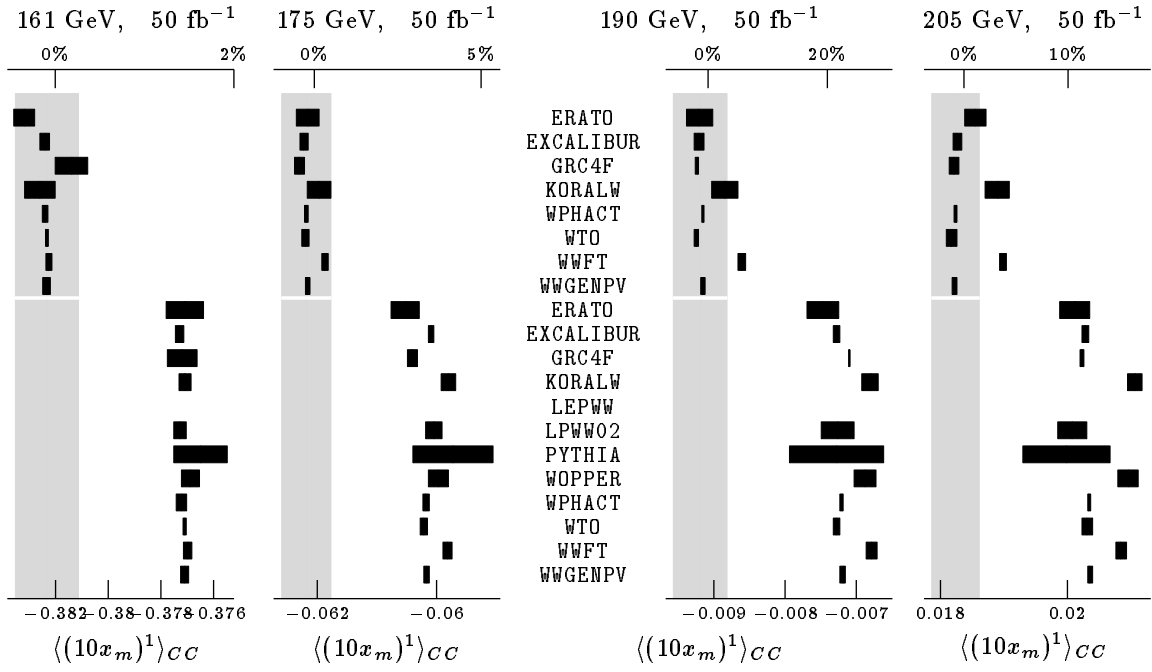
Figure 15: Tuned predictions for the deviation of the sum of invariant W-masses from $2M_W$ in $e^+e^- \to \mu^-\bar{\nu}_\mu u\bar{d}$ after canonical (ADLO/TH) cuts.
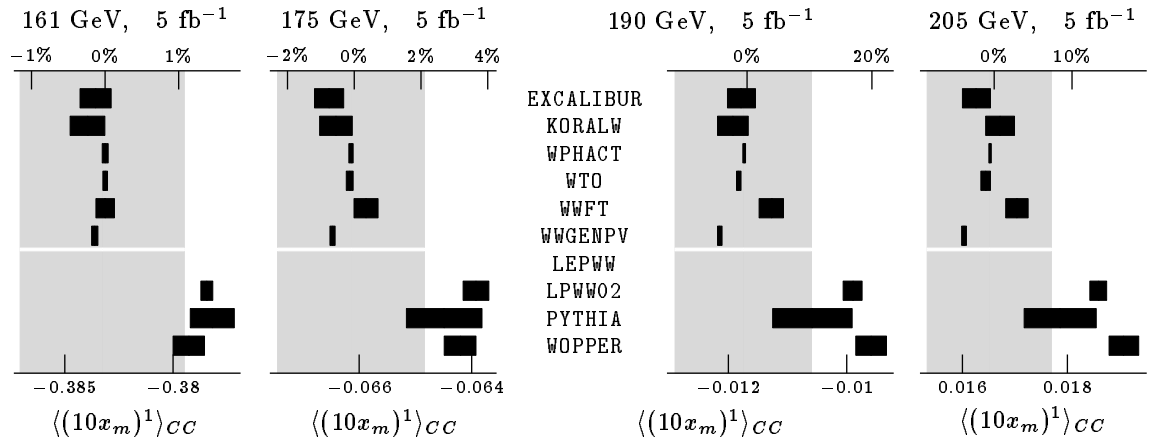
Figure 16: Unleashed predictions for the the deviation of the sum of invariant W-masses from $2M_W$ in $e^+e^- \to \mu^-\bar{\nu}_\mu u\bar{d}$ after canonical (ADLO/TH) cuts.
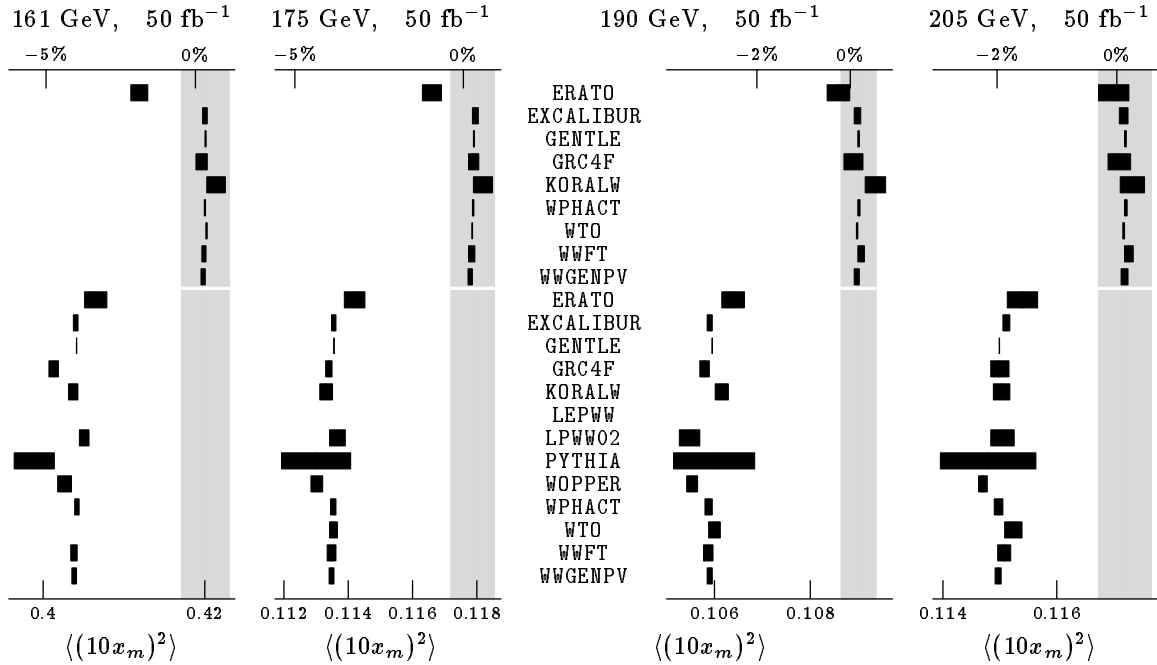
Figure 17: Tuned predictions for the square of the deviation of the sum of invariant W-masses from $2M_W$ in $e^+e^- \to \mu^-\bar{\nu}_\mu u\bar{d}$ without cuts.

cuts for reducing the non-$W^\pm$ background, all programs which are still restricted to the *CC03* set ought to attempt to lift this restriction.

As has been discussed before, this observable vanishes in the zero width approximation and we have to expect *relative* errors which are substantially larger than those for the other observables.

Comparing figures 13 and 15, we observe a nontrivial effect of using a finite p_T for photons. At the higher energies, where a substantial number of hard photons is radiated, the first moment of the invariant masses is slightly higher for the programs with finite photonic p_T (KORALW, WOPPER and WWF), when the ADLO/TH cuts are applied. WWGENPV gives also finite p_T to the photons, but the numbers quoted in the figures have been produced with an intermediate version of the code, in which the p_T is not transferred to the beam particles. Hence, this small effect is absent in this particular case.

3.1.12 γ Energy

The trend continues for the total energy radiated by photons. Here, it should be noted that the *incompleteness error* caused by leaving out the *CC10* diagrams is most notable in the *second* moment, while it is hardly noticeable in the first moment.
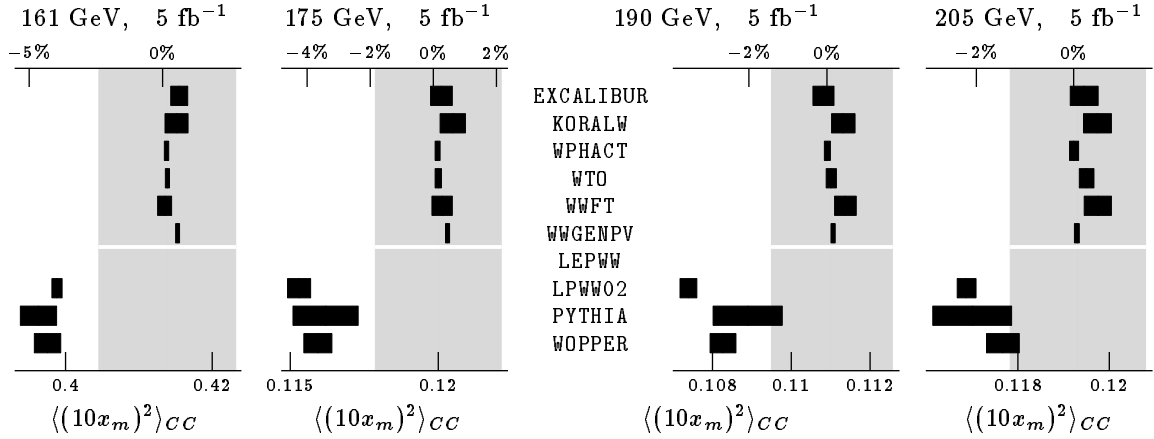
Figure 18: Unleashed predictions for the square of the deviation of the sum of invariant W-masses from $2M_W$ in $e^+e^- \rightarrow \mu^- \bar{\nu}_\mu u\bar{d}$ after canonical (ADLO/TH) cuts.
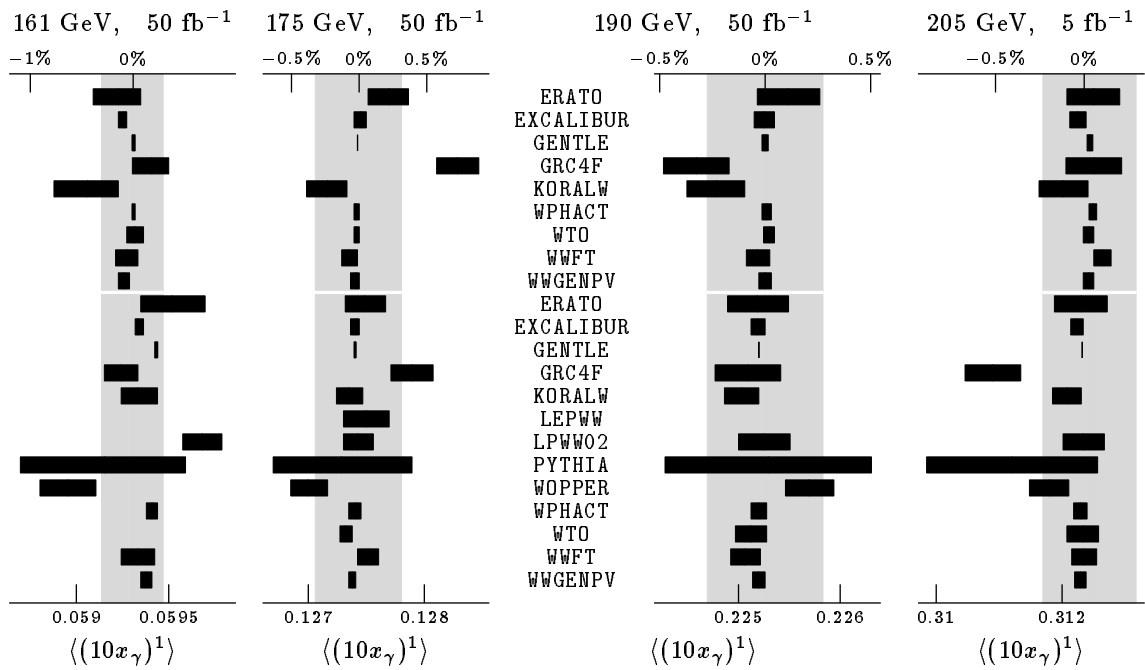
Figure 19: Tuned predictions for the total radiated γ energy in $e^+e^- \rightarrow \mu^- \bar{\nu}_\mu u\bar{d}$ without cuts.
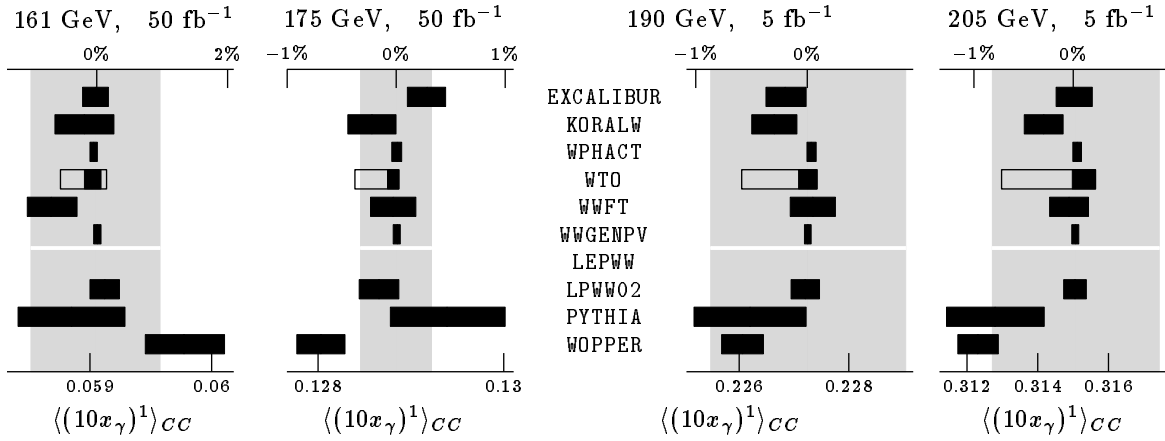
Figure 20: Unleashed predictions for the total radiated γ energy in $e^+e^- \rightarrow \mu^- \bar{\nu}_\mu u\bar{d}$ after canonical (ADLO/TH) cuts. The transparent, framed error bars are theoretical errors (cf. page 72).
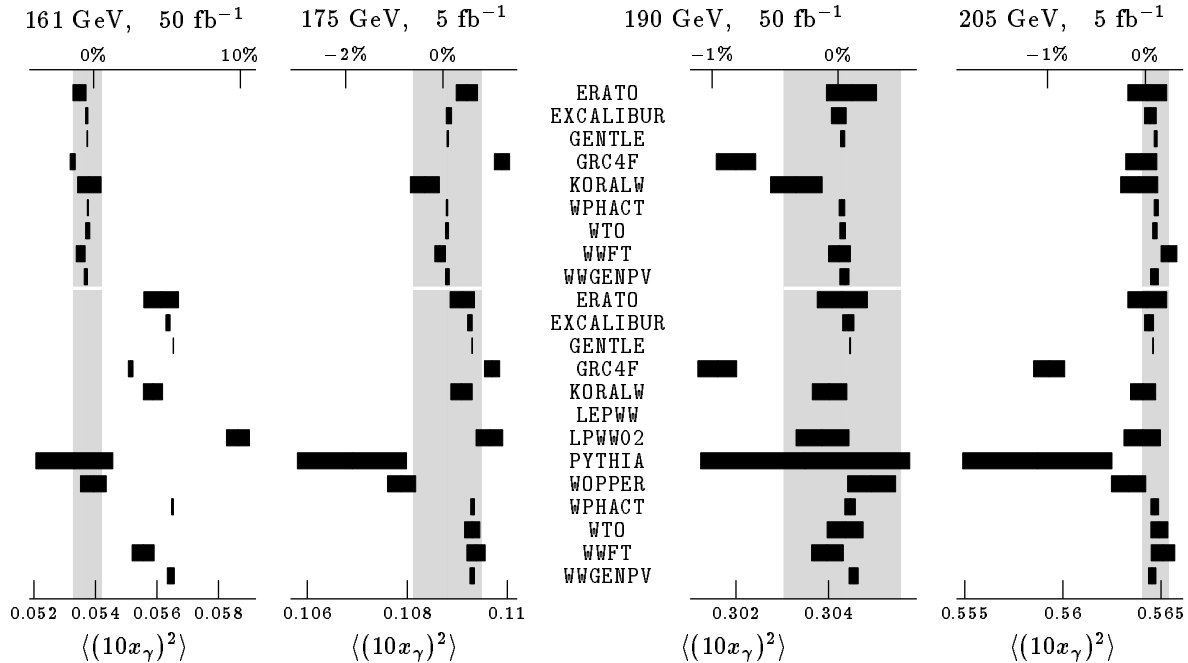
Figure 21: Tuned predictions for the square of the total radiated γ energy in $e^+e^- \rightarrow \mu^- \bar{\nu}_\mu u\bar{d}$ without cuts.

We must keep in mind that this quantity is somewhat artificial and has been used only for comparing the implementation of initial-state radiation among programs which have finite p_T and those who have not. Without the inclusion of final-state radiation, this quantity is not measurable.

0%   5%   −2%   0%   −1%   0%   −2%   0%

ERATO
EXCALIBUR
GRC4F
KORALW
WPHACT
WTO
WWFT
WWGENPV
ERATO
EXCALIBUR
GRC4F
KORALW
LEPWW
LPWW02
PYTHIA
WOPPER
WPHACT
WTO
WWFT
WWGENPV

0.052 0.054 0.056   0.106 0.108 0.11   0.302 0.304 0.306   0.555 0.56 0.565

$\langle (10x_\gamma)^2 \rangle_{CC}$ $\langle (10x_\gamma)^2 \rangle_{CC}$ $\langle (10x_\gamma)^2 \rangle_{CC}$ $\langle (10x_\gamma)^2 \rangle_{CC}$
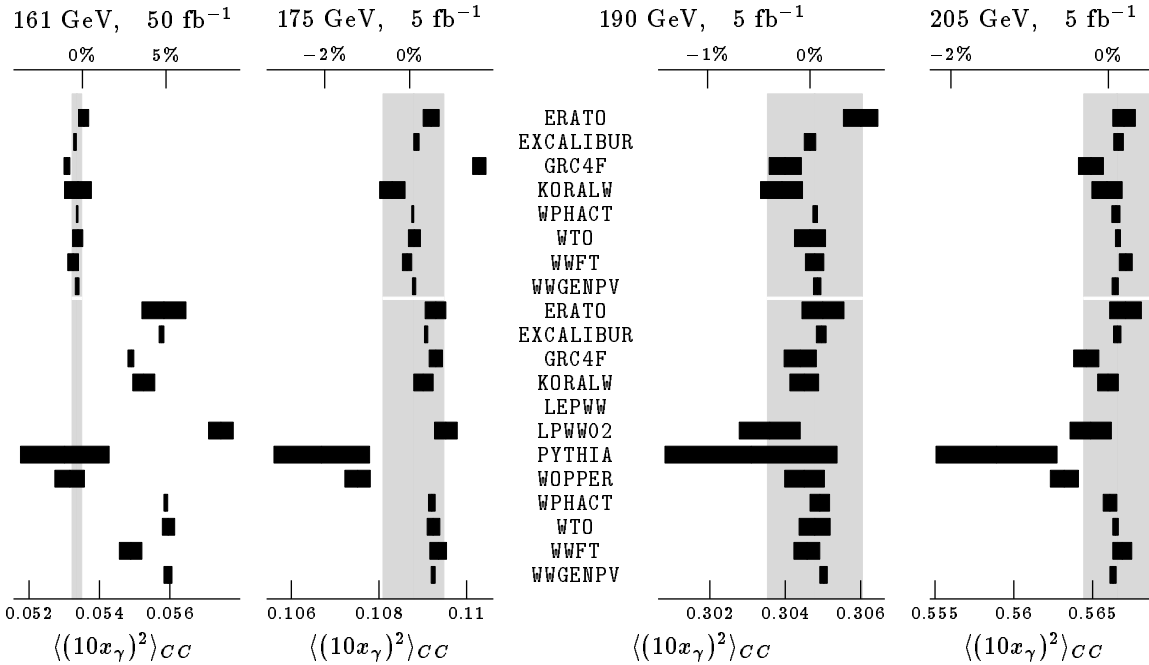
Figure 22: Tuned predictions for the square of the total radiated γ energy in $e^+e^- \rightarrow \mu^-\bar{\nu}_\mu u\bar{d}$ after canonical (ADLO/TH) cuts.

3.1.13   Leptonic Observables

The lepton angles and lepton energies are very well under control. For the lepton energies, the effect of the *incompleteness error* from leaving out the *CC11* diagrams is not even noticeable.

The *incompleteness error* for the lepton angles is noticeable, but hardly measurable. PYTHIA's predictions are significantly different from the other programs.

3.1.14   Visible γ Energy

The situation for exclusive photonic observables is much less satisfactory than the situation for the other observables studied. This should not be surprising, however. The leading-logarithmic approximation is theoretically justified using the renormalization group and an operator product expansion for observables which are totally inclusive in the photons. A majority of programs implements this result with structure functions and treats photons inclusively, treating *all* photons as emitted collinearly.

It is nevertheless possible to investigate the structure of the Feynman diagrams contributing to the renormalization group evolution of the structure functions. This investigation shows that

81

| 161 GeV, 50 fb^{-1} | 175 GeV, 5 fb^{-1} | | 190 GeV, 5 fb^{-1} | | 205 GeV, 5 fb^{-1} |

ERATO			
EXCALIBUR			
GRC4F			
KORALW			
WPHACT			
WTO			
WWFT			
WWGENPV			
ERATO			
EXCALIBUR			
GRC4F			
KORALW			
LEPWW			
LPWW02			
PYTHIA			
WOPPER			
WPHACT			
WTO			
WWFT			
WWGENPV			

$\langle T_1(\cos\theta_\mu)\rangle_{CC}$ $\langle T_1(\cos\theta_\mu)\rangle_{CC}$ $\langle T_1(\cos\theta_\mu)\rangle_{CC}$ $\langle T_1(\cos\theta_\mu)\rangle_{CC}$
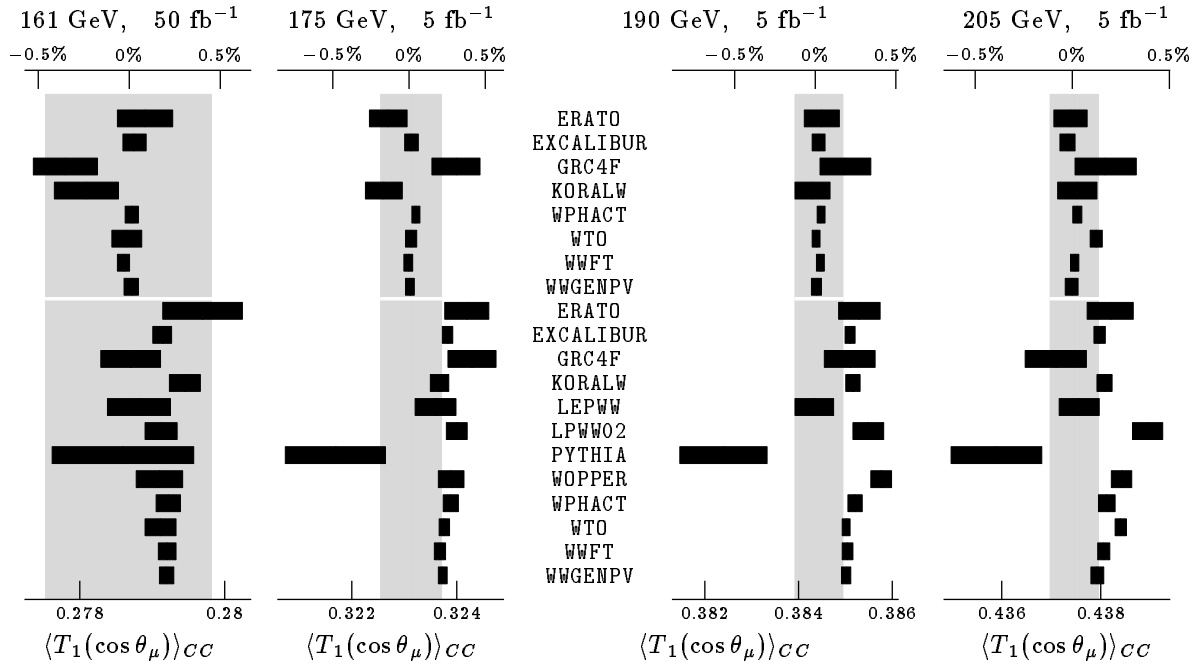
Figure 23: Tuned predictions for the first Chebyshev polynomial of the μ production angle in the laboratory frame in $e^+e^- \rightarrow \mu^- \bar{\nu}_\mu u\bar{d}$ after canonical (ADLO/TH) cuts.

| 161 GeV, 50 fb^{-1} | 175 GeV, 5 fb^{-1} | | 190 GeV, 5 fb^{-1} | | 205 GeV, 5 fb^{-1} |

$\langle T_1(\cos\theta_\mu^*)\rangle_{CC}$ $\langle T_1(\cos\theta_\mu^*)\rangle_{CC}$ $\langle T_1(\cos\theta_\mu^*)\rangle_{CC}$ $\langle T_1(\cos\theta_\mu^*)\rangle_{CC}$
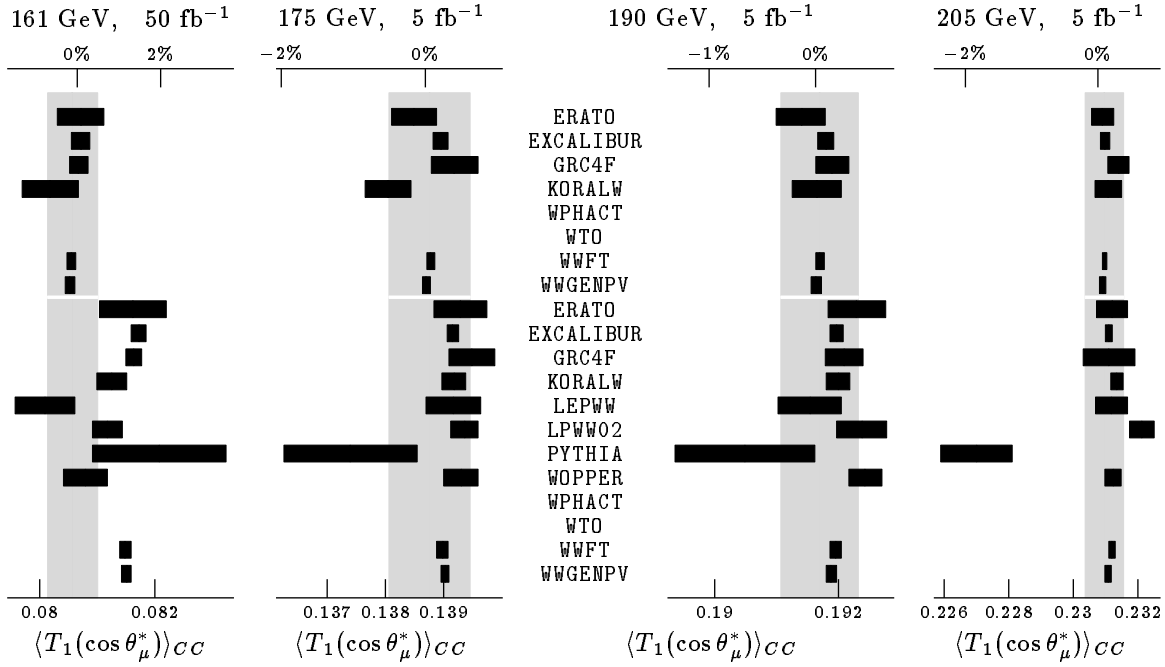
Figure 24: Tuned predictions for the first Chebyshev polynomial of the μ decay angle in the rest frame of the W^- in $e^+e^- \rightarrow \mu^- \bar{\nu}_\mu u\bar{d}$ after canonical (ADLO/TH) cuts.

82
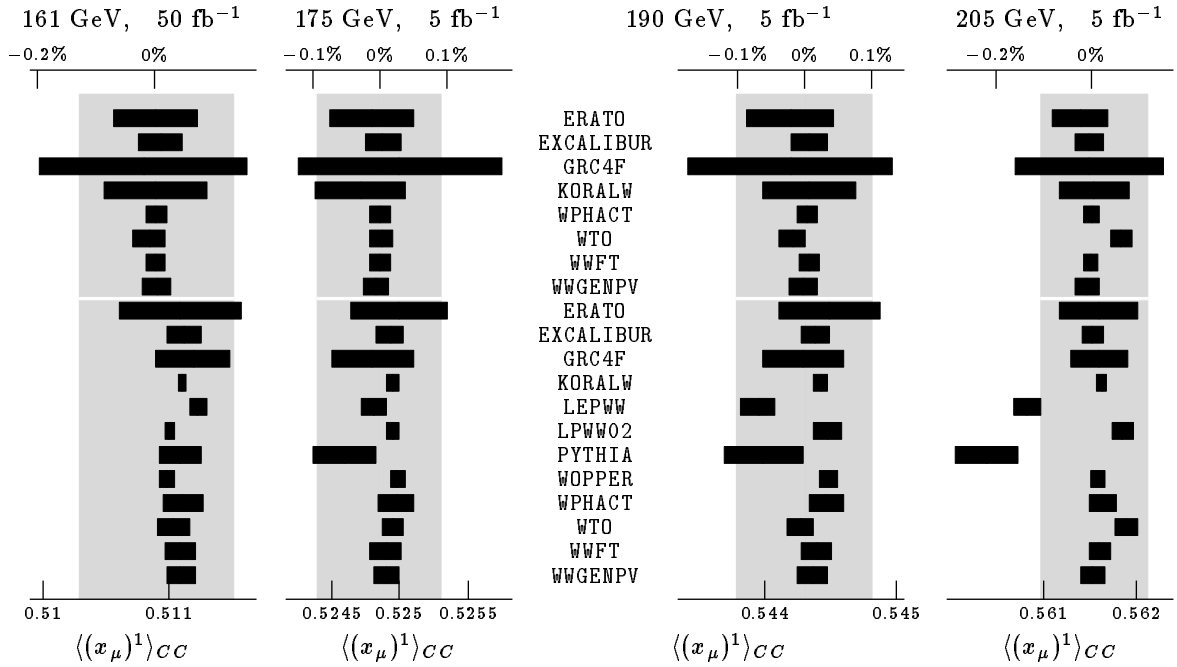
Figure 25: Tuned predictions for the μ energy in $e^+e^- \to \mu^-\bar{\nu}_\mu u\bar{d}$ after canonical (ADLO/TH) cuts.
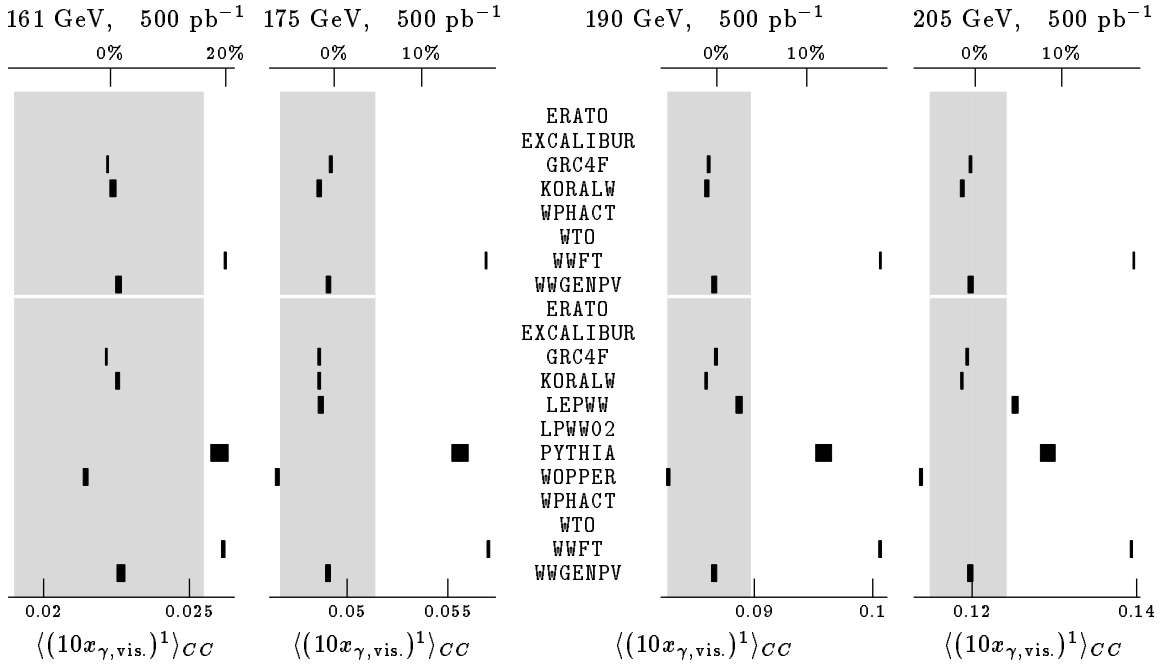
Figure 26: Tuned predictions for the visible γ energy in $e^+e^- \to \mu^-\bar{\nu}_\mu u\bar{d}$ after canonical (ADLO/TH) cuts.

83

the leading logarithms originate from a propagator pole

$$\ln\left(\frac{s}{m_e^2}\right) = \int_{m_e^2}^{s} \frac{d(pk)}{pk} \tag{25}$$

caused by the emission of almost collinear photons. This observation can be used to implement various parton shower algorithms for such photons. Another approach is to use p_T-dependent structure functions that recover the p_T-dependence of the first-order matrix element.

In contrast to the structure function method which is unambiguously defined by the renormalization group, these explicit resummations of Feynman diagrams are not uniquely defined and can lead to differing results. These differences are reflected in our results.

3.1.15 Final State Radiation

The canonical (ADLO/TH) cuts are of calorimetric nature, i.e. photons are combined with nearby charged particles. Therefore we should expect the effect of final-state radiation to be very small and furthermore the leading-logarithmic approximation to be sufficient. Since some programs have implemented final-state radiation, this assertion has to be checked.

We must, of course, again stress the fact that a theoretically meaningful (i.e. gauge invariant) separation of initial and final-state radiation is *not* possible in $e^+e^- \to 4f + \gamma$. The leading logarithmic corrections, however, can be traced back to the mass singularities in initial-state radiation, and do form a gauge invariant subset. From a pragmatical point of view, it is also possible to calculate the bremsstrahlung from the charged final-state particles. The radiation from off-shell intermediate states will likely contribute less than the radiation from on-shell final states, because the latter contains infrared and mass singularities. Therefore one can argue that the dominant radiative corrections will come from these diagrams.

This procedure has some pragmatical merit, but it should be kept in mind that it could be justified only *a posteriori*, after a full calculation of the non-logarithmic terms is available.

At the time of the final meeting, a rather substantial effect for exclusive observables was reported from a preliminary study using the ADLO/TH cuts. The separation cut of 5 degrees for photons from charged particles is rather tight, however. For a realistic assessment of the effect, a looser separation cut should be used. A study [56] from 1994 (comparing version 1.1 of WOPPER and version 1.0 of WWF) had shown that about 20 degrees are required for cutting the effect of final-state radiation at LEP2 energies.

Therefore, another study with modified canonical cuts has been performed. These cuts are identical to ADLO/TH, except for the photonic separation cuts. In the results shown below, a photon is counted as initial-state radiation if it is closer to a beam than to any charged particle. All other photons are counted as final-state radiation and are combined with the closest charged particle.

In order to finish the study before the deadline, it was agreed to perform only tuned comparisons, for the *CC03* subset of diagrams.

The plots feature eight data sets:

- **KORALW/FSR** and **KORALW**: results from **KORALW**, with and without final-state radiation, using the *CC03* diagrams. The final-state radiation is generated using the **PHOTOS** package [36]. **PHOTOS** has been modified to generate final-state radiation for quarks as well.

- **LPWW02/FSR** and **LPWW02**: results from **LPWW02**, with and without final-state radiation, using the *CC03* diagrams. The final-state radiation is generated using again the modified **PHOTOS** version. **LPWW02** does not include a finite p_T for the initial-state radiation. This will reduce the effect from final-state radiation considerably.

- **WWF/FSR** and **WWF**: results from **WWF**, with and without final-state radiation, using the *CC03* diagrams. **WWF/FSR** is the only data set in this study which uses a complete $\mathcal{O}(\alpha)$ matrix element for hard radiation. The virtual corrections are not complete but the most important contributions have been included consistently by demanding the cancellation of infrared and mass divergences, leaving a theoretical uncertainty of $\mathcal{O}(\alpha)$.

- **WWGENPV/FSR** and **WWGENPV**: results from **WWGENPV**, with and without final-state radiation, using the *CC03* diagrams. The final-state radiation is generated in leading-logarithmic approximation, using fragmentation functions (the final state equivalent of structure functions).

For some programs, another set of cuts has also been studied: **ADLO/TH** with a separation cut of 20 degrees. These results will not be shown, because they do not reveal anything unexpected. They are inbetween the results from fully inclusive and those from the **ADLO/TH** cuts, but closer to the former.

For completely inclusive observables like the total cross section, we should not expect any effect from final state parton showers, as implemented in **PHOTOS** or in **WWGENPV**. The sum of the probabilities for radiating zero or N photons has to add up to one. This expectation is confirmed in figure 27. Since we are applying acceptance cuts, a small residual effect will remain from charged particles, that are "kicked" out of, or into, the acceptance cuts.

This is different for calculations including the complete $\mathcal{O}(\alpha)$ matrix element for hard radiation, where non-trivial effects are possible. The result from **WWF** in figure 27 shows that there is an uncertainty, because the non -(infrared or mass)-divergent virtual contributions are not taken into account and the total cross section is expected to have a theoretical error almost as big as the apparent deviation.

The phenomenologically most important issue is certainly the effect of final-state radiation on the measured $W^{\pm}$ masses. If a final-state particle radiates a sufficiently hard photon that is not included in the corresponding "jet", a smaller invariant mass will be measured. We have
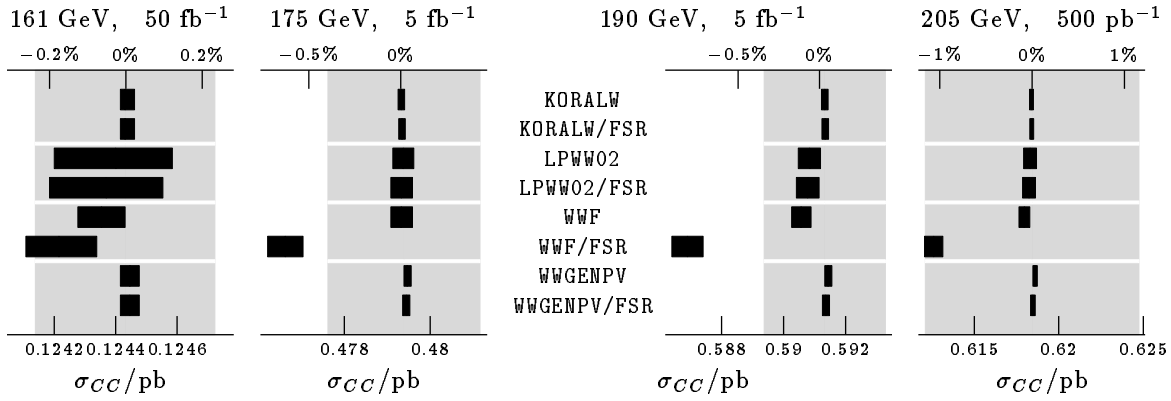
Figure 27: The total cross sections with cuts are not affected by the inclusion of leading logarithmic final-state radiation. See page 85 for comments.
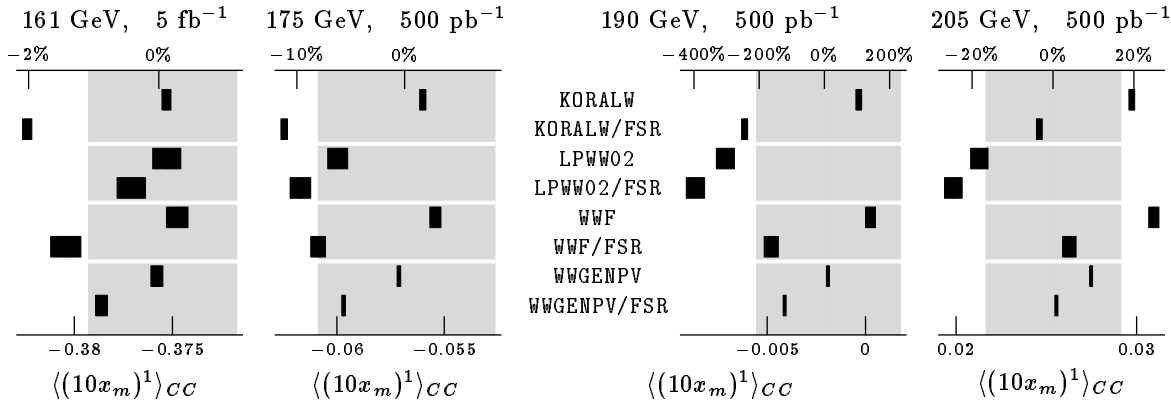
Figure 28: The seemingly large shifts in $\langle x_m \rangle$ correspond to rather moderate shifts in the absolute values of the sum of invariant masses. For the case of WWF we have shifts of $\approx 90\,\mathrm{MeV}$. See page 86 for comments.

to answer the question of whether this shift is numerically important, and whether it is under control.

From figure 28, we see that both KORALW and WWF predict a shift in the sum of invariant masses in the 80–90 MeV range. Toggling options in WWF, it can be verified that this shift is dominated by the leading logarithms and that non-factorizable contributions are negligible.

On the other hand, WWGENPV and LPWW02 predict smaller shifts of 40 MeV and 30 MeV, respectively. For LPWW02, the difference can, presumably, be traced back to the missing p_T in the initial-state radiation. As for WWGENPV, the difference is probably due to differences in the formulations.

As already observed in figures 13 and 15, a finite p_T of the hard scattering system has
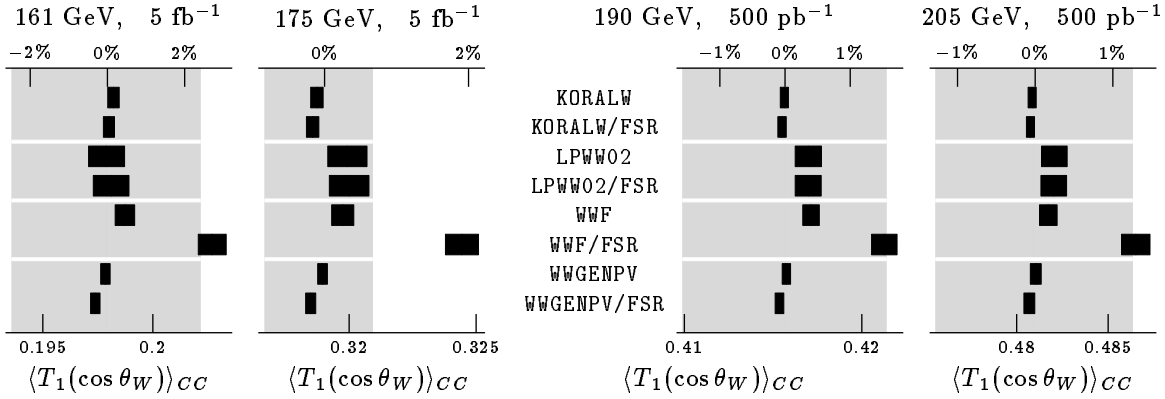
Figure 29: The programs based on leading logarithms show no measurable effect in the $W^\pm$ production angle.
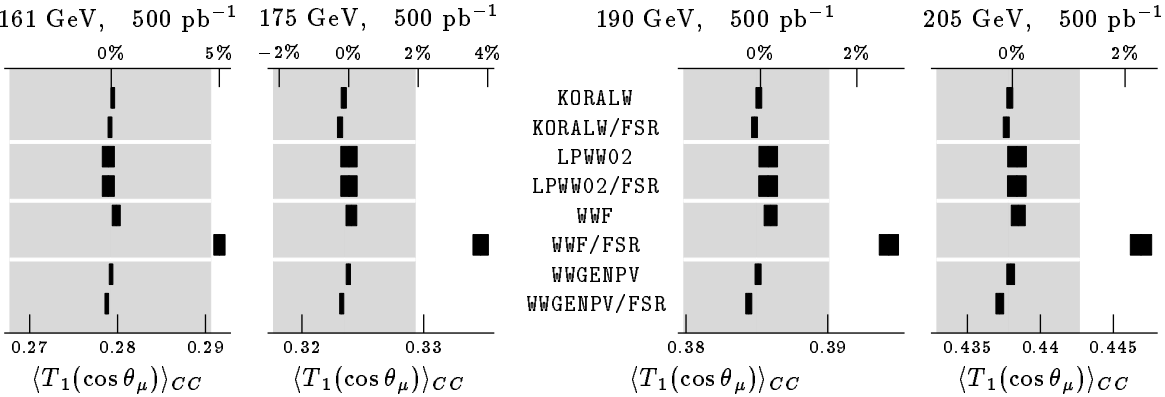
Figure 30: The programs based on leading logarithms show no measurable effect in the μ production angle.

a noticeable effect on the invariant masses if `ADLO/TH` cuts are applied. It must be noted, however, that these results are still very fresh, and the work on this issue must be considered as still in progress. Still, it can be said that all the p_T codes give (apart from small differences in particularly sensitive observables) consistent results on the FSR issue.

Extrapolating the shift predicted by `KORALW` and `WWF` naively to a single $W^\pm$, we have an effect of about $40\,\mathrm{MeV}$. Measuring exclusive photons and making use of constraints, the experiments should be able to control this shift if event generators include final-state radiation in leading logarithmic approximation and initial-state radiation with finite p_T. At the end of the day, the uncertainty from final-state radiation will drop well below the anticipated experimental resolution.

There is a hardly measurable effect of the hard-radiation matrix element in `WWF` on the $W^\pm$ production angle, as shown in figure 29. This effect is of the order of $1\% \approx 4\alpha/\pi$ and

corresponds to non-logarithmic contributions, which can not be reproduced in the structure function and parton shower calculations.

There is a similar effect of the hard-radiation matrix element on the μ production angle, as shown in figure 30, where the μ's are pulled towards the forward direction.

For the decay angle of the μ in the $W^\pm$'s decay frame as well as for its energy in the laboratory frame, there is a tiny effect from final-state radiation, which is neither measurable nor different for the LL programs from WWF. It is completely absent in LPWW02.

About one of the important quantities, the 'lost' photon energy, we want to remark the following. All four programs that enter this comparison have studied the total energy lost to 'initial-state' radiation. This, however, being not an unambiguously defined quantity, we have settled on a definition as described above, where a photon is deemed to be ISR if its angle with respect to one of the beams is smaller than that with respect to any other charged particle. We have studied the average value of both the *total* energy of emitted bremsstrahlung and that of the *lost* amount of energy. The total energy results from the four programs are in a rather good agreement, with about twice as much energy lost under ISR + FSR than under ISR alone. If, however, we impose the cuts intended to define the more meaningful 'lost' bremsstrahlung energy, the agreement is not so good at this moment. We ascribe this to yet remaining differences in the cuts' implementation, and we refrain from presenting a plot here, since we feel that it does not adequately reflect the situation, which has to be clarified in the near future.

Summing up, we see that the effects of final-state radiation are at the level of the experimental resolution or below. They have to be studied in particular for a reliable determination of the $W^\pm$ mass. Therefore an inclusion of final-state radiation in the event generators is desirable from a pragmatical point of view, even before a theoretically satisfactory $\mathcal{O}(\alpha)$ matrix element calculation is available.

It has, however, to be noted that the effect of final-state radiation beyond the collinear approximation is crucially dependent on the details of the cuts, and that the quantitative determination of it has to rely on the use of those codes which implement such an effect.

The differences between the leading logarithms and the $\mathcal{O}(\alpha)$ matrix element for hard radiation in the total cross section and some angular distributions will have to be reevaluated when the virtual contributions in the latter calculation will be complete.

3.1.16 Conclusions

Most Monte Carlo event generators, integration programs and semi-analytic programs are ready for physics at LEP2, at least for the early, low-luminosity stages. However, once enough integrated luminosity has been collected, only the high precision programs should be used:

- Programs with *incompleteness errors*, i.e. omission of Feynman diagrams will have to be upgraded or retired. This effort is known to be under way in some cases and users are encouraged to ask the authors for updated versions once in a while.

- We have concentrated on a typical *CC10* process, which is dominated by the *CC03* diagrams. For processes with electrons in the final state, and also for processes like $u\bar{u}d\bar{d}$, the *incompleteness errors* could be much larger. For these processes, the high-precision complete programs are relevant, unless fairly stringent invariant mass cuts are applied. Of course, to *prove* that such cuts indeed allow for the use of an incomplete program, one has again to rely on a complete program after all.

- For several observables, the effect of finite p_T on both initial and final-state radiation is important. For these observables the programs implementing the effect of finite p_T on photonic radiation are relevant, unless particular experimental cuts are applied.

- Authors of programs with bugs are encouraged to fix them. *At the very least, the results of this comparative study should be mentioned in the respective user manuals.* Let us again repeat that deviations in the *tuned comparisons* are *not* theoretical errors but symptoms of bugs.

- From the considerations of the effect of changes in the theoretical approach (SF versus FF, or the use of η versus that of β in the ISR), it is clear that the theoretical error is *not* much smaller than the expected experimental one, at least for several important quantities. Therefore we conclude that the calculation of the complete one-loop electroweak radiative correction is of much more than purely academic interest.

In any case, it is safe to say that the perfect, all-round Ultimate Monte Carlo event generator for $W^{\pm}$-physics at LEP2 does *not* exist. In all likelihood it will *never* exist because different implementation strategies lead to different strengths and weaknesses. Usually this reflects more of the preferences and interests of the respective authors than their ability to provide complete and bug-free codes.

One important issue that has not been studied in detail by our group is the implementation of *anomalous couplings* [73]. While a precise experimental determination of such couplings will in all likelihood not be possible at LEP2, a similarly detailed analysis would be valuable and might be performed in the future.

3.2 *CC11* processes

E_{cm}	GE/4fan	WPHACT	WTO	WWGENPV
Born				
95	.52886(0)	.52890(10)	—	.52895(8)
100	.63217(0)	.63220(10)	—	.63218(6)
130	9.0560(0)	9.0559(5)	—	9.0560(7)
	9.0517(1)	*9.0522(4)*	*9.0530(25)*	*9.0515(4)*
160	.38447(0)	.38447(1)	—	.38446(1)
161	.53580(0)	.53581(2)	—	.53580(2)
175	1.77062(0)	1.77061(6)	—	1.77061(6)
176	1.80481(0)	1.80483(7)	—	1.80483(7)
	1.80445(2)	*1.80450(5)*	*1.80446(4)*	*1.80447(7)*
190	2.04049(0)	2.04053(8)	2.0403(1)	2.04048(10)
205	2.05733(0)	2.05738(8)	—	2.05743(10)
	2.05631(2)	*2.05640(6)*	*2.05637(8)*	*2.05641(10)*
300	1.49733(0)	1.49742(8)	—	1.49735(7)
500	.81482(0)	.81483(7)	—	.81480(6)
1000	.32607(0)	.32607(5)	—	.32602(6)
2000	.16684(0)	.16683(5)	—	.16682(7)
	.10734(0)	*.10737(7)*	*.10782(6)*	*.10727(5)*
With ISR				
95	.55170(1)	.55170(10)	.55190(70)	.55140(55)
100	.57908(1)	.57910(10)	.57930(50)	.57937(34)
130	7.5225(1)	7.5221(7)	7.5219(13)	7.5214(15)
	7.5187(1)	*7.5195(5)*	*7.5215(15)*	*7.5186(17)*
160	.27563(1)	.27563(2)	—	.27563(3)
161	.38090(2)	.38090(2)	.38092(4)	.38092(4)
175	1.46646(1)	1.46649(6)	—	1.46643(6)
176	1.50459(2)	1.50457(9)	1.50464(10)	1.50453(7)
	1.50430(2)	*1.50433(6)*	*1.50423(12)*	*1.50426(6)*
190	1.81236(2)	1.81235(7)	1.81229(11)	1.81235(7)
205	1.89984(2)	1.89986(12)	1.89995(8)	1.89996(10)
	1.89897(2)	*1.89900(7)*	*1.89896(34)*	*1.89899(10)*
300	1.51351(2)	1.51353(10)	1.51353(20)	1.51349(11)
500	.86950(1)	.86956(9)	.86960(25)	.86956(14)
1000	.36514(1)	.36515(5)	.36554(49)	.36530(35)
2000	.18247(1)	.18250(4)	—	.18247(13)
	.12800(0)	*.12797(12)*	*.12858(48)*	*.12806(13)*

Table 9: *CC11* process. Cross sections are in *fb* for $E_{cm} = 95, 100, 130$ GeV, in *pb* for higher energies. Numbers in *italics* correspond to constant Z width.

E_{cm}	175	190	205
Born			
ALPHA	0.8152 ± 0.0004	9.505±0.005	12.505±0.006
CompHEP	0.8160 ± 0.0013	9.514±0.011	12.506±0.014
EXCALIBUR	0.8162 ± 0.0011	9.514±0.008	12.499±0.010
GENTLE/4fan	0.8157 ± .00001	9.511±.0001	12.500±.0001
HIGGSPV	0.8159 ± 0.0004	9.506±0.005	12.505±0.008
WPHACT	0.8150 ± 0.0008	9.509±0.006	12.501±0.007
WTO	0.8168 ± 0.0003	9.517±0.002	12.509±0.013
with ISR			
EXCALIBUR	0.6478 ± 0.0004	7.371±0.003	10.789±0.004
GENTLE/4fan	0.6481 ± 0.0001	7.370±0.001	10.791±0.001
HIGGSPV	0.6481 ± 0.0003	7.371±0.003	10.789±0.006
WPHACT	0.6482 ± 0.0006	7.367±0.007	10.784±0.008
WTO	0.6477 ± 0.0010	7.373±0.003	10.792±0.005
Born			
ALPHA	0.7724 ± 0.0004	9.036±0.005	11.804±0.006
CompHEP	0.7732 ± 0.0014	9.058±0.012	11.834±0.016
EXCALIBUR	0.7728 ± 0.0004	9.036±0.003	11.809±0.003
HIGGSPV	0.7728 ± 0.0003	9.034±0.006	11.814±0.006
WPHACT	0.7723 ± 0.0006	9.034±0.006	11.810±0.007
WTO	0.7739 ± 0.0002	9.042±0.002	11.818±0.001
with ISR			
EXCALIBUR	0.6119 ± 0.0004	7.004±0.003	10.199±0.004
HIGGSPV	0.6128 ± 0.0003	7.002±0.004	10.199±0.005
WPHACT	0.6129 ± 0.0006	7.000±0.007	10.193±0.008
WTO	0.6128 ± 0.0010	7.007±0.002	10.203±0.006

Table 10: Cross sections for the process $e^+e^- \rightarrow \mu^+\mu^- b\bar{b}$, with invariant mass cuts: $M_Z - 15 < m_{\mu\mu} < M_Z + 15$ GeV, $m_{bb} > 30$ GeV, $m_b = 0$. The two lower parts have additional cuts: lepton momenta > 10 GeV, lepton polar angles with beams $> 15^0$.

A few codes have performed a very precise ($\simeq 10^{-4}$) *tuned comparison* of the total cross section of a *CC11* process, $e^+e^- \rightarrow u\bar{d}s\bar{c}$, in a broad CM energy range, $130 \div 2000$ GeV, using the input parameters of tuned comparison, as in table 5 both with *running* and *constant Z* widths. The results are given in table 9.

An interesting conclusion can be drawn from comparing these two cases. There is practically no difference between running at constant Z widths result at LEP2 energies, whereas at $E_{cm} = 2000$ GeV the running Z width results starts to blow up. This is an illustration of gauge-invariance violation, see [71].

This comparison was attempted at an early phase of our work. The extreme accuracy served

E_{cm}	175	190	205
Born			
ALPHA	1.5863 ± 0.0009	18.375 ± 0.009	24.138 ± 0.012
CompHEP	1.5785 ± 0.0030	18.352 ± 0.030	24.180 ± 0.039
EXCALIBUR	1.5916 ± 0.0020	18.398 ± 0.020	24.141 ± 0.015
GENTLE/4fan	1.5878 ± 0.00002	$18.381 \pm .0002$	$24.150 \pm .0002$
HIGGSPV	1.5876 ± 0.0011	18.376 ± 0.014	24.150 ± 0.021
WPHACT	1.5868 ± 0.0013	18.383 ± 0.011	24.151 ± 0.013
WTO	1.5864 ± 0.0024	18.378 ± 0.002	24.159 ± 0.008
with ISR			
EXCALIBUR	1.2770 ± 0.0008	14.243 ± 0.008	20.840 ± 0.010
GENTLE/4fan	1.2782 ± 0.0001	14.243 ± 0.001	20.838 ± 0.002
HIGGSPV	1.2781 ± 0.0008	14.248 ± 0.009	20.846 ± 0.014
WPHACT	1.2773 ± 0.0010	14.235 ± 0.014	20.827 ± 0.017
WTO	1.2799 ± 0.0027	14.246 ± 0.004	20.833 ± 0.005
Born			
ALPHA	1.4204 ± 0.0008	16.767 ± 0.008	21.784 ± 0.010
CompHEP	1.4141 ± 0.0032	16.748 ± 0.032	21.851 ± 0.044
EXCALIBUR	1.4197 ± 0.0009	16.750 ± 0.008	21.782 ± 0.010
HIGGSPV	1.4199 ± 0.0009	16.771 ± 0.012	21.782 ± 0.016
WPHACT	1.4197 ± 0.0014	16.775 ± 0.013	21.785 ± 0.015
WTO	1.4169 ± 0.0021	16.766 ± 0.002	21.776 ± 0.004
with ISR			
EXCALIBUR	1.1423 ± 0.0008	12.995 ± 0.008	18.812 ± 0.010
HIGGSPV	1.1437 ± 0.0007	13.001 ± 0.011	18.799 ± 0.017
WPHACT	1.1430 ± 0.0010	13.001 ± 0.009	18.813 ± 0.018
WTO	1.1449 ± 0.0021	13.003 ± 0.003	18.814 ± 0.007

Table 11: Cross sections for the process $e^+e^- \rightarrow \nu_\mu \bar{\nu}_\mu b\bar{b}$ with invariant mass cuts: $M_Z - 25 < m_{\mu\mu} < M_Z + 25$ GeV, $m_{bb} > 30$ GeV, $m_b = 0$. The lower parts have an addition cut of 20 degrees on the angle of the b's with respect to both beams.

as a very efficient tool for hunting down many tiny bugs. Furthermore, it demonstrates that a level of precision of the order 10^{-4} is now within the reach of not only semi-analytical but also adaptive Monte Carlo integrators.

4   Comparisons of NC processes

Here we present the results of the *tuned* comparison for three *NC* processes *NC24, NC10, NC21*. We computed only cross sections at three c.m.s energies: 175, 190 and 205 GeV with

E_{cm}	175	190	205
Born			
ALPHA	1.3940 ± 0.0007	18.299±0.009	26.361±0.013
CompHEP	1.3909 ± 0.0029	18.309±0.031	26.470±0.051
HIGGSPV	1.3946 ± 0.0005	18.294±0.011	26.348±0.011
WPHACT	1.3955 ± 0.0010	18.314±0.012	26.384±0.017
WTO	1.3937 ± 0.0029	18.304±0.004	26.386±0.008
with ISR			
HIGGSPV	1.1444 ± 0.0004	14.053±0.009	22.490±0.012
WPHACT	1.1440 ± 0.0010	14.064±0.010	22.505±0.020
WTO	1.1483 ± 0.0028	14.068±0.003	22.508±0.009
Born			
ALPHA	1.2466 ± 0.0007	16.732±0.008	23.843±0.012
CompHEP	1.2430 ± 0.0031	16.761±0.034	23.965±0.054
EXCALIBUR	1.2458 ± 0.0008	16.727±0.008	23.862±0.015
HIGGSPV	1.2463 ± 0.0005	16.715±0.009	23.822±0.013
WPHACT	1.2473 ± 0.0010	16.749±0.013	23.855±0.018
WTO	1.2457 ± 0.0023	16.735±0.004	23.855±0.006
with ISR			
EXCALIBUR	1.0227 ± 0.0007	12.865±0.008	20.381±0.015
HIGGSPV	1.0239 ± 0.0004	12.853±0.008	20.306±0.042
WPHACT	1.0229 ± 0.0010	12.865±0.010	20.378±0.015
WTO	1.0263 ± 0.0022	12.864±0.003	20.377±0.008

Table 12: Cross sections for the process $e^+e^- \to \nu_e\bar{\nu}_e b\bar{b}$ under the same cuts as table 11.

simple cuts. Seven codes participated in this comparison.

We have concentrated on processes where a $b\bar{b}$ pair is produced together with two leptons, since these can form an important background for the production and decay of a light Higgs boson. All cross sections are given in fb: since they are quite small, we have not pursued detailed comparisons of other quantities as we have done for the CC processes.

From the tables it is apparent that the agreement among the various codes is very good, both at the Born level and after inclusion of ISR. The cuts have been chosen so as to be more or less realistic in an experimental Higgs search.

5 All four-fermion processes

In the following two subsections we present the cross sections for many four fermion processes at only one center-of-mass energy, $\sqrt{s} = 190$ GeV, in the massless approximation $m_f = 0$, with the Standard LEP2 Input, see table 5. In the first subsection, *all* 32 four-fermion processes are presented. They are calculated with the standard Canonical Cuts. The four-fermion processes are ordered in accordance with the classification of tables 1-2. For historical reasons, the Born cross sections are presented in the Report of the Working Group on Standard Model Processes, [69]. The tables of the next subsection contain numbers computed *with* the ISR radiation (SF) and *with* gluon exchange diagrams for non-leptonic processes.

Since this is a tuned comparison all codes have used a fixed strong coupling constant, $\alpha_s = 0.12$. Obviously, any further study of the non-leptonic processes must include some educated guess on the scale of α_s, e.g. $\alpha_s(s_\pm)$ (running) or $\alpha_s(2M_W)$ (fixed).

The precision of the computation is quite high, normally better than .1%. These numbers are supposed to provide benchmarks for future calculations of four-fermion processes.

5.1 AYC, Canonical Cuts

final state	CompHEP	EXCALIBUR	grc4f	WPHACT	WTO	WWGENPV
$\mu^-\bar{\nu}_\mu\nu_\tau\tau^+$	.1947(5)	.1941(1)	.1941(2)	.1942(2)	.1941(0)	.1941(1)
$\mu^-\bar{\nu}_\mu u\bar{d}$	.5917(11)	.5916(3)	.5919(5)	.5921(5)	.5919(0)	.5920(6)
$u\bar{d}s\bar{c}$	1.791(5)	1.788(1)	1.791(2)	1.789(1)	1.788(0)	1.789(1)

Table 13: *CC11, CC10, CC09* family. Cross sections in pb.

final state	CompHEP	ERATO	EXCALIB	grc4f	WPHACT	WTO	WWGENPV
$e^-\bar{\nu}_e\nu_\mu\mu^+$	.2012(6)	—	.2014(1)	.2014(3)	.2015(1)	.2014(2)	.2013(4)
$e^-\bar{\nu}_e u\bar{d}$	.6131(12)	.6139(6)	.6140(4)	.6135(4)	.6135(6)	.6137(6)	.6134(12)

Table 14: *CC20, CC18* family. Cross sections in pb.

final state	CompHEP	EXCALIBUR	grc4f	WPHACT	WTO
$\mu^+\mu^-\nu_\mu\bar{\nu}_\mu$	.2018(8)	.2049(1)	.2029(4)	.2050(0)	.2032(3)
$u\bar{u}d\bar{d}$	1.967(8)	1.992(2)	1.985(4)	1.992(0)	1.980(6)

Table 15: `mix43` family. Cross sections in pb.

final state	CompHEP	EXCALIBUR	grc4f	WPHACT
$e^-e^+\nu_e\bar{\nu}_e$	.2244(12)	.2294(2)	.2289(7)	.2292(2)

Table 16: `mix56` process. Cross sections in pb.

final state	CompHEP	EXCALIB	grc4f	HIGGSPV	WPHACT	WTO
$\mu^+\mu^-\tau^+\tau^-$	13.19(9)	13.38(3)	13.28(4)	13.32(1)	13.33(2)	13.26(14)
$\nu_\tau\bar{\nu}_\tau\mu^+\mu^-$	10.75(4)	10.71(2)	10.71(1)	10.720(4)	10.72(1)	10.76(13)
$\nu_\mu\bar{\nu}_\mu\nu_\tau\bar{\nu}_\tau$	6.366(8)	6.377(3)	6.373(4)	6.377(5)	6.376(1)	6.375(0)
$\mu^+\mu^-u\bar{u}$	27.09(9)	27.29(5)	27.20(2)	27.22(2)	27.24(3)	27.16(24)
$\mu^+\mu^-d\bar{d}$	25.39(17)	25.49(5)	25.44(2)	25.48(1)	25.49(2)	25.37(13)
$\nu_\mu\bar{\nu}_\mu u\bar{u}$	18.17(6)	18.22(1)	18.20(3)	18.22(1)	18.21(1)	18.22(5)
$\nu_\mu\bar{\nu}_\mu d\bar{d}$	15.80(5)	15.84(1)	15.85(2)	15.83(1)	15.83(1)	15.83(1)
$u\bar{u}c\bar{c}$	210.7(15)	206.8(7)	208.3(4)	207.8(2)	208.0(2)	208.9(5)
$u\bar{u}s\bar{s}$	203.6(13)	203.5(8)	203.7(6)	203.0(2)	203.2(2)	204.4(5)
$d\bar{d}s\bar{s}$	183.8(19)	182.2(10)	181.0(4)	181.2(2)	181.3(2)	182.6(5)

Table 17: *NC32, NC24, NC10, NC06 family. Cross sections in fb.*

final state	CompHEP	EXCALIB	grc4f	HIGGSPV	WPHACT	WTO
$\nu_e\bar{\nu}_e\mu^+\mu^-$	18.07(8)	18.03(5)	17.98(5)	18.07(1)	18.05(2)	17.83(13)
$\nu_e\bar{\nu}_e\nu_\mu\bar{\nu}_\mu$	6.408(9)	6.417(3)	6.408(5)	6.364(91)	6.416(1)	6.439(5)
$\nu_e\bar{\nu}_e u\bar{u}$	20.78(5)	20.74(1)	20.74(4)	20.78(16)	20.72(3)	20.95(9)
$\nu_e\bar{\nu}_e d\bar{d}$	16.12(4)	16.48(1)	16.48(2)	16.37(17)	16.46(2)	16.67(15)

Table 18: *NC21, NC12 family. Cross sections in fb.*

final state	CompHEP	EXCALIBUR	grc4f	HIGGSPV	WPHACT
$e^+e^-\mu^+\mu^-$	.1231(15)	.1251(2)	.1247(5)	.1192(21)	.1253(2)
$e^+e^-\nu_\mu\bar{\nu}_\mu$	.01421(8)	.01426(2)	.01421(2)	.01445(18)	.01429(2)
$e^+e^- u\bar{u}$	.09070(76)	.09234(11)	.09226(12)	.09003(89)	.09244(14)
$e^+e^- d\bar{d}$	.04259(45)	.04427(6)	.04425(4)	.04491(46)	.04429(8)

Table 19: *NC48 family. Cross sections in pb.*

final state	CompHEP	EXCALIBUR	grc4f	HIGGSPV	WPHACT
$\mu^+\mu^-\mu^+\mu^-$	—	.006650(17)	.006643(30)	.006671(85)	.006622(13)
$\nu_\mu\bar{\nu}_\mu\nu_\mu\bar{\nu}_\mu$	.003176(7)	.003142(1)	.003141(4)	.003142(7)	.003142(1)
$u\bar{u}u\bar{u}$	—	.1017(3)	.1020(5)	—	.1014(1)
$d\bar{d}d\bar{d}$	—	.08765(38)	.08767(17)	—	.08788(22)

Table 20: *NC4x16, NC4x12 family. Cross sections in pb.*

final state	CompHEP	EXCALIBUR	grc4f	WPHACT
$e^+e^-e^+e^-$	—	.1169(2)	.1156(11)	.1169(2)
$\nu_e\bar{\nu}_e\nu_e\bar{\nu}_e$	.003194(18)	.003123(1)	.003128(3)	.003125(1)

Table 21: *NC4x36 and NC4x9 processes. Cross sections in pb.*

95

5.2 AYC, Simple Cuts

final state	ALPHA	EXCALIB	GE/4fan	grc4f	WPHACT	WTO	WWGENPV
Born							
$\mu^- \bar{\nu}_\mu \nu_\tau \tau^+$	.2264(2)	.2267(1)	.2267(0)	.2267(1)	.2267(0)	.2267(0)	.2267(0)
$\mu^- \bar{\nu}_\mu u \bar{d}$	.6804(4)	.6801(4)	.6801(0)	.6799(2)	.6801(1)	.6801(0)	.6801(0)
$u \bar{d} s \bar{c}$	2.040(1)	2.040(1)	2.040(0)	2.040(1)	2.041(0)	2.040(0)	2.040(0)
With ISR							
$\mu^- \bar{\nu}_\mu \nu_\tau \tau^+$	—	.2013(1)	.2014(0)	.2014(1)	.2014(0)	—	.2014(0)
$\mu^- \bar{\nu}_\mu u \bar{d}$	—	.6036(4)	.6041(0)	.6041(3)	.6041(0)	.6041(0)	.6041(1)
$u \bar{d} s \bar{c}$	—	1.811(1)	1.812(0)	1.812(1)	1.812(0)	1.812(0)	1.812(0)

Table 22: *CC11, CC10, CC09* family. Cross sections in pb.

final state	ALPHA	EXCALIB	grc4f	HIGGSPV	WPHACT
Born					
$\nu_e \bar{\nu}_e \mu^+ \mu^-$	12.40(1)	12.38(1)	12.37(1)	12.37(1)	12.38(1)
$\nu_e \bar{\nu}_e \nu_\mu \bar{\nu}_\mu$	8.335(4)	8.336(3)	8.335(6)	8.342(5)	8.339(1)
$\nu_e \bar{\nu}_e u \bar{u}$	24.95(2)	24.92(1)	24.92(2)	25.01(3)	24.91(1)
$\nu_e \bar{\nu}_e d \bar{d}$	20.91(2)	20.92(1)	20.91(1)	20.90(3)	20.92(1)
With ISR					
$\nu_e \bar{\nu}_e \mu^+ \mu^-$	—	11.59(1)	11.59(1)	11.59(1)	11.60(0)
$\nu_e \bar{\nu}_e \nu_\mu \bar{\nu}_\mu$	—	6.412(3)	6.408(5)	6.411(7)	6.416(1)
$\nu_e \bar{\nu}_e u \bar{u}$	—	21.87(1)	21.88(2)	21.94(2)	21.86(1)
$\nu_e \bar{\nu}_e d \bar{d}$	—	16.75(1)	16.76(1)	16.74(2)	16.75(1)

Table 23: *NC21, NC12* family. Cross sections in pb.

In this subsection, only those processes are given that were treated within the semi-analytic approach with Simple Cuts on the invariant mass of any charged fermion-antifermion pair. The latter cut value is chosen to be 5 GeV. Every table contains two sets of numbers which are computed:
1. in the Born approximation and without gluon exchange diagrams for non-leptonic processes;
2. with the ISR radiation (SF) and with gluon exchange diagrams for non-leptonic processes.

5.3 Conclusions

We want to stress that many of the codes contributing to the "all you can" comparison have been developed during this workshop. The level of agreement documented in these tables

final state	ALPHA	EXCALIB	GE/4fan	grc4f	HIGGSPV	WPHACT	WTO
Born, without gluon exchange diagrams							
$\mu^+\mu^-\tau^+\tau^-$	10.06(9)	10.08(0)	10.07(0)	10.07(0)	10.07(0)	10.07(0)	10.14(7)
$\nu_\tau\bar{\nu}_\tau\mu^+\mu^-$	9.894(10)	9.872(3)	9.871(0)	9.875(4)	9.872(3)	9.873(3)	9.884(10)
$\nu_\mu\bar{\nu}_\mu\nu_\tau\bar{\nu}_\tau$	8.245(4)	8.242(3)	8.241(0)	8.240(4)	8.237(6)	8.241(1)	8.241(1)
$\mu^+\mu^- u\bar{u}$	23.99(2)	24.04(1)	24.03(0)	24.04(2)	24.03(1)	24.04(1)	—
$\mu^+\mu^- d\bar{d}$	23.46(2)	23.45(1)	23.45(0)	23.46(2)	23.45(1)	23.46(1)	—
$\nu_\mu\bar{\nu}_\mu u\bar{u}$	21.59(2)	21.59(1)	21.59(0)	21.58(1)	21.58(1)	21.59(1)	21.63(3)
$\nu_\mu\bar{\nu}_\mu d\bar{d}$	20.00(2)	19.99(1)	19.99(0)	20.00(1)	20.00(1)	19.99(1)	20.00(1)
$u\bar{u}c\bar{c}$	54.80(5)	54.75(2)	54.74(0)	54.73(4)	54.69(4)	54.74(2)	—
$u\bar{u}s\bar{s}$	51.83(5)	51.86(1)	51.86(0)	51.85(2)	51.85(5)	51.87(2)	—
$d\bar{d}s\bar{s}$	48.30(5)	48.33(2)	48.33(0)	48.34(1)	48.27(6)	48.34(1)	—
With ISR, with gluon exchange diagrams							
$\mu^+\mu^-\tau^+\tau^-$	—	10.29(0)	10.30(0)	10.29(1)	10.30(0)	10.30(0)	—
$\nu_\tau\bar{\nu}_\tau\mu^+\mu^-$	—	9.279(3)	9.284(1)	9.278(7)	9.283(3)	9.284(4)	—
$\nu_\mu\bar{\nu}_\mu\nu_\tau\bar{\nu}_\tau$	—	6.379(3)	6.376(1)	6.373(4)	6.377(5)	6.377(1)	6.379(2)
$\mu^+\mu^- u\bar{u}$	—	23.74(1)	23.76(0)	23.77(2)	23.75(1)	23.75(1)	—
$\mu^+\mu^- d\bar{d}$	—	22.31(1)	22.34(0)	22.33(1)	22.33(1)	22.34(1)	—
$\nu_\mu\bar{\nu}_\mu u\bar{u}$	—	18.83(1)	18.84(0)	18.84(1)	18.85(1)	18.84(1)	—
$\nu_\mu\bar{\nu}_\mu d\bar{d}$	—	16.00(1)	15.99(0)	15.99(1)	16.00(1)	15.99(0)	—
$u\bar{u}c\bar{c}$	—	272.6(9)	272.3(0)	271.4(9)	272.1(1)	272.2(1)	—
$u\bar{u}s\bar{s}$	—	267.0(10)	266.8(0)	266.5(6)	266.8(1)	266.8(1)	—
$d\bar{d}s\bar{s}$	—	240.7(11)	240.8(0)	240.5(6)	240.6(4)	240.8(1)	—

Table 24: *NC32, NC24, NC10, NC06* family. Cross sections in fb.

demonstrates a substantial progress in our understanding of the general $e^+e^- \to 4f$ cross section.

However, this comparison revealed also some problems, e.g.: some numbers still disagree within declared errors; during the collection of these tables, some codes exhibited fluctuations much larger than the statistical errors; we didn't attempt a comparison of CPU times, needed by different codes to reach a given accuracy. All these items deserve a more thorough study in the future.

Acknowledgments

References

[1] T. Muta, R. Najima and S. Wakaizumi, *Mod. Phys. Letters* **A1** (1986) 203.

[2] D. Bardin and T. Riemann, preprint DESY 95–167 (1995), to appear in *Nucl. Phys.* **B**, [hep-ph/9509341].

[3] E.N. Argyres et al., *Phys. Lett.* **B358** (1995) 339;
C.G. Papadopoulos, *Phys. Lett.* **B352** (1995) 144;
U. Baur and D. Zeppenfeld, *Phys. Rev. Lett.* **75** (1995) 1002.

[4] E. Boos et al., `CompHEP`: computer system for calculation of particle collision characteristics at high energies, version 2.3 (1991), Moscow State Univ. preprint MGU-89-63/140 (1989); preprint KEK 92-47 (1992).

[5] D. Bardin, M. Bilenky, D. Lehner, A. Olchevski and T. Riemann, in: T. Riemann and J. Blümlein (eds.), Proc. of the Zeuthen Workshop on Elementary Particle Theory – Physics at LEP200 and Beyond, Teupitz, Germany, April 10–15, 1994, *Nucl. Phys.* (Proc. Suppl.) **37B** (1994) p. 148.

[6] D. Bardin, A. Leike and T. Riemann, *Phys. Lett.* **B353** (1995) 513.

[7] F.A. Berends, R. Kleiss and R. Pittau, *Nucl. Phys.* **B424** (1994) 308; *Nucl. Phys.* **B426** (1994) 344; *Nucl. Phys.* (Proc. Suppl.) **37B** (1994) 163-168;
R. Pittau, *Phys. Lett.* **B335** (1994) 490-493.

[8] F. Caravaglios and M. Moretti, *Phys. Lett.* **B358** (1995) 332;

[9] G.P. Lepage, *J. Comp. Phys.* **27** (1978) 192.

[10] E. Boos, M. Dubinin, V. Edneral, V. Ilyin, A. Kryukov, A. Pukhov, S. Shichanin, in: "New Computing Techniques in Physics Research II", ed.by D. Perret-Gallix, World Scientific, Singapore, 1992, p. 665
in: Proc. of the XXVI Recontre de Moriond, ed. by Tranh Than Van, Editions Frontieres, 1991, p. 501

E.Boos, M.Dubinin, V.Ilyin, A.Pukhov, V.Savrin, preprint INP MSU 94-36/358, 1994 (hep-ph/9503280)

[11] S. Kawabata, *Comp. Phys. Comm.* **41** (1986) 127.

[12] V.Ilyin, D.Kovalenko, A.Pukhov, preprint INP MSU 95-2/366, 1995

[13] E.Kuraev, V.Fadin, *Yad. Phys.* **41** (1985) 733

[14] E.N. Argyres and C.G. Papadopoulos, *Phys. Lett.* **B263** (1991) 298.

[15] C.G. Papadopoulos, writeup in preparation.

98

[16] T. Stelzer (Durham U.) and W.F. Long (Wisconsin U., Madison), *Comp. Phys. Comm.* **81** (1994) 357-371.

[17] G. Marchesini *et al. Comp. Phys. Comm.* **67** (1992) 465-508.

[18] R. Kleiss and R. Pittau, *Comp. Phys. Comm.* **83** (1994) 141.

[19] F.A. Berends and A.I. van Sighem, Leiden preprint INLO-PUB-7/95.

[20] D. Bardin, A. Leike, T. Riemann and M. Sachwitz, *Phys. Letters* **206B** (1988) 539.

[21] D. Bardin, A. Leike, T. Riemann, report of the *Searches Event Generators Working Group*, these proceedings.

[22] D. Bardin, M. Bilenky, A. Olchevski and T. Riemann, *Phys. Lett.* **B308** (1993) 403; E: [hep-ph/9507277].

[23] D. Bardin, D. Lehner and T. Riemann, preprint DESY 94–216 (1994), to appear in the proceedings of the IXth *International Workshop "High Energy Physics and Quantum Field Theory", Zvenigorod, Moscow Region, Russia, September 1994* [hep-ph/9411321];
D. Lehner, Ph.D. thesis, Humboldt-Universität zu Berlin (1995), unpublished, available from `http://www.ifh.de/~lehner`.

[24] D. Bardin, A. Leike and T. Riemann, *Phys. Lett.* **B344** (1995) 383.

[25] D. Bardin, W. Beenakker, A. Denner, *Phys. Lett.* **B317** (1991) 213.

[26] Minami-Tateya collaboration, "`GRACE` manual ver 1.0", KEK Report **92-19**, 1993,
Minami-Tateya collaboration, Brief Manual of `GRACE` system ver $2.0/\beta$, 1995.

[27] Y.Kurihara, J.Fujimoto, T.Munehisa, Y.Shimizu, KEK CP-035, KEK 95-126, 1995.

[28] T. Sjöstrand, *Comp. Phys. Comm.* **39** (1986) 347;
T. Sjöstrand and M. Bengtsson, *Comp. Phys. Comm.* **43** (1987) 367.
T. Sjöstrand and H.-U. Bengtsson, *Comp. Phys. Comm.* **46** (1987) 43.

[29] S. Kawabata, *Comp. Phys. Comm.* **88** (1995) 309.

[30] CERN CN Division, KUIP, CERN Program Library Long Writeup I102, 1993.

[31] CERN CN Division, PAW++, CERN Program Library Long Writeup Q121, 1993.

[32] CERN CN Division, HBOOK, CERN Program Library Long Writeup Y250, 1995.

[33] M. Skrzypek, S. Jadach, W. Płaczek, and Z. Wąs, Monte Carlo program `KORALW 1.02` for W-pair production at LEP2/NLC energies with Yennie-Frautschi-Suura exponentiation, CERN preprint CERN-TH/95-205 to appear in *Comp. Phys. Comm.*

[34] M. Skrzypek *et al.*, Initial state QED Corrections to W-pair Production at LEP2/NLC – Monte Carlo Versus Semianalytical Approach, CERN preprint CERN-TH/95-246 (unpublished).

[35] R. Decker, S. Jadach, J.H. Kühn, Z. Wąs, CERN-TH 6793/93, *Comp. Phys. Comm.* **76** (1993) 361.

[36] E. Barberio, B. van Eijk, Z. Wąs, *Comp. Phys. Comm.* **79** (1994) 291.

[37] V. Fadin, V. Khoze, A. Martin, and W. Stirling, Higher-order Coulomb Corrections to the Threshold $e^+e^- \to W^+W^-$ Cross Section (unpublished), preprint DTP/95/64.

[38] M. Aguilar-Benitez *et al.*, *Phys. Rev.* **D50** (1994) 1173.

[39] R. Kleiss, Private Communication.

[40] F.A. Berends and R. Kleiss, "Radiative Effects in Higgs Production at LEP", Leiden Preprint, see also *Nucl. Phys.* **178** (1981) 141.

[41] K. Hagiwara, R. D. Peccei, D. Zeppenfeld and K. Hikasa, *Nucl. Phys.* **B282** (1987) 253.

[42] R. Kleiss, program `LEPWW`, unpublished.

[43] R. Miquel, M. Schmitt, CERN-PPE/95-109 (*Z. Phys.* **C**, in press).

[44] E. .A. Kuraev, V. S. Fadin, *Sov. J. Nucl. Phys.* **41** (1985) 466.

[45] O. Nicrosini, L. Trentadue, *Phys. Lett.* **B196** (1987) 551.

[46] V. S. Fadin, V. A. Khoze, A. D. Martin and A. Chapovskii, *Phys. Rev.* **D52** (1995) 1377.

[47] T. Sjöstrand, *Comp. Phys. Comm.* **82** (1994) 74.

[48] T. Sjöstrand, Lund University report LU TP 95–20 (1995).

[49] R. Kleiss et al., in Z Physics at LEP 1, eds. G. Altarelli, R. Kleiss and C. Verzegnassi, CERN 89–08 (Geneva, 1989), Vol. 3, p. 1.

[50] T. Sjöstrand, *Phys. Lett.* **157B** (1985) 321.

[51] M. Bengtsson and T. Sjöstrand, *Phys. Lett.* **B185** (1987) 435.

[52] J.F. Gunion and Z. Kunszt, *Phys. Rev.* **D33** (1986) 665.

[53] V.A. Khoze and T. Sjöstrand, DTP/95/68 and LU TP 95–18, to appear in *Z. Phys.* **C**.

[54] V.S. Fadin, V.A. Khoze and A.D. Martin, *Phys. Lett.* **B311** (1993) 311.

[55] H. Anlauf, J. Biebel, H. D. Dahmen, A. Himmler, P. Manakos, T. Mannel, W. Schönau, *Comp. Phys. Comm.* **79** (1994) 487 and references cited therein.

[56] H. Anlauf, H. D. Dahmen, A. Himmler, P. Manakos, T. Mannel, T. Ohl, *Nucl. Phys.* **B** (Proc. Suppl.) **37B** (1994) 81.

[57] H. Anlauf, H. D. Dahmen, A. Himmler, P. Manakos, T. Mannel, T. Ohl, hep-ex/9504006, IKDA 95/14, SI 95-3. (Updated versions of this writeup are part of the WOPPER distribution.)

[58] A. Ballestrero, E. Maina, *Phys. Lett.* **B350** (1995) 225.

[59] A. Ballestrero, in preparation.

[60] F.A. Berends, P.H. Daverveldt and R. Kleiss *Nucl. Phys.* **B253** (1985) 441; R. Kleiss and W.J. Stirling, *Nucl. Phys.* **B262** (1985) 235.

[61] G. Passarino, *Nucl. Phys.* **B237** (1984) 249.

[62] G. Montagna, O. Nicrosini, G. Passarino and F. Piccinini, *Phys. Lett.* **B348** (1995) 178.

[63] G. Montagna, O. Nicrosini and F. Piccinini, *Comp. Phys. Comm.* **90** (1995) 141.

[64] NAG Fortran Library manual Mark 15 (Numerical Algorithms Group, Oxford, 1991).

[65] G. J. van Oldenborgh, P. J. Franzini, and A. Borrelli, *Comp. Phys. Comm.* **83**(1994)14. This describes the original, hard-photon only version of WWF (1.0).

[66] *Hard photons in W pair production at LEP 2*, G. J. van Oldenborgh, INLO-PUB-95/04 (revised). Here the extensions to include the soft matrix element, and the combination of hard photon matrix element and structure functions is discussed.

[67] F. Jegerlehner in: T. Riemann and J. Blümlein (eds.), Proc. of the Zeuthen Workshop on Elementary Particle Theory – Physics at LEP200 and Beyond, Teupitz, Germany, April 10–15, 1994, *Nucl. Phys.* (Proc. Suppl.) **37B** (1994) p. 129.

[68] WWGENPV - Technical and Physical upgrades, by D. Charlton, G. Montagna, O. Nicrosini and F. Piccinini, in preparation.

[69] *Report of the Working Group on Standard Model Processes* , this report.

[70] *Electroweak Working Group Report* in *Reports of the Working Group on Precision Calculations for the Z-Resonance*, D. Bardin, W. Hollik, G. Passarino (eds.), Yellow Report, CERN 95-03, Geneva, 1995.

[71] *Report of the Working Group on $W^{\pm}$ Physics*, this report.

[72] *Report of the Working Group on W mass*, this report.

[73] *Report of the Working Group on Triple Gauge Boson Couplings*, this report.

QCD EVENT GENERATORS

Conveners: I.G. Knowles and T. Sjöstrand

Working group: A. Blondel, A. Boehrer, C.D. Buchanan, D.G. Charlton, S.-L. Chu, S. Chun, G. Dissertori, D. Duchesneau, J.W. Gary, M. Gibbs, A. Grefrath, G. Gustafson, J. Häkkinen, K. Hamacher, K. Kato, L. Lönnblad, W. Metzger, R. Møller, T. Munehisa, R. Odorico, Y. Pei, G. Rudolph, S. Sarkar, M.H. Seymour, J.C. Thompson, Š. Todorova and B.R. Webber.

Contents

1 Introduction

This section is devoted to QCD generators, relevant for LEP 2 processes where hadrons may be found in the final state: $e^+e^- \rightarrow \gamma^*/Z^0 \rightarrow q\bar{q}$, $e^+e^- \rightarrow W^+W^- \rightarrow q\bar{q}q'\bar{q}'$, $e^+e^- \rightarrow Z^0h^0 \rightarrow \nu\bar{\nu}b\bar{b}$, *etc.* In fact, almost all interesting processes at LEP 2 give hadronic final states, ensuring that QCD generators will remain of vital importance.

It is instructive to contrast the EW and QCD generator perspectives for LEP 2. In the EW physics program, the main emphasis is on four-fermion final states. This is different from LEP 1, where the Z^0 line shape was a major focus of attention [1]. Dedicated four-fermion generators are new creations, that have to stand on their own and cannot be tested at LEP 1. Therefore there is little sense of continuity with respect to the LEP 1 workshop [2] and subsequent LEP 1 activities. QCD physics, by contrast, extrapolates logically from LEP 1. New aspects may enter, such as colour reconnection, but these are expected to be relatively small perturbations on the basic picture (though of importance for precision physics). Therefore the QCD generators write-up for the LEP 1 workshop [3] is still partly relevant and subsequent LEP 1 experience very much so. The high Z^0 statistics will make LEP 1 a significant testing ground for many new QCD physics ideas also in the LEP 2 era.

It is thus logical to begin this section with an assessment of experience from LEP 1, with emphasis on areas where generators are known to have shortcomings. Any improvements for LEP 1 will directly benefit LEP 2. This is followed by a comparison of extrapolations to LEP 2 energies, from which the current range of uncertainty can be estimated. Next comes a survey of existing generators, ranging from major programs, with coverage of the full generation chain, to shorter pieces of code for specific purposes. Finally, there is a section on standardization efforts, to help ease life for users who rely on several generators.

This report is not a complete description of the topic. However it should provide a convenient starting point, with ample references to further relevant literature.

2 Experience from LEP 1

2.1 Event shapes and inclusive distributions

A large quantitative improvement in the description of event shape and inclusive distributions has been made at LEP 1 with respect to the era of PETRA and PEP. This is due mainly to the vast amount of high quality data available and the need to achieve good agreement in model/data comparisons so as to obtain small systematic errors for the high precision electroweak measurements. To help facilitate this goal flexible fitting algorithms were developed, based on previous work [4, 5]. In many cases the dependence of the model's response to its parameters is analytically interpolated [6, 7, 8, 9]. This strategy is flexible, allows easy exchange of input distributions but also the simultaneous fitting of very many, 10–15, parameters [9, 10].

Evidently the choice of input distributions used to constrain the model parameters is important. In general a distribution depends on very many parameters, thus the parameters resulting from a fit are in general correlated. A survey has been undertaken to determine which distributions have the highest sensitivity to the individual model parameters [9, 11]. It turns out that semi-inclusive spectra are most important, as has been observed before [8]. The charged particle momentum and transverse momentum spectra strongly constrain the fragmentation function or, alternatively, the cluster parameters. However their dependence on the fragmentation parameters is not exclusive. Inclusive distributions may depend even more strongly on Λ_{QCD} and/or the parton shower cut-off. In fact, the latter parameter strongly influences the high-momentum tail of the momentum spectrum. The 3-jet rate as defined using the Durham or JADE algorithms almost only depends on Λ_{QCD}. This emphasizes the reliability of α_{s} determinations using this quantity. In contrast, and somewhat surprisingly, the AEEC depends strongly on very many model parameters. Measures of the general event topology, e.g. thrust and sphericity, depend mainly on Λ_{QCD} and only in the 2-jet regime on fragmentation parameters. Shape measures sensitive to radiation out of the event plane, like minor or aplanarity, show strong dependence both on fragmentation parameters and on Λ_{QCD}. In summary, model parameters are best determined by fitting the model to inclusive distributions, jet rates and shape distributions simultaneously.

It appears that the "partonic" phase of the models is best tested by studying the properties of jets defined using jet algorithms [12]. At large resolution parameter y_{cut}, when dealing with few jets or the emission of the "first" hard gluons at large angles, fragmentation effects are almost negligible. In contrast at smaller y_{cut}, where higher jet rates are sizable i.e. when the subjet structure described by multiple emission of soft and collinear gluons is important, also fragmentation effects are of increasing importance.

The parton shower models ARIADNE [13], HERWIG [14] and JETSET [15] describe well the general evolution of the individual jet rates with y_{cut}, especially the 3-jet rate [9] (see Fig. 1 [16] and Fig. 2 [9]). A more detailed 3-jet Dalitz plot study using the ordered normalized jet energies x_i ($i = 1, 2, 3$) and $\mathcal{Z} = (x_2 - x_3)/\sqrt{3}$ unveiled slight differences among the models

4

n-jet(Durham) rates
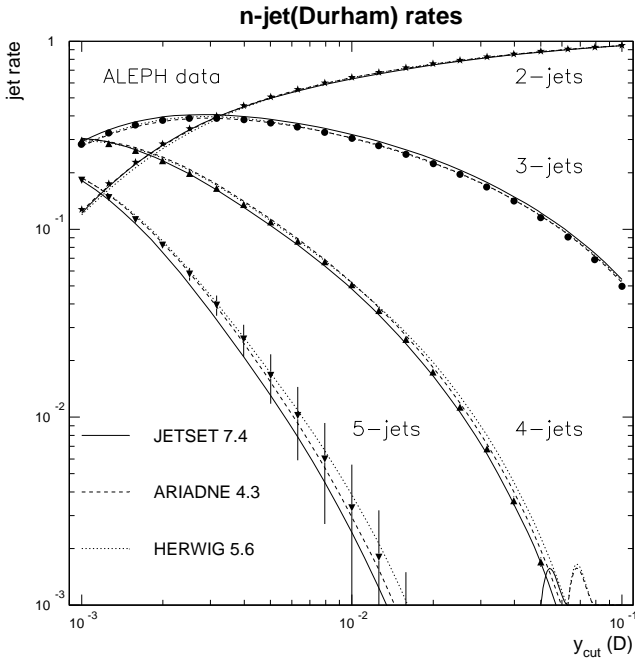
Figure 1: Differential n-jet rates compared to ARIADNE, HERWIG and JETSET PS.

$\mathbf{D_2^{Durham}}$

DELPHI
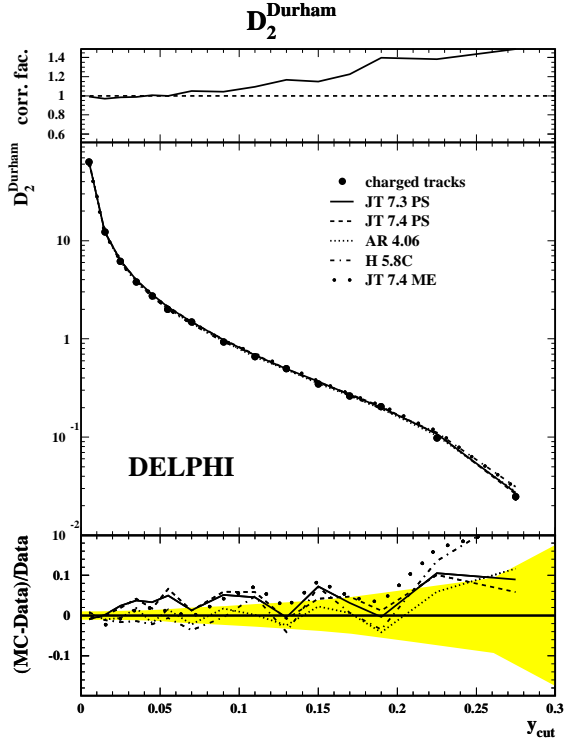
Figure 2: Differential 2-jet rate compared to ARIADNE, HERWIG and JETSET PS & ME.

[17]. ARIADNE is in perfect agreement with the data, JETSET is slightly below the data in the almost 2-jet like case ($\mathcal{Z} \to 1/\sqrt{3}$) and slightly above when the lower energetic jets have similar energies ($\mathcal{Z} \to 0$). HERWIG shows a somewhat bigger deviation along the diagonal (i.e. the x_3 direction) of the Dalitz plot. Also the $\mathcal{O}(\alpha_s^2)$ ME option of JETSET is in good agreement with the data. It is interesting to observe that the agreement is less good when optimized scales are used to achieve a better agreement for the 4-jet rate.

The discrepancies observed are due either to the different shower evolution strategies used or can be traced back to way in which the PS models perform the matching of the first splitting to the first order matrix element. In ARIADNE this matching is performed naturally, since the splitting function is just the lowest order matrix element expression. If no matching is performed (a possible option in HERWIG and JETSET) the agreement with the data is poor.

The 4- and 5-jet rates predicted by JETSET PS (HERWIG) decrease more (less) rapidly with y_{cut} than the data (see Fig. 1). At large y_{cut} the discrepancy is up to 20% [9]. ARIADNE however is in perfect agreement with the data.

Clear discrepancies have been observed at PEP and PETRA comparing the JETSET ME model to the 4-jet rate. This discrepancy has been resolved by introducing optimized scales [18]. Today using optimized scales the 4-jet rate is perfectly described by the JETSET ME

model [8, 9]. However the 5-jet rate predicted by the ME model, as is to be expected, decreases far too rapidly and is one order of magnitude below the data at large $y_{\rm cut}$. Recently it has been shown that the 5-jet rate is also correctly described [19] when the $\mathcal{O}(\alpha_{\rm s}^3)$ tree-level graphs are included in the model [20]. The scale in this case can be chosen similarly to that for the standard $\mathcal{O}(\alpha_{\rm s}^2)$ case.

The observations made for the jet rates consistently lead to the following picture if the models are compared to event shape distributions: general event shape measures, mainly sensitive to hard gluon radiation, like thrust, sphericity, $M_{\rm high/sum}^2/\sqrt{s}$ or $B_{\rm max/sum}$, are reproduced extremely well by all PS models [9]. The only significant discrepancy is a slight overestimation of very spherical events by HERWIG. Observables sensitive to higher order radiation like minor, aplanarity, $M_{\rm low}^2/\sqrt{s}$ and $B_{\rm min}$ are consistently overestimated (underestimated) by HERWIG (JETSET) for large values of the observables. Due to the normalization of the distributions this must also lead to (in general smaller) deviations at intermediate or small values of these observables. For example the minor distribution in the case of HERWIG is predicted to be too wide. ARIADNE is in perfect agreement for most distributions. As JETSET and ARIADNE both use the JETSET string fragmentation model, it is evident that the discrepancies observed for JETSET are due to the parton shower part of the model.

The general fragmentation part of the models are best tested using inclusive charged particle distributions which depend strongly on the interplay between the partonic and fragmentation phases of the models. The average charged multiplicity $\langle n_{\rm ch}\rangle$ is the integral of the scaled momentum (x) distribution. Both quantities have to be described simultaneously by the models. When fitting only to the scaled momentum spectrum, HERWIG predicts $\langle n_{\rm ch}\rangle \approx 20.8$ close to the the very precisely known LEP 1 average $\langle n_{\rm ch}\rangle = 20.92 \pm 0.24$ [21]. ARIADNE and JETSET PS give values that are too small (≈ 20.3) and JETSET ME gives too high a multiplicity (≈ 22.7) [11].

The HERWIG x distribution oscillates slightly around the data distribution. For small x it is below, for $0.3 \leq x \leq 0.7$ it is above (max. 10%) and for larger x again below the data. If the multiplicity is constrained to the measured value, the x spectrum is well described by the JETSET PS and ARIADNE for $x \leq 0.5$ but drops 20%–30% below the data for large x. This should not to be overinterpreted because experimental smearing is important in this momentum range and systematic errors increase. The data so far available from ALEPH and DELPHI [9, 22] agree here only within the full experimental error. The JETSET ME result also oscillates slightly around the data curve ($\pm 5\%$).

Thus the multiplicity distribution is described well by ARIADNE and JETSET (compare Fig. 4). HERWIG predicts a slightly too wide distribution thus overestimating the dispersion of the number of hadrons; in HERWIG this is strongly coupled to the number of primary partons.

The transverse momentum in the event plane, $p_{\perp\rm in}$, is strongly sensitive to hard gluon radiation and almost correctly described by all models. Only the large $p_{\perp\rm in}$ tail is slightly underestimated. The predicted $p_{\perp\rm out}$ distribution for $p_{\perp\rm out} > 0.8$ GeV falls off more rapidly than the data in all models and at large $p_{\perp\rm out}$ is $\approx 30\%$ below the data! This fact is shown in

6
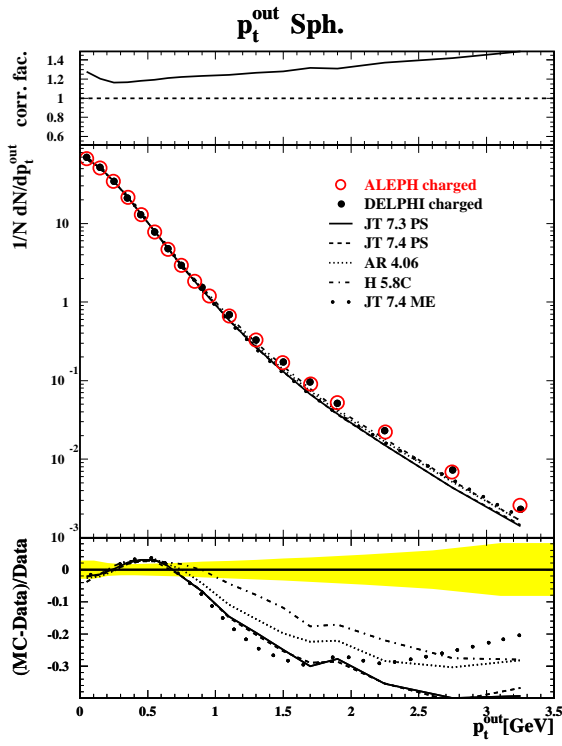
Figure 3: Distribution of $p_{\perp \text{out}}$ with respect to the sphericity axis compared to ARIADNE, HERWIG and JETSET PS & ME [9].
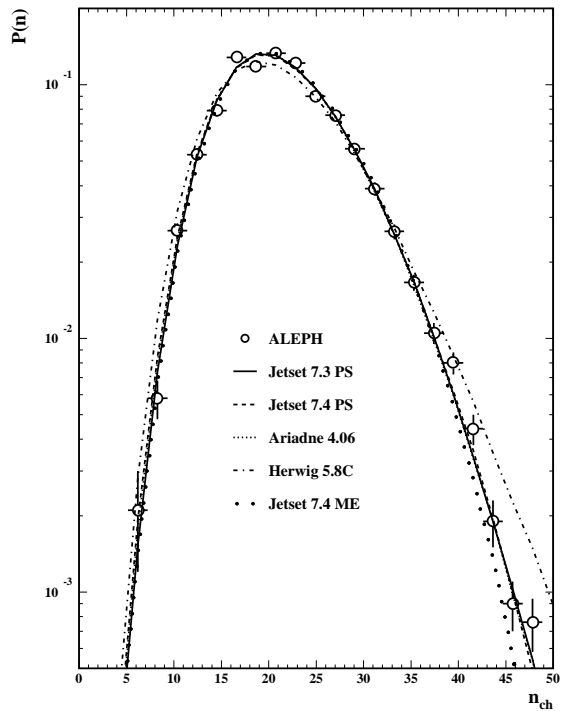
Figure 4: Multiplicity distribution [25] compared to the DELPHI tuning of ARIADNE, HERWIG and JETSET PS & ME [9].

figure 3 which also compares the data of ALEPH [23] and DELPHI [9] to depict the precision of the experimental data. The large $p_{\perp \text{out}}$ tail is mainly due to gluon radiation. This failure of the shower models is presumably due to missing large angle contributions in the basic LLA used by the models. A matching of the second order matrix element and the LLA shower formalism should lead to an improved description similar to that of the matched NLLA and $\mathcal{O}(\alpha_{\text{s}}^2)$ calculations used in α_{s} determinations [24]. For the ME model the situation can be improved by including higher order terms as has been shown recently by OPAL [19].

2.2 Particle composition and spectra

Experimental studies of the spectra and composition of particles in hadronic jets provide an unique way to understand the fragmentation of quarks and gluons into hadrons. Thanks to the excellent performance of the detectors and high statistics available, very careful work by all four LEP experiments has given us a very complete picture of the production of identified particles from e^+e^- annihilation. All states in the $SU(3)$ pseudoscalar and vector meson nonets, except

the ρ^+, and at least one state per isospin multiplet in the baryon octet and decuplet, plus the scalar $f_0(980)$ and the tensors $f_2(1270)$, $K_2^*(1430)$ and $f_2'(1525)$ [26] have been measured. The average production rates per hadronic Z event, together with the predictions from the tuned [9] JETSET 7.4 and HERWIG 5.8, are listed in table 1 [21]. The measurements are in good agreement between experiments for all mesons and octet baryons. However for the decuplet baryons there are still discrepancies between experiments, reflecting difficulties in the measurements. In particular, the Δ^{++} signal is difficult to measure because of its large width and the large combinatorial background in combinations of π^+p. The Ω^- rate seems to be established around the value expected from JETSET, contrary to the old claims of an anomalously high production rate.

Particle rates could depend on many things, such as flavor content, spin, mass, phase space, hadron wave functions, Bose-Einstein interference and other collective effects. The two most frequently used models HERWIG and JETSET use different ways to account for the particle production rates. In the Lund/JETSET approach (similarly to the old Field & Feynman model [27]), the production rate of a specific hadron type depends principally on its flavor content and spin. One can also use essentially pure phase space as in the case of the HERWIG cluster fragmentation approach.

Studies of general features of particle production, such as the strangeness suppression factor s/u or the fraction of mesons produced in spin-1 states, $V/(V+P)$, or in orbitally excited states provide useful information about the main production mechanisms. The (one dimensional) string model suggests the production of orbitally excited states is small $\approx 10\%$ [28] whilst $V/(V+P) = 3/4$ is expected from simple spin counting.

Measurements of the $f_0(980)$, $f_2(1270)$, $K_2^*(1430)^0$ [21] and $f_2'(1525)$ [26] as well as of D^{**} and B^{**} mesons indicate that orbitally excited states, most of which so far were not included in HERWIG, JETSET and other models, are copiously produced ($\approx 30\%$ of the primary hadrons). Thus a quite large fraction of the observed stable particles come from decays of these numerous states. As a result, the $V/(V+P)$ ratio can differ significantly from that when no orbitally excited states are considered. From a global tuning, where the orbitally excited meson states are included, a value of $V/(V+P) \approx 0.4 - -0.6$ is obtained for light mesons [9, 29]. This low value of $V/(V+P)$ could be explained by mass differences between the vector and pseudoscalar mesons, i.e. by the relatively larger binding energy of pseudoscalar mesons[28]. The measured ratio of $V/(V+P) = 0.75 \pm 0.04$ [30] for B mesons agrees well with the expected value of $3/4$. However for D mesons the much lower value 0.46 ± 0.06 [31] is still not understood.

In the string fragmentation model, one expects the strangeness suppression factor s/u to be around 0.3 using the typical values of (constituent) quark masses. This parameter can be measured from the production rates of strange compared with non-strange mesons and from the momentum spectrum of strange mesons. The results, which are summarized in table 2, are very consistent with the expectation[1]. It is interesting to see that s/u determined from

---

[1]However, neutrino experiments at lower energies [32] and recently both ZEUS [33] and H1 [34] require a lower value of about 0.2 for s/u. More careful studies in this area are needed in the future.

8

Particle	Rate Measured	Experiments	Rate JETSET 7.4	Rate HERWIG 5.8
All charged	20.92 ± 0.24	ADLO	20.81	20.94
π^0	9.19 ± 0.73	DL	9.83	9.81
π^+	8.53 ± 0.22	O	8.55	8.83
K^0	1.006 ± 0.017	ADLO	1.09	1.04
K^+	1.185 ± 0.065	DO	1.12	1.06
η	0.95 ± 0.11	AL	1.10	1.02
η'	0.22 ± 0.07	AL	0.09	0.14
$f_0(980)$	0.140 ± 0.034	DL	0.16	—
ρ^0	1.29 ± 0.13	AD	1.27	1.43
K^{*0}	0.380 ± 0.021	ADO	0.39	0.37
K^{*+}	0.358 ± 0.034	DO	0.39	0.37
ω	1.11 ± 0.14	AL	1.32	0.91
ϕ	0.107 ± 0.009	ADO	0.107	0.099
$f_2(1270)$	0.25 ± 0.08	DL	0.29	0.26
$K_2^*(1430)^0$	0.095 ± 0.035	O	0.075	0.0785
$f_2'(1525)$	0.0224 ± 0.0062	D	0.026	0.03
p	0.49 ± 0.05	DO	0.485	0.39
Λ	0.186 ± 0.008	ADLO	0.175	0.184
Σ^0	0.0355 ± 0.0065	DO	0.036	0.0265
Σ^+	0.044 ± 0.006	DO	0.0343	0.0298
Ξ^-	0.0129 ± 0.0007	ADO	0.015	0.0247*
Δ^{++}	0.064 ± 0.033	DO	0.080	0.077
$\Sigma(1385)^+$	0.011 ± 0.002	ADO	0.009	0.0163
$\Xi(1530)^0$	0.0031 ± 0.0006	ADO	0.00345	0.0125*
Ω^-	0.00080 ± 0.00025	ADO	0.00095	0.00385*
$\Lambda\bar{\Lambda}$	0.089 ± 0.007	ADO	0.085	0.134*
$\Lambda\Lambda + \bar{\Lambda}\bar{\Lambda}$	0.0249 ± 0.0022	ADO	0.023	0.029

Table 1: Average particle production rates in hadronic Z decays (excluding charge conjugates and antiparticles), compared to the predictions of JETSET and HERWIG. A * indicates that the predicted rate differs from measurement by more than three standard deviations.

heavy mesons agrees well with the values obtained from light mesons. This suggests that the strangeness suppression occurs at the quark level.

Technique	Results	References
$\dfrac{K^{*0}}{\rho^0 + \omega}$, $\dfrac{K^{*\pm}}{\rho^0 + \omega}$, $\dfrac{2\phi}{K^{*0}}$, $\dfrac{2\phi}{K^{*\pm}}$, $\sqrt{\dfrac{2\phi}{\rho^0 + \omega}}$	0.29 ± 0.03	table 1 [35]
$\dfrac{K^+}{\pi^+}$ at high momentum	$0.35 \pm 0.07 (\text{stat})$	[35, 36]
$\dfrac{K^+}{\pi^+}$ at high momentum	$0.25 \pm 0.03 (\text{stat})$	[35, 37]
K^0 momentum spectrum	0.285 ± 0.035	[38]
K^0 momentum spectrum	$0.30 \pm 0.02 (\text{stat})$	[39]
Ratio $\dfrac{2f(\text{c} \to \text{D}_s^+)}{f(\text{c} \to \text{D}^+ + f(\text{c} \to \text{D}^0)}$	0.31 ± 0.07	[40]
Ratio $\dfrac{2\text{B}_s}{\text{B}_{u,d}}$	0.32 ± 0.08	[41]
Ratio $\dfrac{2\text{B}_s^{**}}{\text{B}_{u,d}^{**}}$	0.28 ± 0.11	[42]
$\text{B}^0\bar{\text{B}}^0$ mixing $(\chi_{\text{B}}, \chi_{\text{B}_d})$, f_{Λ_b}	~ 0.3	[43]

Table 2: Measurements of s/u at LEP

The relative rates of the decuplet baryons as well as those of the $\Sigma^{0,+}$ and Ξ^- provide a clean test of models, since they are less affected by resonance decays. From table 1, we obtain the following ratios:

Ratio	Measured	JETSET	HERWIG
Ξ^- / Σ^+	0.29 ± 0.04	0.44	0.84
Ξ^- / Σ^0	0.36 ± 0.07	0.42	0.93
$\Sigma(1385)^+ / \Delta^{++}$	0.17 ± 0.09	0.11	0.21
$\Xi(1530)^0 / \Sigma(1385)^+$	0.28 ± 0.07	0.38	0.77
$\Omega^- / \Xi(1530)^0$	0.26 ± 0.09	0.28	0.31

One obtains from the above ratios a suppression factor of about 0.28 per s quark for baryons (0.24 if only the decuplet baryons are considered). This is similar to the value obtained for mesons, suggesting that the additional suppression for diquarks might be small.

After being tuned to LEP 1 data, HERWIG and JETSET[2] describe well the measured rates in the meson sector. There is a fairly good agreement in the baryon octet, except that the proton rate is slightly underestimated and the Ξ^- rate is overestimated by about a factor of

---

[2]New parameters have to be introduced, as attempted in [9], to treat the quark type dependent production probabilities for pseudoscalar, vector and orbitally excited mesons.

10

two by HERWIG. In the baryon decuplet JETSET predictions are consistent with the data while the predictions of HERWIG differ from the data in most of the cases. Differences in the ratios of the baryon rates between HERWIG and data, as shown above, can not be solved simply by tuning the cluster fragmentation parameters, indicating the need for real dynamics beyond phase space and spin counting.

Although in general JETSET describes the measured rates better than HERWIG, it contains a large number of free parameters. As a result, it has little predictive power. The UCLA model [44], a variant of JETSET with less parameters, does a good job in many cases but has problems in the baryon decuplet. Also the copiously produced orbitally excited mesons so far are not included in the UCLA model. In [45] an interesting regularity in production rates is shown for all particles (except pions) belonging to the pseudoscalar and vector meson nonets and the baryon octet and decuplet. The particle multiplicity can be described by a simple exponential fall off in mass squared and $2J + 1$ spin counting factors. This regularity seems to be energy independent and has recently been established similarly also in $\bar{\text{p}}$p interactions [46]. However it is necessary to use generalized isospin multiplets and to not seperate the contributions from resonance decays. Recently a new approach [47] has been proposed which uses only three free parameters but reproduces the measured rates quite well. The basic assumption used is that hadrons reach complete thermal and chemical equilibrium, in contrast to the general belief that $e^+e^- \rightarrow$ hadrons is a rapidly expanding process and during fragmentation the hadronic density is rather low. More tests are needed to check this thermodynamic approach.

Since all fragmentation models contain a number of parameters which can be tuned according to data (more dramatic in the case of JETSET), measurements of production rates do not provide a high discriminating power among different models. A more effective method is to look at baryon correlations. In JETSET the major source of baryon production is the creation of a diquark-antidiquark pair within the fragmentation. The baryon-antibaryon ($\mathcal{B}\bar{\mathcal{B}}$) rate is much higher than the $\mathcal{B}\mathcal{B}$ and $\bar{\mathcal{B}}\bar{\mathcal{B}}$ rate (see table 1) and $\mathcal{B}\bar{\mathcal{B}}$ are more likely to occur close in phase space than $\mathcal{B}\mathcal{B}$ or $\bar{\mathcal{B}}\bar{\mathcal{B}}$. Correlations between $\mathcal{B}\bar{\mathcal{B}}$ can be reduced by the *popcorn* mechanism, allowing a meson to be created in between a $\mathcal{B}\bar{\mathcal{B}}$ pair. As can be seen from table 1, HERWIG overestimates the $\Lambda\bar{\Lambda}$ rate (note that the prediction for the Λ is quite good), while JETSET with popcorn describes the data well. It has been shown in [48] that $\mathcal{B}\bar{\mathcal{B}}$ correlations, for example in rapidity, are overestimated by HERWIG, whilst JETSET with a high probability of the popcorn occurrence ($\sim 80\%$) reproduces the data well. A more impressive test is to study the angle between the baryon and the event axis in the $\mathcal{B}\bar{\mathcal{B}}$ rest frame. The string model predicts that baryon production is preferentially lined up along the event axis, while the cluster model predicts an isotropic distribution. Data [48] clearly favor the string model. Also measurements of baryon and antibaryon production in quark and antiquark jets with polarized beams by SLD [49] and jet charge studies [10] support the string model but disfavor the idea of isotropic cluster decays.

Identified particle spectra have been studied as function of both the scaled momentum $x_p = p/p_{\text{beam}}$ and the variable $\xi_p = \log\frac{1}{x_p}$. In general all models describe the data fairly well, with few discrepancies remaining:

- Data show a harder momentum spectrum for the η produced in gluon jets [50].
- $K^\pm$ momentum spectra predicted by the models are too soft [36, 37, 51]. This might be caused by wrong branching fractions of b hadrons in the models.
- Momentum spectra of light quark baryons predicted by the models are too hard [36, 37, 48, 51, 52]. This indicates a different production mechanism for baryons than for mesons. Partly it may also be due to missing orbitally excited baryon states in the models. However, so far these states have not been observed in e^+e^- annihilation.

The heavy quark fragmentation function has been measured at LEP 1 mainly using $D^{(*)}$ reconstruction in the c-quark case [53] and using high-$p_\perp$ lepton spectra [54], D^*–lepton combinations [55], and exclusive [56] and inclusive b-reconstruction [57] in the case of b-quark fragmentation. The D-meson distributions are obscured by contributions from b-hadron decays. Today the (experimentally involved) inclusive b-hadron reconstruction yields the best statistical precision. It allows for the first time (besides a precise determination of the average b-hadron energy $\langle x_E \rangle$) a decisive comparison to different fragmentation models. This, so far incomplete comparison, gives best agreement for LLA based parton shower models (ARIADNE, JETSET and HERWIG) combined with Peterson fragmentation [58]. The HERWIG cluster fragmentation as well as the Lund-symmetric and the modified Lund-Bowler ansatz give less satisfactory results. In the case of JETSET ME with Peterson fragmentation a too narrow energy distribution indicates the lack of soft gluon emission.

2.3   Differences between q and g jets

In QCD, the gluon is associated with a color charge $C_A = 3$ and the quark with a charge $C_F = 4/3$. The larger color charge of the gluon means that it is more likely to radiate an additional gluon than a quark, leading to differences in the expected properties of quark- and gluon-induced jets. For quark and gluon jets produced with the same energy and under the same conditions, gluon jets are expected to have a larger mean particle multiplicity than quark jets [59]. The larger multiplicity of the gluon jet implies that its particle energy spectrum, known as the fragmentation function, is softer. A related prediction is that the mean opening angle of particles in a gluon jet is larger than in a quark jet [60]: thus the gluon jets are broader. Much experimental effort has been invested in an attempt to observe these predicted differences (for a recent compilation, see [61] and references therein). Before LEP 1, there were experimental indications that gluon jets were indeed broader than quark jets, based on measurements of the mean transverse momentum of particles in a jet with respect to the jet axis, or similar variables. However, contradictory results were published concerning differences between the quark and gluon jet fragmentation functions, while no evidence was found for a multiplicity difference between the two jet types. In general, it proved difficult to obtain conclusive results on quark-gluon jet differences at facilities before LEP 1 either because biases were introduced by assuming the gluon jets to be the lowest energy jets in e^+e^- three-jet events or else because there was no event-by-event identification of gluon jets with a resulting lack of sensitivity.

Due to large event statistics and good detector capabilities, the LEP experiments have been able to settle the experimental question of quark and gluon jet differences [62, 63]. Three aspects of the LEP 1 studies allow this success. (1) Symmetric events were selected in which the quark and gluon jets being compared had the same energy and angles relative to the other jets, allowing a direct, model independent comparison of the jet properties. (2) The quark jets were tagged, leading to identification of the gluon jets with better than 90% purity through anti-tagging. (3) The anti-tagged gluon jet data were combined algebraically with the quark and gluon jet data from the untagged, symmetric events, leading to separated quark and gluon jet measurements with essentially no biases except from the jet definition. In the first LEP 1 studies, the quark jet samples were the natural ones for Z^0 decay, given by the Z^0 coupling strength to the individual flavors, corresponding to roughly 20% d, u, s, c and b quarks. In later studies, b quark jets and uds quark jets were explicitly selected to compare to gluon jets [64].

These studies resulted in a confirmation of the qualitative differences between quark and gluon jets given above. Selecting 24 GeV jets in a so-called "Y" symmetric event topology, it was shown that gluon jets were 60–80% broader than quark jets as measured by the full width at half maximum of the differential energy and multiplicity profiles [65]. The fragmentation function of the gluon jet was observed to be much softer than that of the quark jet. The mean charged particle multiplicity of gluon jets was found to exceed that of quark jets by 20–25%. Besides the Y events, DELPHI [63] studied 30 GeV jets from three-fold symmetric "Mercedes" events and obtained similar results. The comparison of the fragmentation function of quark and gluon jets in Y and Mercedes events shows the expected stronger energy dependence for gluon jets. Extensive comparisons of Monte Carlo predictions to the quark and gluon jet data are presented in [65] and [64]. ARIADNE, HERWIG and JETSET were found to be in good agreement with the measurements. The COJETS agreement was somewhat less good.

ALEPH [66] extended these studies by including a measurement of sub-jet multiplicities [67]. For small values of the sub-jet resolution scale, y_0 (defined using the $k_\perp$ jet finder), the ratio of the gluon to quark jet mean sub-jet multiplicity was found to be similar to the hadron level value of about 1.2 discussed above. After subtracting one from the mean sub-jet multiplicities to account for the contributions of the initiating quarks and gluons, the sub-jet multiplicity ratio of gluon to quark jets was observed to reach a much larger value of about 2.0 as y_0 approached the resolution scale y_1 at which the jets were defined. The explanation for this is that the mean sub-jet multiplicity of the quark jets approaches unity slightly before that of the gluon jets as $y_0 \to y_1$. ARIADNE, HERWIG, JETSET and NLLJET were all found to reproduce the measurement.

Beyond these studies based on symmetric events, ALEPH and DELPHI have examined quark and gluon jet properties in non-symmetric three-jet event configurations. The DELPHI approach [63] is to identify gluon jets in three-jet events using anti-tagging methods as mentioned above. The gluon jet properties were compared to those of quark jets with similar energies found in radiative QED $q\bar{q}\gamma$ events. The qualitative differences discussed above between quark and gluon jets were observed to be present for jet energies between 5 and 40 GeV

13

and were well reproduced by JETSET. ALEPH [68] introduced a new method to study the multiplicity difference between quark and gluon jets in three-jet events, by examining the mean charged particle multiplicity of the entire event as a function of the energies and opening angles of the jets in the event. Assuming each event to be composed of a gluon jet and two quark jets, and that every particle in an event could be associated with one of these jets, a fit was made to extract a value for the ratio of the mean charged particle multiplicity values of gluon to quark jets, r_{ch}. The result for all jet energies and event topologies was $r_{ch} = 1.48$. The fit results were found to agree well with those from the symmetric Y analyses when they were restricted to that geometric situation.

Thus the basic differences expected between quark and gluon jets — a larger mean multiplicity, a softer fragmentation function and a larger angular width of gluon relative to quark jets — are now all well established by the LEP 1 experiments. The QCD models are in good overall agreement with the measured differences. Future effort in this field at LEP 1 will probably include studies of differences in the identified particle rates in gluon and quark jets, differences in particle correlation phenomena and attempts to reduce the reliance of the analysis method on the jet definition (as the ALEPH study [68] discussed above attempts to do). Already, L3 has presented results which indicate an enhanced η meson production rate in gluon jets compared to the rates predicted by HERWIG and JETSET [50]. This suggests that the models for gluon jets may need to be modified to allow for an enhanced production of isosinglet mesons [69].

2.4 Coherence

Gluon radiation in the parton shower should be coherent. However, gluon interference only becomes apparent when one goes beyond the Leading Log Approximation (LLA). A number of such effects are found in the next simplest approximation, the Modified LLA (MLLA) [70]. Due to the non-abelian nature of QCD, the overall result of this interference is "angular ordering" of the gluon radiation [71], which constrains the angles between the radiator and the radiated gluon to decrease as the evolution proceeds to lower scales.

In parton-shower Monte Carlos gluon interference is either: imposed as an *a posteriori* constraint on gluon opening angles as in JETSET [15]; built into the choice of evolution variable as in HERWIG [14]; or neglected in independent fragmentation models such as COJETS [72]. ARIADNE [13], on the other hand, employs a formulation based on a cascade of q$\bar{\text{q}}$, qg and gg dipoles which naturally incorporates interference phenomena. In JETSET the angular-ordering constraint can be turned off. By comparing JETSET with and without angular ordering one can obtain an idea of the importance of the effect.

Some consequences of gluon interference have been calculated directly in perturbative QCD as well as by Monte Carlo. Such calculations apply, strictly speaking, only to partons. Comparison with data relies on the additional assumption of Local Parton Hadron Duality (LPHD) [73, 74], which posits that many distributions of hadrons rather closely follow the corresponding parton distribution, with non-perturbative effects affecting mainly the normalization rather

than the shape of the distributions. However, we shall not emphasize such calculations here, since our main purpose is to evaluate the adequacy of current Monte Carlo programs.

The first effect to be explained [75] as a consequence of gluon interference was the so-called string effect; first predicted using (non-perturbative) string fragmentation phenomenology [76] and later discovered by the JADE experiment [77]. In terms of gluon interference it is explained as a purely perturbative effect at the parton level. The string effect has been extensively studied, most recently by DELPHI [63], L3 [78] and OPAL [79]. These analyses have compared $q\bar{q}g$ and $q\bar{q}\gamma$ events taking care to have samples of comparable kinematic configurations. The string effect appears as a smaller particle flow in the region between the quark jets in $q\bar{q}g$ than in $q\bar{q}\gamma$ events. ALEPH [80] instead compared the particle flow between the quarks with that between quark and gluon. The string effect is found to be rather well reproduced by the coherent Monte Carlo models but not by the incoherent ones. However this success is not entirely due to the coherence at parton level; the non-perturbative modelling in the programs also contributes.

It is also worth mentioning that evidence of gluon interference is also seen in $p\bar{p}$ interactions at the Tevatron. Using events with 3 high-$p_{\perp}$ jets CDF examined the differences in rapidity and in azimuthal angle between quark and gluon jets [81]. HERWIG, which incorporates coherence in both space-like and time-like showers, reproduced the data well. PYTHIA/JETSET, with coherence only in time-like showers did less well, although it improved when modified to partially incorporate coherence in space-like showers. ISAJET, with no coherence, performed poorly.

As is well known [70], gluon interference leads to suppression of soft gluons in the shower, which in turn should lead to a suppression of soft hadrons. The distribution of $\xi_p = -\ln x_p = -\ln p/p_{\rm jet}$ is expected to have a roughly Gaussian shape and its peak position, ξ^*, should increase with $\sqrt{s}$. The dependence of ξ^* on $\sqrt{s}$ is strikingly different in the MLLA from that in the LLA. Assuming LPHD, ξ^* is expected to show similar behaviour. Many comparisons have been made, for many types of particle, using data from PETRA/PEP, TRISTAN, and LEP; they support the form predicted by MLLA and clearly reject the LLA form.

From MLLA+LPHD it is expected [82] that ξ^* decrease with the mass of the hadron. This is indeed found to be the case with ξ^* being approximately proportional to $-\ln M_{\rm hadron}$. However, the proportionality constant is quite different for mesons and baryons [51]. This difference is due to decays. When the ξ_p distributions are corrected for decays [37, 51, 83], using JETSET, the ξ^* values of mesons and baryons are found to lie on a universal curve [51]. The conclusion is clearly that we must be cautious about the interpretation of LPHD, in particular with the inclusion of decays.

The $\sqrt{s}$ dependence of ξ^* is support for MLLA, but says little about the quality of the Monte Carlo programs, since they are retuned at each value of $\sqrt{s}$. However, accepting the validity of MLLA, the improvement seen in the previous paragraph supports the description of non-perturbative hadronization in the model.

The angular ordering resulting from gluon interference effectively moves the radiated gluons

15

closer to the jet axis. The size of the effect depends on the colour charge of the radiator and on the initial configuration of the event (i.e. 2 or 3 jets, there being interference effects in the interjet region for 3-jet events as seen in the string effect). The total number of (sub-)jets found in an event has been calculated [67] in the Next-LLA (NLLA) as a function of the jet resolution parameter, $y_{cut} = y_0$, for 2- and 3-jet events classified using $y_{cut} = y_1 > y_0$. Of course, if y_1 becomes too small non-perturbative processes become important and the calculation breaks down. The perturbative and non-perturbative regions are rather clearly separated and the sub-jet multiplicities thus provide a test not only of perturbative QCD calculations and their incorporation into Monte Carlo programs, but also of the non-perturbative models in the programs.

Sub-jet multiplicities have been studied [84, 85] at LEP 1. Quite good qualitative agreement is found between the data and the NLLA calculations in the perturbative region while a simple $\mathcal{O}(\alpha_s)$ calculation clearly disagrees. Of the Monte Carlo programs, ARIADNE does quite well; HERWIG 5.5 and JETSET 6.3 perform somewhat less well; and the incoherent model COJETS gives the worst agreement. Both versions 6.12 and 6.23 of COJETS disagree in the perturbative region while only 6.23 disagrees in the non-perturbative region. JETSET was compared [85] using various combinations of fragmentation and parton shower schemes. Incoherent parton showers resulted in poor agreement in both perturbative and non-perturbative regions independently of the fragmentation scheme. Coherent showers gave much better agreement in the perturbative region. In the non-perturbative region agreement was poor for independent fragmentation whilst good for string fragmentation.

The MLLA predicts [86] a suppression of gluon emission within a cone of angle $\theta < \theta_0 = M_q/E_q$ about the quark direction in a parton shower. This should lead to a lower *primary* multiplicity for heavy quark events. However, the total multiplicity is higher because of the high multiplicity of heavy flavour decays. The difference in multiplicity between heavy and light quark events is predicted to be independent of $\sqrt{s}$, contrary to the naïve expectation that the difference would decrease as the quark mass difference becomes smaller compared to the total energy. Results from PEP/PETRA, TRISTAN, and LEP/SLC agree reasonably well with the MLLA value, both for charm and beauty, particularly when the recent work of Petrov and Kisselev [87] is taken into account. The results [88, 89, 90] at $\sqrt{s} = M_Z$ agree reasonably well with the predictions of JETSET, with the possible exception of light (uds) quarks.

Given the appearance of angular ordering in MLLA, the effects of gluon interference should be apparent in angular correlations. Assuming LPHD, the correlations should persist in the hadrons. Besides the angular ordering in the polar angle, also the azimuthal angular distribution is affected by gluon interference. OPAL [91], has studied two-particle correlations in the azimuthal angle within restricted rapidity intervals. To avoid defining a jet axis they, and more recently ALEPH [92], have also studied such correlations using the Energy-Multiplicity-Multiplicity Correlation (EMMC) [93]. Taking in turn each track's direction as an axis the correlation calculated, the EMMC is the average of these correlations weighted by the axis defining track's energy. The EMMC has been calculated analytically in leading [93] and next-to-leading [94] order; the corrections are large. LPHD must be assumed to apply these calculations to

16

those calculated from hadrons. Nevertheless, qualitative agreement is obtained for $\phi > \pi/2$, where Monte Carlo models show hadronization to be relatively unimportant. Agreement with the data is even better for Monte Carlo models which incorporate gluon interference. Models not incorporating this interference fail to describe the data.

ALEPH [92, 95] and L3 [96, 97] have studied two-particle angular correlations in the full spatial angle using the Asymmetry in the Particle-Particle Correlation (APPC). In addition, L3 has studied the Asymetry in the Energy-Energy Correlation AEEC. The APPC is defined in analogy to the well-known AEEC by simply removing the energy weighting. This results in a correlation which is sensitive to all branchings of the shower, whereas the AEEC is primarily sensitive to the earliest branchings. The APPC is less sensitive to systematics in the correction for detector effects. On the other hand, the energy weighting makes the AEEC less sensitive to the Bose-Einstein effect. The use of the asymmetry serves to cancel some of the correlations arising from other effects as well as some detector effects and Monte Carlo uncertainties.

These correlations have been compared with Monte Carlo models. The conclusion is that the models containing gluon interference agree much better with the data than do the incoherent models. However neither version of NLLJET can be said to agree well.

All of these studies favour the Monte Carlo models ARIADNE, HERWIG and JETSET, which incorporate the gluon interference expected in MLLA. In general the agreement of data with these models is quite good. On the other hand, models that do not incorporate gluon interference, such as COJETS and incoherent JETSET do not in general agree well with the data. Both coherent and incoherent versions of NLLJET have been found also not to agree well with data.

2.5   Prompt photons

The principal source of observable prompt photons in hadronic decays of the Z (i.e. those with energies greater than a few GeV) is final state radiation (FSR) emitted at an early stage in the parton evolution process initiated by the primary quark–antiquark pair. To reduce large backgrounds from non-prompt sources, the first measurements reported by OPAL [98] and followed later by the other LEP experiments selected events with photons well isolated from the hadrons by a geometrical cone followed by a 2-step jet reconstruction process. In this procedure, the candidate photon is first removed from the event and all the hadrons reconstructed into jets. Then, the photon is replaced and its isolation from the jets tested in a second application of the clustering algorithm. It was soon realized that the cross sections are substantially less than those predicted from fractionally charged fermion pairs due to the influence of gluons. Thus, the measurement of prompt photons has become a sensitive test of the predictions of both perturbative QCD matrix element calculations and the Monte Carlo shower models free from the direct effects of fragmentation.

After tuning the parameters of these models in recent versions, namely ARIADNE 4.2, HERWIG 5.4 and JETSET 7.3 to the properties of the hadrons observed in non-FSR events,

there is no freedom to adjust the photon emission parameters with the exception of the infra-red cut-off. In the following reported analyses, these cut-off values are chosen to be similar to those employed to terminate the parton evolution, but in any case do not significantly influence the isolated hard photon rates.

All the published high statistics analyses from ALEPH, L3 and OPAL [99] show that both ARIADNE and HERWIG give acceptable descriptions of the total and individual n-jet $+\ \gamma$ cross sections as a function of the jet resolution parameter, y_{cut} (JADE E0), as well as the distributions in $p_\perp$ and fractional energy z_γ of the photon. A more critical test to differentiate between these two models is based on their predictions for the rate of low energy photons (< 15 GeV) at large angles ($> 75°$) to the event thrust axis, where the evolution scale ordering used in HERWIG predicts a larger cross section than ARIADNE [100]. Preliminary data from ALEPH indicate that ARIADNE gives the better description but more statistics are needed. However, the above published results show that JETSET is less satisfactory predicting cross sections that are 20-30% low (3σ's). ALEPH showed that this can be improved by either switching off the $\mathcal{O}(\alpha_{\mathrm{s}})$ matching or by keeping α_{s} constant indicating that virtuality as the scale controlling the parton evolution is not the best choice. More recently, DELPHI has also shown [101] that their data are in excess of JETSET by 18±7% in the low energy region of the photon spectrum below 15 GeV. After clustering the hadrons with the Durham ($k_\perp$) algorithm in a similar 2-step procedure, their respective jet rates above $y_{\mathrm{cut}} \geq 0.01$ are in reasonable agreement with JETSET. The excess is largely eliminated since most low energy photons are no longer isolated when the clustering algorithm is applied a second time. This appears to be a different conclusion from the other experiments. However, careful examination shows that the discrepancy between JETSET and data for ALEPH and L3 are largely at low y_{cut} in the total cross section where the use of different algorithms for jet-finding makes comparison difficult with DELPHI. It should be noted also that DELPHI compare with JETSET at *hadron* level before fragmentation corrections are applied.

The 2-step analysis procedure to select isolated photon events does not prevent a significant number of non-isolated hard photons from contaminating the $\gamma + 1$-jet event topology. Each of these photons remain within the hadron jet formed from the remnant of the radiating quark and are better separated from the isolated radiation by a "democratic" analysis [102]. Here, the prompt photon candidate is not removed from the event and thus becomes a member of a hadron jet with fractional energy z_γ of its total energy. The true isolated component is now concentrated at $z_\gamma = 1$ broadened downwards in z_γ by hadronization effects to overlap with the high energy tail of the collinear quark fragmentation component. For the $\gamma + 1$-jet (ie: 2-jet) cross section, this is well separated from the fragmentation tail when $z_\gamma \geq 0.95$. Fig. 5 shows the comparison as a function of y_{cut} (Durham E0 scheme) between the data measured by ALEPH and the predictions of ARIADNE and JETSET for this isolated component. The continuous curve is a prediction of a leading order calculation dominated by perturbative terms which are derived from a pure QED calculation. HERWIG (not shown) is in close agreement with the data. JETSET falls well below the data in this case showing that its treatment of radiation as independent emission from either quark at the first branching is quite inadequate. This discrepancy diminishes as the jet multiplicity increases. There is more satisfactory agreement
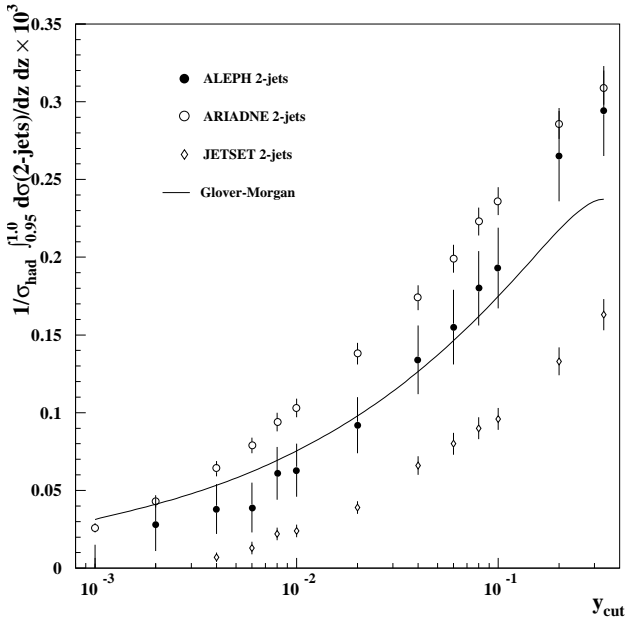
Figure 5: Integrated 2-jet rate above $z_\gamma = 0.95$ as a function of y_{cut}, compared with ARIADNE, JETSET and a QCD calculation.

in the fragmentation region below $z_\gamma = 0.95$.

Overall, the conclusion is that HERWIG gives the best description of all prompt photon data at the Z closely followed by ARIADNE.

In this review it is appropriate to mention the difficulties faced in determining the non-prompt photon background coming from hadrons decaying into γ's (mainly π^0). The isolation and energy cuts applied to the prompt photon candidates in the 2-step analyses are insufficient to eliminate this background entirely even when the full granularity of the electromagnetic calorimeters is exploited to recognize single from multiple γ showers. Hence, an irreducible non-prompt component must be subtracted statistically using QCD models or inferred from other data. However, the selection cuts applied choose a region of phase space that is not well understood in these models as they correspond to tails in the fragmentation process which cannot be tuned precisely.

The early analyses made at LEP 1 showed a clear discrepancy in the hadronic background yield predicted by the HERWIG and JETSET models [104]. The magnitude of the differences depends strongly on the isolation and energy cuts. A substantial effort has been made to quantify these discrepancies in detail, most recently by L3 [105]. They are able to reconstruct well resolved π^0s and ηs from two identified photons isolated by a geometric cone in which no other particles are found with energies above 50 MeV. JETSET reproduces the observed rate of π^0s and ηs with energies above 3 GeV for $10°$ isolation, but significantly underestimates the rate for $25°$ isolation. This study was restricted to 8 GeV maximum energy where the direct meson reconstruction procedure is efficient, but has been extended to 45 GeV using a neural network. The observed background rate of non-prompt photons is about a factor 2 larger than the predicted rate over the full energy range and the discrepancy increases with tighter isolation cuts. HERWIG tends to give a slightly better prediction but still underestimates the rate.

In other studies at the Z of the non-prompt photon background both ALEPH [99] and

DELPHI [101] have reported that JETSET underestimates the isolated π^0 yields but only in the lower part of the energy spectrum below 20 GeV. In these analyses, the limit allowed for the maximum particle energy accompanying the photon in the cone is set to 500 MeV. They are not inconsistent with the L3 results but instead demonstrate that the comparison with the generators is sensitively dependent on the isolation parameters. In the alternative "democratic" analysis without isolation cones of ALEPH [102] some activity is allowed in the vicinity of the γ which results in a better description by JETSET of the region of phase-space considered for the fragmentation.

2.6 Bose–Einstein effects

Most of the Bose–Einstein interference studies at LEP 1 have concentrated on two-particle correlations between identical charged pions [106] using the quantity

$$R(M) = \frac{\rho_2(M)}{\rho_1 \otimes \rho_1(M)} \tag{1}$$

Here, $\rho_2(M)$ is the two-particle correlation function, usually given as a function of Q, $Q^2 = M^2 - 4m_\pi^2$, and $\rho_1 \otimes \rho_1(M)$ is a reference sample. This sample should resemble $\rho_2(M)$ except for the Bose-Einstein correlations being studied.

Two choices for the reference sample are made, unlike-sign pion pairs or uncorrelated pairs from track mixing. Both alternatives have disadvantages. Unlike-sign pion pairs suffer from correlations due to resonances not present in like-sign pion pairs and the contribution of resonances with poorly known rates, especially η and η' at low Q. Furthermore residual effects of Bose–Einstein interference may also be visible in the unlike-sign pairs (see below). The track mixing has the disadvantage that correlations, other than from Bose-Einstein interference, are missing. In addition cuts to suppress gluon radiation must be applied. For both methods the systematic uncertainties are reduced using the double ratio $R^{\text{data}}(M)/R^{\text{MC}}(M)$. Additional corrections for background, e.g., Coulomb interactions are applied.

Assuming a spherical and Gaussian source the enhancement at low Q is parameterized as $R(M) \sim 1 + \lambda \exp(-r^2 Q^2)$. The chaoticity parameter λ is expected to vary between 0 and 1, and is extracted from data in the range from 0.4 to 1.5; the radius r of the source is measured to be 0.4 fm to 1 fm. In Fig. 6 the background-corrected measurements are displayed for the mesons $\pi^\pm$, π^0, $K^\pm$, and K^0.

Only identical mesons, that are prompt, i.e. do not originate from long-lived resonances, can contribute to the enhancement at low Q. It has been pointed out that the measured value of λ is about the maximum you could expect from direct pairs or even higher [107].

In more recent analyses the fraction $f(Q)$ of direct pions as a function of Q has been parameterized using Monte Carlo and included in the fit. For example DELPHI uses $f(Q) = 0.17 + 0.26Q - 0.12Q^2$, obtained from JETSET, to fit λ and r for charged pions: $R(M) \sim$

20
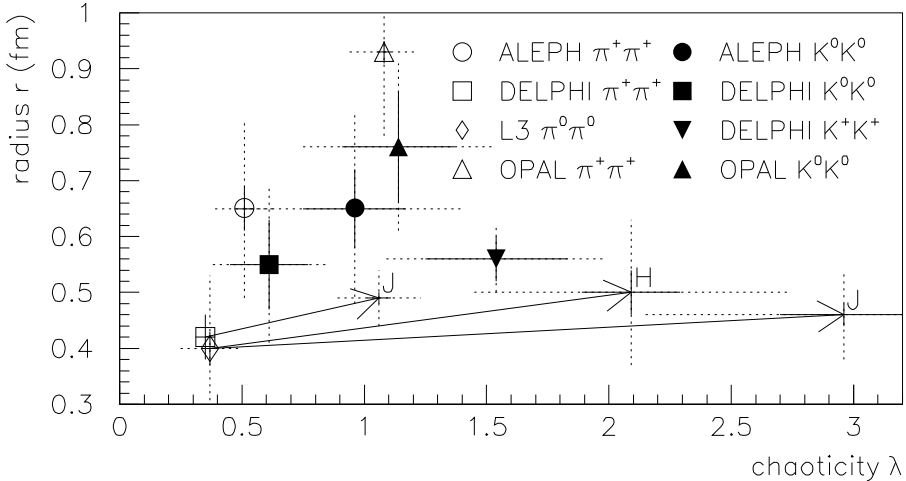
Figure 6: Chaoticity parameter λ versus radius r measured at LEP 1. Measured values are corrected for background with statistical (solid line) and total errors (dots) shown. The arrows indicate the changes, when corrected for non-prompt meson-pairs estimated with HERWIG or JETSET, when it is calculated by the experiment [106, 108, 109].

$1 + \lambda f(Q) \exp(-r^2 Q^2)$ [106]. Whilst the change in the radius is small, λ is changed by a factor 3. A bigger change is reported by L3 for $\pi^0 - \pi^0$ correlations [108]. The corrections are very sensitive to the model used. The corrections for non-prompt mesons are indicated by arrows in Fig. 6. The kaons have higher chaoticity values than pions before correction [109]. Only DELPHI has estimated the corrections for non-prompt kaons. The correction for kaons from c- and b-decay increases λ by $\approx$ 25 to 30%.

Three-particle correlations have been studied by DELPHI. Whilst JETSET without Bose-Einstein correlations fails to describe the data, JETSET with Bose-Einstein correlations enabled gives a fair description of unlike-sign triplets; the shape is reproduced, but the magnitude is too small [110].

Bose-Einstein correlation affect the unlike-sign spectra as well. In the invariant mass distribution of pions the ρ^0 meson appears shifted towards lower masses [111]. In the framework of the model this can be interpreted as coming from Bose-Einstein correlations between like-sign pion pairs, which induces correlations between unlike-sign combinations, for example seen as a distortion of the ρ^0 line shape. OPAL finds nice agreement between data and JETSET including Bose-Einstein correlations, when the chaoticity parameter is set to 2.5. This value of λ was obtained with a fit to the ratio $R(M)$. ALEPH agrees with this observation and extracts a ρ^0 rate with λ and r as free parameters. The value of $\lambda = 2.1$ is compatible with OPAL in view of the different η' rate and choice of the coherence time parameter χ. (χ gives the minimum width of resonances whose daughters contribute to the Bose-Einstein enhancement). DELPHI,

21

which observes a shift of the ρ^0, uses its λ value extracted from the Bose-Einstein analysis, after correction, for the ρ^0 analysis. Also with this parameter choice the agreement of data and model mass spectra is satisfactory [112].

Concerns have to be raised about the implementation of Bose-Einstein correlations in JET-SET. The implementation treats them as a classical force, which violates energy-momentum conservation. The rescaling applied to restore the total energy and momentum, however, twists the event shape variables and the model description becomes worse. Multijet rates for larger y_{cut} are reduced by up to 20% and the tails of the thrust and minor distributions are decreased by 5-10%. The amount of particles with low rapidities is depleted by $\approx$5%. A small but significant improvement is observed for small $p_{\perp \text{out}}$. The wave structure visible for $p_{\perp \text{out}} <$ 0.8 GeV vanishes when well tuned BE parameters are used and the $p_{\perp \text{out}}$ distribution here can be perfectly described [11]. Studies on a modified implementation, which also moves unlike-sign pairs to avoid rescaling (additional ϵ parameter) improves the situation but the description of the ρ^0 mass shift is in the wrong direction (positive).

Another new simulation, based on the area spanned by the string, is in preparation. A first result with a toy Monte Carlo predicts that the reconstructed λ should be 2 for π^0, when $\lambda = 1$ is used for event generation [113].

At first glance, the experimental results are different, $\lambda \approx 1$ for corrected direct measurements (DELPHI) and $\lambda \approx 2$ for an extraction tuning the JETSET model. However the following differences must be kept in mind. The use of track mixing for a reference distribution tends always to give lower λ values than the use of the unlike-sign meson sample. The uncorrected values for DELPHI are lower than for the other experiments. For kaons, corrections are estimated for c- and b-decays only, but not for strong decays. ALEPH has used daughters of resonances wider than $\Gamma = 100\,\text{MeV}/c^2$ as prompt pions, excluding the K* which seems not to be affected by Bose-Einstein correlations. Ignoring this and correcting OPAL for the η' rate would bring the values down to $\lambda = 1.7$ in these two analyses.

On the model side more understanding is needed of how to include the correlation without twisting the event shape distribution. The new ϵ parameter is a first step but there is no real success yet. Taking the decay amplitudes, i.e. string area, may be another promising approach.

22

3 Extrapolation to LEP 2 Energies

A question of interest for LEP 2 is that of how well the characteristics of QCD events are understood at large energies. By QCD events, it is here meant those that are produced through the s-channel decay of a Z^0/γ^* into quark and gluon jets. This question is of interest because W^+W^- events lead to multi-jet states for which one of the principal backgrounds will be QCD events, because QCD events will also form a principal source of background for higgs, chargino and other particle searches, and because QCD events will be interesting in their own right as a means to test perturbation theory in a regime with particularly small hadronization uncertainties. The principal tools to test how well QCD event characteristics are understood are Monte Carlo generators. The main generators, ARIADNE, COJETS, HERWIG and PYTHIA, have been tuned by the LEP experiments or by the Monte Carlo authors to describe global features of hadronic Z^0 data. In many cases, the generators have proven able to describe detailed features of these data as well. It is thus relevant to extrapolate the predictions of the QCD generators to LEP 2 energies and to compare their level of agreement for distributions likely to be of importance at LEP 2. In this section, such an extrapolation and comparison is presented.

For this study, members of each of the LEP experiments generated Monte Carlo event samples at $E_{\mathrm{cm}}=$ 175 GeV using parameter sets determined within their Collaboration. The Monte Carlo parameter sets used at LEP 1 are continually revised in order to yield as accurate a description of the Z^0 data as possible. Therefore, the parameter sets employed for this study do not necessarily represent official versions which will be published by the Collaborations. The parameter sets used for ARIADNE, HERWIG and PYTHIA are given in tables 3–5. For COJETS, L3 and OPAL results were made available using the parameter values given in table 6. There are numerous parameters and strategies involved in the optimization of the parameters. Comparison of the results obtained using the parameter sets of the different Collaborations therefore provides a systematic check of effects associated with the optimization choice. Samples of 100,000 events were generated without initial-state photon radiation or detector simulation, treating all charged and neutral particles with mean lifetimes greater than $3 \cdot 10^{-10}$ s as stable.

The following distributions were examined using charged particles only:
1. charged particle multiplicity, n_{ch},
2. scaled particle momentum, $x_p = 2p/E_{\mathrm{cm}}$,
3. component of particle momentum in the event plane, $p_{\perp\mathrm{in}}$, and
4. component of particle momentum out of the event plane, $p_{\perp\mathrm{out}}$.

The event plane was defined by the two vectors associated with the two largest eigenvalues of the Sphericity tensor.

The following distributions were examined using both charged and neutral particles:
1. Thrust, T [114],
2. Thrust major, T_{major} [115],
3. Thrust minor, T_{minor} [115],
4. jet rates R_n defined using the $k_\perp$ jet finder [116],

Parameter	Name	Default	ALEPH	DELPHI	L3	OPAL
Λ_{LLA}	PARA(1)	0.220	0.218	0.237	0.220	0.200
$p_\perp$ cutoff	PARA(3)	0.60	0.58	0.64	1.00	1.00
Fragmentation function	MSTJ(11)	4	3	3	3	4
Baryon model option	MSTJ(12)	2	2	3	2	2
$\mathcal{P}(\mathrm{qq})/\mathcal{P}(\mathrm{q})$	PARJ(1)	0.100	0.100	0.096	0.100	0.100
$\mathcal{P}(\mathrm{s})/\mathcal{P}(\mathrm{u})$	PARJ(2)	0.300	0.300	0.302	0.300	0.300
$(\mathcal{P}(\mathrm{us})/\mathcal{P}(\mathrm{ud}))/(\mathcal{P}(\mathrm{s})/\mathcal{P}(\mathrm{d}))$	PARJ(3)	0.400	0.400	0.650	0.400	0.400
$(1/3)\mathcal{P}(\mathrm{ud}_1)/\mathcal{P}(\mathrm{ud}_0)$	PARJ(4)	0.050	0.050	0.070	0.050	0.050
$\mathcal{P}(S{=}1)_{\mathrm{d,u}}$	PARJ(11)	0.500	0.500	—	0.500	0.500
$\mathcal{P}(S{=}1)_{\mathrm{s}}$	PARJ(12)	0.600	0.600	—	0.600	0.600
$\mathcal{P}(S{=}1)_{\mathrm{c,b}}$	PARJ(13)	0.750	0.750	—	0.750	0.750
Axial, $\mathcal{P}(S{=}0,L{=}1;J{=}1)$	PARJ(14)	0.000	0.000	—	0.100	0.000
Scalar, $\mathcal{P}(S{=}1,L{=}1;J{=}0)$	PARJ(15)	0.000	0.000	—	0.100	0.000
Axial, $\mathcal{P}(S{=}1,L{=}1;J{=}1)$	PARJ(16)	0.000	0.000	—	0.100	0.000
Tensor, $\mathcal{P}(S{=}1,L{=}1;J{=}2)$	PARJ(17)	0.000	0.000	—	0.250	0.000
Extra baryon suppression	PARJ(19)	1.000	1.000	0.500	1.000	1.000
σ_{q}	PARJ(21)	0.360	0.354	0.390	0.500	0.370
extra η suppression	PARJ(25)	1.000	1.000	0.650	0.600	1.000
extra η' suppression	PARJ(26)	0.400	0.400	0.230	0.300	0.400
a	PARJ(41)	0.300	0.500	0.391	0.500	0.180
b	PARJ(42)	0.580	0.810	0.850	0.650	0.340
ϵ_{c}	PARJ(54)	-0.050	-0.050	-0.0378	-0.030	—
ϵ_{b}	PARJ(55)	-0.0050	-0.0060	-0.00255	-0.0035	—

Table 3: Optimized parameter sets for ARIADNE, version 4.06 (for ALEPH, version 4.05), from the LEP Collaborations. The parameters listed are those which were changed from their default values by at least one of the groups. The ARIADNE events were generated using PYTHIA version 5.7 to describe the hadronization and hadron decays. The DELPHI Collaboration implements its own procedure to specify the relative rate at which mesons are produced in different multiplets [9], in place of the PYTHIA parameters PARJ(11)-PARJ(17).

Parameter	Name	Default	ALEPH	DELPHI	L3	OPAL
Λ_{MLLA}	QCDLAM	0.180	0.149	0.163	0.170	0.160
Cluster mass parameter 1	CLMAX	3.35	3.90	3.48	3.20	3.40
Cluster mass parameter 2	CLPOW	2.00	2.00	1.49	1.45	1.30
Effective gluon mass	RMASS(13)	0.750	0.726	0.650	0.750	0.750
Photon virtuality cutoff	VPCUT	0.40	1.00	0.40	0.50	0.40
Smearing of cluster direction	CLSMR	0.00	0.56	0.36	0.00	0.35
Weight for decuplet baryons	DECWT	1.00	1.00	0.77	1.00	1.00
s quark weight	PWT(3)	1.00	1.00	0.83	1.00	1.00
diquark weight	PWT(7)	1.00	1.00	0.74	1.00	1.00

Table 4: Optimized parameter sets for HERWIG, version 5.8, from the LEP Collaborations. The parameters listed are those which were changed from their default values by at least one of the groups.

5. normalized heavy jet mass for events divided into hemispheres by the plane perpendicular to the Thrust axis, $M_{\mathrm{heavy}}/E_{\mathrm{cm}}$ [117],

6. normalized difference between the heavy and light jet masses, $M_{\mathrm{diff}}/E_{\mathrm{cm}}$,

7. total jet broadening, B_T [118],

8. wide jet broadening, B_W [118],

9. Sphericity, S [119],

10. Aplanarity, A [120],

11. the modified Nachtmann-Reiter four-jet angular variable, $|\cos\theta^*_{\mathrm{NR}}|$ [121], with four-jet events defined using the $k_\perp$ jet finder with y_{cut}=0.01, and

12. the cosine of the angle between the two lowest energy jets in the four-jet events, $\cos\alpha_{34}$. In addition, the mean values of n_{ch}, T, T_{major} and T_{minor} were examined as a function of E_{cm}.

The results for $\langle n_{\mathrm{ch}}\rangle$, T, T_{major} and T_{minor} as a function of E_{cm} are shown in Fig. 7. For those cases in which the results of at least three Collaborations are similar to each other, the Monte Carlo predictions are shown as shaded or hatched bands. The widths of the bands show the maximum deviations between the results found by the different Collaborations. The widths of the bands are generally much larger than the statistical uncertainties. In a few cases, the Monte Carlo prediction obtained by one of the Collaborations differs significantly from those obtained by the other three groups and is shown as a separate curve. The COJETS predictions are likewise shown as separate curves for purposes of clarity. The results found by the four LEP experiments are labelled A, D, L and O in the figure legends.

Representative measurements from PEP, PETRA, TRISTAN and LEP 1 are included in Fig. 7. For E_{cm}= 175 GeV, an indicative "data point" is also shown, which is taken to be equal to the mean of the PYTHIA predictions from the four groups. The size of the symbol for the LEP 2 point is larger than the statistical uncertainty for 10 000 QCD events. Systematic terms were generally found to dominate the statistical ones for the experimental measurements shown in Fig. 7. The total experimental uncertainties at 175 GeV can therefore be expected to

Parameter	Name	Default	ALEPH	DELPHI	L3	OPAL
Fragmentation function	MSTJ(11)	4	3	3	3	3
Baryon model option	MSTJ(12)	2	2	3	2	2
Azimuthal correlations	MSTJ(46)	3	0	3	3	3
$\mathcal{P}(qq)/\mathcal{P}(q)$	PARJ(1)	0.100	0.095	0.099	0.100	0.085
$\mathcal{P}(s)/\mathcal{P}(u)$	PARJ(2)	0.300	0.285	0.308	0.300	0.310
$(\mathcal{P}(us)/\mathcal{P}(ud))/(\mathcal{P}(s)/\mathcal{P}(d))$	PARJ(3)	0.400	0.580	0.650	0.400	0.450
$(1/3)\mathcal{P}(ud_1)/\mathcal{P}(ud_0)$	PARJ(4)	0.050	0.050	0.070	0.050	0.025
$\mathcal{P}(S{=}1)_{d,u}$	PARJ(11)	0.500	0.550	—	0.500	0.600
$\mathcal{P}(S{=}1)_{s}$	PARJ(12)	0.600	0.470	—	0.600	0.400
$\mathcal{P}(S{=}1)_{c,b}$	PARJ(13)	0.750	0.600	—	0.750	0.720
Axial, $\mathcal{P}(S{=}0,L{=}1;J{=}1)$	PARJ(14)	0.000	0.096	—	0.100	0.430
Scalar, $\mathcal{P}(S{=}1,L{=}1;J{=}0)$	PARJ(15)	0.000	0.032	—	0.100	0.080
Axial, $\mathcal{P}(S{=}1,L{=}1;J{=}1)$	PARJ(16)	0.000	0.096	—	0.100	0.080
Tensor, $\mathcal{P}(S{=}1,L{=}1;J{=}2)$	PARJ(17)	0.000	0.160	—	0.250	0.170
Extra baryon suppression	PARJ(19)	1.000	1.000	0.500	1.000	1.000
σ_q	PARJ(21)	0.360	0.360	0.408	0.399	0.400
extra η suppression	PARJ(25)	1.000	1.000	0.650	0.600	1.000
extra η' suppression	PARJ(26)	0.400	0.400	0.230	0.300	0.400
a	PARJ(41)	0.300	0.400	0.417	0.500	0.110
b	PARJ(42)	0.580	1.030	0.850	0.848	0.520
ϵ_c	PARJ(54)	-0.050	-0.050	-0.038	-0.030	-0.031
ϵ_b	PARJ(55)	-0.0050	-0.0045	-0.00284	-0.0035	-0.0038
Λ_{LLA}	PARJ(81)	0.290	0.320	0.297	0.306	0.250
Q_0	PARJ(82)	1.000	1.220	1.560	1.000	1.900

Table 5: Optimized parameter sets for PYTHIA, version 5.7, from the LEP Collaborations. The parameters listed are those which were changed from their default values by at least one of the groups. The DELPHI Collaboration implements their own procedure to specify the relative rate at which mesons are produced in different multiplets [9], in place of the PYTHIA parameters PARJ(11)–PARJ(17).

Parameter	Name	Default	L3	OPAL
b_g	FRALOG(2)	46.6	100.0	46.6
d_g	FRALOG(4)	1.52	2.10	1.52
b_q	FRALOQ(2)	30.5	43.0	30.5
d_q	FRALOQ(4)	1.52	2.10	1.52

Table 6: Optimized parameter sets for COJETS, version 6.23, from the L3 and OPAL Collaborations. The parameters listed are those which were changed from their default values by at least one of the groups.
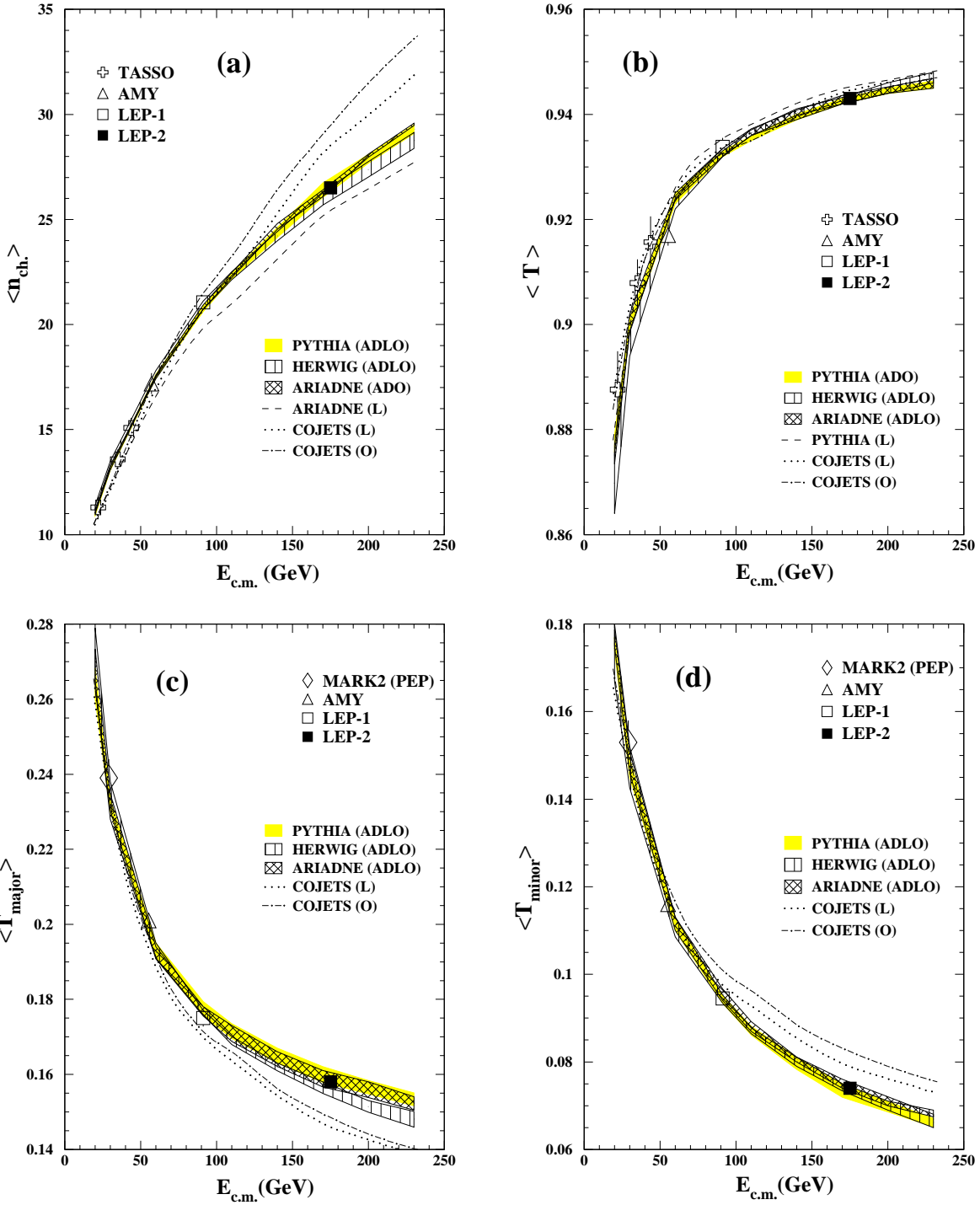
Figure 7: The mean values of n_{ch}, Thrust T, T_{major} and T_{minor} predicted by ARIADNE, COJETS, HERWIG and PYTHIA as a function of E_{cm} in comparison with measurements from PEP, PETRA, TRISTAN and LEP 1. The LEP 2 point is indicative only, based on the PYTHIA prediction. The total uncertainty expected at LEP 2 assuming 10 000 QCD events is smaller than the symbol size.

27

be comparable to those found for the LEP 1 data.

From the distribution of $\langle n_{\rm ch} \rangle$ versus $E_{\rm cm}$ (Fig. 7(a)), it is seen that, with the exception of the L3 ARIADNE curve, the predictions of ARIADNE, HERWIG and PYTHIA are similar. The widths of the ARIADNE, HERWIG and PYTHIA bands are narrow for energies at and below the Z^0 mass, showing that the results from the four Collaborations are in close agreement (with the exception of the L3 curve for ARIADNE). For energies above about 150 GeV, the HERWIG band becomes broader, indicating that there is some divergence in the predictions obtained by the different groups. From Fig. 7(a) it is also seen that COJETS predicts a substantially larger value of $\langle n_{\rm ch} \rangle$ than the other models for energies above the Z^0 mass. This difference is suggestive of coherence effects in the parton shower, which are absent in COJETS but present in the other three models. Coherence reduces the mean soft gluon multiplicity in the parton shower. It is generally expected that coherence will lead to a reduction in the mean hadron multiplicity as well. Thus, a measurement of $\langle n_{\rm ch} \rangle$ at LEP 2 could help to establish the existence of coherence phenomena in the data.

Figs. 7(b)–(d) show the corresponding distributions for the T, $T_{\rm major}$ and $T_{\rm minor}$ variables. Again, ARIADNE, HERWIG and PYTHIA are seen to exhibit similar behavior. COJETS agrees well with the other models for T, but lies below them for $T_{\rm major}$ and above them for $T_{\rm minor}$ in the LEP 2 energy range. Thus the jets from COJETS are less oblate than those from ARIADNE, HERWIG or PYTHIA. (The Oblateness O of an event is given by $O = T_{\rm major} - T_{\rm minor}$.) The differences between COJETS and the other three models become larger as $E_{\rm cm}$ increases.

In Fig. 8, the Monte Carlo predictions for $n_{\rm ch}$, x_p, $p_{\perp \rm in}$ and $p_{\perp \rm out}$ at 175 GeV are shown. The corresponding results for T, $T_{\rm major}$, $T_{\rm minor}$ and R_n, for $M_{\rm heavy}/E_{\rm cm}$, $M_{\rm diff}/E_{\rm cm}$, B_T and B_W, and for S, A, $|\cos \theta^*_{\rm NR}|$ and $\cos \alpha_{34}$ are shown in Figs. 9, 10, and 11, respectively. Overall, the models are seen to be in general agreement with each other. Some of the more notable exceptions to this agreement are discussed below.

1. A striking difference is observed between COJETS and the other models for the $n_{\rm ch}$ and $p_{\perp \rm in}$ distributions (Figs. 8(a) and (c)). Smaller but visible differences are observed between COJETS and the other models for a number of the other distributions as well. At the Z^0 mass, these differences between COJETS and the other models are either not present or are much smaller. This implies that the energy scaling behavior of COJETS differs from that of ARIADNE, HERWIG and PYTHIA.

2. For HERWIG, the x_p distribution is much harder using the L3 parameter set than it is using the parameter sets of the other Collaborations (Fig. 8(b)). This feature is also observed at the Z^0 energy. The primary reason for this difference between L3 and the other groups is the different treatment of the parameter CLSMR (see table 4).

3. From Fig. 9(d), it is seen that the three-jet rate from PYTHIA is significantly larger than that of the other models for $y_{\rm cut}$ values below about 0.02. Correspondingly, the two jet rate from PYTHIA is smaller. This difference is also observed at $E_{\rm cm} = 91$ GeV. From this same figure, COJETS is seen to predict a three-jet rate which is smaller than that of the other models: this last difference is not observed at LEP 1 energies.

4. COJETS exhibits a clear deviation with respect to the predictions of the other models for
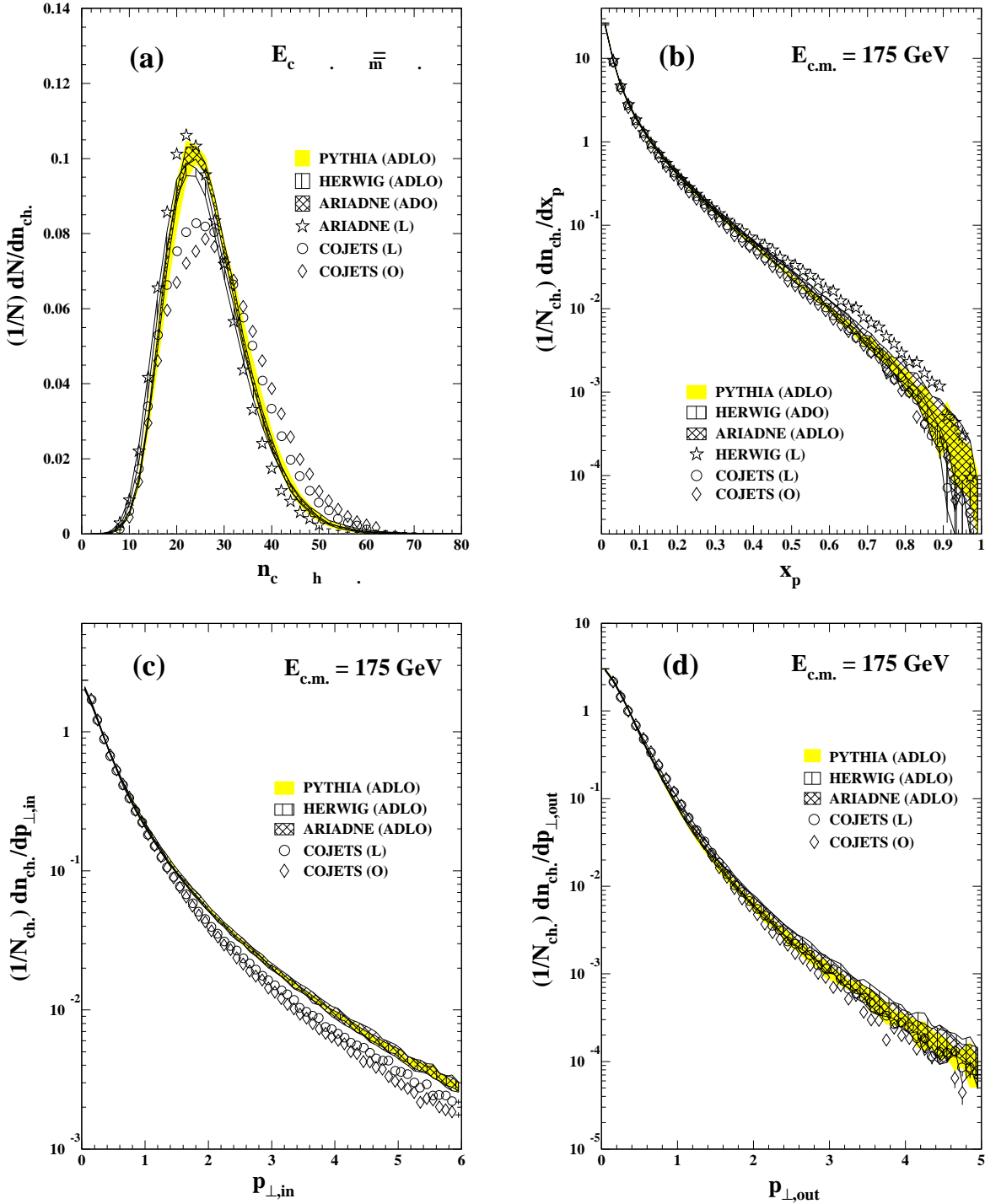
Figure 8: Comparison of the predictions of QCD event generators at $E_{\mathrm{cm}} = 175$ GeV.
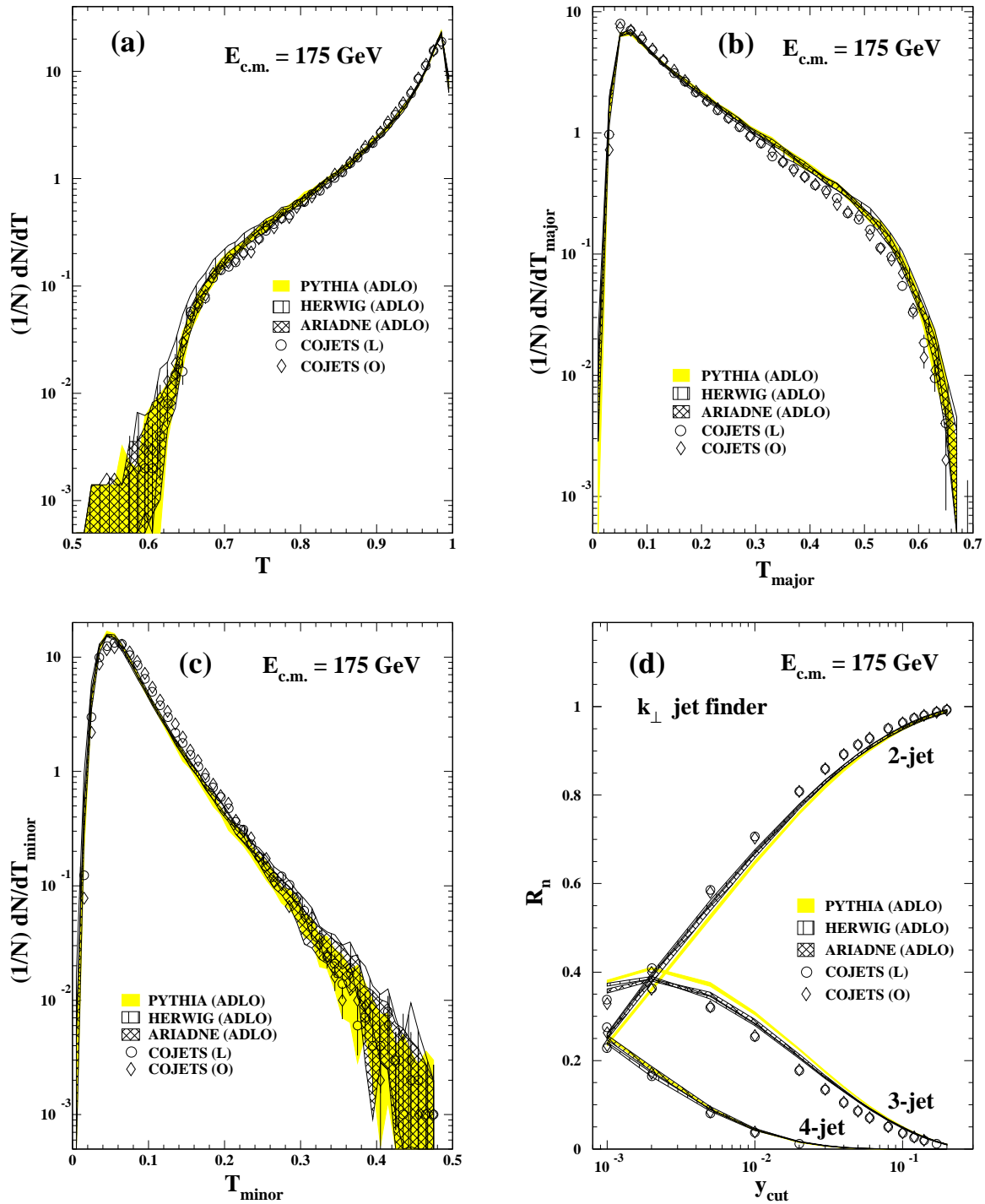
Figure 9: Comparison of the predictions of QCD event generators at $E_{cm} = 175$ GeV.

the jet mass distributions, $M_{\text{heavy}}/E_{\text{cm}}$ and $M_{\text{diff}}/E_{\text{cm}}$ (Figs. 10(a) and (b)). Less of a deviation is present for the jet broadening variables, B_T and B_W (Figs. 10(c) and (d)). This suggests that these last two variables may be less subject to uncertainties related to the modelling of QCD and hadronization than the first two variables.

5. COJETS and HERWIG are seen to exhibit a somewhat flatter distribution in $|\cos\theta^*_{\text{NR}}|$ than ARIADNE and PYTHIA (Fig. 11(c)).

The general conclusion that can be drawn from this study is that there is relatively little uncertainty in the predictions of QCD generators for event characteristics at LEP 2. Such basic features of events as charged multiplicity, Thrust and Oblateness are described in an almost identical manner by ARIADNE, HERWIG and PYTHIA. Only COJETS deviates significantly from the predictions of the other models. On the other hand, there is modest disagreement between the models for variables which require use of a jet finding algorithm: R_n (Fig. 9(d)) and $|\cos\theta^*_{\text{NR}}|$ (Fig. 11(c)). This could have some implication for the W mass determination based on the reconstruction of jets.
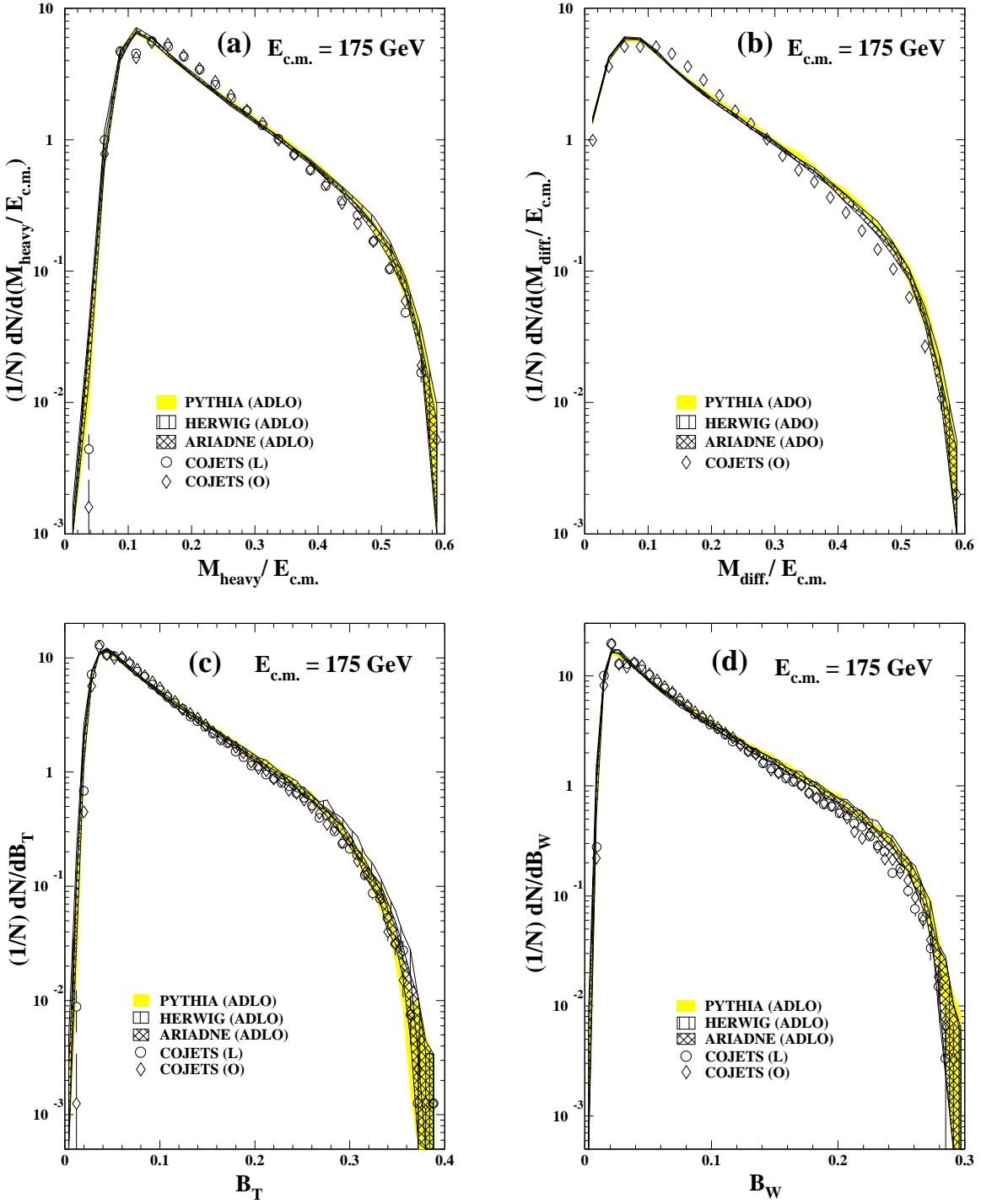
Figure 10: Comparison of the predictions of QCD event generators at $E_{cm}=$ 175 GeV.
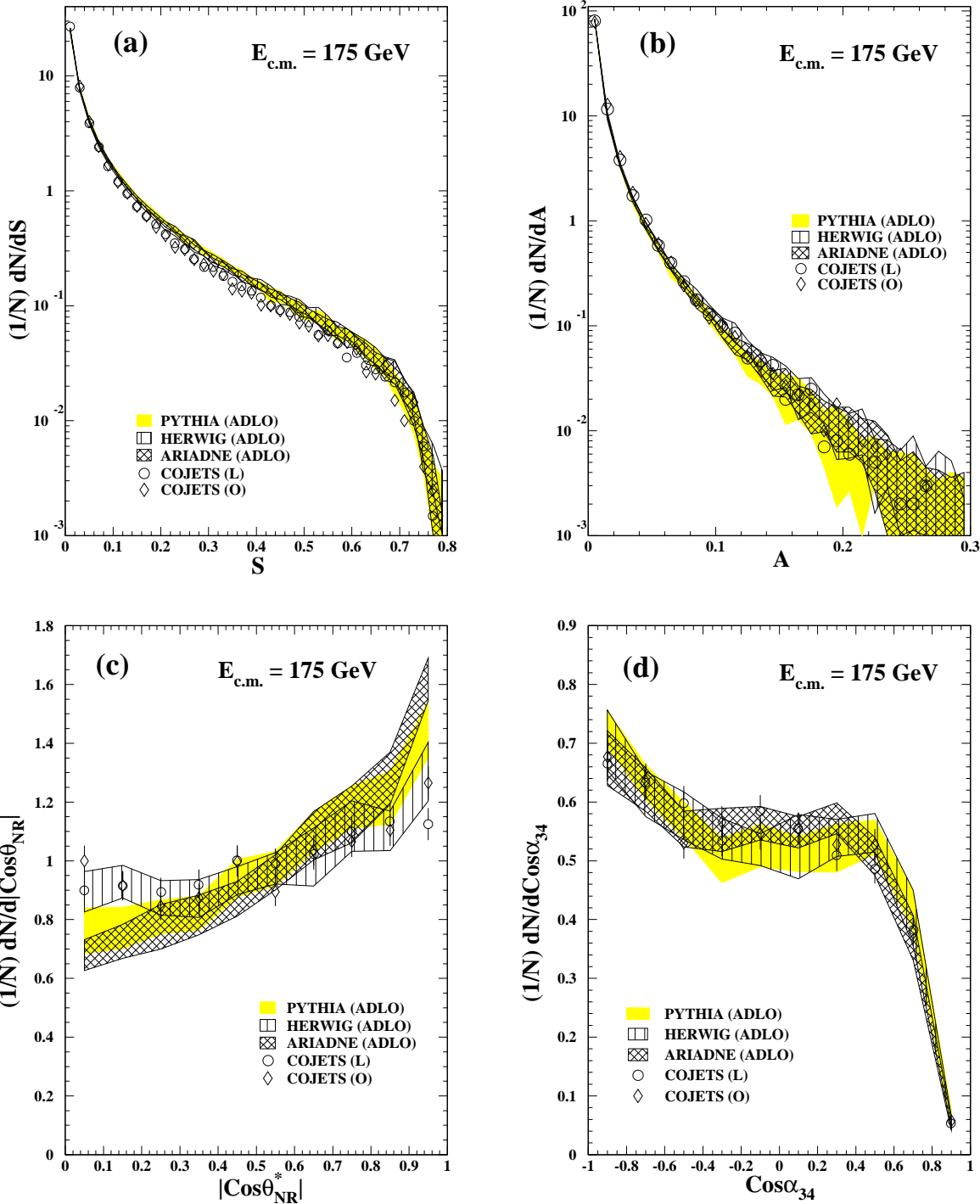
Figure 11: Comparison of the predictions of QCD event generators at E_{cm}= 175 GeV.

4 Monte Carlo descriptions

In this section we have collected brief descriptions for the main QCD generators and other pieces of QCD code. These writeups are intended to introduce the main physics ideas and give further references to manuals and codes — a full coverage of all physics and programming aspects is excluded for space reasons. The compilation below should be rather complete for programs intended for the main QCD-related processes, such as γ^*/Z^0 and W pair production. Special emphasis is put on HERWIG and PYTHIA/JETSET, which have been used extensively at LEP 1 and are equipped with a simulation both of electroweak and QCD aspects. A few programs include QCD aspects but have still been judged to better belong elsewhere, e.g. PHOJET is a $\gamma\gamma$ physics generator and ISAJET is mainly of interest (in the e^+e^- sector) as a supersymmetry generator.

4.1 ARIADNE

Basic Facts

Program name:	ARIADNE [13]
Version:	4.08 of 30 November 1995
Author:	Leif Lönnblad
	NORDITA, Blegdamsvej 17,
	DK 2100 Copenhagen Ø, Denmark
	Phone: + 45 – 35325285
	E-mail: leif@nordita.dk
Program size:	12853 lines
Program location:	http://surya11.cern.ch/users/lonnblad/ariadne/

The ARIADNE program implements the Dipole Cascade Model (DCM) for QCD cascades [122]. In this model the emission of a gluon g_1 from a $q\bar{q}$ pair created in an e^+e^- annihilation event can be described as radiation from the colour dipole between the q and $\bar{q}$. A subsequent emission of a softer gluon g_2 can be described as radiation from two independent colour dipoles, one between the q and g_1 and one between g_1 and $\bar{q}$, neglecting the contribution from the $q\bar{q}$ dipole, which is suppressed by $1/N_C^2$. Further gluon emissions are given by three independent dipoles, *etc.* In this way, the end result is a chain of dipoles, where one dipole connects two partons, and a gluon connects two dipoles. This is in close correspondence with the Lund string picture, where gluons act as kinks on a string-like field stretched between the $q\bar{q}$ pair.

This formulation of the partonic cascade in terms of colour dipoles means that the coherence effects, handled by introducing angular ordering in conventional parton showers, is correctly taken into account. Also, the DCM has the advantage that the first gluon emission is done according to the correct first-order matrix element, so that an explicit matching procedure like the ones introduced in HERWIG and JETSET is not needed.

Although the model has been developed a lot since the last LEP workshop, much of this development has been related to the description of Deep Inelastic Scattering and hadron-hadron collisions and will be described in some detail in the report from the $\gamma\gamma$ generator working group. Here only aspects relevant to e^+e^- annihilation will be discussed.

The basic DCM only describes gluon emission, and the process of splitting a gluon into a $q\bar{q}$ pair has therefore been added according to [123]. Although this procedure reproduces fairly well the amount of secondary $c\bar{c}$ production observed at LEP [124], there has been some criticism [125] that the model may be overestimating the phase space available for this process. Therefore an extra restriction of this phase space suggested in [125] has been implemented as an option in the last versions.

The radiation of photons from quarks is handled by allowing the process of emitting a photon from the *electro-magnetic* dipole between the original $q\bar{q}$ to compete with the gluon emission from the colour dipoles [126]. This competition is governed by the ordering in transverse momenta of the emitted gluons/photons, which is different from JETSET and HERWIG, where virtuality and angle, respectively, is used for ordering.

In the latest version, a scheme for colour reconnections has been added to the program. The model is described fully in [127] and briefly in section 4.7. Unfortunately, the manual included in the code distribution has not yet been updated to describe this new feature, and users who want to try it are advised to contact the author by e-mail before doing so.

Since ARIADNE only handles the perturbative QCD cascade in an event, it has to be interfaced to the PYTHIA/JETSET programs for generation of the hard sub-process, the hadronization and the particle decays. Such an interface is included in the code, and only very minor changes to the steering program is needed to replace the parton showers in PYTHIA/JETSET with the dipole shower in ARIADNE for any type of process. In a typical steering program for running PYTHIA, the changes needed are as follows.

- Immediately before the call to PYINIT there should be inserted a call to ARTUNE('4.07') to set up default parameters in ARIADNE and PYTHIA/JETSET, followed by a call to ARINIT('PYTHIA') to initialize the PYTHIA interface. To change the default behavior of ARIADNE, changes may be made to the ARDAT1 common block *between* the calls to ARTUNE and ARINIT.
- Immediately after a call to PYEVNT, a call to AREXEC should be made to perform the actual dipole cascade. If PYTHIA is set up to handle fragmentation and decays in the PYEVNT call, this is now handled in AREXEC instead.

Sample programs for how to do this is included in the distribution. The distribution also includes a subroutine AR4FRM which is an interface to four-fermion generators according to the standard presented in section 5.3. Except for what is needed to run PYTHIA/JETSET, no additional software is required to run ARIADNE.

4.2 COJETS

Basic Facts
Program name: COJETS [128]
Version: COJETS 6.23 of 10 February 1992
Author: Roberto Odorico
Department of Physics
University of Bologna
Via Irnerio 46, I-40126 Bologna, Italy
Phone: + 39 − 51 - 24 20 18
E-mail: odorico@bo.infn.it
Program size: 19742 lines
Program location: http://www.bo.infn.it/preprint/odorico.html

COJETS simulates electron-positron annihilation into jets of hadrons. (It also simulates proton-proton and antiproton-proton interactions.) The simulation is based, at the parton level, on the standard model with perturbative QCD treated in the leading-log approximation. QED radiation off beam particles is treated according to the BKJ program. Partons from parton showers are independently fragmented into jets of hadrons according to a Field-Feynman model extended to include heavy quarks and baryons and modified in the generation of soft particles. Gluons are fragmented as a pair of light quark and antiquark jets of opposite random flavors, each one having half the energy of the gluon and its same direction and with fragmentation parameters distinct from those of quark jets. Jet non-perturbative masses are limited by bounds originated by an approximate treatment of global phase-space effects at the multi- jet level. A previous version of the program, COJETS 6.12, in which quarks and gluons share the same fragmentation model is also available. The jet fragmentation model adopted goes hand in hand with the setting of the minimum parton-mass cutoff to a value of 3 GeV, which is substantially larger than those used in string- and cluster-based fragmentation models.

The output common block, containing the generated particle stream, has the standard /HEPEVT/ format, with PDG codes used for particles.

COJETS is maintained with the PATCHY code management system. The appropriate FORTRAN77 codes are obtained by means of suitable pilot patches. The program file also includes the documentation.

Recently, the program has been mainly used to check the relevance of evidence for string fragmentation, parton coherence and quark/gluon differences in jet fragmentation. Its usage to study the signal/background enrichment for bottom non-leptonic decay events by means of neural networks has shown that differences in internal correlations between signal and background are fuzzier in COJETS than in JETSET [129]. Thus for LEP 2 COJETS could be useful when studying ways of disengaging events with W pairs decaying non-leptonically from background.

COJETS had its fragmentation parameters sensibly tuned to reproduce basic experimental distributions. So far the tuning has been done by the author, mimicking experimental apparatus

effects but without a proper GEANT simulation. That can be done by the user by means of the program TUNEMC, based on Minuit's Simplex algorithm (a more advanced version of the program is in preparation).

Programs COJETS 6.12 and TUNEMC can be found at the same WWW URL as COJETS 6.23.

4.3 HERWIG

Basic Facts

Program name:	HERWIG [14]
Version:	HERWIG 5.9 from 1 January 1996
Authors:	G. Marchesini[1], B.R. Webber[2], G. Abbiendi[3], I.G. Knowles[4],
	M.H. Seymour[5], L. Stanco[3]
	1, Dipartimento di Fiscia, Universita di Milano.
	2, Cavendish Laboratory, University of Cambridge.
	3, Dipartmento di Fisica, Universita di Padova.
	4, Department of Physics and Astronomy, University of Glasgow.
	5, Theory Division, CERN.
	E-mail: webber@hep.phy.cam.ac.uk, knowles@v6.ph.gla.ac.uk,
	seymour@surya11.cern.ch.
Program size:	15500 lines
Program location:	http://surya11.cern.ch/users/seymour/herwig/

4.3.1 Introduction

HERWIG (Hadron Emission Reactions With Interfering Gluons) is a large, multipurpose Monte Carlo event generator which has been extensively used at LEP 1. Version 3.2, as applied to e^+e^- annihilation, was described in detail for the LEP 1 workshop [130], here we concentrate principally on program developments and new aspects of relevance to LEP 2 physics.

QCD Monte Carlo event generators utilize the fact that any hard scattering processes can be factorized into separate components at leading twist. These are: the hard sub-process itself; perturbative initial and final state showers; non-perturbative hadronization; resonance decays; and beam remnant fragmentation. In HERWIG great emphasis is placed on making available a very sophisticated, partonic treatment of the calculable QCD showers. In contrast the description of the at present uncalculable hadronization and beam remnant components is in terms of very simple models. Since HERWIG contains many hard sub-processes and supports all combinations of hadron, lepton and photon beams this allows the physics of many types of particle collisions to be simulated in the same package. In view of the universality of the factorized components that build up HERWIG events this allows experience gained at HERA and the TEVATRON, for example, to be made directly available to LEP physicists.

Since version 3.2 was released the HERWIG code was reorganized to isolate the shower, cluster hadronization and unstable particle decay routines. This modularity facilitates the creation of hybrid programs in which sections of code are replaced with interfaces to other Monte Carlo programs. To identify HERWIG code the names of all options statements now begin HW****. The /HEPEVT/ standard proposed in [131] is also now used throughout the program in DOUBLE PRECISION. The random number generator has been upgraded to a l'Ecuyer's algorithm as recommended in [132]. Discussion of physics changes are contained in the following sections.

4.3.2   Hard Sub-processes

An extensive range of hard sub-processes are available in the HERWIG program allowing the full spectrum of standard model LEP 2 physics to be simulated. These are illustrated in table 7; for a complete listing see the program release notes in the text file HERWIGnm.DOC.

The matrix elements used for the continuum processes IPROC=100–153 now allow for arbitrary polarization of the lepton beams, an additional Z' including complete $\gamma^\star/Z^0$ interference and full mass effects ($IQ \neq 0$). When the ZPRIME=.TRUE. option is set the Z' weak couplings used are taken from the arrays AFCH(*,2) and VFCH(*,2), see HWIGIN for details. The arrays Q/V/AFCH(*,1) are used consistently throughout the program for the standard model electric, weak vector and axial-vector fermion couplings. A running electromagnetic coupling $\alpha_{\mathrm{em}}(Q^2)$ is used for internal photons [133] with the hadronic part taken from [134]. It is normalized to the Thomson limit ($Q^2 = 0$) value ALPHEM. Process 107 is included to facilitate q/g studies; in analogy with quarks the gluons are given a $1 + \cos^2\theta$ distribution. The difference between processes 100–106 and the original 120–126 lies in the treatment of hard gluon emission. The massless matrix element matching scheme used by HERWIG is discussed under parton showers.

Specialist Matrix Element programs for W^+W^-/Z^0Z^0 production, more properly four fermion generators, employ the full set of gauge invariant diagrams. In comparison HERWIG only includes the subset of diagrams containing W^+W^- ("CC03") or Z^0Z^0 ("NC02") pairs but does provide realistic hadronic final states. These matrix elements are taken from the program of Kunszt [135] and correctly include spin correlations in the gauge boson decays. Additionally a model for colour re-arrangement within the context of HERWIG is available, see 4.7 for details. The decays of the vector bosons are controlled via the array MODBOS, as detailed in HWIGIN, and include spin correlations. Please also see the detailed prescription, discussed in section 5.3, for interfacing HERWIG to specialist four fermion Monte Carlos.

At LEP 2 the principal Higgs production mechanism is the Bjorken process, IPROC=300+ID, where one or both Z^0's may be off-shell, $Z^{0(\star)} \rightarrow Z^{0(\star)}h^0$; also available is vector boson fusion, IPROC=400+ID. In both cases the exact leading order matrix element is used in the improved s-channel approximation [136]. At LEP 2 a discoverable Higgs would be narrow; in the program the actual mass used is taken from within the range $[M_{\mathrm{h}} - \mathtt{GAMMAX}\star\Gamma_{\mathrm{h}}, M_{\mathrm{h}} + \mathtt{GAMMAX}\star\Gamma_{\mathrm{h}}]$ (default GAMMAX=10) using a 'Breit-Wigner' distribution corrected for an energy dependent width. The event weight is the product of the cross-section (in nb) multiplied by the branching ratio to the

channel specified by `ID`. The Higgs' partial widths are calculated in `HWDHIG`: the quark decay channels include next–to–leading logarithmic corrections and the vector boson decay modes allow for off-shell WW/ZZ pairs.

The cross-sections for $\gamma\gamma$ interactions rise with c.m. energy to become the commonest physics processes at LEP 2. When considering hadronic final states each photon may be viewed as interacting either as a point-like particle or as being resolved into constituent (anti-)quarks and gluons. This leads to three basic sets of hard sub-processes (zero, singly or doubly resolved), a division adopted in the wide selection of sub-processes made available in HERWIG. Note that this separation is in fact artificial and all three components must be combined to obtain the full cross-section. Discussion of these processes can be found in the HERWIG description provided in the gamma-gamma section of this report.

4.3.3 Initial State Radiation

In e^+e^- scattering real photons are radiated from the incoming lepton lines. At LEP 1 any effects were mitigated against by the penalty involved in going off the Z^0 resonance. However photon bremsstrahlung is expected to be an important feature at LEP 2 energies where the basic cross-section typically rises as $\hat{s}$ decreases. HERWIG uses an electron structure function approach to write the total cross-section for a process as:

$$\sigma(s) = \int_0^1 \mathrm{d}x_1 \int_0^1 \mathrm{d}x_2 f_e^e(x_1) f_e^e(x_2) \hat{\sigma}(x_1 x_2 s) \tag{2}$$

Employing a natural choice of variables, $\tau = x_1 x_2 (= \hat{s}/s)$ and $x = x_1$, this can be written:

$$\sigma(s) = \int_T^1 \mathrm{d}\tau \hat{\sigma}(\tau s) \int_\tau^1 \frac{\mathrm{d}x}{x} f_e^e(x) f_e^e\left(\frac{\tau}{x}\right) \tag{3}$$

where $\tau > T$ (`TMNISR`) is a physical cut-off used to avoid the $1/s$ pole in the cross-section's photon exchange term.

The actual structure function used is the second order solution to the full Altarelli-Parisi equation with exponentiated coefficients:

$$
\begin{aligned}
f_e^e(x) &= \beta(1-x)^{\beta-1} \exp\left\{\beta\frac{x}{2}\left(1+\frac{x}{2}\right)\right\}\left(1 - \beta^2\frac{\pi^2}{12}\right) \qquad\qquad \beta = \frac{\alpha_{\mathrm{em}}}{\pi}\left[\log\left(\frac{Q^2}{m_e^2}\right) - 1\right] \\
&+ \frac{\beta^2}{8}\left[(1+x)[(1+x)^2 + 3\log x] - \frac{4\log x}{1-x}\right] + \mathcal{O}(\alpha_{\mathrm{em}}^3)
\end{aligned}
\tag{4}
$$

This is equivalent[3] to the expression, eqs. (58,60), given on p. 34 of [1]. This means that the single photon emission allowed for in HERWIG gives equivalent energy and $p^\perp$ spectra as

---

[3]A discrepancy in the coefficient of the π^2 term, a factor 2 too large, is believed to be their typographic error.

IPROC	Process	
	$\gamma^\star / Z^0 / Z'$ Continuum Processes	
100+IQ	$e^+e^- \to q\overline{q}(g)$	IQ=1-6: q = d,...,t; IQ=0: all flavours
107	$e^+e^- \to gg(g)$	
110+IQ	$e^+e^- \to q\overline{q}g$	IQ as above, includes masses exactly
120+IQ	$e^+e^- \to q\overline{q}$	IQ as above $\Big\}$ no correction to hard
127	$e^+e^- \to gg$	gluon branching
150+IL	$e^+e^- \to \ell\overline{\ell}$	IL=2,3: $\ell = \mu, \tau$
	Di-Boson Production	
200	$e^+e^- \to W^+W^-$	$\Big\}$ $W^\pm / Z^0$ decays controlled
250	$e^+e^- \to Z^0 Z^0$	by MODBOS
	Bjorken process: $e^+e^- \to Z^0 h^0$	
300+IQ	$+h^0 \to q\overline{q}$	IQ as above
300+IL	$+h^0 \to \ell\overline{\ell}$	IL=1,2,3: $\ell = e, \mu, \tau$
310,311	$+h^0 \to W^+W^-, Z^0 Z^0$	
312	$+h^0 \to \gamma\gamma$	
399	$+h^0 \to$ anything	
	Vector Boson Fusion	
400+ID	$e^+e^- \to \nu\bar{\nu}h^0 + e^+e^- h^0$	ID as IPROC=300+ID
	Zero Resolved Gamma-Gamma: $e^+e^- \to (e^+e^-)\gamma\gamma$	
500+ID	$\gamma\gamma \to q\overline{q}/\ell\overline{\ell}/W^+W^-$	ID=0-10 as for IPROC=300+ID
	Gamma-W Fusion: $e^+e^- \to (e^+\nu_e)\gamma W^-$	
550+ID	$\gamma W^- \to q\overline{q}'/\ell\bar{\nu}_\ell$	ID=0-9 as for IPROC=300+ID
	Doubly Resolved Gamma-Gamma	
1500	$gg \to gg, qg \to qg$, etc.	31 $\mathcal{O}(\alpha_s^2)$ two-to-two QCD scatterings
1700+IQ	$gg \to Q\overline{Q}, gQ \to gQ$, etc.	16 $\mathcal{O}(\alpha_s^2)$ heavy quark production processes
1800	$gq \to \gamma q, gg \to \gamma g$, etc.	17 $\mathcal{O}(\alpha_s\alpha_{em}, \alpha_s^3\alpha_{em})$ direct photon processes
2200	$q\overline{q} \to \gamma\gamma, gg \to \gamma\gamma$	3 $\mathcal{O}(\alpha_{em}^2, \alpha_s^2\alpha_{em}^2)$ di-photon processes
	Singly Resolved Gamma-Gamma	
5000	$\gamma q \to gq, \gamma g \to q\overline{q}$, etc.	3 $\mathcal{O}(\alpha_s\alpha_{em})$ dijet processes
5100+IQ	$\gamma g \to Q\overline{Q}$	heavy flavour pair production, IQ as above
5200+IQ	$\gamma Q \to gQ, q\overline{Q} \to q\overline{Q}$	heavy flavour excitation, IQ as above
5500	$gg \to Vg, gq \to Vq'$, etc.	6 $\mathcal{O}(\alpha_s^2\alpha_{em})$ light (u,d,s) $L = 0$ meson production
5510,5520		$J(= S) = 0, 1$ mesons only
8000	Minimum bias soft collision	
	Charged lepton Deep Inelastic Scattering	
9000+IQ	$eq \to eq, e\overline{q} \to e\overline{q}$	NC DIS on flavour IQ as above
9010+IQ	$eq \to \nu_e q', e\overline{q} \to \nu_e \overline{q}'$	CC DIS on flavour IQ as above
10000+IP	As IPROC=IP but with suppressed SUE	

Table 7: The principal HERWIG hard sub-process of importance for LEP 2 physics. In QCD scatterings `IHPRO` labels the actual sub-process, allowing for colour decomposition, generated.

multiple photon emission. In the soft photon limit $f_e^e(x)$ simplifies significantly to the following form, used to efficiently generate the $\{x_i\}$ via importance sampling:

$$f_e^e(x, Q^2) \approx \beta(1-x)^{\beta-1} \tag{5}$$

In practical situations one has: $\alpha_{\text{em}}/\pi \ll \beta \ll 1$, so that $f_e^e(x)$ has an integrable singularity in the soft photon limit, $x \to 1$; $1-x$ is the energy fraction carried by the photon. To regularize this divergence HERWIG employs a resolution parameter, $x < X$, called ZMXISR (default $1 - 10^{-6}$), and includes a fraction of events with no emission, so that:

$$f_e^e(x) \mapsto \bar{f}(x) = \Theta(X - x)f(x) + \delta(1-x)(1-X)^\beta \tag{6}$$

Here X is only an internal parameter and unphysical in the sense that cross-sections should not depend on it. Observe that even for $1 - X = \mathcal{O}(10^{-6})$ the non-emission probability is $\approx 45\%$ at LEP 2. Note also setting ZMXISR=0 has the effect of switching off the initial state photon radiation.

After the emission of a photon the electron entering the hard sub-process is off-shell. In HERWIG its negative virtuality is selected from a logarithmic distribution, dq^2/q^2, bounded in magnitude by eq.(8).

Allowing for the virtualities of the electron lines and treating x as a lightcone momentum fraction $\hat{s}$ is reconstructed as:

$$\hat{s} = \tau s - q_1^2 - q_2^2 + \frac{q_1^2 q_2^2}{s} - 2\underline{p}_1^\perp \underline{p}_2^\perp \tag{7}$$

Since $\hat{\sigma}$ is a rapidly varying function of $\hat{s}$ near the Z^0 HERWIG slightly shifts the $\{x_i\}$ fractions to preserve $\hat{s} = \tau s$. Specifically the highest $p^\perp$ photon is taken to be emitted first and its $x \mapsto x' = x + q^2/s$ (x' is the energy fraction) so that $\hat{s}$ would be preserved in the absence of emission from the other lepton. The x of the lower $p^\perp$ photon is then shifted so as to give exactly $\hat{s}$. For simplicity the program requires photon emission to be in the forward hemisphere which imposes the condition:

$$q^2 < \frac{x'}{1+x'}(1-x)s \tag{8}$$

This inequality is applied to both leptons. Note that this still allows the possibility for on resonance γZ^0 states to be produced but only to the accuracy of the leading logarithm approximation.

The use of the Equivalent Photon Approximation for the case of virtual photon emission in which it is the photon which enters the hard sub-process is again discussed in the report of the gamma-gamma working group.

4.3.4 Parton Showers

HERWIG employs highly developed parton shower algorithms to provide an accurate description of the perturbative QCD jet evolution. Coherence, due to leading infrared singularities [70], is

automatically included through the choice of evolution variables, ordering in which naturally restricts the branching phase space to an angular ordered region. Further angular screening due to heavy quark masses, the *dead cone*, is also fully included [137]. At each branching the azimuthal angles are distributed according to the eikonal dipole distribution for soft gluons [138], including mass effects, and to the full collinear leading logarithm accuracy for hard emission [139]. At large momentum fractions the coherent algorithm used also correctly describes next-to-leading contributions [140]. By using a two-loop expression for α_s this allows the Monte Carlo Λ to be related to $\Lambda_{\overline{MS}}$ as $x \to 1$

$$\Lambda_{MC} = \exp\left\{ \frac{C_A(67 - 3\pi^2) - 10n_f}{6(11C_A - 2n_f)} \right\} \Lambda_{\overline{MS}} \approx |_{n_f=5} 1.569\Lambda_{\overline{MS}}^{(5)} \tag{9}$$

Since the time of the LEP 1 workshop significant progress has been made in the study of final states involving photons [103], leading to the implementation of final state photon radiation in HERWIG [141]. The momentum sharing in $q \to q\gamma$ branchings and relative rate compared to $q \to qg$ branchings are controlled by the following splitting function and Sudakov form factor:

$$
\begin{aligned}
P_{q \to q\gamma}(z) &= e_q^2 \frac{\alpha_{em}}{2\pi} \frac{1 + z^2}{1 - z} \\
\log \Delta_s(Q^2, Q_0^2) &= -e_e^2 \frac{\alpha_{em}}{\pi}[(\log(Q/Q_\gamma) - 3/4)^2 - (\log(Q_0/Q_\gamma) - 3/4)^2] \tag{10}
\end{aligned}
$$

where, since the photon is in the final state, a fixed α_{em} is used (allowing analytic integration of the Sudakov form factor) and $Q_0 = Q_q + Q_\gamma$ with Q_q and Q_γ the cut-offs on the quark and photon scales respectively. The branching $\gamma \to q\bar{q}$ is expected to be small and is not included. Competition between the two types of quark branching is handled in the standard way. That is the Q^2 scales at which the two types of branching attain a preselected probability of occurring are found, the larger is taken to occur first and if its Q^2 is above $(Q_q + Q_\gamma)^2$ it is accepted. The scale Q^2 of any branching is bounded above by that of the last emission, irrespective of type. However the opening angle is bounded from above by the opening angle of the last emission of the same type; this is exact in the case when azimuthal photon-gluon correlations are integrated out.

Due to the choice of evolution variables in HERWIG, configurations in which a very hard gluon or photon recoils against the $q\bar{q}$ pair are not generated by the showering algorithm, that is a 'dead zone' exists [141]. This is particularly important in the photon case due to the relative ease with which they can be identified in the final state. The HERWIG solution is to find what fraction of events are missing by integrating the three parton matrix element over the dead zone and then add back this fraction starting the evolution from a correctly distributed $q\bar{q}g/\gamma$ configuration. The algorithm of [142] is used to exactly include initial/final state correlations starting from a massless $q\bar{q}$ configuration.

The matching of a hard gluon or photon to the exact matrix element is controlled by the logical HARDME (default .TRUE.). Additionally there is a 'soft' matrix element correction, where soft here means inside the phase space region accessible to the branching algorithm; SOFTME

(default .TRUE.) controls the matching of the hardest emission, not necessarily the first, to the exact matrix element [143].

4.3.5 Hadronization

The basic preconfinement inspired [73] cluster hadronization model used in HERWIG remains little changed from its original formulation [144]. The principle criterion for selecting the flavours and spins of the primary hadrons in the cluster two body decays is the phase space available; though weights PWT(1-6), VECWT, TENWT and DECWT can be used to alter the flavour/spin compositions. The cluster decays are isotropic, in their own rest frame, except when a perturbative quark is involved, that is one from the hard sub-process or a g $\rightarrow$ q$\bar{\text{q}}$ splitting. If (CLDIR=1), the default, then the hadron containing this quark is aligned with the quark direction in the cluster rest frame. The main effect is to stiffen the spectrum of heavy charm and bottom hadrons. It is possible to partially decorrelate this direction retention using the parameter CLSMR (default 0), the width of an exponential distribution in $1 - \cos\theta_{\text{qh}}$; thus increasing CLSMR increases the smearing.

New parameters have been introduced to control the treatment of clusters with anomalous masses. CLPOW (default 2) influences the decision on whether a heavy cluster $q_1\bar{q}_2$ should first be split in two prior to hadronization according to if its mass satisfies the inequality:

$$M_{cl}^{CLPOW} > CLMAX^{CLPOW} + (m_{q_1} + m_{\bar{q}_2})^{CLPOW} \tag{11}$$

Using smaller values of CLPOW leads to an increased yield of heavy clusters containing heavy quarks and thence to more heavy baryons; light quark clusters are affected less. The parameter B1LIM (default 0) can be used to increase the number of relatively light bottom clusters that undergo a one-body decay. If M_{thr} is the threshold for two-body decay then the probability of a one-body decay becomes:

$$\mathcal{P} = \begin{cases} 1 & M_{cl} < M_{thr} \\ 1 - \frac{M_{thr} - M_{cl}}{B1LIM \star M_{thr}} & M_{thr} < M_{cl} < (1 + B1LIM)M_{thr} \\ 0 & (1 + B1LIM)M_{thr} < M_{cl} \end{cases} \tag{12}$$

For light quark clusters the one-body decay criterion remains equivalent to the above with B1LIM=0. In practice CLPOW proves more effective in controlling the spectrum of both bottom and charm hadrons. When one-body decays do occur a Lorentz covariant treatment is now used to effect the necessary momentum rearrangement.

In the default version of HERWIG the quark–antiquark pairs which form the colour singlet clusters are taken to be nearest neighbour pairs, in a sense defined by the shower. However a colour reconnection model is now available. It is based upon minimizing the spatial sizes of pairs of clusters as determined from the semi-classical positions of the partons at the end of the showers. This model is discussed more fully in 4.7.

More recently the number of hadrons supported has been enlarged to incorporate all $L = 0, 1$ mesons (including the $0^{+(+)}$ and $1^{+(+)}$ states) composed of d,u,s,c,b quarks and all $J = 1/2$

43

('octet') and $J = 3/2$ ('decuplet') baryons composed of the form $q_1q_2q_3$ or Qq_1q_2, $(Q = c,b)$. Should the user wish to add any new particles it is sufficient to simply specify their properties: name, PDG code number, mass, spin and flavour compositions in the arrays `RNAME`, `IDPDG`, `RMASS`, `RSPIN` and `IFLAV` and they will be included automatically in cluster decays. Using the array `VTOCDK` it is also possible to veto a particular hadron's production in cluster decays.

4.3.6 Decay Tables

The HERWIG decay routines have been largely re-written to make them more user friendly and to adopt the proposals made in section 5.2. Up to five body decays are supported with a number of standard matrix elements made available. Specific hadronic decay channels for B hadrons can now be included. This is in addition to the original partonic model based on spectator decays [137]; note this may involve some double counting. The production of a selected particle via unstable particle decays can be vetoed by specifying it in the array `VTORDK`; any branching ratio sums affected because of excluded channels are automatically reset to unity. The subroutine `HWIODK` has been added to allow the HERWIG decay tables to be inputted and outputted in the proposed standard format. When read in the program checks that the decay is kinematically allowed and does not violate electric charge conservation; if necessary the sum of branching ratios is reset to one. The use of this subroutine makes it simple for the users to adapt the provided tables for their own use. The subroutine `HWMODK` allows individual channels in the decay tables to be added or modified between events. The actual default decay tables themselves have also been updated to include modes at the one *per mille* level.

Interfaces to the EURODEC [145] and CLEO [146] B hadron decay packages are also built into HERWIG. The selection is made by setting `BDECAY='EURO'`, `'CLEO'` or `'HERW'` (the default is of course `'HERW'`).

The production vertices of hadrons are now calculated by HERWIG and stored using the `VHEP` array of `/HEPEVT/`. This is based on the particle lifetimes in the `RLTIM` array. A particle is set unstable if its lifetime is less than `PLTCUT` however when `MAXDKL=.TRUE.` all decays are tested in the routine `HWDXLM` and required to occur within a volume specified by `IOPDKL` else left undecayed. If `BOMIX=.TRUE.` then neutral $B^0_{d,s}$ mesons are allowed to mix before decaying.

4.3.7 Source Code

In addition to the WWW site quoted above copies of the HERWIG source code and supporting files are maintained in the following VAX directories:

```
CBHEP::DISK$THEORY:[THEORY.HERWIG]HERWIGnm.*
FNALV::USR$ROOT2:[BWEBBER.HERWIG]HERWIGnm.*
VXCERN::DISK$CR:[WEBBER.HERWIG]HERWIGnm.*
```

The files supplied are `HERWIGnm.COM`, `*.DOC`, `*.FOR`, `*.INC`, `*.MSG`, `*.SUD` and `*.TST`. The command file `HERWIGnm.COM` runs a test job `*.TST` containing the main program. This uses the source code subroutines found in `*.FOR` with the declarations and common blocks in `*.INC` and default Sudakov form factors in `*.SUD`. Release notes are found in `*.MSG` and more complete documentation in `*.DOC`.

4.4   NLLjet

Basic Facts

Program names:	NLLJET [147]
Versions:	NLLJET 3.0 of September 1992
Author:	Kiyoshi Kato
	Kogakuin University
	Nishi-Shinjuku 1-24, Shinjuku, Tokyo 160, Japan
	Phone: + 81 – 3 - 3342 - 1211
	E-mail: kato@sin.cc.kogakuin.ac.jp
	Tomo Munehisa
	Yamanashi University
	Takeda 4-3, Kofu 400, Japan
	Phone: + 81 – 552 - 20 - 8584
	E-mail: munehisa@top.esb.yamanashi.ac.jp
Program size:	7742 lines
Program location:	ftp.kek.jp : kek/minami/nlljet

NLLJET is a Monte Carlo code for the generation of jet events in e^+e^- annihilation based on the parton shower method. The events are parton final states in the form of a list with particle codes and four-momenta. Connection to the hadronization is open for the user, and a standard interface to Lund hadronization is provided.

Generation of QCD jets by the parton-shower method was born of Konishi, Ukawa and Veneziano in 1979 as the "jet calculus" in which the method to make systematic summation of the collinear singularity in QCD was given. Here, the factorization of the mass singularity works well and the choice of physical gauge leads to a suppression of interference terms, so that a stochastic treatment for jets becomes possible.

Soon after that, models of the QCD parton shower in the leading-logarithmic (LL) approximation were developed. These models are good for the description of jets in high energy. However, they have no chance to determine the fundamental parameter of QCD, $\alpha_s(\mu^2)$ (or QCD Λ), because starting from *any* renormalization scheme in QCD, you obtain the *same* formula for physical quantities in LL approximation. This limits the analysis for the determination of the strong coupling constant in jet phenomena only to the calculation based on the

QCD matrix elements. However, the Monte-Carlo simulation of jets by matrix elements is not appropriate for the global description of jets since it has an avoidable defect, the discontinuity between n- and $(n+1)$-parton states.

The idea of NLLJET was spawned from observation above. In this parton-shower model, the collinear singularity of QCD is summed up to the next-to-leading logarithmic(NLL) order. All components in NLL order are computed in the $\overline{\text{MS}}$ scheme, and they are implemented in the model. Thus NLLJET has the potential to determine the QCD $\Lambda_{\overline{\text{MS}}}$ through a comparison of generated events with experiments [148]. The basic ingredients of NLLJET are as follows:

- Sudakov factor which is defined by the integral of the P function up to $O(\alpha_{\text{s}}^2)$.
- Two-body branching by the two-body vertex function up to $O(\alpha_{\text{s}}^2)$.
- Three-body branching by the three-body vertex function in $O(\alpha_{\text{s}}^2)$.
- Hard cross section of the primary $q\overline{q}g$ process up to $O(\alpha_{\text{s}}^2)$.
- Kinematical conditions and correction terms.

The effect of soft-gluon contribution is an important issue in perturbative QCD. In NLLJET, the strong coupling constant in the Sudakov factor is defined to be $\alpha_{\text{s}}(x(1-x)Q^2)$, and it corresponds to the inclusion of soft gluon resummation. The angular ordering is not introduced to all branchings but only to those in which the angular ordering is really required.

The important point of the formulation beyond LL order is that each kinematical modification is always controlled properly through the introduction of a correction term in the NLL order functions. The three-body vertex functions become positive with the correction for the angular ordering in $q \to q + g + g$ and $g \to g + g + g$ and that for the momentum conservation. The double cascade scheme, which is necessary to recover the symmetry between q and $\overline{q}$, also gives another correction term.

The parton shower method still has a few ambiguous points which are hard to determine from the theoretical view point in perturbative QCD. For example, the virtuality of partons in final states should be less than a cutoff value, Q_0^2. Normally, one sets it equal to Q_0^2. However, sometimes better agreement with experiments is found by taking it to be 0. In this version, this modification is included by setting KINEM -1 parameter.

The effect of a quark mass is only counted kinematically by replacing Q^2 by $Q^2 + m_{\text{q}}^2$. Neither azimuthal correlations nor the parton polarization are considered.

Essential input parameters of NLLJET are W, Λ, Q_0^2, δ, and C. Here W stands for the center-of-mass energy. Physics should not depend strongly on the cutoff Q_0^2 and its dependence is to be counted as a systematic error of the theory. Parameter δ is specific to NLL parton shower and it is absent in LL order. The distribution is expected to be independent of δ. However, detailed study shows that there is small bend at the region connected by δ. If one sets δ large (~ 0.5), the events are free from the bend at the expense of the exclusion of $q\overline{q}g$ primary vertex. The scheme parameter C is available in order to replace μ^2 in $\alpha_{\text{s}}(\mu^2)$ from $\mu^2 = Q^2$ to $\mu^2 = CQ^2$. However, it is not possible to change C in large. In the matrix element, QCD is studied at $Q^2 = W^2$ while in parton shower, it is done for $Q^2 = W^2 \sim Q_0^2$.

46

4.5 PYTHIA/JETSET

Basic Facts

Program names:	PYTHIA and JETSET [15]
Versions:	PYTHIA 5.720 of 29 November 1995
	JETSET 7.408 of 23 August 1995
Author:	Torbjörn Sjöstrand
	Department of Theoretical Physics
	University of Lund
	Sölvegatan 14A, S-223 62 Lund, Sweden
	Phone: + 46 – 46 - 222 48 16
	E-mail: torbjorn@thep.lu.se
Program size:	19936 + 11541 lines
Program location:	http://thep.lu.se/tf2/staff/torbjorn/

4.5.1 Introduction

The JETSET program has been used frequently for QCD physics studies at LEP 1. For applications at LEP 2, JETSET should be complemented with the PYTHIA program. While JETSET only gives access to one hard process, $e^+e^- \rightarrow \gamma^*/Z^0 \rightarrow q\overline{q}$, PYTHIA contains a wealth of different processes. The two programs are fully integrated, in that a call to PYTHIA will not only generate a hard process but also automatically call JETSET routines to perform (timelike) parton showers and fragmentation. Output is in the normal LUJETS commonblock (with easy translation to the HEPEVT standard) and can be studied with the JETSET analysis routines. The emphasis of the PYTHIA/JETSET package is to provide a realistic description of varying hadronic final states, but also non-hadronic processes may be generated.

In addition to the briefer published description of the programs, there is a complete manual and physics description of over 300 pages [15]. The programs, the manual, update notes and sample main programs can be picked up from the web address given above; additionally the CERN program library provides the programs and hardcopies of the manual. The description given here therefore only contains some highlights, with special emphasis on the aspects of relevance for LEP 2 applications.

For the description of a typical high-energy event, a generator should contain a simulation of several physics aspects. If we try to follow the evolution of an event in some semblance of a time order, one may arrange these aspects as follows:

1. Initially the e^+ and e^- are coming in towards each other. An electron contains virtual fluctuations into photons, quarks, gluons, and so on. It is useful to employ the same parton-distribution and parton-shower language as for hadrons. Thus also electrons and photons are included in the parton concept. An initial-state parton shower develops by branchings such as $e \rightarrow e\gamma$, $\gamma \rightarrow q\overline{q}$ and $q \rightarrow qg$.

2. One parton from each of the e^+- and e^--initiated showers enters the hard process, where then a number of outgoing partons/particles are produced. It is the nature of this process that determines the main characteristics of the event. (Also some soft processes are included in the program; since much of the same framework can be used we do not here belabour the differences.)

3. If the hard process produces massive electroweak particles, such as the Z^0, the $W^{\pm}$ or a Higgs, the decay into lighter objects must be considered.

4. The outgoing partons may branch, to build up final-state showers.

5. Further semihard interactions may occur between the other partons in the case of two incoming resolved photons.

6. When a shower initiator is taken out of a beam particle, a beam remnant is left behind.

7. The QCD confinement mechanism ensures that the outgoing quarks and gluons are not observable, but instead fragment to colour-neutral hadrons.

8. Many of the produced hadrons are unstable and decay further.

The time-order above does not have to coincide with the generation sequence. Typically the hard process is selected first.

4.5.2 Hard processes

Close to a hundred subprocess cross sections have been encoded in PYTHIA. Lepton, hadron and photon beams are allowed; thus the program can be used for $p\overline{p}$/pp physics at the Tevatron or LHC or for ep physics at HERA. Here we concentrate on processes of relevance for LEP 2. Some of the more interesting ones are listed in table 8 and discussed below. Further comments may be found in other sections of this report.

It it important to note that PYTHIA is not intended to be a precision program for electroweak physics. The philosophy is to provide sensible first approximations to a wide selection of hard processes, as a starting point for a detailed simulation of the subsequent QCD steps, i.e. parton showers, fragmentation and decay. It is therefore orthogonal in philosophy to many dedicated electroweak generators, that attempt to provide the hard-scattering cross section with very high precision but do not go beyond a parton-level description.

Subprocess 1 is the familiar γ^*/Z^0 process that dominates LEP 1 physics. The full interference structure between the γ and Z^0 propagators is included. It supersedes the LUEEVT generator of JETSET. The main differences are:

- LUEEVT uses a matrix-element approach to generate at most one initial-state photon, while PYTHIA allows for multiple photon emission in a parton-shower approach;
- LUEEVT allows only hadronic final states, while PYTHIA also includes leptonic ones;
- LUEEVT contains a simple Breit-Wigner with the width Γ_Z as input, while PYTHIA contains an s-dependent Breit-Wigner that is dynamically calculated from electroweak parameters; and
- the option to simulate first- or second-order MEs currently only exists with LUEEVT.

Table 8: Main LEP 2 physics processes available in PYTHIA.

ISUB	Process
Gauge boson production	
1	$e^+e^- \to \gamma^*/Z^0$
18	$e^+e^- \to \gamma\gamma$
19	$e^+e^- \to \gamma(\gamma^*/Z^0)$
22	$e^+e^- \to (\gamma^*/Z^0)(\gamma^*/Z^0)$
25	$e^+e^- \to W^+W^-$
35	$e\gamma \to e(\gamma^*/Z^0)$
36	$e\gamma \to \nu W$
69	$\gamma\gamma \to W^+W^-$
70	$\gamma W \to Z^0 W$
Higgs production	
24	$e^+e^- \to Z^0 h^0$
103	$\gamma\gamma \to h^0$
110	$e^+e^- \to \gamma h^0$
123	$e^+e^- \to e^+e^- h^0$
124	$e^+e^- \to \nu_e \overline{\nu}_e h^0$
141	$e^+e^- \to \gamma^*/Z^0/Z'^0 \to H^+H^-, h^0A^0, H^0A^0$
171	$e^+e^- \to Z^0 H^0$
173	$e^+e^- \to e^+e^- H^0$
174	$e^+e^- \to \nu_e \overline{\nu}_e H^0$
Other processes	
10	$e^+e^- \to e^+e^-, \nu_e\overline{\nu}_e$
141	$e^+e^- \to \gamma^*/Z^0/Z'^0$

ISUB	Process
$\gamma\gamma$ physics	
58	$\gamma\gamma \to q\overline{q}, \ell^+\ell^-$
33	$\gamma q \to qg$
54	$\gamma g \to q\overline{q}$
11	$qq' \to qq'$
12	$q\overline{q} \to q'\overline{q}'$
13	$q\overline{q} \to gg$
14	$q\overline{q} \to g\gamma$
18	$q\overline{q} \to \gamma\gamma$
28	$qg \to qg$
29	$qg \to q\gamma$
53	$gg \to q\overline{q}$
68	$gg \to gg$
91	$\gamma\gamma \to VV'$
92	$\gamma\gamma \to XV$
93	$\gamma\gamma \to VX$
94	$\gamma\gamma \to X_1 X_2$
95	$\gamma\gamma \to \text{low-}p_\perp$
85	$\gamma\gamma \to Q\overline{Q}, \ell^+\ell^-$
84	$\gamma g \to Q\overline{Q}$
81	$q\overline{q} \to Q\overline{Q}$
82	$gg \to Q\overline{Q}$
DIS	
10	$eq \to eq$

Subprocess 19 contains a photon in addition to the γ^*/Z^0. This means double counting, since already process 1 can contain initial-state-radiation photons, so results from the two processes should not be added. The usage of process 19 should be restricted to events that contain a high-$p_\perp$ photon, where generation then is more efficient (and accurate) than what is offered by process 1.

Subprocess 25 describes W pair production, including subsequent decay into four fermions with full angular correlations. The formalism includes s-dependent widths in the Breit-Wigners and options to pick the set of independent electroweak parameters. However, it is restricted to the basic graphs of W pair production ("CC03").

Subprocess 22 describes γ^*/Z^0 pair production in a similar approximation ("NC02"). Note that interference terms between process 22 and 25 are not found anywhere. This is in accor-

dance with the basic philosophy of a reasonable but not exhaustive description of electroweak processes.

Subprocesses 35 and 36 describe the production of a single γ^*/Z^0 or W in the approximation of an effective photon flux. A process such as $e^+\gamma \to \overline{\nu}_e W^+$ thus is convoluted with the parton-shower approximation of the $e^- \to e^-\gamma$ branching to give an effective process $e^+e^- \to \overline{\nu}_e e^- W^+$. Process 35 has a singularity when the scattered electron has vanishing $p_\perp$ (in principle this is regularized by the electron mass, but in practice the m_e has been neglected). Therefore it is necessary to run with some minimum $p_\perp$ cut-off; for numerical reasons at least 0.01 GeV. An alternative description can be obtained by using an electron-inside-photon-inside-electron parton distribution (MSTP(12)=1) in process 1. For process 36 the decay of the W is assumed isotropic since the appropriate matrix elements have not been coded. Also subprocesses 69 and 70 assume isotropic W/Z decay. Furthermore, process 70 does not include contributions from γ^* but only from Z^0. The process implementations in this paragraph thus are less sophisticated than the single γ^*/Z^0, W pair and γ^*/Z^0 pair processes above.

PYTHIA is equipped with an extensive selection of production processes for the standard model Higgs, here denoted "h^0". (It is called "H^0" in the program, which confuses matters when two Higgs doublets are introduced, but for this report we stay with the conventional terminology.) Not all available processes have been listed, but only those of some interest. The most important by far (at LEP 2) is process 24, $e^+e^- \to Z^0 \to Z^0 h^0$. Both Z^0's in the graph have been included with a Breit-Wigner shape, so there is no formal restriction that either of them need be on or close to the mass shell. For a Higgs with $m_h + m_Z > E_{cm}$ process 124 takes over, $e^+e^- \to \nu_e \overline{\nu}_e W^+ W^- \to \nu_e \overline{\nu}_e h^0$, but at a much smaller rate. Processes 110, 123 ($Z^0 Z^0$ fusion) and 103 are even further suppressed.

All major h^0 decay modes are included: $h^0 \to q\overline{q}$, $h^0 \to \ell^+\ell^-$, $h^0 \to W^+W^-$, $h^0 \to Z^0Z^0$, $h^0 \to gg$, $h^0 \to \gamma\gamma$ and $h^0 \to \gamma Z^0$. The branching ratios are automatically recalculated based on the Higgs mass. One point that should be noted is that the parton-shower algorithm matches to the same three-jet matrix element that is used for γ^*/Z^0 decays. This gives a somewhat incorrect rate for three-jet production in Higgs decay.

In the minimal supersymmetric extension to the standard model the number of production processes is further increased. The full set of Higgs particles is included in the program: h^0, H^0, A^0 and $H^\pm$. Masses and couplings can be set by the user; this is a somewhat lengthy process, however, since currently the one-loop mass relations are not built into the program. The H^0 have the same production processes as the h^0; the list in table 8 only shows the more interesting. Higgs pair production, H^+H^-, h^0A^0 and H^0A^0, proceeds only through s-channel graphs and has been included as part of $\gamma^*/Z^0/Z'^0$ decays, process 141. The Z'^0 part can easily be switched off (MSTP(44)=4), so that processes 1 and 141 become identical except for the larger selection of decay modes in the latter. (Technically, this way the program can distinguish the Z' decaying to Higgses from a Z produced in Higgs decay, and accommodate different decay modes for the two.)

Subprocess 141 is also useful for the study of virtual corrections caused by the existence of

a Z'^0 somewhere above the LEP 2 energy range. Vector and axial couplings may be set freely to simulate various scenarios, and interference with γ^*/Z^0 is automatically included.

$\gamma\gamma$ physics is a large area, in that a wealth of different subprocesses is involved. A photon may act as a pointlike particle or as a resolved, hadronlike state. A simple subdivision of processes is therefore into direct (58, 85), once-resolved (33, 54, 84) and twice-resolved (the rest, that is all processes allowed e.g. in pp collisions). The resolved part of the photon may be further subdivided into a VMD (vector meson dominance) and anomalous part. In total therefore six classes of events can be separated [149]. An automatic mix to provide a "minimum bias" sample of events is obtainable as an option (MSTP(14)=10). Processes 81–85 include masses in the matrix elements, and thus are convenient to study e.g. heavy-flavour production. It should be noted that several aspects remain to be solved, for instance that of (slightly) off-shell incoming photons. Furthermore, on a technical note, PYTHIA is originally designed for fixed energies of the incoming particles, and so the process of having $\gamma\gamma$ "hadronic" collisions at varying energies is not yet fully automated.

Finally, note that process 10 can be used both as a Bhabha and a deep-inelastic-scattering generator. In neither respect is it competitive with dedicated programs, but it may be useful for first estimates.

4.5.3 Hard process generation

The cross section for a process $ij \to k$ is given by

$$\sigma_{ij \to k} = \int \mathrm{d}x_1 \int \mathrm{d}x_2 \, f_i^{\mathrm{e}^+}(x_1, Q^2) \, f_j^{\mathrm{e}^-}(x_2, Q^2) \, \hat{\sigma}_{ij \to k}(\hat{s}) \ . \tag{13}$$

Here $\hat{\sigma}$ is the cross section for the hard partonic process, as codified in the matrix elements for each specific process. For processes with several particles in the final state it would be replaced by an integral over the allowed final-state phase space. The $f_i(x, Q^2)$ are the parton distribution functions, which describe the probability to find a parton i inside an $\mathrm{e}^\pm$ beam particle, with parton i carrying a fraction x of the total $\mathrm{e}^\pm$ momentum, when the $\mathrm{e}^\pm$ is probed at some squared momentum scale Q^2 that characterizes the hard process. The hard scattering therefore only involves a squared invariant mass $\hat{s} = x_1 x_2 s = x_1 x_2 E_{\mathrm{cm}}^2$, where E_{cm} is the c.m. energy of the event.

The electron-inside-electron parton distributions are based on a next-to-leading order exponentiated description, see [2]. The approximate behaviour is

$$f_{\mathrm{e}}^{\mathrm{e}}(x, Q^2) \approx \frac{\beta}{2}(1 - x)^{\frac{\beta}{2} - 1}; \qquad \beta = \frac{2\alpha_{\mathrm{em}}}{\pi}\left(\ln\frac{Q^2}{m_{\mathrm{e}}^2} - 1\right) . \tag{14}$$

The form is divergent but integrable for $x \to 1$, i.e. the electron likes to keep most of the energy. To handle the numerical precision problems for x very close to unity, the parton distribution is set, by hand, to zero for $x > 0.999999$, and is rescaled upwards in the range $0.9999 < x < 0.999999$, in such a way that the total area under the distribution is preserved.

In the γe or $\gamma\gamma$ processes, an equivalent flow of photons is assumed, based on first-order formulae. There is some ambiguity in the choice of Q^2 range over which emissions should be included. In the probably most appropriate alternative (MSTP(13)=2) the form is

$$f_\gamma^{\mathrm{e}}(x, Q^2) = \frac{\alpha_{\mathrm{em}}}{2\pi} \frac{1 + (1 - x)^2}{x} \ln\left(\frac{Q_{\mathrm{max}}^2(1 - x)}{m_{\mathrm{e}}^2 \, x^2}\right). \tag{15}$$

Here Q_{max}^2 (PARP(13)) is a user-defined cut for the range of scattered electron kinematics that is counted as photoproduction. Note that we now deal with two different Q^2 scales, one related to the hard subprocess itself, which appears as the argument of the parton distribution, and the other related to the scattering of the electron, which is reflected in Q_{max}^2. In the default alternative (MSTP(13)=1) only one scale is assumed, i.e. $Q_{\mathrm{max}}^2(1 - x)/x^2$ is replaced by Q^2 above.

Resolved photoproduction also involves the distributions of quarks and gluons inside the photon inside the electron. By default the SaS 1D set [150] is used for the parton distributions of the photon, but several alternatives are available.

4.5.4 Parton showers

In every process that contains coloured and/or charged objects in the initial or final state, gluon and/or photon radiation may give large corrections to the overall topology of events. The philosophy of PYTHIA is to stay with the lowest-order cross sections (modulo trivial loop corrections such as the running of coupling constants) and then generate higher-order corrections in the parton-shower approach. This is less exact than the explicit calculation of higher-order matrix elements, but has the advantage that it can be applied also to processes where higher orders have not yet been calculated; additionally it includes multiple emissions.

Showers may be subdivided into initial- and final-state ones, depending on whether they precede or follow the hard scattering. Of course, the subdivision often contains an element of arbitrariness, since interference terms may exist. In both initial- and final-state showers, the structure is given in terms of branchings $a \to bc$, specifically e $\to$ eγ, q $\to$ qg, q $\to$ qγ, g $\to$ gg, and g $\to$ q$\overline{\mathrm{q}}$. The kernel $P_{a \to bc}(z)$ of a branching gives the probability distribution of the energy sharing, with daughter b taking a fraction z and daughter c the remaining $1 - z$ of the a energy. Once formed, the daughters b and c may branch in their turn, and so on.

Each parton is characterized by some virtuality scale Q^2, which gives an approximate sense of time ordering to the cascade. In the initial-state shower, spacelike Q^2 values are gradually increasing as the hard scattering is approached, while timelike Q^2 values are decreasing in the final-state showers. Shower evolution is cut off at some lower scale Q_0, typically around 1 GeV for QCD branchings and around m_{e} for initial-state QED ones. From above, a maximum scale Q_{max} is introduced, where the showers are matched to the hard interaction itself. Unfortunately the selection of Q_{max} for a given hard scattering is not unique, but gives rise to some slop.

Despite a number of common traits, the initial- and final-state radiation machineries are in fact quite different. The JETSET final-state algorithm has been used extensively for Z^0 hadronic decays at LEP 1, and is not significantly altered since the LEP 1 writeup [3].

Initial-state radiation is handled within the backwards evolution scheme [151]. In this approach, the choice of the hard scattering is based on the use of evolved parton distributions, which means that the inclusive effects of initial-state radiation are already included. What remains is therefore to construct the exclusive showers. This is done starting from the two incoming partons at the hard interaction, tracing the showers "backwards in time", back to the two shower initiators. In other words, given a parton b, one tries to find the parton a that branched into b. The evolution in the Monte Carlo is therefore in terms of a sequence of decreasing space-like virtualities Q^2 and increasing momentum fractions x. Branchings on the two sides are interleaved in a common sequence of decreasing Q^2 values. The definition of the x and z variables for off-mass-shell partons is not unique; in PYTHIA the $z = x_b/x_a$ of a branching tells how much the scattering subsystem invariant mass-squared is reduced by the branching. If originally parton b was assumed to have vanishing $p_\perp$, the reconstruction of the branching $a \to bc$ introduces a $p_\perp$ for b, which is compensated by c.

4.5.5 Beam remnants and multiple interactions

The initial-state radiation algorithm reconstructs one shower initiator in each beam. Together the two initiators delineate an interaction subsystem, which contains all the partons that participate in the initial-state showers, the hard interaction, and the final-state showers. Left behind are two beam remnants. In some cases a remnant is a single object, as when a γ is taken out of an e beam, leaving behind an e. When taking an e out of an e, a soft γ is left behind, which is then more related to the cutoff of $f_e^e(x, Q^2)$ at $x = 0.999999$ than to the ordinary beam-remnant concept, but is handled with the same machinery. In other cases a remnant consists of two objects, as when a q is taken out of an e, leaving behind e + $\overline{\text{q}}$. The latter example has a coloured remnant, meaning that the fragmentation of the hard-process partons is connected with that of the beam remnants.

A resolved photon contains many partons. In a twice-resolved $\gamma\gamma$ event there is thus the possibility of multiple interactions, i.e. of multiple semi-hard parton–parton processes in the same event. A model for this phenomenon is included in PYTHIA [149], and will be further developed to better represent differences between the VMD and anomalous states.

4.5.6 Fragmentation and decay

The Lund string fragmentation description [28] and the decay routines in JETSET have not changed significantly since the LEP 1 writeup [3], and so are not described here. The string fragmentation approach has been generally successful in comparisons with LEP data, although some shortcomings have shown up. See section 2 for further details.

The issue of Bose-Einstein effects has received increased attention in recent years, e.g. in connection with possible consequences for the W mass determinations [152]. The existing algorithm [3] works well in many respects, but is by no means to be considered as a definite solution to the problem. A somewhat different approach has been implemented to allow some cross-checks, and further alternatives may appear in the future. In the current standard algorithm, identical particles are pulled closer together in such a way as to enhance the two-particle correlation at small relative momentum separation. This makes jets slightly narrower, so that fragmentation parameters have to be retuned for reasonable agreement with data. In the alternative, the shift of identical particles is somewhat reduced, while non-identical particles are pushed apart a bit, so that the average properties of jets remain unchanged. This alternative does not yet come with JETSET, but is available as a plug-in replacement for the LUBOEI routine, at http://thep.lu.se/tf2/staff/torbjorn/test/main10.f.

Also colour rearrangement has been extensively discussed in recent years. Code that allows this has not yet been integrated in the standard PYTHIA/JETSET libraries, but is obtainable separately, see section 4.7.

4.5.7 Final comments

PYTHIA/JETSET are likely to be among the major event generators at LEP 2: access to a broad selection of hard scattering subprocesses is combined with a well-tested description of parton showers and fragmentation. Limitations exist, however. PYTHIA is not a program for precision extraction of electroweak parameters; for instance, no (non-trivial) loop corrections are included in the matrix elements. One may well imagine hybrid arrangements, where dedicated generators are used to provide an improved description of some especially interesting hard scattering processes, such as four-fermion final states, while the rest of the PYTHIA/JETSET machinery is used to turn a simple parton configuration into a complex hadronic final state. An example of such an interface is discussed in section 5.3. Furthermore, the ARIADNE program for colour dipole radiation offers an alternative to the parton-shower description of JETSET, and can be used for all the hard processes in PYTHIA.

While there are no major additions planned for PYTHIA/JETSET, the intention is to continue a steady development and support activity. The $\gamma\gamma$ sector maybe is the area where most further studies are required to complete the picture, but also other aspects deserve attention.

4.6 UCLA ansatz

Basic Facts

Program names:	UCLA [44, 153]
Versions:	UCLA 7.41 of 1 October 1995
Author:	Sebong Chun and C.D. Buchanan
	Department of Physics

UCLA
405 Hilgard Ave, Los Angeles, CA 90024
USA
Phone: (310) 815-1992, 7466
E-mail: chun@physics.ucla.edu,
            buchanan@physics.ucla.edu
Program size: 1922 lines
Program location: http://www.physics.ucla.edu/~chuns

The goal of the UCLA hadronization modeling is to study and develop the underlying principles of e⁺e⁻ annihilation into hadrons, constructing a simple phenomenology which can be used both as a "target" for non-perturbative QCD calculations and also to accurately predict data.

The UCLA7.41 program, a spin-off of the Lund relativistic string Monte Carlo program JETSET, is the manifestation of this modelling to be used in comparing predictions with e⁺e⁻ data. As JETSET has upgraded to new versions, the UCLA program has likewise been adapted with a parallel nomenclature.

The modern UCLA modeling [44] presumes that, by making a few assumptions which can be rationalized within a QCD context (for example, a strong coupling expansion in lattice QCD), one can construct a Weight Function for any specified e⁺e⁻ → hadrons event. That is, given the center-of-mass energy of the e⁺e⁻ system and the flavor and momenta of the primary hadrons produced, the UCLA modeling attaches a weight to the entire event, to be used in comparison with other possible events at that $E_{\rm cm}$.

The general structure of the Weight Function (in addition to kinematics of energy/momentum conservation and phase space with limited transverse momentum) depends on (a) an area law in space–time, (b) possible suppression factors at the vertices where a virtual $q\bar{q}$ pair is created from the colorfield, (c) "knitting factors" to knit a quark and antiquark together into the spatial wave function of a meson (or quark and diquark into a baryon), and (d) Clebsch–Gordon coefficients to knit the quark and antiquark (diquark) together into the flavor and spin state of the meson (baryon).

a) The area law is $\exp(-b'A)$ where b' is a constant and A is the area enclosed by the quark and antiquark trajectories in a space-time plot of the event. Almost any strong-coupling interaction will, in fact, give this sort of dependence.

b) The UCLA modeling assumes that there is no significant vertex suppression for $q\bar{q}$ pairs if the quark mass is less than the hadronic scale of $\simeq 1$ GeV; that is, $u\bar{u}$, $d\bar{d}$ *and* $s\bar{s}$ all have probability $\simeq 1.0$ of virtual creation from the colorfield.

c) The UCLA modeling assumes that all knitting factors are comparable, whether the hadron to be constructed is a spin 0 or 1 meson or a spin 1/2 or 3/2 baryon. (Probability

55

normalization on the fragmentation function derived below yields a value of the knitting factor of $\simeq (40 \text{ Mev})^{-2}$.)

d) The Clebsch-Gordon coefficients are simply the relevant flavor/spin coupling of a quark and antiquark (diquark) into a meson (baryon). Note that (c) and (d) taken together describe the coupling of a quark and antiquark or diquark into the complete state function of a hadron.

Although, in principle, knowing the Weight Function for the final state is enough to select an event, it is practically impossible to implement in this form. In order to implement this simple event Weight Function approach into a working Monte Carlo program, it is necessary to derive a fragmentation function for an "outside-in iterative one-particle-at-a-time" implementation such as JETSET uses.

By somewhat lengthy but straightforward algebra, this can be accomplished. The result so derived turns out to be the Lund Symmetric Fragmentation Function (LSFF) [153], with normalizing parameters of the vertex suppression, the spatial knitting factor, and the Clebsch-Gordon coefficient (see [44]). That is, the UCLA modeling simply amounts to using the LSFF as a hadronic production density weighted by Clebsch-Gordon coefficients, where the suppression of heavy mass particle production arises entirely from the $\exp(-bm^2/z)$ factor in the LSFF. (Note: the general structure of the Weight Function and the subsequent derivation of the fragmentation function can also be used to describe the Lund JETSET treatment. The difference is that JETSET presumes an $s\bar{s}$ vertex suppression of about 0.3 and a knitting factor for vector mesons of about 30% of that for pseudoscalar mesons, does not in general use Clebsch-Gordon coefficients, and adopts a normalization scheme that does not incorporate the $\exp(-bm^2/z)$ factor.)

The UCLA7.41 program uses the parton shower and decay table parts of JETSET, but replaces the flavor and momentum selection part with the UCLA modeling ansatz described above. Default values for the parton shower are $\Lambda = 0.2$ GeV and $Q_0 = 1.0$ GeV. Meson production is controlled by the two natural parameters of the LSFF with default values of $a = 2.1$ and $b = 1.1$ GeV^{-2}. Local transverse momentum compensation is approximated by a factor of $\exp(-\frac{n}{n-1}bp_\perp^2/z)$, where n is a parameter of default value 2.0. For baryon production, with "popcorn" mesons produced between baryon and antibaryon, an additional popcorn suppression factor of $\exp(-\eta m_{\text{pop}})$ is introduced with the default value of $\eta = 10$ GeV^{-1}. For more details, please refer to refs. [44].

This structure and values gives a rather good description of multiplicities, inclusive distributions, and correlations for hadron production from E_{cm} of 10 to 91 GeV, with the possible exception of the spin 3/2 baryons at 91 GeV. The description of heavy flavor (c, b) production distributions also seems reasonably good, with no additional parameterization or parameters.

For a detailed instruction on how to set up parameters and use the program, please refer to the manual at WWW location http://www.physics.ucla.edu/~chuns. A short set of instructions is available in the header to the actual program.

4.7 Colour reconnection codes

One of the QCD questions that has attracted attention in recent years is that of colour reconnection (or colour rearrangement) [127, 154, 155, 156]. This issue has implications for W mass studies, but is also of interest for our general understanding of QCD.

The concept may be illustrated by the process $e^+e^- \rightarrow W^+W^- \rightarrow q_1\overline{q}_2 \, q_3\overline{q}_4$. To first approximation, the hadronic final state can be viewed as coming from the incoherent superposition of two sources of particle production: the $q_1\overline{q}_2$ and the $q_3\overline{q}_4$ ones. If colours are reconnected, the sources would instead be $q_1\overline{q}_4$ and $q_3\overline{q}_2$. The picture is complicated by the possibility of gluon emission. Gluons with an energy above the W width can be viewed as independently emitted from the respective W source, to a good first approximation: propagator effects ensure that interference terms are suppressed. No similar suppression exist for soft gluons or in the nonperturbative régime. Therefore standard calculational techniques are of limited interest, and the phenomenon mainly has to be studied within the context of specific models. By now, several independent codes exist, some part of existing QCD generators, others available as add-ons. Below we list the known ones and give some specific details.

4.7.1 A PYTHIA-based implementation
(code by T. Sjöstrand)

The code used for the studies in [155] has not (yet) been incorporated in the PYTHIA/JETSET programs. A sample main program and the colour rearrangement subroutines can be obtained at web address http://thep.lu.se/tf2/staff/torbjorn/test/main01.f. Several different options are available, among others:
- scenario I, where strings are considered as extended colour flux tubes and the reconnection probability is proportional (up to saturation corrections) to the space–time overlap of the W^+ and W^- strings;
- scenario II, where strings are considered as thin vortex lines and reconnection may occur when strings cross;
- scenario II′, a variant of scenario II where only those reconnections are allowed that reduce the total string length; and
- the instantaneous scenario, where reconnections are allowed before the parton-shower evolution [154]; unphysical but handy for comparisons.

At most one reconnection is performed per event, in scenario II the one that occurs first in time, in scenario I selected according to relative probabilities given by the overlaps. Reconnections within a W system are not considered.

4.7.2 Another PYTHIA-based implementation
(code by Š. Todorova)

The code follows the physical approach of [155]. The reconnection phenomenon is simulated

with the help of the string model, where strings are considered to be either flux tubes or vortex lines with arbitrary diameter of the core. In order to get a more realistic estimation of the effect of colour reconnection, the following features (not found in the preceding code) were incorporated in the simulation:

- space-time evolution of parton shower;
- multiple reconnections; and
- self-interaction of a string (production of glueballs).

It should be noticed that the space-time evolution of a shower together with the self-interaction of a string allow the study of string reconnection effects in a single parton shower (decay of a single Z^0).

The search for candidates for reconnection is processed in parallel with the shower development (reconnection can take place before the emission of the last partons). Overlaps of the colour fields of flux tubes are calculated numerically (using multichannel MC integration with importance sampling). The method is slow but this is the price to be paid for (relative) accuracy and individual treatment of each event. The minimal distance between "vortex lines" is found by a minimization procedure based on parabolic fit.

The code is available in the directory crnvax:[nova.colour_ reconnection].

4.7.3 An ARIADNE-based implementation
(code by J. Häkkinen)

The aim of the simulation program presented in [156] is not so much to study the effect of recoupling on the average events, but to study if rare recoupled events can be identified. Perturbative QCD favours states which correspond to "short strings", i.e. parton states which produce few hadrons. This string "length" can here be specified by the λ measure, defined in [157], which correspond to an effective rapidity range. If recoupling occurs it is conceivable that it is favoured when the recoupling produces a state with lower λ measure, and such states may also be more easy to identify. For this reason the program produces recoupling such that the λ measure for the reconnected final state is minimized. Gluons with $E \gtrsim \Gamma_W$ are emitted independently within the original $q\bar{q}$ systems [158, 155]. This emission is simulated using the Dipole Cascade Model [122] implemented in ARIADNE [13]. For gluons with c.m. energy below $\Gamma_W \approx 2$ GeV there may be unknown interference effects due to emission from the two W systems. These low-energy gluons give very little effect on the hadronic final state, however, if the hadronization phase is described by the Lund string model [28] implemented in JETSET [15]. They are therefore disregarded in the parton states, which implies that a small fraction of the energy ($\approx 4\%$) will be lost in the simulations. During minimization of λ all possible final state configurations, obtained by cutting the original gluon chains in one place only before reconnecting to two new systems, are compared with each other. In this program reconnection between the two strings occur once in every event while reconnections within the strings are not considered. Thus, the program is not expected to reproduce average events, but possibly a small admixture of recoupled events.

The C code used in [156] is available at http://thep.lu.se/tf2/hep/hep.html or through anonymous ftp at thep.lu.se:/pub/LundPrograms/Misc/wwpair.tar.Z. The code contains two more models; the instantaneous scenario of [154], and random reconnection of the strings. These models are only used for comparison with the "main" model.

4.7.4   Another ARIADNE-based implementation
(code by L. Lönnblad)

The model in [127] for colour reconnections, implemented in the ARIADNE program [13], is similar to the one in [156] in that it reconnects colour dipoles within the framework of the Dipole Cascade Model (DCM) [122] with a probability $1/N_C^2$ only if the total string length becomes reduced. The main differences are that reconnections within each W system (and also among the partons from a Z decay) is allowed, that several such reconnections are allowed in each event, and that reconnections are allowed during the perturbative cascade.

To achieve this, colour indices are assigned to each dipole, and after each emission, dipoles with identical indices are allowed to reconnect. The indices are chosen randomly, but restrictions are made to ensure physical colour flows, e.g. two gluons created by a gluon splitting should not be allowed to form a colour singlet. In the DCM, however, a gluon is radiated coherently by the dipole between two partons, and a procedure has to be introduced, where the emitted gluon is said to have been radiated off one of the two emitting partons with some probability depending on which is closer in phase space.

In the case of $e^+e^- \rightarrow W^+W^-$ reconnections are initially only allowed within each W system separately. After all gluons with $E_g > \Gamma_W$ have been emitted, reconnections between the W systems is switched on and gluon emission with $E_g < \Gamma_W$ is performed in the possibly reconnected systems before hadronization.

4.7.5   A HERWIG-based implementation
(code by B.R. Webber)

A model for colour reconnection has been implemented in a package of subroutines that can be used with HERWIG (version 5.8). The new integer parameter IRECO=0,1,2 determines the reconnection option used. IRECO=0 means no reconnection and IRECO=2 gives "immediate" reconnection of the quark–antiquark pairs in hadronic WW events, before parton shower generation, with probability PRECO (default value = 1/9). In HERWIG this changes the evolution of the showers, as well as the colour connections, because the initial opening angles are different.

The most serious option is IRECO=1, which invokes a model based on the assumption that reconnection occurs locally in space–time. First, a space–time structure is computed for each parton shower in the event. This is done using a package written by Mike Seymour to store the internal lines of showers, which is turned on by setting INTLIN=.TRUE.. The algorithm is semi-classical, but qualitative features and orders of magnitude should be correct. In the case

of W hadronic decays, each W decay point is generated with the appropriate exponential decay distribution. Then the locations of all the vertices in the showers are computed by assigning a space-time separation $\Delta x_i = q_i/(q_i^2 - m_i^2)$ to vertices joined by an internal line i of 4-momentum q_i and on-shell mass m_i.

The HERWIG cluster hadronization model, normally called immediately after showering has terminated, involves splitting each final-state gluon into a quark–antiquark pair. For each quark i there is a colour partner antiquark j, with which the quark would normally be paired to form a colour singlet cluster (ij). The IRECO=1 option introduces a reconnection phase before cluster formation. In this phase the program looks for another colour-connected quark-antiquark pair (kl) such that (il) and (kj) could be colour singlets and

$$|\Delta x_{il}|^2 + |\Delta x_{kj}|^2 < |\Delta x_{ij}|^2 + |\Delta x_{kl}|^2 \ , \tag{16}$$

where Δx_{ij} is the (ij) cluster size, defined as the separation of the *production* vertices of i and j (note that this can be zero, e.g. if i and j come from a W decay that did not radiate any gluons). If such a pair exists, the reconnection $(ij)(kl) \rightarrow (il)(kj)$ would reduce the cluster sizes, and so it is performed with probability PRECO. Note that reconnection can happen inside a single shower and not just between different showers. Thus some retuning of parameters to fit data on $e^+e^- \rightarrow Z^0 \rightarrow$ hadrons will be necessary when using IRECO=1.

The code can be obtained by anonymous ftp from

> hep.phy.cam.ac.uk $\equiv$ 131.111.66.27

The following files should be copied from directory disk\$alpha1:[public.herwig]:

- hwwmas58.for – sample main program and analysis routines;
- hwreco58.for – modified HERWIG routines HWBFIN, HWBJCO, HWCFOR which *replace* those in HERWIG version 5.8, plus *new* routines HWGCLU, HWGCMO, HWUPIP, HWVHEP.

There is a new common block containing relevant parameters and counters:

> COMMON/HWRECO/PRECO,EXAG,IRECO,MEVTS,MCLUS,MRECO,MSWCH,INTLIN

PRECO is the reconnection probability (default 1/9); EXAG is an 'exaggeration factor' for the W lifetime, to study effects of the WW separation (default 1.0); IRECO is the reconnection option (see above, default 1); MEVTS *etc.* are integer counters for number of events, clusters, reconnections, and WW reconnections; INTLIN is set to .TRUE. when IRECO=1 (see above).

The code is still under development; please notify webber@hep.phy.cam.ac.uk of any problems, bugs and/or peculiarities.

4.8 Monte Carlo Implementations of Exact Next-to-Leading Order Calculations

Basic Facts

Program name:	EVENT	EERAD	EVENT2
Authors:	Zoltan Kunszt	Walter Giele	Stefano Catani
	Paolo Nason	Nigel Glover	Mike Seymour
email:	nason@surya11.cern.ch	E.W.N.Glover@dur.ac.uk	seymour@surya11.cern.ch

There are now three publicly-available programs for calculating next-to-leading order corrections to arbitrary infrared-safe two- and three-jet quantities in e^+e^- annihilation. Although these use Monte Carlo integration techniques, they should be contrasted with Monte Carlo Event Generators in several ways. Firstly, they calculate the *exact* result in perturbation theory for the $\mathcal{O}(\alpha_s)$ corrections to a given quantity — no more nor less. Secondly, the phase-space configurations generated do not have positive-definite weights, so a probabilistic interpretation is not possible. Finally, for both these reasons, the programs only ever consider the partonic final state, and no treatment of hadronization is attempted.

There are many advantages of implementing higher-order QCD calculations as matrix-element Monte Carlo programs. For all but the simplest observables, the required phase-space integrals are not analytically tractable, and some form of numerical integration becomes mandatory. Since each phase-space point sampled by the program has a direct correspondence to a set of final-state momenta, any infrared-safe jet or event-shape definition may be used, and can be implemented exactly as in an experimental analysis. Many event properties can be analyzed simultaneously, simply by adding code to the analysis routine of the program to histogram the quantity of interest.

However as is well-known, the real and virtual corrections are separately divergent but with finite sum, so naïve numerical integration of each matrix element would fail. Thus a regularization scheme must be used to render the integrals finite. It is principally in the definitions of regularization scheme that the three programs differ, although there are other important differences.

The difference between the regularization schemes can be illustrated using a simple one-dimensional example. In dimensional regularization using $(4 - 2\epsilon)$ dimensions, the integrals we encounter are typically of the form

$$\langle O \rangle = \int_0^1 \frac{\mathrm{d}x}{x^{1+\epsilon}} O(x) + \frac{1}{\epsilon} O(0), \qquad (17)$$

where the first part represents the real cross-section, the second the virtual, and x would typically be a gluon energy or parton-parton invariant mass. The function $O(x)$ represents a final-state observable that is infrared safe, i.e. with the requirement that $O(x)$ tends smoothly to $O(0)$ as x tends to 0. If the integral were analytically tractable, it would yield an ϵ-pole

61

that canceled the virtual term, leaving a finite result. However, in general it is not, and we must manipulate it into a form in which the physical limit $\epsilon \to 0$ can be taken *before* numerical integration, without making any assumption about $O(x)$.

The phase-space *slicing method* does this by introducing an unphysical parameter x_0,

$$\langle O \rangle = \int_0^{x_0} \frac{\mathrm{d}x}{x^{1+\epsilon}} O(x) + \int_{x_0}^1 \frac{\mathrm{d}x}{x^{1+\epsilon}} O(x) + \frac{1}{\epsilon} O(0) \approx \int_{x_0}^1 \frac{\mathrm{d}x}{x} O(x) + \log(x_0) O(0) + \mathcal{O}\left(x_0 O'(0)\right). \quad (18)$$

The result becomes exact in the limit $x_0 \to 0$, which practically means $x_0 \ll x_{\text{physical}}$, where x_{physical} is the smallest physical scale in the problem.

The *subtraction method* works by subtracting and adding a term derived by projecting each point in four-parton phase-space onto some point in three-parton phase-space, and calculating the observable at this phase-space point together with an approximate matrix element. This must be such that it matches all the divergent terms of the full matrix element. In our simple example this corresponds to

$$\langle O \rangle = \int_0^1 \frac{\mathrm{d}x}{x^{1+\epsilon}} O(x) - \int_0^1 \frac{\mathrm{d}x}{x^{1+\epsilon}} O(0) + \int_0^1 \frac{\mathrm{d}x}{x^{1+\epsilon}} O(0) + \frac{1}{\epsilon} O(0) = \int_0^1 \frac{\mathrm{d}x}{x} \left(O(x) - O(0)\right). \quad (19)$$

Note that this is exact and does not depend on any unphysical parameters.

The matrix elements for $\gamma^* \to q\bar{q}g$ have been known to next-to-leading order for many years[159]. These were later checked by other groups, and used for specific calculations of a variety of event shapes. For the 'QCD at LEP' report [160], Kunszt and Nason wrote a general-purpose Monte Carlo program using the subtraction method that could calculate the next-to-leading correction to any event shape or jet definition, EVENT[161]. This has been considered the standard calculation for many years, but has two significant shortcomings owing to the matrix elements used: they have been summed over permutations of the outgoing partons, which means that quarks and gluons cannot be distinguished in the final state; and they consider the decay of a virtual photon, so can only predict quantities averaged over orientations of hadronic events, losing all information on their lab-frame directions and lepton-hadron correlations. Furthermore they neglect specific axial-axial contributions that as a point of principle are essential for describing Z^0 decays, although in practice these are never numerically significant.

More recently two groups have proposed general algorithms for calculating next-to-leading order corrections in arbitrary processes, and both have used three-jet production in e^+e^- annihilation as a simple first proving ground for their methods. These have resulted in the EERAD program by Giele and Glover[162], which uses the slicing method, and the imaginatively-titled EVENT2 program by Catani and Seymour[163], which uses the subtraction method. Both of these use the full next-to-leading order matrix elements for $e^+e^- \to q\bar{q}g$, avoiding the shortcomings of EVENT. Although EVENT2 uses the matrix elements of the Leiden group[164] by default, it has options to use the same matrix elements as EVENT or EERAD as a cross-check. Numerical results of the three algorithms are discussed in [165] and shown to be in good agreement. Since they are supposed to be exact calculations of the same quantity, rather than models, any differences between them should be treated as bugs.

5 Standardization

5.1 Particle codes and /HEPEVT/ update

The /HEPEVT/ standard [166] has been widely adopted by Monte Carlo authors for storing information on generated events. In practice the real variables are commonly declared to be DOUBLE PRECISION and often the size is expanded to NMXHEP=4000. We propose that these are now added to the standard.

In /HEPEVT/ it was intended for particles to be identified using the PDG numbering scheme [167]. However the conventional numbers assigned have deficiencies, particularly concerning the neglect of particles expected according to the quark model but not yet identified in experiment, for example the h_b. This proves troublesome for those program authors who include such states and has lead to *ad hoc* solutions. Further the higher, orbitally excited $L = 2, 3, \ldots$ and radially excited $n = 2, 3, \ldots$ mesons are labelled in a somewhat unsystematic way. In order to preserve the concept of uniqueness, allow for the missing quark model states, systematize the numbering and remain true to the spirit of the PDG scheme we suggest the following revised numbering.

Table 9 lists the $n = 1$, $L = 0, 1$ mesons and indicates their numbering, for these states this is largely in accord with the PDG scheme and with the STDHEP (JETSET) implementation [168]. In the pairs of $I = 0$, (u, d, s) mesons: (η, η'), (ω, ϕ), $(h_1(1170), h_1(1380))$, *etc.* the lighter state is labelled 22 and the heavier 33, reflecting the naive, dominant quark contents. Bound states involving top quarks are not expected, due to the quark's high mass, and therefore are not considered. The mixed K_S^0 and K_L^0 states are still labelled 310 and 130 respectively. The table should be extended to include $n = 1$, $L = 2, 3, \ldots$ states; this leads to up to four mesons of the same total spin. It is proposed to reserve the fifth digit to differentiate these states by continuing the sequence established for the $L = 1$ mesons. That is, for a given $J > 0$ the numbers would be: $(L, S) = (J - 1, 1) : \star \star m$, $(J, 0) : 10 \star \star m$, $(J, 1) : 20 \star \star m$ and $(J + 1, 1) : 30 \star \star m$, where as usual $m = 2J + 1$. The $J = 0$ states represent an exceptional case, here we propose $(L, S) = (0, 0) : \star \star 1$ and $(1, 1) : 10 \star \star 1$, as done in table 9; this may be thought of as $L0 \star \star 1$. Radially excited mesons, $n = 2, 3 \ldots$, are effectively copies of the the above states, it is proposed to introduce a sixth digit to differentiate them as follows: $n = 1 : \star \star \star \star \star$, $n = 2 : 1 \star \star \star \star \star$, $n = 3 : 2 \star \star \star \star \star$, *etc.* Thus for example the $K^{*+}(1680)$, a 1^3D_1 state would be numbered 30323 and the $\rho^0(1450)$, a 2^3S_1 state 100113. The numbering of excited mesons suggested here differs significantly from the original PDG scheme.

Table 10 lists the lowest lying $J = 1/2$, $3/2$ baryons, including the anticipated charm and bottom states. Two $J = 1/2$ states exist for baryons containing three different flavours of quarks. When the two lighter flavours are in a symmetrical ($J = 1$) state the baryon is called a Σ, Ξ' or Ω' and a Λ, Ξ, or Ω if they are in an antisymmetric ($J = 0$) state. To distinguish the lighter, antisymmetric states the light quark numbers are reversed; for example[4] $\Xi_b'^-$ has

---

[4] Actually the PDG naming rules do not make it clear which state to put the prime on, we have provisionally chosen to place it on the heavier state.

		L = 0		L = 1				
		S = 0	S = 1	S = 0	S = 1			
		J = 0	J = 1	J = 1	J = 0	J = 1	J = 2	
q_1	$\overline{q}_2$	★★1	★★3	10★★3	10★★1	20★★3	★★5	
d	$\overline{d}$	π^0	ρ^0	b_1^0	a_0^0	a_1^0	a_2^0	11
	$\overline{u}$	π^-	ρ^-	b_1^-	a_0^-	a_1^-	a_2^-	−21
	$\overline{s}$	K^0	$K^{\star 0}$	$K_1^0(1270)$	$K_0^{\star 0}$	$K_1^0(1400)$	$K_2^{\star 0}$	31
	$\overline{c}$	D^-	$D^{\star -}$	$D_1^-(2420)$	$D_0^{\star -}$	$D_1^-(H)$	$D_2^{\star -}$	−41
	$\overline{b}$	B^0	$B^{\star 0}$	$B_1^0(L)$	$B_0^{\star 0}$	$B_1^0(H)$	$B_2^{\star 0}$	51
u	$\overline{u}$	η	ω	$h_1(1170)$	$f_0(980)$	$f_1(1285)$	$f_2(1270)$	22
	$\overline{s}$	K^+	$K^{\star +}$	$K_1^+(1270)$	$K_0^{\star +}$	$K_1^+(1400)$	$K_2^{\star +}$	32
	$\overline{c}$	$\overline{D}^0$	$\overline{D}^{\star 0}$	$\overline{D}_1^0(2420)$	$\overline{D}_0^{\star 0}$	$\overline{D}_1^0(H)$	$\overline{D}_2^{\star 0}$	−42
	$\overline{b}$	B^+	$B^{\star +}$	$B_1^+(L)$	$B_0^{\star +}$	$B_1^+(H)$	$B_2^{\star +}$	52
s	$\overline{s}$	η'	ϕ	$h_1(1380)$	$f_0(1300)$	$f_1(1510)$	$f_2'(1525)$	33
	$\overline{c}$	D_s^-	$D_s^{\star -}$	$D_{s1}^-(2536)$	$D_{s0}^{\star -}$	$D_{s1}^-(H)$	$D_{s2}^{\star -}$	−43
	$\overline{b}$	B_s^0	$B_s^{\star 0}$	$B_{s1}^0(L)$	$B_{s0}^{\star 0}$	$B_{s1}^0(H)$	$B_{s2}^{\star 0}$	53
c	$\overline{c}$	η_c	J/ψ	h_c	χ_{c0}	χ_{c1}	χ_{c2}	44
	$\overline{b}$	B_c^+	$B_c^{\star +}$	$B_{c1}^+(L)$	$B_{c0}^{\star +}$	$B_{c1}^+(H)$	$B_{c2}^{\star +}$	54
b	$\overline{b}$	η_b	$\Upsilon(1S)$	h_b	χ_{b0}	χ_{b1}	χ_{b2}	55

Table 9: Proposed numbering scheme for the lowest lying mesons: for example the a_1^- has the number −20213. The names of the pseudovector particles are distinguished by their masses, if these are not currently established L and H are used to indicate light and heavy. The pseudo-vector states $K_1(1270)$ and $K_1(1400)$ are believed to be admixtures of the K_{1B} 1^1P_1 and K_{1A} 1^3P_1; in such situations the lighter state is given the lower number.

number 5312 and the Ξ_b^- number 5132. This extends the convention that heavier states are given larger numbers. Excited states are not yet incorporated into event generators and thus are not covered here.

Increasingly supersymmetric particles are found in event generators, we therefore take his opportunity to put forward the following numbering scheme for them. A seventh digit is added being: either 1 (1★★★★★★) for the partner of a boson or left-handed fermion; or 2 (1★★★★★★) for the partner of a right-handed fermion. When left-right mixing occurs the ordering should be by mass. Examples include:

1000011	$\tilde{e}_L^-$	−2000006	$\overline{\tilde{t}}_R$	1000022	$\tilde{\gamma}/\tilde{\chi}_1^0$
2000011	$\tilde{e}_R^-$	1000021	$\tilde{g}$	1000023	$\tilde{Z}^0/\tilde{\chi}_2^0$
1000012	$\tilde{\nu}_e$	1000024	$\tilde{W}^+/\tilde{\chi}_1^+$	1000025	$\tilde{H}_1^0/\tilde{\chi}_3^0$
2000006	$\tilde{t}_R$	1000037	$\tilde{H}^+/\tilde{\chi}_2^+$	1000035	$\tilde{H}_2^0/\tilde{\chi}_4^0$

$q_1 q_2 q_3$	$J = 1/2$		$J = 3/2$	
	$\star n_3 n_2 2$	$\star n_2 n_3 2$	$\star\star\star 4$	
ddd			Δ^-	111
udd		n	Δ^0	211
uud		p	Δ^+	221
uuu			Δ^{++}	222
sdd		Σ^-	$\Sigma^{\star -}$	311
sud	Λ	Σ^0	$\Sigma^{\star 0}$	321
suu		Σ^+	$\Sigma^{\star +}$	322
ssd		Ξ^-	$\Xi^{\star -}$	331
ssu		Ξ^0	$\Xi^{\star 0}$	332
sss			Ω^-	333
cdd		Σ_c^0	$\Sigma_c^{\star 0}$	411
cud	Λ_c^+	Σ_c^+	$\Sigma_c^{\star +}$	421
cuu		Σ_c^{++}	$\Sigma_c^{\star ++}$	422
csd	Ξ_c^0	$\Xi_c^{\prime 0}$	$\Xi_c^{\star 0}$	431
csu	Ξ_c^+	$\Xi_c^{\prime +}$	$\Xi_c^{\star +}$	432
css		Ω_c^0	$\Omega_c^{\star 0}$	433

$q_1 q_2 q_3$	$J = 1/2$		$J = 3/2$	
	$\star n_3 n_2 2$	$\star n_2 n_3 2$	$\star\star\star 4$	
ccd		Ξ_{cc}^+	$\Xi_{cc}^{\star +}$	441
ccu		Ξ_{cc}^{++}	$\Xi_{cc}^{\star ++}$	442
ccs		Ω_{cc}^+	$\Omega_{cc}^{\star +}$	443
ccc			$\Omega_{ccc}^{\star ++}$	444
bdd		Σ_b^-	$\Sigma_b^{\star -}$	511
bud	Λ_b^0	Σ_b^0	$\Sigma_b^{\star 0}$	521
buu		Σ_b^+	$\Sigma_b^{\star +}$	522
bsd	Ξ_b^-	$\Xi_b^{\prime -}$	$\Xi_b^{\star -}$	531
bsu	Ξ_b^0	$\Xi_b^{\prime 0}$	$\Xi_b^{\star 0}$	532
bss		Ω_b^-	$\Omega_b^{\star -}$	533
bcd	Ξ_{bc}^0	$\Xi_{bc}^{\prime 0}$	$\Xi_{bc}^{\star 0}$	541
bcu	Ξ_{bc}^+	$\Xi_{bc}^{\prime +}$	$\Xi_{bc}^{\star +}$	542
bcs	Ω_{bc}^0	$\Omega_{bc}^{\prime 0}$	$\Omega_{bc}^{\star 0}$	543
bcc		Ω_{bcc}^+	$\Omega_{bcc}^{\star +}$	544
bbd		Ξ_{bb}^-	$\Xi_{bb}^{\star -}$	551
bbu		Ξ_{bb}^0	$\Xi_{bb}^{\star 0}$	552
bbs		Ω_{bb}^-	$\Omega_{bb}^{\star -}$	553
bbc		Ω_{bbc}^0	$\Omega_{bbc}^{\star 0}$	554
bbb			$\Omega_{bbb}^{\star -}$	555

Table 10: The proposed numbering scheme for the baryons. In the first $J = 1/2$ column the order of the light quark numbers is reversed; for example Λ has number 3122 whilst Σ^0 is 3212.

The possibility of numbering potential SUSY mesons and baryons in the same spirit is left open at present.

5.2   Decay Tables

The study of identified particle production and the physics underlying the hadronization mechanism continues to be an active area of research at LEP 1. In hadronic Monte Carlo event generators final state particles are produced in two stages. Primary hadrons come directly from the clusters/strings/*etc.* that model the non-perturbative parton to hadron transition. Subsequently chains of secondary particles arise from the decays of the unstable primary hadrons. Note this separation is well defined in the context of MC programs but in reality for the short lived, strongly decaying resonances it may be only semantics.

Thus a major common component of hadronic MCs are routines to do the decay of unstable particles. These are based on the use of tabulated branching ratios and basic matrix elements, though in the case of τ's and b-hadrons specialized packages are also available. The construction of these decay tables is not a simple task and requires much per-in-spiration to fill in gaps in

present measurements [169] and deal with problematic cases. It would save much duplication of effort if one basic table could be used by all programs. This implies the ability to swap decay tables and thereby would allow some control over a (spurious) source of apparent variation in the rates of primary hadron production in the different hadronization models. A common, user friendly, interface would also enable easy maintenance and modification of the tables by users.

To achieve such a goal requires a unique way of identifying the particles, and any associated matrix elements, together with a standard format for outputting and inputting the tables. The revised PDG codes above provide a unique and logical means of identifying the particles. To identify the matrix elements we propose developing a set of standard three-digit integer codes, following the convention of table 11.

Code	Matrix Element
0	Isotropic decay
1-99	Standard codes to be agreed
≥ 100	Program specific options

Table 11: Proposed convention for matrix element codes

It is reasonable to restrict both the number of decay products to five, using zeros to complete an entry, and also numerical branching ratios to five decimal places. A more than five body decay can be stored, realistically, as a sequence of decays involving intermediate resonances. In studies involving very rare decays it is sensible to use a higher branching ratio and then apply a compensating normalization factor. It is then proposed to write out the following information,

> Number of decays listed
> Decaying particle, branching ratio, matrix element code, 1–5 decay products

using the following FORMAT statements,

```
100 FORMAT(1X,I4)
200 FORMAT(1X,I8,1X,F7.5,1X,I3,5(1X,I8))
```

An example is provided by the π^0 decays:

2								
111	0.98800	0	22	22	0	0	0	$(\pi^0 \rightarrow \gamma\gamma)$
111	0.01200	101	22	11	-11	0	0	$(\pi^0 \rightarrow \gamma e^- e^+)$

It must be recognised that b-hadrons represent a special case. In the absence of detailed knowledge about a significant fraction of their decays MC programs resort to models based

66

on partonic decays and fragmentation. Partonic decay modes may also be stored in the above format. Suppose in a $b\overline{q}$ hadron (here $\overline{q}$ may represent a diquark) the decay is $b \rightarrow cW^- \rightarrow cq_1\overline{q}_2$, this can be coded in one of two sequences either '$q_1,\overline{q}_2,c$' or '$c,\overline{q}_2,q_1$'. These two options can be exploited to refer to the two possible colour connections separately: $(c\overline{q})(q_1\overline{q}_2)$ and $(c\overline{q}_2)(q_1\overline{q})$ respectively, at the discretion of program authors[5].

It is now simply a matter of providing a .DAT file containing the decay table listed in the above format. To standardize the interface to the individual MC programs the following two subroutines are proposed:

```
**IODK(IUNIT,IFORMAT,IOPT)                    and
**MODK(IDK,BR,ME,IPRD1,IPRD2,IPRD3,IPRD4,IPRD5)
```

were ** identifies the MC program. The first is used to read IUNIT<0 or write IUNIT>0 the decay table to the given unit number with IFORMAT specifying how the particles are identified. The standard is IFORMAT=1, that is use the revised PDG codes; nonportable program specific options may include: =2 use the internal numbering or =3 use the internal character string names. Authors and users may prefer the later options as more transparent than the PDG numbers. If IOPT=1 then matrix element codes ≥ 100 (program specific) are accepted, if IOPT=0 then such codes are treated as not recognised and set to zero, isotropic decay. The subroutine **MODK is intended to allow individual lines of the table to be modified or added, before or during event generation; the arguments follow the standard format. Note that when a new mode is added or an existing branching ratio modified the sum of the remaining branching ratios should be rescaled to preserve unit sum. This means that when two modes of the same particle are altered the order of the calls is important for their resultant branching ratios.

The provision of such an interface rests with the actual program authors who need to convert between the standard format and their own internal structures. These interfaces may be expected to be robust against unrecognized or blank particle names and provide basic checks of the allowed kinematics, electric charge conservation and unit sum of branching ratios. Such an interface has been established for HERWIG and successfully used to import the JETSET decay table. However if program users do modify the provided decay tables then they must accept responsibility for them making sense.

5.3   Interfaces to electroweak generators

A number of dedicated four-fermion generators are being written for LEP 2 applications. The good ones will do the electroweak theory much better than standard general-purpose QCD generators. On the other hand, they do not contain any QCD physics aspects, i.e. neither perturbative parton showers nor nonperturbative hadronization. This makes the electroweak

---

[5]Observe that if the $V - A$ matrix element was constructed as $(p_0.p_2)(p_1.p_3)$ these would both give $(b.\overline{q}_2)(q_1.c)$.

(EW) generators well suited for some applications, such as total cross sections and leptonic final states, but generally unsuited for the study of hadronic or mixed hadronic–leptonic final states. It is therefore logical to interface them with parton-shower and hadronization programs. To some extent, this is already happening. However, in writing these interfaces there are certain dangers involved. There may also be a lot of work involved.

It would therefore be advantageous if the event generator authors involved could agree on a common approach: EW authors provide the four-fermion configuration in a standard format and QCD authors provide a standard interface that converts this to a set of final hadrons. Then only one interface needs to be written for each program, instead of one for each combination of EW and QCD programs. In this section we propose such a standard and report on progress in implementing it.

5.3.1   The basic problem

In the electroweak sector, fermions can be viewed as asymptotically free final state particles. This means that the production of a specific final state is fully calculable perturbatively. Many different intermediate states can contribute to the same final state, without any ambiguities being introduced by this. The total probability for a final state is given by squaring the sum of amplitudes

$$|A|^2 = |A_1 + A_2 + \ldots + A_n|^2 \tag{20}$$

(suppressing the issue of helicity sums, *etc.* — these aspects are not important for the general discussion). Interference effects therefore are included automatically.

QCD is different. Quarks are *not* asymptotic states. The final state consists of colour singlet hadrons, not coloured partons. The transition from perturbative to non-perturbative physics is not understood from first principles, but is at present modelled. The model used describe well what happens to a simple quark-antiquark pair, e.g. $Z^0 \to q\overline{q}$ at LEP 1. At LEP 2, four-quark states $q_1\overline{q}_2q_3\overline{q}_4$ have to be mastered. If we want to make use of our hard-won phenomenological experience, it is therefore essential that the $q_1\overline{q}_2q_3\overline{q}_4$ system can be subdivided into two colour singlet subsystems, either $q_1\overline{q}_2 + q_3\overline{q}_4$ or $q_1\overline{q}_4 + q_3\overline{q}_2$. Each subsystem can then be described in the same way as a LEP 1 event. On the contrary, if we are not allowed to use such a subdivision into singlets, a completely new hadronization formalism would have to be invented (with brand new parameters to be tuned to the LEP 2 data).

Unfortunately, there are complications. As a simple illustration, consider a system $u\overline{d}d\overline{u}$. The production obtains contributions from several possible intermediate states. One is a W^+W^- pair, with $W^+ \to u\overline{d}$ and $W^- \to d\overline{u}$. Another is a Z^0Z^0 pair, with the first $Z^0 \to u\overline{u}$ and the second $Z^0 \to d\overline{d}$. These two alternative intermediate states correspond to different colour singlets, and therefore would differ with respect to the treatment of subsequent parton showers and hadronization. That is, the final state contains a "memory" of the intermediate state. Furthermore, $|A|^2$ contains an interference term between the two alternatives, where the colour flow is not well-defined in perturbation theory. This is reflected in a relative colour factor

68

$1/(N_C^2 - 1)$ for the interference term, meaning e.g. that both $u\bar{u}$ and $u\bar{d}$ are in relative colour singlet states. Kinematical factors are not likely to compensate for the colour suppression, so numerically the interference terms may not be large. However, when the aim is to make a precision measurement of the W mass (to better than one *per mille*), one cannot rashly neglect their possible contribution. Since we know of no "correct" procedure to calculate it the reasonable approach is to adopt a "good bet" default with a method to define a "band of uncertainty".

5.3.2 Flavour and kinematics specification

It is natural to use the HEPEVT common block specification [166] to transfer flavour and kinematics information from the electroweak generator to the QCD one. After all, the HEPEVT standard was devised specifically with this kind of tasks in mind. The original standard has been changed so that real variables are given in DOUBLE PRECISION.

For the current interface, only NHEP, IDHEP and PHEP are actually mandatory. EW generator authors are invited to fill also the other information, such as mother–daughter pointers, but that is optional. Furthermore, any number of entries may be used in the event record to indicate the incoming e^+e^- pair and intermediate states, but the only objects allowed to have status code ISTHEP= 1 are the two final fermion–antifermion pairs and an arbitrary number of photons. The fermions may be interspersed with photons in the listing, but the relative order of fermions is strict:

1 one outgoing fermion, i.e. $q/\ell^-/\nu_\ell$;
2 one outgoing antifermion, i.e. $\bar{q}/\ell^+/\bar{\nu}_\ell$;
3 another outgoing fermion; and
4 another outgoing antifermion.

The pairing of the outgoing fermions and antifermions should be done so that, when W^+W^- intermediate states can contribute, the pair 1 and 2 corresponds to a possible decay of the W^+, and the pair 3 and 4 to a possible decay of the W^-. An example of an allowed order is $u\bar{d}d\bar{u}$, while $u\bar{u}d\bar{d}$ is not correct. When a W^+W^- pair cannot contribute, the ordering should be instead made consistent with the decay of of one Z^0 to the pair 1 and 2, and another Z^0 to the pair 3 and 4, e.g. $u\bar{u}c\bar{c}$. This way, coloured and uncoloured fermions can not be mixed in a pair, i.e. $ue^-\bar{\nu}_e\bar{d}$ is not an allowed ordering.

Of course, adopting the fixed order above is not crucial, but it avoids the need for QCD generators to do a lot of rearrangements, and establishes a standard for the colour flow weights in the next section.

5.3.3 Colour flow specification

As was already mentioned above, the colour flow is not uniquely specified when both outgoing fermion pairs are of quark-antiquark type. A QCD event generator is therefore required to

make a choice. We propose the following procedure.

The acceptance of a kinematical configuration by the electroweak generator (including specific helicities for some generators) is based on the total squared amplitude, $|A|^2$, so this number is available "for free". Internally, a generator has access to the subamplitudes, $A = A_1 + A_2 + \ldots + A_n$. Each subamplitude does correspond to a well-defined colour flow, so split the amplitudes into two classes, I and II, with I corresponding to colour singlets $1+2$ and $3+4$, and II to singlets $1 + 4$ and $3 + 2$. The total squared amplitude can then be written as

$$|A|^2 = |A_{\mathrm{I}} + A_{\mathrm{II}}|^2 = |A_{\mathrm{I}}|^2 + |A_{\mathrm{II}}|^2 + 2\mathrm{Re}(A_{\mathrm{I}}A_{\mathrm{II}}^*) = |A_{\mathrm{I}}|^2 + |A_{\mathrm{II}}|^2 + \Delta \ . \tag{21}$$

This subdivision should be gauge invariant.

Each electroweak event generator should return the three (positive) numbers $|A|^2$, $|A_{\mathrm{I}}|^2$ and $|A_{\mathrm{II}}|^2$. Then the colour-suppressed interference term Δ is easily found as $\Delta = |A|^2 - |A_{\mathrm{I}}|^2 - |A_{\mathrm{II}}|^2$.

A "good bet" approach to the colour assignment problem is for the QCD generator to neglect the interference term, and use the relative magnitude of $|A_{\mathrm{I}}|^2$ and $|A_{\mathrm{II}}|^2$ to make a choice at random between the two possible colour flows.

More sophisticated recipes are used for QCD processes like qg $\to$ qg in HERWIG and PYTHIA, where the interference terms are split between the non-interference ones in accordance with the pole structure. However, such an approach presupposes a detailed study for each specific combination of allowed graphs, and so cannot be part of a generic interface. Should a generator provide such a subdivision, maybe as an option, it would be easy to represent by modified numbers $|A_i|^2 \to |A_i|^2 + \Delta_i$ so that $\Delta \to \Delta - \Delta_{\mathrm{I}} - \Delta_{\mathrm{II}} = 0$.

When Δ is nonvanishing, the uncertainty can be estimated by assigning the interference terms so that either class I or class II is maximized. Specifically, class I is maximized when the choice of colour flow is based on the relative magnitude of R_{I} and R_{II}, where

$$\begin{aligned} R_{\mathrm{I}} \ &= |A_{\mathrm{I}}|^2 + \Delta \quad R_{\mathrm{II}} \ = |A_{\mathrm{II}}|^2 && \text{if } \Delta > 0 \\ &= |A_{\mathrm{I}}|^2 && = \max(0, |A_{\mathrm{II}}|^2 + \Delta) \quad \text{else} \end{aligned} \tag{22}$$

and correspondingly with I$\leftrightarrow$II for class II maximized. If the difference between these two extremes is small, then presumably the default procedure can be trusted.

5.3.4 Further problems

A number of potential problems exist, where the current approach may not be enough. These are discussed in the following.

It has implicitly been assumed that the scale of perturbative QCD parton-shower evolution is set by the mass of the respective colour singlet. An example of a process where this need not be the case is $e^+e^- \to \gamma^*/Z^0 \to u\bar{u} \to u\bar{u}Z^0 \to u\bar{u}d\bar{d}$. The $u\bar{u}$ pair here has a large original mass,

which is reduced by the emission of a Z^0. It is not clear whether the QCD radiation can be well approximated by that of the final $u\bar{u}$ mass, or whether the original mass is somehow felt e.g. by a larger rate of hard-gluon emission. A study of the matrix element for $e^+e^- \to q\bar{q} \to q\bar{q}Z^0g$ would here be necessary. However, these graphs are not expected to give a major contribution, so presumably the uncertainty from this source is not significant.

When QCD processes are introduced, interference terms need not be colour-suppressed. Specifically, the graph $e^+e^- \to \gamma^*/Z^0 \to u\bar{u} \to u\bar{u}g \to u\bar{u}d\bar{d}$ gives two colour singlets $u\bar{d}$ and $d\bar{u}$, just like a W^+W^- intermediate state would. Therefore a suppression of interference contributions has to be based entirely on kinematical considerations.

Since separation of quark and gluon jets is very difficult on an individual basis, also $q\bar{q}gg$ gives a background to four-fermion final states. Here, of course, there can be no interference with the other processes.

The addition of parton showers to a QCD four-jet event, either $q\bar{q}gg$ or $(q\bar{q}g \to)q\bar{q}q'\bar{q}'$, has to follow quite different rules from that of other four-fermion events, e.g. with respect to angular-ordering constraints in the parton shower. These rules have not yet been worked out for any of the QCD generators. The input that electroweak generators can give here is therefore not so meaningful. The main thrust in this area should be an improved matching between the matrix-element and the parton-shower strategies already present in QCD generators. Electroweak generators (if they contain QCD graphs) should therefore have the option of switching off all QCD contributions, i.e. (the amplitudes for) the graphs above.

Some further input parameter may be required to specify whether QCD showers should be allowed also to involve the emission of photons. At LEP 1 we have learned that the "competition" between photon and gluon emission is a not unimportant aspect, that tends to reduce the total amount of photon radiation compared to the no-QCD-radiation scenario. Something similar is likely to hold at LEP 2. However, the situation is far worse here, since the number of charged particles is much larger, and the presence of intermediate charged states (W^+W^-) makes a subdivision of the full emission rate much more complicated. One could therefore consider two extremes:

- If an EW generator attempts to do the full job of photon radiation from all charged legs, then the QCD generator should not add further photon radiation. In fact, if anything, one may question whether the EW generator overestimated the amount of photon radiation off the quarks.
- If an EW generator only claims to have initial-state photon radiation, then the QCD generator could add final-state radiation inside each fermion-antifermion pair (also leptons, if implemented). This would still not be the full answer, but likely to be better than having no final-state radiation at all. (Since there is no unique, gauge-independent definition of final-state γ radiation in four-fermion processes, the usefulness of such an approach should be checked from case to case.)

Traditionally, QCD generators are not good at handling the polarization of τ's in the decay treatment. This is better done by dedicated τ decay packages. Therefore EW generators that

do provide the spin of outgoing τ's should give this information for the τ entries in

    COMMON/HEPSPN/SHEP(4,NMXHEP)

using the standard conventions [166]. A flag could be set by the EW generator, and used by the QCD generator to inhibit it from decaying the τ's.

We remind the reader that the production vertices at the femtometer level may be of interest for physics such as colour reconnection and Bose-Einstein effects. If any generator should provide such output, the VHEP part of HEPEVT can be used to define vertices. The original objective was for vertices at the scale of mm, but also numbers of order 10^{-12} mm could be stored with maintained precision so long as the primary event vertex is designed to be at the origin.

5.3.5   Existing codes:

Several interfaces now exist that are based on the philosophy outlined above.
- Output from EXCALIBUR, with amplitude information for the different colour singlets. Can be obtained at
  http://wwwcn.cern.ch/~charlton/excalibur/excalibur.html.
- Input into HERWIG. Can be obtained at
  http://surya11.cern.ch/users/seymour/herwig/.
- Input into JETSET. Can be obtained at
  http://thep.lu.se/tf2/staff/torbjorn/test/main07.f.
- Input into ARIADNE. Is part of the standard ARIADNE distribution.

Further information is available in the respective files.

5.4   Systematic errors

At LEP 2, several physics issues will involve hadronized quarks, both for QCD studies and for Electroweak measurements or searches. The following can be envisaged as case studies:
- Establish the running of α_s from the Z pole to LEP 2 energies.
- Measurement of hadronic cross-sections, e.g. $e^+e^- \to Z/\gamma \to q\bar{q}$ or $e^+e^- \to W^+W^- \to q_1\bar{q}_2q_3\bar{q}_4$, and discrimination between the two.
- Reconstruction of jet-jet invariant masses in the above two processes, or even in $e^+e^- \to ZH \to q\bar{q}b\bar{b}$.

The first item seems the easiest case. α_s has been measured using a great variety of observables at the Z peak, with nearly infinite statistics. The *variation* with $\sqrt{s}$ of well defined quantities such as energy-energy correlations or their asymmetry, or jet rates for a given y_{cut} should be much less prone to systematic errors than their relationship to α_s itself.

Two difficulties can be expected here. First, the flavour composition of the sample will be different at LEP 2. In particular, the rate of $b\bar{b}$ production will decrease from 22% down to less than 10%. The fact that the specific fragmentation parameters for b quarks [170] have been measured at LEP 1 should be of great help. In order to extrapolate to higher energies, these results have to be incorporated in the simulation in one way or another. The three-jet rate has been used at the Z peak to test the universality of the strong coupling [171] with an accuracy of about 0.005. The argument can be turned around as, the sensitivity of a determination of α_s to flavour composition, leading to a rough uncertainty estimate of about 0.0005 on the difference in α_s from the Z peak to LEP 2.

The second difficulty will arise when one tries to go from establishing the running to more quantitative estimates of it. The running will be compared to the expectation from the QCD fragmentation models. Given that the most popular generators are presently based on $\mathcal{O}(\alpha_s)$ exponentiated showers, one can rightfully challenge their capability to predict the $\sqrt{s}$ evolution, because of missing higher orders. The solution to this issue will probably have to come from a better mapping of the shower models to second order matrix elements.

The impact on acceptance corrections was limited at the Z peak by two positive factors: large statistics and limited initial state radiation. A simple event rotation technique [172] was sufficient to reduce the uncertainty on event selection down to 10^{-3} or better. The precision required at LEP 2 for such studies is less stringent, statistical errors being at the level of 1%, so that the same method applied to high energy annihilation events should be adequate. One difficulty will arise from initial state radiation (ISR): the optimum sensitivity for electroweak effects is obtained by removing the radiative return to the Z peak using an s' cut. Most of the ISR photons being emitted at small angles, the invariant mass of the hadronic system has to be used to implement this cut. The issue here is to understand how accurately one can reconstruct an invariant mass from a system of boosted jets. An important experimental constraint can presumably be placed by using $e^+e^- \rightarrow Z + \gamma \rightarrow q\bar{q} + \gamma$ events. However the issue of flavour dependence will come up again here, as the mass of the b quark and missing energy from neutrinos are expected to have sizeable effects on the jet angles and energies after a boost. A similar problem will be encountered when reconstructing $W \rightarrow q\bar{q}$ invariant mass, where the difference in flavour composition is even more drastic.

Finally one last but important issue is the discrimination between $e^+e^- \rightarrow Z/\gamma \rightarrow q\bar{q}$ and $e^+e^- \rightarrow W^+W^- \rightarrow q_1\bar{q}_2 q_3\bar{q}_4$ events for the determination of the W^+W^- cross-section at threshold [173]. There is a finite probability that a four-jet event from the first process with two hard QCD-radiated partons will mimic the second process. In the present state of QCD generators with only $\mathcal{O}(\alpha_s)$ exponentiated showers, it is not obvious that the Monte Carlo gives the right answer. One way to obtain direct experimental information is to see how often a hadronic Z decay can be reconstructed as two heavy systems of 45 GeV mass and compare with the predictions of the fragmentation model. The extrapolation to the appropriate center-of-momentum energies and invariant mass requires a fragmentation Model.

In most of these problems, an experimental constraint can be found in e.g. Z decays. However every time fragmentation event generators are needed to perform the necessary extrapolations. Evaluating the corresponding systematic errors has been performed traditionally by either i) varying some (well chosen) input parameters within "reasonable limits" or ii) comparing the results obtained when using two different models. Recently, a more complex situation has emerged for the analysis of the jet charge asymmetries in Z decays [174]. This is a clear example of an electroweak measurement performed using jets. The jet charge separations are ultimately obtained from a fragmentation model, upon which many constraints are imposed: measured production spectra for pions, kaons and baryons (p and Λ), resonances such as ρ, K^* and η, average jet charge measured from opposite hemisphere charge correlation, *etc.* Imposing these constraints immediately leads to extremely strong correlations among fragmentation parameters. In JETSET, it is possible to find enough parameters to describe very completely the production of each particle species. The weak points remain the transverse momentum distributions and the baryon spectra. In HERWIG fewer parameters are available and the χ^2 is worse. Nevertheless the value of the electroweak asymmetry can be extracted for both models, with systematic errors related to the goodness of fit. A consistency check is supplied by the agreement of the values obtained from the two models within the systematics pertaining to each model. Similar procedures can be envisaged for measurements of electroweak quantities at LEP 2.

To conclude, there is no unique prescription for evaluating systematic errors. In each problem specific sources of errors and the corresponding fragmentation model parameters have to be found. Incorporating experimental constraints generally leads to very strong correlations among parameters, but this can be solved by for example using a combined linearized fit. The most general problem in extrapolating results obtained at the Z pole to LEP 2 will be the change in flavour composition. A mapping of the parton shower models to the second order matrix elements would be most useful.

6 Summary and Recommendations

It is useful to remember the last words of the LEP 1 QCD generators report [3]: *Due to the large uncertainty present in any realistic Monte Carlo, physics studies must be based on the use of at least two complete and independent programs.* Nothing has been changed in this regard; QCD is still not solved and the need for models is as large as ever.

The QCD generators of today may be considered more mature than the pre-LEP ones, in that they have successfully survived a number of experimental tests. However, there is always the danger that "incorrect" models do not just fade away — they are only modified and retuned for agreement. The increased energy lever arm provided by LEP 2 could give additional discrimination power, or at lease necessitate further fine tuning of programs.

Furthermore, in comparing with the LEP 1 data, we see that no generator is perfect. Depending on the physics area studied, it is therefore important to beware of generators with known shortcomings in that area. These shortcomings may indicate basic problems in the models, but could also come from further effects (e.g. higher-order matrix-element corrections) that authors never claimed to include. Generator authors are encouranged to sort out known problems in the light of LEP 1 experience, and in particular those with implications for LEP 2 studies. For some areas, such as colour reconnection and Bose-Einstein effects, the modelling is only in its infancy, and further efforts obviously are required.

The World Wide Web offers new opportunities to make programs accessible, including manuals, update notes, sample main programs and so on. To the extent authors did not yet adapt their distribution practices to the new opportunities, they are encouraged to do so. A common practice of having a "home page" for each generator will allow the construction of useful generator directories.

Standardization is as important as ever, in order to avoid confusion among experimentalists required to run a multitude of different codes. We have here proposed modifications to the /HEPEVT/ standard, extensions and a few corrections to the PDG particle code, a standardized decay table and an interface between electroweak four-fermion generators and QCD generators. A continued dialogue about possible standards would be very useful.

References

[1] G. Altarelli, R. Kleiss and C. Verzegnassi, Z Physics at LEP 1, CERN yellow report 89-08.

[2] R. Kleiss *et al.*, in [1], vol.3, p.1.

[3] T. Sjöstrand *et al.*, in [1], vol.3, p.143.

[4] TPC Collaboration: H. Aihara *et al.*, Zeit. Phys. **C28** (1985) 31;
J.W. Gary, Ph. D. Thesis, U. of California, LBL-20638, 1985.

[5] TASSO Collaboration: M. Althoff *et al.*, Zeit. Phys. **C26** (1984) 157 and W. Braunschweig *et al.*, Zeit. Phys. **C41** (1988) 359.

[6] OPAL Collaboration: M.Z. Akrawy *et al.*, Zeit. Phys. **C47** (1990) 505.

[7] L3 Collaboration, B. Adeva *et al.*, Zeit. Phys. **C55** (1992) 39.

[8] ALEPH Collaboration: D. Decamp *et al.*, Zeit. Phys. **C55** (1992) 209.

[9] DELPHI Collaboration: K. Hamacher *et al.*, contribution 548 to EPS HEP95, Brussels; Wuppertal Preprint WU B 95-07 and internal note DELPHI 95-80 PHYS 515.

[10] ALEPH Collaboration, contribution 449 to EPS HEP95, Brussels.

[11] M. Weierstall, Dissertation, Bergische Univ. – G.H., WUB-DIS 95-11, Wuppertal.

[12] S. Bethke *et al.* Nucl. Phys. **B370** (1992) 310.

[13] L. Lönnblad, Comp. Phys. Comm. **71** (1992) 15.

[14] G. Marchesini *et al.*, Comp. Phys. Comm. **67** (1992) 465.

[15] T. Sjöstrand, Comp. Phys. Comm. **82** (1994) 74 and Lund University report LU TP 95–20.

[16] R. Vogl, Dissertation, Universität Innsbruck, Innsbruck 1995.

[17] ALEPH Collaboration: contribution 529 to ICHEP 94, Glasgow.

[18] G. Kramer and B. Lampe, Zeit. Phys. **C39** (1989) 101;
N. Magnussen, Dissertation, Bergische Univ. – G.H., WUB-DIS 88-4, Wuppertal;
DESY int. report F22-89-01, 1989.

[19] OPAL Collaboration: contribution 319 to EPS HEP95, Brussels.

[20] D. Michelsen, H. Müller and F. Wäckerle, IEKP-KA/94-11, Karlsruhe;
F. Wäckerle, Diplomarbeit, IEKP-KA/93-19, Karlsruhe.

[21] A. De Angelis, CERN-PPE/95-135.

[22] ALEPH Collaboration: D. Busculic. *et al.*, CERN-PPE/95-96.

[23] ALEPH Collaboration: to be published, data kindly supplied by G. Rudolph.

[24] ALEPH Collaboration: D. Decamp, *et al.*, Phys. Lett. **B284** (1992) 163;
DELPHI Collaboration: P. Abreu, *et al.*, Zeit. Phys. **C59** (1993) 21;
OPAL Collaboration: P.D. Acton, *et al.*, Zeit. Phys. **C55** (1992) 11;
SLD Collaboration: F. Abe, *et al.*, Phys. Rev. **D51** (1995) 962.

[25] ALEPH Collaboration: D. Busculic, *et al.*, CERN-PPE/95-82.

[26] DELPHI Collaboration: P. Abreu *et al.*, to be published.

[27] R.D. Field and R.P. Feynman, Nucl. Phys. **B136** (1978) 1.

[28] B. Andersson, G. Gustafson, G. Ingelman and T. Sjöstrand, Phys. Rep. **97** (1983) 31.

[29] R.J. Hemingway, OPAL technical note, TN279.

[30] ALEPH Collaboration: D. Buskulic, *et al.*, CERN-PPE/95-108;
DELPHI Collaboration: P. Abreu, *et al.*, CERN-PPE/95-53;
L3 Collaboration: M. Acciarri, *et al.*, Phys. Lett. **B345** (1995) 589.

[31] ALEPH Collaboration: D. Buskulic, *et al.*, Zeit. Phys. **C62** (94) 1;
DELPHI Collaboration: P. Abreu, *et al.*, contribution xyz to ICHEP94.

[32] G.T. Jones, *et al.*, Zeit. Phys. **C27** (1985) 43;
V. Ammosov, *et al.*, Phys. Lett. **B93** (1980) 210;
EMC Collaboration: M. Arneodo, *et al.*, Zeit. Phys. **C34** (1987) 283 and Phys. Lett.
B145 (1984) 156;
N.J. Barker, *et al.*, Phys. Rev. **D34** (1986) 1251.

[33] ZEUS Collaboration: M. Derrick, *et al.*, DESY 95-084.

[34] H1 Collaboration: S. Aid, *et al.*, contribution 479 to EPS HEP95, Brussels.

[35] Y.J. Pei, "Studies of meson production in Z decays", CERN Seminar, September 6 1994
(unpublished).

[36] OPAL Collaboration: R. Akers, *et al.*, Zeit. Phys. **C63** (1994) 181.

[37] ALEPH Collaboration: D. Buskulic, *et al.*, Zeit. Phys. **C66** (1995) 355.

[38] OPAL Collaboration: G. Alexander, *et al.*, Phys. Lett. **B264** (1991) 467.

[39] DELPHI Collaboration: P. Abreu, *et al.*, Phys. Lett. **B275** (1992) 231.

[40] ALEPH Collaboration: D. Buskulic, *et al.*, CERN-PPE/95-92;
     DELPHI Collaboration: P. Abreu, *et al.*, Zeit. Phys. **C59** (1993) 533;
     OPAL Collaboration: G. Alexander, *et al.*, contribution 284 to EPS HEP95, Brussels.

[41] ALEPH Collaboration: D. Buskulic, *et al.*, CERN-PPE/95-94.

[42] DELPHI Collaboration: M. Feindt, *et al.*, contribution 563 to EPS HEP95, Brussels.

[43] L3 Collaboration: B. Adeva, *et al.*, Phys. Lett. **B288** (1992) 395.

[44] C.D. Buchanan and S.B. Chun, UCLA-HEP-95-02;
     C.D. Buchanan and S.B. Chun, Phys. Lett. **B308** (1993) 153.

[45] P.V. Chliaponikov and V.A. Uvarov, Phys. Lett. **B345** (1995) 313.

[46] M. Szczerkowski, Phys. Lett. **B359** (1995) 387.

[47] F. Becattini, Firenzi preprints: DFF 234/10/1995 and F. Becattini *et al.*, DFF
     233/10/1995.

[48] ALEPH Collaboration: D. Buskulic, *et al.*, Zeit. Phys. **C64** (1994) 361;
     DELPHI Collaboration: P. Abreu, *et al.*, Phys. Lett. **B318** (1993) 249;
     OPAL Collaboration: P.D. Acton, *et al.*, Phys. Lett. **B305** (1993) 415.

[49] SLD Collaboration: K. Abe, *et al.*, SLAC-PUB-95-6920.

[50] L3 Collaboration: M. Acciarri, *et al.*, contribution 92 to EPS HEP95, Brussels.

[51] DELPHI Collaboration: P. Abreu, *et al.*, CERN-PPE/95-28.

[52] DELPHI Collaboration: P. Abreu, *et al.*, CERN-PPE/95-39;
     L3 Collaboration: M. Acciarri, *et al.*, Phys. Lett. **B328** (1994) 223;
     OPAL Collaboration: P.D. Acton, *et al.*, Phys. Lett. **B291** (1992) 503.

[53] ALEPH Collaboration: D. Buskulic, *et al.*, Zeit. Phys. **C62** (1994) 1;
     DELPHI Collaboration, P. Abreu, *et al.*, contribution 557 to EPS HEP95, Brussels;
     OPAL Collaboration: P.D. Acton, *et al.*, CERN-PPE/94-217 and G. Alexander, *et al.*,
     contribution 284 to EPS HEP95, Brussels.

[54] ALEPH Collaboration: D. Buskulic, *et al.*, Zeit. Phys. **C62** (1994) 179;
     DELPHI Collaboration: P. Abreu, *et al.*, CERN-PPE/95-08;
     L3 Collaboration: O. Adeva, *et al.*, Phys. Lett. **B261** (1991) 177;
     OPAL Collaboration: R. Akers, *et al.*, Zeit. Phys. **C60** (1993) 199.

[55] ALEPH Collaboration: D. Buskulic, *et al.*, CERN-PPE/95-113;
     OPAL Collaboration: contribution 666 to EPS HEP95, Brussels.

[56] ALEPH Collaboration: contribution 403 to EPS HEP95, Brussels.

[57] DELPHI Collaboration: O. Podobrin, *et al.*, contribution 560 to EPS HEP95, Brussels.

[58] C. Peterson, D. Schlatter, I. Schmitt and P. Zerwas Phys. Rev. **D27** (1983) 105.

[59] S.J. Brodsky and J. Gunion, Phys. Rev. Lett. **37** (1976) 402;
K. Konishi, A. Ukawa and G. Veneziano, Phys. Lett. **B78** (1978) 243.

[60] M.B. Einhorn and B.G. Weeks, Nucl. Phys. **B146** (1978) 445.

[61] J.W. Gary, Phys. Rev. **D49** (1994) 4503.

[62] OPAL Collaboration: G. Alexander, *et al.*, Phys. Lett. **B265** (1991) 462 and P.D. Acton, *et al.*, Zeit. Phys. **C58** (1993) 387.

[63] DELPHI Collaboration: CERN-PPE/95-164.

[64] OPAL Collaboration: G. Alexander, *et al.*, CERN-PPE/95-126.

[65] OPAL Collaboration: R. Akers, *et al.*, Zeit. Phys. **C68** (1995) 179.

[66] ALEPH Collaboration: D. Buskulic, *et al.*, Phys. Lett. **B346** (1995) 389.

[67] S. Catani, Yu. Dokshitzer, F. Fiorani and B.R. Webber, Nucl. Phys. **B383** (1992) 419.

[68] ALEPH Collaboration: contribution 589 to EPS HEP95, Brussels.

[69] C. Peterson and T.F. Walsh, Phys. Lett. **B91** (1980) 455.

[70] Yu. Dokshitzer, V.A. Khoze, S.I. Troyan and A.H. Mueller, Rev. Mod. Phys. **60** (1988) 373 and Basics of Perturbative QCD, Editions Frontières, Paris, 1991.

[71] B.I. Ermolaev and V.S. Fadin, JETP Lett. **33** (1981) 269;
A.H. Mueller, Phys. Lett. **B104** (1981) 161;
A. Bassetto, M. Ciafaloni, G. Marchesini and A.H. Mueller, Nucl. Phys. **B207** (1982) 189;
G. Marchesini and B.R. Webber, Nucl. Phys. **B238** (1984) 1.

[72] R. Odorico, Comp. Phys. Comm. **72** (1992) 235.

[73] D. Amati and G. Veneziano, Phys. Lett. **83B** (1979) 87.

[74] Ya.I. Azimov, Yu.L. Dokshitzer, V.A. Khoze and S.I. Troyan, Zeit. Phys. **C27** (1985) 65.

[75] Ya.I. Azimov, Yu.L. Dokshitzer, V.A. Khoze and S.I. Troyan, Phys. Lett. **B165** (1985) 147.

[76] B. Andersson, G. Gustafson and T. Sjöstrand, Phys. Lett. **B94** (1980) 211.

[77] JADE Collaboration: W. Bartel, *et al.*, Phys. Lett. **B101** (1981) 129.

[78] L3 Collaboration: M. Acciarri, *et al.*, Phys. Lett. **B345** (1995) 74.

[79] OPAL Collaboration: CERN-PPE/95-83.

[80] ALEPH Collaboration: contribution 518 to EPS HEP95, Brussels.

[81] CDF Collaboration: F. Abe, *et al.*, Phys. Rev. **D50** (1994) 5562.

[82] Yu.L. Dokshitzer, V.A. Khoze and S.I. Troyan, Zeit. Phys. **C** (1992) 107.

[83] OPAL Collaboration: R. Akers, *et al.*, Zeit. Phys. **C68** (1995) 1.

[84] L3 Collaboration: O. Adriani, *et al.*, Phys. Rep. **236** (1993) 1.

[85] OPAL Collaboration: R. Akers, *et al.*, Zeit. Phys. **C63** (1994) 363.

[86] B.A. Schumm, Yu.L. Dokshitzer, V.A. Khoze and D.S. Koetke, Phys. Rev. Lett. **69** (1992) 3025.

[87] V.A. Petrov and A.V. Kisselev, Zeit. Phys. **C66** (1995) 453.

[88] DELPHI Collaboration: P. Abreu, *et al.*, Phys. Lett. **B347** (1995) 447.

[89] OPAL Collaboration: R. Akers, *et al.*, Phys. Lett. **B352** (1995) 176.

[90] SLD Collaboration: SLAC-PUB-95-6924.

[91] OPAL Collaboration: P.D. Acton, *et al.*, Zeit. Phys. **C58** (1993) 207.

[92] ALEPH Collaboration: contribution 455 to EPS HEP95, Brussels.

[93] Yu.L. Dokshitzer, *et al.*, Phys. Lett. **B245** (1990) 243.

[94] Yu.L. Dokshitzer, *et al.*, Nucl. Phys. **B387** (1992) 675.

[95] M. Chmeissani, ALEPH internal note 93-097.

[96] Aly Aamer Syed, Ph.D. thesis, Univ. of Nijmegen (1994), ISBN 90-9007038-9.

[97] L3 Collaboration: M. Acciarri, *et al.*, Phys. Lett. **B353** (1995) 145.

[98] OPAL Collaboration: G. Alexander, *et al.*, Phys. Lett. **B264** (1991) 219.

[99] ALEPH Collaboration: D. Buskulic, *et al.*, Zeit. Phys. **C57** (1993) 17;
L3 Collaboration: O. Adriani, *et al.*, Phys. Lett. **B292** (1992) 472;
OPAL Collaboration: P.D. Acton, *et al.*, Zeit. Phys. **C58** (1993) 405.

[100] M.H. Seymour, Lund preprint, LU TP 94-6.

[101] DELPHI Collaboration: P. Abreu, *et al.*, CERN-PPE/95-101.

[102] ALEPH Collaboration: D. Buskulic, *et al.*, CERN-PPE/95-089.

[103] S. Cartwright, Workshop on Photon Radiation from Quarks, CERN yellow report 92-04.

[104] P. Perez, in [103] p.14;
F. Marion, *ibid.* ,p.97.

[105] D. Kirkby, in Perturbative QCD and Hadronic Interactions, ed. J. Tran Thanh Van,
Editions Frontières, 1995 and A study of Final-State Radiation in Hadronic Z Decays,
Ph.D. thesis, California Institute of Technology, September 1995.

[106] ALEPH Collaboration: D. Decamp, *et al.*, Zeit. Phys. **C54** (1992) 75;
DELPHI Collaboration: P. Abreu, *et al.*, Phys. Lett. **B286** (1992) 201 and Zeit. Phys.
C63 (1994) 17;
OPAL Collaboration: P.D. Acton, *et al.*, Phys. Lett. **B267** (1991) 143.

[107] S. Haywood, RAL-94-074.

[108] E.A. de Wolf, in Multiparticle Dynamics 1994, eds. A. Giovannini *et al.*, World Scientific,
Singapore, 1995, p. 15;
Y.F. Wang, L3 Internal Note 1621, 1994.

[109] ALEPH Collaboration: D. Buskulic, *et al.*, Zeit. Phys. **C64** (1994) 361;
DELPHI Collaboration: P. Abreu, *et al.*, contribution to ICHEP94, Glasgow;
OPAL Collaboration: R. Akers, *et al.*, CERN-PPE/95-024.

[110] DELPHI Collaboration: P.Abreu *etal.*, Phys. Lett. **B355** (1995) 415.

[111] ALEPH Collaboration: D. Buskulic, *et al.*, CERN-PPE/95-100;
DELPHI Collaboration: P. Abreu, *et al.*, Phys. Lett. **B298** (1993) 236, Zeit. Phys. **C65**
(1995) 587 and Zeit. Phys. **C63** (1994) 17;
OPAL Collaboration: P.D. Acton, *et al.*, Zeit. Phys. **C56** (1992) 521.

[112] K. Münich, Diplomarbeit, Bergische Univ. – GH, WU-D 95-5, Wuppertal.

[113] B. Andersson, Presented at the 25th International Symposium on Multiparticle Dynamics,
Stara Lesna, 1995.

[114] S. Brandt, *et al.*, Phys. Lett. **12** (1964) 57;
E. Fahri, Phys. Rev. Lett. **39** (1977) 1587.

[115] A. De Rújula, *et al.*, Nucl. Phys. **B138** (1979) 387.

[116] S. Catani, *et al.*, Phys. Lett. **B269** (1991) 432.

[117] T. Chandramohan and L. Clavelli, Nucl. Phys. **B184** (1981) 365;
L. Clavelli and D. Wyler, Phys. Lett. **B103** (1981) 383.

[118] S. Catani, G. Turnock and B.R. Webber, Phys. Lett. **B295** (1992) 269.

[119] J.D. Bjorken and S.J. Brodsky, Phys. Rev. **D1** (1970) 1416;
SLAC-LBL Collaboration: G. Hanson, *et al.*, Phys. Rev. Lett. **35** (1975) 1609.

[120] PLUTO Collaboration: C. Berger, *et al.*, Phys. Lett. **B82** (1979) 449.

[121] O. Nachtmann and A. Reiter, Zeit. Phys. **C16** (1982) 45;
M. Bengtsson, Zeit. Phys. **C42** (1989) 75.

[122] G. Gustafson, Phys. Lett. **B175** (1986) 453;
G. Gustafson and U. Pettersson, Nucl. Phys. **B306** (1988) 746.

[123] B. Andersson, G. Gustafson and L. Lönnblad, Nucl. Phys. **B339** (1990) 393.

[124] OPAL Collaboration: R. Akers, *et al.*, Phys. Lett. **B353** (1995) 595.

[125] M.H. Seymour, Nucl. Phys. **B436** (1995) 163.

[126] L. Lönnblad, in [103] p.109.

[127] L. Lönnblad, CERN-TH/95-218.

[128] R. Odorico, Comp. Phys. Comm. **72** (1992) 238.

[129] P. Mazzanti and R. Odorico, Zeit. Phys. **C59** (1993) 273.

[130] G. Marchesini and B.R. Webber in [1] vol.3, p.235.

[131] T. Sjöstrand, *et al.*, in [1] vol.3, p.325.

[132] F. James, Comp. Phys. Comm. **60** (1990) 329.

[133] R. Kleiss, *et al.*, in [1] vol.3, p.129.

[134] H. Burkhardt, *et al.*, Zeit. Phys. **C43** (1989) 497.

[135] Z. Kunszt, private communication.

[136] M.H. Seymour, Phys. Lett. **B354** (1995) 409.

[137] G. Marchesini and B.R. Webber, Nucl. Phys. **B330** (1990) 271.

[138] G. Marchesini and B.R. Webber, Nucl. Phys. **B310** (1988) 461.

[139] I.G. Knowles, Nucl. Phys. **B310** (1988) 571 and Comp. Phys. Comm. **58** (1990) 271.

[140] S. Catani, B.R. Webber and G. Marchesini, Nucl. Phys. **B349** (1991) 635.

[141] M.H. Seymour, Zeit. Phys. **C56** (1992) 161.

[142] R. Kleiss, Phys. Lett. **B180** (1986) 400.

[143] M.H. Seymour, Comp. Phys. Comm. **90** (1995) 95.

[144] B.R. Webber, Nucl. Phys. **B238** (1984) 492.

[145] A. Ali and B van Eijk, in [1] vol.3, p.226.

[146] Available by kind permision from the CLEO Collaboration.

[147] K.Kato and T.Munehisa, Comp. Phys. Comm. **64** (1991) 67.

[148] K.B.Lee, *et al.*, Phys. Lett. **B313** (1993) 469;
Y.Ohnishi, *et al.*, Phys. Lett. **B313** (1993) 475.

[149] G.A. Schuler and T. Sjöstrand, Nucl. Phys. **B407** (1993) 539 and in Two-Photon Physics from DAΦNE to LEP200 and Beyond, World Scientific, Singapore, 1994, eds. F. Kapusta and J. Parisi, p. 163.

[150] G.A. Schuler and T. Sjöstrand, Zeit. Phys. **C68** (1995) 607.

[151] T. Sjöstrand, Phys. Lett. **157B** (1985) 321.

[152] L. Lönnblad and T. Sjöstrand, Phys. Lett. **B351** (1995) 293.

[153] B. Andersson, G. Gustafson and B. Söderberg, Zeit. Phys. **C20** (1983) 317.

[154] G. Gustafson, U. Pettersson and P. Zerwas, Phys. Lett. **B209** (1988) 90.

[155] T. Sjöstrand and V.A. Khoze, Phys. Rev. Lett. **72** (1994) 28 and Zeit. Phys. **C62** (1994) 281.

[156] G. Gustafson and J. Häkkinen, Zeit. Phys. **C64** (1994) 659.

[157] B. Andersson, P. Dahlqvist and G. Gustafson, Phys. Lett. **B214** (1988) 604 and Zeit. Phys. **C44** (1989) 455.

[158] Yu.L. Dokshitzer, V.A. Khoze, L.H. Orr and W.J. Stirling, Nucl. Phys. **B403** (1993) 65.

[159] R.K. Ellis, D.A. Ross and A.E. Terrano, Nucl. Phys. **B178** (1981) 421.

[160] Z. Kunszt, P. Nason, G. Marchesini and B.R. Webber, in [1] vol.1, p.373.

[161] Z. Kunszt and P. Nason, unpublished.

[162] W.T. Giele and E.W.N. Glover, Phys. Rev. **D46** (1992) 1980.

[163] S. Catani and M.H. Seymour, in preparation.

[164] E.B. Zijlstra and W.L. van Neerven, Nucl. Phys. **B383** (1992) 525.

[165] QCD working group: P. Nason, *et al.*, these proceedings.

[166] T. Sjöstrand, *et al.*, in [1] vol.3, p.327.

[167] Particle Data Group: G.P. Yost, *et al.*, Phys. Lett. **B204** (1988) 113;
T. Sjöstrand, *et al.*, in [1] vol.3, p.326.

[168] L. Garren, URL `http://fnpspa.fnal.gov/stdhep_manual.ps`.

[169] Particle Data Group: M. Aguilar-Benitez, *et al.*, Phys. Rev. **D50** (1994) 1173.

[170] ALEPH Collaboration: D. Buskulic, *et al.*, CERN-PPE/95-113;
DELPHI Collaboration: P. Abreu, *et al.*, Phys. Lett. **B347** (1995) 447;
OPAL Collaboration: R. Akers, *etal.*, Phys. Lett. **B352** (1995) 176, Zeit. Phys. **C65** (1995) 31 and G. Alexander *et al.*, CERN-PPE/95-126.

[171] ALEPH Collaboration: D. Buskulic, *et al.*, Phys. Lett. **B355** (1995) 381;
DELPHI Collaboration: P. Abreu, *et al.*, Phys. Lett. **B307** (1993) 221;
OPAL Collaboration: R. Akers *et al.*, Zeit. Phys. **C65** (1995) 31.

[172] ALEPH Collaboration: D. Buskulic, *et al.*, Zeit. Phys. **C62** (1994) 539.

[173] W mass working group: Z. Kunszt, *et al.*, these proceedings.

[174] ALEPH Collaboration: D. Decamp, *et al.*, Phys. Lett. **B259** (1991) 377 and contribution 449 to EPS HEP95, Brussels;
DELPHI Collaboration: P. Abreu, *et al.*, Phys. Lett. **B307** (1993) 221;
OPAL Collaboration: P.D. Acton *et al.*, Phys. Lett. **B294** (1992) 436 and internal physics note PN195 (1995).

γγ Event Generators

Conveners: Leif Lönnblad, Mike Seymour

Working group: Edouard Boudinov, Jon Butterworth, Ralph Engel, Alex Finch, Suen Hou, Maria Kienzle-Focacci, Mark Lehto, Ed McKigney, David Miller, Denis Perret-Gallix, Johannes Ranft, Gerhard Schuler, Torbjörn Sjöstrand, Rod Walker, Alison Wright.

Contents

1 Introduction

At LEP 2, two-photon collisions make up by far the largest class of events. These are processes in which the incoming electrons each radiate a photon, which collide to produce a hadronic or leptonic final state. A photon can obviously interact electromagnetically with any charged object. However, since it has the same quantum numbers as a vector meson, it can fluctuate into one, and can therefore also be considered as an incoming hadron, interacting strongly through its partonic constituents. The interplay between these two ways of interacting is unique to the photon and provides much of the interest in $\gamma\gamma$ physics.

The two-photon invariant mass spectrum is peaked at low mass, so the bulk of events only produce a few particles, and resonances and exclusive final states can be studied. The total cross-section is so large however, that there are enough events to study deep inelastic $e\gamma$ scattering and high-$p_\perp$ jets and heavy quark production in $\gamma\gamma$ collisions.

LEP 2 is the highest energy and luminosity $e\gamma$ and $\gamma\gamma$ collider available, and many of the same studies as at electron-hadron and hadron-hadron colliders can be made here. However, one essential difference is that, since the beam remnants (the electrons and positrons) typically leave the detectors undetected, the energies of the incoming photons are not known and must be reconstructed from the properties of the final state. In events in which most of the final-state particles are visible in the detector, this is easily done. However, at high energies the final-state distribution becomes increasingly forward-peaked and much of the energy goes into the very forward parts of the detector, or is even missed in the beam pipe. It is therefore essential that as much of the final state as possible is measured, in particular to detect hadrons in the forward detectors that have hitherto only been used for electron tagging.

It is also essential that we are able to understand the details of the multi-particle final states in these interactions, which puts very high demands on the event generators used in the analysis. During the course of this workshop, some of the standard general purpose event generator programs on the market have been developed to also handle $e\gamma$ and $\gamma\gamma$ collisions. This means that we can use our experience from ep and pp collisions to give a more complete description of the hadronic final state of two-photon collisions. These models can now be tested at LEP 1 and should give reliable extrapolations to LEP 2 energy.

In section 2 of this report, we will describe briefly the models of the generators we have studied during the workshop. Then, in section 3 some comparisons between the programs are presented for different classes of events. In section 4, the main programs are presented in some detail, followed by section 5 where some other generators are presented more briefly. Finally in section 6 we present our conclusions. Related work is presented in the reports of the "$\gamma\gamma$ Physics" [1] and "QCD Event Generator" [2] working groups.

2   General Features

The event generators used for $\gamma\gamma$ physics can be divided into two main groups. One deals with low multiplicity final states, like resonances, exclusive channels and leptonic channels and the other with high mass multi-particle final states.

When there are few particles in the final state, the fully differential cross-section for a given process can usually be derived directly from a model of that process. Event generators can then be viewed as a particularly convenient numerical implementation of that cross-section, in which arbitrarily complicated phase-space cuts and detector simulation can be incorporated. In this group are 'four-fermion generators', which incorporate the full set of QED matrix elements for $\mathrm{e^+e^-} \to \mathrm{e^+e^- f\bar{f}}$, and more general programs that use a $\gamma\gamma$ luminosity function to separate the process $\mathrm{e^+e^-} \to \mathrm{e^+e^- X}$ into two stages, $\mathrm{e^+e^-} \to \mathrm{e^+e^-}\gamma\gamma$ and $\gamma\gamma \to \mathrm{X}$.

The other group of generators describe multi-particle production, for which cross-sections cannot be directly calculated in quantum mechanics. They use semi-classical probabilistic models to separate the process into several phases. First photons are radiated from the incoming electrons to give beams of quasi-real photons. Then a hard sub-process is generated, using partonic $2 \to 2$ matrix elements folded with the parton densities of the photon. The emission of additional partons from the incoming partons is generated by evolving them "backwards" in an initial-state parton shower, and from outgoing partons by generating a final-state parton shower. Finally, the partons are converted to hadrons, which are then allowed to decay.

2.1   Photon generation

A two-photon reaction can be factorized into photon fluxes of radiation from incoming $\mathrm{e^\pm}$ and the final state of two-photon collisions. The decomposed differential cross-section for

$$\mathrm{e^+}(p_1)\mathrm{e^-}(p_2) \to \mathrm{e^+}(p_1')\mathrm{e^-}(p_2')\gamma(q_1)\gamma(q_2) \to \mathrm{e^+}(p_1')\mathrm{e^-}(p_2')\mathrm{X}(q_1 + q_2) \tag{1}$$

is [3–5]

$$\begin{aligned}
d\sigma &= \frac{\alpha^2}{16\pi^4 q_1^2 q_2^2} \left(\frac{(q_1 q_2)^2 - q_1^2 q_2^2}{(p_1 p_2)^2 - m_1^2 m_2^2} \right)^{1/2} \left(4\rho_1^{++}\rho_2^{++}\sigma_{TT} + 2|\rho_1^{+-}\rho_2^{+-}|\tau_{TT}\cos(2\tilde{\phi}) \right. \\
&\quad \left. + 2\rho_1^{++}\rho_2^{00}\sigma_{TL} + 2\rho_1^{00}\rho_2^{++}\sigma_{LT} + \rho_1^{00}\rho_2^{00}\sigma_{LL} - 8|\rho_1^{+0}\rho_2^{+0}|\tau_{TL}\cos(\tilde{\phi}) \right) \frac{d^3 p_1'}{E_1'} \frac{d^3 p_2'}{E_2'}, \tag{2}
\end{aligned}$$

where the σ's and τ's are linear combinations of the cross-sections for $\gamma\gamma \to X$ of transverse(T) and longitudinal(L) photons, the flux factor ρ_i^{ab} has photon helicities labelled by $+, -, 0$. Some dedicated $\gamma\gamma$ generators such as Twogam [6] use the full form of Eq. 2, while most models simplify further by taking the $q^2 \to 0$ approximation. At $q^2 \to 0$, the photons are quasi-real and transversely polarized and after integration over $\tilde{\phi}$, the angle between lepton scattering

planes, the only remaining term is σ_{TT}. Expressed in terms of a luminosity function we have

$$\sigma(e^+e^- \to e^+e^- X) = \frac{d^4\mathcal{L}_{\gamma\gamma}}{d\omega_1 d\omega_2 d\theta_1 d\theta_2}\sigma_{TT}, \tag{3}$$

where $w_i = E_b - E'_i$ is the photon energy in the lab frame. The luminosity function can be decomposed as the product of a factor for each of the photons,

$$\frac{d^4\mathcal{L}_{\gamma\gamma}}{d\omega_1 d\omega_2 d\theta_1 d\theta_2} = \frac{d^2\mathcal{L}_{\gamma}}{d\omega_1 d\theta_1} \frac{d^2\mathcal{L}_{\gamma}}{d\omega_2 d\theta_2}, \tag{4}$$

where, apart from a trivial kinematic factor, $d^2\mathcal{L}$ is the Equivalent Photon Approximation (EPA) flux factor,

$$\frac{d^2\mathcal{L}_{\gamma}}{d\omega d\theta} = 2p_t\, f(x, P^2), \tag{5}$$

with x the light-cone momentum fraction and P^2 the photon virtuality, $P^2 = |q^2|$. As discussed in Ref. [7], there are two important corrections to the usual EPA formula. The first is to include the sub-leading term of relative order m_e^2/P^2,

$$f_{\gamma/e}(x, P^2) = \frac{\alpha}{2\pi}\left(\frac{1 + (1-x)^2}{xP^2} - 2m_e^2\frac{x}{P^4}\right), \tag{6}$$

which can give corrections of order 10% for untagged and anti-tagged cross-sections. At present, of the QCD event generators, only PHOJET includes this correction. The second important correction is to include the correct, process-dependent, dynamic upper limit on P^2. However, this is only important for untagged cross-sections, and when an anti-tag condition is imposed, as it is throughout this report, this corrections become small.

2.2   Photon distribution functions

In resolved-photon processes we need parametrizations of the distribution functions for partons inside the photon. These obey an inhomogeneous form of the usual evolution equations. As discussed in more detail in the report of the "$\gamma\gamma$ Physics" working group [1], their solution can be written as the sum of a hadronic or VMD part, which evolves according the usual homogeneous equation, and a point-like or anomalous part.

There are a number of parametrizations available for the parton distribution functions of on-shell photons. Most of them are contained in a single package, PDFLIB [8], to which most of the event generators are interfaced. At present none use the recent models of the structure of virtual photons, although HERWIG does implement a simple P^2-suppression model. In the following when comparing different generators, we use the fairly similar SaS 1D [9] or GRV LO [10] sets.

direct	$\gamma\gamma \to q\bar{q}$
single resolved	$\gamma q \to qg$
	$\gamma g \to q\bar{q}$
double resolved	$qq' \to qq'$
	$gg \to q\bar{q}$
	$\vdots$
DIS	$eq \to eq$

Table 1: *The standard hard sub-processes used by event generators for different event classes*

2.3   Hard sub-processes

Having defined the structure functions and parton densities, we can now use the same machinery as for pp or ep collisions to generate hard sub-processes, with the exception that we here have additional processes where the photon couples directly in the hard interaction. In $\gamma\gamma$ collisions we therefore talk about three kinds of events, direct, single-resolved and double resolved, depending on whether the photons couple directly or not. In Table 1 the standard hard sub-processes are listed for different event classes. Some programs, like PYTHIA, make a further distinction between the anomalous and VMD–like part of the resolved photon and therefore have six different event classes.

In deep inelastic $e\gamma$ scattering, the exchanged photon is usually more virtual than the struck quark, so the EPA is no longer a good approximation (in other words the process-dependent dynamic upper limit on P^2 mentioned in Section 2.1 is exceeded). One therefore needs, in principle, to use the full $2 \to 3$ processes eq $\to$ eqg, eg $\to$ eq$\bar{q}$ and eγ $\to$ eq$\bar{q}$. However, when the quark line is much less virtual than the photon, it can be approximated by the DGLAP probability distribution to find the quark inside a higher-x quark, q $\to$ qg, gluon, g $\to$ q$\bar{q}$ or photon, γ $\to$ q$\bar{q}$ and hence can be absorbed into the evolution of the photon distribution functions. Thus we are again left with a $2 \to 2$ process, eq $\to$ eq, for which one uses the lowest-order matrix element.

Other processes that are usually treated separately are the ones involving heavy quarks, where the matrix elements are different from the massless case. Here there are also event generators that use the next-to-leading order matrix elements, incorporating one additional parton. These can be considered as an exact treatment of the first step of a parton shower and can be compared with the usual algorithms discussed below, which contain approximate treatments of all steps.

2.4   Soft processes

The cross-section for quasi-real $\gamma\gamma$ scattering is dominated by processes in which there is no hard scale. Several models exist for the subdivision of the soft cross-section into separate components, typically: elastic, $\gamma\gamma \to$ VV; single diffractive dissociation, $\gamma\gamma \to$ VX; double diffractive dissociation, $\gamma\gamma \to$ XX; and inelastic, $\gamma\gamma \to$ X. The cross-section for each is given by the model, and the total cross-section is simply their sum. Clearly the separation is model specific, for example the difference between diffractive dissociation and inelastic scattering is the presence of a rapidity gap between the two systems in the former and not in the latter and the cross-sections depend on the size of this gap, and only the sum of the processes can be directly compared between models. Nevertheless, the available models use fairly similar definitions and comparisons between components can prove useful. Since most of these reaction types cannot be calculated from first principles, they are characterized by a rather large number of adjustable parameters. Nevertheless, since the models assume photon-hadron duality and hadron universality, parameters can be fixed in hadron-hadron and photon-hadron collisions, giving parameter-free predictions for LEP 2. PHOJET and PYTHIA contain rather complete soft interaction models, while HERWIG contains only the non-diffractive part of the cross-section.

2.5   Multiple interactions

At increasing centre-of-mass energies most sub-process cross-sections grow faster than the total cross-section, eventually overtaking it. Important examples include (supercritical) soft pomeron exchange and hard two-parton scattering above any given $p_{t\min}$ cut. This corresponds to the possibility of *multiple* soft or hard scatterings within a single $\gamma\gamma$ collision. At present only PHOJET implements both soft and hard multiple scattering in the same package with $p_{t\min}$ forming the boundary between the two. PYTHIA and HERWIG (through an interface to the JIMMY generator) both implement multiple hard scattering above $p_{t\min}$, but with soft models that do not vary with $p_{t\min}$, so that it becomes a critical parameter of the model. Although the general ideas of the models are similar, there are many specific differences in their implementation. For example, the current models only allow multiple interactions in the hadronic cross-section, but since the definition of anomalous and hadronic events differs (see below), so do the multiple scattering results. In all three cases however, the models are essentially identical for $\gamma\gamma$ and γp collisions, so experience gained at HERA will certainly help constrain the predictions for LEP 2.

2.6   Parton showers

The hard scattering disturbs the colour fields of the incoming partons and as a result they partially 'shake off' the cloud of gluons that normally surrounds colour charges. This gives rise to a shower of accompanying radiation, which is conventionally modelled as a series of emissions from the incoming parton, starting from the parton entering the hard interaction and tracing

its history back towards the incoming photon. During this 'backwards evolution', the emission at each step is required to be at a lower scale than the previous one until, near the incoming photon, no more radiation is resolvable above the infrared cutoff. This procedure is governed by the splitting functions of the DGLAP evolution equation and is guided by the input set of parton distribution functions.

This is the way it is done in the two standard generators HERWIG and PYTHIA where the main difference between the two is the choice of evolution, or ordering variable – PYTHIA uses the virtuality of the evolving parton, while HERWIG uses a generalized emission angle, which incorporates colour-coherence effects.

Another important difference between the two programs is the way they distinguish between the anomalous and VMD–like part of the structure functions. In PYTHIA this distinction is done beforehand, and the shower is identical in both cases, only using different parton densities corresponding to the two parts of the structure functions. In HERWIG, however, the two parts are treated together, and an additional branching is introduced into the parton shower, where a quark may be evolved back to the incoming photon. If this happens before the shower is cut off, the event is called anomalous, if not, it is a VMD–like event. In both cases, the photon remnant will have a larger transverse momentum in the anomalous case — this is automatic in the perturbative treatment of HERWIG, while in PYTHIA it is put in by hand.

In both programs the generated partons may continue to branch in a final-state shower, in the same way as is done in e^+e^- annihilation. This is discussed in more detail in the report from the "QCD generator" group [2].

In contrast to HERWIG and PYTHIA, which use backward-evolution algorithms, the GGPS1 and GGPS2 programs evolve forwards, i.e. upwards in scale toward the hard process. This has the advantage that the evolution of the structure function is generated by the Monte Carlo algorithm itself, allowing a non-trivial test, whereas backward evolution is guaranteed to reproduce whatever distribution function is input. Like most implementations of forward evolution, GGPS1 and GGPS2 produce weighted events, which can be inconvenient for detector simulation. Forward evolution can also be extremely inefficient, particularly at small x, but this problem is solved in GGPS1 and GGPS2, as described in Section 4.3.

In the Dipole Cascade Model, implemented in the ARIADNE program, there is no explicit initial state radiation. Instead, in DIS, all gluon emissions are described in terms of dipole radiation from the colour dipole between the struck quark and the photon remnant. The radiation is suppressed in the remnant direction because of its spatial extension.

2.7 Hadronization

The hadronization of the produced partons is done according to the Lund string fragmentation model [11] except in HERWIG, where a cluster fragmentation model is used [12]. Both these models are explained in detail in the report from the "QCD generator" group [2].

The difference in hadronization between $\gamma\gamma$ and e^+e^- events is the presence of the photon remnant in the former. In PYTHIA the remnant is taken to be a single parton (optionally quark and an antiquark in case a gluon is taken out of the photon) which is treated like any other parton. In HERWIG, however, the cluster containing the remnant is treated a bit differently from the others as described in section 4.4.

The hadrons are subsequently decayed. Those produced by the hadronization process are generally taken to be unpolarized and thus decay according to pure phase-space, with standard decay tables as described in Ref. [2]. On the other hand, when vector mesons are produced elastically they are strongly transverse polarized, so they are decayed accordingly, with the two pions predominantly taking similar energies.

3   Comparisons

In the following, we will compare the predictions for LEP 2 of different generators for different kinds of processes. Unless specified otherwise, comparisons are made on the generator level, using a beam energy of 87.5 GeV, a total integrated luminosity of 500 pb^{-1} and requiring at least an invariant mass of 2 GeV of particles in the region $|\cos\theta| < 0.97$.

3.1   Exclusive channels and resonances

Lepton pair production, $e^+e^- \to e^+e^-\ell^+\ell^-$ is well described by the exact matrix elements, which are dominated by the multiperipheral diagram. In terms of the luminosity function, the lepton pair production is given by the QED structure function for $\gamma\gamma \to \ell^+\ell^-$. We have compared muon pair production by PC [13] applying the luminosity function to the exact calculations of matrix elements by DIAG36 [14] and Vermaseren [15]. The mass threshold imposed on the pair is $W > 300$ MeV. The distributions of $Q^2 = \max(-q_1^2, -q_2^2)$ and W obtained are shown in Fig. 1.

The cross-section of $\gamma\gamma \to R$ for a narrow resonance of spin-J is given by [3,16]

$$\sigma(\gamma\gamma \to R) = 8\pi(2J+1)F^2(q_1^2, q_2^2)\frac{\Gamma_{\gamma\gamma}\Gamma}{(m_R^2 - W^2)^2 + m_R^2\Gamma^2}. \tag{7}$$

Here the resonance has mass m_R, radiative width $\Gamma_{\gamma\gamma}$, and energy dependent width Γ. For a wide resonance the Breit-Wigner term of Eq. 7 is multiplied by $(m_R/W)^n$ [16], with $n=1,2$ for the resonance decaying into two, three stable particles respectively. The q^2 dependence is given by the form factor function that satisfies $F^2(0,0) = 1$. The VMD model predicts

$$F^2(q_1^2, q_2^2) = \sum_{V_1, V_2} \frac{A_{V_1}}{(1 - q_1^2/m_{V_1}^2)^2} \frac{A_{V_2}}{(1 - q_2^2/m_{V_2}^2)^2}, \qquad \sum_V A_V \equiv 1, \qquad V = \rho, \omega, \phi, J/\psi \ldots \tag{8}$$

8
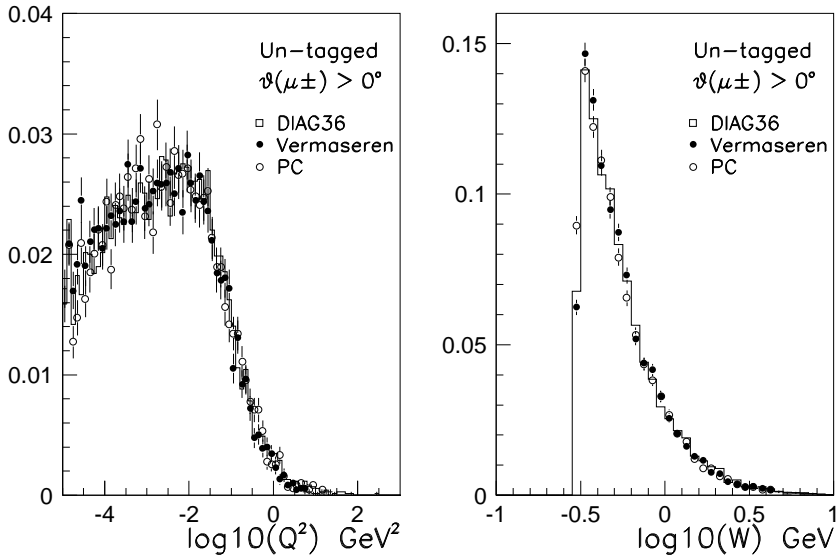
Figure 1: *The Q^2 and W distributions of $e^+e^- \to e^+e^-\mu^+\mu^-$ at $\sqrt{s} = m_Z$.*
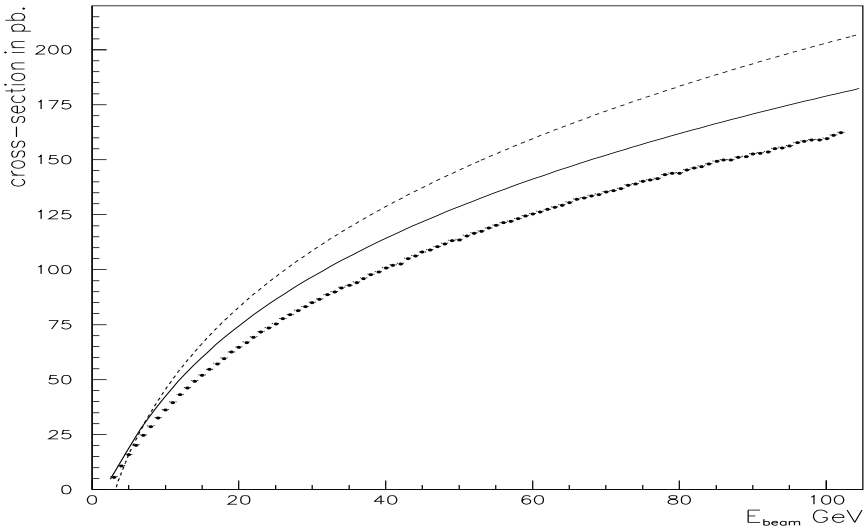
Figure 2: *The η_c cross-section versus beam energy: Low approximation, dashed; narrow-width approximation, solid;* RESPRO *results, points.*

In generating two-photon resonances, the mass spectrum is the product of the Breit-Wigner distribution and the two-photon invariant mass spectrum obtained from the luminosity function. The decay products are further described by the matrix element according to the spin-parity and helicity state that couple to the angular distributions of the final state particles.

9
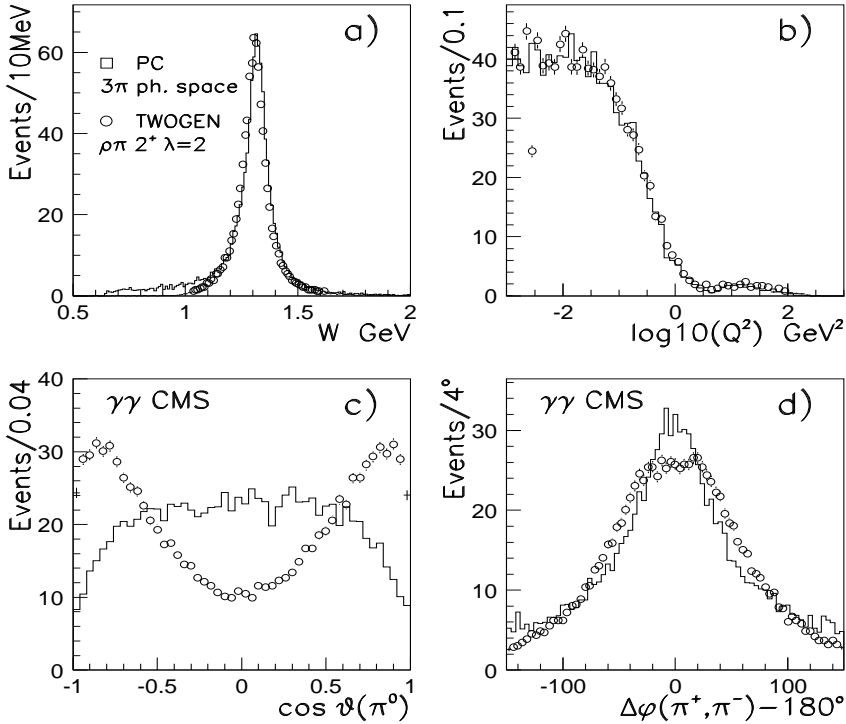
Figure 3: *The $a_2(1320)$ simulations of PC in 3π phase space and* TWOGEN *with $J^P = 2^+$, helicity $\lambda = 2$ and intermediate state $\rho\pi$. Detector acceptance are set to $\theta > 10°, 25°$ for calorimeter and central tracker respectively.*

We have compared the cross-section generated for η_c resonance as a function of beam energy which is shown in Fig. 2. The dashed line is the Low approximation [17] (i.e. the narrow-width approximation and the leading term of the EPA, but with the x-dependence of the P^2 integration neglected: $\int dP^2/P^2 \rightarrow \log s/m_e^2$), the solid line is the luminosity function of Eq. 2 using the approximation of $W^2 = 4w_1 w_2$ for small q^2, and the points are the RESPRO [18] calculation using exact $w_1 w_2$ without form factor.

We have instrumented the photon flux generated by PC and TWOGEN [19] to simulate $a_2(1320)$ mesons in $\pi^+\pi^-\pi^0$ final states at LEP 1 with detector acceptance set to $\theta > 10°, 25°$ from the beam direction for calorimeter and central tracker respectively. Shown in Fig. 3a and b are the invariant mass and Q^2 distributions of $a_2(1320)$ generated by PC and TWOGEN. Instrumented in PC is a narrow resonance of Eq. 7 decaying into 3π phase space, while in TWOGEN the Breit-Wigner of a wide resonance is multiplied by a matrix element of $J^P = 2^+$ with helicity $\lambda = 2$ and intermediate state of $a_2 \rightarrow \rho\pi \rightarrow \pi^+\pi^-\pi^0$. A second Breit-Wigner term for ρ suppresses events at low W. Within the detector acceptance good agreement is seen. The coupling to spin-parity and helicity state is demonstrated in Fig. 3c and d in which the π^0 distribution in polar angle and acollinear azimuthal angle of the two charged pion tracks are compared with the phase space distributions of PC.

10
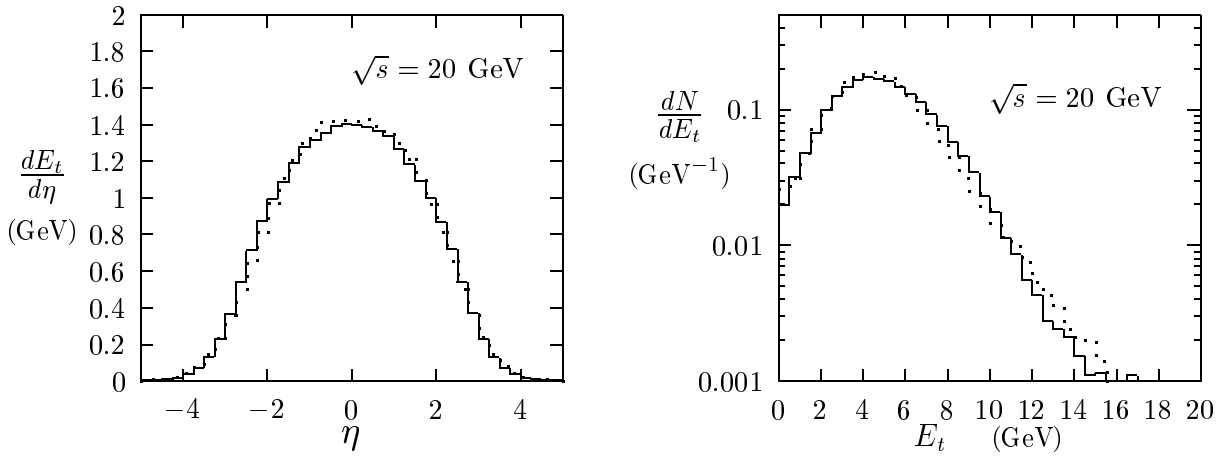
Figure 4: *Transverse energy flow and transverse energy distribution for photon-photon colli-sions. The full (dotted) line presents the predictions by* PYTHIA *(*PHOJET*).*
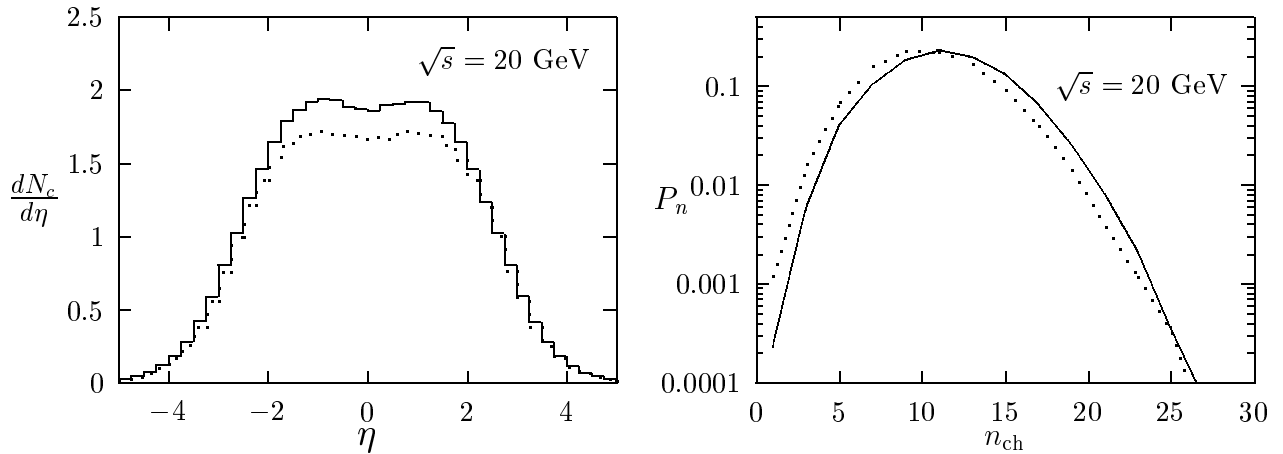
Figure 5: *Pseudorapidity distribution of charged particles and multiplicity distribution for non-single diffractive photon-photon collisions. The full (dotted) line presents the predictions by* PYTHIA *(*PHOJET*).*

3.2 Minimum bias events

In the following, some predictions for photon-photon collisions of the two minimum bias generators PYTHIA and PHOJET are compared at fixed photon-photon energy. The calculations have been done for inelastic, non-diffractive events, using the photon parton distribution functions SaS 1D [9] (PYTHIA) and GRV LO [10] (PHOJET). The transverse energy is one of the typical minimum bias quantities which can be measured without collecting very high statistics. In Fig. 4a the transverse energy flow as function of the pseudorapidity is shown. The transverse energy distribution is shown in Fig. 4b. Both generators give similar predictions.

In Fig. 5a the charged particle distribution as function of the particle pseudorapidity is

11
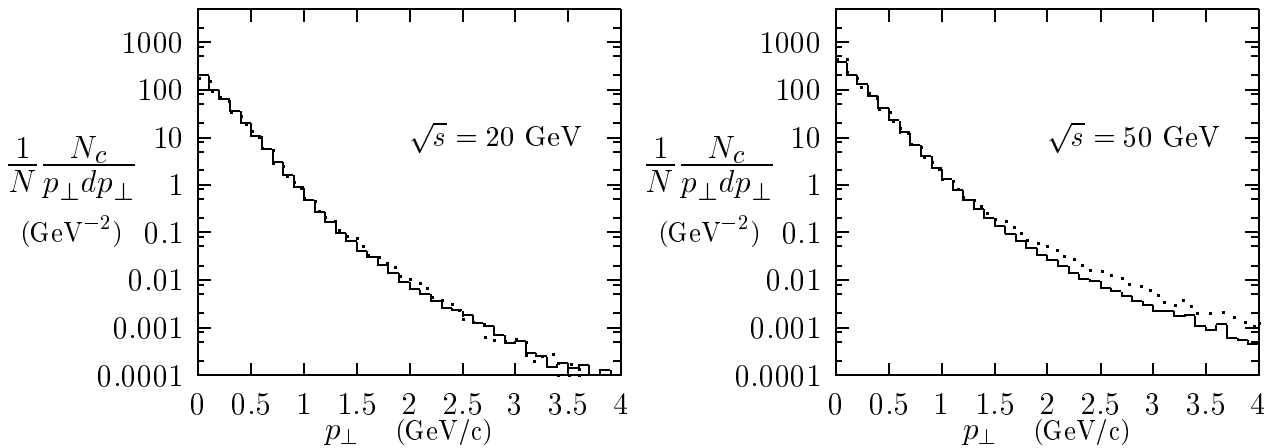
Figure 6: *Transverse momentum distributions of charged particles predicted by* PYTHIA *(full line) and* PHOJET *(dotted line).*

shown. PYTHIA predicts a higher charged particle density than PHOJET. This can be compared to the experimental value $dN_{\mathrm{ch}}/d\eta = 1.4 \pm 0.1$ for inelastic proton-proton collisions [20] at $\sqrt{s} = 24$ GeV. The shapes of the charged particle multiplicity distribution calculated with the generators (shown in Fig. 5b) are similar, however PHOJET predicts a lower value for the average multiplicity.

In general PYTHIA gives a larger difference between $\gamma\gamma$ and pp (and γp) collisions than PHOJET but this discrepancy is expected to diminish once both programs have been properly tuned to HERA data.

Finally, the transverse momentum distribution of charged particles is shown in Fig. 6. Whereas at low energies the generator results agree, PHOJET predicts at $\sqrt{s} = 50$ GeV more charged particles at high transverse momentum than PYTHIA.

3.3 Deep inelastic scattering

When measuring the photon structure function in deep inelastic eγ scattering, it is of course necessary to be able to accurately measure the Q^2 and the Bjorken-x in each event. The Q^2 is easily obtained from the energy and angle of the scattered electron, but since the energy of the target photon is unknown, x must be determined from the hadronic final state. Thus one measures the distribution of visible hadronic mass, W_{vis}, and hence $x_{\mathrm{vis}} \equiv Q^2/(W_{\mathrm{vis}}^2 + Q^2)$. This is then converted into the distribution of x using an unfolding procedure, typically based on Refs. [21] or [22].

It is clear that the more of the solid angle over which we detect hadrons, the better correlated W_{vis} will be with the true hadronic mass, W_{true}, so the less work the unfolding procedure will have to do. For now we simply define W_{vis} to be the total invariant mass of all the hadrons
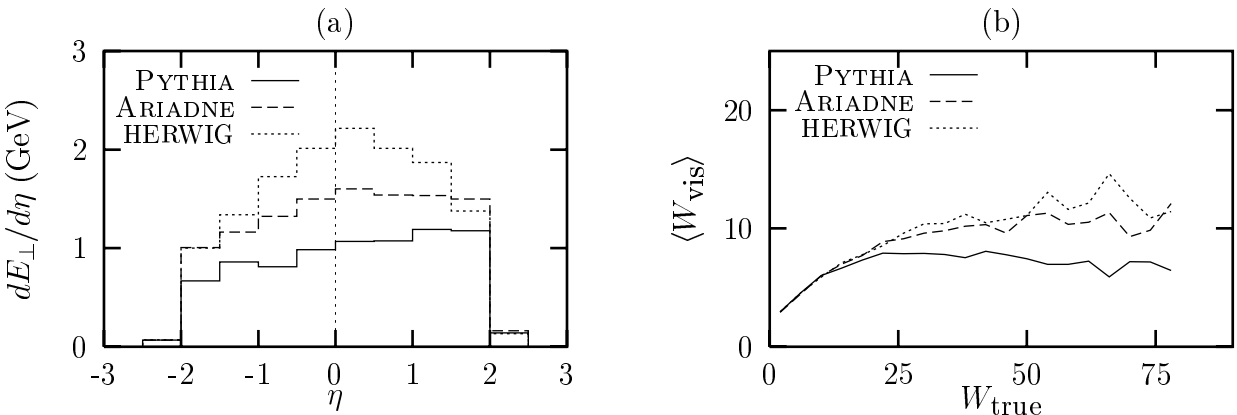
Figure 7: *(a) The transverse energy flow in deep inelastic $e\gamma$ scattering at LEP 2 as predicted by different generators for $x < 0.01$. (b) The mean value of W_{vis} as a function of W_{true} at LEP 2 as predicted by different generators.*

within the angle covered by the tracking system of a typical LEP detector, $|\cos\theta| < 0.97$, as done in most previous analyses, and return to this point later.

The unfolding procedure relies heavily on the event generator's ability to correctly model the hadronic final state. In previous analyses (see for example Refs. [23,24]), the consistency of the generators used for the unfolding has been checked using inclusive distributions of the data, such as the distributions in Q^2, W_{vis} and particle multiplicity and momentum distributions. The problem is that such distributions can be fitted with basically any generator by adjusting the number of events in each x and Q^2 bin, i.e. by modifying the input parton distribution. To really check the generator's description of the final states, one needs to investigate less inclusive distributions.

Experience from HERA shows that at small x, the distribution of transverse energy, $E_\perp$, in the proton direction is very difficult to describe. Indeed, programs with conventional "DGLAP-like" initial-state parton showers cannot explain the measured $E_\perp$ perturbatively and are dominated by the non-perturbative components. On the other hand, the dipole cascade in the ARIADNE program describes the $E_\perp$ flow rather well at the perturbative level, with only small hadronization corrections. While more detailed measurements might hope to distinguish them, the most recent versions of all models are in good agreement with current data.

In Fig. 7a we show the $E_\perp$ flow for small-x events at LEP 2 predicted by some event generators. The reach in x is not as large as at HERA, but the differences are still large. In the forward and central regions, the differences are mostly due to the fact that HERWIG corrects the hardest emission to reproduce the full $\mathcal{O}(\alpha^2\alpha_S)$ and $\mathcal{O}(\alpha^3)$ matrix elements, while this is only done partly in ARIADNE and not at all in PYTHIA. In the backward (photon remnant) direction, PYTHIA is expected to be lower than ARIADNE because of the differences in the parton showers as explained above. HERWIG is here higher than PYTHIA due to the special treatment of the remnant fragmentation.

13
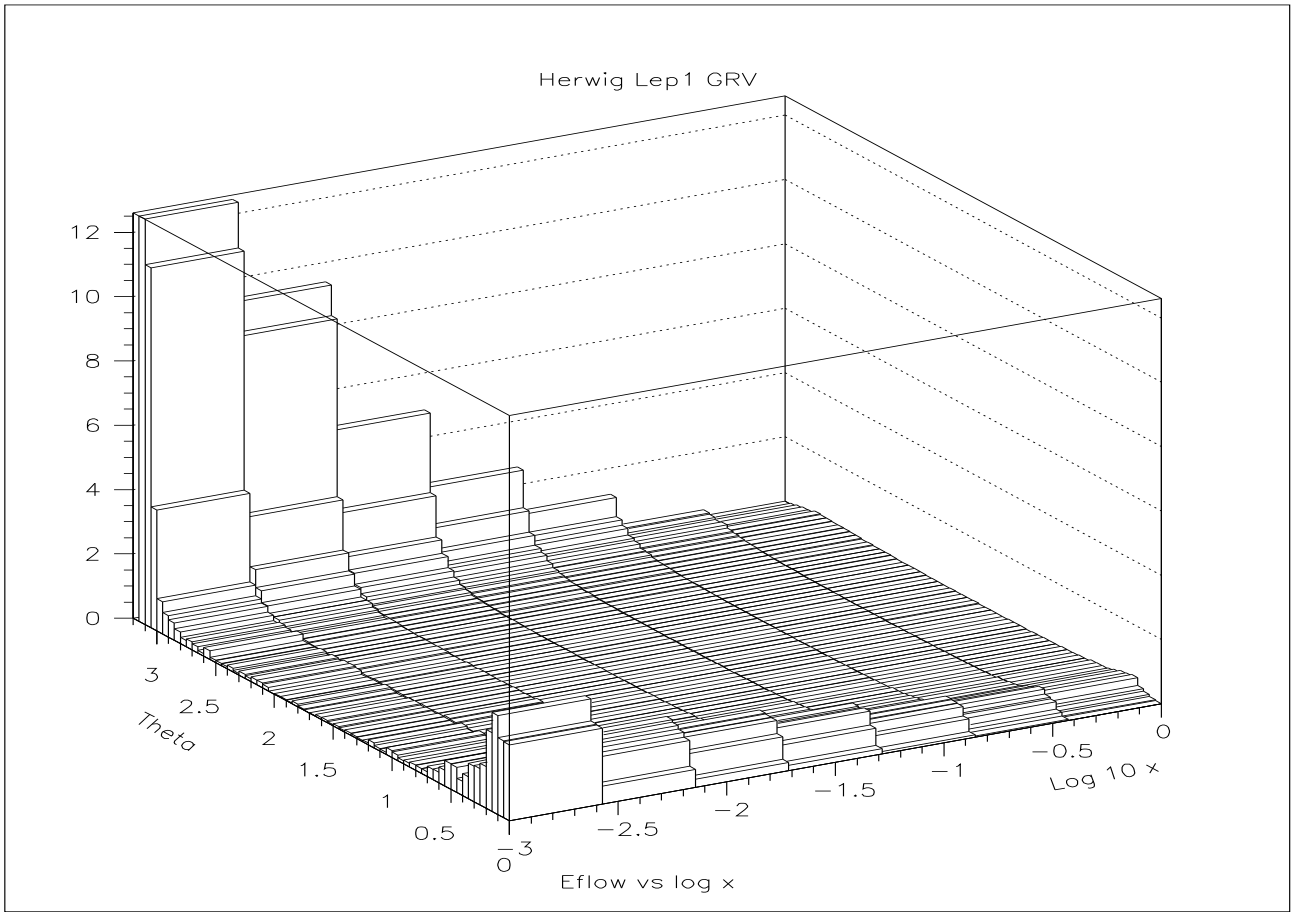
Figure 8: *The angular distribution of energy flow as a function of x at LEP 1 as predicted by HERWIG for events with $4 < Q^2 < 30$ GeV^2. The axes are such that the tagged electron is always on the forward, $0°$ side, while the photon remnant goes in the backward direction.*

It is clear that the relationship between W_{vis} and W_{true} is closely related to the energy flow, and in Fig. 7b we see that the models that give higher $E_\perp$ flow also give a stronger correlation between W_{vis} and W_{true} as expected. Also, all models predict a very weak correlation at large W_{true}, because more and more of the photon remnant falls outside the assumed acceptance as x gets smaller. This is demonstrated more clearly in Fig. 8, where the angular distribution of energy flow as a function of x is shown for LEP 1. The situation is even more extreme at LEP 2. The amount of energy falling into the central regions of the detector hardly increases with W, while almost all the increase is concentrated in the far forward and backward regions.

Our assumed detector acceptance covers all but the last five bins at each end, but we see that this is where most of the energy increase lies. However, all the LEP experiments have detectors in this region, which are used to tag electrons, and cover all but the very last bin of this plot. Thus if these could be used, even just to sample some of the hadronic energy in this region, a greatly improved W measurement could be made. Preliminary studies indicate

that in addition to the neutral pions, which can be measured because they decay to photons, a significant fraction of charged pions deposit some of their energy on the way through the detector. As a generator-level prescription to get some measure of how big an improvement this will make, we assume that neutral pions are perfectly measured, while no other hadrons are measured at all. In addition, we multiply all π^0 energies by a factor of three to arrive at an estimate of the total hadronic energy in the forward region.

In addition to extending our angular coverage, we can use additional kinematic variables of the final state to improve our W measurement. Defining the light-cone components of the particle momenta $p_\pm \equiv E \pm p_z$ we can write the invariant mass of the hadronic system as

$$W^2 = \left(\sum_i p_{i+} \right) \left(\sum_i p_{i-} \right) - \left| \sum_i \vec{p}_{i\perp} \right|^2, \tag{9}$$

where i runs over all hadrons. Using energy-momentum conservation (and neglecting the virtuality of the target photon) we can get some of the terms in Eq. 9 from the scattered electron, to define

$$W^2_{\text{rec}} \equiv \left(p_{e+} - p_{e'+} \right) \left(\sum_i p_{i-} \right) - \left| \vec{p}_{e'\perp} \right|^2. \tag{10}$$

This is equivalent to the well-known Jacquet-Blondel idea in photoproduction [25] except for the inclusion of the transverse momentum component. The sum over i now runs over hadrons in the central region, $|\cos\theta| < 0.97$, and π^0s in the forward region, $0.97 < |\cos\theta| < 0.9996$, and we include an extra factor of three for the forward π^0s.

Using Eq. 10 has two advantages over the naïve method of just using the invariant mass of detected hadrons. Firstly, the detector resolution enters as the product of hadronic and leptonic resolutions, rather than as hadronic-squared which, since the leptonic resolution is usually much better than the hadronic, gives improved overall resolution. Secondly, the effect of missing particles in the current direction $\theta \sim 0$ is minimized, because they give a negligible contribution to $E - p_z$. This, in addition to the inclusion of forward π^0s, means that W_{rec} is much better correlated with the true W, as seen in Fig. 9a. Also the differences between the models is much smaller.

In anomalous events, the photon remnant typically has larger transverse momentum, which means that in such events the correlation between W_{vis} and W_{true} is higher, as is seen in Fig. 9b. The definition of anomalous is, however, not the same in all generators, and in HERWIG, where anomalous events are defined by having a large transverse momentum remnant, the differences are larger than in PYTHIA, where the remnant has larger transverse momentum only on average.

Finally in double-tag events, we have more accurate information about the target photon energy, and hence the $W_{\gamma\gamma}$, as is seen in Fig. 10. It may be possible to use such events to calibrate the unfolding procedure for single-tag events. However, care must be taken, as in double-tag events, the target photon is more off-shell and the fraction of anomalous events are expected to be higher. See also sections 2 and 5 of the report from the "$\gamma\gamma$ Physics" [1] working group for more discussions of double-tag events.
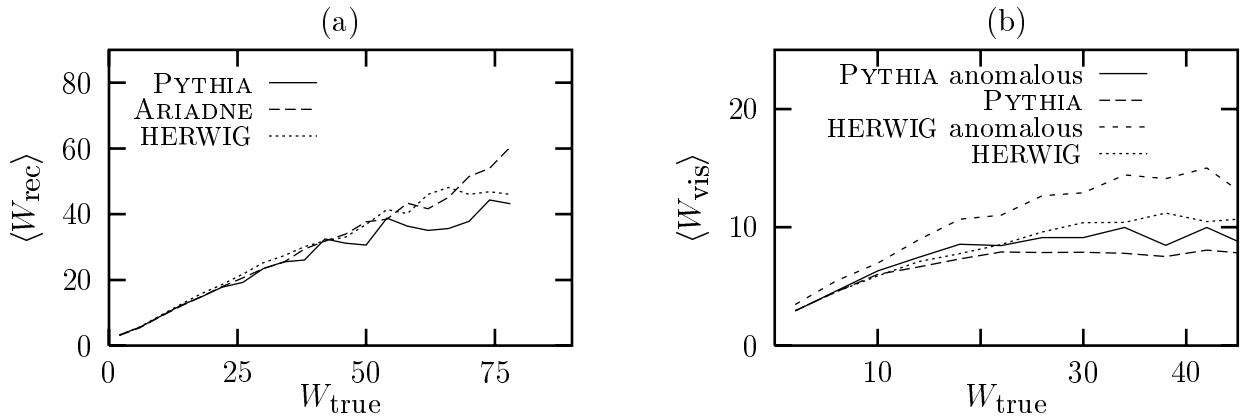
Figure 9: *(a) The mean value of W_{rec} as a function of W_{true} at LEP 2 as predicted by different generators. (b) The mean value of W_{vis} for anomalous and normal events as a function of W_{true} at LEP 2 as predicted by different generators.*
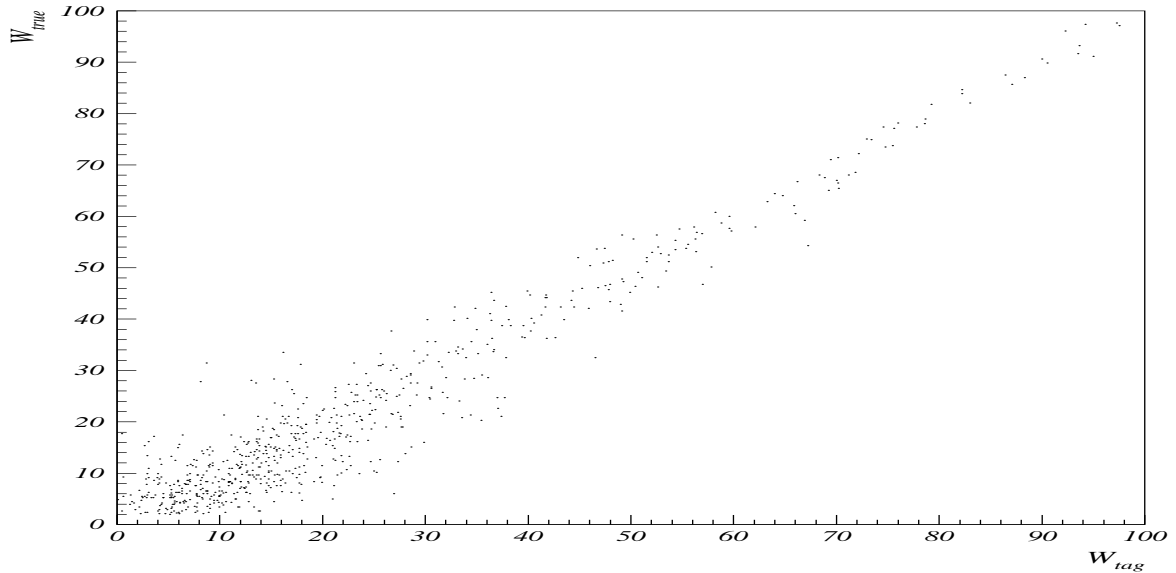
Figure 10: *Scatterplot of W_{true} vs. W_{tag} at LEP 2 as predicted by HERWIG for double-tag events after detector simulation.*

(a)

(b)
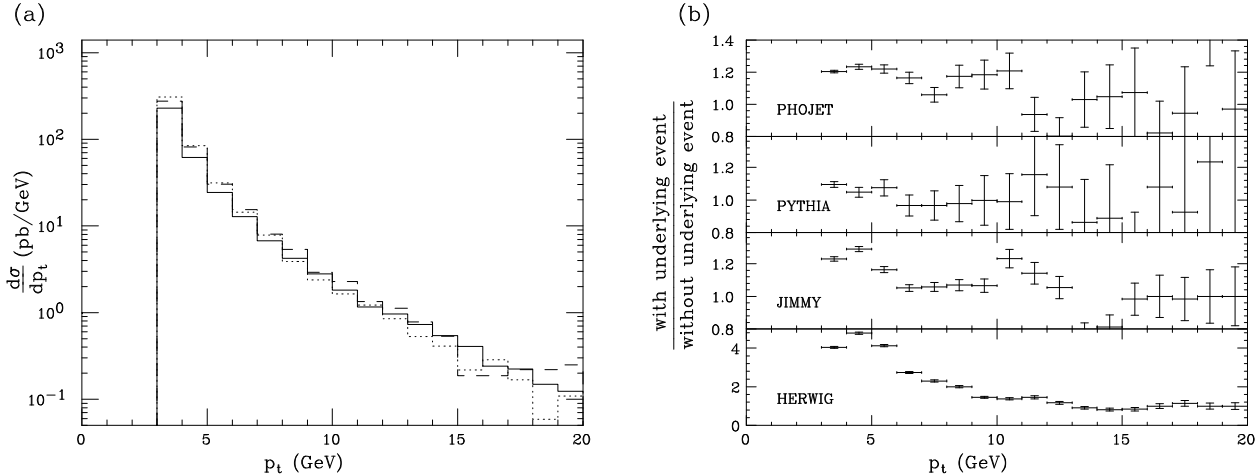
Figure 11: *The inclusive jet cross-section as a function of p_t according to HERWIG (solid),* PYTHIA *(dashed) and* PHOJET *(dotted), when all their underlying event models are turned off (a), and the relative changes when they are turned on (b). Errors shown come purely from the statistics of the Monte Carlo samples.*

3.4 High-$p_\perp$

Next-to-leading order QCD predictions are now available for both hadron and jet distributions in $\gamma\gamma$ collisions. Comparisons of data with these predictions are hoped to provide additional constraints on the parton content of the photon, particularly the gluon. However they apply to the partonic final state, consisting of at most three quarks or gluons, and cannot be compared to data without incorporating hadronization effects. For this to be done meaningfully, it is important to use general purpose QCD event generators, so that the parton level is as accurate a representation of the calculation as possible, while the hadronization is well-constrained by other reactions. Indeed the problems faced in $\gamma\gamma$ are almost identical to those in γp photoproduction at HERA, and we can expect that they will have been explored in detail by the time LEP2 analysis starts.

The hadronization effects can be broadly split into two groups: hadronization itself, and 'underlying event' effects, the latter coming principally from twice-resolved events in which the two photon remnants interact with each other in addition to the main scattering. Of course this separation is model-dependent, as hadrons described as coming from initial-state radiation in one model could be described as an underlying event in another, but it is a useful guide to where we expect the models to be more or less reliable. Hadronization itself is expected to be largely process-independent so models tuned to e^+e^- annihilation should give a reasonable description of data. Underlying event effects are much more poorly understood and the models are almost completely unconstrained at present. Their main effect is to spray additional transverse energy around the event, which can severely distort jet measurements, principally by adding extra transverse momentum to the jets. Because the jet spectrum is so rapidly falling, this increases the jet cross-section considerably at any given jet transverse momentum.

17

In Fig. 11, we show the inclusive jet cross-section, as a function of the jet transverse momentum. Jets are reconstructed using the CDF cone algorithm with a cone size of 1.0 and a minimum transverse momentum of 3 GeV, using all hadrons within the angular acceptance, $|\cos\theta| < 0.97$. We see reasonable agreement between PYTHIA, PHOJET and HERWIG when their underlying event and multiple scattering models are turned off. However, while all of them predict a significant increase with multiple scattering and the underlying event, there is little agreement about its size. It is worth pointing out that HERWIG's soft underlying event model produces far too big an effect to fit HERA photoproduction data, one of the motivations for incorporating the JIMMY multiple hard interaction model into HERWIG instead. Amongst the three other models the relative effect of multiple interactions is comparable to the differences between the models. It is clear that these effects must be understood before an accurate jet measurement can be made below about 10 GeV.

Of course the data itself can be used to study the effects and constrain the models. The jet energy profile is particularly sensitive to the underlying event, since perturbative radiation and hadronization are concentrated at the core of jets, while the underlying background is much more diffuse. Furthermore, since one expects the underlying event to mainly be important in the twice-resolved process, if we make a physical separation of direct and resolved photons we can test this picture. At HERA, a cut is made on x_γ, the fraction of the photon's light-cone momentum carried by the reconstructed jets [26]. In fact the HERA experiments define this in dijet events from the two hardest jets, while we propose a slightly different approach for $\gamma\gamma$ collisions: to use *all* the reconstructed jets, regardless of how many there are. Clearly when this fraction is close to 1 there can be no photon remnant, whereas when it is much smaller than 1 there must be one. The cut is typically set at around 0.7. For $\gamma\gamma$ collisions, we define a *pair* of momentum fractions by analogy, as

$$x_\gamma^\pm = \frac{\sum_{\text{jets}}(E \pm p_z)}{\sum_{\text{particles}}(E \pm p_z)}, \tag{11}$$

where, following the discussion in section 3.3, we include three times the forward π^0 energy in the sum over particles, which significantly improves the measurement of the denominator of Eq. 11. We define the axes such that $x_\gamma^+ > x_\gamma^-$.

In Fig. 12, we show the E_T profile of the hardest jet in the central region, $|\eta| < 1$, where η is the jet rapidity. We only include the transverse energy within the azimuthal region $|\Delta\phi| < 1$, so in a two-jet event the E_T of the other jet should not contribute to the pedestal of this jet. We see that for the direct events, in which both light-cone momentum fractions are large so there is no significant underlying event, the multiple scattering makes very little difference. On the other hand, for twice-resolved events, in which both photons have remnants, it makes a lot more difference. The jet pedestal is sufficiently raised to increase a jet's transverse momentum by about 200 MeV. While this may not seem a large shift in absolute terms, the jet cross-section actually decreases by about 25% in going from 3 to 3.2 GeV, giving rise to the correction predicted by PHOJET in Fig. 11b. Because of the strong correlation between the shape of the jet and the shift in the cross-section, it seems hopeful that the models can be constrained by data, to provide a reliable unfolding of these effects. Indeed this is already in progress at HERA.

18

(a) (b)
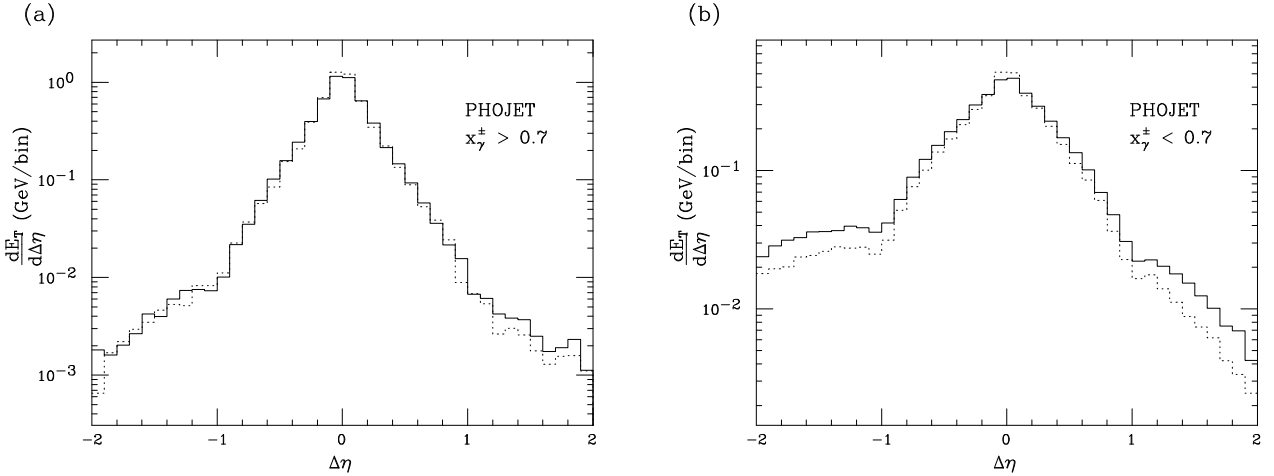
Figure 12: *The jet profile of central jets divided into (a) direct events and (b) double-resolved events according to a physical definition, as predicted by* PHOJET *with (solid) and without (dotted) multiple interactions.* $\Delta\eta$ *is the rapidity relative to the jet's, with the axes defined such that* $x_\gamma^+ > x_\gamma^-$ *such that there is always more of a remnant to the left than the right.*

Of course, one would like to make a more direct measurement of the nature of the underlying event, to differentiate between soft and multiple-hard interaction models. However it is extremely difficult to find event features that are unambiguous in this respect, as one's naïve picture of four jets in back-to-back pairs does not survive hadronization and realistic jet definition, so one is forced to look in the hard tails of distributions that are usually not well predicted anyway. Nevertheless, if direct evidence of multiple hard interactions could be found it would be extremely important for our understanding of photon and hadron collisions as a whole, and it is certainly worth continuing to search for such signals.

3.5 Heavy quarks

In this study we have compared five different generators of charm production in two-photon events: Vermaseren; PYTHIA; HERWIG; GGHV01 [27, 28]; and MINIJET [29]. All of these can generate the direct process, but only the last 4 the resolved process. For the comparison we chose the same parameters for each model: charm mass=1.7 GeV; minimum $c\bar{c}$ invariant mass=4.0 GeV; beam energy=85.0 GeV; and the GRV parton distribution set (for the resolved process).

We generated 10000 events with each program and compared the following distributions: scattered electron energy; final state invariant mass; energy, p_t and rapidity of the charm quark; p_t^2 of charm quarks with $\cos(\theta) < 0.9$ and energy > 2.0 GeV. In most cases the differences between the generators turn out to be rather small, so only a small selection are shown here (Figs. 13–15). Since they are so similar, we emphasize the differences by plotting the absolute distribution for only one generator (Vermaseren/PYTHIA for direct/resolved production) and
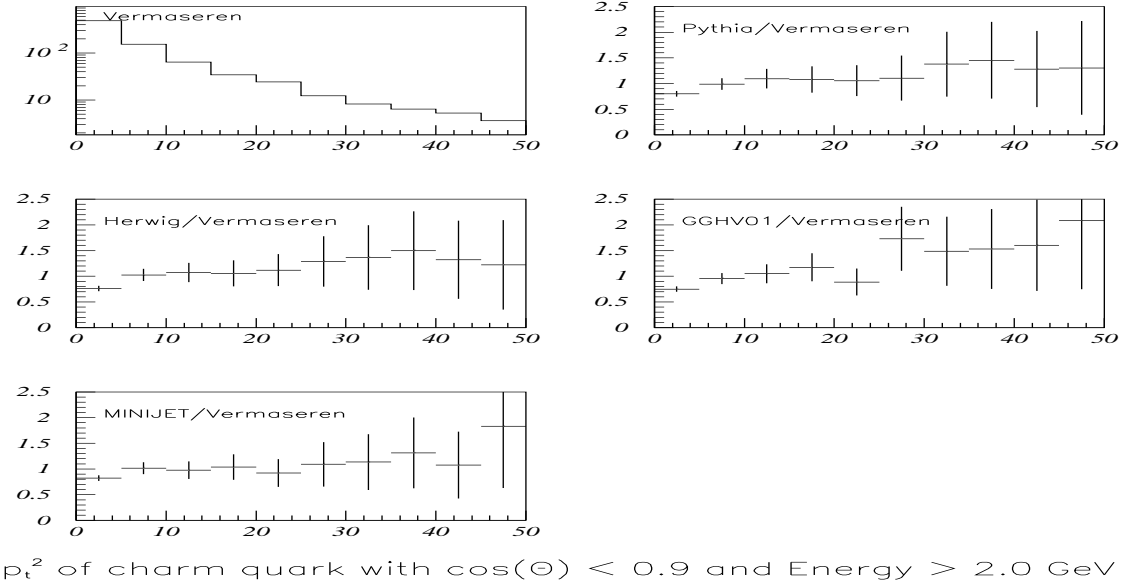
Figure 13: *Comparison of five generators of the direct production of charm quarks in two photon collisions. The top left histogram is the distribution for the Vermaseren generator. Other generators are shown as a ratio to the Vermaseren distribution in remaining plots.*

showing the results for the other generators as a ratio to it.

It can be seen that in the case of direct production the programs produce very consistent results. It should be noted that the Vermaseren generator is a full matrix element calculation while all the other generators involve a convolution of some version of the Equivalent Photon Approximation luminosity function with a cross-section for real photons. Thus it should be considered the correct answer to which the other calculations should be compared.

For the resolved process there is a larger variation between the generators. Unfortunately at this stage it is not clear which if any of these should be regarded as standard. The distribution that most clearly shows the differences is that of the rapidity of the charm quark (Fig. 15), where the MINIJET generator produces quarks that are more forward peaked, while GGHV01 produces more quarks in the central region. PYTHIA and HERWIG are fairly similar and lie somewhere in between.

Experimental charm measurement is generally restricted to the central region, with rapidity less than about 2. In Table 2, we show the selection efficiency of an imaginary experiment with 100% tagging efficiency for all charm quarks within the acceptance cuts, $\cos(\theta) < 0.9$ and $p_\perp > 2.0$ GeV. The differences in the rapidity distribution for resolved events are directly reflected in the selection efficiencies. One can see that an experiment using MINIJET to correct their data would 'measure' a resolved cross-section almost a factor of two larger than one using GGHV01, with PYTHIA and HERWIG lying between the two. It is therefore clearly a
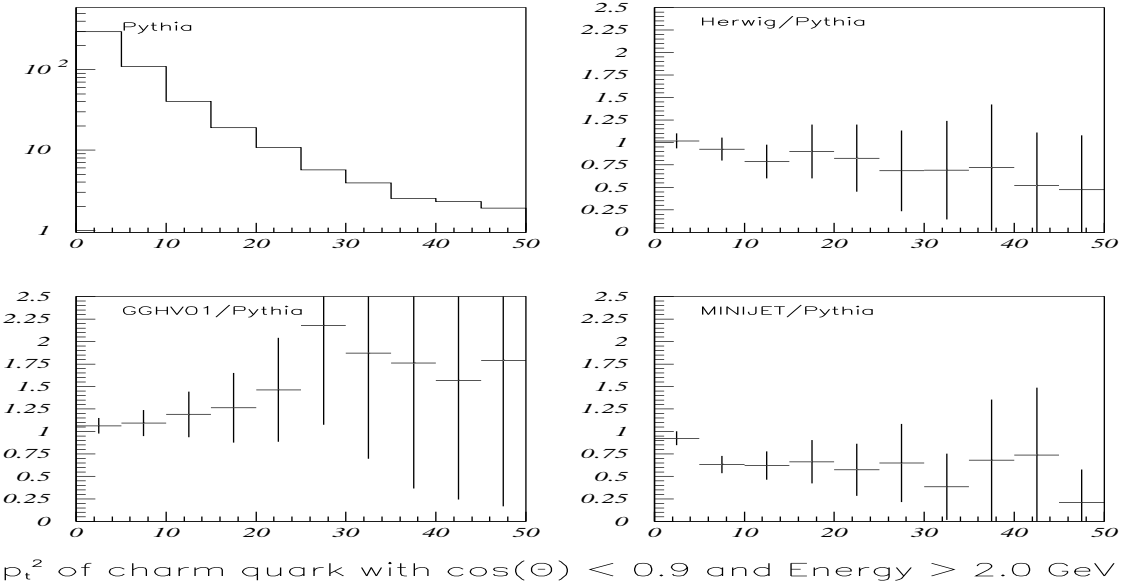
Figure 14: *Comparison of four generators of the production of charm quarks via the single resolved process in two photon collisions. The top left histogram is the distribution for the* PYTHIA *generator. Other generators are shown as a ratio to the* PYTHIA *distribution in remaining plots.*
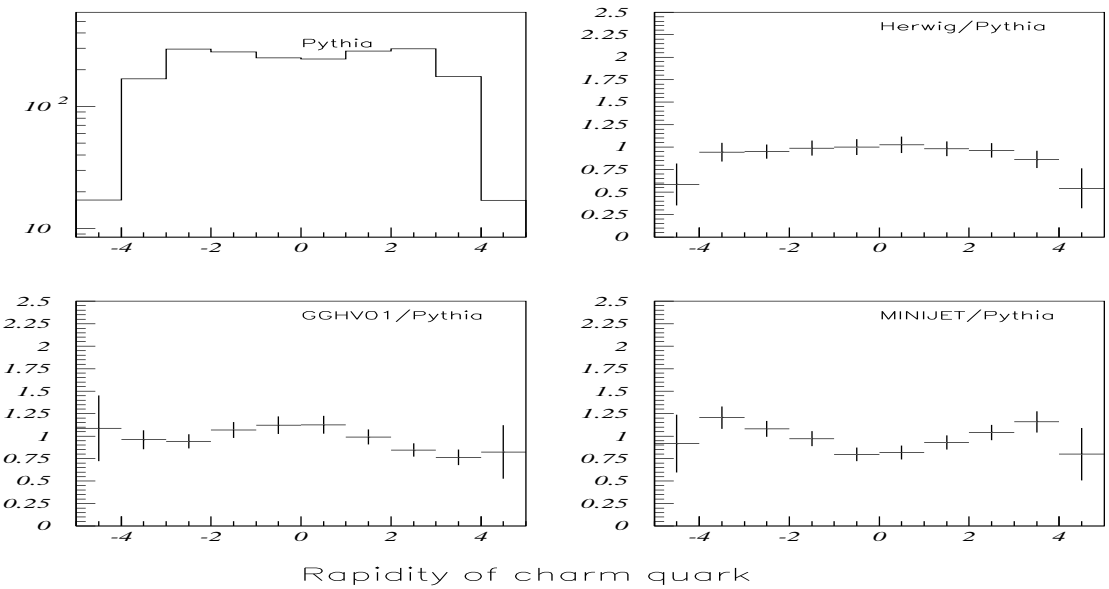
Figure 15: *Comparison of four generators of the production of charm quarks via the single resolved process in two photon collisions. The top left histogram is the distribution for the* PYTHIA *generator. Other generators are shown as a ratio to the* PYTHIA *distribution in remaining plots.*

21

Generator	Direct	Resolved
Vermaseren	42	-
GGHV01	39	28
PYTHIA	39	24
HERWIG	40	21
MINIJET	37	16

Table 2: *Percentage of events passing 'acceptance' cuts.*

high priority to understand where these differences arise and in particular whether the spread represents a genuine uncertainty in the measurement or is simply an indication that we should not trust one or some of the models. Unfortunately little progress has been made with this during the workshop.

Comparisons with data for the event features, rather than just the total cross-section, should also help to resolve this discrepancy. Within the limited statistics (33 events) Aleph found that GGHV01 gave a better description of data than the Vermaseren generator alone [27].

4   Description of programs

In this section we detail some of the event generators for $\gamma\gamma$ physics, concentrating mainly on those in which there has been significant development during this workshop. Other programs are commented on and described briefly in section 5.

4.1   Ariadne

Version: 4.07 of 15 August 1995 [30]
Author: Leif Lönnblad
                      NORDITA, Blegdamsvej 17,
                      DK 2100 Copenhagen Ø, Denmark
                      Phone: $+ 45 - 35325285$
                      E-mail: leif@nordita.dk
Program size: 12839 lines
Program location: http://surya11.cern.ch/users/lonnblad/ariadne/

The ARIADNE program implements the Dipole Cascade Model (DCM) for QCD cascades [31,32]. In this model the emission of a gluon g_1 from a $q\bar{q}$ pair created in an e^+e^- annihilation event can be described as radiation from the colour dipole between the q and $\bar{q}$. A subsequent emission of a softer gluon g_2 can be described as radiation from two independent colour dipoles,

22

one between the q and g_1 and one between g_1 and $\bar{q}$. Further gluon emissions are given by three independent dipoles etc. In this way, the end result is a chain of dipoles, where one dipole connects two partons, and a gluon connects two dipoles. This is in close correspondence with the Lund string picture, where gluons act as kinks on a string-like field stretched between the $q\bar{q}$ pair.

Further details of how ARIADNE generates the QCD cascade in e^+e^--annihilation can be found in Ref. [30] and elsewhere in these proceedings [2]. Here only the parts relevant for eγ DIS and high-$p_\perp$ $\gamma\gamma$ is presented.

The treatment of DIS is very similar to e^+e^- [33] gluon emission is described in terms of radiation from the colour dipole stretched between the quark, struck by the electroweak probe, and the photon remnant. The difference is that, while q and $\bar{q}$ are both point-like in the case of e^+e^-, the photon remnant in DIS is an extended object. This results in an extra suppression of radiation in the remnant direction.

The suppression depends on the transverse size of the remnant, which is taken to be inversely proportional to its intrinsic transverse momentum $k_{i\perp}$. In anomalous events where $k_{i\perp}$ is larger, the suppression is therefore smaller than in VMD–like events. Also in events where the target photon is significantly off-shell, the transverse size is taken to be the inverse of the maximum of $k_{i\perp}$ and the photon virtuality. Similarly in the case of events with $Q^2 \ll W^2$, where gluons may be radiated with transverse momentum larger than Q, also the struck quark may be treated as extended with a transverse size $\propto 1/Q$.

The DCM is evidently very different from conventional initial-state parton shower models. Tracing emissions "backwards" from the struck quark as in an initial-state shower, these would be unordered in transverse momentum, while in a program like PYTHIA these emissions would be ordered in falling transverse momentum. In the DCM, the transverse momentum of gluons far away from the struck quark, i.e. close to the remnant, can be much larger than in an initial-state parton shower.

The first emission in the dipole cascade is corrected to match the $\mathcal{O}(\alpha_S)$ matrix element for gluon emission. The gamma-gluon fusion diagram is, however, not yet included for the eγ DIS, because of technical difficulties in the current interface to PYTHIA.

The interface to PYTHIA, described in the report from the QCD generator group [2], also enables ARIADNE to generate high-$p_\perp$ $\gamma\gamma$ scattering. Here, PYTHIA is used to generate the hard sub-process. The outgoing partons and remnants are then connected with dipoles, which are allowed to radiate, restricting the transverse momentum of the emissions to be smaller than that of the hard interaction and treating all remnants as extended objects as in DIS.

For $\gamma\gamma$ it is also possible to run ARIADNE with PYTHIA using multiple interactions. However, this part of the interface is still preliminary, and more studies are needed.

4.2 GGHV01

Version:	Version 1.0 of 1/11/1994
Author:	M. Krämer, P. Zerwas (DESY),
	J. Zunft (formerly of DESY, no longer in HEP) and
	A.Finch,
	School of Physics and Materials,
	University of Lancaster,
	Lancaster LA1 4YB United Kingdom
	Phone: (+44) 1524 593618
	E-mail: A.Finch@lancaster.ac.uk
Program size:	Interface routines:1148 lines
	Physics routines: 2639 lines
	Integration package (BASES): 4432 lines
Program location:	ftp://lavhep.lancs.ac.uk/

GGHV01 was developed by the above authors as a Monte Carlo implementation of the calculation in Ref. [28] of heavy flavour quark production in gamma gamma collisions at next to leading order. It can either produce direct or single resolved events at a range of beam energies, but is restricted to real photons only.

The program is not a complete NLO generator. It does generate the $2 \rightarrow 3$ process according to the NLO matrix elements, which is cut off against soft and collinear divergences. The remaining events are, however, approximated with $2 \rightarrow 2$ processes generated only to leading order, but rescaled so that the total NLO cross-section is reproduced.

During the initialization stage the routine FANDK calculates the factor by which the $2 \rightarrow 2$ process should be increased to achieve the correct cross-section. In order to do this it needs to know beforehand the total cross-section. This it finds from a parameterization of the total cross-section from Ref. [28]. This is a quick method but less flexible than recalculating the total cross-section from scratch. The latter approach may be adopted in a later version. The chief criticism of this approach is that there is just one global correction factor whereas a more sophisticated approach would be to calculate a different factor for different regions of phase space.

The main event generation loop uses the coupled routines BASES and SPRING [34] which together constitute a general purpose integration and event generation package. The input to both routines is a function to be integrated as a function of n random variables. In this case the routine GENHVY. This routine uses the input random numbers to first pick whether to generate a 2 or 3 body event, it then calculates the fraction of the energy of the incoming beam electrons taken by each photon. In the resolved photon case the fraction of the photon's energy taken by a gluon is also found using the Glück Reya and Vogt next to leading order parton distribution functions [10]. Momenta for the outgoing particles are then chosen using the subroutine RAMBO. The weight for the event is found using routines based on the NLO calculation of Ref. [28]

multiplied by the phase space weight from RAMBO. The 2 body ('Born term') contributions is additionally scaled by the factor calculated in the initialization step as described above.

During the BASES stage the program first optimizes a 'map' of the function to provide efficient calculation, and then calculates the total cross-section (for GGHV01 this simply provides a check as the total cross-section is already known). During the SPRING stage the function is repeatedly called to generate unit weight events which are put in the LUJETS common for fragmentation by the LUEXEC routine from the JETSET package. The map generated by BASES is written out to a file, which means the program can later be run from the SPRING step only. In this case it reads back the map produced in a previous run and by simply varying the random number seed a fast event generation can be achieved..

4.3 GGPS1, GGPS2

Version:	1.0 [35]
Author:	T. Munehisa, K. Kato, D. Perret-Gallix
	Phone: +81-552208584 (TM), +81-333421264 (KK),
	+33-50091600, +41 22 7676293 (DPG)
	E-mail: munehisa@hep.esb.yamanashi.ac.jp,
	kato@sin.kogakuin.ac.jp, perretg@cernvm.cern.ch
Program size:	2213 (GGPS1) and 2841 (GGPS2) lines
Program location:	ftp://lapphp8.in2p3.fr/pub/keklapp/ggps/ggps.tar.gz

This generator simulates jet productions in two-photon process based on the leading-log (LL) parton shower (PS) technique [36]. Two cases are separately treated, namely, the deep inelastic scattering of the photon (GGPS1) and the scattering of two quasi-real photons (GGPS2) [35]. Both processes begin by the PS space-like evolution, then the hard scattering of partons takes place, followed by the time-like evolution of the final state partons.

The non-singlet quark distribution in the photon, $q_{NS}(x, Q^2)$, obeys [37]

$$\frac{dq_{NS}(x, Q^2)}{d \ln Q^2} = \frac{\alpha_s}{2\pi} \int_x^1 \frac{dy}{y} P_{qq}^{(0)}(x/y) q_{NS}(y, Q^2) + \frac{\alpha}{2\pi} k_{NS}^{(0)}(x), \qquad (12)$$

The inhomogeneous term, $k_{NS}^{(0)}(x)$, is proportional to $x^2 + (1 - x)^2$. α is the QED coupling constant, the QCD coupling constant α_s is defined as: $\alpha_s(Q^2) = 4\pi/(\beta_0 \ln Q^2/\Lambda^2) = \alpha_0/(\ln Q^2/\Lambda^2)$ with $\beta_0 = 11 - (2/3)N_F$. N_F is the number of flavours. Eq. 12 can be brought into the integral equation

$$q_{NS}(x, Q^2) = \int_x^1 \frac{dy}{y} K_{NS}^{(0)}(x/y, \overline{s}) q_{NS}(y, Q_0^2) + \int_{Q_0^2}^{Q^2} \frac{dK^2}{K^2} \int_x^1 \frac{dy}{y} K_{NS}^{(0)}(x/y, \eta(K^2)) \frac{\alpha}{2\pi} k_{NS}^{(0)}(y), \quad (13)$$

where $\overline{s} \equiv \ln(\alpha_s(Q_0^2)/\alpha_s(Q^2)) = \ln(\ln(Q^2/\Lambda^2)/\ln(Q_0^2/\Lambda^2))$ and $\eta = \ln(\ln(Q^2/\Lambda^2)/\ln(K^2/\Lambda^2))$. The first term represents the vector meson dominant part (VMD) while the second corresponds

to the perturbative photon. Here $K_{NS}^{(0)}(x, \overline{s})$ is the QCD kernel function [38] defined by the inverse Mellin transformation

$$K_{NS}^{(0)}(x, \overline{s}) = \int_{r_0 - i\infty}^{r_0 + i\infty} \frac{dn}{2\pi i} x^{-n} e^{\alpha_0 d(n)\overline{s}}, \tag{14}$$

where $d(n)$ is the moment of $P_{qq}^{(0)}(x)/(2\pi)$.

The singlet distribution is handled in the similar manner.

Due to the inhomogeneous term in Eq. 12, the total energy is conserved *only if* the photon energy is included,

$$\int_0^1 dx x [\sum_f (q_f(x, Q^2) + \overline{q}_f(x, Q^2)) + G(x, Q^2)] = \int_{Q_0^2}^{Q^2} \frac{dK^2}{K^2} \frac{\alpha}{2\pi} \int_0^1 dx x k_{NS}^{(0)}(x). \tag{15}$$

In the generation the right-hand side is used as *the weight of the event.*

Let us summarize the main steps present in the algorithm generating the partons in the course of the evolution.

1. Selection of a Q^2.

2. Calculation of the energy of the VMD part (independent of Q^2) and of the energy of the perturbative photon part by using Eq. 15. The sum of these energies is used as the weight of the event.

3. Selection of the actual process, either VMD or perturbative photon, according to the ratio of energies.

4. If VMD is chosen, the usual QCD evolution from Q_0^2 (the cut-off momentum) to Q^2 is performed.

5. In the case of a perturbative photon, the virtual mass squared K^2 according to the probability dK^2/K^2 is determined. Then the flavour of the partons are selected according to the ratio of charges squared.

6. For each quark or anti-quark, the usual QCD evolution from K^2 up to Q^2 is performed.

This algorithm is common to the deep inelastic photon scattering and to the two quasi-real photon scattering with large p_T^2. The hard scattering parts are, however, different. In quasi-real photon collision the initial states q-q, q-$\overline{q}$, q-G, G-G, q-γ G-γ and γ-γ are taken into account for the hard scattering, although in the virtual-quasi-real case only the γ^*-q and γ^*-G subprocesses are considered.

The reference cross-section used to select events is the differential cross-section:

$$d\sigma^0/dp_T^2 = \pi/p_T^4. \tag{16}$$

26

The ratio of the hard cross-section to Eq. 16 is counted as the weight of the event. The argument of α_s in the hard cross-section is set to be p_T^2, because there are some processes whose cross-section is dominated by the t-channel contribution. After the time-like evolution of the produced partons has been performed, the energy of the initial photons is fixed and thus the four-momenta of all partons are determined.

Events are generated with a weight whose maximum is unknown at the beginning of a run. A maximum value is arbitrary fixed by the user, overweight events are rejected and counted. At the end of the run, if the number of overweight events is too large, compromising the generation accuracy, the user must increase the maximum weight, reducing consequently the generation efficiency.

Finally the generated partons are hadronized following the JETSET [39] mechanism. Colour flows are properly matched and adopt the JETSET definition. Two types of colour singlet exist: a string beginning and ending with quarks possibly embedding one or many gluons or a closed colour loop of gluons.

4.4 HERWIG

Version: 5.8d of October 1995 [40] (and 5.9 of December 1995)
Authors: G. Marchesini[1], B.R. Webber[2], G. Abbiendi[3], I.G. Knowles[4],
M.H. Seymour[5], L. Stanco[3]
[1]Dipartimento di Fisica, Universita di Milano.
[2]Cavendish Laboratory, University of Cambridge.
[3]Dipartmento di Fisica, Universita di Padova.
[4]Department of Physics and Astronomy, University of Glasgow.
[5]Theory Division, CERN.
E-mail: webber@hep.phy.cam.ac.uk, knowles@v6.ph.gla.ac.uk,
seymour@surya11.cern.ch.
Program size: 15500 lines
Program location: http://surya11.cern.ch/users/seymour/herwig/

HERWIG is a general-purpose QCD Monte Carlo event generator for simulating **H**adron **E**mission **R**eactions, **W**ith **I**nterfering **G**luons. Its general design philosophy is to provide as complete as possible an implementation of perturbative QCD, combined with as simple as possible a model of non-perturbative QCD. It does this uniformly for a very wide range of processes, allowing the parameters to be fitted in one reaction, principally e$^+$e$^-$ annihilation, and applied to other reactions. Although HERWIG has been capable of simulating $\gamma\gamma$ collisions for some time, there were many technical deficiencies, which practically prevented experiments from using it. Many of these have been rectified during the workshop, resulting in the preliminary versions 5.8a, 5.8c and 5.8d. However work is still ongoing, and some of the features described below will not be available until the full version release towards the end of this year. Since

much of HERWIG is described in Ref. [2], we concentrate on the additional features relevant to $\gamma\gamma$ collisions here. Original references can be found in Ref. [40].

Event generation proceeds much like the general case described in the introduction. The equivalent photon approximation (EPA) is used, correctly generating the P^2 dependence. Since this means that the photons no longer collide head-on, they are boosted to their centre-of-mass frame, where the remainder of the event generation is performed. At the end of the event they are automatically boosted back to the lab frame.

Since the user can control the P^2 range generated (through the variables `Q2WWMN` and `Q2WWMX`), it is in principle possible to generate all event classes using the EPA. However, to provide a more accurate description of high-Q^2 tagged events, these are described as deep inelastic scattering, e$\gamma \rightarrow$ e+hadrons including the full electron kinematics, rather than as $\gamma^*\gamma \rightarrow$hadrons using the EPA.

The treatment of deep inelastic lepton-photon scattering is essentially identical to that of lepton-hadron, except for the inclusion of the point-like photon-quark coupling in the initial-state parton shower. The hard process is generated as eq $\rightarrow$ eq according to whichever parton distribution function is selected from PDFLIB. This is controlled by the variables `AUTPDF` and `MODPDF`, which hold the 'author group' and set number respectively, for example `GRVph` and `3` for the leading-order photon set of Glück, Reya and Vogt.

The outgoing quark produces a parton shower exactly like that in the final state of e$^+$e$^-$ annihilation, described in Ref. [2]. The incoming quark also produces a parton shower, which is generated using the 'backward evolution' algorithm. One can imagine this as an evolution in the factorization scale from the large scale of the hard process down towards zero — as it is reduced, more and more radiation is resolved, i.e. transferred from the evolution of the parton distribution function to the coefficient function. The inhomogeneous term in the evolution equation corresponds directly to the addition of a $\gamma \rightarrow q\bar{q}$ vertex, which is straightforwardly included by considering the photon to be an additional parton type with a delta-function distribution. This results in a dynamic separation of events into point-like and hadronic. At small and medium x values ($x \lesssim 0.3$), this separation is similar to that made in the input distribution functions, demonstrating the self-consistency of the backward evolution algorithm, but at large x it becomes increasingly different from them, classifying almost all large-x events as hadronic, whereas most distribution function sets classify them as point-like. The difference can be traced to the fact that HERWIG uses a cutoff in transverse momentum to separate the perturbative and non-perturbative regions, whereas the distribution functions make a cut on the virtuality of the internal line. At large x, the two differ by a factor of $(1-x)$ giving large differences in the separation scales. While it could be argued that transverse momentum is a more physical scale to use, as in the FKP model, a more conservative approach is to simply say that this indicates a region of uncertainty, and any analysis that relies on the classification of this large x region into the two components should be considered highly model-dependent.

All partons produced by the initial-state cascade undergoing further parton showering just like any other outgoing parton.

Colour coherence is as important in initial-state cascades as it is in the final state. However it is less well understood and only an approximate treatment is implemented in HERWIG. At large x, all emitted gluons must be soft, the emission pattern is identical to a final state dipole, and the emission is angular-ordered. At small x, rather than restricting soft gluon momenta, we actually 'look inside' the soft gluons, resulting in a different coherence structure. At 'fairly small' x, this can be approximated by imposing transverse momentum ordering, which is how it is implemented in HERWIG, but at very small x the correct approach is to use angular ordering and modified emission probabilities. Although this has never been implemented as a full Monte Carlo event generator, a partial implementation was discussed in Ref. [41] and shown to give similar results to the HERWIG algorithm at the x values expected at LEP 2 or even HERA. The actual evolution variable used by HERWIG smoothly interpolates the two regions.

Just as in e^+e^- annihilation, HERWIG is not capable of covering the whole of phase-space with its parton shower emission. This is corrected using the methods proposed in Ref. [42], which ensure that the *hardest* emission (which is not necessarily the first owing to the ordering of opening angles) agrees with the exact matrix element (the sum of higher-order resolved, $g \to q\bar{q}$, $q \to qg$, and point-like, $\gamma \to q\bar{q}$). It is worth noting that azimuthal correlations [1] are correctly included within the 'dead-zone' region of x_p and z_p defined in Ref. [43], but not within the parton shower itself.

After the parton cascade, the system is hadronized according to the cluster model. For outgoing partons, this is identical to e^+e^- annihilation, described in Ref. [2], but for hadronic events, the photon remnant is treated specially. It is given a limited transverse momentum of width `PTRMS`, and the cluster that contains it is given a Gaussian mass-squared distribution, resulting in a limited p_t spectrum of produced hadrons, as expected for such a soft object. An 'underlying event' model is provided, which increases the energy released during the break-up of the remnant, but it seriously overestimates HERA data on DIS at small x, and it is recommended that it be switched off by running process `IPROC=19000` rather than 9000[1].

Untagged and low-Q^2 tagged events are generated using the equivalent photon approximation to split both beams to photons. One hard process type is selected from those listed in Ref. [2]. At present there is no facility to mix events of different types in the same run, although it is clear that this would improve the utility of the program and it is a planned improvement. Events are generated according to the leading order matrix elements for $2 \to 2$ scattering, and initial-state and final-state showers are added exactly as in deep inelastic scattering. Another current problem is that the phase-space cuts accessible to the user are completely different for direct and resolved processes, making it difficult to generate both uniformly. Fixing this is another planned improvement.

In all event classes except deep inelastic scattering, it is recommended that the soft underlying event be selected. This models the collision between the photon remnants as a soft hadron-hadron scattering, which produces a uniform rapidity plateau of extra hadrons on top

---

[1]This applies to versions 5.8d onwards. In earlier versions, the two processes would be expected to bracket the correct result.

of those from the perturbative event. This is based on the UA5 minimum bias model, and is essentially just a parametrization of data. The soft VMD scattering process, `IPROC=8000`, uses the Donnachie-Landshoff cross-section and generates events as in the soft underlying event.

As discussed earlier, one would expect multiple hard scattering to be an important effect in untagged $\gamma\gamma$ collisions at LEP 2. Its contribution to the underlying event is also a major source of uncertainty in the measurement of jets at HERA and it is important to have several different models of it, to get some estimate of the uncertainty in the predictions. Although such scattering is not included in HERWIG at present, there is an interface to the JIMMY Generator [44] (which can also be obtained from the web-page listed above). However, there is not yet a smooth transition between hard and soft multiple scattering, and JIMMY and s.u.e. should be considered mutually exclusive at present.

The default parameter set that comes with HERWIG is tuned to OPAL data in the case of parameters that affect e^+e^- annihilation, but are simply theoretically prejudiced guesses for the others. At present the HERA experiments are involved with tuning the additional parameters and these will be included in future releases, hopefully improving the predictivity for $\gamma\gamma$ physics.

4.5 PHOJET

Version:	1.04 of 20 October 1995 [45]
Author:	Ralph Engel
	Institute of Theoretical Physics
	University Leipzig
	Augustusplatz 10, D-04109 Leipzig, Germany
	Phone: $+ 49 - 341$ - 97 32444
	E-mail: eng@tph200.physik.uni-leipzig.de
Program size:	31000 lines
Program location:	http://www.physik.uni-leipzig.de/~engel/phojet.html

PHOJET is a minimum bias event generator for hadronic pp, γp and $\gamma\gamma$ interactions. The interactions are described within the Dual Parton Model (DPM) [46] in terms of reggeon and pomeron exchanges. The realization of the DPM with a hard and a soft component in PHOJET is similar to the event generator DTUJET-93 [47, 48]. Regge arguments are combined with perturbative QCD to get an almost complete description of the leading event characteristics. Special emphasis is taken on diffractive and soft interactions. Soft and hard interactions are unitarized together leading to the possibility to have multiple soft and hard scatterings in one event.

In the following, some comments on LEP 2 specific aspects are given. In the model [45], the dual nature of the photon is taken into account by considering the physical photon state as a superposition of a "bare photon" and virtual hadronic states having the same quantum numbers as the photon. Two generic hadronic states $|q\bar{q}\rangle$ and $|q\bar{q}^\star\rangle$ have been introduced to describe the

hadronic piece of the photon. The low-mass state $|q\bar{q}\rangle$ corresponds to the superposition of the vector mesons ρ, ω and ϕ and a $\pi^+\pi^-$ background. The state $|q\bar{q}^\star\rangle$ is used as an approximation for hadronic states with higher masses. The physical photon reads

$$|\gamma\rangle = \sqrt{Z_3}\,|\gamma_{\text{bare}}\rangle + \frac{e}{f_{q\bar{q}}}\,|q\bar{q}\rangle + \frac{e}{f_{q\bar{q}^\star}}\,|q\bar{q}^\star\rangle. \tag{17}$$

The interaction of the hadronic states via pomeron/reggeon exchange is subdivided into processes involving only *soft* processes and all the other processes with at least one large momentum transfer (*hard* processes) by applying a transverse momentum cutoff $p_\perp^{\text{cutoff}}$ to the partons. On Born-graph level, for example, the photon-photon cross-sections is built up by: **(i)** soft reggeon and pomeron exchange, **(ii)** hard resolved photon-photon interaction, **(iii)** single direct interactions, and **(iv)** double direct interactions. The soft pomeron cross-sections is parametrized using Regge theory. The hard cross-sections are calculated within the QCD Parton Model using lowest order matrix elements. For soft processes, photon-hadron duality is assumed. The energy-dependence of the reggeon and pomeron amplitudes is assumed to be the same for all hadronic processes. Therefore, data on hadron-hadron and photon-hadron cross-sections can be used to determine the parameters necessary to describe soft photon-photon interactions.

The amplitudes corresponding to the one-pomeron exchange between the hadronic fluctuations are unitarized applying a two-channel eikonal formalism similar to Ref. [47]. The probabilities $e^2/f_{q\bar{q}}^2$ and $e^2/f_{q\bar{q}^\star}^2$ to find a photon in one of the generic hadronic states, the coupling constants to the reggeon and pomeron, and the effective reggeon and pomeron intercepts cannot be determined by basic principles. These quantities are treated as free parameters and determined by cross-section fits [45]. Once the parameters are fitted, the model allows for predictions on photon-photon collisions without new parameters.

The probabilities for the different partonic final state configurations are calculated from the discontinuity of the scattering amplitude (optical theorem). Using the Abramovski-Gribov-Kancheli cutting rules [49] the cross-section for graphs with k_c soft pomeron cuts, l_c hard pomeron cuts, m_c triple- or loop-pomeron cuts, and n_c double-pomeron are estimated. For pomeron cuts involving a hard scattering, the complete parton kinematics and flavours/colours are sampled according to the Parton Model using a method similar to Ref. [50], extended to direct processes. For pomeron cuts involving parton configurations without a large momentum transfer, the partonic interpretation of the Dual Parton Model is used: photons or mesons are split into a quark-antiquark pair whereas baryons are approximated by a quark-diquark pair. The longitudinal momentum fractions of the soft partons are given by Regge asymptotics [51]. One obtains for the valence quark (x) and diquark ($1-x$) distribution inside the proton $\rho(x) \sim (1-x)^{1.5}/\sqrt{x}$ and for the quark antiquark distribution inside the photon $\rho(x) \sim 1/\sqrt{x(1-x)}$. For multiple interaction events, the sea quark momenta are sampled from a $\rho(x) \sim 1/x$ distribution. The transverse momenta of the soft partons are sampled from an exponential distribution in order to get a smooth transition between the transverse momentum distributions of the soft constituents and the hard scattered partons.

In diffraction dissociation or double-pomeron scattering, the parton configurations are generated using the same ideas described above applied to pomeron- photon/pomeron scattering processes. According to the kinematics of the triple- or loop-pomeron graphs, the mass of the diffractively dissociating systems is sampled from a $1/M_D^{2\alpha_{I\!P}(0)}$ distribution. The momentum transfer in diffraction is obtained from an exponential distribution with mass-dependent slope (see Ref. [45]). For the parton distributions of the pomeron, the CKMT parametrization with a hard gluonic component [52] is used. The low-mass part of diffraction dissociation is approximated by the superposition of high-mass vector mesons. In order to take into account the transverse polarization of quasi-elastically produced vector mesons, diffractively scattered ρ, ω and ϕ are decayed anisotropically.

Finally, the fragmentation of the sampled partonic final states is done by forming colour neutral strings between the partons according to the colour flow. In the limit of many colons in QCD, this leads to the two-chain configuration characterizing a cut pomeron and a one-chain system for a cut reggeon. In hard interactions the colour flow is taken from the matrix elements directly [53]. The leading contributions of the matrix elements give a two-chain structure which corresponds to a cut pomeron. The chains are fragmented using the Lund fragmentation code JETSET 7.3 [39].

In order to get the LEP 2 kinematics, the complete lepton-photon vertex for transversally polarized photons is simulated in the program. The lepton (anti-) tagging conditions can be specified by the user. However, in the model only photons with very low virtualities are considered at the moment. The extension to virtual (and longitudinally polarized) photons is in progress.

An example input file for a $\gamma\gamma$ run can be in found in the PHOJET manual [54].

4.6 PYTHIA/JETSET

Versions:	PYTHIA 5.720 of 29 November 1995 [39]
	JETSET 7.408 of 23 August 1995
Author:	Torbjörn Sjöstrand
	Department of Theoretical Physics
	University of Lund
	Sölvegatan 14A, S-223 62 Lund, Sweden
	Phone: $+ 46 - 46$ - 222 48 16
	E-mail: torbjorn@thep.lu.se
Program size:	19936 + 11541 lines
Program location:	http://thep.lu.se/tf2/staff/torbjorn/

PYTHIA/JETSET is a general-purpose generator of high-energy particle physics reactions. An introduction and a survey of processes of interest for LEP 2 physics are found in the QCD generators section, while the full description is in Ref. [39]. Here only aspects specific to $\gamma\gamma$

physics will be summarized. These have been developed together with Gerhard Schuler, and are described extensively elsewhere [55, 56].

To first approximation, the photon is a point-like particle. However, quantum mechanically, it may fluctuate into a (charged) fermion–antifermion pair. The fluctuations $\gamma \leftrightarrow q\overline{q}$ can interact strongly and therefore turn out to be responsible for the major part of the $\gamma\gamma$ total cross-section. The spectrum of fluctuations may be split into a low-virtuality and a high-virtuality part. The former part can be approximated by a sum over low-mass vector-meson states, customarily restricted to the lowest-lying vector multiplet. Phenomenologically, this Vector Meson Dominance (VMD) ansatz turns out to be very successful in describing a host of data. The high-virtuality part, on the other hand, should be in a perturbatively calculable domain. Based on the above separation, PYTHIA distinguishes three main classes of interacting photons: direct, VMD and anomalous.

For a $\gamma\gamma$ event, there are therefore three times three event classes. By symmetry, the 'off-diagonal' combinations appear pairwise, so the number of distinct classes is only six. These are:

1. VMD×VMD: both photons turn into hadrons, and the processes are therefore the same as allowed in hadron–hadron collisions.
2. VMD×direct: a bare photon interacts with the partons of the VMD photon.
3. VMD×anomalous: the anomalous photon perturbatively branches into a $q\overline{q}$ pair, and one of these (or a daughter parton thereof) interacts with a parton from the VMD photon.
4. Direct×direct: the two photons directly give a quark pair, $\gamma\gamma \rightarrow q\overline{q}$. Also lepton pair production is allowed, $\gamma\gamma \rightarrow \ell^+\ell^-$, but will not be considered here.
5. Direct×anomalous: the anomalous photon perturbatively branches into a $q\overline{q}$ pair, and one of these (or a daughter parton thereof) directly interacts with the other photon.
6. Anomalous×anomalous: both photons perturbatively branch into $q\overline{q}$ pairs, and subsequently one parton from each photon undergoes a hard interaction.

In a complete framework, there would be no sharp borders between the six above classes, but rather fairly smooth transition regions that interpolate between the extreme behaviours. However, at our current level of understanding, we do not know how to do this, and therefore push our ignorance into parameters of the model. From a practical point of view, the sharp borders on the parton level are smeared out by parton showers and hadronization. Any Monte Carlo event sample intended to catch a border region would actually consist of a mixture of the three extreme scenarios, and therefore indeed be intermediate.

The main parton-level processes that occur in the above classes are:
- The 'direct' processes $\gamma\gamma \rightarrow q\overline{q}$ only occur in class 4.
- The '1-resolved' processes $\gamma q \rightarrow qg$ and $\gamma g \rightarrow q\overline{q}$ occur in classes 2 and 5.
- The '2-resolved' processes $qq' \rightarrow qq'$ (where q' may also represent an antiquark), $q\overline{q} \rightarrow q'\overline{q}'$, $q\overline{q} \rightarrow gg$, $qg \rightarrow qg$, $gg \rightarrow q\overline{q}$ and $gg \rightarrow gg$ occur in classes 1, 3 and 6.
- Elastic, diffractive and low-$p_\perp$ events occur in class 1.

33

The notation direct, 1-resolved and 2-resolved is the conventional subdivision of $\gamma\gamma$ interactions. The rest is then called 'soft-VMD'. The subdivision in PYTHIA is an attempt to be more precise and internally consistent than the conventional classes allow.

The cross-sections for the above components are based on a number of considerations. The VMD×VMD ones are derived from a Regge theory ansatz, with a pomeron plus reggeon form for the total cross-section, plus parametrizations of elastic and diffractive components [57]. The other five cross-sections are obtained by a direct integration of parton-level cross-sections above lower cut-offs $k_0 \approx 0.6$ GeV for $\gamma \leftrightarrow q\overline{q}$ fluctuations and $p_{\perp\min}^{\mathrm{anom}} = 0.7 + 0.17\log^2(1 + E_{\mathrm{cm}}/20)$ [GeV] for QCD processes in the anomalous sector. The latter is a purely phenomenological fit based on consistency arguments in the γp sector. It does not include possible eikonalization effects, and would therefore change in a more complete treatment (studies under way). Taken all together, one obtains a reasonable description of the total $\gamma\gamma$ cross-section.

The program comes with several parton-distribution sets for the photon. The default is SaS 1D [9]. In view of the above event classification, the SaS sets have the advantage that the separation into VMD and anomalous parts is explicit.

Currently only real incoming photons are considered. Eventually PYTHIA should be extended to (moderately) virtual photons. A separate treatment exists of the DIS region, e$\gamma \to$ eX, i.e. with one real and one very virtual γ, but this option is less well developed (especially for parton showers). Furthermore, the program does not yet generate the spectrum of real photons internally, i.e. it is easiest to run for a fixed energy of the $\gamma\gamma$ system. It is possible to use the varying-energy and weighted-events options of the program to obtain a reasonable photon spectrum, however.

Some main switches and parameters of interest for $\gamma\gamma$ physics are:
- `MSEL` selects allowed processes; a change to 2 would include also elastic and diffractive VMD events.
- `MSTP(14)` sets the $\gamma\gamma$ event class among the six possibilities listed above. The most useful option is `MSTP(14) = 10`, where the six classes are automatically mixed in the proper proportions. Note that some variables, such as `CKIN(3)`, differ between the event classes and therefore automatically are reset internally.
- `MSTI(9)` tells which event class the current event belongs to.
- `MSTP(55)` and `MSTP(56)` gives choice of parton-distribution set and library for the photon.
- `PARP(15)` is the k_0 scale, i.e. minimum $p_\perp$ for $\gamma \leftrightarrow q\overline{q}$ fluctuations.
- `CKIN(3)` sets $p_{\perp\min}$ scale of hard interactions; for `MSTP(14) = 10` only to be set when studying high-$p_\perp$ jet production.
- `PARP(81)` (alternatively `PARP(82)`, depending on `MSTP(82)` value) sets the $p_{\perp\min}$ scale of multiple interactions in VMD×VMD events.

5   Other generators

Most of the general-purpose QCD event generators described above have only become available for $\gamma\gamma$ physics during the last year or two. Therefore most existing analyses have used generators written specifically for $\gamma\gamma$ physics with little or no overlap with other processes. This means that they are extremely hard to test thoroughly, except on the very data they are used to unfold. Although of course the different programs have different strengths and weaknesses, they are mainly based on the same general design. In this section we describe it and make a few general comments on when and why it is expected to be adequate or inadequate.

The principle way in which the older programs differ from the QCD generators is the lack of a parton shower stage. A hard scattering is typically generated according to the leading order matrix element, often taking great care with their accuracy and including many effects that are not yet included in the QCD programs. The final state described by these matrix elements ranges from a simple quark-antiquark pair in the case of DIS to up to two jets and two remnants in the case of high-p_t scattering. These simple partonic states are then given directly to the JETSET program, which implements the Lund string fragmentation model.

It may at first sight appear that parton showers are a luxurious frill that can be added to the model to slightly improve event simulation, for example by including the small fraction of events in which a third jet accompanies the two hard jets in an event. However in the modern view of hadronization, they are an essential precursor to the confinement of partons into hadrons, which does not take place globally between the main few hard partons in an event but locally between nearby soft partons. It is only by adopting the latter view that one can have any expectation that the hadronization process is universal. Quite apart from these theoretical issues, as a practical issue it is certainly the case that the parameters of the string model need to be retuned to fit to data at different energies and in different reactions when it is not preceded by a parton shower, but that coupled with a parton shower a reasonable description of all current data can be achieved with a single parameter set. This alone is enough to mean that any model that uses string fragmentation without a parton shower should be considered descriptive rather than predictive.

In addition to their rôle in setting the initial conditions for the hadronization process, parton showers are crucial for determining certain event features, for example the hadronic final state of DIS at small x, where the predictions of a 'QPM model', i.e. hard matrix element plus string fragmentation were found to give an extremely poor description of the HERA data [58].

Another closely related difference between the two groups of programs is in the assumptions made about the photon structure function. The older programs generally make an FKP-like [59] separation into the point-like and hadronic parts, a scheme with strong physical motivation, but then neglect the QCD evolution in the hadronic part. While one might suppose that this is unimportant if we only use the event generator as an unfolding tool, this is not in fact the case because structure functions do not just evolve by themselves, they do so by emitting gluons, which have an effect on the structure of the hadronic final state. QCD not only predicts that

changing Q^2 changes the structure function, but also the features of the hadronic final state. This should therefore be included in any model used to unfold data.

One possible solution would be to incorporate parton showers into the existing programs. However this is far from straightforward, because the evolution of a shower is strongly dependent on its initial conditions, namely on how the hard partons were formed. For example in DIS, simply setting up a q$\bar{\text{q}}$ pair and calling JETSET with its final state parton shower option switched on will result in emission with transverse momenta up to $W/2$, producing far too much hadronic activity. The correct solution, roughly speaking, is that the current jet produces a shower with upper scale of order Q, the photon remnant produces one of order its p_t and the internal line produces an initial-state shower. There are additional complications in the high-p_t case as there are contributions that contribute to different event classes depending on their kinematics, so one must impose additional constraints on the parton shower in order to avoid double-counting. Eventually, one realizes that to build in all the relevant conditions, the parton shower has to know so much about the hard process that one ends up almost having to write ones own parton shower algorithm from scratch.

Should we therefore conclude that existing programs are wrong and existing analyses need to be redone? No, because in the kinematic regions explored so far they have several advantages. Firstly the range in W has been rather limited so that the move into regions in which parton showers and QCD effects become important has been limited. Secondly for reasonably low W, most of the hadronic event is actually seen in the detector, so the actual reliance on the models is rather small. Thirdly, this means that the models can be well constrained and tested by fitting to the majority of the event so that they are fairly predictive for the unseen remainder of it. Finally, and very importantly, the low energy range has many problems associated with it that are rather carefully treated in the dedicated generators, such as exact kinematics, target mass effects, higher order terms in the EPA and other polarization states of the photon. This is in contrast with the QCD programs, which were traditionally oriented towards the high energy limit and are only now starting to 'catch up' in their treatment of effects important at lower energy.

In conclusion, we would say that at pre-LEP energies existing programs are perfectly adequate. At LEP 1, they have proved sufficient for most tasks, but problems are beginning to become apparent. For example, in DIS if one studies the energy flow in the detector as a function of x_{vis}, similar to what is shown in Fig. 8, one obtains predictions that are reasonably insensitive to the shape of the structure function and hence can make a fairly stringent test of the model. Preliminary results seem to indicate that existing models already have problems [60]. One can fairly confidently predict that at LEP 2 these problems will be sufficiently severe that using the QCD models will become essential, both because of the huge leap to smaller x and higher Q^2 and simply because of the higher statistical precision that will require better control of systematic errors.

Below we give a few basic facts about some of the programs used at present.

5.1 DIAG36

Author: F.A. Berends, P.H. Daverveldt and R. Kleiss [14]
E-mail: t30@nikhef.nl
Program size: 4335 lines
Program location: CPC program library

DIAG36 is an event generator for the full set of QED diagrams for $e^+e^- \to e^+e^-f\bar{f}$, including all fermion masses. Phase-space generation can cover the whole kinematically-allowed phase-space, or cuts can be applied for typical single- or double-tagged configurations.

5.2 MINIJET

Author: A. Miyamoto and H. Hayashii [29]
E-mail:hayashii@naras1.kek.jp

The MINIJET program generates the direct and the resolved photon events in two-photon processes of e^+e^- collisions. It calculates the cross-section of light- and heavy-quark production according to the EPA approximation for the photon flux and the leading-order matrix elements for the sub-process cross-sections. It uses the BASES program for the cross-section calculation and SPRING for the generation of four-momenta of final state partons. The generated parton are hadronized using the JETSET program. It has been used in the analysis of two-photon data by the TOPAZ group and in background studies for the JLC. Multiple interactions are not included in the program.

5.3 PC

Author: F.L. Linde [13]
E-mail: z66@nikhef.nl

The PC program generates two-photon events according to Eq. 2. It provides event generation of fermion pairs and resonance states in phase space of up to 4 final state particles with many dominant resonant states. The form factor is chosen between ρ, π, and J/ψ poles. It provides a cross-section calculation of all terms in Eq. 2.

5.4 RESPRO

Author: E.R. Boudinov and M.V. Shevlyagin [18]
       E-mail: BOUDINOV@vxcern.cern.ch

The RESPRO program generates explicitly the two-photon resonance in a very efficient way and calculates the cross-section according to Eqs. 3 and 7.

5.5 TWOGAM

Authors: S. Nova, A. Olshevski, T. Todorov [6]
       E-mail: todorovt@vxcern.cern.ch

TWOGAM implements Eq. 2 exactly for leptonic final states and for the direct, QPM, component of quark production, including all helicity states and the exact $2 \rightarrow 4$ kinematics. Single- and double-resolved components are added to the transverse–transverse scattering cross-section according to any parton distribution function selected from PDFLIB, and include a simple P^2-suppression model. The resulting partonic states are hadronized by the Lund string model, as implemented in JETSET. The user can select from several different soft VDM scattering models.

5.6 TWOGEN

Author: A. Buijs, W.G.J. Langeveld, M.H. Lehto, D.J. Miller [19]
       E-mail: buijs@fys.ruu.nl
Program size: 1800 lines
Program location: http://www.fys.ruu.nl/ buijs/twogen/twogen.for

TWOGEN samples the transverse-transverse luminosity function for real and virtual photons of the multiperipheral diagram. The events are then weighted with any user supplied cross-section $\sigma_{TT}(\gamma\gamma \rightarrow X)$ and chosen using a simple "hit or miss" sampling. Thus, for example, the program can generate according to a chosen F_2 or can produce resonances. Final state partons are fragmented using the Lund string model in JETSET.

5.7   Vermaseren

Author: J.A.M. Vermaseren [15]
                     E-mail: t68@nikhef.nl

The Vermaseren Monte Carlo has become the *de facto* standard calculation of $e^+e^- \to e^+e^- f\bar{f}$ via $\gamma\gamma$ collisions. It uses the subset of the exact $2 \to 4$ matrix elements in which the electron and positron lines do not annihilate (i.e. formally they apply to the process $e^+\mu^- \to e^+\mu^- f\bar{f}$ with equal electron and "muon" masses).

6   Conclusions

$\gamma\gamma$ physics at LEP 2 is virtually impossible without event generators. Not only are they needed for modelling detector effects, as in almost all high energy physics analyses, but also because in $\gamma\gamma$ collisions the energy of the incoming photons is generally unknown. This means that we need to reconstruct the basic parameters of events solely from final-state properties. Except for the simplest final states consisting of only a few particles, detailed understanding is presently only possible through models implemented in event generators.

During the course of this workshop, several general purpose QCD generators have been developed to better handle $\gamma\gamma$ and eγ interactions, enabling us to use experience gained from experiments with e^+e^-, ep and pp collisions, where these programs have been used extensively. A lot more work needs to be done however. In contrast to the special purpose generators used so far in $\gamma\gamma$ physics, which in the case of high energy multi-particle production are less theoretically advanced, the general purpose ones have not yet been extensively confronted with available data. Such comparisons have already been started for γp data from HERA with promising results, and it is important that this is also done with LEP 1 $\gamma\gamma$ data in preparation for LEP 2.

References

[1] Report of the $\gamma\gamma$ physics working group, these proceedings.

[2] Report of the QCD event generator working group, these proceedings.

[3] V.M. Budnev, et al., *Phys. Rep.* **15** (1975) 181.

[4] G. Bonneau, et al., *Nucl. Phys.* **B54** (1973) 573.

[5] J.H. Field, *Nucl. Phys.* **B168** (1980) 477; **B176** (1980) 545; **B187** (1981) 585.

[6] S. Nova, A. Olshevski, T. Todorov, DELPHI Note 90-35 (1990).

[7] S. Frixione, et al., *Phys. Lett.* **B319** (1993) 339.

[8] H. Plothow-Besch, *Comput. Phys. Commun.* **75** (1993) 396.

[9] G.A. Schuler and T. Sjöstrand, *Z. Phys.* **C68** (1995) 607.

[10] M. Glück, E. Reya, A. Vogt, *Phys. Rev.* **D46** (1992) 1973.

[11] B. Andersson, et al., *Phys. Rep.* **97** (1983) 31.

[12] B.R. Webber, *Nucl. Phys.* **B238** (1984) 492.

[13] F.L. Linde, "Charm production in two-photon collisions", RX-1224 (LEIDEN), (1988) thesis.

[14] F.A. Berends, P.H. Daverveldt, R. Kleiss, *Nucl. Phys.* **B253** (1985) 421; *Comput. Phys. Commun.* **40** (1986) 271, 285, and 309.

[15] J.A.M. Vermaseren, *Nucl. Phys.* **B229** (1983) 347.

[16] M. Poppe, *Int. J. of Mod. Phys.* **1** (1986) 545.

[17] F. Low, *Phys. Rev.* **120** (1960) 582; P. Kessler, *Nuovo Cim.* **17** (1960) 809.

[18] E.R. Boudinov and M.V. Shevlyagin, DELPHI 95-49 PHYS 487.

[19] A. Buijs, et al., *Comput. Phys. Commun.* **79** (1994) 523.

[20] W. Thomé, et al., *Nucl. Phys.* **B129** (1977) 365.

[21] V. Blobel, Proc. CERN school of computing, Aiguablava, Spain, September 1984.

[22] G. d'Agostini, *Nucl. Instrum. Meth.* **A362** (1995) 487.

[23] OPAL Collaboration, R. Akers, et al., *Z. Phys.* **C61** (1993) 199.

[24] DELPHI Collaboration, P. Abreu, et al., CERN-PPE/95-87, June 1995 (to be published in *Z. Phys. C*).

[25] F. Jacquet and A. Blondel, "Proc. of the study for an ep facility for Europe", DESY 79/48 (1979) 391.

[26] ZEUS Collaboration, M. Derrick, et al., *Phys. Lett.* **B348** (1995) 665.

[27] ALEPH Collaboration, D. Buskulic, et al., *Phys. Lett.* **B355** (1995) 595.

[28] M. Drees, et al., *Phys. Lett.* **B306** (1993) 371;
M. Krämer, proceedings of the Photon 95 conference, Sheffield, UK.

[29] A. Miyamoto, H. Hayashii, KEK Preprint 94-204, to appear in *Comput. Phys. Commun.*

[30] L. Lönnblad, *Comput. Phys. Commun.* **71** (1992) 15.

[31] G. Gustafson, *Phys. Lett.* **B175** (1986) 453.

[32] G. Gustafson, U. Pettersson, *Nucl. Phys.* **B306** (1988) 746.

[33] B. Andersson, et al., *Z. Phys.* **C43** (1989) 625.

[34] S. Kawabata, *Comput. Phys. Commun.* **41** (1986) 127.

[35] T. Munehisa, et al., KEK CP-034, KEK preprint 95-51, ENSLAPP-A-522/95, LPTHE-Orsay 95/37, to appear in *Z. Phys. C.*

[36] R. Odorico, *Nucl. Phys.* **B172** (1980) 157;
G. Marchesini and B.R. Webber, *Nucl. Phys.* **B238** (1984) 1;
K. Kato, T. Munehisa, *Comput. Phys. Commun.* **64** (1991) 67.

[37] E. Witten, *Nucl. Phys.* **B120**(1977)189;
Ch. Berger and W. Wagner, *Phys. Rep.* **146** (1987) 1.

[38] K. Kato, Y. Shimizu, H. Yamamoto, *Prog. Theor. Phys.* **63**(1980)1295;
K. Kato, Y. Shimizu, *Prog. Theor. Phys.* **64** (1980) 703; **68** (1982) 862;
K. Kato, Y. Shimizu, H. Yamamoto, preprint, UT-370 (1982), unpublished.

[39] T. Sjöstrand, *Comput. Phys. Commun.* **82** (1994) 74;
T. Sjöstrand, Lund University report LU TP 95–20 (1995).

[40] G. Marchesini, et al., *Comput. Phys. Commun.* **67** (1992) 465.

[41] G. Marchesini and B.R. Webber, *Nucl. Phys.* **B386** (1992) 215.

[42] M.H. Seymour, *Comput. Phys. Commun.* **90** (1995) 95.

[43] M.H. Seymour, contribution gls0258 to the "27th International Conference on High Energy Physics", Glasgow, U.K., 20–27 July 1994.

[44] J.M. Butterworth, J.R. Forshaw, *J. Phys.* **G19** (1993) 1657;
J.M. Butterworth, J.R. Forshaw, M.H. Seymour, CERN–TH/95–82, in preparation.

[45] R. Engel, *Z. Phys.* **C66** (1995) 203;
R. Engel. "Multiparticle Photoproduction within the two-component Dual Parton Model", in preparation, 1995;
R. Engel, J. Ranft, "Hadronic photon-photon collisions at high energies", ENSLAPP-A-540/95 (hep-ph/9509373), 1995.

[46] A. Capella, et al., *Phys. Rep.* **236** (1994) 227.

[47] P. Aurenche, et al., *Phys. Rev.* **D45** (1992) 92.

[48] P. Aurenche, et al., *Comput. Phys. Commun.* **83** (1994) 107.

[49] V.A. Abramovski, V.N. Gribov, O.V. Kancheli, *Yad. Fis.* **18** (1973) 595.

[50] K. Hahn and J. Ranft, *Phys. Rev.* **D41** (1990) 1463.

[51] A. Capella, et al., *Z. Phys.* **C10** (1980) 249;
A.B. Kaidalov, *Phys. Lett.* **B116** (1982) 459.

[52] A. Capella, et al., *Phys. Lett.* **B343** (1995) 403;
R. Engel, J. Ranft, S. Roesler, **Phys. Rev. D52** (1995) 1459.

[53] H.U. Bengtsson, *Comput. Phys. Commun.* **31** (1984) 323.

[54] R. Engel, PHOJET manual, 1995.

[55] G.A. Schuler, T. Sjöstrand, *Phys. Lett.* **B300** (1993) 169; *Nucl. Phys.* **B407** (1993) 539.

[56] G.A. Schuler and T. Sjöstrand, in "Two-Photon Physics from DAΦNE to LEP200 and Beyond", World Scientific, Singapore, 1994, eds. F. Kapusta and J. Parisi, p163;
T. Sjöstrand, in "XXIV International Symposium on Multiparticle Dynamics 1994", World Scientific, Singapore, 1995, eds. A. Giovannini, S. Lupia and R. Ugoccioni, p221.

[57] G.A. Schuler and T. Sjöstrand, *Phys. Rev.* **D49** (1994) 2257.

[58] H1 Collaboration, I. Abt, et al., *Z. Phys.* **63** (1994) 377.

[59] J.H. Field, F. Kapusta, L Poggioli, *Phys. Lett.* **B181** (1986) 362; J.H. Field, F. Kapusta, L Poggioli, *Z. Phys.* **C36** (1987) 121; F. Kapusta, *Z. Phys.* **C42** (1989) 225.

[60] F. Kapusta, I. Tyapkin, N. Zimin and A. Zinchenko, DELPHI note in preparation.

Event Generators for Bhabha Scattering

Conveners: S. Jadach and O. Nicrosini

Working Group: H. Anlauf, A. Arbuzov, M. Bigi, H. Burkhardt, M. Cacciari, M. Caffo,
H. Czyż, M. Dallavalle, J. Field, F. Filthaut, F. Jegerlehner, E. Kuraev, G. Montagna,
T. Ohl, B. Pietrzyk, F. Piccinini, W. Płaczek, E. Remiddi, M. Skrzypek, L. Trentadue,
B. F. L. Ward, Z. Wąs,

Contents

1 Introduction

The main goals of the Bhabha working group are to make an inventory of all the available Monte Carlo (MC) event generators for small-angle (SABH) and large-angle (LABH) Bhabha processes at LEP1 and LEP2, and to improve our understanding of their theoretical uncertainties through systematic comparisons of the MC event generators (developed independently) among themselves and with other non-MC programs. The presented activity is of course an obvious continuation of the previous workshops on LEP1 physics [1, 2]. In the beginning of the present workshop the theoretical uncertainty at LEP1 for the SABH process was typically estimated as 0.16%, and for the LABH process was estimated at 0.2% level at Z peak and 1% on the wings of the Z resonance. There were no estimates specific to LEP2.

We shall concentrate on the comparison of all the presently available theoretical calculations (published and unpublished). This will be done for several kinds of event selection (ES), defined as a set of experimental cuts and apparatus acceptances, starting from ES's unrealistic, but useful for some studies oriented towards the QED matrix element, and ending on ES's very close to the experimental ones.

Let us add a few comments to clarify our priorities and to set the proper perspective for our work. In spite of the considerable effort of several theoretical groups, at present the theoretical error on the small-angle Bhabha cross section dominates the luminosity error at LEP1. This inhibits from taking full advantage of the high experimental precision of the final LEP1 data for precision tests of the Standard Model. As a consequence, the reduction of the theoretical error in the SABH process at LEP1 is the biggest challenge, and was the main objective of our working group. The precision requirements of LEP2 are lower than those of LEP1. The total cross section of W pair production will be measured with 1.0% to 0.5% precision at best, so it is sufficient to keep the theoretical uncertainty of the SABH process at the 0.25% level. Furthermore, at LEP2 the detectors and experimental techniques for measuring the SABH process are almost the same as for LEP1[1]. Radiative corrections to the SABH cross section depend on the center of mass energy, but smoothly; moreover, in the small-angle regime the center of mass energy is not so important from the point of view of the physics involved: we are always faced with a t-channel photon-exchange dominated process; hence, improving the small-angle Bhabha generators for LEP1 is generally a sufficient condition for improving them also for LEP2. The only subtle point concerns the error estimate: a 0.1% error at LEP1 does not guarantee such a small error also at LEP2, so that an additional analysis has to be performed. For the LABH process, the final LEP1 data analysis requires a theoretical uncertainty of the codes used to be at the 0.5% level. The LABH process at LEP2 is not of major interest, and we think that a precision of the order of 2% is enough. Nevertheless, the physics of the LABH process at LEP2 is significantly different from LEP1 (different Feynman diagrams rise to importance), so performing additional study for the LABH process at LEP2 is a new nontrivial

---

[1]Actually, the main difference is that, due to machine background radiation, the internal part of luminosity detectors may be obscured by special masks. We shall discuss the impact of such modification on the theoretical errors. This aspect was brought to our attention by B. Bloch-Devaux during our WG meeting in January 95.

work[2].

In view of the above, our strategy was to do all the work for the SABH and the LABH processes first for LEP1 experimental conditions, and to supplement it with all necessary work/discussion which would assure control of the precision at the level sufficient for LEP2 experiments. This practically means that all the numerical comparisons were done for LEP1 and repeated for LEP2, or, in rare cases, a convincing argument was given that it is not necessary (sometimes numerical results for LEP2 were obtained, but are not shown in full form because they were trivially identical to those for LEP1).

We include in our report two main parts: one part on the SABH process and a second one on the LABH process, with the cases of LEP1 and LEP2 discussed in parallel. These two processes are governed by different physics (i.e. dominated by different Feynman diagrams). Also, the theoretical precision requirements in calculating SABH and LABH cross sections are different by a factor of five-ten. These two parts are followed by a section including short descriptions of all the involved Monte Carlo (MC) event generators or other codes, and a final section on conclusions and outlook.

2   Small-angle Bhabha scattering

Small-angle Bhabha (SABH) scattering is used at LEP1 and LEP2 to measure the accelerator luminosity. The LEP1 experiments have reached in 1993-1994 a systematic uncertainty of better than 0.10% in selecting luminosity Bhabha events, see Ref. [3] and Refs. [4,5].

On the theory side, QED calculations have still an uncertainty larger than 0.16% [6] in determining the Bhabha cross section in the detector acceptance, which is caused mostly by the non-existence of a Monte Carlo program including complete $\mathcal{O}(\alpha^2)$ next-to-leading terms. Actually, there exist $\mathcal{O}(\alpha^2)$ calculations with complete next-to-leading contributions [7,8] which claim a precision of the order of 0.1%, but they can not be used in a straightforward way, because they are not implemented in the Monte Carlo event generators. The size of the $\mathcal{O}(\alpha^2)$ contributions depends not only on the angular range covered by the detector and on the electron energy cut-off, but also on crucial experimental aspects, such as the sensitivity to soft photons or such as the electron cluster size. This means that the main interest is in the theoretical predictions for the Bhabha process, including as many higher order radiative corrections at it is necessary to reach a precision of 0.05%, in a form of a Monte Carlo *event generator*.

Monte Carlo event generators are very powerful tools because they are able to provide a theoretical prediction, cross sections and any kind of distribution, for arbitrary ES's. However, event generators are difficult to construct and, what is even more serious, they are very difficult to test – one has to have at least two of them to compare with one another for a wide range of

---

[2]The radiative LABH process is an important background to other processes, like τ-pair production, $W^+W^- - > ee\nu\nu$, "new physics" like SUSY processes and so on, but a detailed analysis of these items goes beyond the aims of the present study.

4

ES's.

For the SABH process, the task of comparing various Monte Carlo event generators was the *main goal* of the Bhabha Working Group. There were only a few comparisons of independently developed Monte Carlo event generators for the SABH process in the past. A few examples can be found in Ref. [2]. However, we shall include in the comparisons results from non-Monte Carlo calculations, as well. They are usually limited to certain special (primitive) ES's. Nevertheless they provide additional valuable cross-checks.

What shall we learn from these comparisons? The calculations from various Monte Carlo event generators will of course differ. The differences have to be understood. In a certain class of the comparisons, the underlying QED matrix element will be the same and in that case the differences will be only due to numerical effects. The results from two or more computer programs will differ due to rounding errors, programming bugs, numerical approximations. The difference measures uncertainties of this kind, and we say that we are determining the *technical precision* of the tested programs. One has to remember that the technical precision is dependent on the ES, and it is therefore absolutely necessary to use several at least semi-realistic, quite different, examples of ES's. In other cases, we shall compare Monte Carlo event generators which are based on different QED matrix elements. In this case, the difference between results will tell us typically about higher order effects which are *not included* in some of these event generators, or which are *approximated* differently in these programs. In this situation we shall talk about exploring the *physical precision* of the tested Monte Carlo event generators. Needless to say, the physical precision is the main goal, but one has to remember that without a technical precision of at least a factor of two better than the physical precision it is pointless to discuss the physical precision at all!

Before we come to the actual comparisons of the programs, let us characterize various contributions/corrections to the SABH process. We shall also characterize briefly the various Monte Carlo event generators and non-Monte-Carlo calculations involved in the comparisons.

If we remember that the SABH process was chosen for the luminosity measurement because it is calculable from first principles within quantum electrodynamics (QED), then it is natural to group corrections to the SABH process into *pure-QED* and *non-QED* corrections. The latter ones are due to s-channel Z-exchange, and the corrections induced by low energy strong interactions (QCD) through vacuum polarization and light quark pair production. Among the pure QED corrections, we may distinguish *photonic* (bremsstrahlung) corrections, related to multiple photon emission, and *non-photonic* corrections – for instance lepton pairs, leptonic vacuum polarization, multiperipheral diagrams. Numerically, the biggest ones are the photonic corrections and the vacuum polarization correction. They also contribute the most to the physical precision. Photonic corrections dominate completely the technical precision, due to the MC integration over the complicated multi-body phase space. The QED non-photonic corrections are small, but are difficult to calculate and quite uncertain (technical precision).

For all the comparisons of the event generators it is crucial (especially for SABH) to understand the experimental ES. In the main comparisons we shall compare *all* the available event

generators for four types of ES's. However, the problem of the variation of the parameters in the ES is so important that we include also a separate subsection on this subject, in which, for a limited number of three event generators, we perform a detailed study of the dependence of the higher order corrections on all possible cut-offs involved in the real experiment. This will allow us to see all our work in the proper perspective from the point of view of the experimental analysis, and will also give us clear hints on the dependence of the higher order corrections on the fine details of the ES. This study will be limited to the SABH process.

2.1   Sensitivity of LEP1 observables to luminosity

The importance of the improvement of the theoretical luminosity error on the LEP1 results is shown in Table 1. The results of the lineshape parameter fits made with the theoretical luminosity error of 0.16% and 0.11% are given [9], corresponding to the reduction of error achieved during this workshop. A projection concerning a further reduction of the theoretical luminosity error to 0.06% is also given. The results of the four LEP1 experiments used as input to the fits, as well as the fitting procedure, are described in Ref. [10]. From the five parameter fit, only σ_h^0 is sensitive to the luminosity error. The decreased error in this variable causes a reduction of the errors of the derived parameters shown in the lower part of Table 1. As we see, the above improvement in the theoretical luminosity error influences significantly not only quantities like the "number of light neutrino's" N_ν, but also other LEP1 observables used routinely in the tests of the Standard Model.

	theoretical luminosity error		
	0.16%	0.11%	0.06%
m_Z [GeV]	91.1884 ± 0.0022	91.1884 ± 0.0022	91.1884 ± 0.0022
Γ_Z [GeV]	2.4962 ± 0.0032	2.4962 ± 0.0032	2.4961 ± 0.0032
σ_h^0 [nb]	41.487 ± 0.075	41.487 ± 0.057	41.487 ± 0.044
R_l	20.788 ± 0.032	20.787 ± 0.032	20.786 ± 0.032
$A_{FB}^{0,l}$	0.0173 ± 0.0012	0.0173 ± 0.0012	0.0173 ± 0012
Γ_{had} [GeV]	1.7447 ± 0.0030	1.7447 ± 0.0028	1.7446 ± 0.0027
Γ_{ll} [MeV]	83.93 ± 0.13	83.93 ± 0.13	83.93 ± 0.12
σ_{ll}^0 [nb]	1.9957 ± 0.0044	1.9958 ± 0.0038	1.9959 ± 0.0034
Γ_{had}/Γ_Z [%]	69.90 ± 0.089	69.90 ± 0.079	69.89 ± 0.072
Γ_{ll}/Γ_Z [%]	3.362 ± 0.0037	3.362 ± 0.0032	3.362 ± 0.0028
Γ_{inv} [MeV]	499.9 ± 2.4	499.9 ± 2.1	499.9 ± 1.9
Γ_{inv}/Γ_{ll} [%]	5.956 ± 0.030	5.956 ± 0.024	5.956 ± 0.020
N_ν	2.990 ± 0.015	2.990 ± 0.013	2.990 ± 0.011

Table 1: Line shape and asymmetry parameters from 5-parameter fits to the data of the four LEP1 experiments, made with a theoretical luminosity error of 0.16%, 0.11% and 0.06% [9]. In the lower part of the Table also derived parameters are listed.

At LEP2, the normalization of the total cross section for the WW production process enters

in a nontrivial way into tests of the W boson coupling constants. The precision requirements for the total cross section is limited by statistics of the WW process, and a luminosity error at the 0.25% level is sufficient (see the chapter "WW cross-sections and distributions", these proceedings).

2.2   Higher order photonic corrections at LEP1 and LEP2

Canonical coefficients					
		$\theta_{min} = 30$ mrad		$\theta_{min} = 60$ mrad	
		LEP1	LEP2	LEP1	LEP2
$\mathcal{O}(\alpha L)$	$\frac{\alpha}{\pi}4L$	137×10^{-3}	152×10^{-3}	150×10^{-3}	165×10^{-3}
$\mathcal{O}(\alpha)$	$2\frac{1}{2}\frac{\alpha}{\pi}$	2.3×10^{-3}	2.3×10^{-3}	2.3×10^{-3}	2.3×10^{-3}
$\mathcal{O}(\alpha^2 L^2)$	$\frac{1}{2}\left(\frac{\alpha}{\pi}4L\right)^2$	9.4×10^{-3}	11×10^{-3}	11×10^{-3}	14×10^{-3}
$\mathcal{O}(\alpha^2 L)$	$\frac{\alpha}{\pi}\left(\frac{\alpha}{\pi}4L\right)$	0.31×10^{-3}	0.35×10^{-3}	0.35×10^{-3}	0.38×10^{-3}
$\mathcal{O}(\alpha^3 L^3)$	$\frac{1}{3!}\left(\frac{\alpha}{\pi}4L\right)^3$	0.42×10^{-3}	0.58×10^{-3}	0.57×10^{-3}	0.74×10^{-3}

Table 2: The canonical coefficients indicating the generic magnitude of various leading and subleading contributions up to third-order. The big-log $L = \ln(|t|/m_e^2) - 1$ is calculated for $\theta_{min} = 30$ mrad and $\theta_{min} = 60$ mrad and for two values of the center of mass energy: at LEP1 $\left(\sqrt{s} = M_Z\right)$, where the corresponding $|t| = (s/4)\theta_{min}^2$ are 1.86 and 7.53 GeV^2, and at LEP2 energy $\left(\sqrt{s} = 200$ GeV$\right)$, where the corresponding $|t|$ are 9 and 36 GeV^2, respectively.

For the SABH process, the smallness of the electron mass "ruins" the normal perturbative expansion order in the following sense: for instance, the $\mathcal{O}(\alpha^2)$ QED contributions can be expanded into $\mathcal{O}(\alpha^2 L^2)$, $\mathcal{O}(\alpha^2 L)$ and pure non-log $\mathcal{O}(\alpha^2)$. The non-log $\mathcal{O}(\alpha^2)$ corrections are completely uninteresting, while the $\mathcal{O}(\alpha^3 L^3)$ corrections are as important as the $\mathcal{O}(\alpha^2 L)$ corrections. Here $L = \ln(|t|/m_e^2)$ is the so-called big-log in the leading-logarithmic (LL) approximation, where t is the momentum transfer in the t-channel (of the order of 1 GeV). This phenomenon is illustrated in Tab. 2. From this table, it is clear that for a precision of the order of 0.25% (for calorimetric ES's) it is enough to include the $\mathcal{O}(\alpha^1 L)$, $\mathcal{O}(\alpha^1)$ and $\mathcal{O}(\alpha^2 L^2)$. For a precision of the order of 0.1% or better, one has to add $\mathcal{O}(\alpha^3 L^3)$ and $\mathcal{O}(\alpha^2 L)$. These "scale coefficients" have to be kept in mind when discussing various QED calculations/programs. As we shall see, the higher order effects seen in the numerical results presented in the next sections generally conform to the above scale coefficients.

Table 2 demonstrates also the "scaling laws" for various QED corrections between LEP1 (Z peak) and LEP2 energies. If the angular range is kept the same, then t-channel transfer is proportional to $s = 4E_{beam}^2$. Actually, at LEP2 experiments the luminosity measurement will rely more on the SABH process at larger angles, above 3°, and this is why we also included in

the table another two columns for this angular range. As we see, photonic corrections do not change very much due to the increase of $\sqrt{s}$ from Z-peak energy to LEP2 energy (200 GeV) and due to going to twice larger angles. Actually, the change in canonical coefficients is negligible. One has only to pay attention to the $\mathcal{O}(\alpha^3 L^3)$ corrections, which in the worst case increase by a factor 1.75 (however, as we shall see they are under good control).

One has to remember that, as it was shown explicitly in ref. [11], the radiative corrections to the SABH process with the typical "double tag" detection are proportional to $\ln((\theta_{max}/\theta_{min}) - 1)$, i.e. they are bigger for "narrower" angular acceptance and smaller for "wider" angular acceptance. This has to be remembered, because at LEP2 in some experiments the angular range might be "narrowed" by placing masks in front of the SABH detectors in order to eliminate machine background radiation. We conclude that the change for "narrower" angular acceptance is more dangerous from the point of view of the increase of the pure photonic corrections, and we shall address this problem with a separate numerical exercise.

In ref. [11] it was also shown (numerically), using an $\mathcal{O}(\alpha)$ calculation, that for the purpose of the SABH process below 6° we may neglect the real and virtual QED interference contributions between photon emission from the electron and positron lines, the so called "up-down interference". In the numerical example in ref. [11] it was shown that, for the angular range $3.0° - 4.24°$, the "up-down interference" is below 0.015%. It is even smaller for smaller angles. It means that it is negligible for all practical purposes in the luminosity measurements. This phenomenon was also discussed in ref. [12] beyond $\mathcal{O}(\alpha)$ in the framework of the eikonal approximation.

2.3 Light pairs and other small contributions

To calculate pair corrections to the SABH two approaches have been used. **(1)** The first one is based on direct analysis of Feynman graphs and analytical extraction of graphs and terms contributing to the SABH within the $\mathcal{O}(0.1\%)$ accuracy. Both leading and next-to-leading terms are considered. **(2)** The other method uses the LL approximation to find the dominant pair contributions to SABH and to discard the negligible ones. Having isolated the dominant mechanism, an actual MC program for this particular mechanism is constructed.

(1) The dominant pair production corrections (enhanced by factors of L^2 and L) arise from kinematical configurations where one (or both) of the produced leptons is almost collinear with the incoming or outgoing $e^\pm$. These contributions have been calculated analytically [13, 14]. The analytical calculation [7, 8, 13–15] of the real hard pair production cross-section within logarithmic accuracy takes into account the contributions of the collinear and semi-collinear kinematical regions. All possible mechanisms for pair creation (Singlet and Non-Singlet), as well as the identity of the particles in the final state, are taken into account[3]. In the case of

---

[3]Here we have taken into account only $e^+ e^-$ pair production. An estimate of the muon pair contribution gives less than 0.05% since $\ln(Q^2/m^2) \sim 3\ln(Q^2/m_\mu^2)$. Contributions of pion and tau-lepton pairs give still smaller corrections. Therefore, within the 0.1% accuracy, one may omit any pair production contribution except the
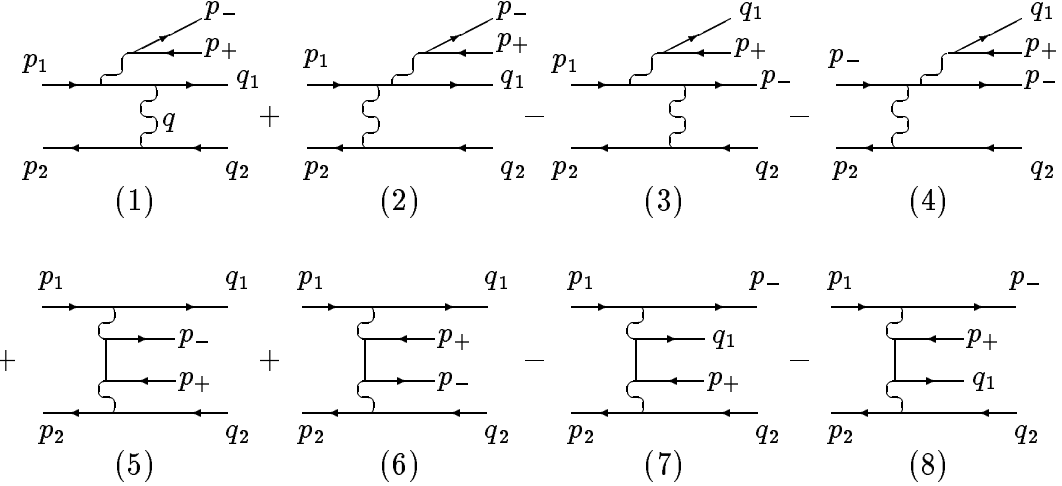
Figure 1: The Feynman diagrams giving logarithmically enhanced contributions in the kinematical region where the created pair goes along the electron direction. The signs represent the Fermi-Dirac statistics of the interchanged fermions.

Channel	e e	$\mu\mu$	$\tau\tau$	$c\bar{c}$	$u\bar{u}, d\bar{d}, s\bar{s}$	total
σ (nb)	0.006	0.006	0.0008	0.0005	0.0011	0.0144

Table 3: Double Tag cross sections for fermion pair production from multiperipheral graphs. $\sqrt{s} = 91.2$ GeV, 30 mrad $< \theta_{e^+}, \theta_{e^-} < 60$ mrad. For u, d, s quarks $W_{\gamma\gamma} > 4$ GeV. The uncorrected Born cross section σ_{Born} is 104 nb.

SABH only a part of the total 36 Feynman diagrams are relevant, i.e. the scattering diagrams[4] shown in Fig. 1.

The analytical formulae for virtual, soft, hard and total pair production contributions can be found in [7, 8, 15]. Numerical results for the pair contribution cross sections based on these formulae can be obtained by using the code NLLBHA (see below for a description of the code). The leading term can be described by the electron structure function $D_e^e(x)$ [16–22]. Numerical results can be found in Refs. [2, 7, 8, 15, 23]. The contribution to SABH of the process of pair production accompanied by photon emission when both, pair and photons, may be real and virtual has also been analyzed and the relevant analytical formulae are given in [2, 23].

With the help of a Monte Carlo generator [24, 25], a dedicated study has been done for the contribution of the multiperipheral graphs, Fig. 1 (5–8), being for many kinematical setups the dominant mechanism of pair production. The total cross sections for the production of fermion pairs as detailed in Table 3 were obtained. The total contribution from the multiperipheral graphs is then estimated to be $1.4 \times 10^{-4} \sigma_{Born}$, with a relative error (from MC statistics) of

---

$e^+ e^-$ one.

[4]It can be verified [7, 8, 15] that the interference between the amplitudes describing the production of pairs moving in the electron direction and the positron one cancels. This is known as up-down (interference) cancelation.

z_{min}	0.3	0.4	0.5	0.6	0.7	.3/175GeV	.7/175GeV
$10^4\sigma_{NN}^{LL}/\sigma_{Born}$	-3.619	-3.655	-3.707	-3.807	-4.191	-4.185	-4.884
$10^4\sigma_{WW}^{LL}/\sigma_{Born}$	-2.748	-2.798	-2.883	-3.175	-3.771	-3.177	-4.405
$10^4\sigma_{NW}^{LL}/\sigma_{Born}$	-2.142	-2.191	-2.264	-2.478	-3.064	-2.489	-3.603

Table 4: LL Non-Singlet $e\bar{e}$ pair correction to SABH, SiCAL angular cuts WW: $1.5° - 3.15°$, NN: $1.61° - 2.8°$, in $10^4\times$ Born units, $\sqrt{s} = 91.1888$ GeV (175 GeV for last two entries), $z_{min} = s'_{min}/s$.

$\pm 50\%$. This correction, which still does not take into account a further reduction factor of $\simeq 20$ coming from a cut on the acoplanarity angle of the detected $e^\pm$, is thus negligible for SABH [26].

(2) The LL calculation of photonic corrections to SABH of Ref. [27] has been extended to pair corrections in [28]. Analytical formulae for arbitrary asymmetric angular cuts, for both Singlet and Non-Singlet corrections have been given in [28][5]. These formulae, based on [22], include both pairs and photons up to the exponentiated second or third order. The semianalytical program BHPAIR based on this calculation has been written [28]. Numerical results for the LCAL type angular cuts have been given in [28]. For the SiCAL type angular cuts the Singlet contribution is negligible (below $5\times10^{-5}\sigma_{Born}$) and the Non-Singlet contribution (up to third order with exponentiation) is calculated in Table 4, also for the LEP2 energies. The strong dependence of the result on angular cuts (WW, NN or NW) may indicate significant effects due to more realistic ES's. This can only be analyzed with the MC simulation. Such a MC program has already been constructed [29]. This program, being an extension of the BHLUMI MC code [30], is based on the extension of the YFS resummation of soft photons to the resummation of infrared and collinear pairs, cf. [31]. Preliminary results [29] show that a calorimetric ES reduces further the pair correction of Table 4.

To summarize, numerical values of pair corrections as given in [7, 8, 15], [2, 23] and Table 4 agree within $4 \times 10^{-4}\sigma_{Born}$ for the NN and WW cuts. The total contribution from pairs and multiperipheral diagrams for the energy cut in the experimentaly interesting range $0.3 < x_c < 0.7$ is also at most $4 \times 10^{-4}\sigma_{Born}$. With the help of a MC simulation of a realistic ES, one should be able to control the pair contribution with an accuracy of $3 \times 10^{-4}\sigma_{Born}$, or better. A similar conclusion is to be expected also for the LEP2 energies.

2.4 Vacuum polarization

Vacuum polarization contributes about 5.3% and 4%, respectively, to the e^+e^- cross-section in the angular region of the first and second generation of the luminosity detectors at LEP [3, 32]. The leptonic part of this contribution is known with excellent precision. The quark

---

[5]Extending further the analysis of Ref. [28], with the help of the 'parton-like' picture together with appropriate choices of structure functions and hard scattering cross-sections, one can calculate the other pair creation mechanisms, including the multiperipheral one, as well as other leptonic backgrounds to SABH resulting from the 'charge blindness' of the detectors. This analysis will appear elsewhere [29].

part, however, is more difficult since the quark masses are not unambiguously defined and perturbative QCD cannot be used for reliable calculations [33–35]. Therefore this part is calculated using a dispersion integral of R_{had}

$$R_{had} = \frac{\sigma(e^+e^- \to hadrons)}{\sigma(e^+e^- \to \mu^+\mu^-)} \tag{1}$$

measured experimentally.

Θ (rad)	$|t|$ (GeV^2)	Ref. [36]	(a) Ref. [33]	(b) Ref. [34]	(b)–(a)
.020	.83	$-.00345$	$-.00340 \pm .00008(2.5\%)$	$-.00339 \pm .00013(3.9\%)$	.00002
.030	1.87	$-.00505$	$-.00494 \pm .00014(2.8\%)$	$-.00493 \pm .00020(4.1\%)$	.00001
.040	3.33	$-.00629$	$-.00612 \pm .00019(3.1\%)$	$-.00613 \pm .00025(4.1\%)$	$-.00001$
.050	5.20	$-.00729$	$-.00711 \pm .00024(3.4\%)$	$-.00714 \pm .00030(4.2\%)$	$-.00003$
.060	7.48	$-.00812$	$-.00795 \pm .00027(3.5\%)$	$-.00801 \pm .00034(4.3\%)$	$-.00006$
.070	10.18	$-.00889$	$-.00869 \pm .00030(3.5\%)$	$-.00876 \pm .00038(4.4\%)$	$-.00006$
.080	13.30	$-.00963$	$-.00936 \pm .00033(3.5\%)$	$-.00941 \pm .00040(4.3\%)$	$-.00005$
.090	16.83	$-.01029$	$-.00997 \pm .00035(3.5\%)$	$-.01000 \pm .00043(4.3\%)$	$-.00003$
.100	20.77	$-.01089$	$-.01052 \pm .00037(3.5\%)$	$-.01058 \pm .00045(4.3\%)$	$-.00006$
.110	25.13	$-.01144$	$-.01103 \pm .00039(3.5\%)$	$-.01110 \pm .00047(4.2\%)$	$-.00007$
.120	29.90	$-.01194$	$-.01150 \pm .00040(3.5\%)$	$-.01157 \pm .00049(4.2\%)$	$-.00008$
.130	35.08	$-.01241$	$-.01193 \pm .00042(3.5\%)$	$-.01201 \pm .00050(4.2\%)$	$-.00008$

Table 5: The hadronic part of the vacuum polarization contribution to the small-angle Bhabha scattering as a function of the scattering angle (and corresponding momentum transfer t). In column 4 and 5 also the ratio of the error to the value of the hadronic contribution is given in brackets. The last column gives the difference between the results of Refs. [34] and [33].

Recently, several reevaluations of the hadronic contribution to the QED vacuum polarization have been performed, mainly to determine the effective QED coupling $\alpha(m_Z^2)$ [33, 37–42] and the anomalous magnetic moment (g-2) of the leptons [33]. At the same time, the vacuum polarization contribution to the small-angle Bhabha scattering has been recalculated [33, 34]. Table 5 compares the results of these two calculations of the hadronic contribution in the angular region of small-angle Bhabha scattering used at LEP for the luminosity measurements. They are in excellent agreement, as is evident from the very small differences listed in the last column. In brackets, the error is given as a percentage of the total hadronic contribution. We see that the error of Ref. [33] varies between 63% and 83% of that of Ref. [34] in the angular region presented here. Numbers have been obtained with the help of FORTRAN routines HADR5 [33] and REPI [34] available from the authors. Finally the values of the previously used hadronic contribution from Ref. [36] are also shown.

Fig. 2 from Ref. [34] shows the contribution of different energy regions of R to the value of the hadronic contribution and its error while the Fig. 3 from Ref. [33] shows the uncertainty

contribution
in magnitude

> 12.GeV
7 - 12.GeV
5 - 7. GeV

2.5 - 5 GeV

1.05 - 2.5 GeV

narrow resonances

ρ

in uncertainty

> 12.GeV
7 - 12.GeV
5 - 7. GeV

2.5 - 5 GeV

ρ

1.05 - 2.5 GeV

narrow resonances
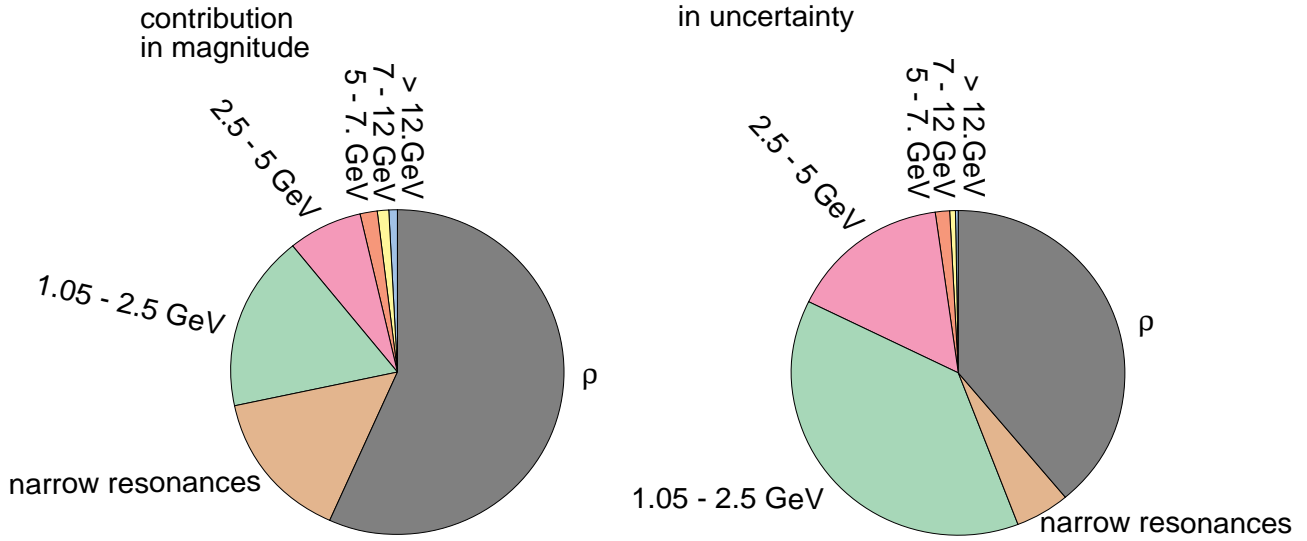
Figure 2: Relative contributions to $\Delta\alpha(t = -1.424 \text{ GeV}^2)$ in magnitude and uncertainty from the Ref. [34].
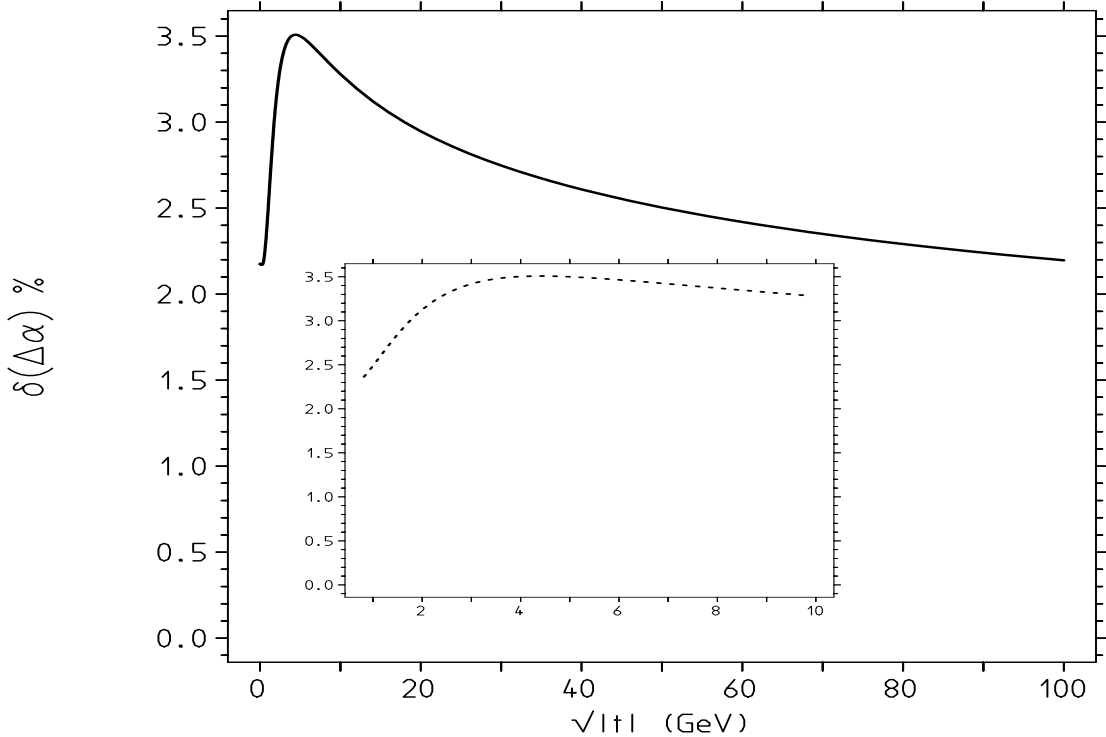
Figure 3: Relative uncertainty in percent of the hadronic vacuum polarization contribution as a function of the momentum transfer in the small-angle Bhabha scattering calculation from the Ref. [33].

Θ (rad)	Ref. [36]	Ref. [33]	Ref. [34]	$\frac{hadronic}{total}$ (%)
.020	−.01590	−.01585 ± .00008	−.01583 ± .00013	21
.030	−.01877	−.01866 ± .00014	−.01865 ± .00020	26
.040	−.02095	−.02078 ± .00019	−.02079 ± .00025	30
.050	−.02271	−.02252 ± .00024	−.02255 ± .00030	32
.060	−.02418	−.02400 ± .00027	−.02406 ± .00034	33
.070	−.02551	−.02531 ± .00030	−.02537 ± .00038	35
.080	−.02674	−.02647 ± .00033	−.02652 ± .00040	36
.090	−.02785	−.02753 ± .00035	−.02756 ± .00043	36
.100	−.02886	−.02849 ± .00037	−.02855 ± .00045	37
.110	−.02979	−.02938 ± .00039	−.02945 ± .00047	38
.120	−.03064	−.03020 ± .00040	−.03028 ± .00049	38
.130	−.03144	−.03096 ± .00042	−.03104 ± .00050	39

Table 6: The vacuum polarization contribution to the small-angle Bhabha scattering as a function of the scattering angle. The last column gives the ratio of the hadronic part to the total vacuum polarization contribution.

Generation	typical Θ (rad)	Ref. [33]	Ref. [34]
first	.060	.0003	.0004
second	.030	.0005	.0007

Table 7: Summary of the uncertainty of the vacuum polarization calculation for the first and second generation of the luminosity detectors of LEP according to Ref. [33, 34].

of the hadronic vacuum polarization contribution to the calculation of the small-angle Bhabha scattering as a function of the momentum transfer.

The total vacuum polarization contribution is obtained as sum of the leptonic contribution and the hadronic one. It is shown in Table 6. The contribution of the vacuum polarization error to the total error of the luminosity measurement is about twice the error given in the Table 6. The typical angular region of the first and second generation of the LEP luminosity detectors is 60 and 30 mrad, respectively [3]. The contribution of the vacuum polarization error to the luminosity calculation for the LEP detector is given in Table 7.

The vacuum polarization correction and its uncertainty are smaller for the lower angles covered by the second generation of luminosity detectors.

In conclusion, the error of the hadronic contribution of Ref. [34] makes a negligible contribution to the total error of the calculation of the small-angle Bhabha scattering. The error of Ref. [33] is even smaller. Thus the error of Ref. [34] can be considered as a conservative one.

2.5   Brief characteristics of the programs/calculations

Here we will very briefly summarize the basic features of the codes involved in the SABH comparisons. The only aim of the following is to just settle the frame, and not to give an exhaustive description of the codes, which can be found in the original literature and/or in the dedicated write-up's at the end of the present report.

BHAGEN95 [43] – It is a Monte Carlo integrator for both small- and large-angle Bhabha scattering. It is a structure function based program for all orders resummation, including complete photonic $\mathcal{O}(\alpha)$ and leading logarithmic $\mathcal{O}(\alpha^2 L^2)$ corrections in all channels.

BHLUMI [44] – Full scale Monte Carlo event generator for small-angle Bhabha scattering. It includes multiphoton radiation in the framework of YFS *exclusive exponentiation*. Its matrix element includes complete $\mathcal{O}(\alpha)$ and $\mathcal{O}(\alpha^2 L^2)$. The program provides the full event in terms of particle flavors and their four-momenta with an arbitrary number of radiative photons.

LUMLOG – It is a Monte Carlo event generator for SABH (part of BHLUMI, see [44]). Photonic corrections are treated at the leading logarithmic level at the *strictly collinear* and inclusive way. Structure functions exponentiated up to $\mathcal{O}(\alpha^3 L^3)$ are included (and without exponentiation up to $\mathcal{O}(\alpha^2 L^2)$).

NLLBHA [2,23] – It is the FORTRAN translation of a fully analytical up to $\mathcal{O}(\alpha^2)$ calculation, including all the next-to-leading corrections. It is also able to provide $\mathcal{O}(\alpha^3 L^3)$ photonic corrections and light pair corrections including simultaneous photon and light pair emission. *Not an event generator.*

OLDBIS – Classical Monte Carlo event generator for SABH from PETRA times [45] (the modernized version is incorporated in the BHLUMI set [44]). It includes photonic corrections at the exact $O(\alpha)$.

OLDBIS+LUMLOG – It is the well known "tandem" developed in order to take into account higher order corrections (LUMLOG) on top of the exact $O(\alpha)$ result (OLDBIS). The matching between $O(\alpha)$ and higher orders is realized in an *additive* form.

SABSPV [46] – It is a new Monte Carlo integrator, designed for small-angle Bhabha scattering. It is based on a proper matching of the exact $O(\alpha)$ cross section for t-channel photon exchange and of the leading logarithmic results in the structure function approach. The matching is performed in a *factorized* form, in order to preserve the classical limit.

2.6   Experimental event selection and theory uncertainty in luminosity measurements

In this section we discuss the interplay between experimental selection and higher-order radiative corrections. All numerical examples are for LEP1 at Z peak energy. The discussion of the results is generally limited to LEP1 but using "scaling rules" from the introduction one may easily extend it LEP2. In particular one has to remember that third order LL corrections

have the strongest energy dependence, and going from the Z-peak to the highest LEP2 energy introduces in them a factor of almost two.

In this subsection three different event generators are used: **i)** a generator based on a complete first-order calculation OLDBIS [6,30], which has at most one photon radiated; it includes $\mathcal{O}(\alpha)$ and $\mathcal{O}(\alpha L)$; **ii)** a generator based on a leading-logarithmic third-order exponentiated calculation LUMLOG [6,30]; it includes $\mathcal{O}(\alpha L)$, $\mathcal{O}(\alpha^2 L^2)$, $\mathcal{O}(\alpha^2 L^2)$ in strictly collinear approximation; the 4-momenta of the final state photons are added to the electrons; **iii)** a truly multi-photon generator based on an exponentiated calculation (BHLUMI) [6,30]; it includes complete $\mathcal{O}(\alpha)$, $\mathcal{O}(\alpha L)$ and $\mathcal{O}(\alpha^2 L^2)$ while $\mathcal{O}(\alpha^2 L)$ and $\mathcal{O}(\alpha^3 L^3)$ are incomplete; it generates explicitly 4-momenta of all photons above an arbitrary (user-defined) energy threshold, typically a fraction k° (typically 10^{-4}) of the beam energy. The Bhabha cross section calculated with BHLUMI will be compared to the one calculated with the hybrid calculation consisting of OLDBIS plus higher-order contributions from LUMLOG (LUMLOG$_{HO}$). The cross section differences BHLUMI $-$ OLDBIS and BHLUMI $-$ (OLDBIS $+$ LUMLOG$_{HO}$) are studied as a function of variations in the event selection parameters. Note that BHLUMI $-$ OLDBIS is dominated by $\mathcal{O}(\alpha^2 L^2)$, $\mathcal{O}(\alpha^2 L)$ and $\mathcal{O}(\alpha^3 L^3)$ while BHLUMI $-$ (OLDBIS $+$ LUMLOG$_{HO}$) is dominated by $\mathcal{O}(\alpha^2 L)$ and $\mathcal{O}(\alpha^3 L^3)$.

Only the QED t-channel part of the generators is used, with photon vacuum-polarization switched off. We use an improved version of the BHLUMI event generator as discussed in Ref. [44]. BHLUMI $-$ OLDBIS is used to estimate the higher-order contributions. We choose BHLUMI because the BHLUMI Monte Carlo distributions are in excellent agreement with the data distributions for all LEP experiments [47–52] A quantitative measurement of doubly radiative events [53] has shown consistency with the BHLUMI expectations and also with OLDBIS $+$ LUMLOG$_{HO}$ expectations, while OLDBIS alone fails to describe this contribution, as expected. However, although the MC differential distributions agree with the data, the absolute scale of the integrated cross section remains uncertain, since the bulk of the radiative corrections are either virtual or involve soft (< 5 MeV) photons.

In order to set the scale for the following numerical investigation let us remind the reader that the LEP1 experiments have reached in 1993-94 a systematic experimental uncertainty in the measuring the SABH luminosity cross section better than 0.10% [3–5].

2.6.1 Reference event selections

We define an imaginary detector, consisting in a pair of cylindrical calorimeters covering the region between 62 and 142 mm radially out from the beam pipe centre and located at 2460 mm from the interaction point, at opposite sides of it. The beams are pointlike and centered within the beam pipe. The calorimeters are each divided into 32 azimuthal segments, subdivided into 32 radial pads. A parton (electron or photon) deposits all its energy in the pad it hits. Photons and electrons from Bhabha events that hit the detector within a region of ±16 radial pads and 5 azimuthal segments centered on the pad struck by the largest energy parton are combined

into a cluster. The cluster energy is the pad energy sum. Coordinates of the cluster centroid are the energy weighted average polar coordinates (R, ϕ), summing over all pads in the cluster. Partons falling outside the principal cluster can originate secondary clusters, with no overlap. Only one cluster, the most energetic of all clusters, is used. Bhabha events are selected using the cluster energy $E_{cluster}$ and the radial coordinate of the cluster centroid in both calorimeters.

We then define a reference small-angle selection for Bhabha events (RSA selection). The radial acceptance edges for Bhabha events are set at pad boundaries. The "Wide" acceptance boundary extends up to two pads away from the detector inner and outer edges ($27.236 < \theta < 55.691$ mrad). The "Narrow" acceptance boundary extends up to six pads away from the detector inner and outer edges ($31.301 < \theta < 51.626$ mrad). A similar angular range is covered by the OPAL, L3, ALEPH luminometers [54–56]. An event is selected when the cluster coordinates are within the Wide acceptance at one side (side 1) and within the narrow acceptance at the opposite side (side 2). Events must satisfy the criterion $0.5(x_1 + x_2) > 0.75$, with $x = E_{cluster}/E_{beam}$. Selection criteria are also applied on the acoplanarity (0.2 rad) and the acollinearity (10 mrad) between the electron and positron clusters.

Another selection is also considered, similar to the previous one but extending over the angular range covered by the DELPHI luminometer [57] (RLA: reference large-angle selection). The calorimeters are located at 2200 mm from the interaction point and cover radially the region between 6.5 and 41.7 cm. A cluster is formed starting from the most energetic particle hitting the calorimeter and considering all particles whose angular distance $(\Delta\theta, \Delta\phi)$ (in radians) from the initial one satisfies the two shower separation condition (determined from the comparison with the data) $(\Delta\theta/0.03)^2 + (\Delta\phi/0.87)^2 < 1$. The cluster energy is the sum over the energies of all particles inside the cluster, while the cluster coordinates are given by the energy weighted sum of their polar coordinates. Bhabha events are selected by cutting on the minimum cluster energy $\min(x_1, x_2)$, on the acoplanarity (20^0) and on the cluster radial coordinate. The radial acceptance is defined on the Narrow side by the condition $43.502 < \theta < 113.151$ mrad and on the Wide side by the condition $38.629 < \theta < 126.592$ mrad.

2.6.2 Comparison of exponentiated and order-by-order calculations

First-Order Calculation
The Bhabha cross-section for the RSA and RLA selections has been calculated with OLDBIS. The results are shown in figure 4 for the RSA selection, where the cross section is subdivided into x-bins, separately for the narrow acceptance side and for the large acceptance side (x_{Narrow}, x_{Wide}). A sample of 3×10^9 events is used. The total Bhabha cross section within the RSA acceptance is 75.589 ± 0.009 nb. Displacing the generation minimum angle θ_{min}^{gen} from 10.4 mrad as recommended in [6,30] to 5.2 mrad changes the accepted cross section by 0.0039(6) nbarns. No sizeable k° ($=E_\gamma/E_{beam}$) dependence is observed when varying k° from 10^{-4} to 10^{-5}.

x_{Narrow}

0.0498(2)			
	0.1050(3)	0.8251(8)	73.009(9)
		0	1.339(1)
	$< 10^{-5}$		0.1774(3)
			0.0836(2)

1.00 — 0.85 — 0.75 — 0.65 — 0.50 (vertical axis)

x_{Wide}: 0.50 0.65 0.75 0.85 1

1.0763(9)	7.053(3)	7.269(3)	41.278(7)
0	0.00180(3)	0.00393(5)	7.331(3)
0	0	0.00175(3)	7.577(3)
0	0	0	1.415(1)

1.00 — 0.999 — 0.99 — 0.90 — 0.85 (vertical axis)

0.85 0.90 0.99 0.999 1 (horizontal axis)
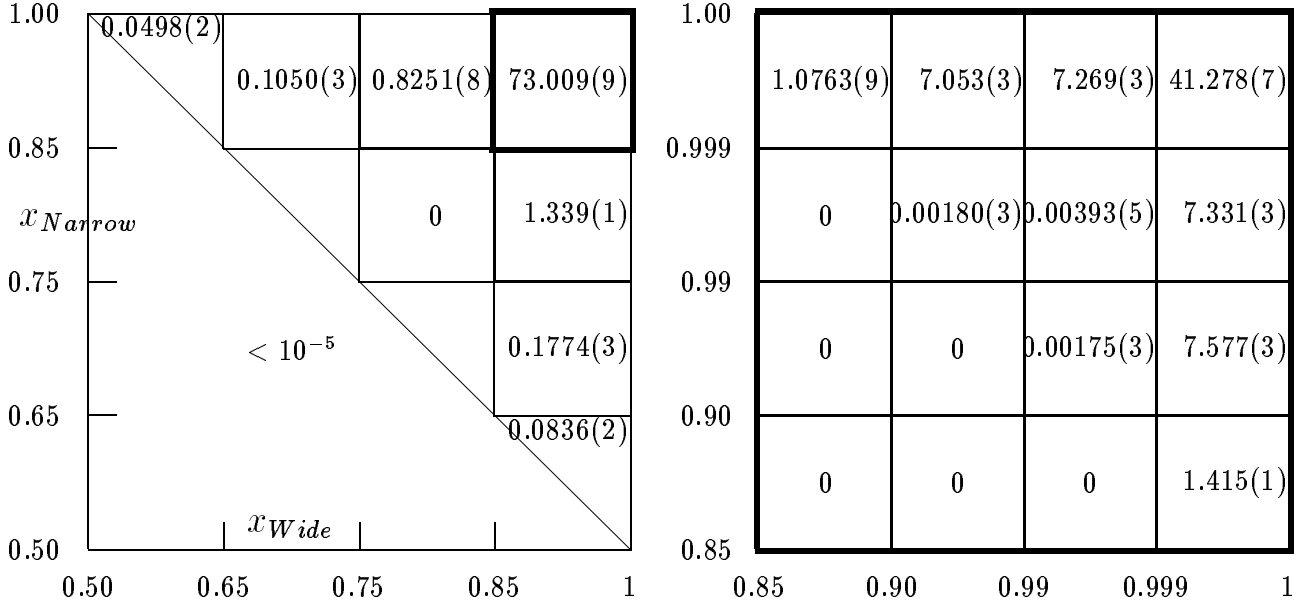
Figure 4: OLDBIS Bhabha cross section (nb) in phase space bins for the RSA selection (see text).

Higher-Order Leading-Log Contribution

The cross section difference $LUMLOG_{HO} = LUMLOG$(all orders) $- LUMLOG$(first order) is used to estimate the higher-order leading-logarithmic contribution (figure 5) for the RSA selection. In LUMLOG only the initial state radiation has an impact on the measured cluster energies and angles, because the 4-momenta of the final state photons are combined together with the electrons. A sample of 2.1×10^9 events is used. There is a total higher-order leading-log contribution of 0.144 ± 0.008 nb to the Bhabha cross section within the RSA acceptance: the higher-order contribution is negative in the phase-space region dominated by singly radiative events; it is positive in the non radiative Bhabha peak and in the phase-space region of hard doubly radiative events.

Exponentiated Calculation

The Bhabha cross-section in phase-space bins for the RSA selection obtained with BHLUMI is presented in figure 6. A sample of 1.6×10^9 events is used. The total Bhabha cross section accepted by the RSA selection is 75.712 ± 0.006 nb. The accepted cross section changes by $< 10^{-5}$ when decreasing the t_{min}^{gen} (minimum generated four-momentum transfer squared) value as recommended in [6,30] to half of it.

Comparison of Exponentiated and Order-by-Order Calculations

The BHLUMI and OLDBIS cross sections differ for the RSA selection by $(0.16 \pm 0.01)\%$, showing that the estimated contribution to the accepted cross section from higher-order radiative effects is very small. This estimate is also in reasonable agreement with the $LUMLOG_{HO}$ expectation of $(0.19 \pm 0.01)\%$.

A similar study for the RLA selection results in a BHLUMI $-$ OLDBIS relative difference

17
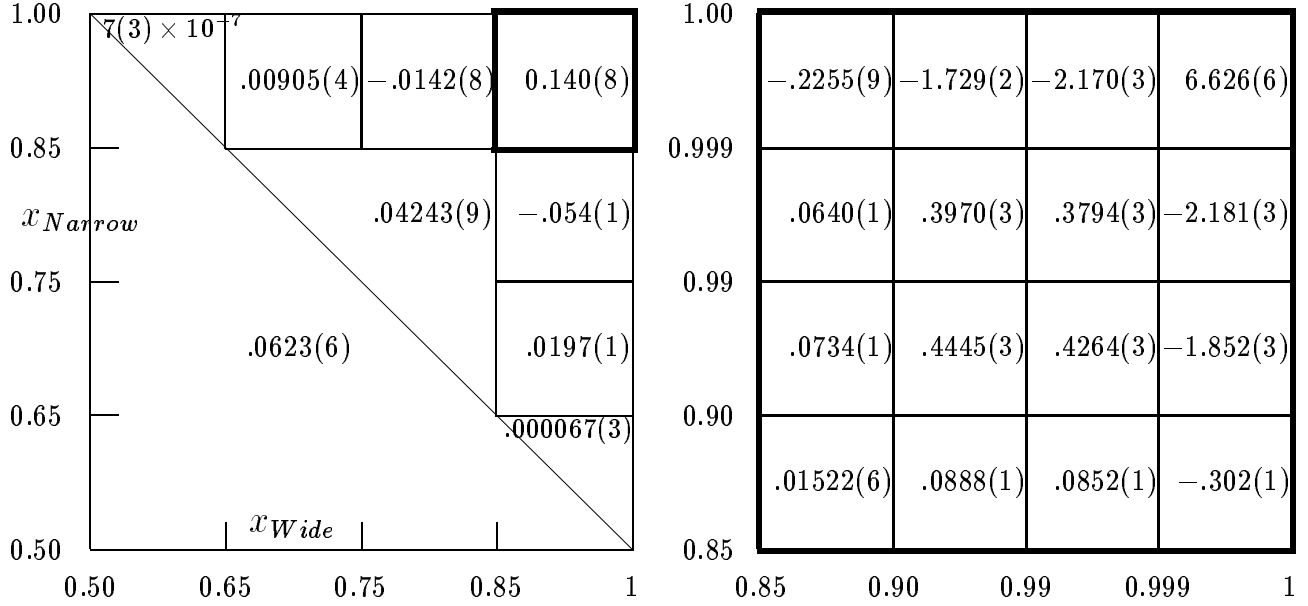
Figure 5: LUMLOG higher-order contribution to the Bhabha cross section (nb) in phase space bins for the RSA selection (see text).
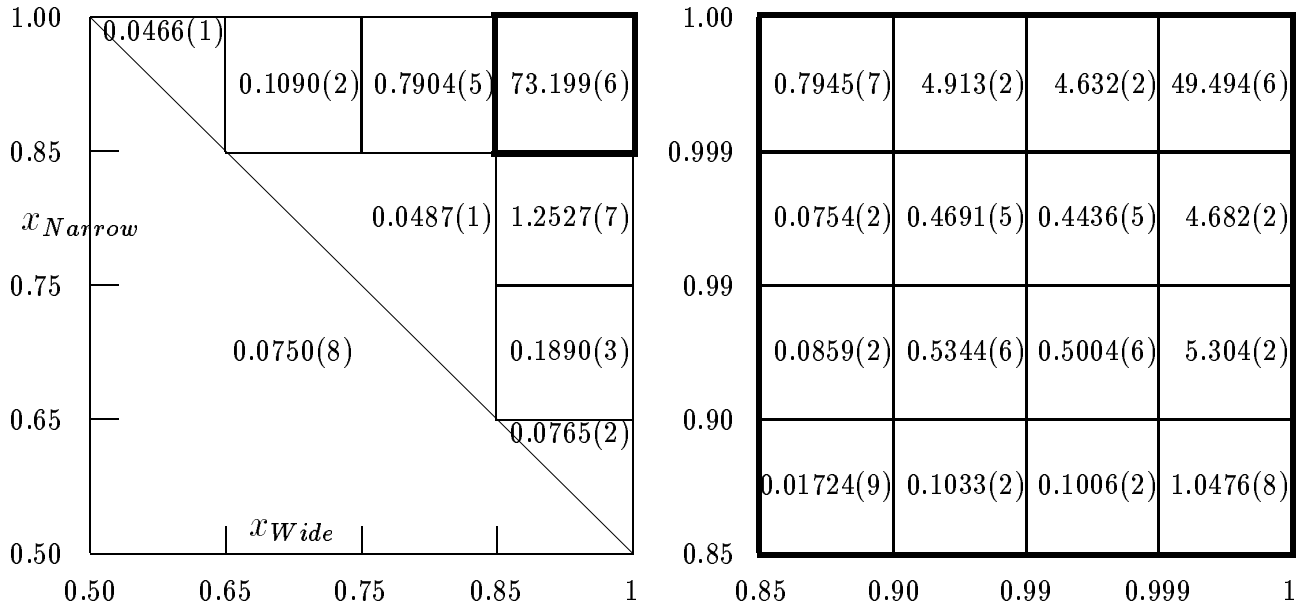
Figure 6: BHLUMI Bhabha cross section (nb) in phase space bins for the RSA selection (see text).

of $(-0.08 \pm 0.01)\%$ to be compared with a LUMLOG$_{HO}$ expectation of $(-0.03 \pm 0.01)\%$.

2.6.3 Dependence on energy and acollinearity cuts

The cross section relative difference $(\mathrm{BHLUMI} - \mathrm{OLDBIS})/\mathrm{BHLUMI(RSA)}$, where BHLUMI(RSA) refers to the RSA selection, is studied in table 8 for several selection criteria on energy and acollinearity. With x_{min}^{cut} we mean that the energy cut $min(x_1, x_2) > x_{min}^{cut}$ is applied. Through transverse momentum conservation, energy and acollinearity cuts are strongly correlated in events with initial state radiation. The relative difference $\mathrm{BHLUMI} - \mathrm{OLDBIS}$ is indicative of the higher-order contribution, which clearly appears in table 8 to be huge for large x_{min}^{cut}. It becomes progressively smaller for smaller x_{min}^{cut}. It should be stressed that the h.o. corrections are small (at the per mille level) over a very broad region of x_{min}^{cut} and acollinearity.

A second estimate of the Bhabha cross section with higher-order radiative corrections can be obtained with $\mathrm{OLDBIS} + \mathrm{LUMLOG}_{HO}$. The three generator relative difference $(\mathrm{BHLUMI} - (\mathrm{OLDBIS} + \mathrm{LUMLOG}_{HO}))/\mathrm{BHLUMI(RSA)}$ in table 8 shows that the h.o. corrections in BHLUMI and in LUMLOG track each other very well, giving confidence that the h.o. contributions are in fact small when they are estimated to be so. The unstable region is limited to very large x_{min}^{cut}. The BHLUMI and $\mathrm{OLDBIS} + \mathrm{LUMLOG}_{HO}$ Bhabha cross sections agree at the 0.1% level over an extremely broad range of energy and acollinearity cuts.

The cross section differences $\mathrm{BHLUMI} - \mathrm{OLDBIS}$ and $\mathrm{BHLUMI} - (\mathrm{OLDBIS} + \mathrm{LUMLOG}_{HO})$ for the RSA selection change by $(-0.013 \pm 0.009)\%$ when the acoplanarity cut is not applied.

For the RLA selection the cross section differences $\mathrm{BHLUMI} - \mathrm{OLDBIS}$ and $\mathrm{BHLUMI} - (\mathrm{OLDBIS} + \mathrm{LUMLOG}_{HO})$ normalized to the BHLUMI result are shown in table 9 as a function of the cut on x_{min}^{cut}. The higher-order contribution to the Bhabha cross section for the RLA selection both in BHLUMI and in LUMLOG is very small over a broad range of x_{min}^{cut}.

BHLUMI−OLDBIS

x_{min}^{cut}	Acollinearity cut (rad)		
	0.005	0.010	no cut
0.999	11.35(1)%	10.86(1)%	10.61(1)%
0.99	4.65(1)%	4.45(1)%	4.35(1)%
0.90	0.69(2)%	0.60(1)%	0.58(1)%
0.85	0.68(1)%	0.25(1)%	0.24(1)%
0.75	0.75(1)%	0.12(1)%	-0.00(1)%
triang.	0.78(1)%	0.16(1)%	-0.09(1)%
0.50	0.83(1)%	0.26(1)%	0.06(1)%

BHLUMI−(OLDBIS+LUMLOG$_{HO}$)

x_{min}^{cut}	Acollinearity cut (rad)		
	0.005	0.010	no cut
0.999	2.19(2)%	2.10(1)%	2.05(1)%
0.99	0.98(2)%	0.94(2)%	0.92(2)%
0.90	0.19(2)%	0.15(2)%	0.14(2)%
0.85	0.15(2)%	0.06(2)%	0.06(2)%
0.75	0.13(2)%	-0.00(2)%	-0.03(2)%
triang.	0.12(2)%	-0.03(2)%	-0.09(2)%
0.50	0.18(2)%	-0.02(2)%	-0.07(2)%

Table 8: Cross section differences BHLUMI−OLDBIS and BHLUMI−(OLDBIS+LUMLOG$_{HO}$) normalized to the BHLUMI Bhabha cross section for the RSA selection. The label "triangular" stands for the cut $0.5(x_1 + x_2) > 0.75$.

x_{min}^{cut}	BHL−OB
0.9	0.76(1)%
0.8	0.10(1)%
0.7	-0.06(1)%
0.6	-0.08(1)%
0.5	-0.05(1)%

x_{min}^{cut}	BHL−(OB+LL$_{HO}$)
0.9	0.21(1)%
0.8	0.03(1)%
0.7	-0.03(1)%
0.6	-0.05(1)%
0.5	-0.06(1)%

Table 9: Cross section differences BHLUMI−OLDBIS and BHLUMI−(OLDBIS+LUMLOG$_{HO}$) normalized to the BHLUMI Bhabha cross section for the RLA selection.

2.6.4 Wide-Wide, Narrow-Narrow versus Wide-Narrow acceptance

In the reference selections (RFA and RLA) an asymmetric acceptance (Wide on one side and Narrow on the opposite side) is used. All 4 LEP experiments use an asymmetric acceptance for the LEP luminosity measurement. We study in table 10 how the results change when using a symmetric (Wide-Wide or Narrow-Narrow). The BHLUMI − OLDBIS cross section difference becomes large (0.77(1)% for the Narrow-Narrow acceptance). A similar result is also obtained using LUMLOG$_{HO}$ and then the BHLUMI − (OLDBIS + LUMLOG$_{HO}$) difference is small. We thus conclude that the higher-order contributions to the accepted Bhabha cross section, as estimated with BHLUMI or LUMLOG, are largely reduced when using an asymmetric Wide-Narrow acceptance.

	WN	WW	NN
BHLUMI	75.712(5)nb	117.918(6)nb	73.344(5)nb
OLDBIS	75.589(8)nb	117.219(9)nb	72.781(8)nb
LUMLOG$_{HO}$	0.144(8)nb	0.568(9)nb	0.465(8)nb
(BHL−OB)/BHL	0.16(1)%	0.59(1)%	0.77(1)%
(BHL−OB−LL$_{HO}$)/BHL	-0.03(2)%	0.11(2)%	0.13(2)%

Table 10: Comparison of BHLUMI, OLDBIS and LUMLOG$_{HO}$ Bhabha cross sections for Wide-Narrow, Wide-Wide, Narrow-Narrow event selections. All other cuts as in the RSA selection.

2.6.5 Multiple photon radiation

A very relevant property of exclusive exponentiation is that there are many more multi-photon events than expected from perturbation theory at a fixed order in α. In a sample of 10^6 BHLUMI Bhabha events, the events have up to eight photons with energy larger than $k^\circ E_{beam} (\approx 5$ MeV), as shown in figure 7. This may enhance the difference between cross section calculations performed with BHLUMI and with OLDBIS + LUMLOG$_{HO}$. In the following we study the stability of the BHLUMI − OLDBIS and BHLUMI − OLDBIS − LUMLOG(ho) differences in

20

table 8 and in table 9 when varying those parameters in the experimental selection which are sensitive to the presence of many photons.

Lower Energy Photon Cut-off
We define a K_c parameter (in MeV) expressing the sensitivity to soft photons: the detector is fully efficient for photons of energy larger than K_c. An implicit K_c cut-off is present in BHLUMI at $K_c = k^\circ E_{beam}$ (5 MeV) for the cross sections calculations presented above. The relative variation of the BHLUMI Bhabha cross section when varying K_c is reported in table 11 for the RSA selection and in table 12 for the RLA selection. The effect is at most of -0.03% for the RSA acceptance in the extreme case of K_c=500 MeV. The relative changes in the BHLUMI and OLDBIS cross sections are compared in figures 8 and 9. The large-x region is very different; most of the difference has already disappeared for x_{min}^{cut}=0.9. LUMLOG remains unaffected: it has in the output only the electron and positron 4-momenta with the final state photons combined with the electrons/positrons. Hence, the effect on the relative cross section differences BHLUMI $-$ OLDBIS and BHLUMI $-$ (OLDBIS + LUMLOG$_{HO}$) for the RSA selection is at most $-0.030(4)\%$.
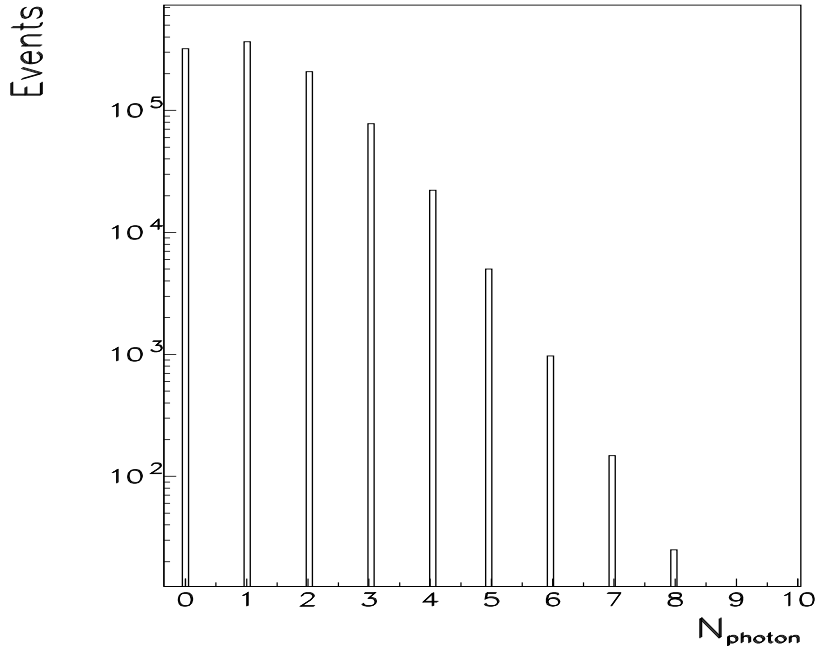
Figure 7: Distribution in number of emitted photons for a sample of 10^6 unweighted BHLUMI events. (The Removal flag is switched on in BHLUMI, with $K_c = k^\circ E_{beam} = 5$ MeV).

Cluster Size
The relative variation of the accepted Bhabha cross section with respect to the RSA selection when changing the cluster size is studied in figure 10 using BHLUMI generated events and using OLDBIS generated events. For large cluster sizes BHLUMI and OLDBIS track each other very well and the BHLUMI $-$ OLDBIS relative difference observed for the RSA selection remains unchanged. On the contrary, for small cluster sizes, the effect of many photons in BHLUMI generated events shows up strongly. The LUMLOG result remains unaffected. Thus, for the

x_{min}^{cut}	K_c (MeV)			
	10	50	100	500
0.999	-0.025(4)%	-0.75(2)%	-3.51(5)%	-9.45(8)%
0.90	-0.001(1)%	-0.002(1)%	-0.004(2)%	-0.029(4)%
0.85	$< 10^{-5}$	-0.003(1)%	-0.003(1)%	-0.012(3)%
triangular	-0.004(2)%	-0.015(3)%	-0.018(3)%	-0.030(4)%

Table 11: Variation of the BHLUMI Bhabha cross section when changing the photon minimum detectable energy K_c. Normalization is with respect to the RSA selection with $K_c = k^\circ E_{beam} = 5$ MeV. The label "triangular" stands for the cut $0.5(x_1 + x_2) > 0.75$.

x_{min}^{cut}	K_c (MeV)			
	10	50	100	500
0.9	-0.0005(2)%	-0.0032(5)%	-0.0067(7)%	-0.033(2)%
0.7	-0.0003(2)%	-0.0010(3)%	-0.0015(3)%	-0.0085(8)%
0.5	$< 10^{-6}$	-0.0002(1)%	-0.0005(2)%	-0.0025(5)%

Table 12: Variation of the BHLUMI Bhabha cross section when changing the photon minimum detectable energy K_c from $K_c = 5$ MeV for the RLA selection.
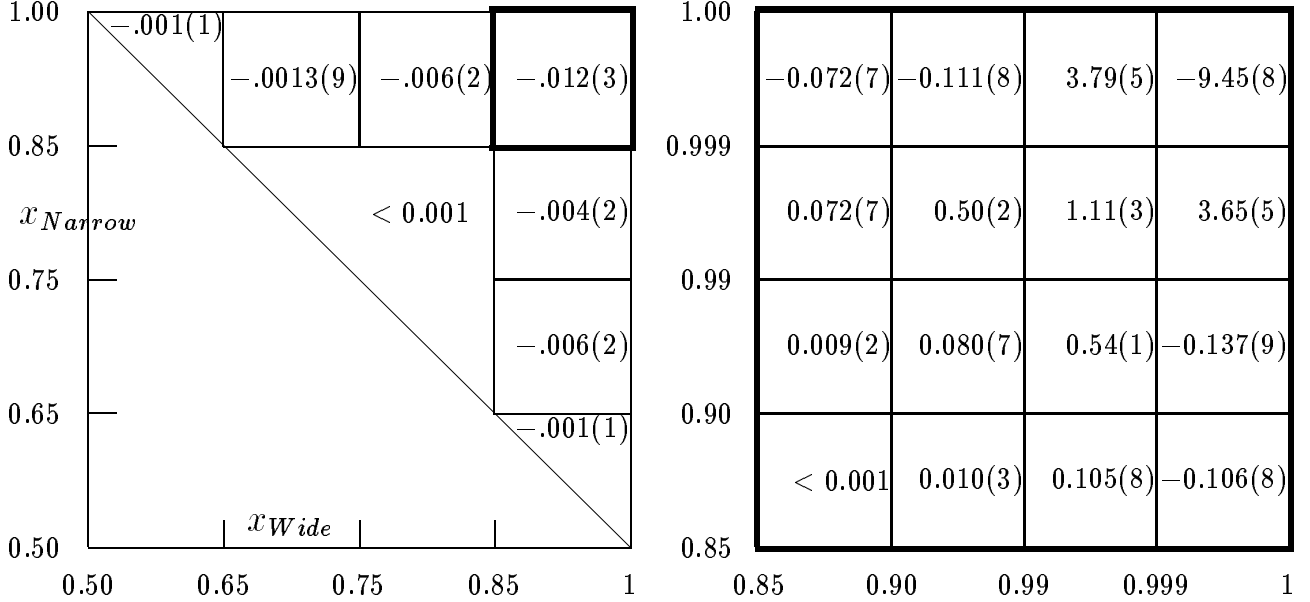
Figure 8: Percentage variation of the BHLUMI Bhabha cross section when setting the photon minimum detectable energy K_c to 500 MeV (see also figure 3) instead of $K_c = 5$ MeV.
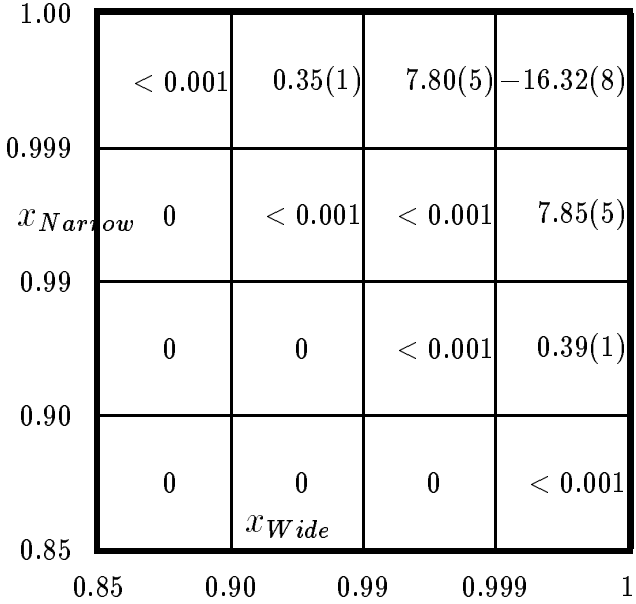
Figure 9: Percentage variation of the OLDBIS Bhabha cross section when setting the photon minimum detectable energy K_c to 500 MeV (see also figure 1) instead of $K_c = 5$ MeV.

RSA selection we can exclude an effect larger than $\pm 0.007\%$ on the BHLUMI − OLDBIS and on the BHLUMI − (OLDBIS + LUMLOG$_{HO}$) cross section differences.

Cluster Coordinate
The energy weighting algorithm for extracting the cluster coordinates couples the coordinates to the cluster size. A different coordinate reconstruction algorithm (PADMAX) is then used: we select the pad with the largest energy deposit and use the 4-momentum sum of the partons which enter that pad to calculate an impact point in the pad; the impact point so calculated defines the cluster coordinates, independent of the cluster dimensions. The BHLUMI cross section when changing from θ (ϕ) energy weighted coordinates to PADMAX coordinates in the RSA selection changes by $(-0.088 \pm 0.003)\%$. The OLDBIS cross section when changing from θ (ϕ) energy weighted coordinates to PADMAX coordinates changes by $(-0.091 \pm 0.005)\%$. The LUMLOG result is unaffected. The effect on the BHLUMI − OLDBIS and on the BHLUMI − (OLDBIS + LUMLOG$_{HO}$) cross section differences in the RSA selection when using the PADMAX coordinates instead of the energy weighted coordinates is $(0.003 \pm 0.006)\%$.

2.6.6 Summary

We have shown that there is a strong correlation between the magnitude of the $O(\alpha^2)$ radiative corrections to the Bhabha cross section and distinctive characteristics of the experimental Bhabha event selection. In particular, we have shown that the Bhabha selections used by the LEP experiments to measure the accelerator luminosity minimize the sensitivity to $O(\alpha^2)$ radiative corrections.

23

BHLUMI

Δ_{PAD}	0	1	2	4	8	12	16(all)
32(all)	$-.071(3)\%$		$+.075(3)\%$	$+.160(4)\%$	$+.270(5)\%$		$+.310(5)\%$
16	$-.086(3)\%$	$-.020(1)\%$	0	$+.044(2)\%$	$+.109(3)\%$	$+.117(3)\%$	$+.119(3)\%$
8			$-.071(3)\%$				
4			$-.099(3)\%$				
0	$-.237(5)\%$		$-.224(5)\%$				$-.221(5)\%$

OLDBIS

Δ_{PAD}	0	1	2	4	8	12	16(all)
32(all)	$-.028(4)\%$		$+.074(6)\%$	$+.156(9)\%$	$+.261(12)\%$		$+.311(13)\%$
16	$-.053(5)\%$	$-.017(3)\%$	0	$+.042(5)\%$	$+.101(7)\%$	$+.118(8)\%$	$+.126(8)\%$
8			$-.069(6)\%$				
4			$-.073(6)\%$				
0	$-.073(6)\%$		$-.072(6)\%$				$-.066(6)\%$
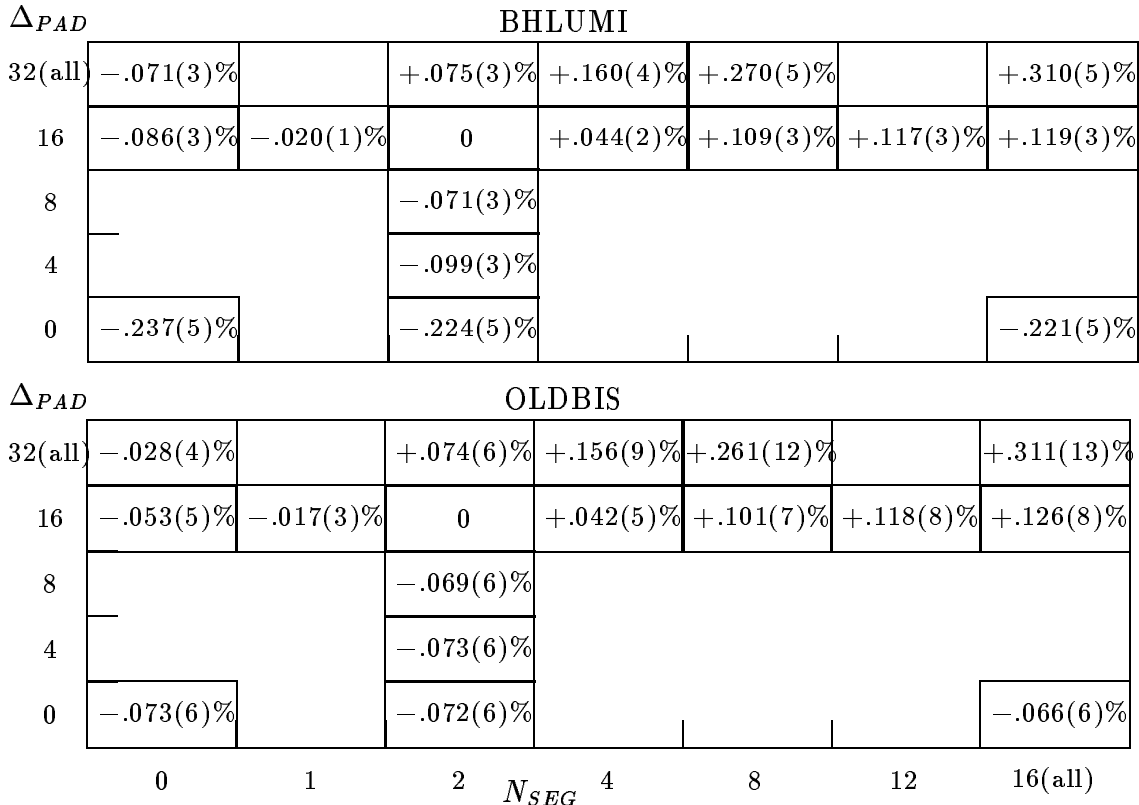
N_{SEG}

Figure 10: Relative variation of the accepted Bhabha cross section with respect to the RSA selection when changing cluster radial (PAD's) and azimuthal (SEGments) dimensions. A cluster extends for $\pm\Delta_{PAD}$ pads and $\pm N_{SEG}$ segments around the pad containing the largest energy deposit. A pad subtends a polar angle of about 1 mrad; a segment covers azimuthally an angle of 11.25 degrees. The RSA selection has $\Delta_{PAD} = 16$ and $N_{SEG} = 2$.

The $O(\alpha^2)$ contributions have been estimated using BHLUMI − OLDBIS and LUMLOG$_{HO}$= LUMLOG$_{all-orders}$ −LUMLOG$_{first-order}$. The cross section differences BHLUMI − OLDBIS and BHLUMI − (OLDBIS + LUMLOG$_{HO}$) are very small (at the per mille level) in a broad region of phase space around the experimental selections. We have considered two angular ranges $27 < \theta < 57$ mrad and $44 < \theta < 113$ mrad, with a variety of energy and acollinearity cuts. The sensitivity to the possible presence of many photons, predicted by exclusive exponentiation, the effect of small or large cluster sizes and different ways of reconstructing the cluster coordinates have been investigated. Large cluster sizes, rather soft energy cuts and a Wide-Narrow method are very effective in minimizing the cross section differences BHLUMI − OLDBIS and BHLUMI − (OLDBIS + LUMLOG$_{HO}$). Vice versa, these same effects could be used to enhance the sensitivity to the $O(\alpha^2)$ radiative corrections in order to perform measurements and test the theory predictions.

24

2.7 Comparisons of event generators for small-angle Bhabha scattering

In contrast to the previous section, where we have seen results from many variants of ES's with varying cut parameters but for only three types of QED calculations, here we shall limit ourselves to "only" four ES's (two of which very close to realistic experimental situations), but we shall discuss *all the available* theoretical calculations. The outline of this section is the following: the actual comparisons will be presented first at the $\mathcal{O}(\alpha^1)$ level, in order to determine the basic technical precision, and later for more advanced QED matrix elements beyond $\mathcal{O}(\alpha^1)$, in order to explore physical precision. These comparisons will be done first for LEP1 energy and later will be also extended to LEP2 energies.

WW: $\theta_i \in (\theta_{\min}^W, \theta_{\max}^W)$, NN: $\theta_i \in (\theta_{\min}^N, \theta_{\max}^N)$

NW: $\theta_1 \in (\theta_{\min}^W, \theta_{\max}^W)$, $\theta_2 \in (\theta_{\min}^N, \theta_{\max}^N)$ $s' > u_{min}s$
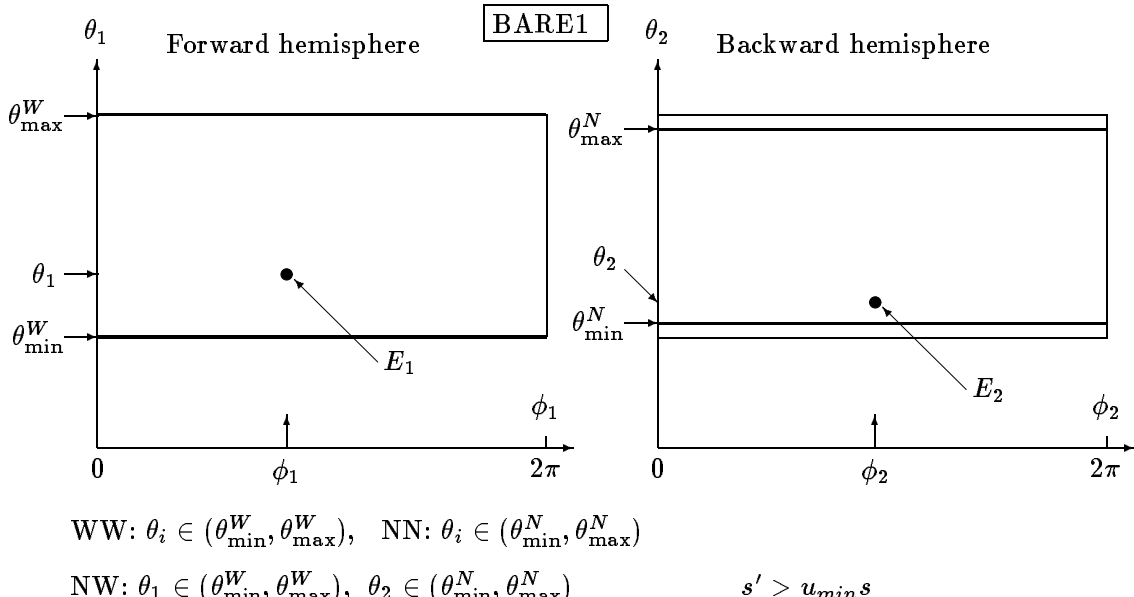
Figure 11: Geometry and acceptance of the simple (non-calorimetric) ES BARE1. This ES restricts polar angles θ_i in the forward/backward hemispheres and requires a certain minimum *energy* to be detected simultaneously in both hemispheres. Photon momentum is not constrained at all. The entire "fiducial" θ-range, i.e. wide (W) range, is $(\theta_{\min}^W, \theta_{\max}^W) = (0.024, 0.058)$ rad and the narrow (N) range is $(\theta_{\min}^N, \theta_{\max}^N)$, where $\theta_{\min}^N = \theta_{\min}^W + \delta_\theta$, $\theta_{\max}^N = \theta_{\max}^W - \delta_\theta$ and $\delta_\theta = (\theta_{\max}^W - \theta_{\min}^W)/16$. This ES can be symmetric Wide-Wide (WW) or Narrow-Narrow (NN), or asymmetric Narrow-Wide (NW), see the description in the figure. The energy cut $s' > u_{min}s$ involves momenta of outgoing $e^\pm$ ($s' = (q^+ + q^-)^2$) only.

2.7.1 Event selections

One cannot talk about the cross section for the small-angle Bhabha (SABH) process without defining precisely all cuts, or, in other terms, without specifying the ES. The most interesting ES is that of the actual experiment. LEP1 and LEP2 experiments employ in the measurement of the small-angle Bhabha scattering cross section a rich family of ES's. They do, however,

θ_1 Forward hemisphere | CALO1 | θ_2 Backward hemisphere

$\theta^W_{\max}$

$\theta^N_{\max}$

$\theta^{cl}_1 \rightarrow$

θ^{cl}_2

$\theta^W_{\min}$

$\theta^N_{\min}$

E^{cl}_1

ϕ_1

E^{cl}_2

ϕ_2

0 ϕ^{cl}_1 2π 0 ϕ^{cl}_2 2π

WW: $\theta^{cl}_i \in (\theta^W_{\min}, \theta^W_{\max})$,   NN: $\theta^{cl}_i \in (\theta^N_{\min}, \theta^N_{\max})$

NW: $\theta^{cl}_1 \in (\theta^W_{\min}, \theta^W_{\max})$, $\theta^{cl}_2 \in (\theta^N_{\min}, \theta^N_{\max})$ $E^{cl}_1 E^{cl}_2 > z_{min} E^2_{beam}$
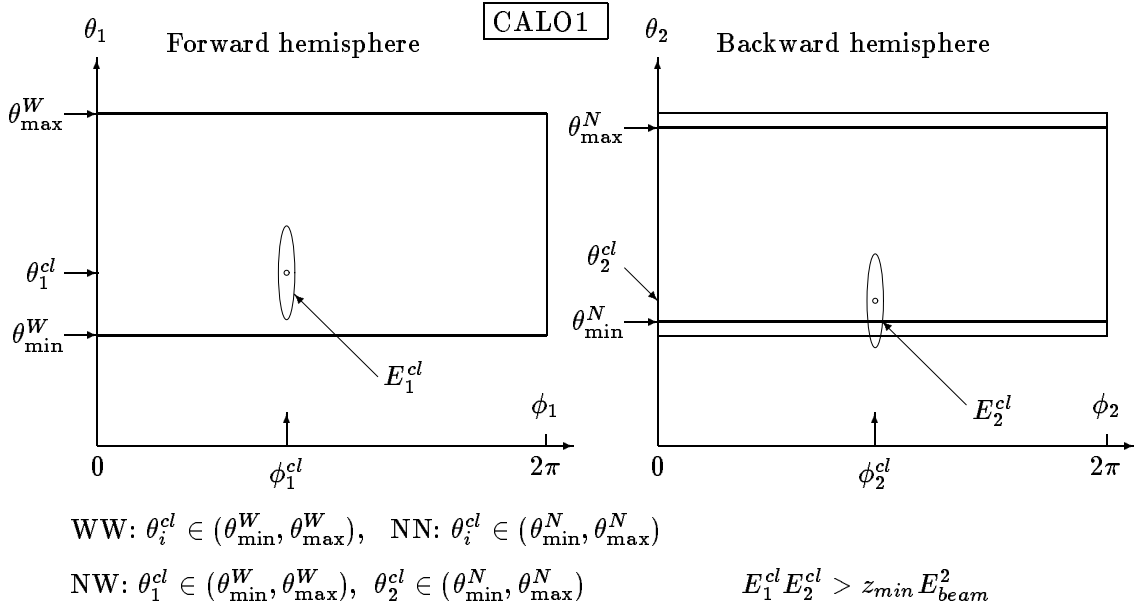
Figure 12: Geometry and acceptance of the calorimetric ES CALO1. This ES restricts polar *angles* θ_i in the forward/backward hemispheres and requires a certain minimum *energy* to be detected simultaneously in both hemispheres. The entire "fiducial" θ-range, i.e. wide (W) range, is $(\theta^W_{\min}, \theta^W_{\max}) = (0.024, 0.058)$ rad and the narrow (N) range is $(\theta^N_{\min}, \theta^N_{\max})$, where $\theta^N_{\min} = \theta^W_{\min} + \delta_\theta$, $\theta^N_{\max} = \theta^W_{\max} - \delta_\theta$ and $\delta_\theta = (\theta^W_{\max} - \theta^W_{\min})/16$. This ES can be symmetric Wide-Wide (WW) or Narrow-Narrow (NN), or asymmetric Narrow-Wide (NW), see the description in the figure. The energy cut involves the definition of the *cluster*: the cluster center $(\theta^{cl}_i, \phi^{cl}_i)$, $i = 1, 2$, is identical to the angular position of the positron in the forward and the electron in the backward hemisphere. The angular "cone" of radius $\delta = 0.010$ rad around $e^\pm$ is called cluster. The cone/cluster in the θ, ϕ plane is an elongated ellipsis, due to smallness of *theta*. The total energy registered in the cluster is denoted by E^{cl}_i. (Note that $\phi_1 = \phi_2$ for back-to-back configuration.)

have essential common features. The most important is the "double tag". It means that e^+ and e^- are *both* detected with a certain minimum energy and minimum scattering angle in the forward and backward direction, close to the beams. The other important feature of the typical experimental ES is that (except for rare cases) the photons and $e^\pm$ cannot be distinguished – only the combined energy and angle is registered. It is said that the typical experimental ES is *calorimetric*. On the other hand, for comparing theoretical calculations it is useful to deal with simplified ES's, in which only $e^\pm$ are measured and the accompanying bremsstrahlung photons ($e^\pm$ pairs) are ignored. The "double tag" is done on "bare $e^\pm$". Actually, in order to compare efficiently numerical results from the various programs, we employed the family of four ES's connecting in an almost continuous way the experimentally unrealistic (but useful for theorists) examples of ES's to experimentally realistic (but difficult for some class of theoretical calculations) ones. In order to compare theoretical results for SABH, we use one simple non-calorimetric ES called BARE1, see Figs. (11), and three calorimetric ES's called CALO1, CALO2 and SICAL2, with increasing degrees of sophistication. They are defined in Figs. (12,13) and Fig. (14). The last one, SICAL2 of Fig. (14), corresponds very closely to the ES of the real silicon detector of OPAL or ALEPH.

CALO2

Forward hemisphere θ_1 ... θ_2 Backward hemisphere

$\theta^f_{\max}$
$\theta^W_{\max}$
$\theta^N_{\max}$
θ^{cl}_2
θ^{cl}_1
$\theta^N_{\min}$
$\theta^W_{\min}$
$\theta^f_{\min}$
E^{cl}_1
E^{cl}_2
ϕ_1
ϕ_2
0 ϕ^{cl}_1 2π
0 ϕ^{cl}_2 2π

WW: $\theta^{cl}_i \in (\theta^W_{\min}, \theta^W_{\max})$,   NN: $\theta^{cl}_i \in (\theta^N_{\min}, \theta^N_{\max})$

NW: $\theta^{cl}_1 \in (\theta^W_{\min}, \theta^W_{\max})$, $\theta^{cl}_2 \in (\theta^N_{\min}, \theta^N_{\max})$ $E^{cl}_1 E^{cl}_2 > z_{min} E^2_{beam}$
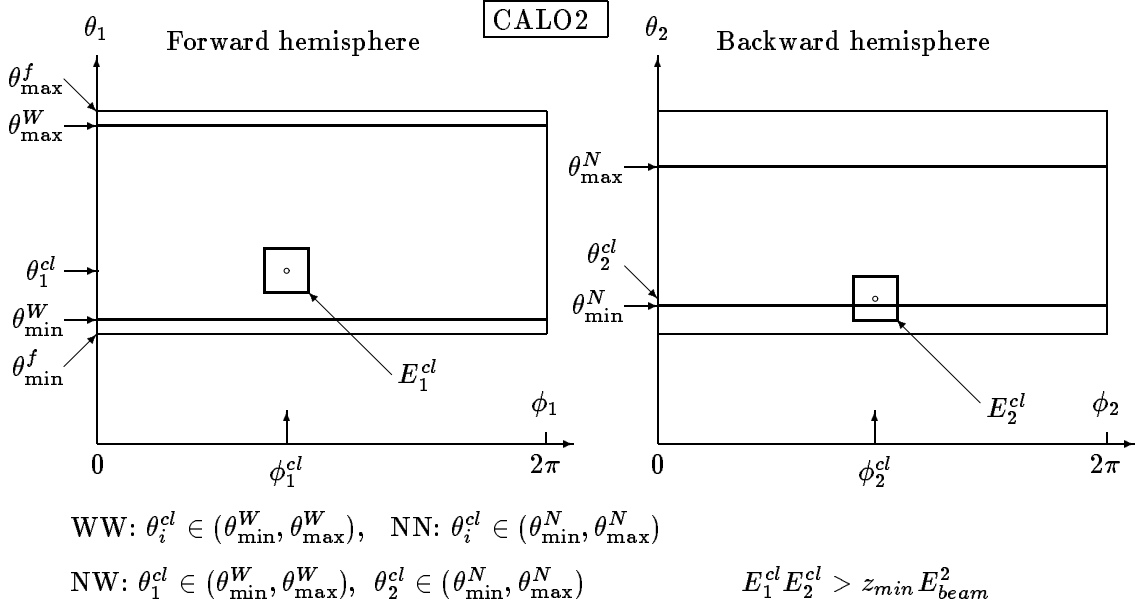
Figure 13: Geometry and acceptance of the calorimetric ES CALO2. This ES restricts polar *angles* θ_i in the forward/backward hemispheres and requires a certain minimum *energy* to be detected simultaneously in both hemispheres. The entire "fiducial" θ-range, $(\theta^f_{\min}, \theta^f_{\max}) = (0.024, 0.058)$ rad, includes the wide (W) range $(\theta^W_{\min}, \theta^W_{\max})$ and the narrow (N) range $(\theta^N_{\min}, \theta^N_{\max})$, where $\theta^W_{\min} = \theta^f_{\min} + \delta_\theta$, $\theta^W_{\max} = \theta^f_{\max} - \delta_\theta$, $\delta_\theta = (\theta^f_{\max} - \theta^f_{\min})/16$, and $\theta^N_{\min} = \theta^f_{\min} + 2\delta_\theta$, $\theta^N_{\max} = \theta^f_{\max} - 4\delta_\theta$. This ES can be symmetric Wide-Wide (WW) or Narrow-Narrow (NN), or asymmetric Narrow-Wide (NW), see the description in the figure. The energy cut involves the definition of the *cluster*: the cluster center $(\theta^{cl}_i, \phi^{cl}_i)$, $i = 1, 2$, is identical to the angular position of the positron in the forward and electron in the backward hemisphere. The angular "plaquette" $(\theta^{cl}_i + 1.5\delta_\theta, \theta^{cl}_i - 1.5\delta_\theta) \times (\phi^{cl}_i + 1.5\delta_\phi, \phi^{cl}_i - 1.5\delta_\phi)$, where $\delta_\phi = 2\pi/32$, around $e^\pm$ is called cluster. The total energy registered in the cluster is denoted by E^{cl}_i. (Note that $\phi_1 = \phi_2$ for back-to-back configuration.)

2.7.2   First order - technical precision

We start the numerical comparisons of the various theoretical calculations with the calibration exercise in which we limit ourselves to strict $\mathcal{O}(\alpha^1)$ with Z exchange, up-down interference and vacuum polarization switched off, i.e. we examine pure photonic corrections without up-down interferences. We calculate the corresponding total cross section for all our four ES's at the LEP1 energy, $\sqrt{s} = 92.3$ GeV. The purpose of this exercise is to eliminate possible trivial normalization problems in the core MC programs and in the testing programs which implement our ES's. Since $\mathcal{O}(\alpha^1)$ is unique and common, the difference of the results will be entirely due to numerical/technical problems and, following ref. [11] where the analogous exercise of this type was done for the first time, we call it the "technical precision" of the involved calculations/programs. The results are shown in Tab. 13. Since tables are hard to read, we always include a figure which contains exactly the same result in the pictorial way. In the figure, one of the cross sections is used as a reference cross section and is subtracted from the other ones. It is plotted however on the horizontal line with its true statistical error.

SICAL2

Forward hemisphere   Backward hemisphere

θ_1 θ_2

$\theta_{\max}^f$

$\theta_{\max}^W$

$\theta_{\max}^N$

θ_1^{cl}

θ_2^{cl}

$\theta_{\min}^W$

$\theta_{\min}^N$

$\theta_{\min}^f$

E_1^{cl} E_2^{cl}

ϕ_1 ϕ_2

0 ϕ_1^{cl} 2π 0 ϕ_2^{cl} 2π

WW: $\theta_i^{cl} \in (\theta_{\min}^W, \theta_{\max}^W)$,   NN: $\theta_i^{cl} \in (\theta_{\min}^N, \theta_{\max}^N)$

NW: $\theta_1^{cl} \in (\theta_{\min}^W, \theta_{\max}^W)$, $\theta_2^{cl} \in (\theta_{\min}^N, \theta_{\max}^N)$ $E_1^{cl} E_2^{cl} > z_{min} E_{beam}^2$
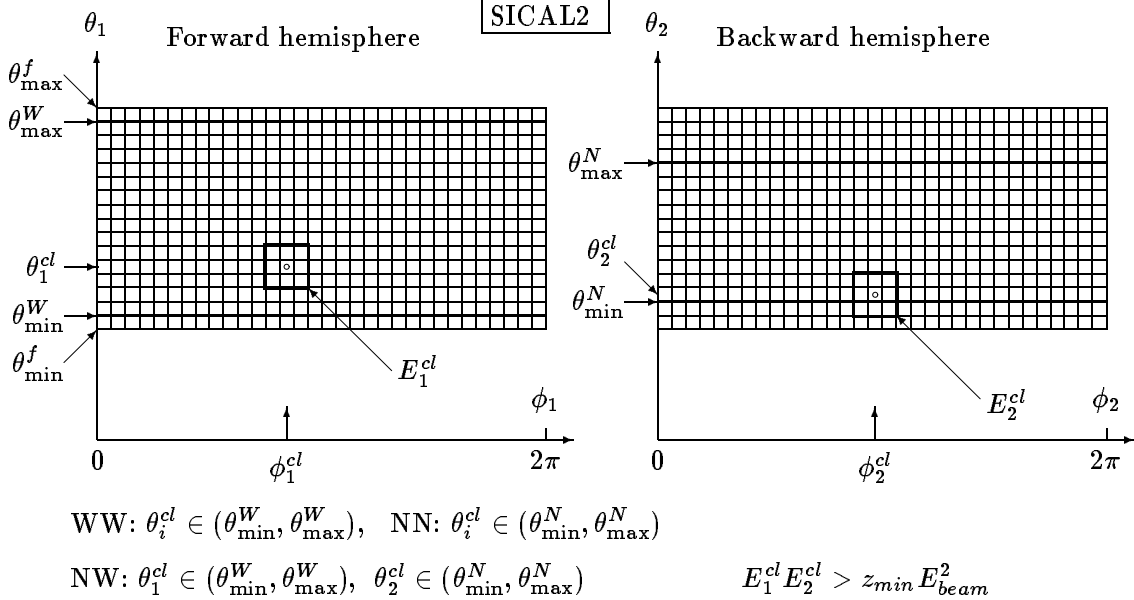
Figure 14: Geometry and acceptance of the calorimetric ES SICAL2. This ES restricts polar *angles* θ_i in the forward/backward hemispheres and requires a certain minimum *energy* to be detected simultaneously in both hemispheres. No restrictions on azimuthal angles ϕ_i are there. The entire "fiducial" θ-range, $(\theta_{\min}^f, \theta_{\max}^f) = (0.024, 0.058)$ rad, includes the wide (W) range $(\theta_{\min}^W, \theta_{\max}^W)$ and the narrow (N) range $(\theta_{\min}^N, \theta_{\max}^N)$ exactly as depicted in the figure. This ES can be symmetric Wide-Wide (WW) or Narrow-Narrow (NN), or asymmetric Narrow-Wide (NW). The energy cut and θ-cuts involve the definition of the *cluster*. Eeach side detector consists of 16×32 equal *plaquetes*. A single plaquete registers the total energy of electrons and photons. The plaquete with the maximum energy, together with its 3×3 neighborhood, is called cluster. The total energy registered in the cluster is E_i^{cl} and its angular position is $(\theta_i^{cl}, \phi_i^{cl})$, $i = 1, 2$. More precisely the angular position of a cluster is the average position of the *centers* of all 3×3 plaquetes, weighted by their energies (the definitions of ϕ's are adjusted in such a way that $\phi_1 = \phi_2$ for back-to-back configuration). The plaquetes of the cluster which spill over the angular range (outside thick lines) are also used to determine the total energy and the average position of the cluster (see backward hemisphere).

Here Tab. 13 is visualized in Fig. 15. In this figure, the cross sections from the Monte Carlo OLDBIS (an improved version of the MC program written originally by Berends and Kleiss in PETRA times, now part of BHLUMI) is used as a reference. As we see, all calculations agree well within 3×10^{-4} relative deviation. The apparent discrepancy of the $\mathcal{O}(\alpha^1)$ SABSPV for the SICAL2 ES is not statistically significant. The cross section from the non-Monte-Carlo type of calculation NLLBHA is available only for the simplest BARE1. As we have already discussed, the photonic radiative corrections for the SABH process scale smoothly with energy, so we regard this test to be valid for LEP2 energies within a factor two, i.e. within 6×10^{-4}.

2.7.3   Beyond first order - physical precision

Having found good agreement of the various calculations at the first order level, we now reinstall the photonic corrections beyond first order. More precisely we keep again Z exchange, up-down

28

$z_{\min}$	OLDBIS [nb]	SABSPV [nb]	BHAGEN95 [nb]	NNLBHA [nb]	BHLUMI [nb]
			(a) BARE1		
.100	$166.079 \pm .013$	$166.070 \pm .024$	$.000 \pm .000$	$166.070 \pm .017$	$166.046 \pm .021$
.300	$164.772 \pm .013$	$164.762 \pm .012$	$164.756 \pm .012$	$164.767 \pm .016$	$164.740 \pm .021$
.500	$162.277 \pm .013$	$162.263 \pm .012$	$162.258 \pm .012$	$162.265 \pm .016$	$162.241 \pm .021$
.700	$155.465 \pm .013$	$155.452 \pm .012$	$155.444 \pm .012$	$155.453 \pm .015$	$155.431 \pm .020$
.900	$134.417 \pm .012$	$134.401 \pm .023$	$134.394 \pm .012$	$134.393 \pm .014$	$134.390 \pm .020$
			(b) CALO1		
.100	$166.361 \pm .013$	$166.353 \pm .024$	$.000 \pm .000$	$.000 \pm .000$	$166.329 \pm .021$
.300	$166.081 \pm .013$	$166.071 \pm .021$	$166.074 \pm .013$	$.000 \pm .000$	$166.049 \pm .021$
.500	$165.319 \pm .013$	$165.311 \pm .012$	$165.312 \pm .013$	$.000 \pm .000$	$165.287 \pm .021$
.700	$161.823 \pm .013$	$161.817 \pm .024$	$161.818 \pm .013$	$.000 \pm .000$	$161.794 \pm .021$
.900	$149.942 \pm .013$	$149.934 \pm .023$	$149.934 \pm .013$	$.000 \pm .000$	$149.925 \pm .020$
			(c) CALO2		
.100	$131.061 \pm .012$	$131.070 \pm .022$	$131.051 \pm .010$	$.000 \pm .000$	$131.032 \pm .019$
.300	$130.769 \pm .012$	$130.778 \pm .022$	$130.758 \pm .010$	$.000 \pm .000$	$130.739 \pm .019$
.500	$130.206 \pm .012$	$130.214 \pm .022$	$130.194 \pm .010$	$.000 \pm .000$	$130.176 \pm .019$
.700	$127.555 \pm .012$	$127.565 \pm .022$	$127.546 \pm .010$	$.000 \pm .000$	$127.528 \pm .019$
.900	$117.557 \pm .011$	$117.572 \pm .025$	$117.543 \pm .010$	$.000 \pm .000$	$117.541 \pm .018$
			(d) SICAL2		
.100	$132.011 \pm .012$	$131.965 \pm .023$	$132.004 \pm .028$	$.000 \pm .000$	$131.984 \pm .019$
.300	$131.900 \pm .012$	$131.862 \pm .021$	$131.893 \pm .027$	$.000 \pm .000$	$131.872 \pm .019$
.500	$131.587 \pm .012$	$131.539 \pm .018$	$131.581 \pm .027$	$.000 \pm .000$	$131.559 \pm .019$
.700	$128.363 \pm .012$	$128.306 \pm .016$	$128.364 \pm .027$	$.000 \pm .000$	$128.338 \pm .019$
.900	$117.843 \pm .011$	$117.795 \pm .012$	$117.811 \pm .027$	$.000 \pm .000$	$117.828 \pm .018$

Table 13: Monte Carlo results for the symmetric Wide-Wide ES's BARE1, CALO1, CALO2 and SICAL2, for the $\mathcal{O}(\alpha^1)$ matrix element. Z exchange, up-down interference and vacuum polarization are switched off. The center of mass energy is $\sqrt{s} = 92.3$ GeV. Not available x-sections are set to zero.

interference and vacuum polarization switched off, but compare numerical results which include $\mathcal{O}(\alpha^2 L^2)$, $\mathcal{O}(\alpha^2 L)$ and $\mathcal{O}(\alpha^3 L^3)$ contributions due to photon bremsstrahlung. We do not include production of light fermion pairs unless stated otherwise. The numerical results are shown in Tab. 14 and Fig. 16. In the figure, the cross section from the second order exponentiated Monte Carlo BHLUMI is used as a reference cross section. The differences between various calculations now represent not only technical precision, but also physical precision because the cross sections are calculated using different QED matrix elements.

The results shown in Tab. 14 and Fig. 16 have remarkable properties. For values of the energy-cut variable in the experimentally interesting range $0.25 < z_{\min} < 0.75$, the cross section from the programs BHLUMI and SABSPV agree throughout all the four ES's, from the unrealistic BARE1 to very realistic SICAL2, to within 1.0×10^{-3} relative deviation. This agreement is definitely better than the difference between BHLUMI and OLDBIS+LUMLOG, which
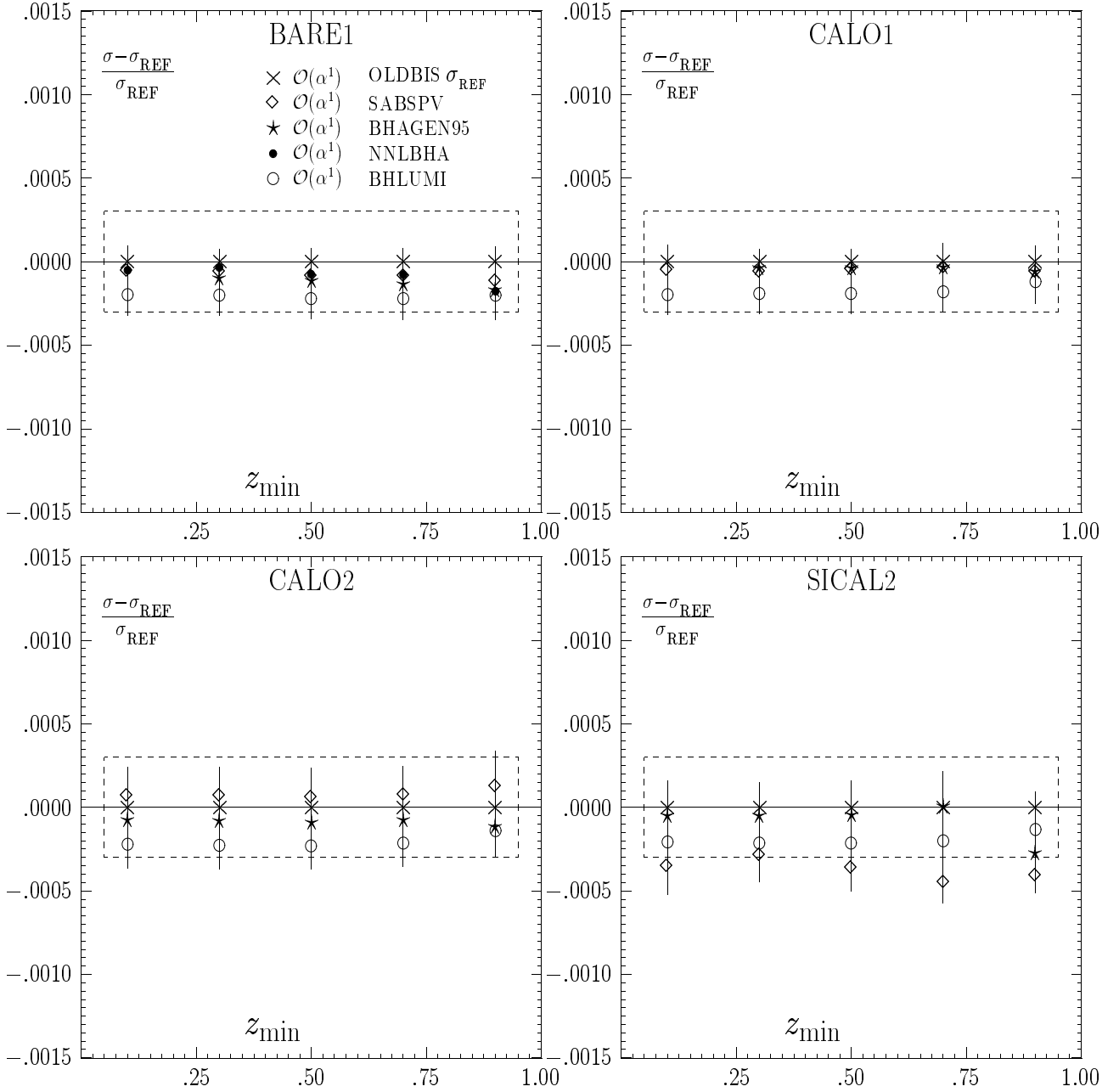
Figure 15: Monte Carlo results for the symmetric Wide-Wide ES's BARE1, CALO1, CALO2 and SICAL2, for the $\mathcal{O}(\alpha^1)$ matrix element. Z exchange, up-down interference and vacuum polarization are switched off. The center of mass energy is $\sqrt{s} = 92.3$ GeV. In the plot, the cross section from the program OLDBIS (part from BHLUMI 4.02.a, originally written by Berends and Kleiss) is used as a reference cross section.

in the last years was routinely used (see Refs. [6,58]) in order to estimate missing higher order and subleading corrections. Remarkably, the OLDBIS+LUMLOG results coincide extremely well with BHAGEN95. Let us note that the OLDBIS+LUMLOG matrix element does not ex-

z_{min}	BHLUMI [nb]	SABSPV [nb]	BHAGEN95 [nb]	OBI+LMG [nb]	NLLBHA [nb]
			(a) BARE1		
.100	$166.892 \pm .006$	$166.795 \pm .028$	$.000 \pm .000$	$166.672 \pm .017$	$166.948 \pm .000$
.300	$165.374 \pm .006$	$165.323 \pm .028$	$165.190 \pm .012$	$165.187 \pm .017$	$165.448 \pm .000$
.500	$162.530 \pm .006$	$162.529 \pm .028$	$162.330 \pm .012$	$162.365 \pm .017$	$162.581 \pm .000$
.700	$155.668 \pm .006$	$155.751 \pm .026$	$155.466 \pm .012$	$155.519 \pm .017$	$155.617 \pm .000$
.900	$137.342 \pm .006$	$137.528 \pm .022$	$137.188 \pm .011$	$137.210 \pm .017$	$137.201 \pm .000$
			(b) CALO1		
.100	$167.203 \pm .006$	$167.106 \pm .028$	$.000 \pm .000$	$167.000 \pm .017$	$.000 \pm .000$
.300	$166.795 \pm .006$	$166.715 \pm .028$	$166.618 \pm .012$	$166.623 \pm .017$	$.000 \pm .000$
.500	$165.830 \pm .006$	$165.768 \pm .014$	$165.661 \pm .014$	$165.686 \pm .017$	$.000 \pm .000$
.700	$162.237 \pm .006$	$162.203 \pm .027$	$162.048 \pm .014$	$162.053 \pm .017$	$.000 \pm .000$
.900	$151.270 \pm .006$	$151.272 \pm .025$	$150.823 \pm .014$	$150.707 \pm .017$	$.000 \pm .000$
			(c) CALO2		
.100	$131.835 \pm .006$	$131.755 \pm .027$	$131.658 \pm .007$	$131.632 \pm .016$	$.000 \pm .000$
.300	$131.450 \pm .006$	$131.393 \pm .027$	$131.285 \pm .012$	$131.274 \pm .016$	$.000 \pm .000$
.500	$130.727 \pm .006$	$130.708 \pm .027$	$130.575 \pm .012$	$130.584 \pm .016$	$.000 \pm .000$
.700	$127.969 \pm .006$	$127.999 \pm .027$	$127.802 \pm .014$	$127.802 \pm .016$	$.000 \pm .000$
.900	$118.792 \pm .006$	$118.879 \pm .029$	$118.293 \pm .013$	$118.201 \pm .015$	$.000 \pm .000$
			(d) SICAL2		
.100	$132.816 \pm .006$	$132.612 \pm .026$	$132.611 \pm .028$	$132.582 \pm .016$	$.000 \pm .000$
.300	$132.553 \pm .006$	$132.427 \pm .025$	$132.420 \pm .028$	$132.405 \pm .016$	$.000 \pm .000$
.500	$131.985 \pm .006$	$131.966 \pm .022$	$131.962 \pm .027$	$131.965 \pm .016$	$.000 \pm .000$
.700	$128.672 \pm .006$	$128.691 \pm .019$	$128.620 \pm .027$	$128.610 \pm .016$	$.000 \pm .000$
.900	$119.013 \pm .006$	$119.075 \pm .015$	$118.561 \pm .027$	$118.488 \pm .015$	$.000 \pm .000$

Table 14: Monte Carlo results for the symmetric Wide-Wide ES's BARE1, CALO1, CALO2 and SICAL2, for matrix elements beyond first order. Z exchange, up-down interference and vacuum polarization are switched off. The center of mass energy is $\sqrt{s} = 92.3$ GeV. Not available x-sections are set to zero.

ponentiate properly $\mathcal{O}(\alpha^2 L)$ corrections, i.e. they are wrong in the soft photon limit. This may explain why BHLUMI and SABSPV, which do not have such problems, agree better. According to the authors, BHAGEN95 does not suffer of the same problem as it has the soft photon limit properly treated by construction, but some corrections are expected due to the approximate treatment of two hard photon emission. The result from NLLBHA is present only for unrealistic BARE1 selection, and for $0.25 < z_{\min} < 0.75$ it agrees to within 0.1% with BHLUMI and SABSPV. It is an interesting result because NLLBHA features complete $\mathcal{O}(\alpha^2 L)$ corrections, while all the other programs have only incomplete $\mathcal{O}(\alpha^2 L)$ contributions. In Tab. 14 and Fig. 16 the results of BHLUMI, SABSPV and BHAGEN95 include exponentiation, and therefore they include necessarily $\mathcal{O}(\alpha^3 L^3)$ effects (incomplete). We therefore compare them with a version of NLLBHA which includes, besides $\mathcal{O}(\alpha^2 L)$, also $\mathcal{O}(\alpha^3 L^3)$ corrections. All the above results will be used as an input in our final estimate of the total theoretical uncertainty of SABH cross

31
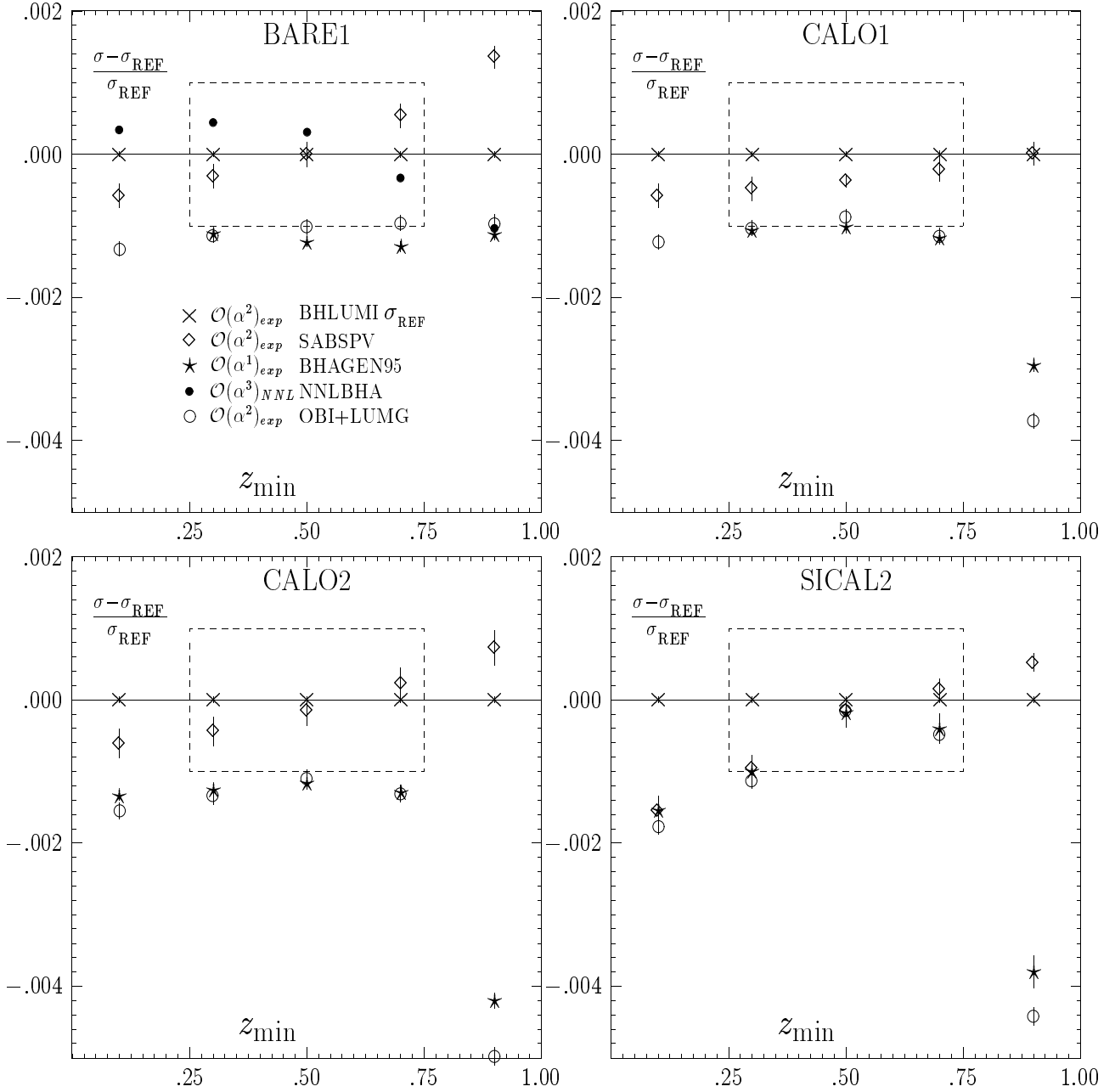
Figure 16: Monte Carlo results for the symmetric Wide-Wide ES's BARE1, CALO1, CALO2 and SICAL2, for matrix elements beyond first order. Z exchange, up-down interference and vacuum polarization are switched off. The center of mass energy is $\sqrt{s} = 92.3$ GeV. In the plot, the $\mathcal{O}(\alpha^2)_{exp}^{YFS}$ cross section σ_{BHL} from BHLUMI 4.02.a is used as a reference cross section.

section for LEP1/LEP2 energies.

Finally, we present similar numerical comparisons of the calculations beyond $\mathcal{O}(\alpha^1)$ at one LEP2 energy $\sqrt{s} = 176$ GeV. As before, since the tables are hard to read, we accompany

z_{min}	BHLUMI [nb]	SABSPV [nb]	BHAGEN95 [nb]	OBI+LUM [nb]
	(a) CALO2 LEP2			
.100	$36.123 \pm .003$	$36.096 \pm .008$	$.000 \pm .000$	$36.060 \pm .006$
.300	$36.013 \pm .003$	$35.992 \pm .008$	$35.963 \pm .005$	$35.958 \pm .006$
.500	$35.807 \pm .003$	$35.796 \pm .008$	$35.762 \pm .005$	$35.761 \pm .006$
.700	$35.001 \pm .003$	$35.005 \pm .008$	$34.951 \pm .005$	$34.948 \pm .006$
.900	$32.324 \pm .003$	$32.341 \pm .008$	$32.173 \pm .006$	$32.145 \pm .006$
	(b) SICAL2 LEP2			
.100	$36.394 \pm .003$	$36.337 \pm .011$	$.000 \pm .000$	$36.322 \pm .006$
.300	$36.316 \pm .003$	$36.284 \pm .010$	$36.271 \pm .009$	$36.270 \pm .006$
.500	$36.150 \pm .003$	$36.147 \pm .009$	$36.139 \pm .009$	$36.142 \pm .006$
.700	$35.193 \pm .003$	$35.203 \pm .008$	$35.173 \pm .009$	$35.171 \pm .006$
.900	$32.383 \pm .003$	$32.405 \pm .006$	$32.243 \pm .009$	$32.224 \pm .006$
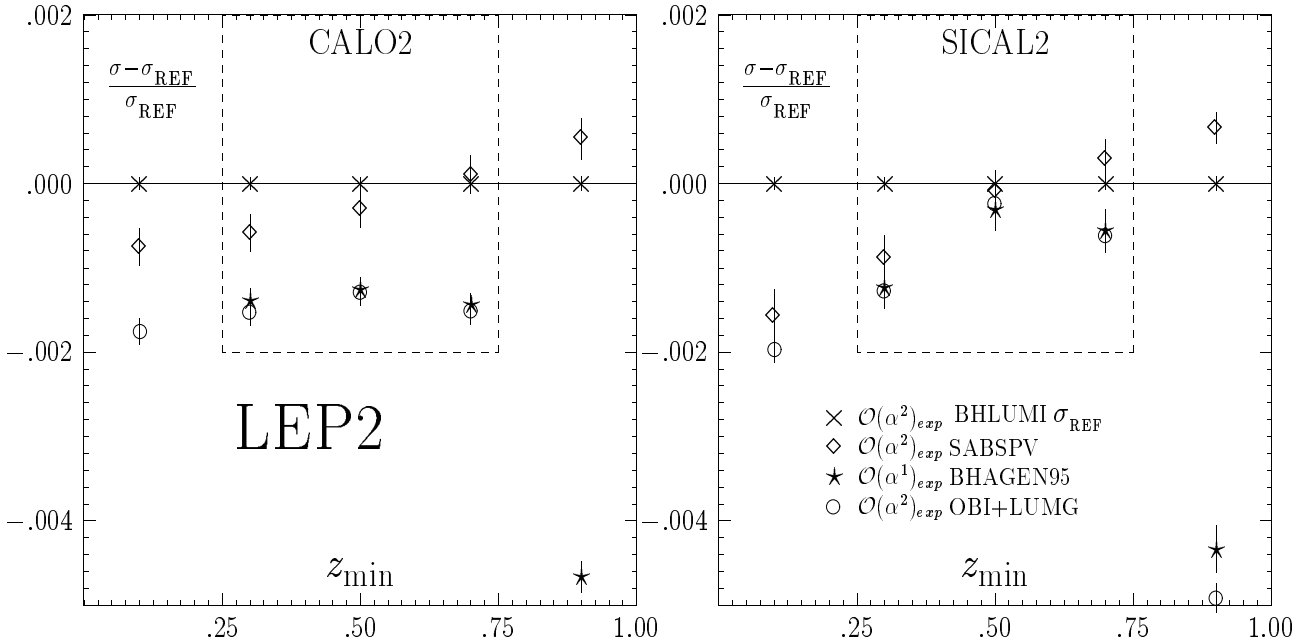
Table 15: In this table/figure we show cross sections for LEP2 center of mass energy, $\sqrt{s} = 176$ GeV. Monte Carlo results are shown for various symmetric Wide-Wide ES's and matrix elements beyond first order. Z exchange, up-down interference and vacuum polarization are switched off. Not available x-sections are set to zero. In the plot, the $\mathcal{O}(\alpha^2)_{exp}$ cross section σ_{BHL} from BHLUMI 4.02.a is used as a reference cross section.

the table with a figure which shows the same numerical result in a pictorial way (the caption is common for the table and figure). This way of presenting results in the form of the twin table/figure will be used often in the following. As before, in the figure one of the cross sections is used as a reference cross section and is subtracted from the other ones. The main result is shown in table/figure 15. Here, results are shown for the symmetric Wide-Wide variant of the CALO2 and SICAL2 ES's. As expected, the difference between the programs is almost the same! The higher order corrections at LEP2 are only slightly stronger. This result was already

anticipated when analyzing "scaling rules" derived from Tab. 2. From the scaling rules we also know that this result will be essentially the same for the wider angular range $3° − 6°$. *The practical message is that, within 20-30%, the precision estimates derived from the numerical exercises for the SABH process at LEP1 should be valid also for LEP2.*

Precision requirements at LEP2 are less stringent. In the figure, we draw a LEP2-type box which spans over 0.2% and extends over the experimentally interesting range $0.25 < z_{min} < 0.75$. All programs come together within the above range. The above 0.2% limit will be used as an input in our final estimate of the total theoretical uncertainty of the SABH cross section for LEP2 energies. This limit has obviously a large safety margin, close to a factor of two.

2.7.4   Asymmetric and very narrow event selections

The numerical comparisons shown in the previous section were done, for pure technical reasons (less chances for programming errors in the testing programs), for the *symmetric* Wide-Wide version of the ES. As we know very well (see the introduction), the higher order contributions are sensitive to the "asymmetricity" of the ES. In order to avoid any danger due to the above simplification, we have done another series of comparisons of the various calculations for the symmetric Narrow-Narrow and asymmetric Narrow-Wide versions of the ES's CALO2, which are defined in Fig. 13. Let us remind the reader that the variation of the difference BHLUMI−(OLDBIS+LUMLOG$_{HO}$) over the WW, NN and NW selection was the cornerstone of the previous estimates [6,58] of the size of uncontrolled higher order photonic corrections (together with technical precision). We believe that CALO2 is close enough to our most realistic ES SICAL2 and the results obtained for CALO2 are valid for SICAL2. Let us also recall that the typical experimental ES is of the asymmetric Narrow-Wide type. The corresponding results are shown in table/figure 16 for the matrix elements in the $\mathcal{O}(\alpha^2)$ class (we have checked that for the $\mathcal{O}(\alpha^1)$ level the same programs agree better than 0.03%, but we omit the corresponding table/plot due to lack of space).

As we see in tables/figures 16 and 14, for all the three types of the CALO2 ES (WW, NN and NW), BHLUMI and SABSPV stay within 0.1% from one another for all the values of the energy-cut variable in the experimentally interesting range $0.25 < z_{min} < 0.75$. This is a new nontrivial result, which will be exploited to decrease the estimated error due to the higher order photonic corrections from 0.15% down to 0.1%. In a sense, we replace the old estimate based on BHLUMI − (OLDBIS + LUMLOG$_{HO}$) with a new one based on BHLUMI−SABSPV. Hybrid Monte Carlo's (OLDBIS + LUMLOG$_{HO}$) and BHAGEN95 are off of about 0.2% in the NN case but, noticeably, they are on the same ground as BHLUMI and SABSPV for the most interesting NW case. The above exercise was done for the LEP1 energy, and in view of the results shown in table/figure 15 and our "scaling rules" (see the introduction), we do not foresee any problem with extending its validity to LEP2 energies.

As we already stressed in the introduction, for the purpose of LEP2 it is more important, however, to check if the change of the "narrowness", i.e. the ratio $\theta_{max}/\theta_{min} − 1$, to smaller

34

z_{min}	BHLUMI [nb]	OBI+LMG [nb]	SABSPV [nb]	BHAGEN95 [nb]
	CALO2 *Symmetric Narrow-Narrow*			
.100	$95.458 \pm .005$	$95.259 \pm .014$	$95.363 \pm .013$	$95.287 \pm .009$
.300	$95.233 \pm .005$	$95.048 \pm .014$	$95.157 \pm .016$	$95.065 \pm .009$
.500	$94.841 \pm .005$	$94.672 \pm .014$	$94.792 \pm .016$	$94.680 \pm .009$
.700	$93.520 \pm .005$	$93.347 \pm .014$	$93.513 \pm .019$	$93.354 \pm .009$
.900	$87.359 \pm .005$	$86.899 \pm .013$	$87.396 \pm .012$	$86.958 \pm .009$
	CALO2 *Asymmetric Narrow-Wide*			
.100	$98.834 \pm .003$	$98.809 \pm .010$	$98.859 \pm .017$	$98.804 \pm .009$
.300	$98.539 \pm .003$	$98.535 \pm .010$	$98.577 \pm .017$	$98.515 \pm .009$
.500	$98.020 \pm .003$	$98.038 \pm .010$	$98.073 \pm .019$	$98.006 \pm .009$
.700	$96.054 \pm .003$	$96.061 \pm .010$	$96.131 \pm .018$	$96.033 \pm .009$
.900	$88.554 \pm .003$	$88.220 \pm .009$	$88.648 \pm .015$	$88.263 \pm .009$
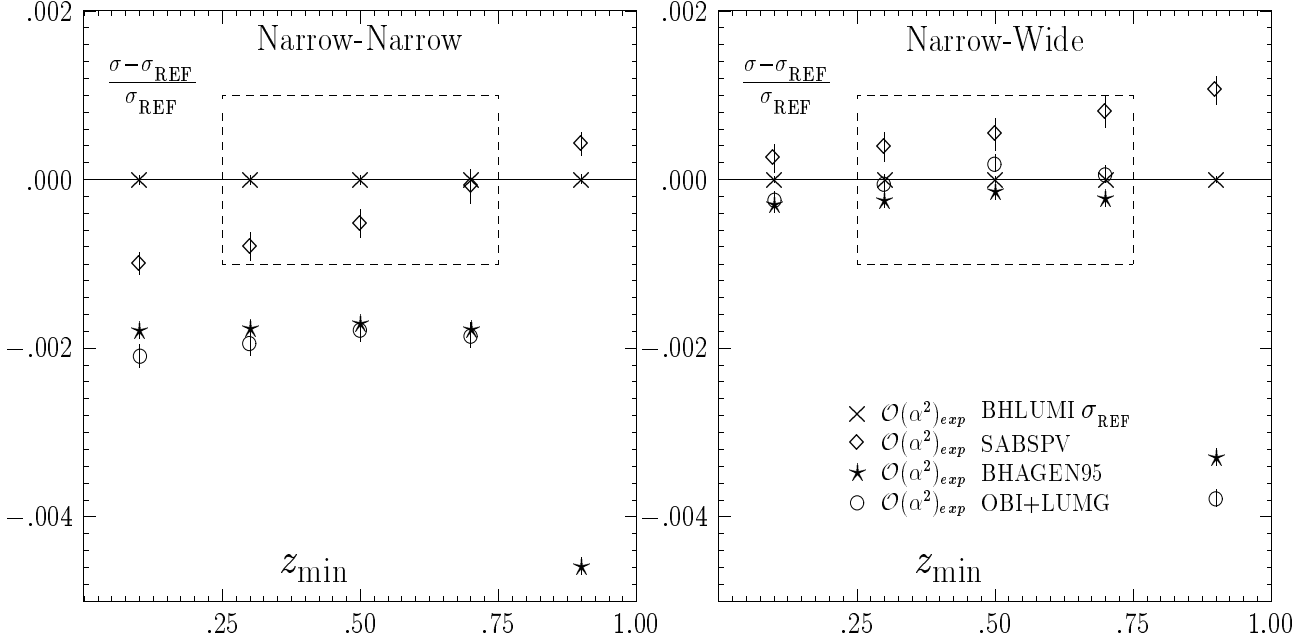
Table 16: In this table/figure we show cross sections for various symmetric/asymmetric versions of the CALO2 ES, for matrix elements beyond first order. Z exchange, up-down interference and vacuum polarization are switched off. The center of mass energy is $\sqrt{s} = 92.3$ GeV. Not available x-sections are set to zero. The wide range is defined by $\theta_{1w} = \theta_{1f} + \delta_{segm}$ and $\theta_{2w} = \theta_{2f} - \delta_{segm}$, and the narrow range by $\theta_{1n} = \theta_{1f} + 2\delta_{segm}$ and $\theta_{2n} = \theta_{2f} - 4\delta_{segm}$; $\delta_{segm} = (\theta_{2f} - \theta_{1f})/16$, $\theta_{1f} = 0.024$ and $\theta_{2f} = 0.058$ rad, respectively.

values does not spoil the agreement of the table/figure 16. As we have already indicated, at LEP2 the decrease of the narrowness $\theta_{max}/\theta_{min} - 1$ may cause a significant increase in the photonic radiative corrections. The relevant cross-check is done in table/figure 17. It represents the *worst possible scenario* at LEP2. The results are shown for the narrower version of the CALO2 ES, which we call CALO3, in the symmetric and asymmetric versions. As we see, BHLUMI and SABSPV differ again for the above ES by less than 0.2%. This result will

35

z_{min}	BHLUMI [nb]	OBI+LMG [nb]	SABSPV [nb]	BHAGEN95 [nb]
	CALO2 *Symmetric Narrow-Narrow LEP2*			
.100	$8.088 \pm .001$	$8.052 \pm .003$	$8.074 \pm .001$	$8.058 \pm .001$
.300	$8.074 \pm .001$	$8.039 \pm .003$	$8.061 \pm .001$	$8.044 \pm .001$
.500	$8.048 \pm .001$	$8.014 \pm .003$	$8.039 \pm .001$	$8.018 \pm .001$
.700	$7.989 \pm .001$	$7.954 \pm .003$	$7.986 \pm .001$	$7.958 \pm .001$
.900	$7.574 \pm .001$	$7.515 \pm .003$	$7.582 \pm .001$	$7.522 \pm .001$
	CALO2 *Asymmetric Narrow-Wide LEP2*			
.100	$8.523 \pm .001$	$8.514 \pm .002$	$8.518 \pm .001$	$8.515 \pm .001$
.300	$8.501 \pm .001$	$8.494 \pm .002$	$8.499 \pm .001$	$8.494 \pm .001$
.500	$8.464 \pm .001$	$8.457 \pm .002$	$8.465 \pm .001$	$8.457 \pm .001$
.700	$8.374 \pm .001$	$8.366 \pm .002$	$8.380 \pm .001$	$8.365 \pm .001$
.900	$7.755 \pm .001$	$7.716 \pm .002$	$7.769 \pm .001$	$7.720 \pm .001$
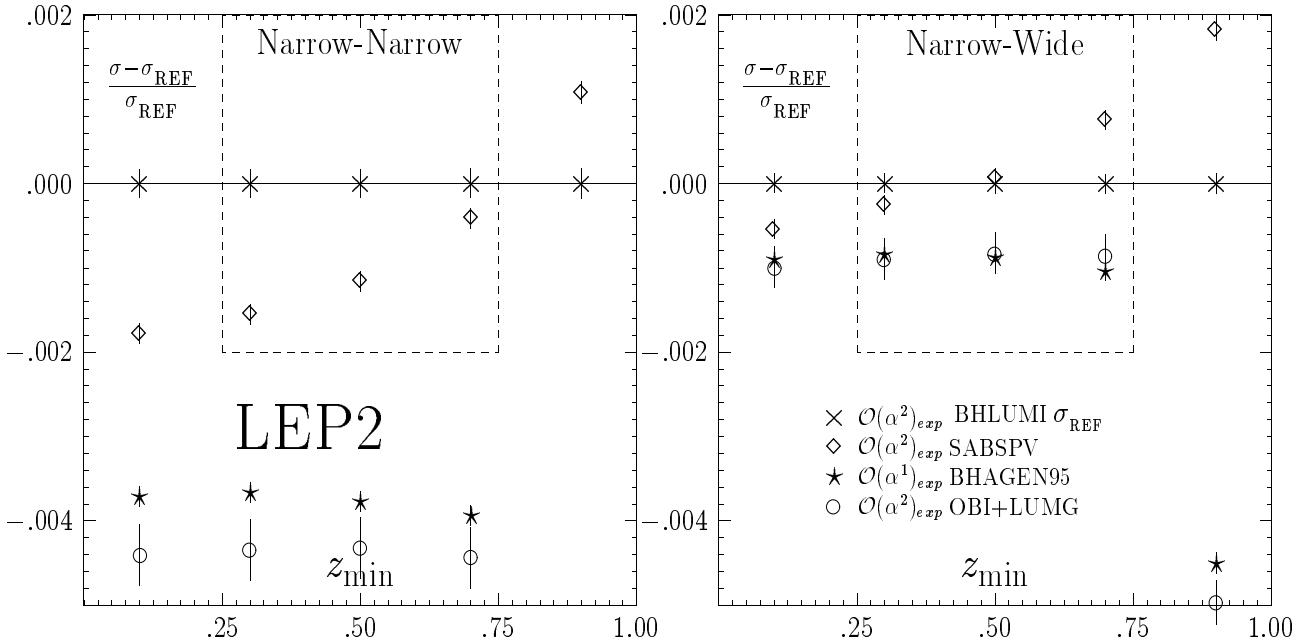
Table 17: In this table/figure we show cross sections for for the symmetric/asymmetric CALO3 ES's (the narrower version of CALO2) for matrix elements beyond first order. Z exchange, up-down interference and vacuum polarization are switched off. The center of mass energy is $\sqrt{s} = 176$ GeV. Not available x-sections are set to zero. The wide range is defined by $\theta_{1w} = \theta_{1f} + 6\delta_{segm}$ and $\theta_{2w} = \theta_{1f} + 16\delta_{segm}$, and the narrow range by $\theta_{1n} = \theta_{1f} + 8\delta_{segm}$ and $\theta_{2n} = \theta_{1f} + 15\delta_{segm}$; $\delta_{segm} = (\theta_{2f} - \theta_{1f})/16$, $\theta_{1f} = 0.024$ and $\theta_{2f} = 0.058$ rad, respectively.

be used for estimating theoretical uncertainty of the SABH process at LEP2. Hybrid Monte Carlo's (OLDBIS + LUMLOG$_{HO}$) and BHAGEN95 are off of about 0.4% in the NN case but, noticeably, they are on the same ground as BHLUMI and SABSPV for the most interesting NW case.

z_{min}	BHLUMI [nb]	SABSPV [nb]	BHAGEN95	VP+Z Bhlumi
	CALO2 *Symmetric Wide-Wide*			
.100	$136.975 \pm .010$	$136.831 \pm .018$	$136.861 \pm .008$	$5.140 \pm .008$
.300	$136.576 \pm .010$	$136.453 \pm .018$	$136.482 \pm .008$	$5.126 \pm .008$
.500	$135.827 \pm .010$	$135.742 \pm .018$	$135.770 \pm .008$	$5.100 \pm .008$
.700	$132.962 \pm .010$	$132.928 \pm .017$	$132.927 \pm .008$	$4.994 \pm .008$
.900	$123.420 \pm .009$	$123.430 \pm .018$	$123.114 \pm .009$	$4.627 \pm .008$
	CALO2 *Symmetric Narrow-Narrow*			
.100	$99.208 \pm .009$	$99.074 \pm .017$	$99.089 \pm .011$	$3.751 \pm .007$
.300	$98.975 \pm .009$	$98.851 \pm .021$	$98.866 \pm .011$	$3.742 \pm .007$
.500	$98.570 \pm .009$	$98.477 \pm .017$	$98.479 \pm .011$	$3.728 \pm .007$
.700	$97.198 \pm .008$	$97.147 \pm .017$	$97.128 \pm .011$	$3.678 \pm .007$
.900	$90.789 \pm .008$	$90.791 \pm .016$	$90.537 \pm .011$	$3.430 \pm .007$
	CALO2 *Asymmetric Narrow-Wide*			
.100	$102.717 \pm .006$	$102.703 \pm .017$	$102.724 \pm .010$	$3.883 \pm .004$
.300	$102.412 \pm .006$	$102.411 \pm .017$	$102.434 \pm .010$	$3.873 \pm .004$
.500	$101.874 \pm .006$	$101.894 \pm .017$	$101.922 \pm .010$	$3.854 \pm .004$
.700	$99.833 \pm .005$	$99.878 \pm .017$	$99.902 \pm .010$	$3.779 \pm .004$
.900	$92.033 \pm .005$	$92.088 \pm .016$	$91.887 \pm .011$	$3.478 \pm .004$

Table 18: Monte Carlo results for various symmetric/asymmetric versions of the CALO2 ES, for matrix elements beyond first order. Z exchange, up-down interference and vacuum polarization are switched ON. The center of mass energy is $\sqrt{s} = 92.3$ GeV. Not available x-sections are set to zero. The wide range is defined by $\theta_{1w} = \theta_{1f} + \delta_{segm}$ and $\theta_{2w} = \theta_{2f} - \delta_{segm}$, and the narrow range by $\theta_{1n} = \theta_{1f} + 2\delta_{segm}$ and $\theta_{2n} = \theta_{2f} - 4\delta_{segm}$; $\delta_{segm} = (\theta_{2f} - \theta_{1f})/16$, $\theta_{1f} = 0.024$ and $\theta_{2f} = 0.058$ rad, respectively.

2.7.5 Z and vacuum polarization included

In all the previous comparisons, the small contributions from s-channel Z-exchange and s-channel photon exchange diagrams were switched off in order to enhance the possibility of seeing more clearly the most important pure photonic higher order corrections. In the following part of numerical comparisons, we restore in the calculations the contributions from these s-channel Z-exchange and s-channel photon exchange diagrams, together with the effect of vacuum polarization. The comparison of various calculations is done for the semi-realistic ES CALO2 in the versions Wide-Wide, Narrow-Narrow and Narrow-Wide, as defined in Fig. 13. The resulting cross sections are shown for a LEP1 energy in Tab. 18 and Fig. 17. Again, BHLUMI and SABSPV, for values of the energy-cut variable in the experimentally interesting range $0.25 < z_{\min} < 0.75$, agree within 0.1% for all the three versions of the ES (WW, NN and WN). BHAGEN95 is also in agreement, in this case, for all the three versions of the ES, due to a slightly bigger correction in these added contributions. We do not expect that switching on the small s-channel Z-exchange and s-channel photon exchange corrections would change our conclusions for LEP2. Vacuum polarization enters essentially only in the normalization of the SABH cross section, and Z contribution at LEP2 can be safely neglected. We therefore extend the validity of the above exercise to LEP2.
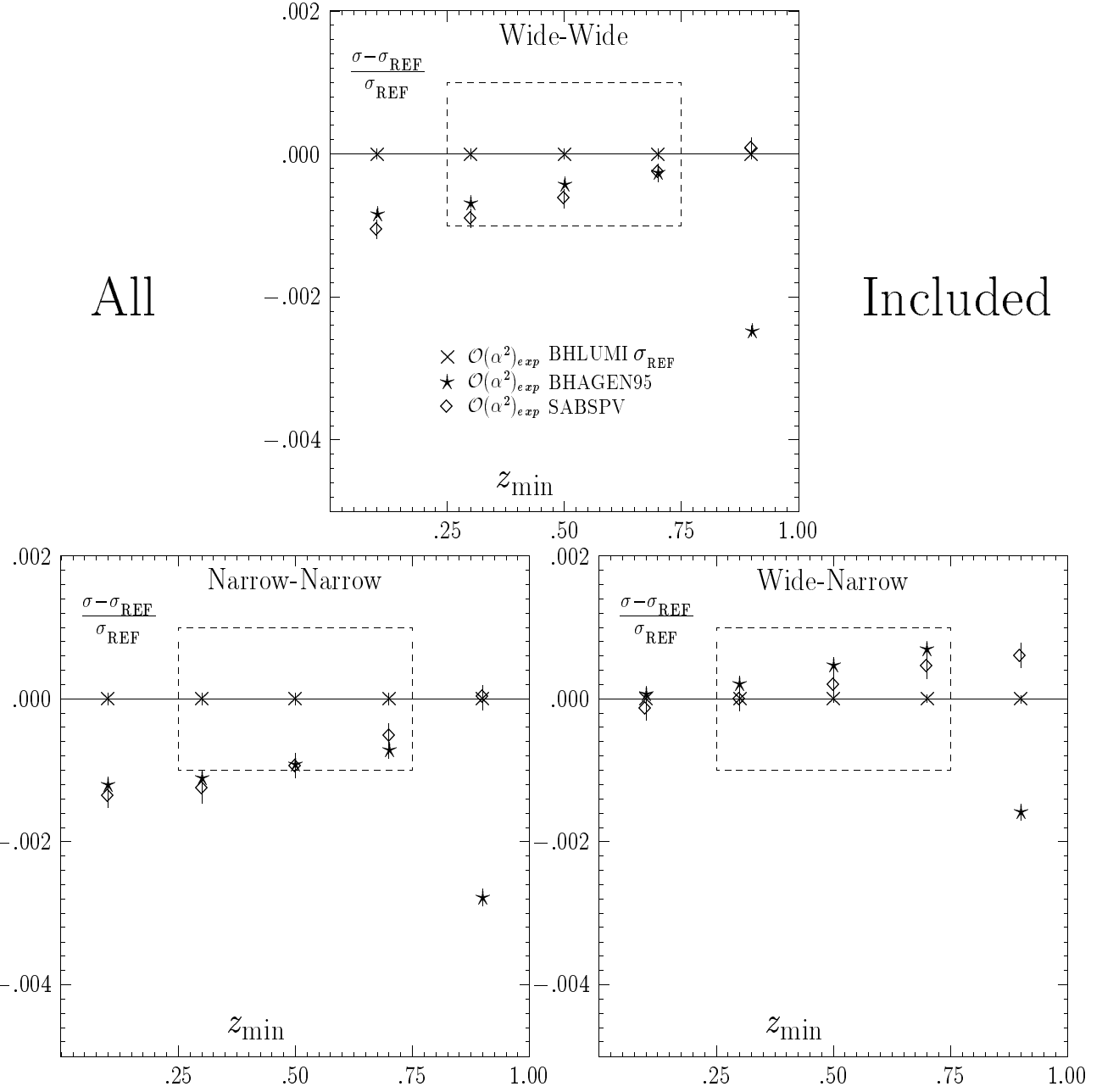
Figure 17: Monte Carlo results for various symmetric/asymmetric versions of the CALO2 ES, for matrix elements beyond first order. Z exchange, up-down interference and vacuum polarization are switched ON. The center of mass energy is $\sqrt{s} = 92.3$ GeV. Not available x-sections are set to zero. In the plot, the $\mathcal{O}(\alpha^2)_{exp}^{YFS}$ cross section σ_{BHL} from BHLUMI 4.x is used as a reference cross section.

2.8 The total theoretical error for small-angle Bhabha scattering

In this section we present some supplementary numerical material concerning higher order corrections from MC and non-MC programs, and we summarize on the total theoretical error

z_{min}	BHLUMI(alf2e)	BHLUMI(alf3e)	BHLUMI(alf2)	NLLBHA(alf2)	NLLBHA(alf3)	NLLBHA(alf3p)
	(a) BARE1					
.100	$166.892 \pm .006$	$-.017 \pm .000$	$166.988 \pm .021$	$167.016 \pm .017$	$166.948 \pm .000$	$166.966 \pm .000$
.300	$165.374 \pm .006$	$-.010 \pm .000$	$165.471 \pm .021$	$165.503 \pm .017$	$165.448 \pm .000$	$165.421 \pm .000$
.500	$162.530 \pm .006$	$-.006 \pm .000$	$162.594 \pm .021$	$162.630 \pm .016$	$162.581 \pm .000$	$162.527 \pm .000$
.700	$155.668 \pm .006$	$-.002 \pm .000$	$155.620 \pm .020$	$155.649 \pm .015$	$155.617 \pm .000$	$155.528 \pm .000$
.900	$137.342 \pm .006$	$.004 \pm .000$	$137.191 \pm .020$	$137.205 \pm .014$	$137.201 \pm .000$	$137.063 \pm .000$
	(b) SICAL2					
.000	$132.816 \pm .006$	$-.017 \pm .000$	$132.912 \pm .019$	$.000 \pm .000$	$.000 \pm .000$	$.000 \pm .000$
.200	$132.553 \pm .006$	$-.018 \pm .000$	$132.645 \pm .019$	$.000 \pm .000$	$.000 \pm .000$	$.000 \pm .000$
.400	$131.985 \pm .006$	$-.019 \pm .000$	$132.061 \pm .019$	$.000 \pm .000$	$.000 \pm .000$	$.000 \pm .000$
.600	$128.672 \pm .006$	$-.017 \pm .000$	$128.711 \pm .019$	$.000 \pm .000$	$.000 \pm .000$	$.000 \pm .000$
.800	$119.013 \pm .006$	$-.012 \pm .000$	$119.014 \pm .018$	$.000 \pm .000$	$.000 \pm .000$	$.000 \pm .000$
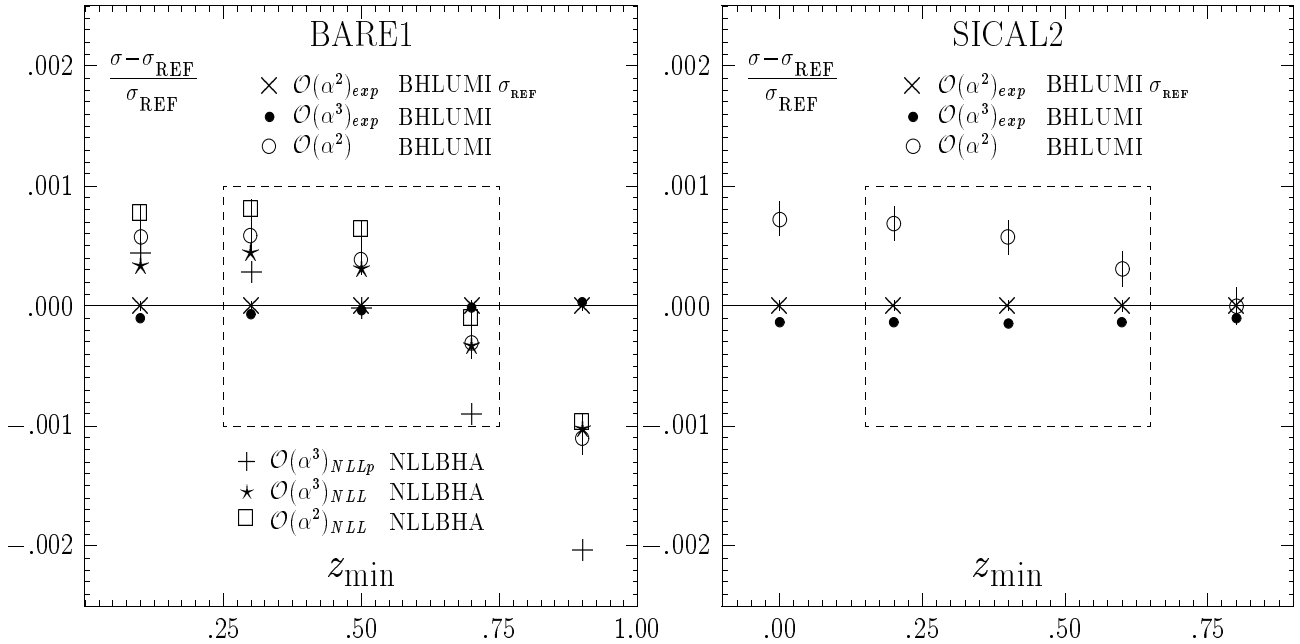
Table 19: In this table/figure we show cross sections for LEP1 center of mass energy, $\sqrt{s} = 92$ GeV. Results from BHLUMI and NLLBHA for the symmetric Wide-Wide ES's BARE1 and SICAL2 are shown. Not available x-sections are set to zero. In the table, column BHLUMI(alf2e) represents $\mathcal{O}(\alpha^2)_{exp}$ BHLUMI 4.02.a, col. BHLUMI(alf2) shows $\mathcal{O}(\alpha^2)$ BHLUMI without exponentiation, col. BHLUMI(alf3e) shows missing $\mathcal{O}(\alpha^3)_{LL}$ in BHLUMI 4.02.a as calulated with the new (unpublished) version of LUMLOG, col. NLLBHA(alf2) shows $\mathcal{O}(\alpha^2)$ result from NLLBHA including NLL corrections, col. NLLBHA(alf3) is the previous plus $\mathcal{O}(\alpha^3)_{LL}$ and col. NLLBHA(alf3p) is the previous plus light pair corrections. In the plot, the $\mathcal{O}(\alpha^2)_{exp}$ cross section σ_{REF} from BHLUMI 4.02.a is used as a reference cross section (except for missing $\mathcal{O}(\alpha^3)_{LL}$, for which we show σ/σ_{REF}).

for the SABH process at LEP1 and LEP2.

Let us discuss again the size of the $\mathcal{O}(\alpha^3 L^3)$ and $\mathcal{O}(\alpha^2 L)$ corrections. In the next ta-

| | LEP1 | | LEP2 |
Type of correction/error	Ref. [6]	Present	Present
(a) Missing photonic $\mathcal{O}(\alpha^2 L)$	0.15%	0.10%	0.20%
(a) Missing photonic $\mathcal{O}(\alpha^3 L^3)$	0.008%	0.015%	0.03%
(c) Vacuum polarization	0.05%	0.04%	0.10%
(d) Light pairs	0.04%	0.03%	0.05%
(e) Z-exchange	0.03%	0.015%	0.0%
Total	0.16%	0.11%	0.25%

Table 20: Summary of the total (physical+technical) theoretical uncertainty for a typical calorimetric detector. For LEP1, the above estimate is valid for the angular range within $1° - 3°$, and for LEP2 it covers energies up to 176 GeV, and angular range within $1° - 3°$ and $3° - 6°$ (see the text for further comments).

ble/figure 19, we address this question showing once again some results from Tab. 14/Fig. 16, and adding some new numerical results from the BHLUMI event generator and the semianalytical program NLLBHA for the unrealistic ES BARE1 and the realistic ES SICAL2, symmetric WW variants. First, let us recall that in Tab. 14/Fig. 16 the $\mathcal{O}(\alpha^3 L^3)$ effects were included through exponentiation in all calculations, but in most cases they were incomplete. In the case of BHLUMI, the recent version of LUMLOG[6] is able to answer the question: how big is the missing $\mathcal{O}(\alpha^3 L^3)$ in BHLUMI 4.02a. In table/figure 19 we see (black dots) that it is below 0.01% for both BARE1 and SICAL2 ES's. According to our "scaling rules", we conclude that it is below 0.02% at LEP2. Hence, from the *practical* point of view, $\mathcal{O}(\alpha^3 L^3)$ in BHLUMI 4.02a is complete. In table/figure 19 we also include, for the unrealistic BARE1 ES, numerical results from NLLBHA (stars), which includes complete $\mathcal{O}(\alpha^2 L)$ and $\mathcal{O}(\alpha^3 L^3)_{LL}$ corrections. The difference between BHLUMI (crosses) and NLLBHA (stars) should be, in principle, due to $\mathcal{O}(\alpha^2 L)$ (and technical precision), because $\mathcal{O}(\alpha^3 L^3)$ should cancel completely. As we see, the above difference is within the "one per mil box", but for stronger cuts, $z_{min} = 0.9$, it grows slightly beyond 0.1%. Luckily enough, we may push the above exercise in the interesting direction – we have also in table/figure 19 the results from BHLUMI (circles) and NLLBHA (boxes), in which exponentiation and $\mathcal{O}(\alpha^3 L^3)_{LL}$ was removed completely. As we see, these results agree better, even for strong energy cut ($z_{min} = 0.9$). Actually, this result (difference between boxes and circles) represents an interesting quantity: missing $\mathcal{O}(\alpha^2 L)$ in BHLUMI. The above result suggests that it is rather small, below 0.03%. One has to keep in mind that, if the above is true, then the former difference, with $\mathcal{O}(\alpha^3 L^3)_{LL}$ (crosses and stars), is a puzzle and needs to be examined further. In any case, the fact that all the four above results from BHLUMI and NLLBHA are within the "one per mil box" is interesting, encouraging and reinforcing our final conclusion that photonic corrections are under control within 0.1%. For the present time the above interesting comparison is limited to BARE1 ES. For SICAL2 and BARE1 ES's, we see that the difference between BHLUMI with and without exponentiation is quite sizeable, 0.08%, and from that we conclude that the inclusive Yennie-Frautschi-Suura exponentiation in BH-

---

[6]The new LUMLOG includes final state radiation (in addition to the initial) up to $\mathcal{O}(\alpha^3 L^3)_{LL}$. It was discussed in the Bhabha Working Group and will be included in the next release of BHLUMI.

LUMI is necessary and instrumental for getting good control over the $\mathcal{O}(\alpha^3 L^3)_{LL}$ corrections, even if they are not complete in the matrix element. As a matter of fact, all the other MC codes involved in the present study include exponentiation, and so are on a firm ground from this point of view. In table/figure 19, we show also results from NLLBHA including pair production in addition to the $\mathcal{O}(\alpha^2 L)$ and $\mathcal{O}(\alpha^3 L^3)$ corrections ("plus" marks in the plot). The difference between pluses and stars represents the net effect of the light fermion pair production. For the BARE1 ES, with z_{min} in the experimentally interesting range, it is 0.06% at most. We expect this effect to be about a factor of two smaller for calorimetric ES's.

The total theoretical error for the SABH process at LEP1/LEP2 is summarized in table 20. The errors in the table are understood to be with respect to the cross section calculated for any typical (asymmetric) ES, for the LEP1 experiment in the angular range $1° - 3°$, with respect to the cross section calculated using BHLUMI 4.02a. In the case of LEP2, the estimate extends to the angular range $3° - 6°$, and to the case of the angular range about twice narrower than usual (see the discussion of the numerical results in the previous sections). The entries include combined technical and physical precision. In this table, entry (a) for Missing $\mathcal{O}(\alpha^2 L)$ is based mainly on the agreement between BHLUMI and SABSPV, as seen in tables 14, 16 and 18. It should be stressed that we rely on the agreement between BHLUMI and SABSPV for *all the three types* of ES, Wide-Wide, Wide-Narrow and Narrow Narrow. The agreement between BHLUMI and SABSPV is now better than the one between BHLUMI and OLDBIS+LUMLOG used in the previous best error estimate of Ref. [6]. Noticeably, albeit the agreement between BHLUMI on the one side and BHAGEN95/(OLDBIS + LUMLOG) on the other side is not always below 0.1% for all the ES's considered, it is at least for the experimentally most interesting NW case. This fact is a further reinforcement of the present theoretical error estimate for the SABH process in the NW case, and it is a suggestion for the experimentalists to continue to choose the NW-ES's. The fact that for the unrealistic ES BARE1 the difference between BHLUMI and NLLBHA, see fig. 19, is also within 0.1% confirms this evaluation. Entry (b) is based on table/figure 19. In entry (c), the new improved uncertainty of the vacuum polarization is taken from Tab. 7. We take the biggest of the results from refs. [33, 34]. The light pair production uncertainty, entry (c), is based on new estimates reported during the workshop (see Ref. [7, 8, 12, 15] and Ref. [26, 28]; see also table/figure 19). In tab. 20, we quote for LEP1 the present error due to light fermion pairs contribution to be 0.03%. This is based on all the references quoted above and on the discussion during the WG meetings [29]. The previous estimate in Ref. [6] is therefore confirmed and improved slightly. This is *under the assumption* that the pair effect is corrected for at least in the LL approximation. If the effect is not corrected for[7], then we recommend to use for LEP1 0.04% as an estimate for the missing pair effect (0.06% for LEP2). The material presented at the workshop suggests that the final uncertainty of the light pair contribution will be at the level of 0.015%. In entry (e), the reduced uncertainty of the Z-exchange contribution is based on Ref. [59], work done during this Workshop.

The improvement of the theoretical luminosity error from 0.16% down to 0.11% is basically

---

[7]Production of the light pairs is not included in the standard version of BHLUMI. It is implemented only in the testing unpublished version [29].

due to successful comparisons of the programs BHLUMI and SABSPV for a wide range (WW, NN and NW) of experimentally realistic ES's (SICAL2), and also due to an encouraging (although limited to the unrealistic ES BARE1) comparison of un-exponentiated BHLUMI and NLLBHA in table/figure 19. Furthermore, the agreement of BHLUMI, SABSPV, BHAGEN95 and (OLDBIS+LUMLOG) within that same 0.11% error in the NW-ES recommends safely this choice in the experimentally relevant cases. At last, the analysis described in subsection 2.6 shows that the actual Bhabha selections used by the LEP experiments to measure the accelerator luminosity minimize the sensitivity to $O(\alpha^2)$ radiative corrections, thus putting the above conclusions on an even firmer ground. We would like to stress very strongly that the above new estimate 0.11% of the total luminosity error is based on new results which, although pretty stable numerically, are generally still quite fresh and they are *unpublished*. We expect these new results to be published in journals shortly after the workshop, together with the corresponding computer programs.

The total theoretical error for the SABH process at LEP2 is also summarized in Tab. 20. We assume that the cross section is calculated for any typical (asymmetric) ES for LEP2 experiment, in the typical angular range $1° - 3°$ or $3° - 6°$. The error estimate covers also the "worst case scenario" of the super-narrow angular range (see the example of ES CALO3 in table/figure 17). In entry (a), the estimate of the total photonic uncertainty is based again upon the agreement between BHLUMI and SABSPV on all the variants of ES's considered, and reinforced by the fact that BHAGEN95/OLDBIS+LUMLOG are on the same ground as BHLUMI and SABSPV in the experimentally more interesting NW case (see tables/figures 15 and 17). Note that, sometimes, in the case of other angular range $3° - 6°$ and higher energies, the "scaling laws" from the introduction were used instead of direct calculation to extend the actual numerical results to these situations (see the comments accompanying the relevant tables/plots). We do not see much danger in this because, usually, the large safety margin close to a factor of two was present. Entry (b) is produced out of LEP1 result using the "scaling rule". The vacuum polarization for LEP2 case in the Tab. 20 is taken from Tab. 5 at the $|t| = 36$ GeV^2, corresponding to LEP2 energy and the angle of $\theta_{min} = 60$ mrad.

Type of correction/error	Error estimate
(a) Missing $\mathcal{O}(\alpha^2 L)$, $\mathcal{O}(\alpha^3 L^3)$	< 0.010 %
(b) Technical precision (photonic)	0.040%
(c) Vacuum polarization	0.030%
(d) Light fermion pairs	0.015%
(e) Z-contribution	0.010%
Total	0.053%

Table 21: *Future* projection of the total (physical+technical) theoretical uncertainty for a typical calorimetric detector, within the $1° - 3°$ angular range at LEP1 energies.

Finally, in view of all the work reviewed during the workshop, we are also able to estimate the precision which will be attained in the next step. It is shown schematically in table 21. At the time when Monte Carlo programs will include the matrix element from $\mathcal{O}(\alpha^2 L)$, the

uncertainty due to higher order corrections will be negligible. The dominant contribution will be of *technical* origin and we think that, as we have seen from $\mathcal{O}(\alpha^1)$ comparisons, it can be reduced to 0.04% (provided we can successfully tune two independent Monte Carlo event generators at that precision level, for the same or very similar $\mathcal{O}(\alpha^2)$ matrix elements). The vacuum polarization is now taken according to Ref. [33], and from the discussions during the workshop meetings it was obvious that a further reduction of the uncertainty due to pairs and Z-exchange is also possible. The corresponding work is in progress.

3 Large-angle Bhabha scattering

In the present section the LABH process is considered, both at LEP1 and LEP2. The aim of the study, rather than updating the conclusions of Ref. [1] concerning the theoretical accuracy of the LABH process at LEP1, is twofold: on the one hand, the comparison between the semi-analytical benchmarks and the Monte Carlo codes used by the LEP collaborations; on the other one, the study of the LABH process at LEP2, accompanied by the development of dedicated software.

3.1 Physics

The main physics interest of Bhabha scattering measurements at large angles (say $\theta > 40°$) around the Z resonance is a precise test of the electroweak sector of the Standard Model. In this angular region more than 80 % of the cross section is due to resonant s-channel Z exchange. For $\sqrt{s} = M_Z$ the interference contributions between s-channel Z exchange and the other diagrams either vanish or are completely irrelevant, and the s-channel photon exchange contribution is small ($\simeq 5 \times 10^{-3}$ of the Z exchange cross section). The only other relevant contribution is t-channel photon exchange. For electroweak analyzes, one thus subtracts the t-channel and $s - t$ interference contributions from the large-angle experimental data, typically calculated using the ALIBABA [60] semi-analytical (SA) program. After correcting for the effects of real and virtual photon radiation using the analytical programs MIBA [61,62], TOPAZ0 [63,64] or ZFITTER [65,66], the Z exchange cross section σ_Z^0 may be extracted. For $\sqrt{s} = M_Z, \sigma_Z^0 = \sigma_Z^{peak}$ where:

$$\sigma_Z^{peak} = \frac{12\pi\Gamma_e^2}{M_Z^2\Gamma_Z^2} \tag{2}$$

For the other charged lepton pair decay modes, $\mu^+\mu^-$, $\tau^+\tau^-$, of the Z the quantity Γ_e^2 in Eqn. (2) is replaced by $\Gamma_e\Gamma_\mu$, $\Gamma_e\Gamma_\tau$, respectively, while for hadronic ($q\bar{q}$) decays it is replaced by $\Gamma_e\Gamma_{had}$. Thus the electronic width of the Z, Γ_e, which appears in the cross section for all decay modes of the Z, is measured directly and with improved sensitivity (because in this case $\sigma_Z^{peak} \propto \Gamma_e^2$) only in large-angle Bhabha scattering. It is worth noting, however, that in principle the so called t-channel subtraction is not unavoidable. Actually, the program TOPAZ0 [63,64] could be

used to fit directly the data for large-angle Bhabha scattering without relying upon t-channel subtracted data.

The resulting sensitivity of the backward-forward charge asymmetry in large-angle Bhabha scattering to the important electroweak parameters[8] $\Delta\kappa^{top}$ and $\Delta\kappa^{HIGGS}$

$$\Delta\kappa^{top} = \frac{3\sqrt{2}G_\mu}{16\pi^2}\frac{c_W^2}{s_W^2}m_t^2 \tag{3}$$

$$\Delta\kappa^{HIGGS} = \frac{\sqrt{2}G_\mu M_W^2}{16\pi^2}\left(-\frac{10}{3}\ln\left(\frac{M_H}{M_W}\right)^2 - \frac{5}{6}\right) \tag{4}$$

is similar to that of the other dilepton channels $\mu^+\mu^-$, $\tau^+\tau^-$. The above formulae of course indicate only the leading dependence of the one-loop corrections on the masses of the top-quark and the Higgs boson. Actually, at the nowadays precision level a complete electroweak library is mandatory [1].

At the Z peak the purely QED corrections to the large-angle Bhabha cross section are, for typical experimental cuts [67]: $O(\alpha)$, -30 % ; $O(\alpha^2)$, +4 %. These corrections are much larger than those in small-angle Bhabha scattering when typical 'wide'/'narrow' cuts are used [32]: $O(\alpha)$, +5 % ; $O(\alpha^2)$, -1.4 %. Thus theoretical errors on QED radiatively corrected cross sections are expected to be considerably larger in large-angle than in small-angle Bhabha scattering. This is indeed found to be the case in the comparisons between different codes shown below.

In the energy regime of LEP2, the Z-boson effects on the large-angle Bhabha cross section are much smaller than at LEP1. Actually, before entering the details of the comparisons, it is worth noting that large-angle Bhabha scattering shows very different physical features depending on the energy regime at which it is considered. As can be seen from Fig. 18, around the Z peak the cross section is largely dominated by Z-boson annihilation, whereas, already some GeV off resonance, the cross section is largely dominated by t-channel photon exchange. From this point of view, large-angle Bhabha scattering at LEP2 is much more similar to small-angle Bhabha scattering than to large-angle Bhabha scattering at LEP1. Hence, at LEP2 the large-angle Bhabha cross section cannot be a useful tool for precise tests of the electroweak sector of the Standard Model, but rather for general QED tests.

The state-of-the-art of large-angle Bhabha scattering up to now can be found in Ref. [1]. In that paper an extensive comparison between two semi-analytical codes, namely ALIBABA [60] and TOPAZ0 [63,64], is shown. On the other hand, although extensive in the sense that cross sections and asymmetries are considered, that comparison is in some sense limited: actually it involves only semi-analytical codes, on very simple, academic ES's, only at the Z peak.

In view of the above considerations, the tasks of the present Working Group, as far as large-angle Bhabha scattering is concerned, are the following ones:

- involving in the comparisons also the Monte Carlo (MC) codes today available and used by the LEP collaborations;

---

[8]See [1] for a discussion of pseudo-observables for precision calculations at the Z peak.
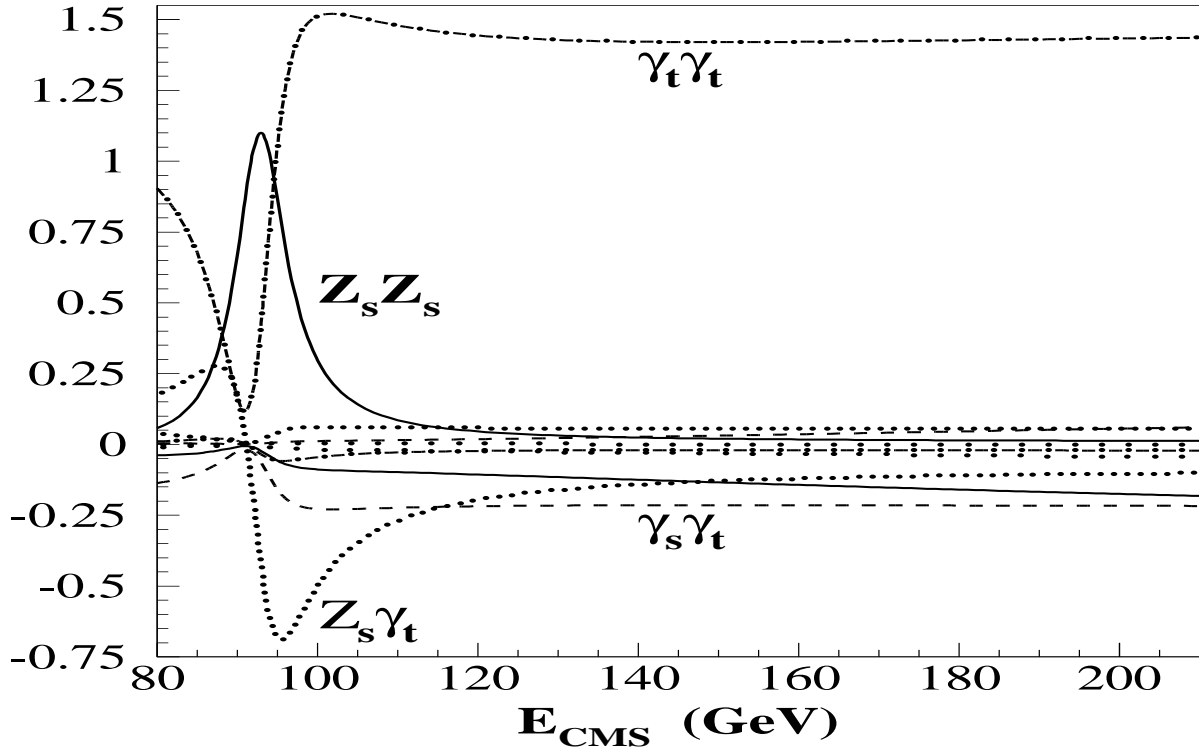
Figure 18: The relative contributions to the integrated cross section at the Born level. The individual contributions are, from top to bottom on the right-hand side of the plot: $\gamma(t)\gamma(t)$, $Z(t)Z(t)$, $\gamma(s)\gamma(s)$, $Z(s)Z(s)$, $Z(s)\gamma(s)$, $Z(s)Z(t)$, $\gamma(s)Z(t)$, $Z(s)\gamma(t)$, $\gamma(t)Z(t)$, and $\gamma(s)\gamma(t)$.

- considering also more realistic, albeit simple, ES's;

- providing results also for the LEP2 energy range, eventually developing dedicated software.

The ES's considered in the present study are the following ones:

- BARE - This ES, for the sake of simplicity, is defined exactly as in [1], namely $40° < \vartheta_- < 140°$, $0° < \vartheta_+ < 180°$, $\vartheta_{acoll}^{max} = 10°, 25°$ and $E_{min} = 1$ GeV for both electron and positron;

- CALO - This ES is defined as above, but with $E_{min} = 20$ GeV for the final fermion energy, which is the electron(positron) energy if there are no photons nearby, whereas it is the electron(positron) plus photon energy if the photon is within a cone of semi-aperture $1°$ from the electron(positron).

For all the cases considered, the input parameters are $M_Z = 91.1887$ GeV, $m_t = 174$ GeV, $m_H = 300$ GeV and $\alpha_s(M_Z) = 0.124$. The predictions by ALIBABA are taken from Ref. [1].

45

Let us now briefly summarize the features of the codes involved in the study. Here only the general features will be highlighted; for more details the reader is referred to the original literature or to the write-ups presented at the end of this section.

ALIBABA [60] – It is a semi-analytical code, implementing exact $O(\alpha)$ QED and weak corrections. The higher-order QED corrections consist of leading log $O(\alpha^2)$ corrections plus soft-photon exponentiation. Moreover, the weak $O(\alpha)$ corrections are folded with the leading log structure functions. The matching between the exact $O(\alpha)$ QED matrix element and the higher order corrections is performed in additive form. The electroweak library is not up to date. Nonetheless, the code has to be considered as a benchmark.

BHAGEN95 [43] – It is a Monte Carlo integrator for both small and large-angle Bhabha scattering. The value for the cross section is obtained from the event generator BHAGEN94, a structure function based program for all orders resummation, including complete photonic $O(\alpha)$ and leading logarithmic $O(\alpha^2 L^2)$ corrections in all channels, and all relevant electroweak corrections according to BHM/WOH basic formulae from Ref. [1]. The approximations, introduced with the collinear kinematics of initial and final radiation and in its angular distribution, are eliminated for the one hard photon emission by substitution with the exact calculation.

BHAGENE3 [67, 68] – It is a Monte Carlo event generator for large-angle Bhabha scattering and muon pair production. The program includes one-loop and the most important two-loop electroweak as well as QED radiative corrections. The $O(\alpha)$ QED correction uses the exact matrix element. Higher order QED corrections are included in an improved soft photon approximation with exponentiation of initial state radiation. Up to three hard final state photons are generated. Events are generated in the full final state phase space including explicit mass effects in the region of collinear mass singularities. The minimum scattering angle for percent level cross section accuracy is $10°$. Extensive use is made in the program of one and two dimensional look-up tables for fast, flexible and efficient Monte Carlo generation. The program was designed for the Z peak region but may also be used at LEP2 energies.

BHWIDE [69] – It is a new Monte Carlo event generator for large-angle Bhabha scattering at LEP1/SLC and LEP2. It includes multiphoton radiation in the framework of $O(\alpha)$ YFS exponentiation. The $O(\alpha)$ virtual (both weak and QED) corrections are in the current version taken from ALIBABA. The program provides the full event in terms of particle flavors and their four-momenta with an arbitrary number of radiative photons. In many aspects it is similar to the program BHLUMI for small-angle Bhabha scattering and can be considered as its extension to large angles. It has been checked that for the pure QED process BHWIDE at $\mathcal{O}(\alpha)$ (no exponentiation) agrees with the MC program OLDBIS within a statistical accuracy of 0.05%.

SABSPV [46] – It is a new Monte Carlo integrator, originally designed for small-angle Bhabha scattering, but adapted to the treatment of large-angle Bhabha scattering at the LEP2 energy range. It is based on a proper matching of the $O(\alpha)$ corrected cross section for t-channel photon exchange and of the leading logarithmic results in the structure function approach. The matching is performed in a factorized form, in order to preserve the classical limit. At present, the effect of up-down interference in the $\gamma(t) - \gamma(t)$ contribution is not taken into

account and all the other contributions are corrected at the leading logarithmic level. Due to the present approximations, the theoretical accuracy of the code is of the order of 1%, as far as large-angle Bhabha scattering at LEP2 is concerned.

TOPAZ0 [63, 64] – It is a semi-analytical code, developed for precision physics at LEP1. It includes the state-of-the-art concerning weak and QCD corrections, according to Ref. [1]. As far as QED corrections are concerned, they are exactly treated at $O(\alpha)$ for s-channel processes (leptonic and hadronic), at the leading logarithmic level for pure t-channel and s-t contributions in the Bhabha scattering case. On top of this, higher order QED corrections are taken into account in the structure functions approach, in a factorized form in order to preserve the classical limit. A particular effort has been performed in order to implement as much analytically as possible the experimental cuts typically applied by the LEP collaborations.

UNIBAB [70] – It is a full Monte Carlo event generator that was originally designed for large-angle Bhabha scattering at LEP1 and SLC energies. The QED corrections are implemented in a fully factorized form by assuming s-channel dominance and using photon shower algorithms for initial- and final-state radiation, and therefore exponentiation of soft photons and resummation of the logarithms from multiple emission of hard collinear photons is automatic. QED initial-final interference corrections are not yet implemented. The electroweak corrections are based on a library also used by ALIBABA, but updated to include the leading m_t^4-dependence and higher order QCD corrections to the Z width.

3.2 On Z peak (LEP1)

The situation of the comparisons for LEP1 is summarized in Figs. 19 (BARE) and 20 (CALO) and corresponding tables. Conventionally, the reference cross section with respect to which the relative deviations are computed is taken from TOPAZ0. It has to be stressed that this choice has no particular meaning at all.

Let us begin with commenting the situation of Fig. 19, i.e. for the BARE ES. As far as the comparison between the two semi-analytical codes, ALIBABA and TOPAZ0, is concerned, the agreement is better than 0.1% at the Z peak (energy points n. 4 and 5, corresponding to the smallest experimental error, which is of the order of 0.3% statistical and 0.3% systematic), and deteriorates on the wings, where, on the other hand, the experimental error is larger (for instance, at peak±2 GeV the experimental error is of the order of 1% statistical and 0.3% systematic). Note that the worst situation is for maximum acollinearity cut of 10°, above the Z peak, where the codes differ from one another of about 1%: this difference is due to higher order QED effects, as pointed out in Ref. [71] (factorized versus additive formulation). As far as the Monte Carlo codes BHAGENE3 and BHWIDE are concerned, their agreement with the semi-analytical codes at peak is within few per mil, whereas off peak BHWIDE is within 1% and BHAGENE3 can deviate up to 2%.

The situation for the more realistic case, the CALO ES (Fig. 20), is generally better from the point of view of the SA/MC comparisons. Note that ALIBABA is no more involved, since

No.	E_{CM}	TOPAZ0	BHWIDE	BHAGENE3	ALIBABA	BHAGEN95
		(a) BARE $acol_{max} = 10^o$				
1.	88.45	$.4579 \pm .0003$	$.4560 \pm .0004$	$.4495 \pm .0016$	$.4575 \pm .0003$	$.4556 \pm .0002$
2.	89.45	$.6452 \pm .0002$	$.6429 \pm .0006$	$.6334 \pm .0023$	$.6440 \pm .0003$	$.6403 \pm .0003$
3.	90.20	$.9115 \pm .0002$	$.9087 \pm .0008$	$.8997 \pm .0033$	$.9090 \pm .0004$	$.9026 \pm .0004$
4.	91.19	$1.1846 \pm .0002$	$1.1797 \pm .0010$	$1.1847 \pm .0033$	$1.1840 \pm .0004$	$1.1715 \pm .0005$
5.	91.30	$1.1639 \pm .0002$	$1.1592 \pm .0009$	$1.1667 \pm .0033$	$1.1636 \pm .0005$	$1.1514 \pm .0005$
6.	91.95	$.8738 \pm .0002$	$.8711 \pm .0007$	$.8856 \pm .0028$	$.8769 \pm .0003$	$.8664 \pm .0003$
7.	93.00	$.4771 \pm .0002$	$.4761 \pm .0005$	$.4808 \pm .0019$	$.4814 \pm .0001$	$.4756 \pm .0002$
8.	93.70	$.3521 \pm .0002$	$.3512 \pm .0004$	$.3521 \pm .0013$	$.3556 \pm .0001$	$.3522 \pm .0001$
		(b) BARE $acol_{max} = 25^0$				
1.	88.45	$.4854 \pm .0003$	$.4808 \pm .0005$	$.4699 \pm .0016$	$.4833 \pm .0003$	$.4833 \pm .0003$
2.	89.45	$.6746 \pm .0003$	$.6699 \pm .0006$	$.6593 \pm .0023$	$.6727 \pm .0003$	$.6727 \pm .0003$
3.	90.20	$.9438 \pm .0003$	$.9387 \pm .0008$	$.9279 \pm .0033$	$.9425 \pm .0003$	$.9425 \pm .0003$
4.	91.19	$1.2198 \pm .0003$	$1.2130 \pm .0010$	$1.2169 \pm .0034$	$1.2187 \pm .0004$	$1.2187 \pm .0004$
5.	91.30	$1.1989 \pm .0003$	$1.1924 \pm .0010$	$1.1995 \pm .0034$	$1.1982 \pm .0004$	$1.1982 \pm .0004$
6.	91.95	$.9054 \pm .0002$	$.9011 \pm .0007$	$.9124 \pm .0026$	$.9089 \pm .0003$	$.9089 \pm .0003$
7.	93.00	$.5040 \pm .0002$	$.5013 \pm .0005$	$.4996 \pm .0019$	$.5054 \pm .0002$	$.5054 \pm .0002$
8.	93.70	$.3777 \pm .0002$	$.3749 \pm .0004$	$.3689 \pm .0013$	$.3782 \pm .0001$	$.3782 \pm .0001$
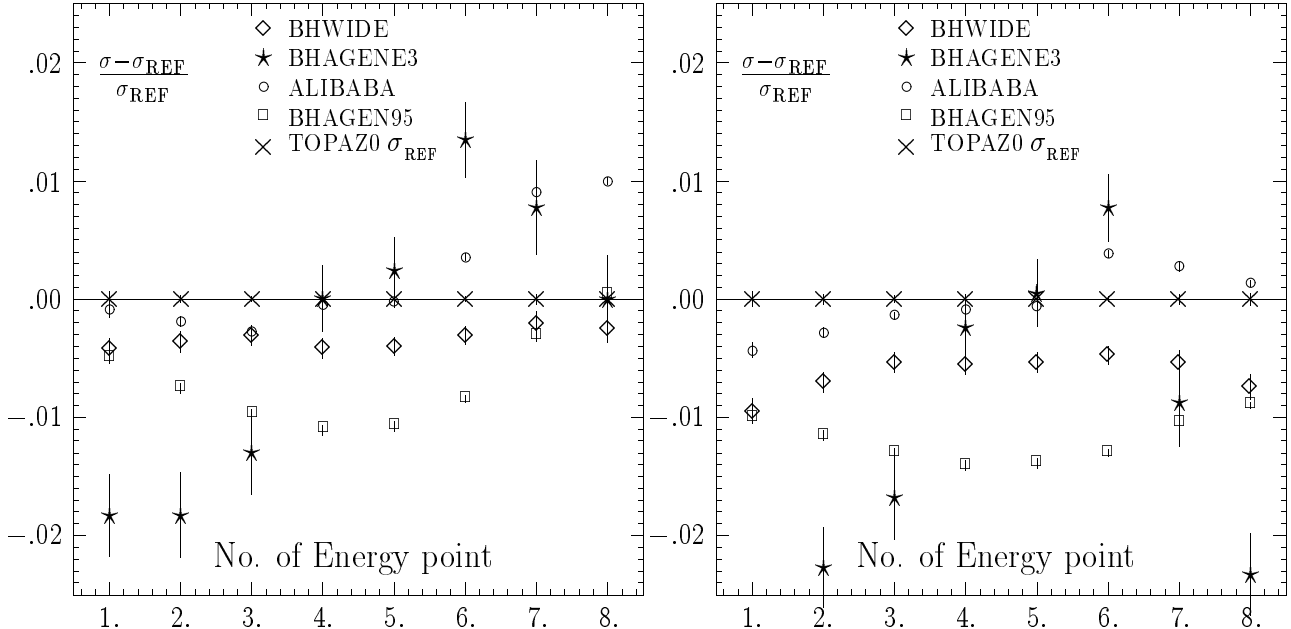
Figure 19: Monte Carlo results for the BARE ES, for two values (10° and 25°) of acollinearity cut. Center of mass energies (in GeV) close to Z peak. In the plots, the cross section σ_{REF} from TOPAZ0 is used as a reference cross section. Cross sections in nb.

it cannot manage calorimetric measurements, whereas UNIBAB appears (it is slow for very small minimum fermion energy and therefore it did not contribute to the BARE case). On peak, the agreement between the codes is at the few per mil level; off peak BHWIDE is within

48

No.	E_{CM}	TOPAZ0	BHWIDE	BHAGENE3	UNIBAB	BHAGEN95
			(a) CALO $acol_{max} = 10^o$			
1.	88.45	$.4533 \pm .0004$	$.4523 \pm .0004$	$.4467 \pm .0008$	$.4490 \pm .0010$	$.4501 \pm .0002$
2.	89.45	$.6387 \pm .0004$	$.6377 \pm .0006$	$.6302 \pm .0011$	$.6358 \pm .0012$	$.6326 \pm .0003$
3.	90.20	$.9023 \pm .0003$	$.9016 \pm .0008$	$.8920 \pm .0015$	$.9021 \pm .0014$	$.8918 \pm .0004$
4.	91.19	$1.1725 \pm .0001$	$1.1707 \pm .0010$	$1.1767 \pm .0021$	$1.1772 \pm .0016$	$1.1582 \pm .0005$
5.	91.30	$1.1520 \pm .0001$	$1.1505 \pm .0009$	$1.1571 \pm .0020$	$1.1559 \pm .0016$	$1.1385 \pm .0005$
6.	91.95	$.8649 \pm .0001$	$.8646 \pm .0007$	$.8795 \pm .0015$	$.8689 \pm .0012$	$.8579 \pm .0003$
7.	93.00	$.4723 \pm .0001$	$.4725 \pm .0005$	$.4796 \pm .0008$	$.4733 \pm .0008$	$.4719 \pm .0002$
8.	93.70	$.3486 \pm .0001$	$.3486 \pm .0004$	$.3507 \pm .0006$	$.3486 \pm .0007$	$.3498 \pm .0001$
			(b) CALO $acol_{max} = 25^o$			
1.	88.45	$.4769 \pm .0004$	$.4742 \pm .0004$	$.4696 \pm .0008$	$.4733 \pm .0010$	$.4717 \pm .0002$
2.	89.45	$.6638 \pm .0003$	$.6615 \pm .0006$	$.6556 \pm .0011$	$.6619 \pm .0012$	$.6554 \pm .0003$
3.	90.20	$.9297 \pm .0003$	$.9278 \pm .0008$	$.9207 \pm .0012$	$.9302 \pm .0014$	$.9164 \pm .0004$
4.	91.19	$1.2025 \pm .0003$	$1.1994 \pm .0010$	$1.2074 \pm .0021$	$1.2073 \pm .0016$	$1.1845 \pm .0005$
5.	91.30	$1.1819 \pm .0003$	$1.1790 \pm .0010$	$1.1879 \pm .0021$	$1.1860 \pm .0016$	$1.1647 \pm .0005$
6.	91.95	$.8924 \pm .0003$	$.8909 \pm .0007$	$.9058 \pm .0016$	$.8965 \pm .0012$	$.8817 \pm .0003$
7.	93.00	$.4964 \pm .0003$	$.4954 \pm .0005$	$.5004 \pm .0009$	$.4976 \pm .0008$	$.4929 \pm .0002$
8.	93.70	$.3717 \pm .0003$	$.3704 \pm .0004$	$.3690 \pm .0006$	$.3720 \pm .0007$	$.3701 \pm .0001$
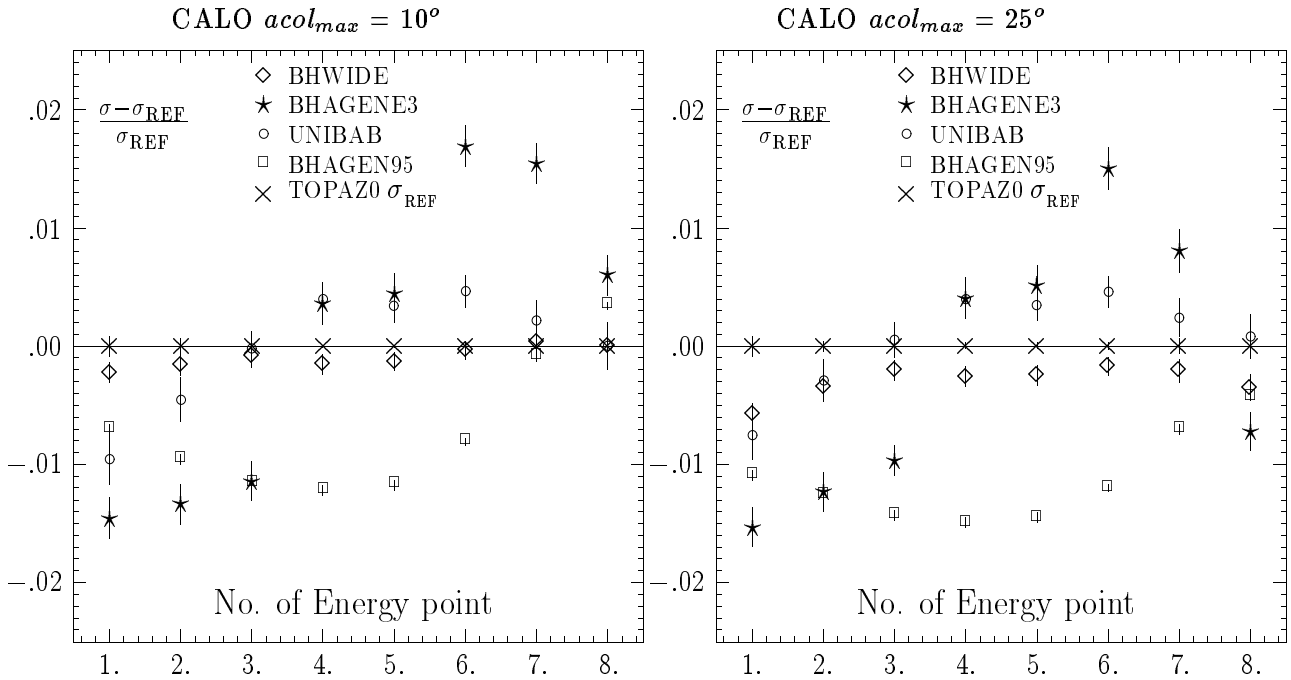
Figure 20: Monte Carlo results for the CALO ES, for two values (10° and 25°) of acollinearity cut. Center of mass energies (in GeV) close to Z peak. In the plots, the cross section σ_{REF} from TOPAZ0 is used as a reference cross section. Cross sections in nb.

0.5% from TOPAZ0, whereas UNIBAB deviates up to 1% below peak, and BHAGENE3 can differ from TOPAZ0 by about 2%.

BHAGEN95 is within 1.5% everywhere for both the BARE and CALO ES's around the Z peak. The agreement is better few GeV above and below the Z resonance. However the implementation of the complete weak and QCD library is very recent and still under tests.

3.3   Far off Z peak (LEP2)

No.	BHWIDE	TOPAZ0	BHAGENE3	UNIBAB	SABSPV	BHAGEN95
	(a) CALO $acol_{max} = 10^o$					
1.	$35.257 \pm .040$	$35.455 \pm .024$	$34.690 \pm .210$	$34.498 \pm .157$	$35.740 \pm .080$	$35.847 \pm .022$
2.	$29.899 \pm .034$	$30.024 \pm .020$	$28.780 \pm .170$	$29.189 \pm .134$	$30.270 \pm .070$	$30.352 \pm .017$
3.	$25.593 \pm .029$	$25.738 \pm .015$	$24.690 \pm .150$	$24.976 \pm .115$	$25.960 \pm .060$	$26.007 \pm .014$
	(b) CALO $acol_{max} = 25^o$					
1.	$39.741 \pm .049$	$40.487 \pm .025$	$39.170 \pm .280$	$39.521 \pm .158$	$40.240 \pm .100$	$40.505 \pm .026$
2.	$33.698 \pm .042$	$34.336 \pm .017$	$32.400 \pm .190$	$33.512 \pm .135$	$34.100 \pm .080$	$34.331 \pm .020$
3.	$28.929 \pm .036$	$29.460 \pm .013$	$27.840 \pm .160$	$28.710 \pm .116$	$29.280 \pm .070$	$29.437 \pm .015$
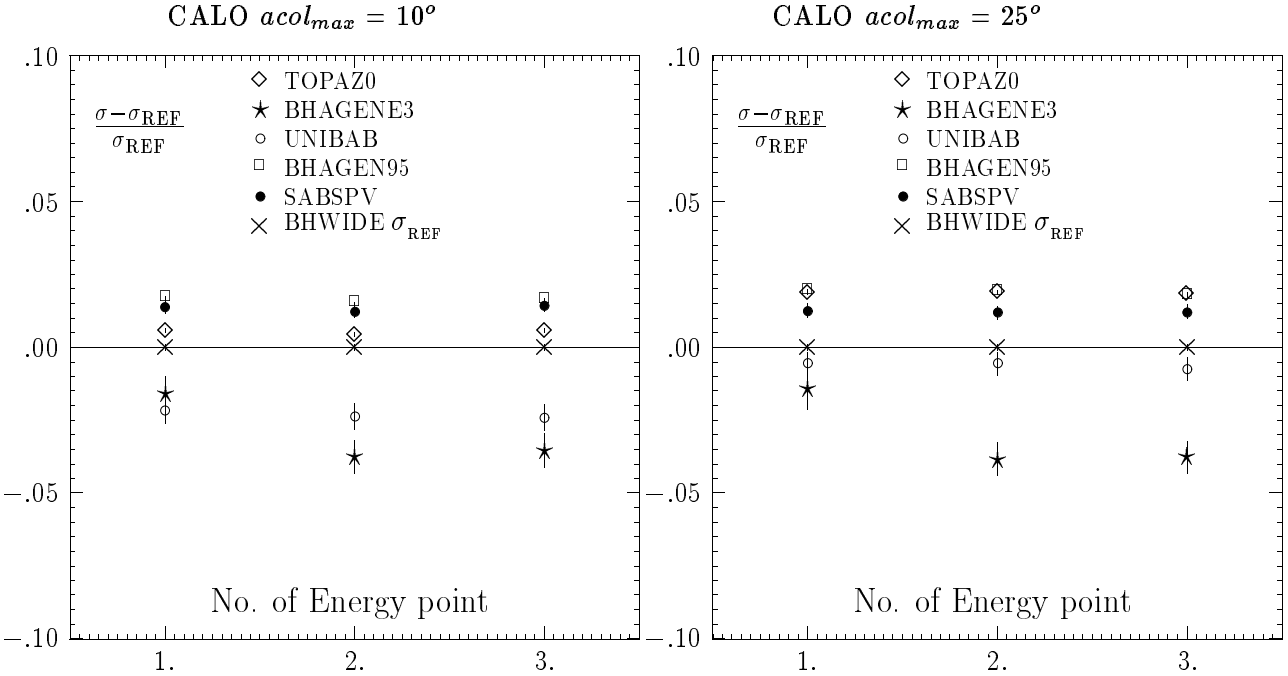
Figure 21: Monte Carlo results for the CALO ES, for two values (10° and 25°) of acollinearity cut. Center of mass energies close to W-pair production threshold (E_{CM}: 1. 175 GeV, 2. 190 GeV, 3. 205 GeV). In the plots, the cross section σ_{REF} from BHWIDE is used as a reference cross section. Cross sections in pb.

The situation of the comparisons for LEP2 is shown in Fig. 21 (CALO) and corresponding table. Conventionally, the reference cross section with respect to which the relative deviations are computed is taken from BHWIDE. It has to be stressed again that this choice has no particular meaning at all. Note that TOPAZ0 has been developed in the Z-dominance approximation, and

UNIBAB does not include initial-final interference effects, so that their results are at the leading logarithmic level in the LEP2 energy range. A new entry appears, namely SABSPV, which has been conceived for small-angle Bhabha scattering, and further improved for large-angle Bhabha at LEP2.

BHAGEN95, BHWIDE and SABSPV stay within 2% from one another. More precisely, SABSPV is steadily around 1.5% above BHWIDE and 0.5% below BHAGEN95. BHAGENE3, for both the acollinearity cuts considered, can deviate from the reference cross section up to 5%.

TOPAZ0 and UNIBAB show deviations from the reference cross section (up to 2% above and 3% below, respectively) which depend on the acollinearity cut, and can be presumably traced back to the approximations intrinsic in these Z-peak designed codes. Anyway, the deviations of the two codes from the reference cross section are consistent with what can be expected from leading logarithmic results.

4   Short-write-up's of the programs

The aim of the following short-write-up's is to provide quick reference for the reader on basic properties of all event generators used in the numerical comparisons throughout this article. The intention was that details are given only on new and/or unpublished features of the programs (including bugs) while other features are described in general terms with help of references to published works.

4.1   BHAGEN95

AUTHORS:

M. Caffo   INFN and Dipartimento di Fisica dell'Università, Bologna, Italy
            `caffo@bo.infn.it`
H. Czyż   University of Silesia, Katowice, Poland, INFN, Università, Bologna, Italy
            `czyz@bo.infn.it`
E. Remiddi   INFN and Dipartimento di Fisica dell'Università, Bologna, Italy
            `remiddi@bo.infn.it`

GENERAL DESCRIPTION:
BHAGEN95 is a collection of three programs to calculate the cross-section for Bhabha scattering for small and large scattering angles at LEP1 and LEP2 energies. In its present form the integrated cross-section σ for a given selection of cuts is calculated as

$$\sigma = \sigma(\text{BHAGEN94}) - \sigma^H(\text{BH94-FO}) + \sigma^H(\text{BHAGEN-1PH}) . \tag{5}$$

$\sigma(\text{BHAGEN94})$ is the integrated cross-section obtained with the Monte Carlo event generator

51

BHAGEN94 [2, 72–76], a structure function based program for all orders resummation, including complete photonic $\mathcal{O}(\alpha)$ and leading logarithmic $\mathcal{O}(\alpha^2 L^2)$ corrections in all channels, and all relevant electroweak corrections according to BHM/WOH basic formulae from [1]. Approximations are introduced with the collinear kinematics of initial and final radiation and in its angular distribution.

σ^H(BH94-FO) is the integrated cross-section of $\mathcal{O}(\alpha)$ for one hard photon emission obtained with the Monte Carlo event generator BH94-FO [76], the $\mathcal{O}(\alpha)$ expansion of BHAGEN94.

σ^H(BHAGEN-1PH) is the integrated cross-section obtained with the one hard photon complete matrix element and exact kinematics, implemented in the Monte Carlo event generator BHAGEN-1PH [77].

The subtraction of σ^H(BH94-FO) and its substitution with σ^H(BHAGEN-1PH) is to eliminate the error in the contribution coming from the one hard photon emission.

FEATURES OF THE PROGRAM:
The three programs provide cross-sections, which are summed as in Eq. (5) or used to obtain other quantities, such as forward-backward asymmetry. Due to the mentioned substitution procedure, the event generator feature of the constituent programs can not be profited and the use is simply that of a Monte Carlo integrator.
At small-angle we estimate the accuracy in the cross-section evaluation, which comes from the uncontrolled higher orders terms $\mathcal{O}(\alpha^2 L)$ and $\mathcal{O}(\alpha^3 L^3)$ and from the incertitude in $\mathcal{O}(\alpha^2 L^2)$ $s - t$ interference to amount comprehensively to a 0.1%. The error due to approximate two hard photon contribution (strongly dependent on the imposed cuts) is estimated on the basis of the correction required for the one hard photon contribution times $\beta(s) = 0.1$, to account for the increase in perturbative order. All included we estimate at small-angle an accuracy of the order of 0.15% for loose cuts ($z_{min} = 0.3$) and of 0.45% for sharp cuts ($z_{min} = 0.9$) for both LEP1 and LEP2 energies.
At large-angle we estimate the $\mathcal{O}(\alpha^2 L^2)$ $s - t$ interference accuracy up to 1% (depending on cuts) at LEP1 energy, but much smaller at LEP2. The error coming from the approximate treatment of two hard photon emission is estimated as above and is smaller for more stringent acollinearity cut. All included we estimate an accuracy of the order of 1% for both LEP1 and LEP2 energies.

HOW DOES THE CODE WORK:
The three programs run separately. They provide initialization and fiducial volume definition according to input parameters, then starts the generation of events according to some variables which smooth the cross-section behavior. Rejection is performed through the routine TRIGGER, where the special cuts can be implemented. The programs stop when the requested number of accepted events is reached or alternatively when the requested accuracy is obtained.

INPUT CARD:
The following data have to be provided in input: mass of the Z^0, mass of the top quark, mass of the Higgs, value of $\alpha_S(M_Z^2)$, value of Γ_Z, the beam energy E_{beam}, the minimum energy for leptons E_{min} (larger than 1 GeV), minimum and maximum angle for the scattered electron

(positron) with the initial electron (positron) direction, maximum acollinearity allowed between final electron and positron, number of accepted events to be produced, numbers to initialize the random number generator. One may also switch on or off: pairs production, the channels to be considered and the recording of the events. For $\mathcal{O}(\alpha)$ programs one has also to specify the minimum and maximum energy allowed for the photon. For the input of BHAGEN-1PH one has to give also the maximum acoplanarity, and minimum angles of the emitted photon with initial and final fermion directions, if one wants to exclude the contributions with the collinear photons.

DESCRIPTION OF THE OUTPUT:
Each program return the input parameters and the values of the cross-section obtained with weighted and unweighted events, with the relative statistical variance (one standard deviation). Of course due to the efficiency the weighted cross-section is usually much more precise than the unweighted one. The total integrated cross-section is then calculated according to Eq. (5).

AVAILABILITY:
On request to the authors and to be posted on WWW at http://www.bo.infn.it/

4.2   BHAGENE3

AUTHORS:

J. Field	Département de Physique Nucl. et Corpusculaire Univ. de Genève
	jfield@cernvm.cern.ch
T. Riemann	DESY, Platanenallee 6, D–15738 Zeuthen
	riemann@ifh.de

GENERAL DESCRIPTION:
BHAGENE3 is a Monte Carlo event generator for muon pairs (at all angles) or for Bhabha scattering in the large angle region ($\theta > 10°$). The program, which is intended for use at, or above, the Z peak region contains all tree level diagrams with complete one loop and the leading two loop virtual corrections [78–81] The running α is included with the correct scale in all amplitudes. The O(α) QED correction uses the exact $ll\gamma$ matrix elements [82,83]. Higher order QED corrections are included in an improved soft photon approximation with exponentiation of initial state radiation. Events with up to three hard photons are generated in the full kinematically allowed phase space including explicit mass effects for near collinear photon radiation. If n_γ^I, n_γ^F are the respective numbers of initial and final state photons, the different final state topologies generated are: $n_\gamma^I/n_\gamma^F = 0/0$, 1/0, 0/1, 2/0, 1/1, 0/2, 0/3 . Initial/Final state interference effects are taken into account only to O(α). The photon energies are described by scaled variables: $y_i = 2E_\gamma^i/\sqrt{s} < 1$. For $y_i < y_0$ (typically $y_0 = 0.005$) a Born topology (0/0) event is generated. The corresponding cross section contains all virtual (V) corrections and is integrated over the phase space of all soft (S) photons with $y_i < y_0$. Exponentiation of initial state radiation is implemented by modifying the O(α) partial cross sections and interference terms in such a way that the derivative of the VS cross-section with respect to y is recovered in

53

the $y \to 0$ limit. For example in the s-channel photon exchange contribution with initial state radiation:

$$\frac{d\sigma(\gamma_s \gamma_s)_{init}}{d\Omega_l dy} = \frac{\alpha^3}{2\pi s} \frac{1}{y} \left[(\frac{s'}{s}) \ln \frac{s}{m_e^2} - 1 \right] \left[\frac{u^2 + t^2 + u'^2 + t'^2}{s'^2} \right] \tag{6}$$

exponentiation is carried out by the replacement $u^2 + t^2 + u'^2 + t'^2 \longrightarrow f(u^2 + t^2) + u'^2 + t'^2$ where $f = 2\, C_V^i\, y^{\beta_e} - 1$. Events with hard photons are generated according to distributions where the soft photon eikonal factors are corrected by the Gribov-Lipatov [84] kernels. The relative probabilities of different topologies of final state photons are chosen according to the Poisson distribution: $P(n|\bar{N})$ where $n = n_\gamma - 1$ and

$$\bar{N}^I = \beta_e \ln(1/y_0), \quad \bar{N}^F = \beta_f \ln(1/y_0) \tag{7}$$

A short description of program together with comparisons with other muon pair and wide angle Bhabha codes has been published [67]. A long write-up is also available [68].

OIMZ	Z mass (GeV)
OIMT	Top quark mass (GeV)
OIMH	Higgs boson mass (GeV)
OMAS	$\alpha_s(M_Z)$
IOCH	$= 0(\mu^+\mu^-), = 1(e^+e^-)$
IOEXP	$= 1$ exponentiated , $= 0$ $O(\alpha)$
OW	collision energy (GeV)
OCTC1	lower $\cos\theta_{l+}$ in the ODLR frame
OCTC2	lower $\cos\theta_{l-}$ in the ODLR frame
IOXI	initial random number

Table 22: Variables of the labelled common ICOM. OCTC1,OCTC2 are used in setting up the LUT of the lepton scattering angles. To allow for the effects of the Lorentz boost the angular range should be chosen somewhat wider than that defined by the cuts in the LAB system.

FEATURES OF THE PROGRAM:
The execution of the program has three distinct phases: initialisation, generation and termination. In the initialisation phase all relevant electroweak quantities are calculated from the input parameters M_Z, M_t M_H and α_s. Also a number of look up tables for quantities such as the lepton scattering angle and photon energies are created for use in the subsequent generation phase. This process is relatively time consuming, so the user should not be surprised if there is some delay between the execution of the program and the start of event generation. In the generation phase events with unit weight are generated by the weight throwing technique. The corresponding 4-vectors are stored in common C4VEC. The user may apply arbitary cuts and produce weighted histograms in subroutine FUSER. Histograms of unit weight events may be produced in subroutine FHIST. In the final, termination, phase the input parameters are printed out together with the exact cross section σ^{CUT} and its error, together with all histograms and plots.

HOW TO USE THE PROGRAM:
The program has a very short main program containing definitions of the most important

NPAR(1)	$\underline{1}$, 0 weak loop corrections ON, OFF
NPAR(2)	2,$\underline{3}$ parameterisations of had. vac. pol.
NPAR(3)	$\underline{0}$,1,2 two-loop $\alpha\alpha_s m_t^2$ correction
NPAR(4)	$\underline{1}$,0 weak box diagrams ON, OFF
NPAR(6)	$\underline{1}$, 0 two-loop terms $\propto m_t^4$ ON,OFF
XPAR(1)	initial lepton charge (-1.D0)
XPAR(2)	final lepton charge (-1.D0)
XPAR(3)	final lepton colour (1.D0)
XPAR(4)	final lepton mass (GeV)
XPAR(9)	QCD correction to Γ_q^Z (non-b quarks)
XPAR(10)	QCD correction to Γ_b^Z
YMA	maximum value of $\sum E_\gamma / E_{beam}$ (0.99D0)
YMI	minimum value of E_γ / E_{beam} (0.005D0)
WTMAX	maximum value of the event weight (2.0D)

Table 23: Control parameters defined in SUBROUTINE BHAGENE3. Default values are underlined or given in parentheses.

input parameters, which are stored in the labelled common block ICOM. These variables are described in Table 22 The execution of the program has three distinct phases: (i) Initialisation, (ii) Generation of a single unit weight event, (iii) Termination. Each of these phases is entered via a call to subroutine BHAGENE3 in the main program:

CALL BHAGENE3(MODE,CTP1,CTP2,CTM1,CTM2,CTAC,EP0,EM0)

MODE is set to $-1, 0, 1$ for the initialisation, generation and termination phases respectively. The other parameters of BHAGENE3 define the kinematical cuts to be applied to the generated events:

$$\text{CTP1} = \text{minimum value of } \cos\theta_{l+}$$
$$\text{CTP2} = \text{maximum value of } \cos\theta_{l+}$$
$$\text{CTM1} = \text{minimum value of } \cos\theta_{l-}$$
$$\text{CTM2} = \text{maximum value of } \cos\theta_{l-}$$
$$\text{CTAC} = \text{maximum value of } \cos\phi_{col}$$
$$\text{EP0} = \text{minimum energy of } l^+ \ (GeV)$$
$$\text{EM0} = \text{minimum energy of } l^- \ (GeV)$$

All these cuts are applied in the laboratory (incoming e^+, e^- centre of mass) system. The angle ϕ_{col} is the collinearity angle between the l^+ and the l^- (CATC = -1 for a back-to-back configuration). In the calls of BHAGENE3 with MODE = 0,1 only this parameter need be specified. Other initialisation parameters of interest to users are defined in BHAGENE3 itself. A list of the most important of these can be found in Table 23.

AVAILABILITY:
From Compure Physics Communications Program Library, see http://www.cs.qub.ac.uk/cpc for more details.

4.3 BHLUMI

AUTHORS:

S. Jadach	Institute of Nuclear Physics, Kraków, ul. Kawiory 26a
	`jadach@cernvm.cern.ch`
E. Richter-Wąs	Institute of Computer Science, Jagellonian University, Kraków
	`erichter@cernvm.cern.ch`
B.F.L. Ward	Department of Physics and Astron., University of Tennessee and SLAC
	`bflw@slac.stanford.edu`
Z. Wąs	CERN and Institute of Nuclear Physics, Kraków, ul. Kawiory 26a
	`wasm@cernvm.cern.ch`

GENERAL DESCRIPTION:

The program is a multiphoton Monte Carlo event generator for low angle Bhabha providing four-momenta of outgoing electron, positron and photons. The first $\mathcal{O}(\alpha^1)_{YFS}$ version was described in ref. [85]. The actual version 4.02.a includes several types of the matrix elements. The most important $\mathcal{O}(\alpha^2)_{YFS}^{prag}$ matrix elements (M.E.) is based on the Yennie-Frautschi-Suura (YFS) exponentiation. This M.E. includes exactly the photonic first order and second order leading-log corrections. In the $\mathcal{O}(\alpha^2)_{YFS}^{prag}$ M.E. the other higher order and subleading contributions are included in the approximate form. The detailed description exists for the version 2.02 in ref. [30]. For the differences between the versions 2.02 and 4.02 the user has to consult ref. [6], the README file in the distribution directory and comments in the main program of the demonstration deck [44]. The only difference between versions 4.02 and 4.02a is correction to an important bug 95a. In order to correct it one has to replace $v_{[1,0]}^{(2)}$ in eq. (3) in Ref. [6] with

$$v_{[1,0]}^{(2)} = (\gamma_p + \gamma_q)\ln\Delta + \frac{3}{2}\gamma - \frac{\alpha}{\pi} - \frac{3}{4}\gamma\ln(1-\tilde{\beta}_1) - \frac{1}{4}\gamma\ln(1-\tilde{\alpha}_1). \tag{8}$$

We also provide patch to correct this in the sorce code of the versions 4.02, see AVAILABILITY below. This correction can affect the result of the program typicaly 0.05%, up to 0.08% for some event selections.

FEATURES OF THE PROGRAM:

BHLUMI consists in fact of the three separate event generators: BHLUM4, OLDBIS and LUMLOG, where OLDBIS is an improved version of the OLDBAB written by Berends and Kleiss at PETRA times, and LUMLOG is an event generator with the inclusive many photons emission strictly collinear to momenta of incomming/outcogoing fermions. M.E. of OLDBIS is limited to $\mathcal{O}(\alpha^1)$ and M.E. of LUMLOG includes exponentiated and non-exponentiated electron structure functions up to $\mathcal{O}(\alpha^3)_{LL}$. BHLUM4 includes four types of the exponentited M.E.: $\mathcal{O}(\alpha^2)_{A,B}^{YFS}$, $\mathcal{O}(\alpha^1)_{A,B}^{YFS}$ and four types of the non-exponentited M.E.: $\mathcal{O}(\alpha^2)_{A,B}$, $\mathcal{O}(\alpha^1)_{A,B}$ where the cases A and B correspond to two kinds of ansatz employed for modeling the $\mathcal{O}(\alpha^2 L)$, second order NNL, contribution. The BHLUM4 program includes vacuum polarization, s-chanel γ and Z exchange contributions, see ref. [59] in the approximation suitable for the low angle (below 0.1rad.) scattering. The BHLUM4 does no include so called up-down interferences. However, OLDBIS does include them so it can be used to check how small they are.

56

HOW DOES THE CODE WORK:

The program ia a full scale Monte Carlo event generator. A single `CALL BHLUMI` produces one event, i.e. the list of the final state four-momenta of electron, positron and photons encoded in the common block. Depending on switch in the input parameters the program provides event with the variable weight WTMOD or with constant weight WTMOD=1. In the constant weight mode the calculation is done for M.E. of the $\mathcal{O}(\alpha^2)_{\mathrm{B}}^{YFS}$ type. In the variable weight mode WTMOD corresponds to the above M.E. but the user has also acces to all six types of the M.E. listed above (and even more) and may perform in a single run calculation for various types of the M.E. The choice of one of three sub-generators BHLUM4, OLDBIS or LUMLOG is decided through one of the input parameters. Program requires initialization before producing first MC event. There are many input parameters. The most important ones define the minimum and maximum angle (t chanel transfer). For weighted events it is possible to cover the angular range down to zero angle but the program is realy designed for "double tag" acceptance. It is possible to stop and restart the program from the next event in the series. The distribution directory incudes example demonstrating how to do it.

DESCRIPTION OF THE OUTPUT:

Program prints certain control output. The basic output of the program is the series of the Monte Carlo events and the user decides by himself which events are accepted or rejected according to his favourite selection criteria. The total cross section in nanobarns can be calculated for arbitrary cuts in a standard way

$$\sigma = \sigma_0 \frac{1}{N} \sum_{Accepted\ Events} W_I \tag{9}$$

where the sum of the weights (variable or constant) is over all accepted events, N is total number of generated events and σ_0 is a reference (normalization) cross section in nanobarns provided by the program at the end of the MC generation. In the analogous standard way one may obtain any arbitrary distribution properly normalized.

AVAILABILITY:

The program is posted on WWW at $\mathtt{http://hpjmiady.ifj.edu.pl}$ in the form of ".tar.gz" file together with all relevant papers and documentation in postscript. The version 4.02.a which was used to produce all numerical results in this workshop consists of the version 4.02 described in ref. [6] and of the error patch posted in the same location $\mathtt{http://hpjmiady.ifj.edu.pl}$. After workshop the equivalent version 4.03 will be released. The new version of BHLUMI will also contain new version of LUMLOG with the final state bremsstrahlung which was used in in the table/figure 19 and improved version of the BHLUMI matrix element without exponentiation which was used in this table/figure.

4.4 BHWIDE

AUTHORS:

S. Jadach   Institute of Nuclear Physics, Kraków, ul. Kawiory 26a
                  `jadach@cernvm.cern.ch`
W. Płaczek   Dept. of Physics and Astron., Univ. of Tennessee
                  `placzek@hephp02.phys.utk.edu`
B.F.L. Ward   Dept. of Physics and Astron., Univ. of Tennessee and SLAC
                  `bflw@slac.stanford.edu`

GENERAL DESCRIPTION:
The program evaluates the large (wide) angle Bhabha cross section at LEP1/SLC and LEP2 energies. The theoretical formulation is based on $\mathcal{O}(\alpha)$ YFS exponentiation, with $\mathcal{O}(\alpha)$ virtual (both weak and QED) corrections taken from ref. [60, 86] as formulated in the program ALIBABA. The YFS exponentiation is realized via Monte Carlo methods based on BHLUMI-type Monte Carlo algorithm, which is explained in refs. [30,85]. Thus, we achieved an event-by-event realization of our calculation in which arbitrary detector cuts are possible and in which infrared singularities are canceled to all orders in α. A detailed description of our work can be found in ref. [69].

FEATURES OF THE PROGRAM:
The code is a full-fledged Monte Carlo event generator, so that the final particle four-momenta for the entire $e^+e^- + n\gamma$ final state are available for each event, which may be generated as a weighted or unweighted event, as the user finds more or less convenient accordingly. Thus, it is trivial to impose arbitrary detector cuts on the events. If the user wishes, he/she may also use the original BABAMC [82,83] type of pure weak corrections (there is a simple switch which accomplishes this). The expected accuracy of the program, when all tests are finished, is anticipated at $\sim 0.2\%$ in the Z-region and $\sim 0.1\%$ in the LEP2 regime.

HOW DOES THE CODE WORK:
The code works entirely analogous to the MC event generator BHLUMI 2.01 described in ref. [30]. A crude distribution consisting of the primitive Born level distribution and the most dominant part of the YFS form factors, which can be integrated analytically, is used to generate a background population of events. The weight for these events is then computed by the standard rejection techniques involving the ratio of the complete distribution and the crude distribution. As the user wishes, these weights may either be used directly with the events, which have the four-momenta of all final state particles available, or they may be accepted/rejected against a constant maximal weight WTMAX to produce unweighted events via again standard MC methods. Standard final statistics of the run are provided, such as statistical error analysis, total cross section, etc.

DESCRIPTION OF THE OUTPUT:
Program prints certain control output. The basic output of the program is the series of the Monte Carlo events. The total cross section in nanobarns can be calculated for arbitrary cuts

in the same standard way as for BHLUMI, i.e. user may imposed arbitrary experimental cuts by rejection.

AVAILABILITY:
The program can be obtained via e-mail from the authors. It will be posted soon on WWW at `http://enigma.phys.utk.edu` as well as on anonymous ftp at `enigma.phys.utk.edu` in the form of ".tar.gz" file together with all relevant papers and documentation in postscript. It will also be available via anonymous ftp at `enigma.phys.utk.edu` in the directory `/pub/BHWIDE`.

4.5 NLLBHA

AUTHORS:

A.B. Arbuzov	Joint Institute for Nuclear Research, Dubna, 141980, Russia
	arbuzov@thsun1.jinr.dubna.su
E.A. Kuraev	Joint Institute for Nuclear Research, Dubna, 141980, Russia
	kuraev@theor.jinrc.dubna.su
L. Trentadue	CERN TH Division, Universitá di Parma, INFN Sezione di Milano
	trenta@vxcern.cern.ch

GENERAL DESCRIPTION:
`NLLBHA` is a semi–analytical program for calculations of radiative QED and electroweak corrections to the small–angle Bhabha scattering at high energies. It takes into account complete (relevant at small angles) first order QED and electroweak corrections, the leading and next–to–leading QED corrections to $\mathcal{O}(\alpha^2)$ and the leading logarithmic contributions to $\mathcal{O}(\alpha^3)$. The corrections due to photon emission as well as the ones due to pair production are included. The theoretical uncertainty of the calculations is less then 0.1%.

FEATURES OF THE PROGRAM:
`NLLBHA` integrates numerically analytical formulae [2,8,23]. For the Born cross–section an expansion for small scattering angles is used. The contributions due to real particle emission are integrated over symmetrical detector apertures. For the case of asymmetrical detectors (narrow–wide case) leading logarithmic contributions are calculated (next–to–leading are estimated to be equal or less the ones in the narrow–narrow case). Cuts on the final particles energies are possible. Calorimetric set–up as well as other special experimental conditions are not implemented.

HOW DOES THE CODE WORK:
The code consists of the main part and of a series of subroutines which calculate separately radiative correction (RC) contributions from different Feynman diagrams and configurations. In the main part the flags, the parameters and the constants are defined. Using the flags one can define with their help the event selection (BARE1 symmetric or asymmetric are possible only), the order of corrections, switch on or off different contributions (like Z-boson exchange, vacuum polarization and light pair production). Then the user have to set the parameters: the

beam energy, the angular range, the energy cut. The electroweak parameters are calculated with the help of the DIZET package [87].

DESCRIPTION OF THE OUTPUT:
At firdt the code prints the information about the chosen set-up, vacuum polarization (on/off), Z-boson contribution (on/off). Then the code prints the beam energy, the angular range and the electroweak parameters. After calculations it prints, for each value of x_c (energy cut), the Born and the radiatively corrected (to different orders and approximations) cross–sections in [nb]; It also prints a line with the values of the different corrections in percent with respect to the Born cross–section. The normalizations and definitions used do directly correspond to the ones given in [2] where also the origin of all RC contributions can be found.

AVAILABILITY:
The code is available upon request from the authors.

4.6 SABSPV

AUTHORS:

M. Cacciari DESY, Hamburg, Germany
cacciari@desy.de
G. Montagna University of Pavia, Italy
montagna@pavia.pv.infn.it
O. Nicrosini CERN - TH Division (Permanent address: INFN Pavia, Italy)
nicrosini@vxcern.cern.ch, nicrosini@pavia.pv.infn.it
F. Piccinini INFN Pavia, Italy
piccinini@pavia.pv.infn.it

GENERAL DESCRIPTION:
SABSPV evaluates small angle Bhabha cross sections, in the angular region used for luminosity measurement at LEP, and large angle Bhabha cross sections at LEP2. The theoretical formulation is based on a suitable matching between an exact fixed order calculation and the resummation of leading log radiative effects provided by the structure function techniques.
The matching between the all-orders leading-log cross section, $\sigma_{LL}^{(\infty)}$, given by the convolution of structure functions with kernel (Born) cross sections, and the $\mathcal{O}(\alpha)$ one is realized according to the following general recipe: the order-α content of the leading-log cross section is extracted by employing the $\mathcal{O}(\alpha)$ expansions of the structure functions, thereby yielding $\sigma_{LL}^{(\alpha)}$. Denoting by $\sigma^{S+V}(k_0)$ the cross section including virtual corrections plus soft photons of energy up to $E_\gamma = k_0 E$, and by $\sigma^H(k_0)$ the radiative $\mathcal{O}(\alpha)$ cross section, the fully corrected cross section can finally be written as

$$\sigma_A = \sigma_{LL}^{(\infty)} - \sigma_{LL}^{(\alpha)} + \sigma^{S+V}(k_0) + \sigma^H(k_0) . \tag{10}$$

Equation (10) is in the additive form. A factorized form can also be supplied. It has the same $\mathcal{O}(\alpha)$ content but also leads to the so-called classical limit, according to which the cross section

60

must vanish in the absence of photonic radiation. It reads

$$\sigma_F = (1 + C_{NL}^H)\sigma_{LL}^{(\infty)}, \quad C_{NL}^H \equiv \frac{\sigma^{S+V}(k_0) + \sigma^H(k_0) - \sigma_{LL}^{(\alpha)}}{\sigma} \equiv \frac{\sigma_{NL}^{(\alpha)}}{\sigma}, \tag{11}$$

σ being the Born cross section; C_{NL}^H contains the non-log part of the $\mathcal{O}(\alpha)$ cross section, represented by $\sigma_{NL}^{(\alpha)}$.

In order to be flexible with respect to the different kinds of experimental cuts and triggering conditions, it makes use of a multi-dimensional Monte Carlo integration with importance sampling. A detailed description of the formalism adopted and the physical ideas behind it can be found refs. [2, 46] and references therein.

FEATURES OF THE PROGRAM:
The code is a Monte Carlo integrator for weighted events. At every step, two kinds of events are fully accessible:
(A) "two-body" events: they include tree-level events and radiative events in the collinear approximation; in this last case, information concerning the equivalent photons lost in the beam pipe is available,
(B) three-body events: they include the radiative events $e^+e^- \rightarrow e^+e^-\gamma$ beyond the collinear approximation.
No explicit photons beyond $\mathcal{O}(\alpha)$ are generated; on the generated events, every kind of cuts can be imposed. $\mathcal{O}(\alpha)$ corrections are available for the $\gamma(t)\gamma(t)$ contribution (see for instance [72] for the soft plus virtual corrections and [88, 89] for the hard bremsstrahlung contribution); all the other channels are treated in the leading logarithmic approximation[9]. This theoretical framework does exploit the fact that the $\gamma(t)\gamma(t)$ channel is by far the most dominant one. It is therefore sufficient to evaluate exact order α corrections for this channel only. The other channels, which at the Born level contribute at the level of one per cent in the small angle region and of some per cents in the large angle region at LEP2 energies, can be evaluated in the leading log approximation. Higher order corrections are implemented in the structure function formalism [2]. The overall accuracy of the predictions performed by the code is, generically, of the order of 0.1% in the small angle regime and of the order of 1% in the large angle regime at LEP2 energies.

HOW DOES THE CODE WORK:
The code generates random integration variables within the "fiducial" cuts supplied via the input card (see below). These values are passed to the kinematics subroutines, which construct the full quadrimomenta for electron, positron and photon. The quadrimomenta are then fed to a trigger routine, which either accepts or rejects the event according to the cuts specified in it by the user. The control is then returned to the main integration routine, which generates weighted events, accumulates the cross section result for each single contribution and compose them as described in eqs. (10) and (11). Once in a given number of events the integrations

---

[9]Actually, in the present version of the program the up-down interference contribution is neglected. This is of no practical relevance for the small angle cross section, whereas it introduces an error of the order of some per mil in the large angle cross section at LEP2.

results and the related error estimates are evaluated and written to the output file. The error is also compared to the accuracy limit required, and the run stops when the latter is reached. The program can be restarted from its own output file, by specifying the same "physical" inputs and either a larger number of events or a higher accuracy.

INPUT CARD:
The following data card has to be provided via standard input:

```
46.15D0                                 ! EBEAM
24.D-3  58.D-3  0.D0                     ! T1MIN, T1MAX, E1MIN
24.D-3  58.D-3  0.D0                     ! T2MIN, T2MAX, E2MIN
0.5D0   1.D-2   0.D0  0.D0  0.D0         ! CALOINPUT(1...5)
1                                        ! ISIM
1                                        ! ICALO
1.D5    0.D0    0     'SABSPV.OUT'       ! EVTS, ACCLIM, IRESTART, OUTFILE
```

These parameters have the following meaning:

[1] `46.15D0` - the electron and positron beam energy, `EBEAM`.

[2] `24.D-3`, `58.D-3`, `0.D0` - the electron minimum and maximum scattering angle (in radians) and the minimum electron energy (in GeV), `T1MIN`, `T1MAX`, `E1MIN`. These cuts are to be interpreted as "fiducial" cuts within which the events are generated, before going through the triggering routine.

[3] the same for the positron, `T2MIN`, `T2MAX`, `E2MIN`.

[4] `0.5D0`, `1.D-2`, `0.D0`, `0.D0`, `0.D0` - inputs that may be required by the cutting routines for the triggers. These values are stored in the vector `CALOINPUT(5)` via the common block `COMMON/CALOS`.

[5] `1` - flag for symmetric cuts, `ISIM`. The user has to specify if the experimental cuts asked for are (1) or not (0) symmetric for electron–positron exchange. If they are, choosing 1 saves computing time.

[6] `1` - flag for choosing the triggering routine, `ICALO`.

[7] `1.D5`, `0.D0`, `0`, `'SABSPV.OUT'` - these are inputs related to the Monte Carlo integration and to the management of the output. Namely, the total number of events, `EVTS`, the relative accuracy limit aimed at, `ACCLIM`, the restarting flag, `IRESTART` (if 1 the program tries to restart execution from the indicated output file, if 0 it reinitializes it), and the output file name, `OUTFILE`.

DESCRIPTION OF THE OUTPUT:
The output file `OUTFILE` contains a description of the inputs provided to the code, the results of the Monte Carlo integrations for the various contributions and the final results with their standard statistical error. Moreover informations concerning the random number generator and the cumulants, that can be used to restart the program from where it stopped, are provided.

AVAILABILITY:
The code is available upon request to one of the authors.

4.7 UNIBAB

AUTHORS:

H. Anlauf TH Darmstadt & Universität Siegen, Germany
  `anlauf@crunch.ikp.physik.th-darmstadt.de`
T. Ohl   TH Darmstadt, Germany
  `ohl@crunch.ikp.physik.th-darmstadt.de`

GENERAL DESCRIPTION:
UNIBAB is a Monte Carlo event generator designed for large angle Bhabha scattering at LEP and SLC energies. In its original incarnation [90,91], it was a simple QED dresser describing only multiphoton initial-state radiation, thus focusing on the exponentiation of soft photons and the resummation to all orders of the leading logarithmic corrections of the form $(\alpha/\pi)^n \ln^n(s/m_e^2)$. The first published version, UNIBAB version 2.0 [70] contains improvements in the exclusive photon shower algorithm used for the description of initial-state radiation, and many enhancements, such as final-state radiation using a similar photon shower algorithm. An electroweak library based on ALIBABA [60] was added. Initial and final state corrections are implemented in a fully factorized form. Version 2.1 of the program features the inclusion of longitudinal beam polarization. During this workshop the current version 2.2 was developed, which uses an implementation of the final state photon shower based on the exact lowest order matrix element for the process $Z \to f\bar{f}\gamma$. Also, the electroweak library has been updated slightly to include the leading m_t^4-dependence and higher order QCD corrections to the Z width, as discussed in detail in [1].

FEATURES OF THE PROGRAM:
The event generator UNIBAB calculates the QED radiative corrections through a photon shower algorithm. The actual implementation is based on an iterative numerical solution of an Altarelli-Parisi type evolution equation for the electron structure function. The effective matrix element for photon emission from the initial state assumes a factorized form of the radiative matrix element. Therefore it is exact for collinear emission. It also allows to generate finite transverse momenta of the radiated photons. For final state radiation, the algorithm employs an iterated form of the first order matrix element for $Z \to f\bar{f}\gamma$, which gives a reasonable description of exclusive distributions that are sensitive to the details of the approximations used for the multiphoton matrix element, such as acollinearity distributions on the Z peak.
UNIBAB generates only unweighted events. It is implicitly assumed that all scales in the hard subprocess are of the same order of magnitude, and the program does not yet include initial-final interference, thus the program is generally limited to the large angle region. Numerically, the effects from initial-final interference are sufficiently small in the vicinity of the Z peak. For details see the long write-up [70].

HOW DOES THE CODE WORK:
UNIBAB consists of two layers, an external layer with a very simple user interface that allows easy interactive and batch control of the program, and an internal layer with a low level interface to the internal routines. It is however recommended to use the high level interface which

automatically takes care of parameter dependencies and properly reinitializes the Monte Carlo when a physics parameter is modified.

In order to run the program, one has to specify several steering parameters that are internally translated into Monte Carlo parameters. The actual physical cuts have to be implemented in an external analyzer. The essential steering parameters are:

- `ctsmin`, `ctsmax`: cuts on $\cos\theta^*$, where θ^* is the scattering angle in the boosted subsystem after taking initial state radiation into account.

- `ecut`: minimum energy of the final state fermions.

- `acocut`: maximum acollinearity of the outgoing e^+e^- pair.

An interactive run may look like:

```
set ebeam    45.65          # Beam energy in GeV
set mass1z   91.1888        # Z mass
set mass1t   174            # top quark mass
set mass1h   300            # Higgs mass
set ctsmin  -0.8
set ctsmax   0.8
set ecut     20
set acocut   30             # acollinearity cut in degrees
init
generate 100000
close
quit
```

Additional switches control the inclusion or omission of certain contributions like weak box diagrams or t-channel diagrams. For more details please consult the manual.

DESCRIPTION OF THE OUTPUT:

UNIBAB stores the generated events and all supplementary information for analysis (cross section, Monte Carlo error) in the proposed standard /hepevt/ common block [72] and must be read from there by a suitable analyzer. A simple yet very flexible tool for implementing a "theorist's detector" is given by HEPAWK [92,93], which easily allows to obtain arbitrary distributions from the generated events.

AVAILABILITY:

The current version of UNIBAB may be downloaded via anonymous ftp from
ftp://crunch.ikp.physik.th-darmstadt.de/pub/anlauf/unibab
along with up-to-date documentation. At the time of this writing (and for historical reasons), the program source and accompanying files are still distributed in the CERN patchy format. Platform-dependent Fortran77 source files will be made available upon request. For the sample test run, UNIBAB has also to be linked with the analyzer HEPAWK [92,93]. A more modern (auto-configuring) and self-contained version of the Monte Carlo generator will be made available in a future release after the end of the workshop.

5 Conclusions and outlook

In this WG, the first systematic comparison of all the existing Monte Carlo event generators for the Bhabha process at LEP1 and LEP2 has been performed. This is one of our main achievements. The other one is that, as a result of these comparisons, the theoretical error of the small-angle Bhabha process is now reduced from 0.16% to 0.11% for typical LEP1 experimental ES's, at the angular range of $1° - 3°$. In parallel, an estimate of the theoretical error of the small-angle Bhabha process at LEP2 has also been fixed at 0.25%, for all possible experimental situations. The theoretical precision of the small-angle Bhabha scattering should be still improved by a factor of two at LEP1, in order to match the experimental precision. From the analysis performed, we conclude that a theoretical error of the order of 0.06% is reasonably feasible at LEP1, and the present study offers a solid ground for the next step in this direction.

As far as the large-angle Bhabha process is concerned, the main result of this WG is that now we have comparisons not only among the semi-analytical benchmarks ALIBABA and TOPAZ0, but also among Monte Carlo event generators and on the Monte Carlo codes versus semianalytical programs. In spite of the fact that the comparisons involving Monte Carlo's do not change the conclusions of the previous LEP1 WG on the theoretical precision of large-angle Bhabha at LEP1 (see [1]), they give information about the performances of the Monte Carlo event generators themselves. In particular (except for some programs which have to be improved, either on the QED libraries or on the pure weak ones), the situation at LEP1 is generally under control with respect to the present experimental accuracy, both on and off Z peak. As far as LEP2 is concerned, a general agreement of the order of 2% has been achieved. There is certainly room for further improvements on this item, but for practical purposes the situation can be considered satisfactory.

References

[1] Part I: "Electroweak Physics", in *Reports of the working group on precision calculations for the Z resonance*, edited by D. Bardin, W. Hollik, and G. Passarino (CERN, Geneva, 1995), CERN Yellow Report 95-03.

[2] Part III: "Small Angle Bhabha Scattering", in *Reports of the working group on precision calculations for the Z resonance*, edited by D. Bardin, W. Hollik, and G. Passarino (CERN, Geneva, 1995), CERN Yellow Report 95-03.

[3] B. Pietrzyk, in *Tennessee International Symposium on Radiative Corrections: Status and Outlook*, edited by B. F. L. Ward (World Scientific, Singapore, 1995), Gatlinburg, Tennessee, USA, June 1994.

[4] LEP Electroweak Working Group, A Combination of Preliminary LEP Electroweak Results from the 1995 Summer Conferences, 1995, CERN report LEPEWWG/95-02.

[5] LEP Collaborations, 1995, Collaboration notes: ALEPH 95-093 PHYSICS 95-086; DEL-PHI 95-137 PHYS 562; L3 Note 1814; OPAL Technical Note TN312, 1 August 1995.

[6] S. Jadach, E. Richter-Wąs, B. F. L. Ward, and Z. Wąs, Phys. Lett **B353**, 362 (1995), CERN preprint CERN-TH/95-38.

[7] A. B. Arbuzov, E. A. Kuraev, N. P. Merenkov, and L. Trentadue, preprint JINR, Dubna, E2-95-110 (unpublished).

[8] A. B. Arbuzov, E. A. Kuraev, N. P. Merenkov, and L. Trentadue, JETPh **108**, 1 (1995).

[9] F. Teubert, 1995, IFAE, Barcelona, private communication.

[10] The LEP Collaborations ALEPH, DELPHI, L3, OPAL and the LEP Electroweak Working Group, preprint CERN-TH-6443-92 (unpublished).

[11] S. Jadach, E. Richter-Wąs, B. F. L. Ward, and Z. Wąs, Phys. Lett. **B253**, 469 (1991).

[12] A. Arbuzov *et al.*, in *Tennessee International Symposium on Radiative Corrections: Status and Outlook*, edited by B. F. L. Ward (World Scientific, Singapore, 1995), Gatlinburg, Tennessee, USA, June 1994.

[13] N. P. Merenkov, Sov. J. Nucl. Phys. **48**, 1073 (1988).

[14] N. P. Merenkov, Sov. J. Nucl. Phys. **50**, 469 (1989).

[15] A. B. Arbuzov, E. A. Kuraev, N. P. Merenkov, and L. Trentadue, preprint CERN-TH/95-241 (unpublished).

[16] L. N. Lipatov, Sov. J. Nucl. Phys. **20**, 94 (1974).

[17] G. Altarelli and G. Parisi, Nucl. Phys. **B126**, 298 (1977).

[18] E. A. Kuraev and V. S. Fadin, Sov. J. Nucl. Phys. **41**, 466 (1985).

[19] E. A. Kuraev and V. S. Fadin, preprint INP 84-44, Novosibirsk, 1984 (unpublished).

[20] O. Nicrosini and L. Trentadue, Phys. Lett. **196B**, 551 (1987).

[21] E. A. Kuraev, N. P. Merenkov, and V. S. Fadin, Sov. J. Nucl. Phys. **47**, 1009 (1988).

[22] M. Skrzypek, Acta Phys. Pol. **B23**, 135 (1992).

[23] A. Arbuzov *et al.*, in preparation.

[24] F. A. Berends, P. H. Daverveldt, and R. Kleiss, Nucl. Phys. **B253**, 421 (1985).

[25] F. A. Berends, P. H. Daverveldt, and R. Kleiss, Comput. Phys. Comm. **40**, 271 (1986).

[26] J. H. Field, presented in the meeting of the Bhabha WG (unpublished).

[27] S. Jadach, E. Richter-Wąs, B. F. L. Ward, and Z. Wąs, Phys. Lett. **B260**, 438 (1991).

[28] S. Jadach, M. Skrzypek, and B. F. L. Ward, Phys. Rev. **D47**, 3733 (1993).

[29] S. Jadach, M. Skrzypek, and B. F. L. Ward, presented in the meeting of the Bhabha WG and to appear.

[30] S. Jadach, E. Richter-Wąs, B. F. L. Ward, and Z. Wąs, Comput. Phys. Commun. **70**, 305 (1992).

[31] S. Jadach, M. Skrzypek, and B. F. L. Ward, Phys. Rev. **D49**, 1178 (1994).

[32] W. Beenakker and B. Pietrzyk, Phys. Lett. **B304**, 366 (1993).

[33] S. Eidelman and F. Jegerlehner, Z. Phys. **C67**, 585 (1995).

[34] H. Burkhardt and B. Pietrzyk, Phys. Lett. **B356**, 398 (1995).

[35] H. Burkhardt, in *Electroweak interactions and unified theories*, edited by J. Tran Than Van (Editions Frontières, Gif-sur-Yvette, 1995), in print.

[36] H. Burkhardt, F. Jegerlehner, G. Penso, and C. Verzegnassi, Z. Phys. **C43**, 497 (1989).

[37] R. B. Nevzorov, A. V. Novikov, and M. . Vysotsky, JETP Lett. **60**, 399 (1994).

[38] B. Geshkenbein and V. Morgunov, preprint HEPPH–9407228 (unpublished).

[39] N. V. Krasnikov, Mod. Phys. Lett **A9**, 2825 (1994).

[40] M. L. Swartz, preprint SLAC–PUB–6710 revised, November 1994 (unpublished).

[41] M. L. Swartz, preprint SLAC–PUB–95–7001, September 1995 (unpublished).

[42] K. Abel and F. J. Yndurain, preprint FTUAM-95-32, September 1995 (unpublished).

[43] M. Caffo, H. Czyż, and E. Remiddi, BHAGEN95 short write-up, these Proceedings.

[44] S. Jadach *et al.*, BHLUMI 4.02 Monte Carlo, to be submitted to Comput. Phys. Commun., available from WWW location http://hpjmiady.ifj.edu.pl, a patch correcting bug 95a can be also found there (unpublished).

[45] F. A. Berends and R. Kleiss, Nucl. Phys. **B228**, 537 (1983).

[46] M. Cacciari, G. Montagna, O. Nicrosini, and F. Piccinini, Comput. Phys. Commun. **90**, 301 (1995), preprint CERN-TH/95-169.

[47] M. Acciarri *et al.*, Z. Phys. **C62**, 551 (1994).

[48] I. C. Brock *et al.*, Luminosity Measurement in L3, 1995, L3 Collaboration, in preparation.

[49] B. Bloch-Devaux *et al.*, The 1992 SiCal luminosity analysis, 1993, ALEPH internal note ALEPH 93-149 PHYSIC 93-129.

[50] D. Buskulic *et al.*, Z. Phys. **C62**, 539 (1994).

[51] OPAL Collaboration, 1994, OPAL Physics Note PN-142.

[52] J. Hart, in *Rencontres de Physique de la Vallee D'Aoste*, edited by [?EDITOR?] ([?PUB-LISHER NAME?], [?PUBLISHER TOWN?], 1994), p. [?PAGE?].

[53] G. M. Dallavalle, in *The Standard Model and Just Beyond, 4th S.Miniato Topical Seminar*, edited by F. L. Navarria and P. Pelfer (World Scientific, Singapore, 1993), San Miniato, Italy, 1-5 June 1992.

[54] D. Bederede *et al.*, Nucl. Instr. and Meth. **A365**, 117 (1995).

[55] B. E. Anderson *et al.*, IEEE Trans. on Nucl. Sci. **41**, 845 (1994).

[56] M. Merk, in *Electroweak interactions and unified theories*, edited by J. Tran Than Van (Editions Frontières, Gif-sur-Yvette, 1994).

[57] [?AUTHOR?], in *EPS-HEP 95*, edited by [?EDITOR?] ([?PUBLISHER?], [?PUBLISHER TOWN?], 1995), Brussels, 27 July - 2 August 1995, in print.

[58] S. Jadach, E. Richter-Wąs, B. F. L. Ward, and Z. Wąs, Phys. Lett. **B268**, 253 (1991).

[59] S. Jadach, W. Płaczek, and B. Ward, Phys. Lett **B353**, 349 (1995), CERN preprint TH-95-74, April 1995.

[60] W. Beenakker, F. A. Berends, and S. C. van der Marck, Nucl. Phys. **B349**, 323 (1991).

[61] M. Martinez and R. Miquel, Z. Phys. **C53**, 115 (1992).

[62] P.Comas and R.Martinez, Z. Phys. **C58**, 15 (1993).

[63] G. Montagna *et al.*, Comput. Phys. Commun **76**, 328 (1993).

[64] G. Montagna, O. Nicrosini, G. Passarino, and F. Piccinini, preprint CERN-TH.7463/94, to appear in Comput. Phys. Commun. (unpublished).

[65] D. Bardin *et al.*, *ZFITTER: An Analytical program for fermion pair production in e+ e-annihilation*, 1992, preprint CERN-TH-6443-92 (unpublished).

[66] D. Bardin *et al.*, Nucl. Phys. **B351**, 1 (1991).

[67] J. H. Field, Phys. Lett. **B323**, 432 (1994).

[68] J. H. Field and T. Riemann, *BHAGENE3 a Monte Carlo Event Generator for Lepton Pair Production and Wide Angle Bhabha Scattering in e^+e^- Collisions near the Z-Peak*, 1995, report UGVA-DPNC 1995/6-166, DESY 95-100, to be published in Comp. Phys. Commun.

[69] S. Jadach, W. Płaczek, and B. F. L. Ward, preprint The University of Tennessee UTHEP-95-1001 (unpublished).

[70] H. Anlauf *et al.*, Comput. Phys. Commun. **79**, 466 (1994).

[71] G. Montagna *et al.*, Nucl. Phys. **B401**, 3 (1993).

[72] M. Caffo et al. "Bhabha Scattering", in *Z Physics at LEP 1*, edited by G. Altarelli, R. Kleiss, and C. Verzegnassi (CERN, Geneva, 1989), p. 171, CERN Yellow Report 89-08.

[73] M. Caffo, H. Czyż, and E. Remiddi, Nuovo Cim. **105A**, 277 (1992).

[74] M. Caffo, H. Czyż, and E. Remiddi, Int. J. Mod. Phys. **4**, 591 (1993).

[75] M. Caffo, H. Czyż, and E. Remiddi, Phys. Lett. **B327**, 369 (1994).

[76] M. Caffo, H. Czyż, and E. Remiddi, 1995, program BHAGEN94, in preparation.

[77] M. Caffo, H. Czyż, and E. Remiddi, 1995, program BHAGEN-1PH, in preparation.

[78] D. Bardinand, W. Hollik, and T. Riemann, Z. Phys. C **49**, 485 (1991).

[79] A. Djouadi and C. Verzegnassi, Phys. Lett. **B195**, 265 (1987).

[80] A. Djouadi, Nuovo Cim. **100A**, 357 (1988).

[81] D. Bardin and A. Chizhov, preprint INR Dubna E2–89–525 (unpublished).

[82] M. Böhm, A. Denner, and W. Hollik, Nucl. Phys. **B304**, 687 (1988), and references therein.

[83] F. A. Berends, R. Kleiss, and W. Hollik, Nucl. Phys. **B304**, 712 (1988).

[84] V. N. Gribov and L. N. Lipatov, Sov. J. Nucl. Phys. **15**, 438 (1972).

[85] S. Jadach and B. F. L. Ward, Phys. Rev. **D40**, 3582 (1989).

[86] W. Beenakker, F. A. Berends, and S. C. van der Marck, Nucl. Phys. **B355**, 281 (1991).

[87] D. Bardin *et al.*, Comp. Phys. Commun. **59**, 303 (1990).

[88] M. Greco, G. Montagna, O. Nicrosini, and F. Piccinini, Phys. Lett. **B318**, 635 (1993), and references therein.

[89] G. Montagna, O. Nicrosini, and F. Piccinini, Comput. Phys. Commun. **78**, 155 (1993), erratum, ibid. **79**.

[90] H. D. Dahmen, P. Manakos, T. Mannel, and T. Ohl, preprint SI 89-8, IKDA 89/28 (unpublished).

[91] H. D. Dahmen, P. Manakos, T. Mannel, and T. Ohl, Z. Phys. C **50**, 75 (1991).

[92] T. Ohl, Comp. Phys. Commun. **70**, 120 (1992).

[93] T. Ohl, report IKDA 95/15, hep-ex/9504007 (unpublished).

hep-ph/9602203

EVENT GENERATORS FOR DISCOVERY PHYSICS

Conveners: M.L. Mangano and G. Ridolfi

Working group: E. Accomando, S. Asai, H. Baer, A. Ballestrero, M. Besançon, E. Boos, C. Dionisi, M. Dubinin, L. Duflot, V. Edneral, K. Fujii, J. Fujimoto, S. Giagu, D. Gingrich, T. Ishikawa, P. Janot, M. Jimbo, T. Kaneko, K. Kato, S. Katsanevas, S. Kawabata, S. Komamiya, T. Kon, Y. Kurihara, A. Leike, G. Montagna, O. Nicrosini, F. Paige, G. Passarino, D. Perret-Gallix, F. Piccinini, R. Pittau, S. Protopopescu, A. Pukhov, T. Riemann, S. Shichanin, Y. Shimizu, A. Sopczak, H. Tanaka, X. Tata, T. Tsukamoto

Contents

1

1 Introduction

This chapter of the report presents a review of Monte Carlo (MC) event generators for signals of new particles. The areas covered include Higgs production, Supersymmetry (SUSY) and leptoquarks. Contrary to other contexts, where MC generators for specific Standard Model (SM) processes are considered, it is not possible to identify a simple common set of features which event generators for new physics should possess. Each new process presents its own theoretical and technical issues, with the emphasis being now equally shared between the precision of the calculations and the completeness of the coverage of exotic phenomena and their parametrization. While the accuracy and the statistical power of the future measurements call for high precision in the Bhabha, WW and QCD generators, a precision of the order of few percent in the determination of the cross sections for new phenomena and for their backgrounds is sufficient in most examples of practical relevance. In this respect, it is important to distinguish between two uses of event generators for new physics. The first one involves the evaluation of the potential signals, *i.e.* the calculation of production cross sections, decay branching ratios (BR's) and detector acceptances and efficiencies. The second one involves the determination of the parameters of the new physics which will be hopefully discovered from the comparison of the properties of the observed signal with what derived from the MC model. Most of the studies carried out by our working group and by the New Physics working groups covered the first issue. In the examples considered, the conclusion was that the current theoretical uncertainties in the various MC's do not affect the projected discovery potential. On the other hand the extraction of the parameters which determine the specific model of new physics could depend strongly on the accuracy of the theoretical description of the production process. For example, features such as the presence or absence of spin correlations, which do not seem to be critical for the discovery of supersymmetric particles, will affect the determination of the EW properties of the new particles, as will be shown explicitly in sect. 3.5.

The plan of this contribution is as follows: we start with Higgs production, shortly describing the main technical issues and presenting the available generators. Results and comparisons are discussed. We then present the SUSY generators, covering both multi-purpose codes which include most of the possible SUSY final states, and single-channel codes, which focus on a given signal trying to incorporate the most accurate theoretical treatment possible today. The description of a leptoquark generator will complete this work.

While this review is by no means complete, it contains most of the tools available to the public. We are aware of many other existing programs, part of which have been used in the extensive cross checks performed as part of the working group activity. Since they have not been developed for distribution, and would not be easily accessible to the public, they have not been included in this report.

2 Higgs

The search for the Higgs boson will have first priority in the LEP2 programme [1], and a large effort has been devoted to the development of reliable MC event generators. In the Standard Model, Higgs production at LEP2 is dominated by the process $e^+e^- \to Z^* \to ZH$ [1]. In the mass range of interest for LEP2 the Higgs boson is expected to decay dominantly into a pair of bottom quarks, leading to final states like $f\bar{f}b\bar{b}$, f being any fermion aside from the top. Because of the large width of the Z boson, the approximation in which the production and decay of the Z boson factorize is not good enough. On the other hand, the small width of the Higgs could justify the factorization approximation. Nevertheless, most of the event generators presented below include the matrix elements for the full 4-fermion process $e^+e^- \to f\bar{f}b\bar{b}$. The evaluation of this process involves not only the diagrams with a Higgs boson, but also all possible SM diagrams leading to the same final state. As an example, assuming $f \neq e, \nu_e$ one should evaluate a total of 25 tree level diagrams: 1 corresponding to the signal, 8 t-channel diagrams relative to ZZ, $Z\gamma$ and $\gamma\gamma$ exchange, and 16 s-channel diagrams relative to the bremsstrahlung of a neutral vector boson from the fermionic final states. If f is a quark, QCD processes should be added to this last category. Likewise, different sets of diagrams appear both in the signal and in the background if $f = e$ or $f = \nu_e$. The presence of several resonating channels in the full amplitude poses some numerical problem, which can be easily overcome by choosing properly the importance sampling, as described later on. In the case of massless final state fermions, the interference between signal and background diagrams is zero, because of the helicity non-conservation induced by the coupling to the Higgs boson. If the mass of the b quarks is kept different from zero in the matrix elements, a finite interference will develop. In addition to including all diagrams, accurate event generators should also include the effects of initial state radiation (ISR), and provide the user with the effective 4-momentum of the final state after initial state photon emission. As a desirable feature, Higgs generators should also contain a description of Higgs production and decay in models beyond the SM, such as two-doublet or SUSY models [1]. Finally, one expects the code to provide unweigthed events with the 4-momenta of all final state particles, in order for the user to process the events through the detector and to apply analysis cuts.

Each code presented in this section embodies all these features to a different degree. A comparison between results obtained using different approximations will allow us to estimate the importance of any given effect, and to assess the limitation of a given approach. It must be pointed out that none of these codes contains the full 1-loop EW radiative corrections. Their evaluation and inclusion in a 4-fermion event generator has not been achieved for any 4-fermion final state. The largest component of the radiative corrections is however incorporated using the so-called Improved Born Approximation [3], in which vector boson self-energy insertions are absorbed by using running EW couplings. A partial calculation of the full EW 1-loop corrections has been performed [4] for the process $e^+e^- \to Hf\bar{f}$. The resulting production cross section never differs from the IBA by more than 2% in the range of interest at LEP2. The agreement improves for Higgs masses near the LEP2 discovery reach. The 1% level is therefore an optimal goal for the agreement between the tree level event generators which will

be described here.

2.1 CompHEP

Program name:	CompHEP – version 3.0
Authors:	E. Boos – boos@theory.npi.msu.su
	M. Dubinin – dubinin@theory.npi.msu.su
	V. Edneral – edneral@theory.npi.msu.su
	V. Ilyin – ilyin@theory.npi.msu.su
	A. Pukhov – pukhov@theory.npi.msu.su
	V. Savrin – savrin@theory.npi.msu.su
	S. Shichanin – shichanin@m9.ihep.su
Availability:	anonymous ftp from theory.npi.msu.su
	Directory: pub/comphep-3.0
	File: 30.tar.Z
Documentation:	Files: install.doc, manual.ps.Z

The main purpose of CompHEP [6] is to allow the automatic evaluation of cross sections and distributions directly from an assigned lagrangian.

The general structure of the CompHEP package is described in the section "Event generators for WW physics" of this Workshop. Here we describe in more detail the feature of the program relevant for the Standard Model (SM) Higgs search at LEP2.

Any kind of three-, four- and five-particle final states can be calculated using CompHEP. In the case of Higgs boson production, the reactions of interest are $e^+e^- \rightarrow f\bar{f}b\bar{b}$, with f any lepton or quark. The main features of the calculations implemented in CompHEP can be summarized in the following way:

- all possible Feynman diagrams contributing to the process are calculated and all interferences between signal and background diagrams are taken into account (at tree level). Fermion masses can be kept nonzero in the calculation of the squared amplitudes.

- final particle phase space with massive fermions is generated explicitly.

CompHEP generates graphically complete sets of Feynman diagrams for the processes mentioned above (for instance, 25 diagrams including one signal diagram for $e^+e^- \rightarrow \mu^+\mu^-b\bar{b}$, 21 diagrams including two signal diagrams for $e^+e^- \rightarrow \nu\bar{\nu}b\bar{b}$, 50 diagrams including two signal diagrams for $e^+e^- \rightarrow e^+e^-b\bar{b}$). Any desired subset of diagrams (for instance, signal only) can be separated for further processing. Squared amplitudes and interference terms are calculated symbolically with the help of a special module for trace calculations. In the next step, optimized FORTRAN codes corresponding to these terms are generated by the package. The codes are

compiled and linked to the special interface program and Monte Carlo integrator program. The FORTRAN loading module created as a result of this process represents by itself the generator of the Higgs signal in the four fermion reaction under consideration. It is driven by the screen menu allowing the user to choose various options of signal and background simulation. A more detailed description of the menu system can be found in ref. [2].

Seven-dimensional adaptive Monte Carlo integration over the phase space and unweighted event generation is performed by the BASES/SPRING package [7]. The output has the standard BASES form (sequence of Monte Carlo iterations for total cross section and a set of histograms for various distributions). The width of the light Higgs boson is small, so the adaptive possibilities of BASES are not sufficient for integration over the phase space. Additional kinematical regularization (integration with probability density concentrated around the resonance peaks) can be introduced for the Higgs as well as vector bosons.

Initial state radiation is implemented in the structure function approach. Non-standard interaction vertices can be introduced by changing the model input (see [6] for details). Any kinematical cuts can be implemented.

At present, versions of CompHEP for different platforms exist: HP Apollo 9000, IBM RS 6000, DECstation 3000, SPARC station, Silicon Graphics and VAX.

2.2   4fan

Program name: **4fan**
Authors: D. Bardin – `bardindy@cernvm.cern.ch`
                  A. Leike – `leike@cernvm.cern.ch`
                  T. Riemann – `riemann@ifh.de`
Availability: Anonymous ftp from `gluon.hep.physik.uni-muenchen.de:4fan`.
                  Files: `4fanv12.f, 4fanv12.dat, readme`
Documentation: D. Bardin, A. Leike and T. Riemann, Phys. Lett. **B344** (1995) 383,
                  D. Bardin, A. Leike and T. Riemann, Phys. Lett. **B353** (1995) 513.

4fan is a semi-analytical program which calculates the process

$$e^+e^- \to f_1\bar{f}_1 f_2\bar{f}_2, \qquad (2.1)$$

where the three involved fermions e, f_1 and f_2 must be in different electroweak multiplets (the so called NC32 process) [9]. SM Higgs production can be included optionally [10]. For calculations at the Born level, **4fan** can be used as a stand-alone program. For the calculation of cross sections including initial state radiation, the initial state radiation environment of the code **GENTLE** has to be used which calls **4fan** as a subroutine. For the description of **GENTLE/4fan**, we refer to [2]. Here we describe the stand-alone program **4fan**.

Six of the eight integrations of the four particle phase space were done analytically. The

6

two remaining integrations over $s_1 = [p(f_1) + p(\bar{f}_1)]^2$ and $s_2 = [p(f_2) + p(\bar{f}_2)]^2$ are performed numerically allowing the inclusion of cuts for these variables.

Finite mass effects are taken into account using the following approximations:

The phase space is treated exactly.

In the Higgs contributions and the conversion diagrams $e^+e^- \to (\gamma\gamma) \to f_1 \bar{f}_1 f_2 \bar{f}_2$, the masses are treated up to order $O[m^2(f_i)/s_i]$.

Fermion masses are treated identically in traces and Higgs couplings.

The Higgs width is calculated including the decays into b-, c- and τ- pairs.

The numbers quoted in the tables of sect. 2.8 are produced for zero fermion masses except in the Higgs couplings. The Higgs propagator is always connected with s_2 by convention.

The initialization routine BBMMIN assigns to the SM parameters the values from the Particle Data Book [11]. In the subroutine DSDSHSZ, the interferences between the three main subsets of the NC32 diagrams are calculated as well as those with the Higgs signal diagram. Their sum gives the double differential cross section. The integration of selected interferences between these subsets is not foreseen.

The numerical integration is done by a twofold application of a one-dimensional Simpson integration with a control over the relative and the absolute error. The singularities due to resonating vector propagators are eliminated by appropriate changes of integration variables. To avoid numerical instabilities, the kinematical functions resulting from the six-fold analytical integration are replaced by Taylor expansions near the borders of the phase space. The shortest calculational time is achieved by a choice of the required absolute and relative errors in such a way that they give approximately equal contributions to the error of the output.

The calculational time of a Born cross section is several seconds on a HP workstation depending on the required accuracy and on the cuts on s_1 and s_2; improving the accuracy by a factor of ten approximately doubles the calculational time.

Input and output are transferred through the arguments of the subroutine only.

Usage of the program:

```
CALL FOURFAN(EPS,ABS,IF1,IF2,S,S1MIN,S1MAX,S2MIN,S2MAX,AMH,IOUT,OUT)
```

Input:

`EPS,ABS`:	The required relative and absolute error. If at least one of the two criteria is fulfilled, the calculation is finished.
`IF1,IF2`:	Integers specifying the two final fermion pairs according to the Monte Carlo particle numbering scheme, see Particle Data Group [11], Chapter 32).
`S`:	The c.m. energy squared of the e^+e^- pair.
`S1MIN,S1MAX`:	The integration bounds of s_1.
`S2MIN,S2MAX`:	The integration bounds of s_2.
`AMH`:	The Higgs mass.
`IOUT`:	Integer, selecting the output, Currently `IOUT`=1, 2, 11 and 12 are implemented:

`IOUT=1`:	Total cross section σ_t without Higgs.
`IOUT=2`:	Differential cross section $d\sigma/ds_2$ without Higgs.
`IOUT=11, 12`:	The same as `IOUT=1, 2` but *with* Higgs.

The units of the input (if required) are GeV^2 or GeV.

Output: OUT Depends on the value of `IOUT`. The output is given in fb or in fb/GeV.

On HP workstations **4fan** must be compiled with the -K option.

2.3 HIGGSPV

Program name:	HIGGSPV
Authors:	G. Montagna – `montagna@pv.infn.it`
	O. Nicrosini – `nicrosini@vxcern.cern.ch`
	F. Piccinini – `piccinini@pv.infn.it`
Availability:	Code available upon request
Documentation:	

General Description. The present version of the four-fermion Monte Carlo code HIGGSPV is an upgrade of the version used in [12], where a general description of the formalism adopted and the physical ideas behind it can be found (see also references therein). All the physical and technical upgrades will be described in detail in [13].

The program is based on the exact tree-level calculation of several four-fermion final states relevant for Higgs search at future e^+e^- colliders. Any cut on the final state configuration can be implemented. Initial- and final-state QED corrections are taken into account at the leading logarithmic level by proper structure functions, including p_T/p_L effects [23]. An hadronization interface is under development. All the relevant presently known non-QED corrections are also taken into account.

Features of the program. The code consists of three Monte Carlo branches, in wich the

importance-sampling technique is employed to take care of the peaking behaviour of the integrand:

- Unweighted event generation. The code provides a sample of unweighted events, defined as the components of the four final-state fermions momenta, plus the components of the initial- and final-state photons, plus $\sqrt{s}$, stored into proper n-tuples. The code returns also the value of the unweigthed-event cross section, together with a Monte Carlo estimate of the error. The program must be linked to CERNLIB for graphical interfaces.

- Weighted event integration. It is intended for computation only. In particular, the code returns the value of the cross section for weighted events together with a Monte Carlo estimate of the errors. The program must be linked to CERNLIB for the evaluation of few special functions.

- Adaptive integration. It is intended for computation only, but offering high precision performances. On top of importance sampling, an adaptive Monte Carlo integration algorithm is used. The program must be linked to NAG library for the Monte Carlo adaptive routines. Full consistency between non-adaptive and adaptive integrations has been explicitly proven. Neither final-state radiation nor p_T splitting are taken into account in this branch.

The non-adaptive branches rely upon the random number generator RANLUX.

The most important features are:

- The processes available are the neutral current reactions $e^+ e^- \rightarrow l\bar{l}q\bar{q}$, namely NC48 (NC50 = NC48 + Higgs signals) NC24 (NC25 = NC24 + Higgs signal), NC19 (NC21 = NC19 + Higgs signals).

- Any kind of cuts can be imposed.

- There is the possibility of getting information on the contribution of subsets of the diagrams by setting proper flags.

At present, final state decays are not implemented and finite fermion mass effects are partially taken into account at the phase space boundary. However it is worth noting that the $\mathcal{O}(\alpha_s^2)$ running quark masses $(m_{c,b}(m_H^2))$ are employed in the $Hq\bar{q}$ coupling. An interface to hadronization packages is presently under development.

How the code works. After the initialization of the SM parameters and of the electromagnetic quantities, the independent variables are generated, according to proper multi-channel importance samplings, within the allowed phase space. By means of the solution of the exact kinematics, the four-momenta of the outgoing fermions, together with the four-momenta of all the generated photons, are reconstructed in the laboratory frame. If the event satisfies the cuts

imposed by the user in SUBROUTINE CUTUSER the matrix element is called, otherwise it is set to zero.

In the generation branch, an additional random number is generated in order to implement the hit-or-miss algorithm and if the event is accepted it is recorded into an n-tuple. In the non-adaptive integration branch, the cross section for weighted events is computed. In the adaptive integration branch (ref.: NAG routine D01GBF), on top of importance sampling the integration routine automatically subdivides the integration region into subregions and iterates the procedure where the integrand is found more variant. The program stops when a required relative precision is achieved.

Input parameters and flags. A sample of input flags that can be used is the following:

OGEN = I choice between integration [I] and generation [G] branch

RS = c.m. energy (GeV)

OFAST = N choice between adaptive [Y] or non adaptive [N] branch

NHITWMAX = number of weighted events

IQED = 1 choice fo Born [0] or QED corrected [1] predictions

OSIGN = Y includes [Y] or does not include [N] the Higgs-boson signal

OBACK = Y includes [Y] or does not include [N] the SM background

NSCH = 2 Renormalization Scheme choice (three possible choices)

ALPHM1 = 128.07D0 $1/\alpha$ value (LEP2 standard input)

ANH = the Higgs-boson mass (GeV)

OBS = 1 option for the required $l\bar{l}q\bar{q}$ channel

The Higgs-boson width is calculated including the decays into c, τ and b pairs. A detailed account of the other relevant possibilities offered by the code (namely, command files for generation and adaptive integration branches) will be given elsewhere [13].

Description of the output. For all three branches the output contains the values of the relevant Standard Model parameters. In the generation branch, an n-tuple containing the generated events is written, in addition to the output file containing the values of the cross sections for unweighted events. In the integration branches, the values of the cross sections with their numerical errors are printed.

2.4 HZHA

Program name:	HZHA
Author:	P. Janot – janot@cernvm.cern.ch
Availability:	JANOT 193 minidisk on CERNVM.
	Files HZHA FORTRAN, HZHA CARDS and HZHA EXEC.
Documentation:	

General description. This generator is designed to provide a complete coverage of possible production and decay channels of SM (h) and MSSM (h, H, A) Higgs bosons at e^+e^- colliders. The complete set of background four-fermion processes is however not included. HZHA allows eight different Higgs production processes to be simulated (only the processes 1, 5 and 7 are relevant for the SM):

1. $e^+e^- \to hZ \to h f\bar{f}$,

2. $e^+e^- \to HZ \to H f\bar{f}$,

3. $e^+e^- \to hA$,

4. $e^+e^- \to HA$,

5. $e^+e^- \to \nu\bar{\nu}h$ *via* WW fusion,

6. $e^+e^- \to \nu\bar{\nu}H$ *via* WW fusion,

7. $e^+e^- \to e^+e^-h$ *via* ZZ fusion,

8. $e^+e^- \to e^+e^-H$ *via* ZZ fusion,

No interference between these channels is as yet included. The following decay modes of each Higgs boson are considered:

1. $\gamma\gamma$	2. gg	3. $\tau^+\tau^-$	4. $c\bar{c}$
5. $b\bar{b}$	6. $t\bar{t}$	7. $W^{+*}W^{-*}$	8. Z^*Z^*
9. $h, H \to AA$, with $A \to Zh$	10. $H \to hh$	11. γZ^*	12. e^+e^-
13. $\mu^+\mu^-$	14. $s\bar{s}$	15. $\tilde{\chi}\tilde{\chi}$	16. $\tilde{\chi}^+\tilde{\chi}^-$.

The squark, slepton, chargino, neutralino masses and mixings are computed in the MSSM framework. The squarks and sleptons are assumed to be sufficiently heavy that no Higgs boson can decay to them. However, decays to $\tilde{\chi}^0$'s and $\tilde{\chi}^\pm$'s are enabled when kinematically allowed. Therefore, the branching ratios of charginos and neutralinos are also computed and their decays simulated in the following channels :

1. $\tilde{\chi}_2^0 \to \tilde{\chi}_1^0 Z^* \to \tilde{\chi}_1^0 f\bar{f}$,

11

2. $\tilde{\chi}_2^0 \to \tilde{\chi}^+ W^{-*} \to \tilde{\chi}_1^0 f\bar{f}'$,

3. $\tilde{\chi}_2^0 \to \tilde{\chi}_1^0 \gamma$,

4. $\tilde{\chi}^+ \to \tilde{\chi}_1^0 W^* \to \tilde{\chi}_1^0 f\bar{f}'$,

where $\tilde{\chi}_1^0$ and $\tilde{\chi}_2^0$ are two lightest neutralinos, and $\tilde{\chi}^+$ is the lightest chargino (with $m_{\tilde{\chi}_2^0}, m_{\tilde{\chi}^+} > m_{\tilde{\chi}_1^0}$). Cascade decays are also simulated. The lightest neutralino $\tilde{\chi}_1^0$ is assumed to be the LSP (if not so, a warning message appears and the program may stop) and R-parity is assumed to be conserved.

In the SM the h $\to \tilde{\chi}\tilde{\chi}$ is allowed to simulate invisible Higgs decays. In the MSSM, the $\gamma\gamma$ and γZ (resp. gg) decay widths are computed with all the charged (resp. coloured) particles in the loops (squarks, leptons, charginos, charged Higgses).

Finally, the MSSM Higgs boson pole masses are computed using by default the improved renormalization group equations at two loops [14] (they may also be computed using the EPA for comparison purposes). An independent computation of Higgs masses [15] will be implemented soon.

Features of the program. HZHA is an event generator based on a Monte-Carlo technique, producing any desired combination of the final states listed above. In addition, any Z decay channel combination can be defined by the users for the processes 1 and 2 ($e^+e^- \to$ hZ and HZ).

The initial state radiation (ISR) is implemented by means of the REMT package by R. Kleiss, modified to account for the α^2 part of the spectrum, and the possibility of the radiation of two initial photons. The final state radiation (FSR) is implemented for the leptonic Z decays in the processes 1 and 2.

All final state fermions are massive. The couplings of the Higgs bosons to the quarks are computed using the two-loop running quark masses evolved to the Higgs boson mass scale. The pole masses chosen for the c- and the b-quark are 1.64 and 4.87 GeV/c^2. More generally, the cross-sections for all requested processes and the decay widths/branching ratios for all three Higgs bosons are computed with all known QED, weak and QCD corrections. In particular, Higgs width effects are taken into account both in the cross-section computation and in the event generation. Finally, the program is fully interfaced with JETSET 7.4 [16] for the hadronization of the final state quarks.

How it works. When the program is called, the initialization part determines the relevant masses, mixing and couplings as mentioned above, computes the decay widths and branching ratios for the Higgs bosons, the neutralinos and the charginos, and gives the total production cross-sections without and with ISR.

Unweighted events are generated according to the user requests (number of events to be generated, choice of the production processes and the decay channels,...). The events are

stored in the LUJETS common blocks for subsequent use, e.g. in an interface with full detector simulation.

The job is closed by some statistics printout (numbers of events generated in each of the processes and of the decay channels).

Input parameters, flags, etc. The inputs are chosen by the user through data cards read by the CERNLIB routine FFREAD. See item 8 to see where the card file can be obtained from. This card file is well documented and self explanatory. The following inputs can be freely set:

1. From the card TRIG, the first and last events to be generated;

2. From the card DEBU, the first and last events to be printed out;

3. From the card TIME, the time to keep at the end of the job;

4. From the card GENE, the general parameters (centre-of-mass energy, ISR flag, SM or MSSM flag...);

5. From the card GSMO, the SM parameters (Z mass and width, Fermi constant, top mass, Higgs boson mass $m_{\rm H}$, $\Lambda_{QCD}^{(5)}$);

6. From the card GSUS, the MSSM parameters (m_A, $\tan\beta$, the universal gaugino mass M, the squark mixing parameters μ, A_t, A_b, and the masses m_Q, m_U, m_D, m_L, m_E);

7. From the card PRYN, the process(es) to be generated;

8. From the card GZDC, the Z decay channels to be enabled;

9. From the card GCH1, the H decay channels to be enabled;

10. From the card GCH2, the h decay channels to be enabled (also used for the SM Higgs boson);

11. From the card GCH3, the A decay channels to be enabled;

Other data cards can be added (in which case the program should be modified to be able to understand them) to set branching ratios, masses, widths of particles for the JETSET running.

A description of the output to be expected. The output contains the values of the Higgs boson production cross-sections and decay branching ratios, followed by the listing of the numbers of events given by the data card DEBU, and terminated by the end-of-run statistics.

Where can the program be obtained? The program (and its subsequent updates) can be obtained upon request by e-mail to janot@cernvm.cern.ch. It can also be found, for the time being, on the JANOT 193 minidisk on CERNVM. Relevant files are named HZHA FORTRAN and HZHA CARDS. An example of EXEC file (HZHA EXEC) can also be found at the same place.

13

2.5 PYTHIA

Program name:	PYTHIA – version 5.720, 29 November 1995
Author:	T. Sjöstrand – `torbjorn@thep.lu.se`
Availability:	http://thep.lu.se/tf2/staff/torbjorn/Welcome.html
Documentation:	address above and Comp. Phys. Commun. 82 (1994) 74

PYTHIA [16] is a general-purpose event generator, with emphasis on a complete description of QCD cascades and hadronization. Therefore it is extensively discussed in the QCD generators report of this report. Among its selection of subprocesses, described there, there are several related to Higgs production (signal and backgrounds). Extensive details can be found in the documentation referred to above.

2.6 WPHACT

Program name:	WPHACT
Authors:	E. Accomando – `accomando@to.infn.it`
	A. Ballestrero – `ballestrero@to.infn.it`
Availability:	Anonymous `ftp` from:
	`ftp.to.infn.it:pub/ballestrero`
Documentation:	To be found in the above directory.

General description. WPHACT is a program created to study four fermion, WW and Higgs physics at present and future e^+e^- colliders. In its present form, it can compute all SM processes with four fermions in the final state.

We will give here a description of the program and his characteristics with particular emphasis to those regarding Higgs physics. We refer to the analogous description in the WW Physics section of this report for what concerns charged current processes and some general features of the program.

For all processes with $b\,\bar{b}$ in the final state together with $\mu\bar{\mu}$, $\nu_\mu\bar{\nu}_\mu$, $\nu_e\bar{\nu}_e$ and $b\,\bar{b}$, finite b masses are properly taken into account both in the phase space and in matrix elements. Higgs contributions are of course included.

Full tree level matrix elements for these processes (as well as for all other four fermion final states) are computed by means of subroutines which make use of the helicity formalism of ref. [17], which is particularly suited for treating massive fermion processes. The code for them has been written semi automatically through the set of routines PHACT [18] (**P**rogram for **H**elicity **A**mplitudes **C**alculations with **T**au matrices) which implements the method in a fast and efficient way. In the above formalism, eigenstates of the fermion propagators are used to simplify matrix expressions. These eigenstates are chosen to be generalizations of the spinors used in ref. [19]. With the introduction of so called tau matrices [17], the numerators of fermion

14

propagators have a very simple expression also in the massive case and one does not have to care about the various mass terms. The computation of fermion lines reduces to evaluating the matrices corresponding to insertions of vector or scalar lines and combining them together. The program PHACT writes automatically the optimized FORTRAN code necessary for every insertion and every combination, given the names of the vectors, couplings, etc. It turns out that the massive case is not more complicated than the massless one. Only more helicity indices are of course needed. As a consequence, the codes for massive amplitudes written in this way are not much slower, as it is normally the case, than those with massless fermions.

The user has the choice among three different ways of sampling the phase space, in order to take into account the peak structure of the Higgs signal and of the other resonating diagrams of the background. The adaptive routine VEGAS [20] is used for integrating over the phase space.

Features of the program. WPHACT is a Monte Carlo program. The integration is performed by VEGAS [20]. For all phase spaces used, all momenta are explicitly computed in terms of the integration variables. This implies that any cut can be implemented, and it can be easily used also as an event generator. The events obtained in this way are of course weighted. Distributions for any variable can also be easily implemented, even if no automatic implementation of distributions has yet been introduced.

All final states computed by WPHACT correspond to four fermions. Thus no stable Z or Higgs are allowed in the final state. They are always considered as virtual particles. The Higgs decay particles are always treated as massive, both in the matrix elements of signal and background and in the phase space. All tree level QCD background processes ($\mathcal{O}(\alpha \; \alpha_\mathrm{s})$) leading to four-quark final states are completely taken into account. Initial state QED radiation is included through structure functions $\mathcal{O}(\alpha^2)$. Anomalous gauge boson couplings are also present, if required. FSR is not implemented and no interface to hadronization is available.

It is easy to obtain contributions from different set of diagrams, as every diagram is evaluated individually for all helicity configuration and then summed to the others before squaring and summing over helicity configurations. In particular contributions to Higgs signal, background and their interference can be evaluated separately.

We give some indicative values about the running time on an ALPHA AXP 2100/4 OVMS, in the massive case:

CPU time per call for $e^+e^- \to b\bar{b}b\bar{b}$ Higgs signal with ISR: 3.0×10^{-4} sec.

CPU time per call for $e^+e^- \to b\bar{b}b\bar{b}$ Higgs background with ISR: 1.3×10^{-3} sec.

CPU time per call for $e^+e^- \to b\bar{b}\mu^+\mu^-$ Higgs signal with ISR: 9.0×10^{-5} sec.

CPU time per call for $e^+e^- \to b\bar{b}\mu^+\mu^-$ Higgs background with ISR: 6.3×10^{-4} sec.

For the same processes without ISR, CPU time per call is about 20% less. On a VAXstation 4000/90 CPU time for these programs has to be multiplied approximately by a factor 5.

15

At LEP2 energies, 2.5 M calls (about 13 minutes for the first process and 4 minutes for the second one) are used on ALPHA AXP to obtain Higgs signal with ISR cross section with a typical estimated error of about 1×10^{-4}. The same processes can be evaluated in about 1.5 minutes and 15 sec. respectively with 0.2 M calls at permill level. At this level 2.5 M calls (30 minutes) are necessary for $e^+e^- \to b\bar{b}\mu^+\mu^-$ Higgs background with ISR while 16 M calls (6 hours) are needed for $e^+e^- \to b\bar{b}b\bar{b}$ Higgs background with ISR.

How the code works. The variables which parametrize the phase space are: the masses of the two virtual Z's (or those of the virtual Higgs and Z), the angle of the two particles with respect to the beam, the decay angles in their rest frames, and x_1, x_2, the fractions of momenta carried by the electrons. Appropriate changes of variables to optimize the sampling of the peaks in x_1, x_2, M_H and M_Z lead to the actual integration variables. For every point chosen by the integration routine, the full set of four momenta are reconstructed and passed to the subroutine which evaluates the differential cross section with the helicity amplitude formalism. For every point in the integration variables, i.e. for every set of four momenta chosen, VEGAS gives a weight which can be used together with the value of the cross section for producing distributions.

Three different ways of sampling the massive phase space are available, which are appropriate for different peaking structures. We can classify them as double resonant, single resonant and non resonant. We have verified that normally the double resonant phase space is accurate enough. The other two can be used to study contributions of a particular subset of diagrams. It is better to run the Higgs signal and background separately, adding the results, as the change of variables necessary to take care of the resonances of the two contributions depends on their masses. The interference is normally added to the background, but it can be separated and evaluated by itself.

The $e^+e^- \to b\bar{b}b\bar{b}$ is in principle a little more complicated to integrate than processes with only one pair of b's in the final state. This is due to the presence of identical particles in the final state which implies that each b can be resonating in some diagrams with the first $\bar{b}$ and in others with the second one. This further complicates the subdivision in double resonant contributions, but we have reduced it to the simpler cases just exploiting the symmetries of the problem. This simplification is exact only in the symmetric case. One cannot thus evaluate at present the four b processes with cuts which are not symmetric under the exchange of the two b's or of the two $\bar{b}$'s among themselves. A cut which does not fulfill the above requirement is in any case unphysical.

After every iteration the integration routine readjusts the grid in the space of integration variables, in order to concentrate evaluations of the integrands in those regions where the integrand is larger in magnitude. It is advised to use a first iteration with few points to "thermalize".

Input parameters, flags, etc. The standard input parameters are M_H, M_W, M_Z, M_b, α, α_s. In the tuned comparisons presented in sect 2.8 $\sin^2 \theta_W$ has been given as an input, while it is usually derived from the relation $\sin^2 \theta_W = 1 - M_W^2/M_Z^2$.

The main flag of the program is `ich`, which chooses among different final states. Other flags allow to compute with or without ISR (`isr`), to choose among signal, background and interference (`isig`), and to choose whether or not to use some thermalizing iterations (`iterm`). The number of iterations (`itmx`) and of points per iteration (`ncalls`) for the thermalizing phase as well as for the normal one and the accuracy required (`acc`) are read from the input.

Output. The output is just the standard VEGAS output, from which one can read the final result and estimated statistical error, as well as the result and error for every iteration. Results with big oscillations among different iterations and corresponding big reported χ^2 have to be discarded and simply mean that the number of evaluations per iteration was not sufficient for the integrand.

Concluding remarks. As already stated, WPHACT makes use of matrix elements which are suitable for massive fermion calculations. One may question how big the mass effects are for Higgs physics. Using WPHACT one can verify that they are normally at the percent level. They however depend on the Higgs mass, and expecially on the cuts introduced. These may change the expected dependence, and any set of realistic cuts has to be studied independently with programs which take masses into account.

WPHACT does not make use of any library, has proven to be reliable over a vast range of statistical errors and can compute in short time exact massive processes of interest for Higgs physics at e^+e^- colliders.

2.7   WTO

Program name:	WTO
Author:	G. Passarino – `giampiero@to.infn.it`
Availability:	
Documentation:	

WTO is a *quasi-analytical, deterministic* code for computing observables related to the process $e^+e^- \rightarrow \bar{f}_1 f_2 \bar{f}_3 f_4$. The full matrix elements are used and in the present version the following final states are accessible (see [21] for a general classification):

1. CC3, CC11, CC20

2. NC19, NC24, NC32

3. NC21 (= NC19 + Higgs), NC25 (= NC24 + Higgs)

4. MIX43

Further extensions will be gradually implemented. To fully specify WTO's setup an option must be chosen for the renormalization scheme (RS). One has:

1. the option commonly used for tuned comparisons, i.e.

$$s_w^2 = \frac{\pi\alpha(2M_w)}{\sqrt{2}G_\mu M_w^2}, \qquad g^2 = \frac{4\pi\alpha(2M_w)}{s_w^2} \qquad (2.2)$$

2. or the default,

$$s_w^2 = 1 - \frac{M_w^2}{M_z^2}, \qquad g^2 = 4\sqrt{2}G_\mu M_w^2 \qquad (2.3)$$

where $\alpha^{-1}(2M_w) = 128.07$ and G_μ is the Fermi coupling constant. Final state QCD corrections are not taken into account in the present version, but for the Higgs width. A more complete description of WTO is given in ref. [2].

Among all four-fermion processes included in WTO [2], those of relevance to Higgs physics are:

$$e^+e^- \to \bar{b}b\bar{X}X, \qquad (X = l, q \neq b) \qquad (2.4)$$

The matrix elements are obtained with the helicity method described in [26]. The whole answer is written in terms of invariants, i.e.

$$
\begin{aligned}
e^+(p_+)e^-(p_-) \quad &\to \quad f(q_1)\bar{f}(q_2)f'(q_3)\bar{f}'(q_4), && (2.5) \\
x_{ij}s \quad &= \quad -\left(q_{i-2} + q_{j-2}\right)^2, \quad x_{1i}s = -\left(p_+ + q_{i-2}\right)^2, && (2.6) \\
x_{2i}s \quad &= \quad -\left(p_- + q_{i-2}\right)^2, \quad s_1 s^2 = \epsilon\left(p_+, p_-, q_1, q_2\right), \dots && (2.7)
\end{aligned}
$$

and the integration variables are chosen to be

$$
\begin{aligned}
m_-^2 \quad &= \quad x_{24}, \quad m_+^2 = x_{56}, \quad M_0^2 = x_{45}, \quad m_0^2 = x_{36}, && (2.8) \\
m^2 \quad &= \quad x_{35}, \quad t_1 = x_{13}, \quad t_w = x_{13} + x_{14} && (2.9)
\end{aligned}
$$

The convention for the final states in WTO is: $e^+e^- \to 1 + 2 + 3 + 4$. For CC processes $1 = d, 2 = \bar{u}, 3 = u', 4 = \bar{d}'$, with $u = \nu, u, c$ and $d = l, d, s, b$. For NC processes the adopted convention is $1 = f, 2 = \bar{f}, 3 = f'$ and $4 = \bar{f}'$. Initial state QED radiation is included through the Structure Function approach up to $O(\alpha^2)$. The code will return results according to three (pre-selected) options, i.e $\beta^2\eta$ (default) [22], β^3 [23] and $\beta\eta^2$ [24] where

$$\beta = 2\frac{\alpha}{\pi}\left(\log\frac{s}{m_e^2} - 1\right), \qquad \eta = 2\frac{\alpha}{\pi}\log\frac{s}{m_e^2} \qquad (2.10)$$

When initial state QED radiation is included there are two additional integrations over the fractions of the beam energies lost through radiation, $x_\pm$. This description of the phase space gives full cuts-availability through an analytical control of the boundaries of the phase space. Upon specification of the input flags it is therefore possible to cut on all final state invariant masses, all (LAB) final state energies $E_i, i = 1, 4$, all (LAB) scattering angles, $\theta_i, i = 1, 4$, all (LAB) final state angles, $\psi_{ij}, i, j = 1, 4$. Both the matrix elements and the phase space are given for massless fermions. There is no interface with hadronization. The integration is performed

with the help of the NAG routine D01GCF. This routine uses the Korobov-Conroy number theoretic approach with a MC error estimate arising from converting the number theoretic formula for the n-cube $[0,1]^n$ into a stochastic integration rule. This allows a 'standard error' to be estimated. Prior to a call to D01GCF the peak structure of the integrand is treated with the appropriate mappings. The typical process considered belong to the NC21 or NC25 classes. In WTO both the phase space and the matrix elements are written for massless fermions, thus there is no interference between the Higgs signal and the background, making particularly easy to include the Higgs boson. The pole quark masses are specified in a DATA BLOCK as $m_q(m_q^2)$ and the code will convert them internally into running masses, i.e. $m_q(m_H^2)$. Whenever needed the input parameter $\alpha_s(M_W)$ is also converted into $\alpha_s(m_H^2)$. The obtained $m_q(m_q^2)$ are then used to generate the couplings $H \to \bar{q}q$. The Higgs width is computed as $\Gamma_H = \Gamma(H \to \tau^+\tau^-, \bar{c}c, \bar{b}b, gg)$ and upon proper initialization of the corresponding flag final state QCD corrections are applied.

Numerical input parameters such as $\alpha(0), G_\mu, M_z, M_w, \ldots$ are stored in a BLOCK DATA. There are various flags to be initialized to run WTO. Here follows a short description of the most important ones:

NPTS   - INTEGER, NPTS=1,10 chooses the actual number of points for applying the Korobov-Conroy number theoretic formulas. The built-in choices correspond to to a number of actual points ranging from 2129 up to 5,931,551.

NRAND   - INTEGER, NRAND specifies the number of random samples to be generated in the error estimation (usually $5 - 6$).

OXCM   - CHARACTER*1, the main decision branch for the process: [C(N)] for CC,(NC) [21].

OTYPEM - CHARACTER*4,Specifies the process, i.e. CC3, CC11, CC20 for CC processes and NC19, NC24, NC21, NC25, NC32 for NC processes.

IOS   - INTEGER, two options [1,2] (1 =default for tuned comparisons) for the RS.

IOSF   - INTEGER, three options $[1-3]$ for the $\eta - \beta$ choice in the structure functions.

CHDM... - REAL, Electric charges, third component of isospin for the final states.

WTO is a robust one call - one result code, thus in the output one gets a list of all relevant input parameters plus the result of the requested observable with an estimate of the numerical error. A very rough estimate of the theoretical error (very subjective to say the least) can be obtained by repeating runs with different IOS, IOSF options. After the following initialization:

```
7 6                      !  NPTS NRAND
175.d0                   !  E_CM OF PROCESS
n                        !  NC PROCESS
```

19

```
nc25                    ! CLASS = NC25
l                       ! MU
65.d0                   ! M_H(GEV)
0.12d0                  ! ALPHA_S(M_W)
y                       ! FS QCD
y                       ! H --> GG INCLUDED
1 1                     ! IOS IOSF
hc                      ! BUILT-IN CHOICE OF CUTS
hl                      !                         "
-1.d0 -0.33333333333d0  ! CHARGES: F=MU, FP=B
-0.5d0 -0.5d0           ! ISOSPINS
1.d0 3.d0               ! COLOR FACTORS
```

corresponding to the process for $e^+e^- \to \mu^+\mu^-\bar{b}b$ with $M_z - 25\,\mathrm{GeV} < M_{\nu\nu} < M_z + 25$ GeV, $M_{\bar{b}b} > 50$ GeV, the typical output will look as follows:

```
This run is with:

NPTS          =   7
NRAND         =   6

E_cm (GeV) =            0.17500E+03
beta       =            0.11376E+00 sin^2       =            0.23103E+00
M_W  (GeV) =            0.80230E+02 M_Z (GeV) =               0.91189E+02
G_W  (GeV) =            0.20337E+01 G_Z (GeV) =               0.24974E+01
M_H  (GeV) =            0.65000E+02 G_H (MeV) =               0.15865E+01

m_b(M_H) (GeV) =          0.29168E+01
m_c(M_H) (GeV) =          0.64862E+00
alpha_s(M_H)   =          0.12402E+00

nc25-diagrams : charges    -1.0000    -0.3333
                isospin     -0.5000    -0.5000

On exit IFAIL = 0 - Cross-Section

CPU time  28 min  37 sec, sec per call  =  0.286E-02
# of calls      =      599946

(Signal) sigma  =  0.2766804E-01   +-              0.1188170E-04
```

Rel. error of   0.043 %

2.8   Comparisons among the programs

In this section we present some "tuned" comparisons between semianalytical/deterministic and Monte Carlo codes for Higgs searches. In the case of SM Higgs production, we will consider the following processes:

$$
\begin{aligned}
e^+ e^- &\rightarrow b\bar{b}\mu^+\mu^- \\
e^+ e^- &\rightarrow b\bar{b}\nu_\mu\bar{\nu}_\mu \\
e^+ e^- &\rightarrow b\bar{b}\nu_e\bar{\nu}_e.
\end{aligned}
$$

(2.11)

The selection criteria adopted involve only invariant-mass cuts, in order to allow also some semianalytical approaches to appear in the comparisons. These cuts are: $M_Z - 25$ GeV $\leq m_{l\bar{l}} \leq M_Z + 25$ GeV; $m_{b\bar{b}} \geq 50$ GeV. Cross section values for different beam energies and different Higgs masses are given in Tables 1 – 12. As a reference, the last column of each Table contains the cross sections in absence of Higgs signal (pure 4-fermion background). The results[1] of the pure non-Higgs channels obtained by the EXCALIBUR [2] and FERMISV[1] [27] code are also shown. The input parameters used in these Tables are the *STANDARD LEP2 INPUT* [2]. The only exception is the choice of fermion masses. Since the $H \rightarrow f\bar{f}$ coupling constant is proportional to m_f, the choice adopted here [1] is to use running fermion masses $m_f = m_f(Q^2 = m_H^2)$ in the Higgs-boson coupling [1]. The codes which can evaluate massive amplitudes (CompHEP, GENTLE/4fan and WPHACT), adopt however different prescriptions for the choice of the b mass appearing in the phase space and in the matrix elements. For example, WPHACT can fix this to be the pole mass, while GENTLE/4fan adopts the same value used for the coupling to the Higgs. The suffix added to the results of the CompHEP and WPHACT programs refers to the value of the b quark mass used in the evaluation of the *production* matrix elements. The effect of the complete inclusion of b-masses in the matrix elements is clearly visible from the Tables, although it never exceeds the % level.

Few comments on the results are in order. With the exception of HZHA, which does not include the full set of SM background diagrams, the agreement between the Higgs codes presented in the Tables is systematically at the level of 1% or better. The exceptions are the processes with $\nu_e\bar{\nu}_e$ in the final state, where CompHEP differs by approximately 2% from the other codes (see Table 5 and 6). Notice that this is the channel where the difference between having and not having the full set of SM diagrams is potentially the largest, as indicated by the results of HZHA, which can differ from the other codes by up to 20%. While discrepancies at the % level are of the order of the net uncertainty coming from higher order corrections, it is clear that they should be studied further in order to make any future full NLO result meaningful. At the same time, it is important to point out that the impact of the discrepancies

---

[1] The numbers for FERMISV were kindly generated by P. Janot.

21

we found on the discovery potential of LEP2 is minimal. Whether these differences could affect the extraction of Higgs properties after its discovery at LEP2 is an interesting question, which however will require further work to be answered.

m_H (GeV)	65	90	115	∞
CompHEP$_0$	32.487(63)	1.593(03)	1.059(02)	1.059(02)
CompHEP$_{4.7}$	32.474(63)	1.578(03)	1.046(02)	1.046(02)
EXCALIBUR	—	—	—	1.0594(03)
FERMISV	—	—	—	0.931(22)
GENTLE/4fan	32.7148(33)	1.59930(16)	1.05949(11)	1.05944(11)
HIGGSPV	32.714(27)	1.607(08)	1.060(02)	1.049(07)
HZHA	32.435(33)	1.570(33)	1.056(33)	1.056(33)
WPHACT$_{4.7}$	32.5604(66)	1.58552(62)	1.04684(56)	1.04679(55)
WPHACT$_0$	32.7141(68)	1.59946(64)	1.05953(56)	1.05948(56)
WTO	32.7268(51)	1.5980(13)	1.0582(12)	1.0581(12)

Table 1: $\sigma(e^+e^- \rightarrow \mu^+\mu^-b\bar{b})$ (fb) at $E_{cm} = 175$ GeV. No ISR.

Only one of the codes presented here (HZHA) allows the generation of SUSY Higgs bosons. We present a set of cross sections for the $e^+e^- \rightarrow b\bar{b}b\bar{b}$ final state for the four cases relative to the following choice of parameters [1]:

(1) $m_A = 75$ GeV , $\tan\beta = 30$;
(2) $m_A = 400$ GeV , $\tan\beta = 30$;
(3) $m_A = 75$ GeV , $\tan\beta = 1.75$;
(4) $m_A = 400$ GeV , $\tan\beta = 1.75$.

The SM input parameters are the same as for the previous comparisons, and all the $b\bar{b}$ pairs are required to have $m_{b\bar{b}} \geq 20$ GeV. The results are shown in Tables 13 – 16. The only comparison possible between the results of HZHA and those of other codes is for the SM backgrounds. For these we present, when available, the separate contribution coming from the purely EW diagrams. The $\mathcal{O}(\alpha_s\alpha)$ QCD background processes, induced by gluon splitting diagrams, have been evaluated using the exact tree level matrix elements in the case of the EXCALIBUR and WPHACT. HZHA can evaluate these processes only in the parton shower approximation. Since this approach gives a very low generation efficiency, the results have a large statistical error. Although consistent with the exact tree level results, the EW+QCD results from HZHA have therefore not been included in the Tables.

m_H (GeV)	65	90	115	∞
CompHEP$_0$	37.264(58)	24.395(46)	10.696(13)	10.634(13)
CompHEP$_{4.7}$	37.147(58)	24.279(46)	10.580(13)	10.518(13)
EXCALIBUR	—	—	—	10.6398(15)
FERMISV	—	—	—	9.49(23)
GENTLE/4fan	37.3975(37)	24.4727(25)	10.7022(11)	10.6401(11)
HIGGSPV	37.393(27)	24.490(21)	10.694(16)	10.65(05)
HZHA	36.79(13)	23.53(13)	10.28(13)	10.22(13)
WPHACT$_{4.7}$	37.1634(64)	24.3245(40)	10.5863(24)	10.5243(24)
WPHACT$_0$	37.3990(64)	24.4727(40)	10.7027(24)	10.6407(24)
WTO	37.4099(32)	24.4765(42)	10.7036(21)	10.6416(21)

Table 2: $\sigma(e^+e^- \to \mu^+\mu^- b\bar{b})$ (fb) at $E_{cm} = 192$ GeV. No ISR.

m_H (GeV)	65	90	115	∞
CompHEP$_0$	64.14(15)	2.341(07)	1.279(04)	1.279(04)
CompHEP$_{4.7}$	64.12(15)	2.325(07)	1.263(04)	1.263(04)
EXCALIBUR	—	—	—	1.2916(04)
FERMISV	—	—	—	1.195(26)
GENTLE/4fan	64.2407(64)	2.36582(24)	1.29239(13)	1.29229(13)
HIGGSPV	64.199(60)	2.375(19)	1.293(09)	1.286(14)
HZHA	63.99(02)	2.258(18)	1.230(18)	1.230(18)
WPHACT$_{4.7}$	63.941(14)	2.3473(10)	1.27611(80)	1.27601(80)
WPHACT$_0$	64.238(14)	2.3661(10)	1.29237(82)	1.29227(82)
WTO	64.262(11)	2.36583(93)	1.29210(92)	1.2950(20)

Table 3: $\sigma(e^+e^- \to \nu_\mu\bar{\nu}_\mu b\bar{b})$ (fb) at $E_{cm} = 175$ GeV. No ISR.

23

m_H (GeV)	65	90	115	∞
CompHEP$_0$	72.64(19)	47.02(14)	19.76(08)	19.62(07)
CompHEP$_{4.7}$	72.41(19)	46.79(14)	19.53(08)	19.41(07)
EXCALIBUR	—	—	—	19.7131(40)
FERMISV	—	—	—	18.57(62)
GENTLE/4fan	72.9256(73)	47.2239(47)	19.8405(20)	19.7171(20)
HIGGSPV	72.867(63)	47.225(50)	19.786(42)	19.67(06)
HZHA	72.83(21)	46.31(21)	19.82(21)	19.71(21)
WPHACT$_{4.7}$	72.475(16)	46.944(12)	19.625(11)	19.502(10)
WPHACT$_0$	72.927(16)	47.222(12)	19.841(11)	19.717(11)
WTO	72.961(11)	47.2341(40)	19.8394(14)	19.7200(70)

Table 4: $\sigma(e^+e^- \to \nu_\mu \bar{\nu}_\mu b\bar{b})$ (fb) at $E_{cm} = 192$ GeV. No ISR.

m_H (GeV)	65	90	115	∞
CompHEP$_0$	70.26(20)	5.03(02)	1.073(04)	1.073(04)
CompHEP$_{4.7}$	70.24(20)	5.02(02)	1.059(04)	1.059(04)
EXCALIBUR	—	—	—	1.0796(03)
FERMISV	—	—	—	1.195(26)
HIGGSPV	71.727(34)	5.100(05)	1.081(01)	1.077(06)
HZHA	69.98(18)	3.572(18)	1.230(18)	1.230(18)
WPHACT$_{4.7}$	71.366(26)	5.0762(22)	1.06615(87)	1.06602(87)
WPHACT$_0$	71.694(27)	5.0996(23)	1.08027(89)	1.08013(89)
WTO	71.679(14)	5.0997(15)	1.07978(81)	1.0820(20)

Table 5: $\sigma(e^+e^- \to \nu_e \bar{\nu}_e b\bar{b})$ (fb) at $E_{cm} = 175$ GeV. No ISR.

24

m_H (GeV)	65	90	115	∞
CompHEP$_0$	79.01(24)	52.37(18)	20.82(08)	19.89(07)
CompHEP$_{4.7}$	78.79(24)	52.15(18)	20.60(08)	19.67(07)
EXCALIBUR	—	—	—	19.9463(44)
FERMISV	—	—	—	18.57(62)
HIGGSPV	80.628(32)	53.353(21)	20.907(13)	19.95(10)
HZHA	80.99(21)	49.80(21)	20.26(21)	19.71(21)
WPHACT$_{4.7}$	80.122(34)	53.039(19)	20.673(12)	19.736(12)
WPHACT$_0$	80.611(34)	53.335(19)	20.893(12)	19.955(10)
WTO	80.629(32)	53.3468(63)	20.8883(15)	19.9540(50)

Table 6: $\sigma(e^+e^- \to \nu_e \bar{\nu}_e b \bar{b})$ (fb) at $E_{cm} = 192$ GeV. No ISR.

m_H (GeV)	65	90	115	∞
EXCALIBUR	—	—	—	0.8256(04)
FERMISV	—	—	—	0.745(19)
GENTLE/4fan	28.4273(28)	1.22507(12)	0.824890(82)	0.824849(82)
HIGGSPV	28.437(14)	1.224(02)	0.8248(06)	0.817(06)
HZHA	28.317(27)	1.252(27)	0.860(27)	0.860(27)
WPHACT$_{4.7}$	28.305(17)	1.21406(85)	0.81492(81)	0.81489(81)
WPHACT$_0$	28.437(17)	1.22479(70)	0.82472(65)	0.82468(65)
WTO	28.456(12)	1.2241(16)	0.8232(15)	0.8232(15)

Table 7: $\sigma(e^+e^- \to \mu^+\mu^- b\bar{b})$ (fb) at $E_{cm} = 175$ GeV. ISR included.

m_H (GeV)	65	90	115	∞
EXCALIBUR	—	—	—	8.4306(29)
FERMISV	—	—	—	7.90(27)
GENTLE/4fan	33.7575(34)	19.4717(19)	8.47729(85)	8.43290(84)
HIGGSPV	33.759(12)	19.480(09)	8.483(05)	8.44(05)
HZHA	33.48(11)	18.91(11)	8.31(11)	8.27(11)
WPHACT$_{4.7}$	33.547(15)	19.3515(90)	8.3842(56)	8.3400(56)
WPHACT$_0$	33.752(16)	19.4692(91)	8.4767(57)	8.4324(57)
WTO	33.777(10)	19.4856(83)	8.4851(78)	8.4409(78)

Table 8: $\sigma(e^+e^- \to \mu^+\mu^- b\bar{b})$ (fb) at $E_{cm} = 192$ GeV. ISR included.

m_H (GeV)	65	90	115	∞
EXCALIBUR	—	—	—	0.9900(05)
FERMISV	—	—	—	0.928(23)
GENTLE/4fan	55.9190(56)	1.78649(18)	0.990681(99)	0.990600(10)
HIGGSPV	55.899(29)	1.786(05)	0.991(02)	0.991(12)
HZHA	55.863(14)	1.733(14)	0.949(14)	0.949(14)
WPHACT$_{4.7}$	55.644(34)	1.77146(97)	0.97777(83)	0.97770(83)
WPHACT$_0$	55.901(34)	1.7858(10)	0.99028(84)	0.99021(84)
WTO	55.947(27)	1.7857(14)	0.9894(13)	0.9893(13)

Table 9: $\sigma(e^+e^- \to \nu_\mu \bar{\nu}_\mu b\bar{b})$ (fb) at $E_{cm} = 175$ GeV. ISR included.

m_H (GeV)	65	90	115	∞
EXCALIBUR	—	—	—	15.5420(64)
FERMISV	—	—	—	15.14(56)
GENTLE/4fan	65.9061(66)	37.4957(37)	15.6302(16)	15.5421(16)
HIGGSPV	65.895(27)	37.504(20)	15.629(13)	15.51(06)
HZHA	65.60(14)	36.45(14)	15.25(14)	15.17(14)
WPHACT$_{4.7}$	65.500(31)	37.270(18)	15.460(12)	15.372(12)
WPHACT$_0$	65.894(31)	37.491(18)	15.631(12)	15.543(12)
WTO	65.922(27)	37.5201(96)	15.6356(50)	15.5474(50)

Table 10: $\sigma(e^+e^- \to \nu_\mu\bar{\nu}_\mu b\bar{b})$ (fb) at $E_{cm} = 192$ GeV. ISR included.

m_H (GeV)	65	90	115	∞
EXCALIBUR	—	—	—	0.8382(05)
FERMISV	—	—	—	0.928(23)
HIGGSPV	62.917(35)	3.903(04)	0.8398(04)	0.844(05)
HZHA	60.96(14)	2.753(14)	0.949(14)	0.949(14)
WPHACT$_{4.7}$	62.589(32)	3.8858(25)	0.82761(65)	0.82751(65)
WPHACT$_0$	62.876(32)	3.9037(25)	0.83849(66)	0.83838(66)
WTO	62.905(65)	3.9056(40)	0.8381(13)	0.8379(13)

Table 11: $\sigma(e^+e^- \to \nu_e\bar{\nu}_e b\bar{b})$ (fb) at $E_{cm} = 175$ GeV. ISR included.

m_H (GeV)	65	90	115	∞
EXCALIBUR	—	—	—	15.5974(69)
FERMISV	—	—	—	15.14(56)
HIGGSPV	73.051(34)	42.682(21)	16.275(12)	15.78(09)
HZHA	72.85(14)	39.35(14)	15.56(14)	15.17(14)
WPHACT$_{4.7}$	72.595(39)	42.439(20)	16.095(13)	15.418(13)
WPHACT$_0$	73.022(39)	42.673(20)	16.268(13)	15.590(13)
WTO	73.003(44)	42.701(17)	16.2675(58)	15.5897(58)

Table 12: $\sigma(e^+e^- \to \nu_e\bar{\nu}_e b\bar{b})$ (fb) at $E_{cm} = 192$ GeV. ISR included.

	(1)	(2)	(3)	(4)	EW	EW+QCD
EXCALIBUR	—	—	—	—	—	6.859(04)
HZHA	90.71(46)	2.902(19)	158.09(79)	4.632(54)	2.760(17)	—
WPHACT$_0$	—	—	—	—	2.580(2)	6.8589(87)
WPHACT$_{4.7}$	—	—	—	—	—	7.1764(84)

Table 13: $\sigma(e^+e^- \to b\bar{b}b\bar{b})$ (fb) at $E_{cm} = 175$ GeV. No ISR. See the text for the meaning of the labels (1) – (4). The last two columns refer to the SM background results, separated in pure EW and full EW+QCD processes.

	(1)	(2)	(3)	(4)	EW	EW+QCD
EXCALIBUR	—	—	—	—	—	25.933(10)
HZHA	135.17(61)	23.286(58)	163.36(75)	74.04(31)	22.816(50)	—
WPHACT$_0$	—	—	—	—	21.897(16)	25.916(18)
WPHACT$_{4.7}$	—	—	—	—	—	25.946(23)

Table 14: $\sigma(e^+e^- \to b\bar{b}b\bar{b})$ (fb) at $E_{cm} = 192$ GeV. No ISR. See comments in the previous figure caption.

	(1)	(2)	(3)	(4)	EW	EW+QCD
EXCALIBUR	—	—	—	—	—	8.490(20)
HZHA	76.74(39)	2.513(20)	140.20(71)	3.903(48)	2.397(18)	—
WPHACT$_0$	—	—	—	—	2.239(2)	8.447(22)
WPHACT$_{4.7}$	—	—	—	—	—	8.993(21)

Table 15: $\sigma(e^+e^- \to b\bar{b}b\bar{b})$ (fb) at $E_{cm} = 175$ GeV. ISR included. See previous figure caption for comments.

	(1)	(2)	(3)	(4)	EW	EW+QCD
EXCALIBUR	—	—	—	—	—	23.045(23)
HZHA	118.60(58)	18.761(87)	151.75(75)	57.74(28)	18.384(80)	—
WPHACT$_0$	—	—	—	—	17.482(14)	22.991(34)
WPHACT$_{4.7}$	—	—	—	—	—	23.258(37)

Table 16: $\sigma(e^+e^- \to b\bar{b}b\bar{b})$ (fb) at $E_{cm} = 192$ GeV. ISR included. See previous figure caption for comments.

3   Supersymmetry

Supersymmetry [28] is considered to be the most likely candidate for new physics within the reach of LEP2 [5]. We assume here that the reader is familiar with the basics of SUSY and with its most common parameters, and we refer to the review articles in ref. [28] or to the New Physics report [5] for definitions and details. A large body of work has been devoted in the past 10 years to the development of event generators for the simulation of SUSY signals. Due to the large interest in the subject, the number of computer programs which calculate cross sections or generate events is very large; however most of these codes have not been designed for distribution, and are not documented here. We will limit ourselves to present codes which have either been developed during the Workshop, or which have been discussed and used within the activity of the New Physics Working group. All of these codes are either already public, or will soon become.

The main difference between SUSY generators for LEP1 and for LEP2 is related to the significant rôle played at LEP2 by t-channel exchange diagrams, which are almost totally negligible at the Z peak. As a typical example, consider the chargino pair production. This can proceed via s-channel γ-Z production, or via t-channel exchange of the electron scalar-neutrino ($\tilde{\nu}_{ee}$). The interference is always destructive, and can significantly reduce the production cross section if the sneutrino mass is in the 50–100 GeV region. Another example, documented in the New Physics section of this report [5], is that of the scalar electron production, where the t-channel exchange of a neutralino can either decrease or increase the rates.

Alhtough documented only in part in this report, extensive cross checks among the different codes used by the experimental groups have been performed. These checks included the study of the proper inclusion of t-channel diagrams, of the dependence of cross sections on the parameters of the models, as well as studies of kinematical distributions and of the effects of the initial state radiation (ISR). Comparisons of decay branching ratios(BR) for unstable particles have also been performed. All tests have been pursued until agreement at the percent level was achieved.

In most SUSY generators, the emphasis is placed on covering as many processes as possible

in a unified framework. By doing so, the simplest approaches have often been pursued. For example, it is generally assumed that production and decay of SUSY states can be factorized, therefore neglecting possible initial–final state spin correlations. This choice is forced upon us by the multitude of possible decays which each SUSY particle has allowed as soon as the parameters of the theory are slightly changed. Each decay channel would in principle call for a new evaluation of matrix elements with many-body final states, including the interference with SM processes and possibly with other SUSY channels. The multitude of channels to be considered for a generic point in parameter space is such that a thorough evaluation of the full matrix elements for all SUSY particles has never been carried out, and finds no place in any multi-purpose SUSY event generator. In order to assess the limit of this approach, several groups have started working on more specific channels, where the structure of the final state is better determined and where full calculations can be performed and compared to the simpler results. We will report here on one such development, namely the construction of an event generator for chargino production and decay which is based on the evaluation of the full matrix elements.

Another important feature of SUSY event generators is the possibility to impose or relax sets of assumptions or constraints on the parameters of the model. Several theoretical frameworks (*e.g.* Minimal Supergravity) predict relations between some of free SUSY parameters, and allow to produce more specific predictions than otherwise possible. At the same time, it is however important to be able to free themselves from relations which could artificially constrain rates or properties of a given process, in order to make the experimental searches as unbiased as possible. The following documentation will describe to which extent the available codes provide such handles.

3.1 SUSYGEN

Program name:	SUSYGEN
Authors:	S. Katsanevas – `katsanevas@vxcern.cern.ch`
	S. Melachroinos – `melachr@vxcern.cern.ch`
Availability:	`vxcern::disk$delphi:[katsanevas.susygen]`
	Files `susygen.for` and `susygen.com`
Documentation:	vxcern::disk$delphi:[katsanevas.susygen]susygen_manual.ps

SUSYGEN is a Monte Carlo generator for the production and decay of all (R-Parity odd) MSSM sparticles in e^+e^- colliders. It is flexible enough that the user can assume or relax different theoretical constraints, and it is easily generalizable to extensions of the MSSM such as the Next to Minimal Supersymmetric Standard Model (NMSSM) or R-Parity violating processes [2]. In particular, R-Parity violating decays [33] of the $\tilde{\chi}_1^0$ (assumed to be the lightest supersymmetric particle) can be selected by the user through data cards. Each of the possible

---

[2]The parts of the code relative to Higgs and radiative decays of neutralinos and charginos were kindly provided by S. Ambrosanio. Those relative to R-Parity violation interactions by H. Dreiner.

45 R-parity violating operators described in the New Physics Chapter of this Report is allowed. The input parameters specifying the SUSY model are chosen to be:

1. m_0, the common mass of the spin 0 squarks and sleptons, at the GUT scale.

2. M_2, the SU(2) gaugino mass parameter at the EW scale.

3. μ, the mixing parameter of the Higgs doublets at the EW scale,

4. $\tan\beta$, the ratio of the vacuum expectation values of the two Higgs doublets.

5. A, the trilinear coupling in the Higgs sector. This is used only for the calculation of the third generation mixing.

6. and m_A, the mass of the pseudoscal Higgs. This is used only for the calculation of the Higgs spectrum.

Initial state radiation and an interface to JETSET [16] are included.

The production and decay matrix elements are taken from ref. [31]. Direct production of R-even MSSM particles, namely the neutral and charged Higgs bosons h, H, A and H$^\pm$, will be included in the next version of the program.

Production and decay of unstable SUSY particles are factorized, and therefore full initial/final state spin correlations are not included. Nevertheless 2- and 3-body decays are generated using the complete matrix elements, including contributions from all possible bosonic and fermionic intermediate states. Decays to Higgs bosons and radiative decays of neutralinos and charginos are included as well [32]. Since all unstable SUSY particles are decayed before the call to JETSET, $\tilde{t}$ hadronization is not included.

SUSYGEN has been tested extensively and found to agree within 1% with ISAJET (see next Section) in what concerns the production cross sections, and to agree with the production and decay branching ratios generated by the code of the authors of ref. [32]. The code and complete documentation, including a detailed list of cross section formulae and sample outputs from the code, can be found in `vxcern::disk$delphi:[katsanevas.susygen]` in the files `susygen.for`, `susygen.com` and `susygen_manual.ps`.

Decays Some detail on the treatment of SUSY particle decays in SUSYGEN is given here. For the decays of the $\tilde{\chi}^0$'s and $\tilde{\chi}^\pm$'s one can in general distinguish two regimes. If all scalar masses are very large, or the fermions are mostly gauginos, the decay occurs through an off-shell W or Z boson, e.g. $\tilde{\chi}_1^\pm \rightarrow W^{*\pm}\tilde{\chi}_1^0$ or $\tilde{\chi}_2^0 \rightarrow Z^*\tilde{\chi}_1^0$ and $\tilde{\chi}_2^0 \rightarrow W^\mp \tilde{\chi}_1^\pm$. In this case the BR's to the different final state leptons or quarks are mostly determined from those of the off-shell Z and W. If instead the SUSY fermions are mostly charginos, and some scalar lepton and/or quark has mass comparable to the masses of W and Z, decays mediated by the virtual scalars can dominate, and the BR's to the corresponding fermions can be enhanced. Since it is assumed that $\tilde{\chi}_1^0$ is the LSP, only two-body prompt decays of scalar particles are considered. Should

other charginos or neutralinos be lighter than a given scalar, cascade decays through them are included.

SUSYGEN does not distinguish between three-body and two-body decays (when e.g the decay to an on-shell scalar is posssible) since it includes the widths of the scalars in the propagators and therefore lets the propagators force the two-body kinematics, including all possible interferences. There is a small region where the decays to Higgses or the radiative decays dominate: these rare decays are included in the list of possible decays. They can be studied separately by setting the other branching ratios to zero through the data card DECSEL. The masses of the Higgses are calculated by using two-loop evolution equations [14].

Program structure. SUSYGEN is divided in three stages. In the first stage the subroutine SCARDS reads the steering cards and the subroutine SBOOK books some standard histograms. The standard histograms in the case of the SCAN option are: the masses, cross-sections and decay branching ratios in 2-d histograms of μ versus M. In the case of the no-SCAN option, the $\cos\theta$ distribution of the produced objects are reproduced.

In the second stage the routine SUSANA initializes the masses and the branching ratios of MSSM sparticles. The masses of sleptons and squarks are evaluated by assuming a common m_0 mass at GUT unification and running it down to electroweak scales through Renormalization Group Equations (RGE's). Chargino and neutralino masses and mixings are evaluated through the diagonalization of the gaugino and Higgsino mass matrices [31].

The double differential cross sections $\frac{d\sigma}{dsdt}$ have been integrated analytically over t, and then integrated numerically over s inside the subroutine BRANCH. Subroutine INTERF stores the results for further generation. Particle codes are assigned by default their LUND values, while the naming used by ISAJET 7.03 [34] has been retained for comparison purposes.

The third stage calculates the cross sections and generates the sparticles requested by the user via data cards. The cross sections are computed from the functions: CHARGI (production cross section for $\tilde{\chi}^{\pm}$), PHOTI (production cross section for all $\tilde{\chi}^0$), GENSEL (production cross section for $\tilde{e}$), GENSELR (production cross sections for $\tilde{e_L}, \tilde{e_R}$), GENSMUS (production cross section for $\tilde{\mu}, \tilde{\tau}, \tilde{q}$), GENSNUE (production cross section for $\tilde{\nu}_{ee}$), GENSNU (production cross section for $\tilde{\nu}_e$). The user can also select through cards the luminosity available, so after this stage the number of events to be generated is calculated.

Unweigthed events generated according to the appropriate $\cos\theta$ distribution are produced by the routine SUSYEVE. Subroutine DECABR using the tabulated branching ratios determines the branching ratio of the decay. SMBOD2 and SMBOD3 generate the 4-vectors of the decay products at each decay vertex. The program loops till DECABR indicates there is no other possible decay. When the RPARITY card is TRUE the above condition is fulfilled when we have the lowest lying neutralino and standard particles in the products. When RPARITY is FALSE routine LSPDECAY is called and the neutralino decays to the prescribed standard particles. The above 4-vectors are interfaced to LUND in subroutine SFRAGMENT where they fragment and decay.

32

The last subroutines of MSSMGENE are SXWRLU which writes the LUND common block to an external file (unit 12) and a small routine USER gives access to the LUND common after generation. The subroutine SUSEND closes the program, and stores the standard histograms to the file SUSYGEN.HIST. SUSYGEN uses routines from the libraries `jetset74, packlib` and `genlib` and it has therefore to be linked to them.

3.2 ISAJET

Program name:	ISAJET 7.16
Authors:	H. Baer – `baer@fsuhep.physics.fsu.edu`
	F. Paige, `paige@bnlux1.bnl.gov"`
	S. Protopopescu `serban@bnlux1.bnl.gov"`
	X. Tata `tata@uhhepj.phys.hawaii.edu"`
Availability:	Patchy source file via anonymous ftp from
	`bnlux1.bnl.gov:pub/isajet`.
	Files: `isajet.car, makefile.unix` (UNIX) and `isamake.com` (VMS)
Documentation:	ISAJET.DOC can be extracted from isajet.car
	via makefile.unix or isamake.com

The program ISAJET [34], originally developed to generate events for hadron colliders, can also be used for event generation at e^+e^- machines. In particular, the latest version, ISAJET 7.15, contains the following SM $2 \rightarrow 2$ subprocesses

$$
\begin{aligned}
e^+e^- &\rightarrow f\bar{f}, \\
e^+e^- &\rightarrow WW, \\
e^+e^- &\rightarrow ZZ,
\end{aligned}
$$

where $f = e, \mu, \tau, \nu_e, \nu_\mu, \nu_\tau, u, d, s, c, b$ and t. ISAJET includes the Fox-Wolfram final state shower QCD radiation [35] and Field-Feynman hadronization [36]. Spin correlations for the $e^+e^- \rightarrow WW$ and ZZ processes are currently neglected, as is initial state photon radiation. ISAJET 7.15 does contain the capability to generate events assuming longitudinally polarized e^+ or e^- beams, although this option may mainly be of interest to linear e^+e^- collider enthusiasts.

ISAJET also contains a large amount of code relevant for Supersymmetry. Currently, one may input into ISAJET either MSSMi or SUGRA keywords, corresponding to two different parameter sets. For MSSM parameters, the inputs are:

$$
\begin{aligned}
MSSM1: \quad & m_{\tilde{g}}, \ m_{\tilde{q}}, \ m_{\tilde{\ell}_L}, \ m_{\tilde{\ell}_R}, \ m_{\tilde{\nu}}, \\
MSSM2: \quad & m_{\tilde{t}_L}, \ m_{\tilde{t}_R}, \ A_t, \ m_{\tilde{b}_R}, \ A_b, \\
MSSM3: \quad & \tan\beta, \ \mu, \ m_A.
\end{aligned}
$$

The various sparticle masses and mixings are then calculated, as well as sparticle decay modes and branching fractions. GUT scale gaugino mass unification is assumed, as is the degeneracy of the first two generations of squarks, and the first three generations of sleptons (although intra-generational slepton splitting is maintained). A complete set of Higgs boson mass and coupling radiative corrections (evaluated in the one-loop effective potential) are included, as well as all Higgs decay modes to particles and sparticles [37]. An independent program ISASUSY can be extracted from ISAJET which yields a hard copy of the various sparticle masses, parameters and decay branching fractions.

ISAJET also can generate a sparticle spectrum given the parameter set of the minimal supergravity (SUGRA) GUT model with radiative electroweak symmetry breaking [38]. In this case, the input parameters are:

$$SUGRA: \ m_0, \ m_{1/2}, \ A_0, \ \tan\beta, \ sgn(\mu).$$

The top mass m_t also needs to be specified. ISAJET will then calculate sparticle masses by evolving 26 renormalization group equations between the weak scale and GUT scale, in an iterative procedure, using Runge-Kutta method. Gauge coupling unification is imposed, but not Yukawa unification. Weak scale sparticle threshold effects are included in the gauge coupling evolution. Two loop RGE's are used for gauge and Yukawa evolution, while one-loop RGE's are used for the other soft-breaking parameters. In the end, radiative electroweak symmetry breaking is imposed, using the one-loop corrected effective potential. A full set of radiative corrections are included for the Higgs boson masses and couplings. In addition, the running gluino mass is converted to a pole gluino mass. An independent program ISASUGRA can be extracted from ISAJET which yields a hard copy of the resultant sparticle masses, parameters and decay branching fractions.

All lowest order $2 \rightarrow 2$ sparticle and Higgs boson production mechanisms have been incorporated into ISAJET. These include the following processes [39] (neglecting bars over anti-particles):

$$
\begin{aligned}
e^+e^- &\rightarrow \tilde{q}_L\tilde{q}_L, \ \tilde{q}_R\tilde{q}_R, \\
e^+e^- &\rightarrow \tilde{\ell}_L\tilde{\ell}_L, \ \tilde{\ell}_R\tilde{\ell}_R, \ \tilde{e}_L\tilde{e}_R, \\
e^+e^- &\rightarrow \tilde{\nu}_\ell\tilde{\nu}_\ell, \\
e^+e^- &\rightarrow \tilde{\chi}_1^\pm\tilde{\chi}_1^\mp, \ \tilde{\chi}_2^\pm\tilde{\chi}_2^\mp, \ \tilde{\chi}_1^\pm\tilde{\chi}_2^\mp, \\
e^+e^- &\rightarrow \tilde{\chi}_i^0\tilde{\chi}_j^0, \ (i,j = 1-4), \\
e^+e^- &\rightarrow Zh, \ ZH, \ Ah, \ AH, \ H^+H^-.
\end{aligned}
$$

In the above, $\ell = e$, μ or τ. All squarks (and also all sleptons other than staus) are taken to be L or R eigenstates, except the stops, for which $\tilde{t}_1\tilde{t}_1$, $\tilde{t}_1\tilde{t}_2$ and $\tilde{t}_2\tilde{t}_2$ (here, $\tilde{t}_{1,2}$ being the lighter/heavier of the top squark mass eigenstates) production is included.

Given a point in SUGRA or MSSM space, and a collider energy, ISAJET generates all allowed production processes, according to their relative cross sections. The produced sparticles

or Higgs bosons are then decayed into all kinematically accessible channels, with branching fractions calculated within ISAJET. The sparticle decay cascade terminates with the lightest SUSY particle (LSP), taken to be the lightest neutralino ($\tilde{\chi}_1^0$). ISAJET currently neglects spin correlations and sparticle decay matrix elements. In the above reactions, spin correlation effects are only important for chargino and neutralino pair production, while decay matrix elements are mainly important for 3-body sparticle decays. ISAJET 7.15 also includes capability to generate SUSY and Higgs processes with polarized beams. Sample results from running ISAJET for LEP2 are given in Ref. [40].

The complete card image PAM file for ISAJET 7.15 can be copied across HEPNET, the high energy physics DECNET, from bnlcl6::2dua14:[isajet.isalibrary]isajet.car. A Unix makefile makefile.unix and a VMS isamake.com are available in the same directory. The same files can be obtained by anonymous ftp from bnlux1.bnl.gov:pub/isajet.

A sample input file for generating all sparticle processes at LEP2 is given below:

```
SAMPLE LEP2 SUGRA JOB
175.,100,0,0/
E+E-
NTRIES
2000/
SEED
999999999956781/
TMASS
180,-1,1/
SUGRA
100,80,0,2,-1/
JETTYPE1
'ALL'/
JETTYPE2
'ALL'/
END
STOP
```

3.3 SUSYXS

Program name:	SUSYXS 1.0, Dec 15 1995
Authors:	M. Mangano – `mlm@vxcern.cern.ch`
	G. Ridolfi – `ridolfi@vxcern.cern.ch`
Availability:	`http://www.ge.infn.it/LEP2` and
	`http://surya11.cern.ch/users/mlm/SUSY`
Documentation:	To be found in the above WWW directories

This is not an event generator, but a collection of simple programs to evaluate total cross sections for SUSY particles in e^+e^- collisions. No decays nor evaluation of decay BR's are included. This set of programs is mostly useful as a reference, to obtain quickly total production rates as a function of the various relevant parameters. It was used during the workshop as a benchmark for the comparisons among the different codes. The following processes are available (each encoded in a different fortran program):

- chargino pair production (`chargino.for`).
  Input parameters: $\sqrt{s}$, M_2, μ, $\tan\beta$, $M(\tilde{\nu}_{ee})$.

- neutralino pair production, for all possible neutralino pairs (`neutralino.for`).
  Input parameters: $\sqrt{s}$, M_2, μ, $\tan\beta$, $M(\tilde{e})$.

- selectron pair production (LL, RR and RL) (`selectron.for`).
  Input parameters: $\sqrt{s}$, $M(\tilde{e}_L)$, $M(\tilde{e}_R)$, M_2, μ, $\tan\beta$,

- smuon pair production (LL, RR) (`smuon.for`).
  Input parameters: $\sqrt{s}$, $M(\tilde{\mu}_L)$, $M(\tilde{\mu}_R)$.

- stop pair production (`stop.for`).
  Input parameters: $\sqrt{s}$, $M(\tilde{t}_1)$, $M(\tilde{t}_2)$, θ_{LR}.

- Higgs production (`higgs.for`).
  Input parameters: $\sqrt{s}$, M_A, $\tan\beta$, $M(\tilde{q})$.

ISR is included, as well as QCD corrections in the case of stop production [29]. All references for the formulas used are included as comments in the fortran files. The Higgs production code includes the one-loop-corrected masses [1], using the formulas of ref. [30].

How the code works. The code relative to the process of interest has to be linked to `phoisr` (which incorporates the ISR corrections) and to the CERN libraries. The executable can be run interactively, and the input parameters can be entered by the user at running time. Results with and without ISR are printed. In the case of chargino, neutralino and higgs production, the mass spectra are given as well. The codes are simple enough that any user can modify them easily to customize the output and produce directly, for example, cross section distributions or scatter plots. Likewise, the extraction of angular distributions for most processes is straightforward, as all needed formulas are collected in the codes.

3.4 SUSY23

Program name:	SUSY23 version 1.0
Authors:	J. Fujimoto, T. Ishikawa, M. Jimbo, T. Kaneko,
	K. Kato, S. Kawabata, T. Kon, Y. Kurihara,
	D. Perret-Gallix, Y. Shimizu, H. Tanaka
	`susy23@minami.kek.jp`
Availability:	Anonymous ftp: `ftp.kek.jp`
	Files in: `/kek/minami/susy23`.
Documentation:	

This is a Monte-Carlo unit-weight event generator for $2 \rightarrow 3$ SUSY processes at LEP2 energies, based on the minimal supersymmetric standard model (MSSM.).

Features of the program:

- Processes available: $e^+ e^- \rightarrow \chi_1^+ \chi_1^-$, $\tilde{\ell}_{L,R}^+ \tilde{\ell}_{L,R}^-$, $\tilde{\nu}_\ell^* \tilde{\nu}_\ell$, $\tilde{t}_1^* \tilde{t}_1$, $\tilde{b}_1^* \tilde{b}_1$, $\chi_1^0 \chi_2^0$, $\chi_2^0 \chi_2^0$, $\gamma \chi_1^0 \chi_1^0$, $e^\pm \tilde{e}^\mp \chi_1^0$, $e^\pm \tilde{\nu} \chi_1^\mp$

- Initial state radiation implemented using the structure function approach, and using QEDPS in some processes [41]

- Final sparticle decays included (see below)

- Hadronization realized via an interface with JETSET [16].

How the code works. FORTRAN source codes are generated by **GRACE** [42] which is a program for automatic computation of Feynman amplitudes. Largely exercised on standard model processes, **GRACE** is being used in the SUSY framework thanks to the addition of a dedicated vertex and propagator library. Tools have been developed to build automatically the SUSY23 event generator from the various processes thus prepared. Based on an open architecture, the generator can easily accommodate the addition of foreseen more complex processes $(2 \rightarrow 4)$. The numerical integration of the differential cross section over the phase space is carried out by the program BASES[7]. All information on the event kinematics and the phase space hyper-cell weight map are then used by the event generation program SPRING[7] to produce unit-weight events.

Helicity informations are available at the parton level. The hadronization is performed through the interface to the JETSET [16] package which has been extended to incorporate SUSY particle codes.

In this version (V1.0), the user may generate only one process per run, in future releases, the possibility will be given to produce events from a selected set of processes accordingly to their respective probability.

Input parameters Two approaches have been developed to better suit the user needs:

- A general program contains all process codes, the selection being performed by setting data cards.

- An interactive tool using menus and requesters gives the user the possibility to build a generator dedicated to a single process.

The following parameters can be set by the user:

- Selection of SUSY processes

- Center of mass energy : $\sqrt{s}$

- Experimental cuts

  - angle cuts for each sparticles
  - energy cuts for each sparticles
  - invariant mass cuts

- SUSY parameters

The program is based on the MSSM and the notation for SUSY parameters in ref. [43] is adopted. The input SUSY parameters are:

- gaugino parameters: $\tan\beta$, M_2, μ

- scalar lepton masses: $m_{\tilde{\ell}_L}$, $m_{\tilde{\ell}_R}$

- scalar (light) quark masses: $m_{\tilde{q}_L}$, $m_{\tilde{q}_R}$

- third generation scalar quark masses: $m_{\tilde{t}_1}$, $m_{\tilde{t}_2}$, θ_t, $m_{\tilde{b}_1}$, $m_{\tilde{b}_2}$, θ_b

General GRACE parameters can be found in the GRACE manual [42] (Helicity amplitude techniques, diagram generation and selection, phase space integration, event generation).

Sparticle decays. Particle widths and decay branching ratios for all possible modes are calculated. Each event final state is then generated according to these probabilities. We have included some possible cascade decays of sparticles as well as 2-body and 3-body direct decays.

Check of results We compared the results for 2-body processes, $e^+e^- \to \chi_1^+\chi_1^-$, $\tilde{\ell}_{L,R}^+\tilde{\ell}_{L,R}^-$, $\tilde{\nu}_\ell\tilde{\nu}_\ell$, $\tilde{t}_1\tilde{t}_1$, $\tilde{b}_1\tilde{b}_1$, $\chi_1^0\chi_2^0$, $\chi_2^0\chi_2^0$ with the analytical exact calculation. As for the 3-body processes, $e^+e^- \to e^\pm\tilde{e}^\mp\chi_1^0$, $e^\pm\tilde{\nu}\chi_1^\mp$, the results were checked against the analytical calculation based on the equivalent photon approximation. For the radiative process, $e^+e^- \to \gamma\chi_1^0\chi_1^0$, we compared the result with the exact calculation for $e^+e^- \to \gamma\tilde{\gamma}\tilde{\gamma}$ by taking a specific parameter points which corresponds to the case $\chi_1^0 \simeq \tilde{\gamma}$. The results for all 2-body processes are consistent with those of SUSYGEN [48].

3.5 DFGT: a chargino MC generator with full spin correlations

Program name: DFGT
Authors: C. Dionisi – `dionisi@vxrm70.roma1.infn.it`
                K. Fujii – `fujiik@jlcux1.kek.jp`
                S. Giagu – `giagu@vxcern.cern.ch`
                T. Tsukamoto – `tsukamot@kekvax.kek.jp`
Availability:
Documentation:

General features. We shortly summarize the features and performances of a new Montecarlo event generator, DFGT [45] which takes properly into account the full spin correlations that occur in the amplitude due to the matching of the spin of the produced and the decaying particle. The choice of SUSY parameters is that of the minimal supergravity scenario, assuming the GUT-relations [43]. The masses and the couplings of the SUSY particles are then specified by the four parameters m_0, M_2, μ and $\tan\beta$.

The events are generated as follows:

- Full helicity amplitudes including decays into final state partons are first calculated at tree level. This is done using HELAS library routines [46], which allows to implement correct angular correlations and effects of the natural widths of unstable partons.

- The effective cross sections are then evaluated by the numerical integration package BASES [7]. Initial state radiation is included in the structure function formalism, using the results of ref. [47].

- The generation of unweighted events is done at the partonic level using the SPRING package [7], and the QCD evolution and hadronization of the final state quarks in performed via an interface with JETSET 7.4 [16].

Chargino pair production takes place via s-channel γ and Z^0 exchange and via t-channel $\tilde{\nu}$ exchange. Only the light chargino and the lightest neutralino (taken as the LSP) are currently described by DFGT . Furthermore, it is assumed that charginos are lighter than all sfermions. The case of a $\tilde{\nu}$ lighter than the chargino [44], the dominant decay mode being then $\tilde{\chi}_1^\pm \rightarrow \tilde{\nu} l^\pm$, will be described in a forthcoming paper [45].

DFGT performance and comparison with SUSYGEN. Some results from the DFGT Montecarlo will now be presented. Figure 1(a) gives the total cross section of the chargino pair production as a function of $m_{\tilde{\nu}}$ showing the well known behaviour due to the interference between the s-channel and the t-channel amplitudes. The total cross sections at $\sqrt{s} = 190$ GeV with and without ISR corrections, and the total chargino widths for six points of the SUSY parameter space are listed in table 17. The six points, all with $\tan\beta = 1.5$, correspond to the the following set of parameter values:

1. $\mu = -190$ GeV, $M_2 = 65$ GeV

2. $\mu = -180$ GeV, $M_2 = 150$ GeV

3. $\mu = -40$ GeV, $M_2 = 240$ GeV

Labels A and B in table 17 correspond to $m_0 = 1000$ GeV and $m_0 = 90$ GeV, respectively.

(a)   (b)
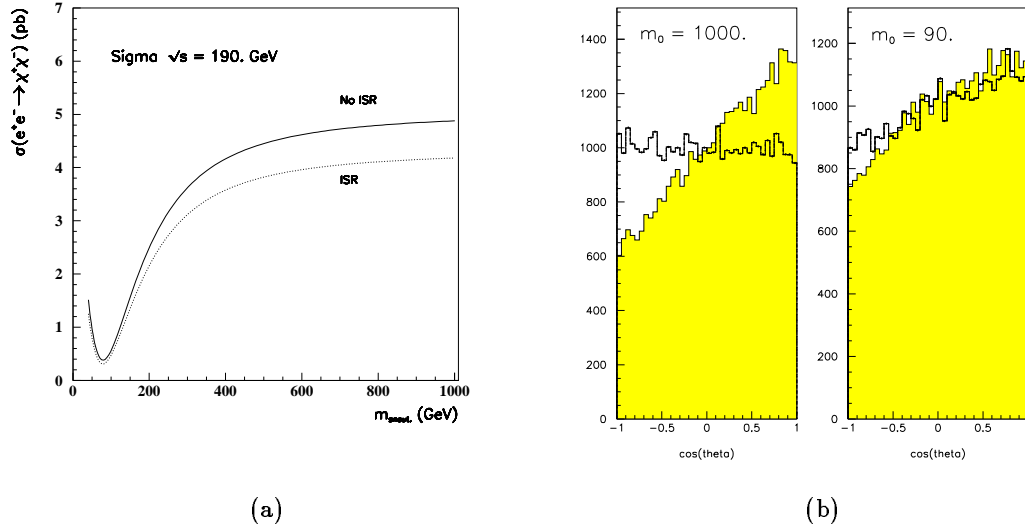
Figure 1: (a) Total cross section for chargino pair production as function of $m_{\tilde{\nu}}$ and (b) angular distributions for the fermions for the set 1A and 1B (Filled histogram: DFGT and histogram+dots: SUSYGEN).

For comparison the cross sections from SUSYXS (see section 3.3) and the total widths from SUSYGEN are also given. The cross sections agree at the percent level, while for the widths the agreement is of the order of few percent.

The effect of the spin correlations will now be shown by comparing some key distributions from DFGT and SUSYGEN at the generator level.

The angular distributions of the final state fermions for the parameter set 1A (which gives $m_{\tilde{\chi}^\pm} = 86$ GeV, $m_{\tilde{\chi}^0} = 37$ GeV, $m_{\tilde{l}} \simeq m_{\tilde{q}} \simeq 1000$ GeV) are shown in fig. 1 (a). Here θ is the angle between the outgoing fermion and the incoming electron. It is worth noticing that because of the large value of $m_{\tilde{\nu}}$ chargino production is dominated by the s-channel contribution, with the decay mode being dominated by $\tilde{\chi}_1^\pm \to W^* \tilde{\chi}^0 \to f\bar{f}'\tilde{\chi}^0$. The peak at $\cos\theta = 1$ is entirely due to the spin correlations, and is completely absent in the SUSYGEN distribution.

40

Set	$\Gamma_{\tilde{\chi}^\pm}$ (keV)		σ (pb)	
	DFGT	SUSYGEN	DFGT	SUSYXS
1A	37.69	37.58	4.849 (born)	4.849 (born)
			4.150 (ISR)	4.144 (ISR)
1B	66.77	66.79	0.538 (born)	0.532 (born)
			0.452 (ISR)	0.449 (ISR)
2A	35.80	36.87	3.630 (born)	3.623 (born)
			3.090 (ISR)	3.038 (ISR)
2B	39.07	40.21	1.656 (born)	1.659 (born)
			1.415 (ISR)	1.419 (ISR)
3A	2.79	2.75	3.503 (born)	3.551 (born)
			3.605 (ISR)	3.640 (ISR)
3B	2.79	2.75	3.287 (born)	3.324 (born)
			3.393 (ISR)	3.419 (ISR)

Table 17: Cross sections and total chargino widths for six points of SUSY parameter space.

The same distributions for the set 1B are given in 1 (b). Contrary to case 1A, now the t-channel contribution to the production and the $\tilde{\chi}_1^\pm \to \tilde{f}^* \nu \to f \bar{f}' \chi 0$ decay are relevant. Although less pronounced than in DFGT , the forward peak in the distribution appears now also in the SUSYGEN case. This reflects the non-trivial chargino angular distribution induced by the t-channel diagram. More work trying to pin down in detail how spin correlations affect the angular distributions is under way [45].

The impact of these differences on the chargino search has been checked by comparing at the generator level the distributions which play a major rôle in separating the signal from the physics backgrounds. Figs. 2 and 3 show, for DFGT and SUSYGEN , the missing p_T, the visible energy, the missing mass and the fermion-momentum distributions for set 1B (for set 1A the agreement is very good and it is not shown here). Although there is a systematic shift of about 1 GeV between the mean values for all the distributions, there is a good agreement in the tails in the regions where the cuts are applied. The importance of such effects has also been evaluated through a complete analysis of the two generators and using a full L3 detector simulation. The two analysis give essentially the same results for the sets of parameters considered here. However it is important to point out that in other points of the SUSY parameter space the conclusion might be different, in particular in regions where the mass splitting between the chargino and the neutralino is small, and where both are Higgsino-like. These cases are currently under investigation [45].
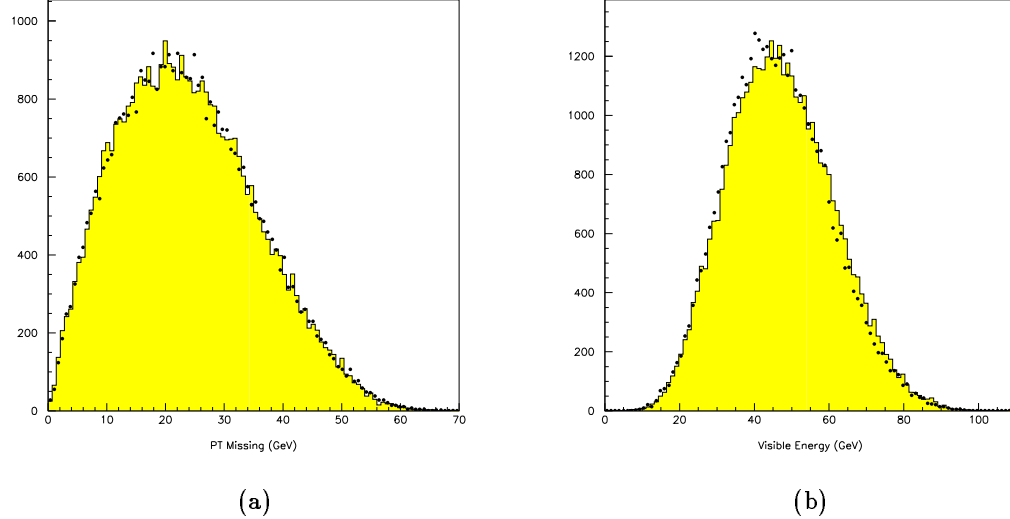
Figure 2: Missing p_T(a) and Visible Energy (b) distributions, for DFGT (histogram) and SUSYGEN (dots).

3.6 Scalar top and scalar bottom event generators

The top quark has two supersymmetric partners, $\tilde{t}_L$ and $\tilde{t}_R$. The mass eigenstates, $\tilde{t}_1$ and $\tilde{t}_2$, are mixtures of the two given by the mixing angle θ_{LR}. In this section we briefly describe and compare the generators developed by different LEP experiments for the production and decay of $\tilde{t}_1$ (from now on simply indicated by $\tilde{t}$) pairs. As discussed in detail ref. [5], the cross section and kinematics of the $\tilde{t}$ production is governed by two free parameters, the stop mass $m_{\tilde{t}}$ and θ_{LR}. The only decay channels which are of potential interest at LEP2 are $\tilde{t} \to \tilde{\chi}_1^0 c$ and $\tilde{t} \to \tilde{\chi}_1^+ b$. The latter decay channel has unit branching ratio when kinematically allowed; otherwise, the dominant final state becomes $\tilde{\chi}_1^0 c$. The decay mode is therefore completely specified by stop, chargino and neutralino masses. The chargino then decays via $\tilde{\chi}_1^+ \to W^{+*} \tilde{\chi}_1^0 \to f \bar{f}' \tilde{\chi}_1^0$; the decay into a real W^+ is almost always forbidden in the LEP2 energy range. The relative values of the stop, neutralino and chargino masses are the most significant parameters for the determination of the detection efficiencies.

The two most significant issues in the development of an event generator for $\tilde{t}$ are the treatment of the perturbative radiation off the $\tilde{t}$, and of the $\tilde{t}$'s hadronization and decay. Since the $\tilde{t}$ is a scalar particle, the spectrum of gluons emitted during the perturbative evolution will differ from that of a quark. Therefore the standard shower evolution codes such as JETSET would in principle require modifications in order to incorporate the correct radiation off the $\tilde{t}$. The Altarelli-Parisi splitting function describing the $\tilde{t} \to \tilde{t}g$ branching as a function of the

42
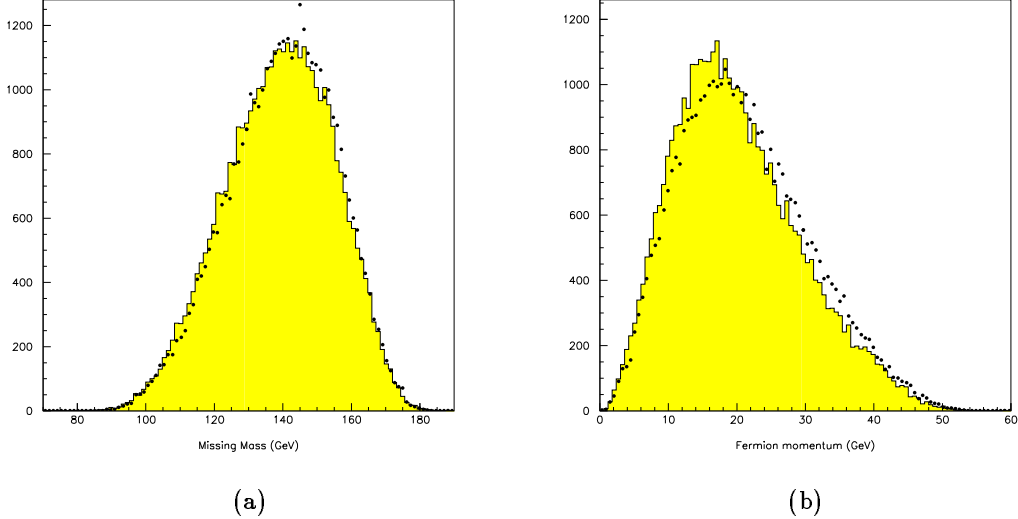
Figure 3: Missing Mass (a) and Fermion Momentum (b) distributions, for DFGT (histogram) and SUSYGEN (dots).

fractional energy carried away by the gluon $(x_g = 1 - x_q)$ is given by:

$$P_{\tilde{q}\tilde{q}}(x_q) = \frac{\alpha_{\rm s} C_F}{2\pi} \left[\left(\frac{1 + x_q^2}{1 - x_q} \right)_+ - (1 - x_q) \right] \tag{3.1}$$

with $C_F = 4/3$, to be compared to the standard spin-1/2 case:

$$P_{qq}(x_q) = \frac{\alpha_{\rm s} C_F}{2\pi} \left(\frac{1 + x_q^2}{1 - x_q} \right)_+ \tag{3.2}$$

Notice that $P_{qq}(x) > P_{\tilde{q}\tilde{q}}(x)$, namely the $\tilde{t}$ fragmentation function will be harder than that of a fermion of the same mass. Notice however that the difference is proportional to the gluon energy, and vanishes in the soft gluon limit $(x_q \to 1)$. Therefore it can be consistently neglected within the approximations used by most shower Monte Carlo programs. More quantitatively, one can estimate the average energy loss due to perturbative gluon emission from a particle of mass m using the well known expression [49]:

$$\langle x_g \rangle = 1 - \left[\frac{\alpha_{\rm s}(m)}{\alpha_{\rm s}(E)} \right]^{P^{(2)}/(2\pi b)} , \tag{3.3}$$

where $P^{(2)}$ is the second moment of the relevant splitting function, $b = (33 - 2N_f)/(12\pi)$ and E is the beam energy. Using the values of $P^{(2)} = -C_F$ for a spin-0 particle and $-4/3 C_F$ for

43

spin-1/2, it is easy to find:

$$\langle x_g \rangle_0 - \langle x_g \rangle_{1/2} = \frac{\alpha_s(E) C_F}{3\pi} \log \frac{E}{m} \tag{3.4}$$

At 190 GeV, this difference ranges between 0.01 and 3×10^{-3} for $45 < m_{\tilde{t}} < 80$ GeV, with average energy losses for the scalar case of 3% and 1%, respectively. Such effects are totally negligible.

As for the issue of $\tilde{t}$ hadronization, it is important to realize that when the dominant decay mode is $\tilde{t} \to \tilde{\chi}_1^0 c$ the $\tilde{t}$ lifetime is longer than the typical time scale of hadron formation, and $\tilde{t}$-hadrons are formed before decay. Therefore, $\tilde{t}$ hadronization must be taken into account by Monte Carlo generator. This has been done within different approaches, which will be described and compared in the following.

Improvements and extentions of the existing codes, in order to achieve a more precise description of $\tilde{t}$ physics, are possible and foreseen. For details on the individual generators, see [50, 51, 52].

3.6.1 The DELPHI event generator.

The DELPHI $\tilde{t}$ and $\tilde{b}_1$ event generators are based on the packages BASES and SPRING [7], which perform the multidimensional phase space integration and the event unweighting. The expression of the differential production cross section for $\tilde{t}$ and $\tilde{b}_1$ pairs has been computed using the results of ref. [29], which include initial state QED radiation in the collinear approximation at the leading order, and QCD corrections.

The event generator has been interfaced with JETSET 7.3 [16] in order to completely describe the evolution and hadronization of the colored partons. Perturbative gluon radiation off the $\tilde{t}$ is implemented according to the $\tilde{t} \to \tilde{t}g$ splitting function given above (see also ref. [53]), together with some additional features such as angular ordering of the gluon shower due to soft gluon interference as described in ref. [54]. The formation and decay of the $\tilde{t}$ hadron is then implemented in the spectator quark approach [55]. After the decay, a color string is pulled between the decay c quark and the spectator quark, giving rise to the standard string fragmentation.

The user can choose the values of the center of mass energy, the $\tilde{t}$ mass, the mixing angle $\theta_{\tilde{t}}$, and the $\tilde{\chi}_1^0$ mass. It is also possible to decide whether or not to include QCD corrections and/or initial state radiation. The decay $\tilde{t} \to b \tilde{\chi}_1^+$ with $\tilde{\chi}_1^+ \to W^* \tilde{\chi}_1^0 \to f \bar{f}' \tilde{\chi}_1^0$ is also implemented; in this case, the $\tilde{\chi}_1^+$ mass is an additional free input parameter.

The $\tilde{b}$ event generator has been implemented along similar lines; the only decay mode in this case is $\tilde{b}_1 \to b \tilde{\chi}_1^0$.

3.6.2 The L3 event generator.

The L3 event generator [51] includes both $\tilde{\chi}^0$ and $\tilde{\chi}^{\pm}$ decay modes. The L3 event generator is based on the calculation of 4-momenta distributions of the final state particles $\tilde{\chi}_1^0 c \tilde{\chi}_1^0 \bar{c}$ or $\tilde{\chi}_1^- b \tilde{\chi}_1^+ \bar{b}$. The large effects of QCD corrections are included in the cross section calculations using the results of ref. [56] (see also [53]). The $\tilde{t}$ production and decay have been defined as new processes in PYTHIA [16]. The event generation process includes modeling of hadronic final states.

In the first step of the event generation, initial state photons are emitted using the program package REMT [16], and the production cross section at the reduced center-of-mass energy is calculated. The effective center-of-mass energy is calculated for the generation of the 4-momenta of the final state particles. These 4-momenta are then boosted according to the momentum of the initial state photon. No perturbative gluon radiation is included before the $\tilde{t}$ decay. This is justified by the fact that less than about 1% of the $\tilde{t}$ energy is expected to be radiated in the form of hard gluons. After the $\tilde{t}$ decay, a color string with the invariant mass of the quark-antiquark-system ($c\bar{c}$ or $b\bar{b}$) is defined. Gluon emission and hadronization is then performed using the Lund model of string fragmentation as implemented in PYTHIA [16]. The Peterson fragmentation parameters [61] for the c and b-quarks are chosen to be $\epsilon_c = 0.03$ and $\epsilon_b = 0.0035$, as determined from L3 event shape distributions. Finally, short-lived particles decay into their observable final state, where the standard L3 particle decay tables are applied.

3.6.3 The OPAL event generator.

The OPAL event generator has been used by OPAL [58] in the LEP1 analyses of $\tilde{t}$ search. It only includes the $\tilde{t} \rightarrow c\tilde{\chi}_1^0$ decay. The production matrix elements are taken from ref. [29, 57], including the effect of QCD corrections. In the first step of the event generation, inital state photons are emitted taking into account the $\tilde{t}\bar{\tilde{t}}$ cross section at the reduced center of mass energy. JETSET [16] is then used to perform the perturbative gluon emission. This is done using the default emission probabilities, evaluated assuming the radiating particle to have spin-1/2. After the perturbative evolution, Peterson fragmentation is introduced, with the parameter $\epsilon_{\tilde{t}}$ set to

$$\epsilon_{\tilde{t}} = \epsilon_b \frac{m_b^2}{m_{\tilde{t}}^2}, \quad \epsilon_b = 0.0057, \ m_b = 5 \text{ GeV}. \tag{3.5}$$

As mentioned above, in the case of the $\tilde{t} \rightarrow c\tilde{\chi}_1^0$ decay the $\tilde{t}$ hadronizes to form a $\tilde{t}$-hadron before it decays. $\tilde{t}$-hadrons are therefore formed, as bound states of a $\tilde{t}$ and a light anti-quark ($\bar{u}, \bar{d}$), $\bar{s}$, or a diquark (uu etc.). As a result of the combined perturbative and non-perturbative evolution, about 1% [0.5%] of the $\tilde{t}$ initial energy goes into ordinary hadrons for a 70 GeV (80 GeV) $\tilde{t}$ at $\sqrt{s} = 190$ GeV. This is consistent with the estimates given earlier.

After the $\tilde{t}$ decay, a colour string is stretched between the charm quark and the spectator. This colour singlet system is again hadronized by JETSET. Additional gluon bremsstrahlung

is allowed in this process. The Peterson fragmentation function is used at the end of the charm quark evolution.

A code based on the same physical principles was also developed by ALEPH, and has been used in their LEP1 $\tilde{t}$ analysis [59].

3.6.4 Comparison of generators for $\tilde{t}\bar{\tilde{t}}$.

We now compare some details of the OPAL, DELPHI, and L3 $\tilde{t}\bar{\tilde{t}}$ generators for the $\tilde{\chi}_1^0 c \tilde{\chi}_1^0 \bar{c}$ channel. Some differences in the features of the final states are observed, and their origin can be found in the different treatment of the hadronization process. In the L3 generator, $\tilde{t}$ production and decay is performed in analogy to the top quark, whose lifetime is much shorter than the hadronization time scale. Connecting the final state c and $\bar{c}$ with a string implicitly assumes that the $c\bar{c}$ system will radiate coherently. This is not the case for radiation whose wave-length is smaller than the $\tilde{t}$ lifetime. OPAL introduces the intermediate step of $\tilde{t}$-hadron formation. The radiating system after $\tilde{t}$ decay is then given not by the $c\bar{c}$ pair, but by the two systems $c\bar{q}$ and $\bar{c}q'$, q and q' being the spectator quarks. Qualitalively this will lead to lower particle multiplicity and more collimated jets than in the L3 approach. DELPHI introduces the emission of a large number of low energy gluons to simulate the fragmentation of the stop bound state. In all codes, we have checked that the effect of varying the ϵ parameter in the Peterson fragmentation effects is very small.

To illustrate the effect of the differences just mentioned, Table 18 shows the total final state charged and neutral multiplicities, as obtained from the different programs. Table 19 shows multiplicities, energies and masses for particles with a minimum energy of 500 MeV, $i.e.$ above the typical detector thresholds. The visible energy is essentially determined by the decay kinematics of the $\tilde{t}$ hadron. The 3-5 GeV difference between the OPAL and L3 generators is due to the energy of hadrons produced during the QCD evolution of the $\tilde{t}$ before it hadronizes. This difference increases for lighter $\tilde{t}$ because of the softer fragmentation function. The particle multiplicity found by L3 is larger than OPAL's by up to 4 charged particles per event, depending on the $\tilde{t}$ and $\tilde{\chi}^0$ masses. This is consistent with what anticipated above. The two-jet structure is expected to be clearer for events generated by OPAL than L3 and DELPHI, because the jet evolution is localized in the $\tilde{t}$-hadron decay. In the DELPHI generator, the cut-off for the gluon emission is a critical parameter and may explain the larger visible energy. The matching of the evolution scale Q^2 where to terminate the gluon emission with the Q_0^2 parameter in the Lund QCD parton shower optimized for the Lund string fragmentation model must be investigated for the DELPHI model.

The DELPHI and L3 generators also include the $b\tilde{\chi}_1^+ \bar{b}\tilde{\chi}_1^-$ channel. A comparison between them appears in table 20. The agreement is good, because the $\tilde{\chi}_1^+$ decay is described in a similar way in the two generators, and in both cases the hadronization takes place in the $b\bar{b}$ system.

The $\tilde{t}$-search studies are documented in [5]. Since the global event signature is the large missing momentum due to the presence of two neutralinos in the final state, the variables in the

(70,50)	neutral	charged	Evis	Mvis
OPAL	10	8.1	50	41
DELPHI	22	19	56	46
L3	15	12	48	37

Table 18: Comparison of LEP2 generators in the $\tilde{\chi}_1^0 c \tilde{\chi}_1^0 \bar{c}$ channel: neutral and charged multiplicity, visible energy (in GeV) and visible mass (in GeV) without a cut on the particle energy. Stop and neutralino masses (in GeV) are given in brackets.

event analysis can be chosen to be largely independent of the generator differences. Differences related to the hadronization properties, which possibly affect the jet structure, can be overcome by choosing different resolution parameters in the jet definitions. As a net result, in spite of the differences currently observed among these three generators the studies of the $\tilde{t}$ discovery potential carried out by the three experiments are consistent with each other [5].

4 Leptoquarks

4.1 LQ2

Program name:	LQ2 – Leptoquark Event Generator 1.00/04
Date of last revision:	29 September 1995
Author:	D. M. Gingrich – `gingrich@phys.ualberta.ca`
Other programs called:	JETSET 7.405 (plus PYTHIA 5.710)
	and CERNLIB (DIVON4, RANECU)
Comments:	source code managed with CMZ
Availability:	The complete code documentation is available from the author

This section describes a Monte Carlo program which generates pair production of scalar or vector leptoquarks in electron-positron annihilation. The leptoquarks are produced according to an effective Lagrangian with the following properties [62]: 1) baryon and lepton number conservation, 2) non-derivative and family diagonal couplings to lepton-quark pairs and 3) $SU(3)_C \times SU(2)_L \times U(1)_Y$ invariance.

The contributions to leptoquark pair production from the s-channel exchange of an electroweak boson, t-channel exchange of a quark and the interference between them are included in the differential cross-section. The angular distribution of the scalar or vector leptoquarks assumes unpolarized beams. Initial state radiation, currently not present, will soon be included. The centre of mass energy is not restricted to the Z-resonance. The leptoquarks are allowed

47

(70,50)	neutral	charged	Evis	Mvis
OPAL	6.6	7.0	48	39
DELPHI	10	16	53	43
L3	9.0	11	45	35
(70,60)	neutral	charged	Evis	Mvis
OPAL	5.0	5.8	28	23
DELPHI	8.3	14	35	28
L3	6.5	7.7	24	19
(70,65)	neutral	charged	Evis	Mvis
OPAL	3.7	4.8	17	14
DELPHI	6.1	11	24	19
L3	4.1	5.3	12	9.6

Table 19: Comparison of LEP2 generators in the $\tilde{\chi}_1^0 c \tilde{\chi}_1^0 \bar{c}$ channel: neutral and charged multiplicity, visible energy (in GeV) and visible mass (in GeV) with a minimum cut on the particle energy of 500 MeV. Stop and neutralino masses (in GeV) are given in brackets.

(70,60,30)	neutral	charged	Evis	Mvis
DELPHI	17	21	81	76
L3	15	20	79	74

Table 20: Comparison of LEP2 generators in the $b\tilde{\chi}_1^+ \bar{b}\tilde{\chi}_1^-$ channel: neutral and charged multiplicity, visible energy (in GeV) and visible mass (in GeV) with a minimum cut on the particle energy of 500 MeV. Stop and neutralino masses (in GeV) are given in brackets.

to decay to lepton-quark or neutrino-quark final states. Decays to all three generations are possible but the massless quark approximation will not be valid for decays to the top quark.

The LUND routines of JETSET [16] are used for the final state parton shower, fragmentation and decay processes. The generator fills the JETSET common block /LUJETS/ and the standard Monte Carlo generator common block /HEPEVT/. The mechanics of the program closely follows that of an analogous generator for simulating leptoquark production and decay in electron-proton collisions [63].

Physics Processes. The lowest order Feynman diagrams for leptoquark production in electron-positron annihilation $(e^+e^- \rightarrow L_Q\overline{L_Q})$ are straightforward to evaluate using the general couplings from the effective Lagrangian [62]. In general, the pair production amplitudes for the s-channel and t-channel processes can interfere and the differential cross-section for the production of scalar leptoquarks is given by three terms:

$$\frac{d\sigma_{\text{scalar}}}{d(\cos\theta)} = \frac{3\pi\alpha^2}{8s}\beta^3\sin^2\theta \sum_{a=\text{L,R}} [|A_\gamma + A_Z|_a^2 + 2\lambda_a^2 Re[(A_\gamma + A_Z)_a(A_q^*)_a] + \lambda_a^4|A_q|_a^2], \qquad (4.1)$$

where A_γ and A_Z denote the photon and Z-boson s-channel exchange terms, and A_q is the t-channel exchange term. The sum is over electron polarizations and $\lambda_{\text{L,R}}$ are the generalized couplings. θ is the polar angle and $\beta = \sqrt{1 - 4m_{\text{LQ}}^2/s}$ is a kinematic threshold factor.

Similarly the differential cross-section for the production of vector leptoquarks is

$$\frac{d\sigma_{\text{vector}}}{d(\cos\theta)} = \frac{3\pi\alpha^2}{8M_{LQ}^2}\beta^3\left(\frac{7 - 3\beta^2}{4}\right)\sum_{a=\text{L,R}} [|A_\gamma + A_Z|_a^2 + 2\lambda_a^2 Re[(A_\gamma + A_Z)_a(A_q^*)_a] + \lambda_a^4|A_q|_a^2], \quad (4.2)$$

From the effective lagrangian one can obtain the various partial leptoquark decay widths, Γ_{LQ}. For the scalar (S) and vector (V) leptoquarks we have

$$\Gamma_{\text{LQ}}^{\text{S}} = \frac{\lambda_{\text{L,R}}^2 m_{\text{LQ}}}{16\pi} \quad \text{and} \quad \Gamma_{\text{LQ}}^{\text{V}} = \frac{\lambda_{\text{L,R}}^2 m_{\text{LQ}}}{24\pi}, \qquad (4.3)$$

where $\lambda_{\text{L,R}}$ denote the leptoquark couplings to a particular final state and m_{LQ} is the leptoquark mass. The total widths are obtained by summing over all possible final states.

Table 21 gives the quantum numbers, couplings and decay channels for all leptoquarks. We have adapted the notation of ref. [64][3].

Generator. The user must supply his own main program to initialize the package and generate events. The initialization routine LQINIT must be called once to perform some initialization and calculate the total cross-section. Some simple checks are make to see that the required leptoquark and decay process are consistent with the requested quantum numbers and couplings.

---

[3]$S_0, \tilde{S}_0, S_1, V_{1/2}, \tilde{V}_{1/2}, V_0, \tilde{V}_0, V_1, S_{1/2}, \tilde{S}_{1/2}$ in ref. [64] correspond to $S_1, \tilde{S}_1, S_3, V_2, \tilde{V}_2, U_1, \tilde{U}_1, U_3, R_2, \tilde{R}_2$ in ref. [62] respectively.

A call is automatically made to the routine TOTSCALAR or TOTVECTOR to calculate the total cross-section. The differential cross-section function XSCALAR or XVECTOR is numerically integrated as a test that the generator is initialized properly. The resonance width and branching ratio are also calculated. A program banner, the value of some parameters and the process to be generated are printed out.

Events are generated by calling the routine LQGEN once per event in the user main program. The routine to create the event record, LQFILL, is then automatically called by LQGEN. Routines from JETSET are used for final state fragmentation and decay processes.

All other subroutines and functions are called internally. But, if so desired, the total cross-section functions or differential cross-section functions (function of polar angle) may be called by the user after initialization.

Numerical integration. The differential cross-sections are integrated and sampled using the CERNLIB package DIVON4 [65]. The package consists of a collection of routines to aid in the numerical integration of functions of several variables and to sample points in a multi-dimensional coordinate space from a specified probability density function. The algorithm adaptively partitions a multi-dimensional coordinate space into a set of axis-oriented hyper-rectangular regions, based on a user provided function. These regions are then used for a stratified sampling estimate of the integral of the function, or to sample random vectors from the coordinate space with probability density that of the function. The integration and importance sampling are extremely fast in LQ2 since the cross-section is a function of a single variable.

Installation and availability. The LQ2 package is managed as a CMZ library. The program needs to be linked with JETSET version 7.4 and PYTHIA version 5.7. The CERN libraries MATHLIB and KERNLIB must also be loaded to include the random number generator RANECU timing routine TIMED and the integration package DIVON4.

The LQ2 CMZ library can be obtained via anonymous ftp at `jever.phys.ualberta.ca` in file `pub/lq2.cmz`.

$^Q\mathrm{LQ}_T$	T_3	Decay	Coupling
$^{-1/3}S_0$	0	$e_L^- u_L$	λ_L
$^{-1/3}S_0$	0	$e_R^- u_R$	λ_R
$^{-1/3}S_0$	0	$\nu_e d_L$	$-\lambda_L$
$^{-4/3}\tilde{S}_0$	0	$e_R^- d_R$	λ_R
$^{+2/3}S_1$	$+1$	$\nu_e u_L$	$\sqrt{2}\lambda_L$
$^{-1/3}S_1$	0	$\nu_e d_L$	$-\lambda_L$
$^{-1/3}S_1$	0	$e_L^- u_L$	$-\lambda_L$
$^{-4/3}S_1$	-1	$e_L^- d_L$	$-\sqrt{2}\lambda_L$
$^{-1/3}V_{1/2}$	$+1/2$	$\nu_e d_R$	λ_L
$^{-1/3}V_{1/2}$	$+1/2$	$e_R^- u_L$	λ_R
$^{-4/3}V_{1/2}$	$-1/2$	$e_L^- d_R$	λ_L
$^{-4/3}V_{1/2}$	$-1/2$	$e_R^- d_L$	λ_R
$^{+2/3}\tilde{V}_{1/2}$	$+1/2$	$\nu_e u_R$	λ_L
$^{-1/3}\tilde{V}_{1/2}$	$-1/2$	$e_L^- u_R$	λ_L
$^{-2/3}V_0$	0	$e_L^- \overline{d}_R$	λ_L
$^{-2/3}V_0$	0	$e_R^- \overline{d}_L$	λ_R
$^{-2/3}V_0$	0	$\nu_e \overline{u}_R$	λ_L
$^{-5/3}\tilde{V}_0$	0	$e_R^- \overline{u}_L$	λ_R
$^{+1/3}V_1$	$+1$	$\nu_e \overline{d}_R$	$\sqrt{2}\lambda_L$
$^{-2/3}V_1$	0	$e_L^- \overline{d}_R$	$-\lambda_L$
$^{-2/3}V_1$	0	$\nu_e \overline{u}_R$	λ_L
$^{-5/3}V_1$	-1	$e_L^- \overline{u}_R$	$\sqrt{2}\lambda_L$
$^{-2/3}S_{1/2}$	$+1/2$	$\nu_e \overline{u}_L$	λ_L
$^{-2/3}S_{1/2}$	$+1/2$	$e_R^- \overline{d}_R$	$-\lambda_R$
$^{-5/3}S_{1/2}$	$-1/2$	$e_L^- \overline{u}_L$	λ_L
$^{-5/3}S_{1/2}$	$-1/2$	$e_R^- \overline{u}_R$	λ_R
$^{+1/3}\tilde{S}_{1/2}$	$+1/2$	$\nu_e \overline{d}_L$	λ_L
$^{-2/3}\tilde{S}_{1/2}$	$-1/2$	$e_L^- \overline{d}_L$	λ_L

Table 21: Quantum numbers (Q is the electric charge, T is the weak isospin and T_3 is the third component of isospin), coupling constants and decay channels for leptoquarks.

References

[1] See the "Higgs Physics" Chapter in vol. I of this Report.

[2] See the "Event generators for WW physics" Chapter in this volume.

[3] M. Consoli, W. Hollik and F. Jegerlehner in: *Z Physics at LEP1*, G. Altarelli, R. Kleiss and C. Verzegnassi eds., CERN Yellow Report No.89-08 (1989) Vol. 1, p.7.

[4] E. Gross, B.A. Kniehl and G. Wolf, *Z. Phys.* **C63** (1994) 417.

[5] See the "Search for New Physics" Chapter in vol. I of this Report.

[6] E. Boos, M. Dubinin, V. Edneral, V. Ilyin, A. Kryukov, A. Pukhov, S. Shichanin, in: "New Computing Techniques in Physics Research II", ed.by D. Perret-Gallix, World Scientific, Singapore, 1992, p. 665
in: Proc. of the XXVI Recontre de Moriond, ed. by Tranh Than Van, Editions Frontieres, 1991, p. 501;
E.Boos, M.Dubinin, V.Ilyin, A.Pukhov, V.Savrin, preprint INP MSU 94-36/358, 1994 (hep-ph/9503280)

[7] S. Kawabata, *Comput. Phys. Commun.* **41** (1986) 127; *ibid.* **88** (1995) 309

[8] E.Boos, M.Sachwitz, H.J.Schreiber, S.Shichanin, *Z. Phys.* **C61** (1994) 675;
M.Dubinin, V.Edneral, Y.Kurihara, Y.Shimizu, *Phys. Lett.* **B329** (1994) 379;
E.Boos, M.Sachwitz, H.J.Schreiber, S.Shichanin, *Int. Jour. Mod. Phys.* **A10** (1995) 2067;
E.Boos, M.Sachwitz, H.J.Schreiber, S.Shichanin, *Z. Phys.* **C64** (1994) 361;
E.Boos, M.Sachwitz, H.J.Schreiber, S.Shichanin, DESY preprint 95-002, 1995.

[9] D. Bardin, A. Leike and T. Riemann, *Phys. Lett.* **B344** (1995) 383.

[10] D. Bardin, A. Leike and T. Riemann, *Phys. Lett.* **B353** (1995) 513.

[11] Review of particle properties, L. Montanet et al., *Phys. Rev.* **D50** (1994) 1173.

[12] G. Montagna, O. Nicrosini and F. Piccinini, *Phys. Lett.* **B348** (1995) 496.

[13] HIGGSPV - in preparation.

[14] M. Carena, M. Quiros, and C.E.M. Wagner, CERN preprint CERN-TH/95-157.

[15] H. Haber, R. Hempfling and A. Hoang, private commmunication.

[16] T. Sjöstrand, *Comput. Phys. Commun.* **82** (1994) 74.

[17] A. Ballestrero, E. Maina, *Phys. Lett.* **B350** (1995) 225.

[18] A. Ballestrero, in preparation.

[19] F.A. Berends, P.H. Daverveldt and R. Kleiss, *Nucl. Phys.* **B253** (1985) 441;
R. Kleiss and W.J. Stirling, *Nucl. Phys.* **B262** (1985) 235.

[20] G.P. Lepage, *Jour. Comp. Phys.* **27** (1978) 192.

[21] D. Bardin et al. in Physics at LEP200 and Beyond, *Nucl. Phys.* **37B** (Proc. Suppl.) (1994), T. Riemann and J. Blümlein eds.

[22] G. Montagna, O. Nicrosini, G. Passarino and F. Piccinini, *Phys. Lett.* **B348** (1995) 178.

[23] G. Montagna, O. Nicrosini and F. Piccinini, *Comput. Phys. Commun.* **90** (1995) 141.

[24] F. A. Berends, R. Kleiss and R. Pittau, *Nucl. Phys.* **B426** (1994) 344.

[25] D. Bardin, W. Beenakker and A. Denner, *Phys. Lett.* **B137** (1993) 213.

[26] G. Passarino, *Nucl. Phys.* **B237** (1984) 249.

[27] J. Hilgart, R. Kleiss and F. Le Diberder, *Comput. Phys. Commun.* **75** (1993) 191.

[28] For references see the review papers: H.-P. Nilles, *Phys. Rep.* **110** (1984) 1;
H.E. Haber, G.L. Kane, *Phys. Rep.* **117** (1985) 75;
R. Barbieri, *Riv. Nuo. Cim.* **11** (1988) 1.

[29] M. Drees and K. Hikasa, *Phys. Lett.* **B252** (1990) 127.

[30] J. Ellis, G. Ridolfi and F. Zwirner, *Phys. Lett.* **B257** (1991) 83; *Phys. Lett.* **B262** (1991) 477.

[31] A. Bartl, H. Fraas, W. Majerotto, *Z. Phys.* **C30** (1986) 411; *Z. Phys.* **C34** (1987) 411; *Z. Phys.* **C41** (1988) 475, *Nucl. Phys.* **B278** (1986) 1; *Z. Phys.* **C55** (1992) 257.

[32] S. Ambrosanio and B. Mele, *Phys. Rev.* **D52** (1995) 3900, and ROME1-1095/95 hep-ph/9508237.

[33] H. Dreiner and S. Lola, DESY 92-123B, p 707.

[34] F. Paige and S. Protopopescu, in *Supercollider Physics*, p. 41, ed. D. Soper (World Scientific, 1986);
H. Baer, F. Paige, S. Protopopescu and X. Tata, in *Proceedings of the Workshop on Physics at Current Accelerators and Supercolliders*, ed. J. Hewett, A. White and D. Zeppenfeld, (Argonne National Laboratory, 1993).

[35] G. Fox and S. Wolfram, *Nucl. Phys.* **B168** (1980) 285.

[36] R. Field and R. Feynman, *Nucl. Phys.* **B136** (1978) 1.

[37] Y. Okada, M. Yamaguchi and T. Yanagida, *Phys. Lett.* **262B** (1991) 54;
H. Haber and R. Hempfling, *Phys. Rev. Lett.* **66** (1991) 1815; J. Ellis, G. Ridolfi and F. Zwirner, *Phys. Lett.* **257B** (1991) 83;
for detailed formulae incorporated into ISAJET, see M. Bisset, University of Hawaii Ph. D. Thesis UH-511-813-94 (1994).

[38] H. Baer, C. H. Chen, R. Munroe, F. Paige and X. Tata, *Phys. Rev.* **D51** (1995) 1046.

[39] H. Baer, A. Bartl, D. Karatas, W. Majerotto and X. Tata, *Int. Jour. Mod. Phys.* **A4** (1989) 4111.

[40] H. Baer, M. Brhlik, R. Munroe and X. Tata, *Phys. Rev.* **D52** (1995) 5031.

[41] Y. Kurihara, J. Fujimoto, T. Munehisa, Y. Shimizu, "QEDPS" in this Yellow Report: KEK CP-035, KEK Preprint 95-126, 1995

[42] Minami-Tateya collabolation, "GRACE manual ver 1.0", KEK Report **92-19**, 1993;
Minami-Tateya collabolation, Brief Manual of GRACE system ver 2.0/β, 1995.

[43] K. Hikasa, *JLC Supersymmetry Manual*, unpublished.

[44] M.Chen,C.Dionisi,M.Martinez and X.Tata, *Phys. Rep.* **159** (1988) 201;
C.Dionisi et al., Proc. of the ECFA workshop on LEP 200, Aachen, 1986, Vol.II, p. 380,
CERN 87-08, ECFA;
A.Bartl, H.Fraas, W. Majerotto and B. Mösslacher, *Z. Phys.* **C55** (1992) 257.

[45] C. Dionisi, K. Fujii, S. Giagu and T. Tsukamoto, in preparation.

[46] H. Murayama, I. Watanabe and K. Hagiwara, KEK Preprint 91-11 (1992)

[47] J.Fujimoto et al., *Progr. of Theor. Phys.*, Supplement No. 100 (1990), Equation (11.200)
on p297.

[48] S. Katsanevas and S. Melachroinos, "SUSYGEN" in this Yellow Report

[49] Ya.I. Azimov, Yu.L. Dokshitzer and V.A. Khoze, *Yad. Fiz.* **36** (1982) 1510.

[50] M. Besançon, DELPHI Note, in preparation.

[51] A. Sopczak, L3 Note 1860, (1995). The generator is implemented in the L3 software under
the name `EGLOv201`.

[52] S. Asai, S. Komamiya and S. Orito, preprint UT-ICEPP 95-10 (1995).

[53] W.Beenakker, R. Hopker and P.M. Zerwas, *Phys. Lett.* **B349** (1995) 468.

[54] G.Marchesini and R.B.Webber, *Nucl. Phys.* **B310** (1988) 461.

[55] A. Ali, *Z. Phys.* **C1** (1979) 25;
M.K. Gaillard, B.W. Lee and J.L. Rosner, *Rev. Mod. Phys.* **47** (1975) 227;
V. Barger, T. Gottschalk and R.J.N Phillips, *Phys. Lett.* **B82** (1979) 445;
M. Suzuki, *Nucl. Phys.* **B258** (1985) 553.

[56] A. Bartl, W. Majerotto, W. Porod, *Z. Phys.* **C64** (1994) 499, and private communication.

[57] K. Hikasa and M. Kobayashi, *Phys. Rev.* **D36** (1987) 724.

[58] OPAL Collaboration, R. Akers *et al.*, *Phys. Lett.* **B337** (1994) 207.

[59] ALEPH Collaboration, Proc. of the International Europhysics Conference on High Energy
Physics, Brussels, Belgium, 27 July - 2 August (1995).

[60] B. Andersson *et al.*, *Phys. Rep.* **97** (1983) 31.

[61] C. Peterson, D. Schlatter, I. Schmitt and P.M. Zerwas, *Phys. Rev.* **D27** (1983) 105.

[62] J. Blümlein & R. Rückl, *Phys. Lett.* **B304** (1993) 337.

[63] D.M. Gingrich, Oxford University preprint OUNP-92-19;
D. Gingrich & N. Harnew, Proceedings of the Workshop, 29-30 Oct. 1991, Hamburg, ed.
W. Buchmüller & G. Ingelman, Vol. 3, pp. 1542-1550.

[64] T. Köhler, Diplomarbeit at the RWTH Aachen (1989);
B. Schrempp, Proceedings of the Workshop, 29-30 Oct. 1991, Hamburg, ed. W. Buchmüller
& G. Ingelman, Vol. 2, pp. 1034-1042.

[65] J.H. Friedman & M.H. Wright, "DIVONNE4 – A Program for Multiple Integration and Adaptive Importance Sampling", CERN D151 DIVON4, 1981.06.01.

[66] "A Source Code Management System CMZ", version 1.37, 1991.07.13.